

LOUGHBOROUGH
UNIVERSITY OF TECHNOLOGY
LIBRARY

AUTHOR/FILING TITLE

CHEUNG, S W

ACCESSION/COPY NO.

010664/02

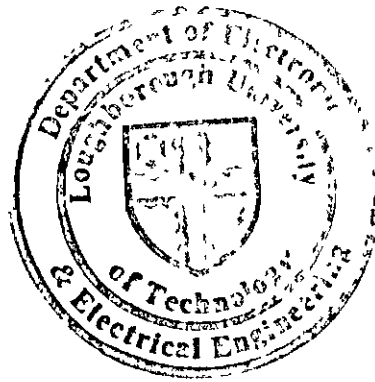
VOL. NO.

CLASS MARK

VOL. NO.	CLASS MARK
- 3 JUL 1987	LOAN COPY
- 6 JUL 1990	
- 3 JUL 1992	
- 2 JUL 1993	
- 1 JUL 1994	
- 2 JUL 1993	

001 0664 02





DIGITAL MODEMS FOR MOBILE SYSTEMS

BY

SING-WAI CHEUNG, B.Sc.

Supervisor: Professor A.P. Clark

Department of Electronic and Electrical Engineering

University of Technology

LOUGHBOROUGH

Leicestershire

© By S.W. Cheung, 1986

Loughborough University	
of T.	Library
Date	May 87
Class	
Acc. No.	010664/02

To
MY
PARENTS



LIST OF CONTENTS

	<u>PAGE</u>
ABSTRACT	I
ACKNOWLEDGEMENTS	III
GLOSSARY	IV
1 INTRODUCTION	1
1.1 Background	1
1.2 Reason for the particular approach adopted	2
1.3 Outline of the investigation	5
REFERENCES	7
2 DATA-TRANSMISSION SYSTEM	8
2.1 Baseband data-transmission system	8
2.2 Baseband signal waveform shaping	17
2.3 Data-transmission system for satellite links	25
2.4 Filters to be used in the satellite transmission systems for computer simulation	30
2.5 Nonlinearity	33
2.6 The baseband equivalent models of quadrature modulation systems	38
REFERENCES	45
3 COHERENT QUATERNARY PHASE-SHIFT KEYING (QPSK) AND DIFFERENTIALLY ENCODED COHERENT QUATERNARY PHASE-SHIFT KEYING (DEQPSK) SYSTEMS OVER A LINEAR OR NONLINEAR SATELLITE CHANNEL	64
3.1 Description of coherent QPSK and DEQPSK systems	64
3.2 Error probability performance of coherent QPSK and DEQPSK signals	70
3.3 Baseband equivalent model of DEQPSK system, with a linear or nonlinear satellite channel, for computer simulation	72
3.4 Baseband equivalent model of DEQPSK system, with a linear or nonlinear satellite channel and in an ACI environment, for computer simulation	78
3.5 Power spectra of QPSK and DEQPSK signals	80
3.6 Spectral estimation of QPSK and DEQPSK signals by computer simulation	81
3.7 Simulation results and discussion	84
REFERENCES	95
4 CONVOLUTIONALLY ENCODED COHERENT 8 PHASE-SHIFT KEYING (CE8PSK) SYSTEM OVER A LINEAR OR NONLINEAR SATELLITE CHANNEL	114
4.1 Introduction	114
4.2 Description of a convolutionally encoded coherent 8PSK (CE8PSK) system	115

4.3	Baseband equivalent model of CE8PSK system, with a linear or nonlinear satellite channel, for computer simulation	120
4.4	Viterbi-algorithm decoder for CE8PSK signals	124
4.5	Baseband equivalent model of CE8PSK system, with a linear or nonlinear satellite channel and in an ACI environment, for computer simulation	126
4.6	Performances of CE8PSK signals	128
4.7	Power spectra of CE8PSK signals	130
4.8	Distance measures for the minimum-distance decoding of CE8PSK signals	131
4.9	Simulation results and discussion	141
	REFERENCES	148
5	BASEBAND PREDISTORTION TECHNIQUE AND CONVOLUTIONALLY AND DIFFERENTIALLY ENCODED COHERENT 8 PHASE-SHIFT KEYING (CDE8PSK) TECHNIQUE	164
5.1	Baseband predistortion technique	164
5.2	Convolutionally and differentially encoded 8 phase-shift keying (CDE8PSK) technique	174
5.3	Simulation results and discussion	185
	REFERENCES	193
6	PHASE DEMODULATION	210
6.1	Phase detector	210
6.2	Amplifier limiter	211
6.3	Optimum filter arrangement for using the amplifier limiter, and the distance measure D	215
6.4	Phase demodulation of the amplifier limited signals	216
6.5	Suboptimum filter arrangement for using the amplifier limiter and the distance measure D	223
6.6	Performances of DEQPSK and CE8PSK signals with the optimum filter arrangement, for the amplifier limiter, phase demodulators and distance measure D, over a linear bandpass channel	225
6.7	Discussion of the simulation results for DEQPSK, CE8PSK and CDE8PSK signals with the use of the suboptimum filters for the amplifier limiter, phase demodulator A or B and the distance measure D	226
7	CARRIER RECOVERY	260
7.1	Introduction	260
7.2	Carrier recovery loops for DEQPSK and CDE8PSK signals	262
7.3	Frequency and phase offsets	279
7.4	Simulation results and discussion	285
	REFERENCES	296
8	COMMENTS ON THE PROJECT	320
8.1	Possible further investigations	320
8.2	Conclusions	323

APPENDICES

A1	MATCHED-FILTER DETECTION	A1
A2	IMPULSE RESPONSES OF THE TRANSFER FUNCTIONS GIVING A RECTANGULAR SPECTRUM AND A SINUSOIDAL ROLLOFF SPECTRUM	A12
A2.1	Rectangular spectrum	A12
A2.2	Sinusoidal rolloff spectrum	A12
A3	THE RELATIONSHIP OF $2E_b/N_0$ BETWEEN THE UPLINK AND DOWNLINK OF A SATELLITE CHANNEL	A17
A4	BASEBAND EQUIVALENT MODELS OF SYMMETRICAL BANDPASS FILTERS	A18
A4.1	Baseband equivalent model of the BPF at the transmitter	A18
A4.2	Baseband equivalent model of the BPF at the receiver	A20
A5	ANALYSIS OF QUADRATURE CROSSTALK IN BANDPASS SIGNALS	A23
A6	PROOF OF THE COMPLEX SIGNAL REPRESENTATION OF SYSTEMS USING QUADRATURE MODULATED SIGNAL	A26
A6.1	Representation of the modulated signal	A26
A6.2	Representation of the demodulated signal	A27
A7	NARROWBAND NOISE REPRESENTATION PROPERTIES	A29
A8	BIT-ENERGY-TO-NOISE POWER DENSITY RATIO ($2E_b/N_0$) CALCULATION FOR COMPUTER SIMULATION	A34
A8.1	$\frac{1}{2}N_0$ determination for computer simulation	A34
A8.2	$2E_b/N_0$ value calculation for computer simulation	A37
A9	THE SCALING RELATIONSHIP BETWEEN THE CONTINUOUS SIGNAL AND THE SAMPLED SIGNAL	A40
A10	PROBABILITY OF ERROR CALCULATION FOR BINARY SIGNALS	A41
A11	FUNDAMENTALS OF CARRIER RECOVERY TECHNIQUES	A44
A11.1	Analog phase-locked loop (APLL)	A44
A11.2	Digital phase-locked loop (DPLL)	A48
A11.3	M^{th} power loop	A52
A11.4	Costas loop	A53
A11.5	Decision-feedback loop	A53
A12	SIMULATOR FOR DEQPSK SIGNALS WITH THE USE OF THE MDFL	A64
A13	SIMULATOR FOR CE8PSK SIGNALS	A79
A13	SIMULATOR FOR CDE8PSK SIGNALS WITH THE USE OF THE DDL	A101
	REFERENCES	A131

ABSTRACT

The thesis is concerned with the design of a digital modem for mobile systems, operating over a satellite link with a highly elliptical orbit, having a transmission rate in the range 64 - 512 kbit/s. The modem uses differentially encoded quaternary phase-shift keying (DEQPSK) or convolutionally encoded 8PSK (CE8PSK) signals.

The transmission system is optimized by sharing the lowpass filtering equally between the transmitter and receiver filters and with a 100%, 75%, 50% or 25% sinusoidal rolloff. Since the impulse response of any of these filters has an infinite length, the minimum truncation lengths of the impulse responses required to approximate to the theoretical ideal are investigated. The bandpass filters are shown to have insignificant effects on the performance of the modem.

The satellite transponder is assumed to be operating in a linear mode. The high power amplifier (HPA) at the earth station introduces AM-AM and AM-PM conversion effects into the transmitted signal. This causes spectral spreading. Since narrow-band signals are used, post HPA filtering is impractical. The effects caused by spectral spreading, nonlinear distortion and adjacent channel interference (ACI) are investigated by means of computer simulation.

A convolutionally encoded 8PSK signal requires a complex Viterbi decoder at the receiver. The thesis describes a method of phase demodulation for use at the receiver that reduces the equipment complexity of the modem. It is shown that only a small degradation in tolerance to additive white Gaussian noise is introduced by this relative to optimum demodulation. Further degradations caused by the HPA and ACI are also investigated.

The thesis describes a method of predistorting the baseband signal in order to reduce the ACI and nonlinear effects caused by the HPA. The results of the improvement are presented.

Finally, the methods of carrier phase recovery for the two signals schemes using data-aided loops are presented. The reference carrier recovered from the convolutionally encoded 8PSK signal has an 8-fold phase ambiguity. A method of resolving the ambiguity, using differential encoding, is described. The degradation in performance is measured by means of computer simulation.

It has been shown that, by using the various techniques studied, a potentially more cost effective modem can be obtained.

ACKNOWLEDGEMENTS

The author would like to express his gratitude to his Supervisor, Prof. A P Clark, for his considerable help and guidance.

The financial support of the Science Research Council, which made the work possible, is gratefully acknowledged.

GLOSSARY

Abbreviations

ACI	adjacent channel interference
AGC	automatic gain controlled
AWGN	additive white Gaussian noise
APLL	analog phase-locked loop
CE8PSK	convolutionally encoded 8 phase-shift keying
CDE8PSK	convolutionally and differentially encoded 8 phase-shift keying
CORPSK	correlative phase-shift keying
8PSK	eight phase-shift keying
D/C	downconverter
DDL	decision-directed loop
D/A	digital-to-analog converter
DPLL	digital phase-locked loop
DTPD	digital-tan-phase-detector
E_b	energy per bit
E_s	energy per symbol
GMSK	Gaussian minimum phase-shift keying
FDMA	frequency-division-multiple-access
FEC	forward-error-correction
FFT	fast Fourier transform
F_{IF}	IF filter
h.f.c.	high frequency components
h.w.r.	half-wave rectifier
HPA	high power amplifier
IBO	input backoff

IDFT	inverse discrete Fourier transform
IF	intermediate frequency
IJF-QQPSK	interference-free offset quaternary phase-shift keying
ISI	intersymbol interference
MDFL	modified decision-feedback loop
MSK	minimum phase-shift keying
OBO	output backoff
OQPSK	offset quaternary phase-shift keying
PD	phase detector
PDMA	Phase Demodulator A
PDMB	Phase Demodulator B
PLL	phase-locked loop
PSK	phase-shift, keying
QPSK	quaternary phase-shift keying
Signals 1A, 2A, 3A and 4A	DEQPSK signals defined in Section 3.7.3
Signals 1B, 2B, 3B and 4B	CE8PSK signals defined in Section 4.9
Signals 1C, 2C, 3C and 4C	CDE8PSK signals defined in Section 5.3.4
SNR	signal-to-noise power ratio
TDM	time-division-multiple-access
TFM	tamed frequency modulation
TWTA	travelling wave tube amplifier
VCO	voltage-controlled oscillator
A/D	analog-to-digital converter
U/C	upconverter

List of principal mathematical symbols

\hat{A}	signal envelope, with the use of the HPA backoff factor H_c , at the input of the input to the HPA
A_1, B_1	i^{th} received samples of $A(t)$ and $B(t)$ from the output of the pre A/D filters in phase demodulator A (in Chapter 6)
\hat{A}_1, \hat{B}_1	i^{th} received samples of $\hat{A}(t)$ and $\hat{B}(t)$ from the output of the pre A/D filters in phase demodulator B (in Chapter 6)
$a_{1,m}, b_{1,m}$	m^{th} real and imaginary samples of the complex-valued signal $s_1(t)$ at the input to the amplifier limiter
$a_{0,m}, b_{0,m}$	m^{th} real and imaginary samples of the complex-valued signal $s_0(t)$ at the output of the amplifier limiter
$AL(t)$	function representing the amplifier limiter
C_1	unitary distance between two vectors (used for decoding a CE8PSK signal)
c_1	incremental distance for the sample received at time $t=iT$, when decoding a CE8PSK signal
$C_1^{(j)}$	unitary distance between two vectors (used for decoding a CDE8PSK signal)
$c_1^{(j)}$	incremental distance for the sample received at time $t=iT$, when decoding a CDE8PSK signal
$D_p(\delta_m), D_q(\delta_m)$	inphase and quadrature components of the conversion function $D(\delta_m)$ of the predistorter
$E[.]$	average of (.)
\hat{E}	signal envelope, with the use of the predistorter backoff factor P_e , at the input to the predistorter.
E_b	energy per bit
E_s	energy per symbol
$e_1^{(j)}$ for $j=1,2,3$	binary coded symbols carried by e_1 (for a CE8PSK or CDE8PSK signal).

Δf and $\Delta\omega$	frequency offset in Hz and rad/s
Δf_p	pull-in-limit
$f(\delta_m)$	AM-PM conversion function of the predistorter
$f(t)$	impulse response of the baseband equivalent model of the transmitter or receiver filter
f_m	$m+1^{\text{th}}$ component of the vector $\{f_n\}$ which is obtained by sampling the impulse response $f(t)$ at a rate of $1/T_s$ samples per second.
f_{IF} and ω_{IF}	intermediate frequency in Hz and rad/s
f_c and ω_c	carrier frequency in Hz and rad/s
f_{c_m} and ω_{c_m}	channel spacing in Hz and rad/s
$F_T(f)$	transfer function of the modulation filter in cascade with the transmitter IF filter
$F(s)$	Laplace transform of the loop filter
$F(z)$	z-transform of the loop filter
$g(\lambda_m)$	AM-PM conversion function of the assumed HPA
$G_p(\lambda_m), G_q(\lambda_m)$	inphase and quadrature components of the conversion function $G(\lambda_m)$ of the assumed HPA
H_c	HPA backoff factor (see Section 2.5)
$H_t(f)$	frequency response (transfer function) of the transmitter filter
$H_r(f)$	frequency response (transfer function) of the receiver filter
$H(f)$	frequency response (transfer function) of the baseband channel, i.e., $H_t(f)$ and $H_r(f)$ in cascade
$H^*(f)$	complex-conjugate of $H(f)$
$h(t)$	impulse response of the resultant transfer function of the baseband channel
$h_t(t)$	impulse response of the transmitter filter

K_d	PD gain factor in volt/rad
K_v	VCO gain factor in rad/sec-v
K_m	a constant with dimension v^{-1}
K	constraint length of the convolutional code
L	number of tested symbols
N	delay in phase estimation in the MDPL and DDL, caused by the demodulation filter (used in Chapter 7)
$\frac{1}{2}N_0$	two-sided power spectral density of zero mean additive white Gaussian noise at the input to the receiver
$N(t)$	bandpass noise function
$n(t)$	baseband equivalent of the noise $N(t)$
$n_c(t)$ and $n_s(t)$	real and imaginary components of the complex valued noise waveform $\hat{n}(t)$
$n_{c,m}$ and $n_{s,m}$	real and imaginary components of $n(t)$ at time $t=mT_s$
$PDMA_m, PDMB_m$	functions representing $PDMA(t)$ and $PDMB(t)$, of phase demodulators A and B, at time $t=mT_s$
$p(t)$	impulse response of the modulation or demodulation filters
P_m	m^{th} component of the vector (p_n) , which are obtained by sampling the impulse response $p(t)$ at the rate of $1/T_s$ samples per second.
P_c	predistorter backoff factor
P_e	probability of bit error in the detection of a received signal element.
q_i	i^{th} 4-level complex-valued symbol in DEQPSK signals or 8-level complex-valued symbol for CE8PSK or CDE8PSK signals.
r_i	i^{th} received sample of the complex-valued signal $r(t)$
$S_i(t)$	bandpass signal at the input of the amplifier limiter (used in Chapter 6)

$S_o(t), \hat{S}_o(t)$	bandpass signal at the input of the phase demodulators A and B (used in Chapter 6)
$S(t)$	bandpass signal
$s(t)$	baseband equivalent signal of $S(t)$
$S_D(t)$	bandpass signal of the desired channel
$s_D(t)$	baseband equivalent signal of $S(t)$
$S_U(t), S_L(t)$	bandpass signals of the upper and lower channels
$s_U(t), s_L(t)$	baseband equivalent signals of $S_U(t)$ and $S_L(t)$
$ s(t) $	magnitude of $s(t)$
$\text{sign}(x)$	1 or -1 depending on whether $x > 0$ or $x < 0$
T	unit of time which represents the length of time between adjacent transmitted symbols
T_m	unit of time which represents the length of time between samples used in computer simulation
u_m	m^{th} transmitted sample of the waveform $u(t)$ at the input to the modulator
v_i	sample value of the filtered noise waveform $v(t)$ at the time $t = iT_m$
X_L	L -component vector of the corresponding data symbol $\{\alpha_L\}$
Y_i	i -component vector of the possible received symbols
z^{-1}	delay of one sample interval
ξ	damping factor
σ^2	variance of the additive white Gaussian noise at the input of the receiver
β	sinusoidal rolloff factor
$\{\alpha_L\}$	L -component data vector to be transmitted
α_i	i^{th} 2-level data symbol in $\{\alpha_L\}$
$\delta(t)$	Unit impulse function (Dirac function)

θ_1	arbitrary carrier phase $\theta(t)$ of the receiving signal at time $t = iT$
$\hat{\theta}_1$	estimate of $\hat{\theta}(t)$ from the local carrier at time $t = iT$
θ_m	initial phase offset
Ω_1	the phase of the received sampled r_1 at the input to the detector at time $t = iT$
Ω^+	phase value of Ω in an anticlockwise direction on the polar coordinate system
ϵ_1	phase error of the local carrier at time $t = iT$
$\Delta\epsilon_1$	difference of ϵ_{1-} , and ϵ_1
$\hat{\epsilon}_1$	estimate of ϵ_1
ψ_1	data phase received at time $t = iT$ in the absence of noise and (phase and frequency) offsets
$\hat{\psi}_1$	estimate of ψ_1
ϕ_1	possible received phase value (used in MDFL and DDL loops) at time $t=iT$
μ	constant used in the loop filter
γ	DCO gain factor

CHAPTER 1

INTRODUCTION

1.1 Background

Conventional cellular land-mobile-radio systems use analog signals whereas the next generation of mobile systems are likely to be digital but probably with low data rates and with frequency division multiplexing of the different channels. The problem with these mobile radio systems is the severe fading that is caused from time to time by multipath propagation. This is the result of reflections from buildings, hills and so on, and is seriously aggravated by the fact that the radio signal travels from the transmitting aerial to the receiving aerial in a straight line, unless blocked by some obstacles, in which case it generally reaches the receiving aerial via one or more reflections. Thus the method of transmitting the radio signal tends to maximize the probability of multipath propagation and the consequent fading. This can, of course, be avoided through techniques for guiding the signal clear of obstacles, such as the use of many short line-of-sight links connected in cascade. Such techniques, however, involve considerable installation costs and are not always very flexible. An alternative approach, which is the subject of the investigation, is the use of a satellite in a highly elliptical orbit, such that the satellite is almost directly overhead during most of its operational period in any one circuit of the earth. This means that the transmitted and received signals travel in an almost vertical direction and so tend to avoid most obstacles, thus minimizing the probability of multipath propagation and the consequent fading. Studies carried out at Bradford University support this conclusion, and link budgets indicate that transmission rates in the range 64-512 kbit/s should be feasible without the need for excessive transmitted signal powers [1]. These transmission rates are considerably higher than those currently used by mobile radio systems, and they should enable a high speed time-division

multiplex service to be provided that is compatible with the integrated subscribers digital network currently being installed in the U.K. and other countries. The mobile system may be used for direct sound broadcasting to vehicles, as a cellular system overlay in sparsely populated rural areas, for the monitoring and perhaps even control of vehicles, and so on. With this in view, large numbers of vehicles will have to be equipped with high performance digital modems, that are small enough to be incorporated into a car radio and cheap enough to keep the vehicle communication-equipment cost comparable with that of a cellular radio set. A high performance could be achieved in the modem through the use of maximum-likelihood detection, but the complexity of this would be prohibitive. However, various near-maximum-likelihood detectors have been developed at Loughborough University, that are capable of achieving almost as good as a performance as a true maximum-likelihood detector but with far less complex equipment. Modems using these techniques for business systems and operating at 1-8 Mbit/s have been designed and are being built at Loughborough University for both UNIVERSE and CERS. At the lower transmission rates appropriate to mobile systems, the same standard of performance as that of the business systems should be achieved, but very much more simply, and this is the aim of the proposed research project.

1.2 Reason for the particular approach adopted

The mobile systems of interest here operate at a speed of 64, 128, 256 or 512 kbit/s over a satellite link. The essential feature of these systems is that the transmitted signal is required to have a constant or near-constant envelope, thus minimizing AM-AM and AM-PM conversion effects and bandspreading of the transmitted signal, when the latter is fed through a nonlinear amplifier. The amplifier could be a high power amplifier (HPA) or satellite repeater that is operating close to saturation.

Many recently proposed signals, such as quaternary phase-shift keying (QPSK), offset quaternary phase-shift keying (OQPSK), minimum phase-shift keying (MSK) [2],[3],[4], Gaussian minimum phase-shift keying (GMSK) [6],[7], tamed frequency modulation (TFM) [8], correlative phase-shift keying (CORPSK) [9], intersymbol-interference-free QPSK (IJF-QPSK) [10],[11],[12], convolutionally encoded 8PSK (CE8PSK) [13],[14] signals, and so on, which have been developed for use over satellite links. Of these, CORPSK, TFM and MSK signals are the ones that achieve a truly constant envelope, the price paid for this being a rather wider bandwidth than that of the others. Bandlimiting of the signals results in the introduction of an envelope ripple and intersymbol interference (ISI). An OQPSK signal is a modified form of a QPSK signal but with a near constant envelope. In an OQPSK signal, the inphase data stream is delayed relatively to the quadrature data stream by half a symbol period. An IJF-QPSK signal [10],[11],[12] is also a near constant envelope scheme derived from an OQPSK signal by employing various transmitted pulse shapes to give a desired compromise between bandwidth and envelope ripple.

Of these proposed signals, the convolutionally encoded 8PSK signal [13],[14] although exhibiting considerable envelope variation, provides a coding gain of greater than 4 dB over an ideal uncoded QPSK signal for a code with a 4-bit memory, hence it can provide high-quality transmission over satellite links. However for the optimum detection of such signal, a complex valued demodulation process is required, involving both inphase and quadrature coherent demodulators. The demodulated baseband signal obtained is complex-valued (having two separate components), and the detector has to compute, for each of a number of possible sequence of received data symbols, the unitary distance between the corresponding received sequence, in the absence of noise, and the sequence actually received. Such computations involve numerous operations of squaring or multiplication. Now, provided only that the transmitted-modulated carrier

signal has a near constant envelope together with a large number of carrier cycles per signal element, then little or no useful information carried by the phase-modulated waveform is lost in the receiver by first slicing the received waveform in an amplifier limiter and then extracting the phase for subsequent use in the detection process.

The important advantages of the arrangement just described are as follows.

1) In a conventional coherent detector, employing inphase and quadrature coherent demodulators, the demodulated baseband signal obtained is complex-valued (having two separate components) whereas, with a slicer and phase demodulator, the phase signal is real-valued (having only one component). This means that in the latter case considerably less signal processing is required for any given degree of accuracy in operation such as multiplication, addition and subtraction and the resulting simplification can make all the difference between the modem being practically viable or not. It is assumed here that the demodulated baseband signal in the receiver is sampled and then processed digitally, thus enabling the receiver to handle the encoding effects of the signal, through the implementation of the Viterbi Decoder.

2) When the received signal is sliced, no automatic gain controlled (AGC) amplifier is required and the correct operation of the receiver is now independent of the received signal level, within the range of levels handled by the slicer.

The aim of the investigation is to determine the combination of the signal design and demodulation process leading to the potentially most cost-effective modem, in a mobile system operating over a satellite link. In the investigation, it is assumed that frequency division multiple access (FDMA) is used at the satellite and that the satellite transponder is operating at less than its full power, so that there will be no further

nonlinear distortion caused by the satellite transponder. It is also assumed that the satellite is used in a highly elliptical orbit and so there is no multipath fading in the channel.

1.3 Outline of the investigation

The investigation is mainly concerned with the tolerance to additive white Gaussian noise (AWGN) of the various data-transmission systems studied, using DEQPSK, CE8PSK and convolutionally and differentially encoded 8PSK (CDE8PSK) signals, with the use of different combinations of the signal design, predistortion process, slicing process, phase demodulation process and carrier recovery technique. The aim is to develop the most cost effective arrangement of the data-transmission system, leading to the potentially most cost effective modem for use over satellite links as part of a mobile system. The investigation is by computer simulation and theoretical analysis (when possible).

The assumed model of the data-transmission system for satellite links and the optimum design of the transmitter and receiver filters are discussed in Chapter 2. The assumed characteristics of the modulation and demodulation filters, the IF filters, the post D/A filters, the pre A/D filters, and the HPA, used for computer simulation, are described. The baseband equivalent models of the quadrature modulation systems, with a nonlinear channel and in an ACI environment, are also derived.

Chapter 3 contains a description of the coherent and differentially coherent QPSK techniques. The baseband equivalent models of the DEQPSK systems, with a linear or nonlinear channel and in an ACI environment, for computer simulation are derived. The results of the simulation tests on the error-rate performances are discussed.

Chapter 4 contains descriptions of the convolutionally encoded 8 phase-shift-keying (CE8PSK) technique and of the Viterbi-algorithm decoder for decoding the signal. Different distance measures for the minimum-distance decoding used at the Viterbi decoder are derived. The baseband equivalent

models of the CE8PSK systems, with a linear or nonlinear channel and in an ACI environment, for computer simulation are derived. The results of the tests on the error-rate performances in different situations are presented and compared with those of the DEQPSK systems.

In Chapter 5, the baseband predistortion technique used to compensate the AM-AM and AM-PM effects of the HPA is described. The baseband equivalent model of the predistorter for computer simulation is derived. The convolutionally and differentially encoded 8PSK (CED8PSK) technique, which is the CE8PSK technique with the phase differentially encoded, used to avoid catastrophic failure in the decoded data symbols, following a sudden large carrier phase change introduced by the transmission path into the received data signal, is described. The suboptimum decoder for the signal is also presented. The results of the error-rate performances of DEQPSK, CE8PSK and CDE8PSK signals, with the use of the predistorter and in an ACI environment, are discussed.

Chapter 6 contains descriptions of the slicing and phase demodulation processes. Two phase demodulators (one using 2 multipliers and the other using 2 EX-OR gates to implement) are described. The optimum and suboptimum filter arrangements for using the slicing process, phase demodulation process and the most promising distance measure (obtained from Chapter 4) are discussed. The results of the error-rate performances of DEQPSK, CE8PSK and CDE8PSK signals, with the use of the suboptimum filter arrangement, the predistorter and the two phase demodulators are presented, compared and discussed.

Chapter 7 is concerned with carrier recovery. Two different data aided carrier recovery loops, the Modified Decision Feedback loop (MDFL) and the Decision Directed loop (DDL), used for the DEQPSK and CDE8PSK signals, respectively, are described. The steady-state performances and transient responses of them are studied. The results of the simulation tests are presented and discussed.

REFERENCES

- [1] Barton, S.K. et al, "Communications Engineering Research", Final Report of Project Definition Phase (PD1) Study of Experimental Payload and Earth Stations, March 1984
- [2] Gronemeyer, S.A. and McBride, A.L., "MSK and Offset QPSK Modulation", *IEEE Trans. on Commun.*, Vol. COM-24, pp.809-820, Aug. 1976
- [3] Buda, R.de, "Coherent Demodulation of Frequency Shift Keying With Low Deviation Ratio", *IEEE Trans. on Commun.*, Vol. COM-20, pp.429-435, June 1972
- [4] Masamura, T., Samejima, S., Morihira, Y. and Fukada, H., "Differential Detection of MSK with Non-redundant Error Correction", *IEEE Trans. Commun.*, Vol. COM-27, pp.912-918, June 1979
- [5] Galko, P and Pasupathy, S, "On a Class of Generalized MSK", *ICC'81 Conf. Rec.*, pp.2.4.1-2.4.5, Denver, June 1981
- [6] Murota, K. and Hirade, K., "GMSK Modulation for Digital Mobile Radio Telephony", *IEEE Trans. on Commun.*, Vol. COM-29, pp.1044-1050, July 1981
- [7] Murota, K., Kimoshita, K. and Hirade, K., "Spectrum Efficiency of GMSK Land Mobile Radio", *IEEE Int. Conf. on Commun.*, pp.23.8.1-23.8.5, June 1981
- [8] Jagar, F. de and Dekker, C.B., "Tamed Frequency Modulation, a Novel Method to Achieve Spectrum Economy in Digital Transmission", *IEEE Trans. on Commun.*, vol. COM-20, pp.534-542, May 1978
- [9] Muilwijk, D., "Correlative Phase Shift Keying - A Class of Constant Envelope Modulation Techniques", *IEEE Trans. on Commun.*, vol. COM-29, pp.226-236, March 1981
- [10] Le-Ngoc, T., Feher, K. and Pham van, H., "New Modulation Techniques for Low-Cost Power and Bandwidth Efficient Satellite Earth Stations", *IEEE Trans. Commun.*, vol. COM-30, Jan. 1982
- [11] Feher, K., *Digital Communications: Satellite/Earth Station Engineering*, Prentice-Hall, Englewood Cliffs, NJ (1983)
- [12] Kato, S. and Feher, K., "XPSK: A New Cross-Correlated Phase-Shift Keying Modulation Technique", *IEEE Trans. Commun.*, vol. COM-31, pp.701-707, May 1983
- [13] Lebowitz, S.H. and Rhodes, S.A, "Performance of Coded 8PSK Signalling for Satellite Communications", *IEEE Int. Conf. on Commun.*, pp.47.4.1-47.4.8, 1981
- [14] Hui, H. and Fang, R.J.F., "Convolutional Code and Signal Waveform Design for Band-Limited Satellite Channels", *IEEE Int. Conf. on Commun.*, pp.47.5.1-47.5.9, 1981
- [15] Girard, H. and Feher, K., "A New Baseband Linearizer for More Efficient Utilization of Earth Station Amplifiers Used for QPSK Transmission", *IEEE Journal on Selected Area in Commun.*, vol. SAC-1, pp.46-56, Jan. 1983

CHAPTER 2

DATA-TRANSMISSION SYSTEM

2.1 Baseband data-transmission system

The derivation of the probability of error, P_e , performance of a matched-filter detector is shown in Appendix A1, where there is no discussion of intersymbol interference (ISI) (i.e., a single signal-element is assumed). The matched-filter detector is optimum for a single-shot transmission, that is, for systems in which only one signal-element is transmitted, and in wideband systems where each signal-element is confined to its duration (i.e., ISI is negligible). However for optimal spectral efficiency, (i.e., in the presence of ISI) the transmitter and receiver filters must be optimized in order to minimize the error probability.

2.1.1 Optimum design of transmitter and receiver filters [1]

It is required to determine the transfer function $H_t(f)$ and $H_r(f)$ of the transmitter and receiver filters, that maximize the signal/noise power ratio at the input to the detector in Fig. 2.1.

A binary polar signal is assumed throughout the following discussion. The transmitted signal-elements being statistically independent and equally likely to have either of the two possible shapes. In the regular sequence of impulses carrying the element values $\{\alpha_k\}$, at the input to the baseband channel, $\alpha_k = \pm k$.

A single transmitted signal-element at the input to the transmission path has the waveform

$$\alpha_k h_c(t - iT)$$

where $h_c(t - iT)$ is the impulse response of the transmitter filter. The Fourier transform (frequency spectrum) of the signal element is

$$\alpha_k \exp(-j2\pi f iT) H_c(f)$$

Thus the energy spectral density of an individual transmitted signal-element, at the input to the transmission path, is

$$|\alpha_1 \exp(-2\pi f1T)H_t(f)|^2 = \alpha_1^2 |H_t(f)|^2 \quad 2.1.1$$

and its energy is

$$E_1 = \alpha_1^2 \int_{-\infty}^{\infty} |H_t(f)|^2 df \quad 2.1.2$$

Since the signal-elements are statistically independent and have zero means, making them statistically orthogonal, the average transmitted energy per signal-element, at the input to the transmission path, is the average of expected value of E_1 and so is

$$E = \overline{\alpha_1^2} \int_{-\infty}^{\infty} |H_t(f)|^2 df \quad 2.1.3$$

where $\overline{\alpha_1^2}$ is the average value of α_1^2 . Clearly, at a given element rate, E is a measure of the transmitted signal power level.

Assume that the signal fed to the transmission path is sufficiently bandlimited by the transmitter filter so that it experiences no further bandlimiting in transmission. Furthermore, the transmission-path is taken to introduce no attenuation, no delay, no amplitude distortion, and no phase distortion, over the signal frequency band, so that the signal experiences no attenuation, delay or distortion in transmission. Thus the transmitter filter, transmission path and receiver filter, in Fig. 2.1, together form a baseband channel with transfer function

$$H(f) = H_t(f)H_r(f) \quad 2.1.4$$

Let

$$\int_{-\infty}^{\infty} |H(f)| df = K \quad 2.1.5$$

where K is a constant.

The impulse response of the baseband channel is

$$h(t) = \int_{-\infty}^{\infty} H(f) \exp(j2\pi ft) df \quad 2.1.6$$

so that a single received signal-element at the detector input has the waveform $\alpha_1 h(t-iT)$ with the Fourier transform $\alpha_1 \exp(-j2\pi fiT) H(f)$. Thus the energy spectral density of an individual received signal-element, at the detector input, is

$$|\alpha_1 \exp(-2\pi fiT) H(f)|^2 = \alpha_1^2 |H(f)|^2 df \quad 2.1.7$$

and its energy is

$$F_1 = \alpha_1^2 \int_{-\infty}^{\infty} |H(f)|^2 df \quad 2.1.8$$

Clearly, the average energy per element of the signal at the detector input is the expected value of F_1 and is

$$F = \alpha_1^2 \int_{-\infty}^{\infty} |H(f)|^2 df \quad 2.1.9$$

The signal waveform at the input to the detector (in the absence of noise) is $\sum_1 \alpha_1 h(t-iT)$, so that the resultant waveform at the detector input is

$$r(t) = \sum_1 \alpha_1 h(t-iT) + v(t) \quad 2.1.10$$

where $v(t)$ is the noise waveform.

Since the noise input to the receiver filter is white Gaussian noise with zero mean and a two-sided power spectral density of $\frac{1}{2}N_0$, $v(t)$ is a sample function of a Gaussian random process with zero mean and a power spectral density $\frac{1}{2}N_0 |H_r(f)|^2$, where $H_r(f)$ is the transfer function of the receiver filter [2]. Thus the average power of the noise waveform $v(t)$ is [2]

$$N = \frac{1}{2}N_0 \int_{-\infty}^{\infty} |H_r(f)|^2 df \quad 2.1.11$$

The signal/noise power ratio at the detector input, expressed as the average per element of the signal divided by the average noise power, is

$$\frac{F}{N} = \frac{\overline{\alpha_1^2} \int_{-\infty}^{\infty} |H(f)|^2 df}{\frac{1}{2} N_0 \int_{-\infty}^{\infty} |H_r(f)|^2 df} \quad 2.1.12$$

Consider now any given transfer function $H(f)$ of the baseband channel, where $H(f)$ satisfies Eqns. 2.1.4 and 2.1.5. Suppose that the value of $H_r(f)$ is multiplied by d , where d is any positive real constant that is independent of frequency. But the average transmitted signal power at the input to the transmission path is a constant fixed by the transmission path, since the transmitted signal power is always assumed to be set at its *maximum* permissible value. Clearly, if the value of N in Eqn. 2.1.12 is multiplied by d^2 , the value of $H_r(f)$ must be multiplied by d^{-1} , in order that Eqns. 2.1.4 and 2.1.5 are still satisfied. Thus, from Eqn. 2.1.3, the value of $\overline{\alpha_1^2}$ is multiplied by d^2 , so that the value of F in Eqn. 2.1.12 is also multiplied by d^2 . It follows that if the value of $H_r(f)$ is multiplied by the constant d , where d may have any real positive value, the value of F/N in Eqn. 2.1.12 remains unchanged.

Assume therefore that the value of $H_r(f)$ is such that

$$\int_{-\infty}^{\infty} |H_r(f)|^2 df = b \quad 2.1.13$$

where b is any positive real constant. It is clear from the previous discussion that F/N is *independent* of b , since $H_r(f)$ may be multiplied by the appropriate constant d so that Eqn. 2.1.13 is satisfied. Now

$$\begin{aligned} \frac{F}{N} &= \frac{\overline{\alpha_1^2} \int_{-\infty}^{\infty} |H(f)|^2 df}{\frac{1}{2} N_0 b} \\ &= \frac{E \int_{-\infty}^{\infty} |H(f)|^2 df}{\frac{1}{2} N_0 b \int_{-\infty}^{\infty} |H_r(f)|^2 df} \end{aligned} \quad 2.1.14$$

from Eqn. 2.1.3, where E is the average transmitted energy per signal-element.

Since for any given application, the values of E, N_0 and $H(f)$ are given and are therefore not subject to modification, and since F/N is independent of b , it can be seen that to maximize F/N , the signal/noise power ratio at the detector input, it is necessary to minimize $\int_{-\infty}^{\infty} |H_t|^2 df$. From a particular case of Holder's inequality [3]

$$\int_{-\infty}^{\infty} |H_t(f)|^2 df \int_{-\infty}^{\infty} |H_r(f)|^2 df \geq \left(\int_{-\infty}^{\infty} |H_r(f)| |H_t(f)| df \right)^2 \quad 2.1.15$$

with equality when

$$|H_r(f)| = d |H_t(f)| \quad 2.1.16$$

From Eqn. 2.1.4

$$|H(f)| = |H_t(f)| |H_r(f)| \quad 2.1.17$$

so that from Eqn. 2.1.5

$$\int_{-\infty}^{\infty} |H_t(f)| |H_r(f)| df = K \quad 2.1.18$$

Thus, from Eqns. 2.1.13 and 2.1.15

$$\int_{-\infty}^{\infty} |H_t(f)|^2 df \geq K b^{-1} \quad 2.1.19$$

with equality when

$$|H_r(f)| = b |H_t(f)| \quad 2.1.20$$

since now $d=b$, as can be seen from Eqns. 2.1.16, 2.1.13 and 2.1.19.

But when equality holds in Eqn. 2.1.19, $\int_{-\infty}^{\infty} |H_t(f)|^2 df$ has its minimum value, so that the signal/noise power ratio at the detector input now has its maximum value. Equation 2.1.20 therefore gives the condition that must be satisfied by the transmitter and receiver filters, in order to maximize the signal/noise power ratio at the detector input. The

signal/noise power ratio is here defined as the ratio of the average energy per signal element to the average noise power. This is not the same as the definition of signal/noise power ratio used for the matched filter in Appendix A1, which is the ratio of the *instantaneous* signal power, at the time instance $t=T$, to the average noise power.

From Eqn. 2.1.20, since $|H_t(f)|$ and $|H_r(f)|$ are the moduli of $H_t(f)$ and $H_r(f)$, respectively, their values are always positive. $H_t(f)$ and $H_r(f)$ are however often complex. The values of $|H_t(f)|$ and $|H_r(f)|$ are clearly independent of the respective phase characteristics. Each filter may therefore introduce any degree of phase distortion and therefore any degree of group delay distortion, so long as Eqns. 2.1.4 and 2.1.20 are satisfied, without affecting the signal/noise power ratio at the detector input.

The linear filter matched to any given signal-element, $\alpha_0 h_t(t)$, where α_0 carries the symbol value and where $h_t(t)$ is nonzero only over the time interval 0 to T seconds, has an impulse response

$$g(t) = c h_t(T-t) \quad 2.1.21$$

where c is any real constant. The transfer function of the linear filter is

$$G(f) = c \exp(-j2\pi fT) H_t^*(f) \quad 2.1.22$$

where $H_t(f)$ is the Fourier transform of $h_t(t)$ and $H_t^*(f)$ is the complex conjugate of $H_t(f)$. $h_t(t)$ is here taken to be the impulse response of the transmitter filter in Fig. 2.1, so that $\alpha_0 h_t(t)$ is the received signal waveform at the input to the receiver filter, corresponding to an individual signal element received in the absence of noise. When the signal element $\alpha_0 h_t(t)$ is received in the presence of AWGN, the matched filter maximizes the output signal/noise power ratio at the time instant $t=T$, as shown in Appendix A1. The received element value is detected by sampling the output signal from the matched filter at the time $t=T$

seconds, and comparing the sample value with the appropriate threshold levels.

The term $\exp(-j2\pi fT)$ in Eqn. 2.1.22 is the Fourier transform of a delay of T seconds. This delay can be neglected without affecting the significant points in the present discussion. Thus the transfer function of the matched filter can be taken to be

$$G(f) = cH_c^*(f) \quad 2.1.23$$

and the received element value is detected here by sampling the output signal from the matched filter at time instant $t=0$. This is a nonphysical system, (i.e., not physically realizable), but it can always be made physically realizable again by re-introducing the appropriate delay of T seconds.

From Eqn. 2.1.23

$$|G(f)| = b|H_c(f)| \quad 2.1.24$$

where $b=|c|$. If the matched filter is now used for the received filter in Fig. 2.1, $H_r(f)=G(f)$ so that Eqn. 2.1.20 is satisfied and the signal/noise power ratio at the output of the filter is maximized. Under these conditions,

$$H_r(f) = cH_c^*(f) \quad 2.1.25$$

and

$$H(f) = cH_c(f)H_c^*(f) \quad 2.1.26$$

so that $H(f)$ is real and even (symmetrical about zero frequency), and the impulse response $h(t)$ of the baseband channel is symmetrical about its central point. It can be seen from Eqn. 2.1.4 that if $H(f)$ is real and even, and if the receiver filter is matched to the received signal and so satisfies Eqn. 2.1.25 and so maximizes the signal/noise power ratio at the detector input. However, Eqn. 2.1.20 can be satisfied for any value of $H(f)$, which means that $H(f)$ need not be real or even. When Eqn. 2.1.20 is

satisfied and $H(f)$ is not real or even, Eqn. 2.1.25 cannot be satisfied, so that the receiver filter cannot now be matched to the received signal.

It is clearly from the preceding discussion that $H_t(f)$ and $H_r(f)$ satisfy Eqn. 2.1.20, $H_r(f)$ is not necessarily the complex conjugate of $H_t(f)$, so that the receiver filter is not necessarily matched to the received signal. However, when it is matched, Eqn. 2.1.20 is necessarily satisfied, so that the matched filter is a particular case for which Eqn. 2.1.20 is satisfied.

An important case for which Eqn. 2.1.20 is satisfied is that where

$$H_r(f) = cH_t(f) \quad 2.1.27$$

where c is any positive or negative real constant and $H_t(f)H_r(f) = H(f)$. The arrangement satisfying Eqn. 2.1.27 is more general than the case where $H_r(f) = cH_t^*(f)$, since Eqn. 2.1.27 can be satisfied for any value of $H(f)$. Furthermore, in the frequently occurring case where $H(f)$ is real, non-negative and even, and Eqn. 2.1.27 is satisfied, both $H_t(f)$ and $H_r(f)$ are real, non-negative and even, and $H_r(f) = cH_t^*(f)$ with c positive, so that the receiver filter is now matched to the receiver signal. Thus the condition given by Eqn. 2.1.27 ensures that the receiver filter is matched to the received signal, whenever $H(f)$ is real, non-negative and even.

2.1.2 Model of the data-transmission system [1]

Since the constant b in Eqns. 2.1.13 and 2.1.20 may be taken to have any positive real value without affecting the signal/noise power ratio at the detector input, it is convenient to set $b=1$. Under these conditions, the signal/noise power ratio at the detector input is then maximum when

$$|H_r(f)| = |H_t(f)| \quad 2.1.28$$

It will be assumed that

$$H_r(f) = \pm H_t(f) \quad 2.1.29$$

As before, $H_t(f) H_r(f) = H(f)$. Under these conditions,

$$\int_{-\infty}^{\infty} |H_t(f)|^2 df = \int_{-\infty}^{\infty} |H_r(f)|^2 df = \int_{-\infty}^{\infty} |H(f)| df = K \quad 2.1.30$$

as can be seen from Eqn. 2.1.5.

The signal/noise power ratio at the input to the detector is now

$$\frac{F}{N} = \frac{E}{\frac{1}{2}N_0} \int_{-\infty}^{\infty} |H(f)|^2 df \quad 2.1.31$$

as can be seen from Eqns. 2.1.14 and 2.1.30. From Eqn. 2.1.3, the average transmitted energy per signal element, at the input to the transmission path, is

$$E = \overline{\alpha_1^2} \quad 2.1.32$$

and, from Eqn. 2.1.11, the Gaussian noise waveform $v(t)$ at the output of the baseband channel has, at any time, zero mean and variance

$$N = \frac{1}{2}N_0 \int_{-\infty}^{\infty} |H_r(f)|^2 df \quad 2.1.33a$$

$$= \frac{1}{2}N_0 \int_{-\infty}^{\infty} |H(f)| df \quad 2.1.33b$$

The data-transmission system is now as shown in Fig. 2.2, which is a particular arrangement of Fig. 2.1, with $H_r(f) = \pm H_t(f)$. A sampler is included at the input to the detector. Clearly $\pm H_t^2(f) = H(f)$. The received waveform $r(t)$ is sampled at the time instants (iT) , for all integer values of i , and the resulting sample values $\{r(iT)\}$ are fed to the detector.

The regular sequence of impulses, at the input to the baseband channel are antipodal signal elements being statistically independent and equally likely to have either of the two possible shapes.

The average energy per signal element at the input to the transmission path is $\overline{\alpha_1^2}$. The transmission path introduces no signal

distortion, attenuation or delay. White Gaussian noise with zero mean and a two-sided power spectral density of $\frac{1}{2}N_0$ is added to the data signal at the output of the transmission path. The baseband channel has a transfer function $H(f)$ and an impulse response $h(t)$. The noise waveform $v(t)$ at the output of the baseband channel is a sample function of a Gaussian random process with zero mean and variance N (Eqn. 2.1.33). Thus the received waveform at the output of the baseband channel is

$$r(t) = \sum_i \alpha_i h(t-iT) + v(t) \quad 2.1.34$$

$r(t)$ is sampled once per symbol, and the detector operates entirely on the sample values $\{r(iT)\}$ to give the detected element values $\{\hat{\alpha}_i\}$. The presence of the noise components in the $\{r(iT)\}$ will, of course, result in occasional errors in the $\{\hat{\alpha}_i\}$.

2.2 Baseband signal waveform shaping

Having determined the best way of sharing the linear filtering of the signal between the transmitter and receiver filters, when the transmission path introduces no signal distortion, it is necessary now to study the effect of the overall transfer function $H(f)$, of the transmitter and receiver filters, on the tolerance of the data-transmission system to white Gaussian noise.

In Fig. 2.2, $H(f)$ is the transfer function of the baseband channel. The spectrum (Fourier transform) of the individual received signal-element at the baseband channel, resulting from the signal-element $\alpha_i \delta(t)$ at the input to the baseband channel, is $\alpha_i H(f)$. Here the "signal spectrum" is taken to mean the spectrum of this individual signal-element. In describing the *shape* of the signal spectrum $\alpha_i H(f)$, it is assumed that $\alpha_i=1$, so that the signal spectrum is equated to the transfer function $H(f)$, of the baseband channel.

2.2.1 Rectangular spectrum

Nyquist has shown that the maximum element rate which may be transmitted over a bandwidth B Hz, for no ISI, is $2B$ bauds (elements per second), and this is sometimes known as the Nyquist rate [4]. This can be seen by considering the receiver and transmitter filters in Fig. 2.2 that gives a rectangular spectrum for an individual received signal-element at the output of the receiver filter. The transfer function of the baseband channel is now

$$H(f) = \begin{cases} T, & -\frac{1}{2T} < f < \frac{1}{2T} \\ 0, & \text{elsewhere} \end{cases} \quad 2.2.1$$

as shown in Fig. 2.3a. The impulse response of it is shown in Appendix 2.1 to be

$$h(t) = \frac{\sin(\pi t/T)}{\pi t/T} \quad 2.2.2$$

as shown in Fig. 2.3b. This signal-element, when spaced (delayed) relative to each other at time intervals which are multiples of T seconds, will cause no ISI if sampled at the central positive peaks [1,p.52]; hence this signal-element is used for Nyquist-rate transmission.

Since $h(t) \neq 0$ for $t < 0$, $h(t)$ is not physically realisable. However, if a large delay of τ seconds is included in the filter characteristics without otherwise changing them, so that $h(t) \approx 0$ for $t < 0$, the filter then becomes physically realisable, for practical purposes, and has an impulse response approximately equal to $h(t-\tau)$, as shown in Fig. 2.3c. The error caused in $h(t-\tau)$ by setting this accurately to zero for $t < 0$, is negligible so long as $\tau \gg T$, and under these conditions a practical filter can be made to approximate closely to the theoretical ideal, the approximation getting better as τ increases. Of course, for the practical filter to have an impulse response exactly equal to $h(t-\tau)$, it is necessary that τ tends to infinity.

There are practical difficulties with this particular waveshape, however:

1. The baseband channel has the characteristics of an ideal lowpass filter which is very difficult to approximate in practice because of the sharp cutoff in its frequency response at $1/(2T)$ Hz.
2. This signal element requires extremely precise synchronization. If the timing at the receiver varies somewhat from exact synchronization, the zero ISI condition disappears. In fact, under certain signal sequences, the tails of adjacent pulses may add up as a divergent series, causing possible errors. Since some timing jitter is inevitable with most synchronization systems, this signal-element is obviously not the one to use.

2.2.2 Spectrum with sinusoidal rolloff

The difficulties of using rectangular spectrum may be greatly overcome by smoothing the abrupt change in $H(f)$ at $f=\pm 1/(2T)$ Hz. In general, for a given bandwidth, the more smooth of $H(f)$ with f , over the whole range of values of f for which $H(f)\neq 0$, the shorter the effective duration of $h(t)$ [1, p.146].

Nyquist's vestigial-symmetry theorem states that if $H(f)$ is real and has odd symmetry about the nominal cutoff frequency $1/(2T)$ Hz, then the corresponding impulse-response $h(t)$ is an even time function, and $h(iT)=0$ for all nonzero integer values of i [4],[5]. Under these conditions, it is possible to transmit data at $1/T$ elements per second without ISI.

The class of signal spectra most often used is that where $H(f)$ is real and has a sinusoidal rolloff centred at $\pm 1/(2T)$ Hz, as shown in Fig. 2.4a.

The transfer function of the baseband channel is now

$$H(f) = \begin{cases} T & , 0 \leq |f| < \frac{(1-\beta)}{2T} \\ \frac{T}{2} [1 - \sin \frac{\pi T}{\beta} (|f| - \frac{1}{2T})] & , \frac{(1-\beta)}{2T} \leq |f| \leq \frac{(1+\beta)}{2T} \\ 0 & , \text{elsewhere} \end{cases} \quad 2.2.3$$

where β is called the rolloff factor. For $\beta = 0$, it becomes the rectangular spectrum previously described. When $\beta = 1$, the spectrum has the shape of an one cycle of a cosine wave, between adjacent negative peaks, the latter being raised to zero. It is often known as a "raised-cosine" spectrum.

The time response $h(t)$, that is, the inverse Fourier Transfer function, of Eqn. 2.2.3 is shown in Appendix A2.2 to be

$$h(t) = \frac{\sin(\pi t/T)}{\pi t/T} \frac{\cos(\beta \pi t/T)}{1 - 4\beta^2 t^2/T^2} \quad 2.2.4$$

This function consists of products of two factors: the factor $[\sin(\pi t/T)]/[\pi t/T]$ associated with the ideal lowpass filter, and a second factor that decreases at $1/|t|^2$ for large $|t|$. The first factor ensures zero crossing of $h(t)$ at the desired sampling instants of time, $t=iT$ with i an integer. The second factor reduces the tails of the signal-element considerably below that obtained from the ideal lowpass filter, so that the pulse is relatively insensitive to sampling timing errors. In fact, the amount of ISI resulting from this timing error decreases as the rolloff factor β is increased from zero to one. Figures 2.4a and b show the spectral characteristics $H(f)$ and the impulse responses $h(t)$ for several values of β . Since $h(t) \neq 0$ for $t < 0$, $h(t)$ is also not physical realisable. However, as said before, a delay of τ seconds can be included in the filter characteristics to make it physical realisable.

In this thesis, all the transmission systems are optimized by sharing the lowpass filtering equally between the transmitter and receiver filters and with a 100%, 75%, 50% or 25% sinusoidal rolloff frequency response, in order to find the best wave shape for data transmission over satellite links.

2.2.3 Probability of error performance of the data-transmission system in an AWGN environment

The data-transmission system in Fig. 2.2 is assumed, with $H_r(f) = \pm H_c(f)$ and $|H_c(f)|^2 = H(f)$. The baseband channel transfer function, $H(f)$, has a sinusoidal rolloff frequency response, as given by Eqn. 2.2.3, with the impulse response, $h(t)$, given by Eqn. 2.2.4. White Gaussian noise with zero mean and a two-sided power spectral density of $\frac{1}{2}N_0$ is added to the data signal at the output of the transmission path. The signal at the output of the baseband channel is the continuous waveform

$$r(t) = \sum_i \alpha_i h(t-iT) + v(t) \quad 2.2.5$$

where $h(t)$ is given by Eqn. 2.2.4. It can be seen from Eqn. 2.2.4 that $h(0)=1$ and $h(iT)=0$ for all values of the integer i other than $i=0$. Thus the i^{th} received signal-element, $\alpha_i h(t-iT)$ may be detected from the sample value of the received waveform $r(t)$, at time instant $t=iT$. The sample value is

$$r(iT) = \alpha_i + v(iT) \quad 2.2.6$$

This may be written more simply as

$$r_i = \alpha_i + v_i \quad 2.2.7$$

where $r_i = r(iT)$ and $v_i = v(iT)$

It is assumed that $\alpha_i = \pm k$. The detection process that minimizes the probability of error in the detection of α_i from r_i , under the assumed conditions, selects the possible value of α_i closest to r_i . This is achieved by comparing r_i with the decision threshold of zero. When $r_i < 0$, α_i is detected as $-k$, and when $r_i > 0$, α_i is detected as k .

An error occurs in the detection of α_i whenever the noise component v_i carries r_i onto the opposite side of the decision threshold with respect to the transmitted α_i . Since v_i is a sample value of a Gaussian random variable with zero mean and variance N (Eqn. 2.1.33), the probability of

an error in the detection of α_1 , when $-k$ is received and r_1 is wrongly detected is

$$\begin{aligned}
 P_{e1} &= \int_k^{\infty} \frac{1}{\sqrt{2N\pi}} \exp\left(-\frac{v^2}{2N}\right) dv = \int_{k/\sqrt{N}}^{\infty} \frac{1}{\sqrt{2\pi}} \exp\left(-\frac{v^2}{2}\right) dv \\
 &= Q\left(\frac{k}{\sqrt{N}}\right)
 \end{aligned}
 \tag{2.2.8}$$

When $+k$ is received and r_1 is wrongly detected, the probability of an error in the detection of α_1 is

$$\begin{aligned}
 P_{e2} &= \int_{-\infty}^{-k} \frac{1}{\sqrt{2N\pi}} \exp\left(-\frac{v^2}{2N}\right) dv = \int_{-\infty}^{-k/\sqrt{N}} \frac{1}{\sqrt{2\pi}} \exp\left(-\frac{v^2}{2}\right) dv \\
 &= Q\left(\frac{k}{\sqrt{N}}\right)
 \end{aligned}
 \tag{2.2.9}$$

P_{e1} and P_{e2} are conditional probabilities with P_{e1} assuming that $-k$ was transmitted and P_{e2} assuming that k was transmitted. Thus assuming the equiprobable case of $\pm k$, the average probability of error P_e in the receiver is given by

$$\begin{aligned}
 P_e &= \frac{1}{2}P_{e1} + \frac{1}{2}P_{e2} \\
 &= Q\left(\frac{k}{\sqrt{N}}\right) = Q\left(\sqrt{\frac{k^2}{N}}\right)
 \end{aligned}
 \tag{2.2.10}$$

where k is the peak voltage at time $t=T$ and N is the noise variance.

2.2.4 Bit-energy-to-noise power spectral density ratio

Appendix A1 shows for systems in which only one signal-element (ISI free) is transmitted, the matched-filter detector is the optimum detector for the received signal-element and the error-rate performance depends on ratio of the received signal energy to the white Gaussian noise power spectral density at the filter input. (Note that, for a matched filter, the variance of a noise sample at the output of the filter is equal numerically to the two-sided power spectral density at the input.) For this reason, the bit-energy-to-noise power spectral density ratio,

$2E_b/N_0$, is frequently used in digital communication systems to enable a comparison of systems having variable transmission rates and of the performances of various modulations and coded systems in a complex interference environment. Here E_b is the energy per bit at the input to the receiver and $\frac{1}{2}N_0$ is the white Gaussian two-sided noise power spectral density measured at the same point.

Equation 2.2.10 shows, under the assumed conditions, the error-rate performance depends on the peak voltage to average noise ratio or the peak power to the noise variance ratio, at time $t=iT$. Now it is to determine the bit-energy-to-noise spectral power density ratio, $2E_b/N_0$, at the receiver input, under the same assumed conditions.

From Eqn. 2.1.3, the average energy per signal-element at the input to the transmission path is

$$E = \overline{\alpha_1^2} \int_{-\infty}^{\infty} |H_t(f)|^2 df$$

Since a binary antipodal signal, $\alpha_1 = \pm k$, is assumed, and the bit energy E_b ($=E$ in this case), can be written as

$$E_b = k^2 \int_{-\infty}^{\infty} |H_t(f)|^2 df \quad 2.2.11$$

From Eqn. 2.1.33a, the average power (mean-square value) of the noise waveform at the detector input (or receiver filter output) is

$$N = \frac{1}{2}N_0 \int_{-\infty}^{\infty} |H_r(f)|^2 df$$

therefore the two-sided power spectral density of the AWGN, in terms of the noise variance N and the receiver filter transfer function $H_r(f)$, can be written as

$$\frac{1}{2}N_0 = \frac{N}{\int_{-\infty}^{\infty} |H_r(f)|^2 df} \quad 2.2.12$$

From Eqns. 2.2.11 and 2.2.12, the ratio of the transmitted-bit-energy to noise-power-spectral-density, at the receiver input, is

$$\begin{aligned} \frac{E_b}{\frac{1}{2}N_o} &= \frac{k^2 \int_{-\infty}^{\infty} |H_t(f)|^2 df \int_{-\infty}^{\infty} |H_r(f)|^2 df}{N} \\ &= \frac{k^2 \int_{-\infty}^{\infty} |H(f)| df \int_{-\infty}^{\infty} |H(f)| df}{N} \end{aligned} \quad 2.2.13$$

as can be seen from Eqn. 2.1.30.

$H(f)$ has a sinusoidal rolloff spectrum, as given by Eqn. 2.2.3, so $\int_{-\infty}^{\infty} |H(f)| df = 1$, and Equation 2.2.13 can be simplified to

$$\frac{2E_b}{N_o} = \left(\frac{k^2}{N} \right) = \left(\frac{k}{\sqrt{N}} \right)^2 \quad 2.2.14$$

It can be seen that, under the assumed conditions, i.e., $H_r(f) = H_t(f)$ and $|H_r(f)|^2 = |H_t(f)|^2 = |H(f)|$ with $H(f)$ a sinusoidal rolloff frequency response, the bit-energy-to-noise power spectral density ratio at the receiver input is equal to the square of the peak voltage to noise variance at the detector input. Using Eqn. 2.2.14, Eqn. 2.2.10 can be rewritten, in term of $2E_b/N_o$, as

$$P_e = Q\left(\sqrt{\frac{2E_b}{N_o}}\right) \quad 2.2.15$$

This is also the error-rate performance of a matched-filter detector which depends upon the value of $2E_b/N_o$ at the input of the filter, as shown in Appendix 1A. The matched-filter detector is only optimum for single-shot transmission, whereas the present arrangement is optimum for even a sequence of signal-element transmission. Note that the bit energy E_b is in joules and the noise power spectral density $\frac{1}{2}N_o$ is in Watts per Hz, so that the ratio $2E_b/N_o$ is dimensionless.

2.3 Data-transmission system for satellite links

The simplest way to achieve frequency division multiple access at a satellite is to give different users different transponders. The trouble with this approach is that the transponders are of fixed capacity, whereas many users want a variable channel assignment. Furthermore, the transponder capacity is much too big for many users. Even when a corporation leases a whole transponder, it still has a demand assignment problem in using that transponder. Some means are needed for geographically dispersed users to share a transponder [6].

When each of many earth stations has access to the same transponder, the bandwidth of that transponder may be shared by frequency-division multiple access or time-division multiple access. These are referred to as FDMA and TDMA, respectively [6].

With FDMA, the transponder bandwidth is divided into smaller bandwidths. An earth station transmits on one or more of these frequency bands [6]. The central mechanism makes sure that no two earth stations transmit on the same frequency band at the same time. A frequency band can be reallocated from one earth station to another as the demand for channels varies [6].

With TDMA, each earth station is allowed to transmit a high-speed burst of bits for a brief period of time. The times of the bursts are carefully controlled so that no two bursts overlap. For the period of its burst, the earth station has the entire transponder bandwidth available to it [6].

TDMA offers a number of advantages over the FDMA systems which have dominated the first generation of multiple-access satellite communication systems. Perhaps its most significant advantage is the presence of only one carrier at a time in the satellite transponder. FDMA requires simultaneous transmission of a multiplicity of carriers through a common TWT in the satellite. It is well known that TWTs are highly nonlinear and the intermodulation products produced by the presence of multiple

carriers generate interference which degrades the individual channel performance if left uncorrected. To avoid this, it is common practice in FDMA systems to back-off the TWTA operating point from maximum power output, consequently forcing a reduction in the amount of traffic capacity that can be realized in that TWTA. With TDMA, since only one carrier appears at a time, the intermodulation distortion is eliminated and the resulting capacity reduction due to TWTA nonlinearity is significantly reduced. But if the number of earth stations is large and the transmission is low, FDMA techniques can provide a more efficient voice or data services. This is because each of the stations does not require the whole bandwidth of the transponder for low-bit rate transmission and a low-bit rate modem is cheaper to build; thus in this thesis, an FDMA system is assumed.

2.3.1 Satellite earth station configuration

A typical satellite earth station configuration is shown in Fig. 2.5. Three independent channels are shown. However, note that the number of channels in an earth station may vary from one to several thousands. The filters $F_{1,1}$, $F_{1,2}$ and $F_{1,3}$ bandlimit the modulated signals S_1 , S_2 and S_3 , respectively. Usually, for common output frequency modems, the first intermediate frequency (IF) f_{IF} may be specified to be the same for all channels [7].

The upconverters (U/Cs) translate the modulated, bandlimited signal to the desired transmitted radio frequencies. The filters $F_{2,1}$, $F_{2,2}$, and $F_{2,3}$ select the required sidebands of the upconverted signals. The center frequencies of these bandpass filters are at $f_c + f_{c_m} + f_{IF}$, $f_c + f_{IF}$, and $f_c - f_{c_m} + f_{IF}$ or at $f_c + f_{c_m} - f_{IF}$, $f_c - f_{IF}$, and $f_c - f_{c_m} - f_{IF}$, depending on whether the upper or the lower sidebands of the modulated and upconverted signals are used. To obtain a high power efficiency, most transmitter high power amplifiers (HPAs) have to operate in a nonlinear mode. This mode of operation spreads the spectrum of the modulated bandlimited signal.

Therefore the filters F_{31} , F_{32} and F_{33} , having the same center frequencies as the filters F_{21} , F_{22} and F_{23} , respectively, are used to prevent spectral spillover into the adjacent channels, i.e., to suppress ACI (adjacent channel interference). Greater ACI suppression is provided by the baseband filtering at both transmitter and receiver.

The sum of the modulated signals is received and amplified by the satellite receiver antenna. They are filtered and further amplified by a low-noise amplifier. A frequency translation is required to prevent in-band interference from the high-power satellite output to the satellite input. If the satellite transponder is not equipped with a frequency translator, then a tremendously high isolation (in the range 100 to 150 dB) between the output and input would be required (practical radio-frequency systems do not even approach this requirement). The signals are then further amplified by a TWTA. The satellite input and output filters F_3 and F_4 have a bandwidth wide enough to accommodate the overall spectrum of the FDMA signal. These two filters are used to bandlimit the signal, and thereby reduce the unwanted out-of-band noise and spectral spreading caused by the TWTA.

The filters F_{41} , F_{42} and F_{43} in the receiver earth stations prevent excessive ACI; that is, they prevent the overloading of the downconverters, which translate the desired radio channels to common IF frequencies before the signals are demodulated. The filters F_{51} , F_{52} and F_{53} preceding the demodulator, having a common center frequency f_{IF} , are used to select the respective downconverted signals.

The heart of the satellite channel is the modulator and the demodulator (i.e., modem). The modulation techniques employed, the filtering strategy and demodulation method have a major impact on the performance of the system. Spectral efficiency, required power, antenna size, and overall performance are significantly influenced by the performance of the modem in both linear and nonlinear channel environments.

2.3.2 Summary of the basic assumptions on the configuration of the low-bit-rate satellite channel

(A) For many applications where the radio-carrier frequency f_c is much higher than the data bit rate ($f_c/f_b > 10^5$, where f_b is the data bit rate), it is very difficult to design spectrally efficiency and temperature-stable radio frequency filters. For example, in a 1.4 GHz uplink using a 64 kbit/s QPSK signal, the filter F_{s1} (Fig. 2.5) requires a center frequency of 1.4 GHz and a two-sided bandwidth of 32 kHz. Because of the complexity of this type of filter design, many satellite earth stations do not utilize spectral shaping filters after the HPA. Thus the restored signal spectra created by these nonlinear amplifiers causes interference in the adjacent satellite channels.

(B) The intermodulation products produced by the presence of multiple carriers in FDMA systems generate interference which degrades the individual channel performance if left uncorrected. To avoid this, the TWTA operating point is backed-off from maximum power output, i.e., to operate the satellite transponder in a more linear mode and so make the problem less serious. F_{s3} and F_{s4} (Fig. 2.5) are wideband filters when compared with the filters F_{s1} , F_{s2} and F_{s3} , so, as far as a single channel is concerned, they have insignificant effects on the signals. In most satellite systems, the value of $2E_b/N_0$ in the uplink is normally made much higher than that in the downlink. Hence it can be assumed that, for the uplink, $2E_b/N_0 = \infty$. This is equivalent to bypassing the satellite transponder and adding the noise only at the input of the receiver at the earth station. It is shown in Appendix A3 that, if the same value of $2E_b/N_0$ is used for both the uplink and downlink, then $2E_b/N_0$ must be at least 3 dB greater than before to achieve the same performance.

(C) At the receiver, the filters F_{d1} , F_{d2} and F_{d3} are used to prevent the overloading of the downconverters (D/Cs). These are also radio-frequency filters and so cannot be narrowband. In order not to introduce

distortion into the signal, they should have a linear phase characteristic over the corresponding signal spectra.

(D) The filters F_{21} , F_{22} and F_{23} are used to select the required sideband of the upconverted signals so that they can be made wideband with a linear phase characteristic over the corresponding signal spectra.

Hence, the basic assumptions of the satellite channel can be summarised as follows.

- 1) Post HPA filtering is not used.
- 2) The filters and TWTA in the satellite do not cause any amplitude or phase distortion in the signal.
- 3) $2E_b/N_0$ for the uplink is made much higher than that for the downlink.
- 4) The radio-frequency filters at the receiver of the earth station do not cause any amplitude or phase distortion in the signal.
- 5) The filters F_{21} , F_{22} and F_{23} do not cause any amplitude or phase distortion in the signal.

Based on these assumptions, the satellite earth station configuration can be simplified as shown in Fig. 2.6, where the post HPA filters, the satellite, and the radio-frequency filters F_{41} , F_{42} and F_{43} have been removed.

Since the filters F_{21} , F_{22} and F_{23} are assumed to be memoryless, this configuration can be further simplified by considering the linear upconverters, the HPAs and the linear downconverters, as a transmission path in an intermediate frequency band. The resultant configuration is shown in Fig. 2.7, where the upconverters, the downconverters and the filters F_{21} , F_{22} and F_{23} are removed. The channels are still separated with a channel spacing of f_{cs} Hz. The IF filters F_{11} and F_{51} , F_{12} and F_{52} , and F_{13} and F_{53} still have the same characteristics, but are centered at $f_{IF}+f_{cs}$, f_{IF} , and $f_{IF}-f_{cs}$ Hz, respectively.

2.4 Filters to be used in the satellite transmission systems for computer simulation

2.4.1 Digital modulation and demodulation filters

Since the transmission system can be optimized by sharing the filtering equally between the transmitter and receiver filters and with a resultant sinusoidal rolloff amplitude response, the modulation and demodulation filters of the satellite system are designed to have the same characteristics and with an overall frequency response having a sinusoidal rolloff. In order to find the best baseband wave shape for data transmission over satellite links, the sinusoidal rolloff of 100%, 75%, 50% and 25% (i.e., $\beta=100\%$, 75%, 50% and 25%, respectively, in Eqn. 2.2.3) are used for investigations. Since it is very difficult to design an analog filter which has the wanted frequency response, these modulation and demodulation filters have to be digital. Provided that their finite sampled impulse responses are long enough and the quantization error is negligible, they can have frequency responses of any desired shapes. So in all the transmission systems described in this thesis, the modulation filter is a pair of digital baseband filters which determine the characteristics of the modulating signal, while the demodulation filter at the receiver is also a pair of digital baseband filters which achieve the matched filtering of the baseband demodulation signal.

The finite sampled impulse responses of the transmitter and receiver filters are designed using IDFT (Inverse Discrete Fourier Transform) to derive the impulse response tap gains for the desired frequency and phase characteristics in frequency domain, as shown in Table 2.1 and plotted in Fig. 2.8. A truncation length of $12T$ has been made and sampling rate of $8/T$ samples per second has been used, where $1/T$ is the signal element-rate. A delay of $6T$ seconds is introduced to make the filters realisable for computer simulation.

In practice, a digital-to-analog (D/A) conversion process is used to obtain the required shape of the analog baseband modulating signal. This will introduce a $[\sin(x)]/x$ amplitude characteristic on the frequency response. Thus an $x/[\sin(x)]$ amplitude characteristic might be required for compensation. However if the sampling rate is several (say 4) times greater than the bandwidth of the signal, the $[\sin(x)]/x$ effect is insignificant and so is neglected in the filter design described in this thesis.

2.4.2 IF bandpass filters F_{IF}

In satellite communication systems, the IF frequency (e.g., 70 MHz) is usually too high to use digital IF filters, so the IF bandpass filters have to be analog. The IF bandpass filters used in the project have the characteristics of a real surface acoustic wave (SAW) bandpass filter (Plessey NO.BP1103) centered at the frequency of 70 MHz with a 3 dB bandwidth of 5.6 MHz. These filters are used in the CERS modem operating at 8 Mbit/s. For the present case, the modem is operating at a speed of 64, 128, 256 or 512 kbit/s, so the bandwidths of the filters have been scaled down by a factor of 1/125, 1/62.5, 1/31.25 or 1/15.625, respectively. The filters have a symmetrical amplitude response (characteristic) as shown in Fig. 2.9a, and an asymmetrical linear phase characteristic over the bandwidth. They have the baseband equivalent model which can easily be obtained by shifting the center frequency to zero frequency, as it is shown in Appendix A4. Since the phase characteristic is linear, without loss of generality, it can be set to zero across the bandwidth; this means that the impulse response will be symmetrical at time $t=0$ and a delay must be re-introduced in the impulse response in order to make the filter physically realizable (Section 2.2.2) for computer simulation. The sampled impulse response of the filter is obtained, using the inverse DFT (IDFT) on the equivalent baseband amplitude response, as shown in Table 2.2 and Fig. 2.9b, where the

sampling rate of $8/T$ samples per second has been used. A truncation length of $6T$ is used to approximate to the ideal impulse responses of the IF filters in all the simulation tests, so that a delay of $3T$ seconds is re-introduced to make the filters realizable. It can be seen that the sampled impulse response shown in Table 2.2 contains only real values. This is because the filter has a symmetrical amplitude characteristic and an asymmetrical phase characteristic around the center frequency, and under these conditions, the filter does not introduce any quadrature crosstalk in the signal (Appendix A5).

2.4.3 Post D/A conversion filters

In practice, the analog baseband signal is obtained by means of a D/A conversion process, so an extra pair of analog post D/A conversion lowpass filters has to be used to reject spurious signals around multiples of the digital sampling frequency. These filters should have a linear phase characteristic over the wanted signal bandwidth. If the cutoff frequency is too low, unwanted ISI will occur. For a sampling rate of $8/T$ samples per second, an acceptable cutoff frequency may be $4/T$ [8]. Since these are wideband filters which do not have any significant effect on the wanted signal, they are not included in the baseband equivalent models of the transmission systems described in this thesis.

2.4.4 Pre A/D conversion filters

The digital baseband signal, at the input of the demodulation filter in the receiver, is obtained by means of A/D (analog-to-digital) conversion process, so that an extra pair of analog pre A/D conversion filter lowpass filters has to be used to remove any unwanted spectral components generated in the demodulation process. These filters should also have a linear phase characteristic over the wanted signal bandwidth. They are wideband filters which do not have any significant effect on the wanted signal, so they are not included in the baseband equivalent models of the transmission systems described in this thesis.

2.5 Nonlinearity

2.5.1 Introduction

In a satellite communication system, the modulated signal passes through the HPA in the earth station prior to transmission to the satellite and through the TWTA prior to retransmission back to an earth station. Typical input/output power and phase characteristics of an HPA and TWTA are shown in Fig. 2.10. It can be seen that the HPA or TWTA introduces nonlinear AM-AM and AM-PM conversion effects. For a low input level, the output power from either device is essentially a linear function of the input power. As the input drive increases, the output power increases nonlinearly until a point is reached at which any additional input level increase results in a decreasing output power. This point of maximum output is referred to as saturation. The operating point of an HPA (or TWTA) is usually given in terms of the input or output backoff below saturation, that is, the input or output power in decibels relative to the level at saturation.

In general, a transponder will carry a single wideband modulation (in TDMA systems) or a number of narrowband carriers (in FDMA systems) regularly spaced in frequency over the transponder bandwidth. Once the signal level approaches the amplifier saturation region, it will cause the following effects: [6],[7],[14]

- 1) For a multicarrier signal, intermodulation occurs. Signals will be suppressed and there will be disproportionate power sharing.
- 2) For a single bandlimited signal, any envelope fluctuation will cause unwanted phase modulation and spectral spreading.

To maximize the available power of the TWTA, it is desirable to have a high input level. However, effect (1) explains why, in FDMA systems, the satellite TWTA is well backed off to avoid intermodulation effects.

Due to the presence of the HPA and TWTA, very few theoretical results are presently available which describe the performance of PSK transmission

over a nonlinear satellite channel. Several results have been calculated to show the performance of a phase-shift keying system through a purely amplitude limiting channel [9],[10],[11]. But the assumption, though greatly simplifying the analysis, does not include the AM-PM conversion effect, which can significantly influence the communication system's performance when angle-modulated signals are employed.

2.5.2 Modelling of HPA for computer simulation

In recent years a considerable effort [9],[11],[12] has been made in attempting to develop analytic expressions that characterise the HPA and TWTA. One technique, as originated by Kaye et al [13], entails determining approximations for the envelope nonlinearities in a quadrature model for the HPA (or TWTA), and is now developed [12] (Fig.2.11a).

An input signal

$$S(t) = \sqrt{2}a(t)\cos\omega_c t - \sqrt{2}b(t)\sin\omega_c t \quad 2.5.1$$

where ω_c is the carrier frequency in rad/s, can be written as

$$S(t) = B(t)\cos[\omega_c t + \theta(t)] \quad 2.5.2$$

where

$$B(t) = \{2[a^2(t) + b^2(t)]\}^{1/2} \quad 2.5.3$$

and

$$\theta(t) = \tan^{-1}[b(t)/a(t)] \quad 2.5.4$$

So that

$$\sqrt{2}a(t) = B(t)\cos\theta(t) \quad 2.5.5a$$

and

$$\sqrt{2}b(t) = B(t)\sin\theta(t) \quad 2.5.5b$$

The HPA output signal is given by

$$Z(t) = G_p(B)B(t)\cos[\omega_c t + \theta(t)] - G_q(B)B(t)\sin[\omega_c t + \theta(t)] \quad 2.5.6$$

$$= |G(B)|B(t)\cos[\omega_c t + \theta(t) + g(B)] \quad 2.5.7$$

where $|G(B)| = \{[G_p(B)]^2 + [G_q(B)]^2\}^{1/2} \quad 2.5.8$

and $g(B) = \tan^{-1}[G_q(B)/G_p(B)] \quad 2.5.9$

with B the input signal envelope, i.e., short-hand notation for B(t) given by Eqn. 2.5.3.

Here $|G(B)|$ and $g(B)$ are the AM-AM and AM-PM conversion functions, respectively, of the HPA for an input signal with an envelope B . If the input signal has a constant envelope, i.e., $B(t)$ in Eqn. 2.5.3 is constant, then $|G(B)|$ and $g(B)$ in Eqns. 2.5.8 and 2.5.9, respectively, remain constant all the time. Hence, it can be seen in Eqn. 2.5.7 that the HPA will have no nonlinear distortion effect on the signal $Z(t)$.

Equation 2.5.6 can be written as

$$\begin{aligned} Z(t) &= [B(t)\cos\theta(t)G_p(B) - B(t)\sin\theta(t)G_q(B)]\cos\omega_c t \\ &\quad - [B(t)\sin\theta(t)G_p(B) + B(t)\cos\theta(t)G_q(B)]\sin\omega_c t \end{aligned} \quad 2.5.10$$

$$\begin{aligned} &= \sqrt{2}[a(t)G_p(B) - b(t)G_q(B)]\cos\omega_c t \\ &\quad - \sqrt{2}[b(t)G_p(B) + a(t)G_q(B)]\sin\omega_c t \end{aligned} \quad 2.5.11$$

as can be seen from Eqn. 2.5.5.

The equivalent baseband signals of $S(t)$ and $Z(t)$, in Eqns. 2.5.1 and 2.5.11 can be represented (Appendix A6) as the complex-valued signals

$$s(t) = a(t) + jb(t) \quad 2.5.12$$

$$\text{and } z(t) = [a(t)G_p(A) - b(t)G_q(A)] + j[b(t)G_p(A) + a(t)G_q(A)] \quad 2.5.13$$

respectively, where $j = \sqrt{-1}$, A is now the envelope of the equivalent baseband signal $s(t)$, i.e., short-hand notation for $A(t)$ given by

$$A(t) = [a^2(t) + b^2(t)]^{1/2} \quad 2.5.14$$

and the conversion functions $G_p(A)$ and $G_q(A)$ are now dependent on the signal envelope A , instead of B (the envelope of the radio-frequency signal). Equation 2.5.13 can be written as

$$z(t) = [a(t) + jb(t)][G_p(A) + jG_q(A)] \quad 2.5.15$$

$$= s(t)G(A) \quad 2.5.16$$

$$\text{where } G(A) = G_p(A) + jG_q(A) \quad 2.5.17$$

and $s(t)$ and $G(A)$ have complex values. The baseband equivalent model of the HPA is shown in Fig. 2.11b, where the HPA is represented by the

conversion function $G(A)$. Since the value of $G(A)$ is dependent on the input signal envelope $A(t)$, it can be varied by multiplying $A(t)$ by a constant factor H_c to give the envelope (Eqn. 2.5.14)

$$\hat{A}(t) = H_c [a^2(t) + b^2(t)]^{1/2} \quad 2.5.18$$

This is equivalent to shifting the operating point along the HPA transfer characteristics by using the value of H_c , so H_c can be used to locate the operating point at the required backoff value. H_c is called the HPA backoff factor.

From Eqns. 2.5.12 and 2.5.15, and with the use of the HPA backoff factor, the signal from the HPA output, for an input signal of

$$s(t) = a(t) + jb(t) \quad 2.5.19$$

is given by

$$z(t) = [a(t) + jb(t)] H_c [G_p(\hat{A}) + jG_q(\hat{A})] \quad 2.5.20$$

$$= s(t) H_c G(\hat{A}) \quad 2.5.21$$

The model can be used to assess the performance of a modulation technique by means of computer simulation. The amplitude and phase characteristics of the HPA are obtained by converting its power and phase characteristics. Samples of $G(\hat{A})$, which provide sufficient resolution, can be stored and used to determine the output signal values by means of interpolation. The samples are obtained as follows.

(1) To represent the HPA amplitude characteristic by, say n , discrete values of $|G(A)|$, the HPA amplitude characteristic is quantized into regular intervals of λ volts along the input axis ($n\lambda$ volts will be the maximum input voltage to the HPA). The values of $|G(\lambda_m)|$, where $\lambda_m = m\lambda$, for $m=1, 2, \dots, n$, are obtained using the amplitude (voltage) characteristic of the HPA and the equation

$$|G(\lambda_m)| = \frac{\text{Output voltage for an input value of } m\lambda \text{ volts}}{m\lambda \text{ volts}} \quad 2.5.22$$

(2) To represent the HPA phase characteristic by n discrete values of $g(\lambda)$, the HPA phase characteristic is quantized into intervals of λ volts along the input axis. The values of $g(\lambda_m)$, where $\lambda_m = m\lambda$, for $m=1, 2, \dots, n$, are obtained from the HPA phase characteristic. The quadrature components, $G_p(\lambda_m)$ and $G_q(\lambda_m)$, for $m=1, 2, \dots, n$, are then obtained using the phase characteristic of the HPA and $|G(\lambda_m)|$ with the use of the following two equations

$$G_p(\lambda_m) = |G(\lambda_m)| \cos[g(\lambda_m)] \quad 2.5.23a$$

and
$$G_q(\lambda_m) = |G(\lambda_m)| \sin[g(\lambda_m)] \quad 2.5.23b$$

(3) The values of $G_p(\lambda_m)$ and $G_q(\lambda_m)$, for $m=1, 2, \dots, n$, are then taken as real and imaginary values, respectively, such that

$$G(\lambda_m) = G_p(\lambda_m) + jG_q(\lambda_m) \quad 2.5.24$$

Hence the $\{G(\lambda_m)\}$ are obtained.

From Eqns. 2.5.19, 2.5.20 and 2.5.21, the signal from the HPA output for an input signal of

$$s(t) = a(t) + jb(t) \quad 2.5.25$$

is given by

$$z(t) = [a(t) + jb(t)]H_c[G_p(\lambda) + jG_q(\lambda)] \quad 2.5.26$$

$$= s(t)H_c G(\lambda) \quad 2.5.27$$

where $s(t)$, $a(t)$, $b(t)$, $z(t)$, $s(t)$ and $G(\lambda)$ are continuous functions. In computer simulation tests, discrete signals are used, so the signals in Eqns. 2.5.25, 2.5.26, 2.5.27 are sampled at the time instants $\{iT_m\}$, where $1/T_m$ is the sampling rate, to give the signal sample values s_i and z_i , at time $t=iT_m$, where

$$s_i = a_i + jb_i \quad 2.5.28$$

and
$$z_i = s_i H_c [G_p(\lambda_i) + jG_q(\lambda_i)] \quad 2.5.29$$

$$= s_i H_c G(\lambda_i) \quad 2.5.30$$

respectively, $s_i = s(iT_m)$, $a_i = a(iT_m)$, $b_i = b(iT_m)$ and $z_i = z(iT)$, and λ_i is the

value of λ_n closest to the signal envelope $|H_c(a_1 + jb_1)|$ at the input, and H_c is the HPA backoff factor. The model of the HPA for discrete signals is shown in Fig. 2.11c.

The values of $\{G(\lambda_n)\}$, for $n=1, 2, \dots, 32$, obtained by quantizing the assumed HPA characteristics (Fig. 2.12) into regular intervals along the input axis and using Eqns. 2.5.22, 2.5.23 and 2.5.24, are shown in Table 2.3. The 20th sample represents the 0 dB OBO (output backoff point). Since none of the samples represents 1 dB OBO, the 12th sample, representing 0.68 dB OBO and marked as 'C' in Fig. 2.12, is used instead. The 15th sample, representing the 0.2 dB OBO and is marked as 'B', is used to determine the nonlinear effects when the HPA is slightly backed off below saturation. In all simulation tests discussed in this thesis, the HPA (when present) is operating at 0 dB, 0.2 dB or 0.68 dB OBO.

2.6 The baseband equivalent models of quadrature modulation systems

In quadrature modulation, the modulated signal consists of the sum of two double sideband suppressed carrier components whose carrier signals have the same frequency but are in phase-quadrature to each other. It is shown in Chapters 3 and 4 that quadrature modulation is used in QPSK, DEQPSK and CE8PSK techniques, so the baseband equivalent model of a quadrature modulation system is considered here.

A) With a nonlinear satellite channel

The model of a quadrature modulation system with a nonlinear satellite channel is shown in Fig. 2.13a, where the transmitter and receiver IF filters are assumed to be the ones described in Section 2.4.2. $a(t)$ and $b(t)$ are two modulating signals in element synchronism and are obtained from two independent data-sources. They are applied to the respective multipliers. The second input to the inphase multiplier is the carrier signal, $\sqrt{2}\cos\omega_c t$, and the second input to the quadrature multiplier is the

carrier signal shifted exactly by $-\pi/2$, i.e., $-\sqrt{2}\sin\omega_c t$. The multiplier outputs are added linearly to give the quadrature signal

$$S(t) = \sqrt{2}a(t)\cos\omega_c t - \sqrt{2}b(t)\sin\omega_c t \quad 2.6.1$$

which is filtered and nonlinearly distorted by the transmitter IF filters and the HPA, respectively.

At the output of the transmitter, the signal is

$$\hat{S}(t) = \sqrt{2}\hat{a}(t)\cos\omega_c t - \sqrt{2}\hat{b}(t)\sin\omega_c t \quad 2.6.2$$

where $\sqrt{2}\hat{a}(t)$ and $\sqrt{2}\hat{b}(t)$ are the inphase and quadrature signal waveforms that have been nonlinearly distorted by the HPA.

The equivalent baseband signal of the quadrature modulated signal, expressed by Eqn. 2.6.1, can be represented (Appendix A6) as the complex-valued signal

$$s(t) = a(t) + jb(t) \quad 2.6.3$$

where $j=\sqrt{-1}$. Likewise, the signal $\hat{S}(t)$, at the output of the transmitter, given by Eqn. 2.6.2, can be represented as the complex-valued signal

$$\hat{s}(t) = \hat{a}(t) + j\hat{b}(t) \quad 2.6.4$$

The noise waveform $N(t)$, at the input of the receiver, is a sample function of a Gaussian random process with zero mean and a two-sided power spectral density of $\frac{1}{2}N_0$ over the signal frequency band. Assume $N(t)$ is a narrowband bandpass noise, so that it can be expanded (Appendix A7) into

$$N(t) = N_c(t)\cos\omega_c t - N_s(t)\sin\omega_c t \quad 2.6.5$$

where $N_c(t)$ and $N_s(t)$ are sample functions of Gaussian random processes

with zero mean, and the two-sided power spectral density of each of them is twice that of $N(t)$ (Appendix A7). The equivalent baseband form of $N(t)$ can be represented as the complex-valued signal

$$n(t) = n_c(t) + jn_m(t) \quad 2.6.6$$

where $n_c(t)$ and $n_m(t)$ all have the same variance and are sample functions of Gaussian random processes with zero mean and a two-sided spectral power density of $\frac{1}{2}N_0$ over the frequency band of the baseband data signal $s(t)$.

So in the model of the quadrature modulation system, since the transmitter and receiver IF filters F_{IF} and the HPA can be represented by their baseband equivalent models, and the bandpass signals $N(t)$, $S(t)$, and $\hat{S}(t)$ can be represented by their equivalent baseband signals $n(t)$, $s(t)$ and $\hat{s}(t)$, respectively, the model of the quadrature modulation system can be simplified by assigning real values to the signals in one of the two parallel channels (that associated with $\sqrt{2}\cos\omega_c t$) and imaginary values to the signals in the other channel, and then considering the linear modulator, the transmitter IF filter, the HPA, the receiver IF filter, the linear demodulator, as a baseband transmission path carrying complex-valued signals. The resultant system is shown in Fig. 2.13b.

In this thesis, three baseband equivalent models of different bandpass channels are used for computer simulation tests. They are (a) linear and memoryless, (b) linear and bandlimited and, (c) nonlinear and bandlimited channels, as shown in Fig. 2.14, which are obtained from Fig. 2.13a by removing the appropriate blocks.

B) With a nonlinear satellite channel and in an ACI environment

In the previous discussion, a single channel is assumed. The interference caused by other channels is neglected. In FDMA systems, the interference caused by adjacent channels has a significant effect on the system performance. This interference is caused by spillover from the adjacent channels and is called adjacent channel interference (ACI). An

illustrative example of ACI is shown in Fig. 2.15, where an ideal brick-wall receiver channel filtering is assumed. The ACI is introduced predominantly by the power spectra of the two adjacent channels overlapping the power spectrum of the desired channel, which cannot be eliminated by the receiver filter.

The model of a quadrature modulation system, with a nonlinear satellite channel in an ACI environment, is shown in Fig. 2.16. The most significant ACI is from the upper and lower adjacent channels, so that only these two channels are considered. The system represents the satellite configuration shown in Fig. 2.7, where the transmitter and receiver IF filters are assumed to be the ones described in Section 2.4.2. Since the ACI effect on the desired channel is considered, the receivers for the upper and lower channels are omitted. It is assumed that the receiver of the desired channel provides the required ideal carrier signal. The modulated signals, at the modulator outputs of the upper, desired and lower channels, are

$$S_U(t) = \sqrt{2}a_U(t)\cos(\omega_c t + \omega_{c_m} t + \theta_U) - \sqrt{2}b_U(t)\sin(\omega_c t + \omega_{c_m} t + \theta_U) \quad 2.6.7a$$

$$S_D(t) = \sqrt{2}a_D(t)\cos\omega_c t - \sqrt{2}b_D(t)\sin\omega_c t \quad 2.6.7b$$

$$\text{and } S_L(t) = \sqrt{2}a_L(t)\cos(\omega_c t - \omega_{c_m} t + \theta_L) - \sqrt{2}b_L(t)\sin(\omega_c t - \omega_{c_m} t + \theta_L) \quad 2.6.7c$$

respectively, where $a_U(t)$ and $b_U(t)$, $a_D(t)$ and $b_D(t)$, and $a_L(t)$ and $b_L(t)$ are the inphase and quadrature baseband signal components in the upper, desired and lower channels, respectively. ω_{c_m} is the channel spacing in rad/s, and θ_U and θ_L are any arbitrary phase angles. The signals are filtered by the respective transmitter IF filters F_{IF} (which all have the same characteristics but are centered at different frequencies), and then

nonlinearly distorted by the respective HPAs (Section 2.5). At the outputs of the transmitters, the signals are

$$\hat{S}_U(t) = \sqrt{2}\hat{a}_U(t)\cos(\omega_c t + \omega_{c_m} t + \theta_U) - \sqrt{2}\hat{b}_U(t)\sin(\omega_c t + \omega_{c_m} t + \theta_U) \quad 2.6.8a$$

$$\hat{S}_D(t) = \sqrt{2}\hat{a}_D(t)\cos\omega_c t - \sqrt{2}\hat{b}_D(t)\sin\omega_c t \quad 2.6.8b$$

$$\text{and } \hat{S}_L(t) = \sqrt{2}\hat{a}_L(t)\cos(\omega_c t - \omega_{c_m} t + \theta_L) - \sqrt{2}\hat{b}_L(t)\sin(\omega_c t - \omega_{c_m} t + \theta_L) \quad 2.6.8c$$

respectively, where $\hat{a}_U(t)$ and $\hat{b}_U(t)$, and $\hat{a}_D(t)$ and $\hat{b}_D(t)$, and $\hat{a}_L(t)$ and $\hat{b}_L(t)$ are the filtered and nonlinearly distorted inphase and quadrature baseband signals in the upper, desired and lower channels, respectively. Assume that the inphase and quadrature signal components of the ACI, from the adjacent channels, affects the inphase and quadrature signal components, respectively, of the desired signal equally all the time. (Results of Computer simulation tests have shown that this is the worst case.) Under these conditions, $\theta_U = \theta_L = 0$, and Equation 2.6.8 becomes

$$\hat{S}_U(t) = \sqrt{2}\hat{a}_U(t)\cos(\omega_c + \omega_{c_m})t - \sqrt{2}\hat{b}_U(t)\sin(\omega_c + \omega_{c_m})t \quad 2.6.9a$$

$$\hat{S}_D(t) = \sqrt{2}\hat{a}_D(t)\cos\omega_c t - \sqrt{2}\hat{b}_D(t)\sin\omega_c t \quad 2.6.9b$$

$$\text{and } \hat{S}_L(t) = \sqrt{2}\hat{a}_L(t)\cos(\omega_c - \omega_{c_m})t - \sqrt{2}\hat{b}_L(t)\sin(\omega_c - \omega_{c_m})t \quad 2.6.9c$$

respectively, which then can be written as

$$\begin{aligned} \hat{S}_U(t) = & \sqrt{2}[\hat{a}_U(t)\cos\omega_{c_m}t - \hat{b}_U(t)\sin\omega_{c_m}t]\cos\omega_c t \\ & - \sqrt{2}[\hat{a}_U(t)\sin\omega_{c_m}t + \hat{b}_U(t)\cos\omega_{c_m}t]\sin\omega_c t \end{aligned} \quad 2.6.10a$$

$$\hat{S}_D(t) = \sqrt{2}\hat{a}_D(t)\cos\omega_c t - \sqrt{2}\hat{b}_D(t)\sin\omega_c t \quad 2.6.10b$$

$$\begin{aligned} \text{and } \hat{S}_L(t) = & \sqrt{2}[\hat{a}_L(t)\cos\omega_{c_m}t + \hat{b}_L(t)\sin\omega_{c_m}t]\cos\omega_c t \\ & - \sqrt{2}[\hat{a}_L(t)\sin\omega_{c_m}t - \hat{b}_L(t)\cos\omega_{c_m}t]\sin\omega_c t \end{aligned} \quad 2.6.10c$$

respectively. The equivalent baseband signals expressed in Eqn. 2.6.10,

with respect to the desired channel, can be represented (Appendix A6) as the complex-valued signals

$$\begin{aligned}\hat{s}_U(t) &= [\hat{a}_U(t)\cos\omega_{c_m}t - \hat{b}_U(t)\sin\omega_{c_m}t] \\ &\quad + j[\hat{a}_U(t)\sin\omega_{c_m}t + \hat{b}_U(t)\cos\omega_{c_m}t]\end{aligned}\quad 2.6.11a$$

$$= [\hat{a}_U(t) + j\hat{b}_U(t)] [\cos\omega_{c_m}t + j\sin\omega_{c_m}t]\quad 2.6.11b$$

$$= [\hat{a}_U(t) + j\hat{b}_U(t)]\exp(j\omega_{c_m}t)\quad 2.6.11c$$

$$\hat{s}_D(t) = \hat{a}_D(t) + j\hat{b}_D(t)\quad 2.6.11d$$

and

$$\begin{aligned}\hat{s}_L(t) &= [\hat{a}_L(t)\cos\omega_{c_m}t + \hat{b}_L(t)\sin\omega_{c_m}t] \\ &\quad + j[\hat{a}_L(t)\sin\omega_{c_m}t - \hat{b}_L(t)\cos\omega_{c_m}t]\end{aligned}\quad 2.6.11e$$

$$= [\hat{a}_L(t) + j\hat{b}_L(t)] [\cos\omega_{c_m}t - j\sin\omega_{c_m}t]\quad 2.6.11f$$

$$= [\hat{a}_L(t) + j\hat{b}_L(t)]\exp(-j\omega_{c_m}t)\quad 2.6.11g$$

respectively, with $j=\sqrt{-1}$, where $\hat{a}_U(t)+j\hat{b}_U(t)$ and $\hat{a}_L(t)+j\hat{b}_L(t)$ are the equivalent baseband signals with respect to the upper and lower channels, respectively, at the outputs of the transmitter IF filters. The resultant equivalent baseband signal (i.e., the sum of the signals in Eqn. 2.6.11), with respect to the desired channel, is (Eqns. 2.6.11a, d and e)

$$s_R(t) = \hat{s}_U(t) + \hat{s}_D(t) + \hat{s}_L(t)\quad 2.6.12$$

$$\begin{aligned} &= [\hat{a}_U(t)\cos\omega_{c_m}t - \hat{b}_U(t)\sin\omega_{c_m}t + \hat{a}_D(t) \\ &\quad + \hat{a}_L(t)\cos\omega_{c_m}t + \hat{b}_L(t)\sin\omega_{c_m}t] \\ &\quad + j[\hat{a}_U(t)\sin\omega_{c_m}t + \hat{b}_U(t)\cos\omega_{c_m}t + \hat{b}_D(t) \\ &\quad + \hat{a}_L(t)\sin\omega_{c_m}t - \hat{b}_L(t)\cos\omega_{c_m}t]\end{aligned}\quad 2.6.13$$

Since $\theta_U=\theta_L=0$ has been assumed, the IF signals at the corresponding modulator outputs, given by Eqn. 2.6.7, can also be represented by the

equivalent baseband signals, with respect to the respective channels, as the complex-valued signals

$$s_u(t) = a_u(t) + jb_u(t) \quad 2.6.14a$$

$$s_p(t) = a_p(t) + jb_p(t) \quad 2.6.14b$$

and
$$s_l(t) = a_l(t) + jb_l(t) \quad 2.6.14c$$

respectively. The noise signal $N(t)$ also can be represented as the equivalent baseband signal (Eqn. 2.6.6).

Hence again, since the transmitter and receiver IF filters F_{IF} (Section 2.4.2) and the HPA can be represented by their baseband equivalent models, and all the bandpass signals have their equivalent baseband signals (Eqns. 2.6.11, 2.6.12 and 2.6.14), the baseband equivalent model of the system can be simplified by assigning, in each of the channels, real values to the signals in one of the two parallel channels (that associated with $\sqrt{2}\cos(\cdot)$), and imaginary values to the other channel, and then considering the linear modulators, the transmitter IF filters, the HPAs, the receiver IF filters, the linear demodulator, as a baseband transmission path carrying complex-valued signals. The resultant system is shown in Fig. 2.17, where all the filters and HPAs are identical. The transmitted signals from the upper and lower channels are multiplied by the factors $\exp(j\omega_c t)$ and $\exp(-j\omega_c t)$, respectively, to take into account ACI. Note that these two factors, $\exp(j\omega_c t)$ and $\exp(-j\omega_c t)$, have a unit gain, so there is no difference in placing them before or after the corresponding HPAs. The baseband equivalent model of the system under two conditions are considered in this thesis. They are (1) when all the transmitters operate the HPAs in a linear mode and, (2) when all the transmitters operate the HPAs in a nonlinear mode.

REFERENCES

- [1] Clark, A.P., *Principles of Digital Data Transmission*, Pentech Press, London (1976)
- [2] Davenport, W.B., *Probability and Random Process*, McGraw-Hill, New York (1970)
- [3] Thomas, J.B., *An Introduction to Statistical Communication Theory*, pp.614-620, Wiley, New York (1969)
- [4] Nyquist, H., "Certain Topics in Telegraph Transmission Theory", *AIEE Trans.*, 47, pp.617-64 (1928)
- [5] Bennett, W.R. and Davey, J.R., *Data transmission*, McGraw-Hill, New York (1965)
- [6] Martin, J. *Communications Satellite Systems*, Prentice-Hall, Englewood Cliffs, NJ (1978)
- [7] Feher, K., *Digital Communications : Satellite/Earth Station Engineering*, Prentice-Hall, Englewood Cliffs, NJ (1983)
- [8] Jagar, F. de and Dekker, C.B., "Tamed Frequency Modulation, A Novel Method To Achieve Spectrum Economy in Digital Transmission", *IEEE Trans. on Commun.*, vol. COM-20, pp.534-542, May 1978
- [9] Lyons, R.G., "The Effect of a Bandpass Nonlinearity on Signal detectability", *IEEE Trans. on Commun. Technol.*, vol. COM-2, pp.51-60, Jan.1973
- [10] Davisson, L.D. and Milstein, L.B., "On The Performance of Digital Communication Systems with Bandpass Limiters - Part I: One link system", *IEEE Trans. on Commun. Technol.*, vol. COM-20, pp.972-975, Oct. 1972
- [11] Jain, P.C. and Blachman, N.M., "Detection of a PSK Signal Transmitted Through a Hard-Limited Channel", *IEEE Trans. Inform. Theory*, vol. IT-19, NO. 5, pp.623-630, Sept. 1973
- [12] Hetrakul, P. and Taylor, D.P., "The Effects of Transponder Nonlinearity on Binary CPSK Signal Transmission", *IEEE Trans. Commun.*, vol. COM-24, pp.546-553, May 1976
- [13] Kaye, A.R., George, D.A. and Eric, M.J., "Analysis and Compensation of Bandpass Nonlinearities for Communications", *IEEE Trans. Commun., Technol.*, vol. COM-20, pp.965-972, Oct. 1972
- [14] Bhargave, U.K., Hacocum, D., Matyas, R. and Nuspl, p.p, *Digital Communications by Satellite*, John Wiley & Sons (1982)

m (unit of T/8 sec.)	Sampled impulse responses of			
	$\beta=100\%$	$\beta=75\%$	$\beta=50\%$	$\beta=25\%$
0	1.000	1.000	1.000	1.000
± 1	0.943	0.954	0.936	0.970
± 2	0.786	0.825	0.858	0.884
± 3	0.566	0.638	0.700	0.751
± 4	0.334	0.425	0.511	0.585
± 5	0.135	0.223	0.316	0.403
± 6	0.000	0.060	0.139	0.227
± 7	0.064	-0.047	-0.001	0.068
± 8	-0.068	-0.095	-0.094	-0.058
± 9	-0.038	-0.096	-0.138	-0.144
± 10	-0.001	-0.067	-0.140	-0.188
± 11	0.024	-0.028	-0.112	-0.192
± 12	0.029	0.005	-0.068	-0.164
± 13	0.017	0.022	-0.022	-0.115
± 14	-0.001	0.022	0.035	-0.056
± 15	-0.014	0.010	0.039	0.002
± 16	-0.017	-0.006	0.030	0.049
± 17	-0.011	-0.018	0.014	0.080
± 18	-0.001	-0.022	0.014	0.091
± 19	0.008	-0.018	-0.003	0.085
± 20	0.010	-0.008	-0.015	0.065
± 21	0.007	0.003	-0.020	0.036
± 22	-0.001	0.011	-0.017	0.006
± 23	-0.007	0.012	-0.008	-0.020
± 24	-0.008	0.009	0.002	-0.039
± 25	-0.006	0.002	0.011	-0.047
± 26	-0.001	-0.004	0.016	-0.045
± 27	0.004	-0.007	0.015	-0.034
± 28	0.005	-0.007	0.010	-0.019
± 29	0.003	-0.003	0.003	-0.003
± 30	-0.001	0.002	-0.005	0.011
± 31	-0.004	0.006	-0.010	0.021
± 32	-0.005	0.006	-0.011	0.024
± 33	-0.004	0.004	-0.009	0.021
± 34	0.000	0.000	-0.005	0.014
± 35	0.003	-0.005	0.001	0.004
± 36	0.004	-0.007	0.005	-0.005
± 37	0.002	-0.008	0.008	-0.012
± 38	0.000	-0.005	0.007	-0.016
± 39	-0.003	-0.002	0.003	-0.015
± 40	-0.004	0.001	-0.001	-0.011
± 41	-0.003	0.003	-0.005	-0.004
± 42	-0.001	0.002	-0.008	0.003
± 43	0.002	0.000	-0.008	0.009
± 44	0.003	-0.002	-0.006	0.013
± 45	0.002	-0.004	-0.002	0.013
± 46	0.000	-0.004	0.002	0.010
± 47	-0.003	-0.002	0.005	0.005
± 48	-0.003	0.001	0.006	-0.002

Table 2.1 Sampled impulse responses of the modulator (or demodulator) filters, with different values of β . The truncation lengths have been made to be $\pm 8T$ with sampling rate of $8/T$.

m (unit of T/8 seconds)	SIR	m	SIR
±0	1.000	±13	0.052
±1	0.935	±14	0.039
±2	0.758	±15	0.017
±3	0.512	±16	-0.004
±4	0.256	±17	-0.017
±5	0.041	±18	-0.021
±6	-0.099	±19	-0.017
±7	-0.157	±20	-0.008
±8	-0.146	±21	0.002
±9	-0.094	±22	0.009
±10	-0.031	±23	0.011
±11	0.020	±24	0.008
±12	0.048		

Table 2.2 Sampled impulse response of the equivalent baseband model of the transmitter (or receiver IF) filter. The truncation length has been made to be ±3T with sampling rate of 8/T samples per second. SIR means sampled impulse response.

m	$G(\lambda_m)$ $= G_p(\lambda_m) + jG_q(\lambda_m)$		m	$G(\lambda_m)$ $= G_p(\lambda_m) + jG_q(\lambda_m)$	
1	3.570	0.170	21	0.630	0.750
2	3.170	0.340	22	0.580	0.730
3	2.830	0.480	23	0.540	0.700
4	2.550	0.580	24	0.500	0.670
5	2.330	0.650	25	0.460	0.650
6	2.150	0.700	26	0.430	0.610
7	1.990	0.750	27	0.400	0.580
8	1.830	0.780	28	0.370	0.560
9	1.690	0.820	29	0.352	0.530
10	1.550	0.840	30	0.352	0.500
11	1.440	0.850	31	0.332	0.480
12	1.300	0.850	32	0.332	0.430
13	1.200	0.840			
14	1.090	0.830			
15	1.000	0.840			
16	0.920	0.850			
17	0.860	0.830			
18	0.800	0.820			
19	0.740	0.800			
20	0.780	0.680			

Table 2.3 Sampled representation of the HPA transfer characteristics shown in Fig. 2.12.

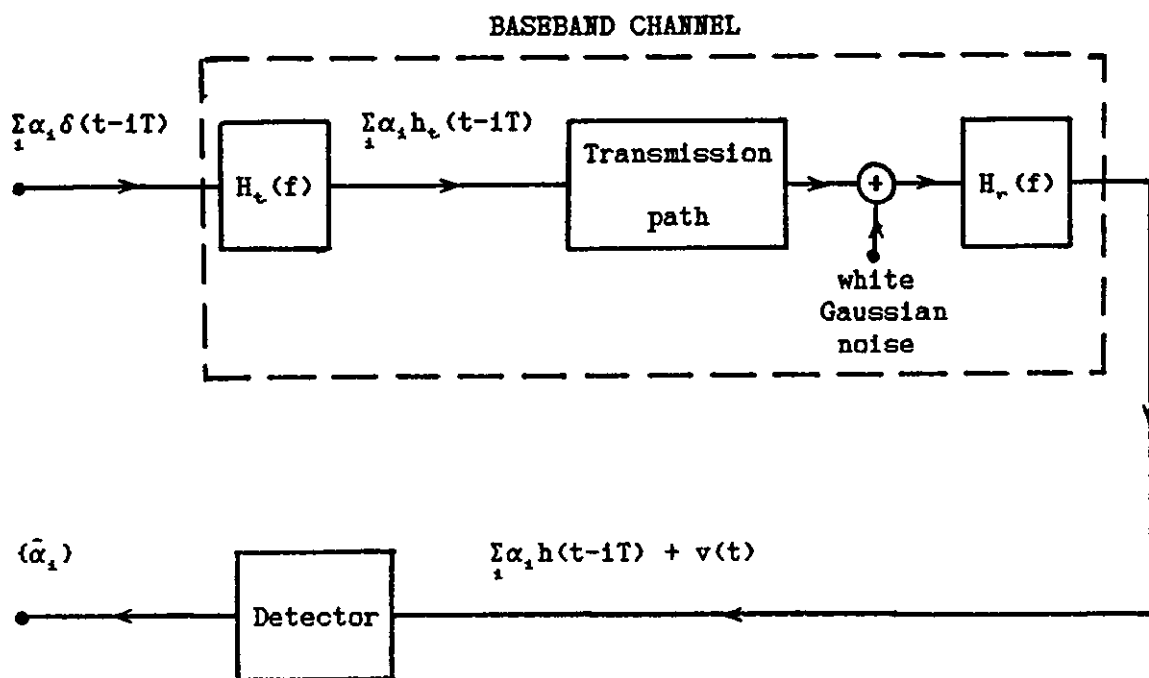


Figure 2.1 Baseband model of the data-transmission system.

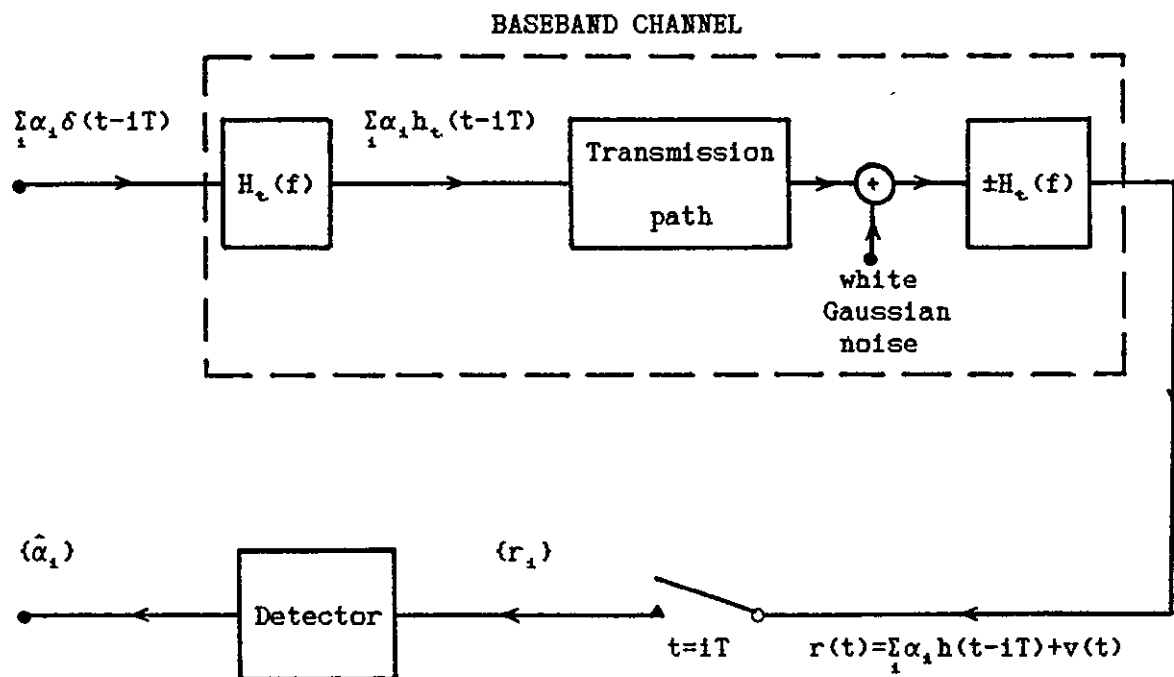


Figure 2.2 Assumed model of the data-transmission system.

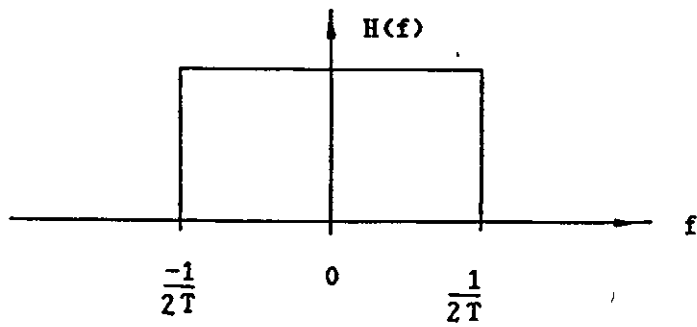


Figure 2.3a Channel transfer-function giving a rectangular signal-spectrum.

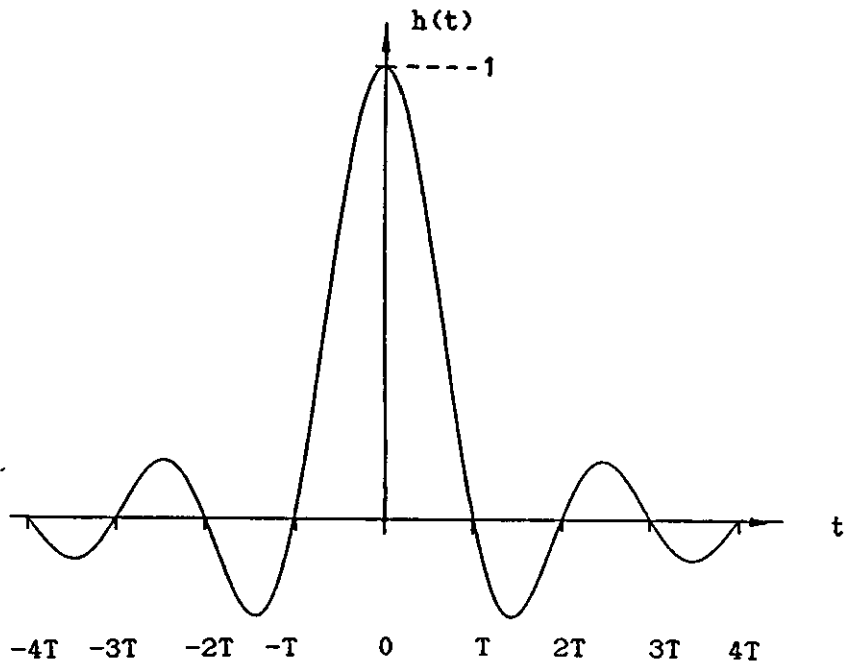


Figure 2.3b Impulse response of baseband channel.

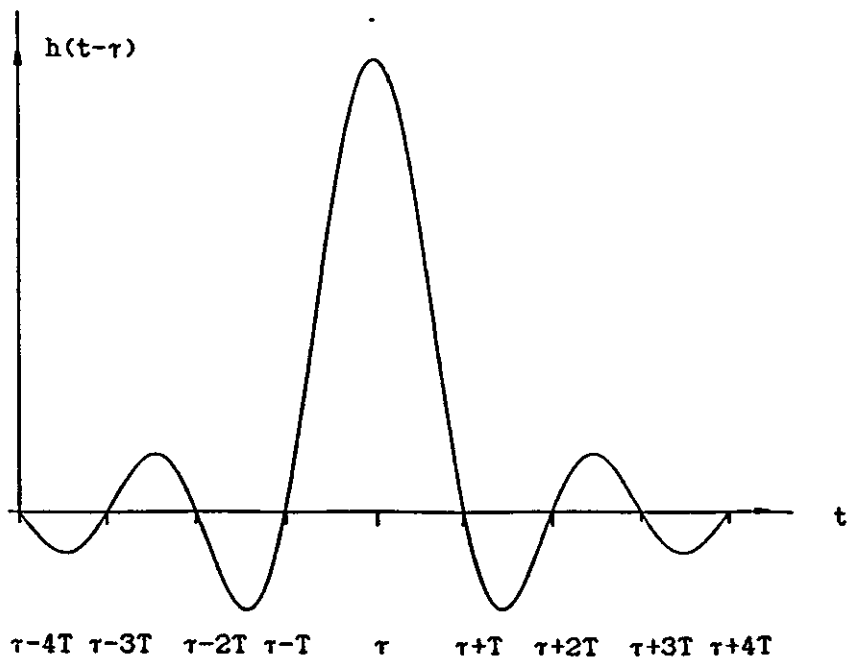
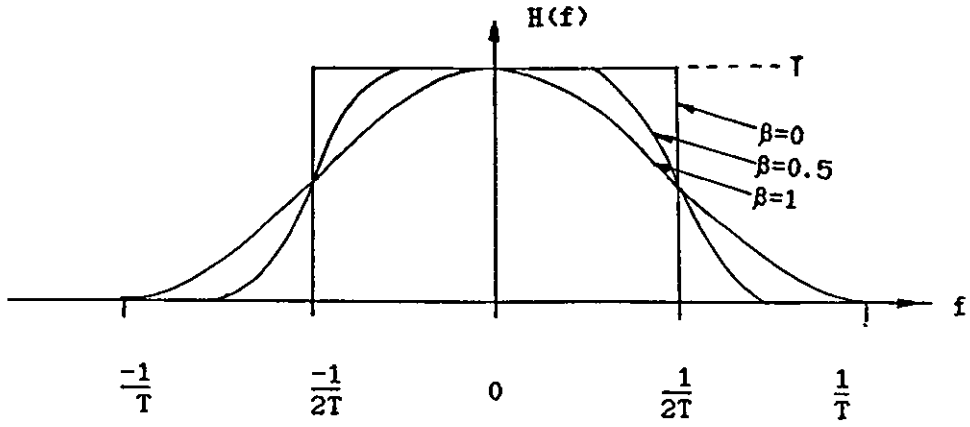
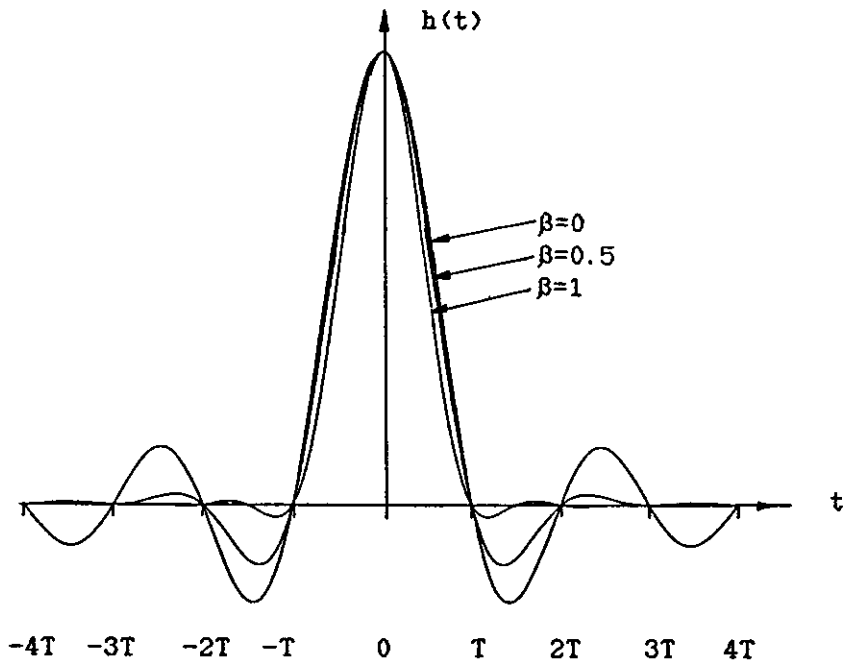


Figure 2.3c Physically realisable impulse response.



(a)



(b)

Figure 2.4
Time response

Responses for different rolloff factor. a) Frequency response. b)

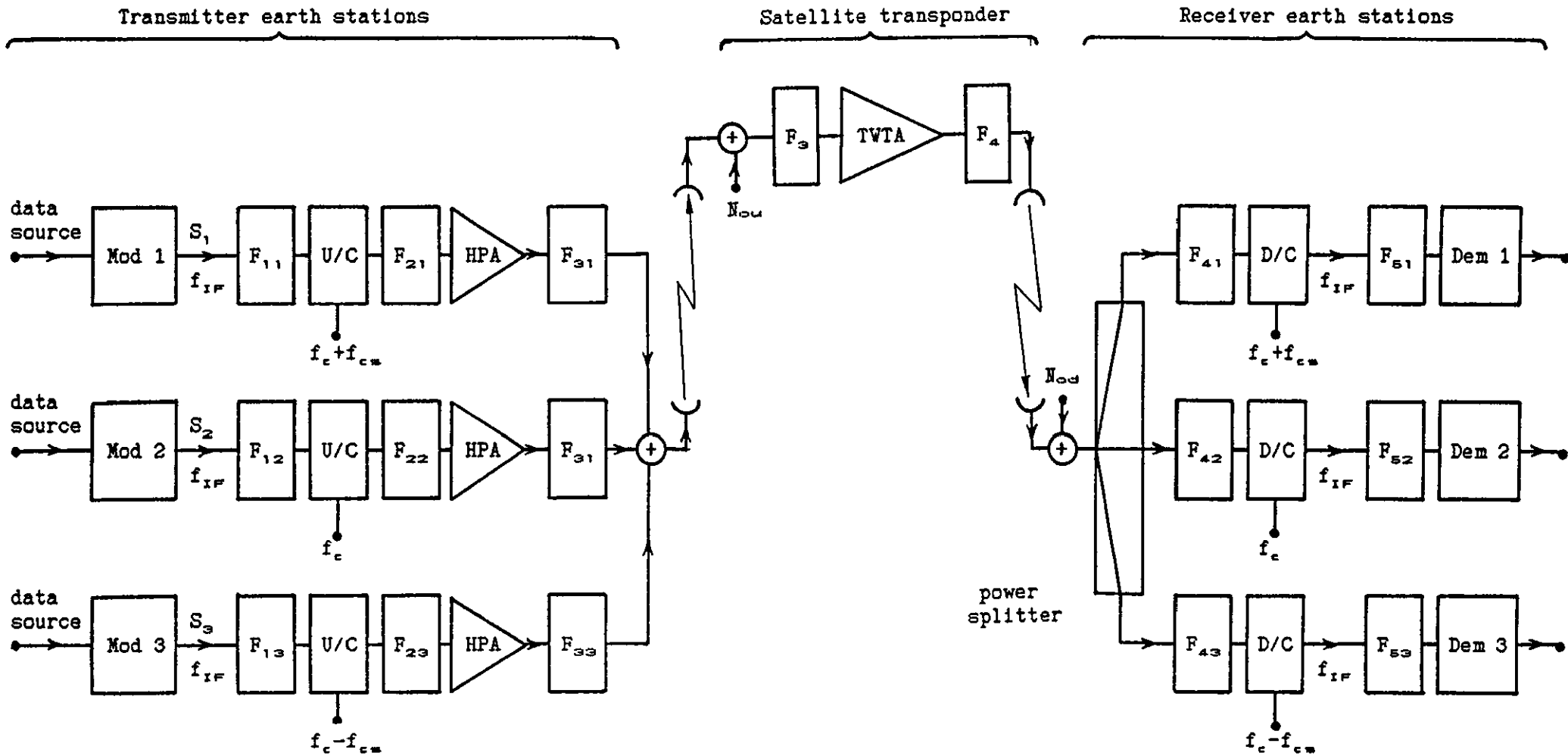


Figure 2.5 Typical satellite earth station configuration. Mod and Dem mean modulator and demodulator, U/C and D/C mean up-converter and down-converter, and N_{ou} and N_{od} mean uplink noise and downlink noise, respectively.

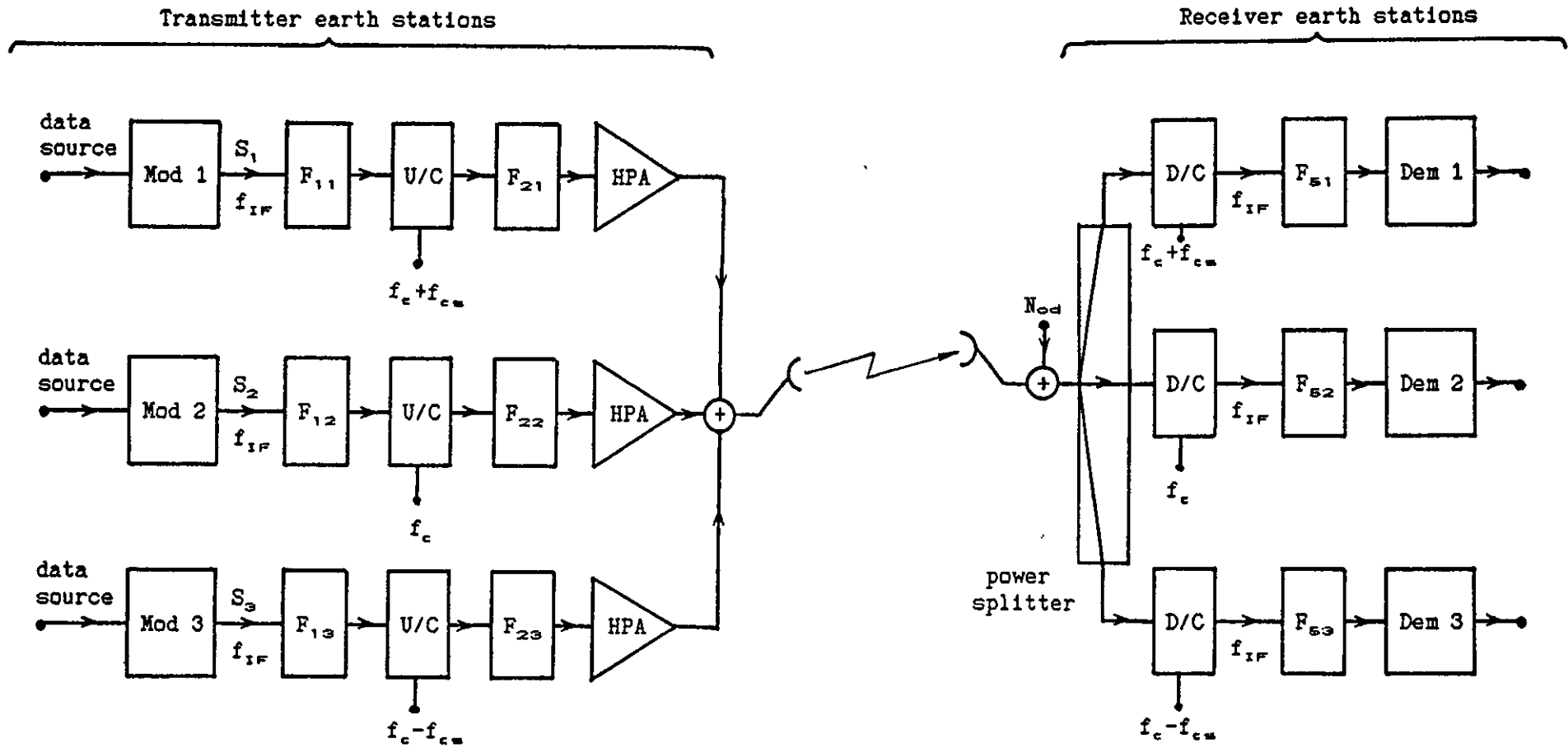


Figure 2.6 Low-bit rate satellite earth station system. (See Fig. 2.5 for abbreviations.)

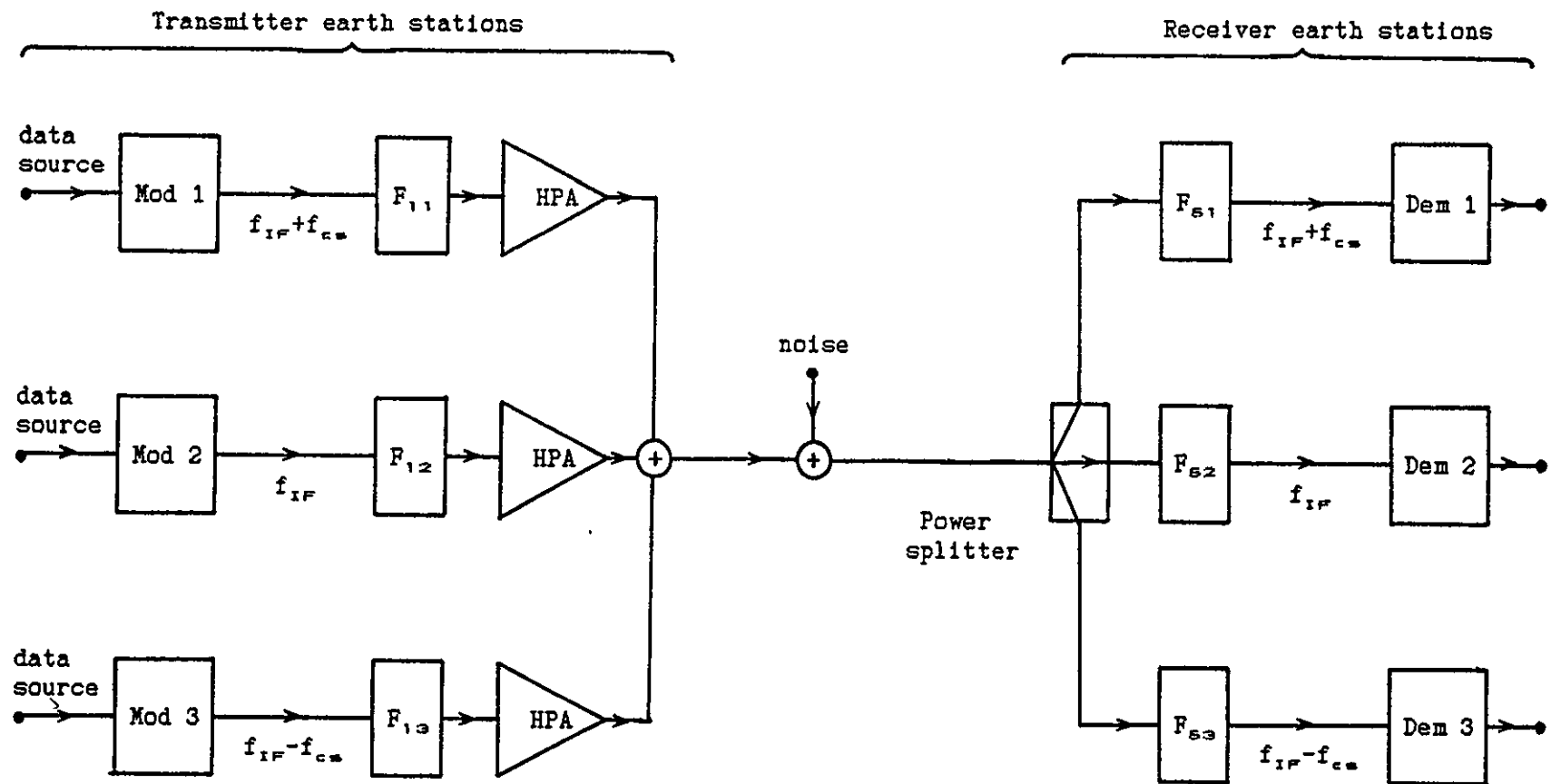


Figure 2.7 Simplified model of the low-bit rate satellite earth station system at IF frequency band. (See Fig. 2.5 for abbreviations.)

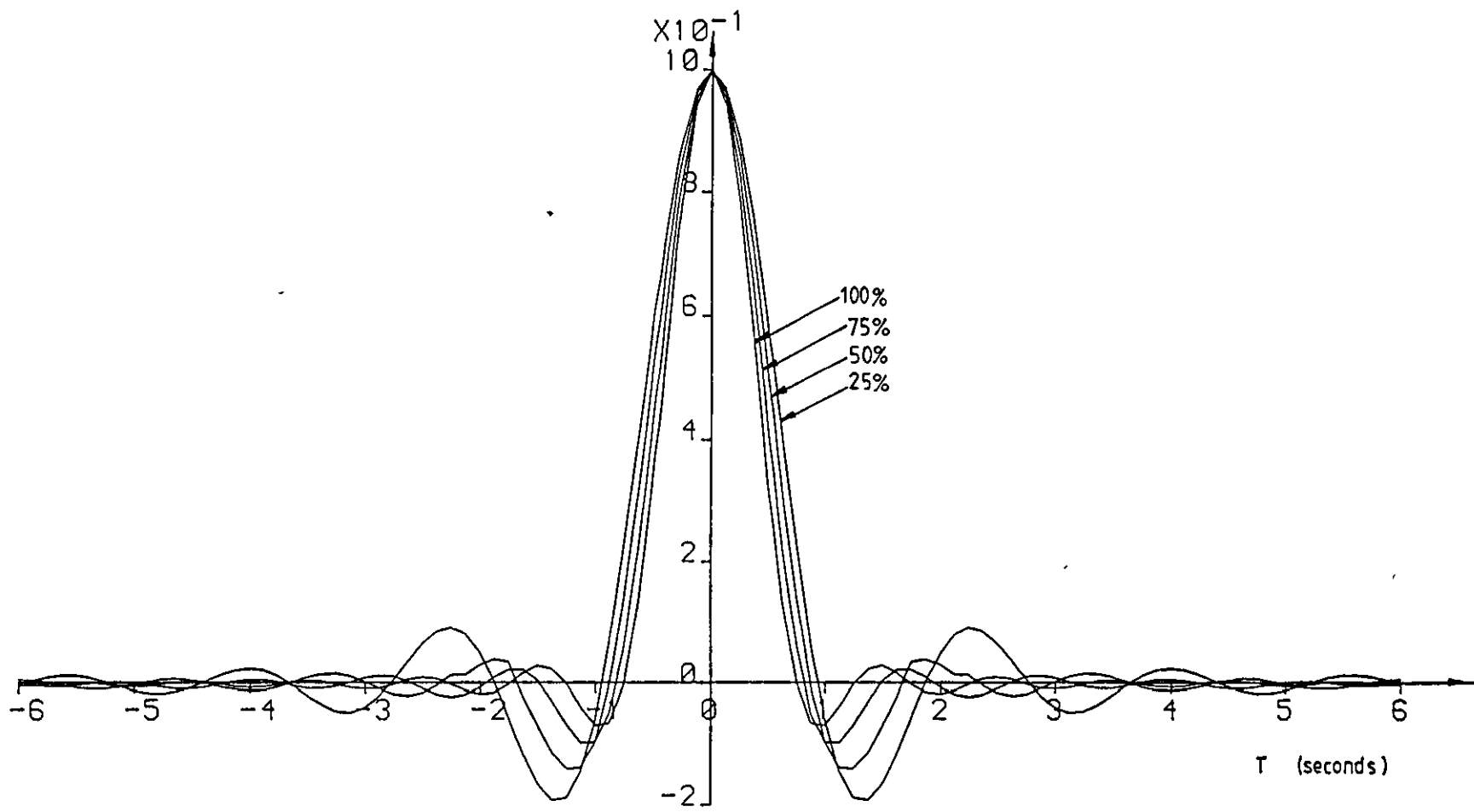


Figure 2.8
50% and 25%.

Impulse responses of the modulation and demodulation filters with $\beta=100\%$, 75%,

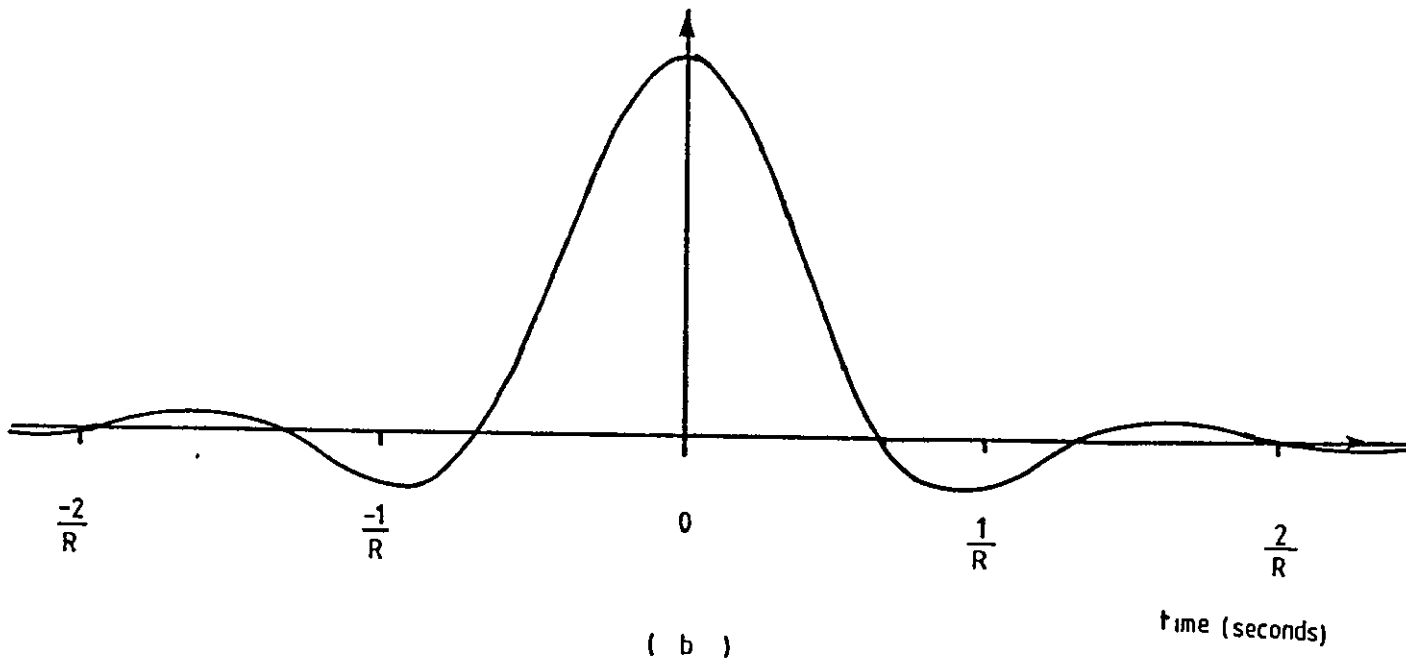
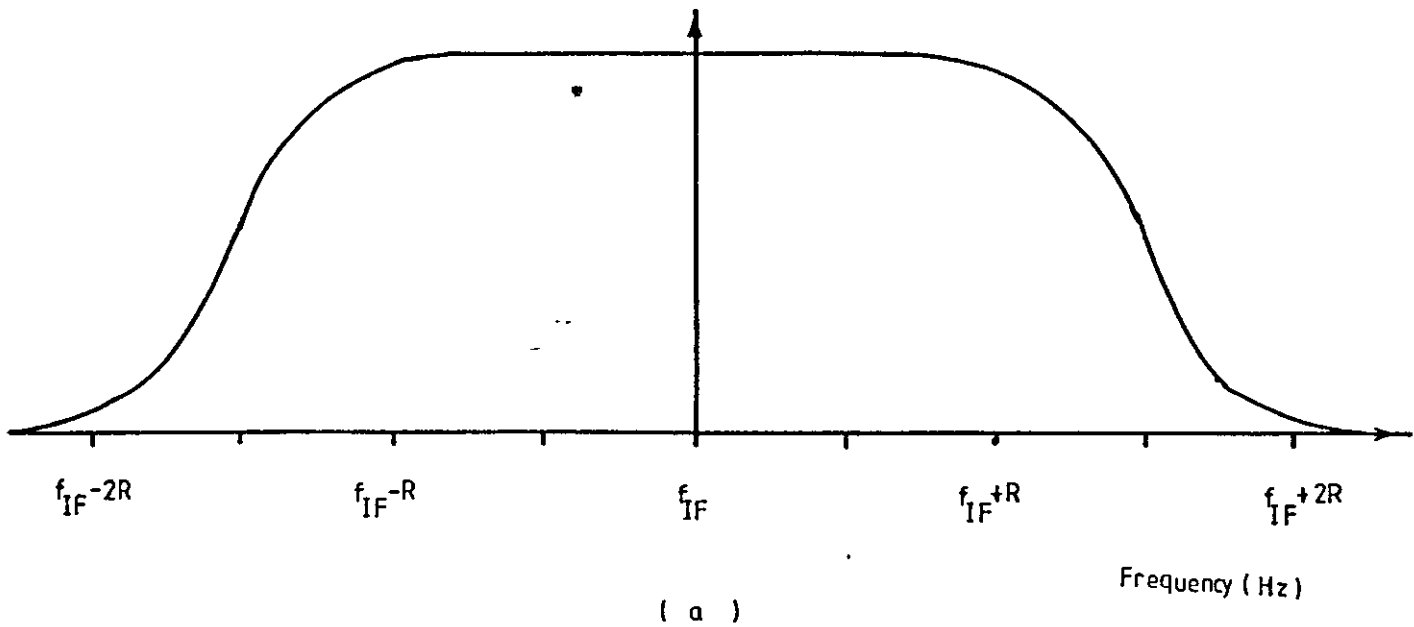


Figure 2.9 Characteristics of the assumed IF filter. a) The actual frequency responses. b) The impulse response of the baseband equivalent model.

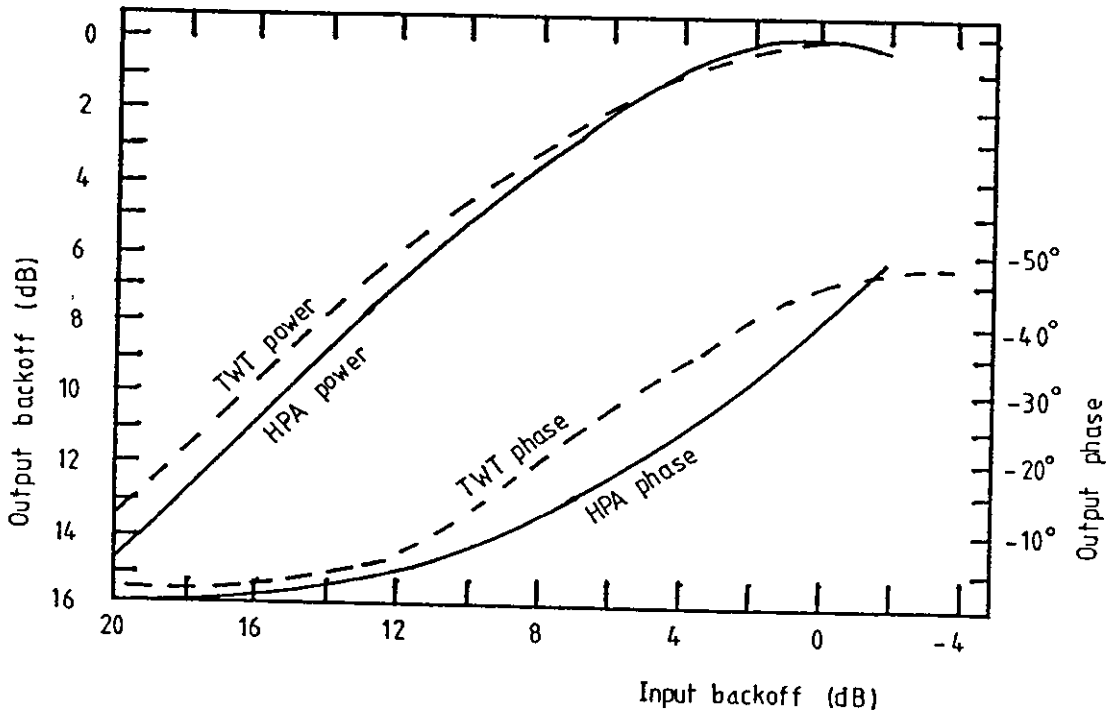


Figure 2.10 Typical input/output power and phase characteristics of an HPA and TWTA - used in the INTELSAT-V TDMA 6/4-G Hz system.

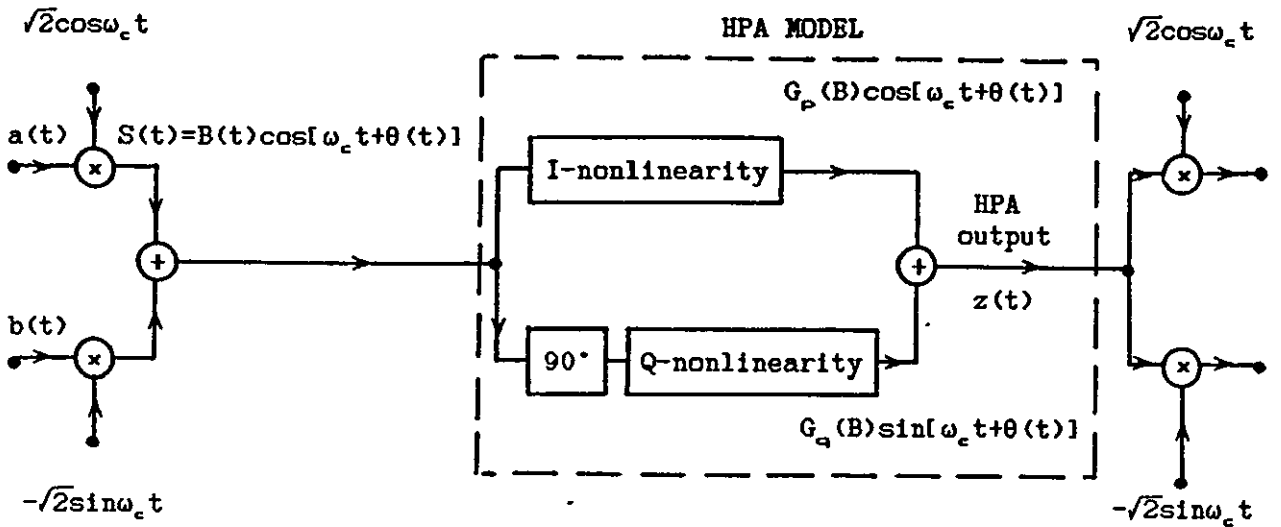


Figure 2.11a Quadrature model of HPA in a quadrature modulation system.

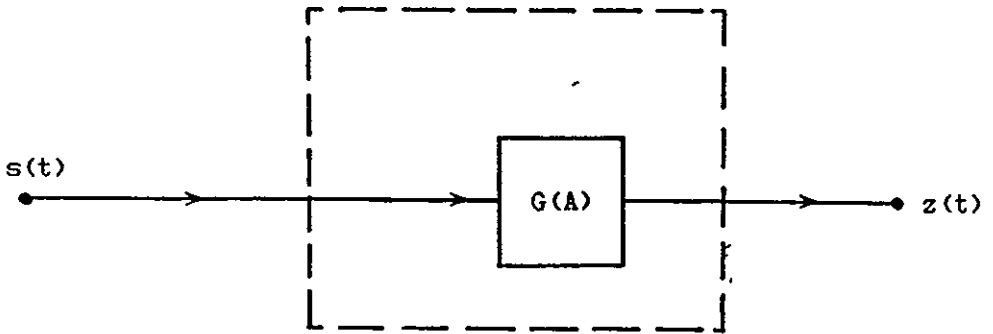


Figure 2.11b Baseband equivalent model of HPA.

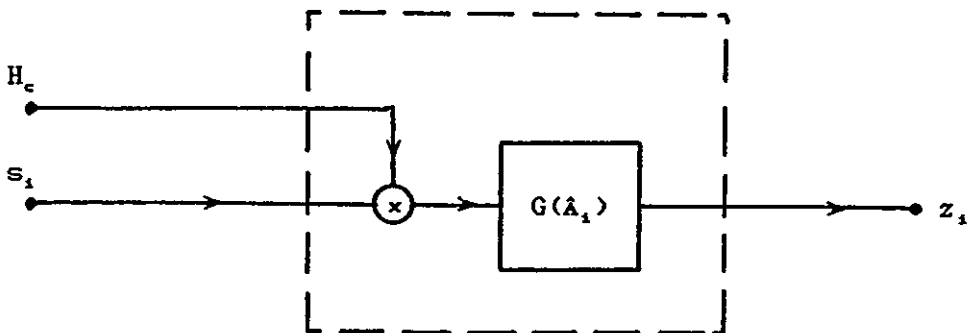


Figure 2.11c Baseband equivalent model of HPA for discrete signals.

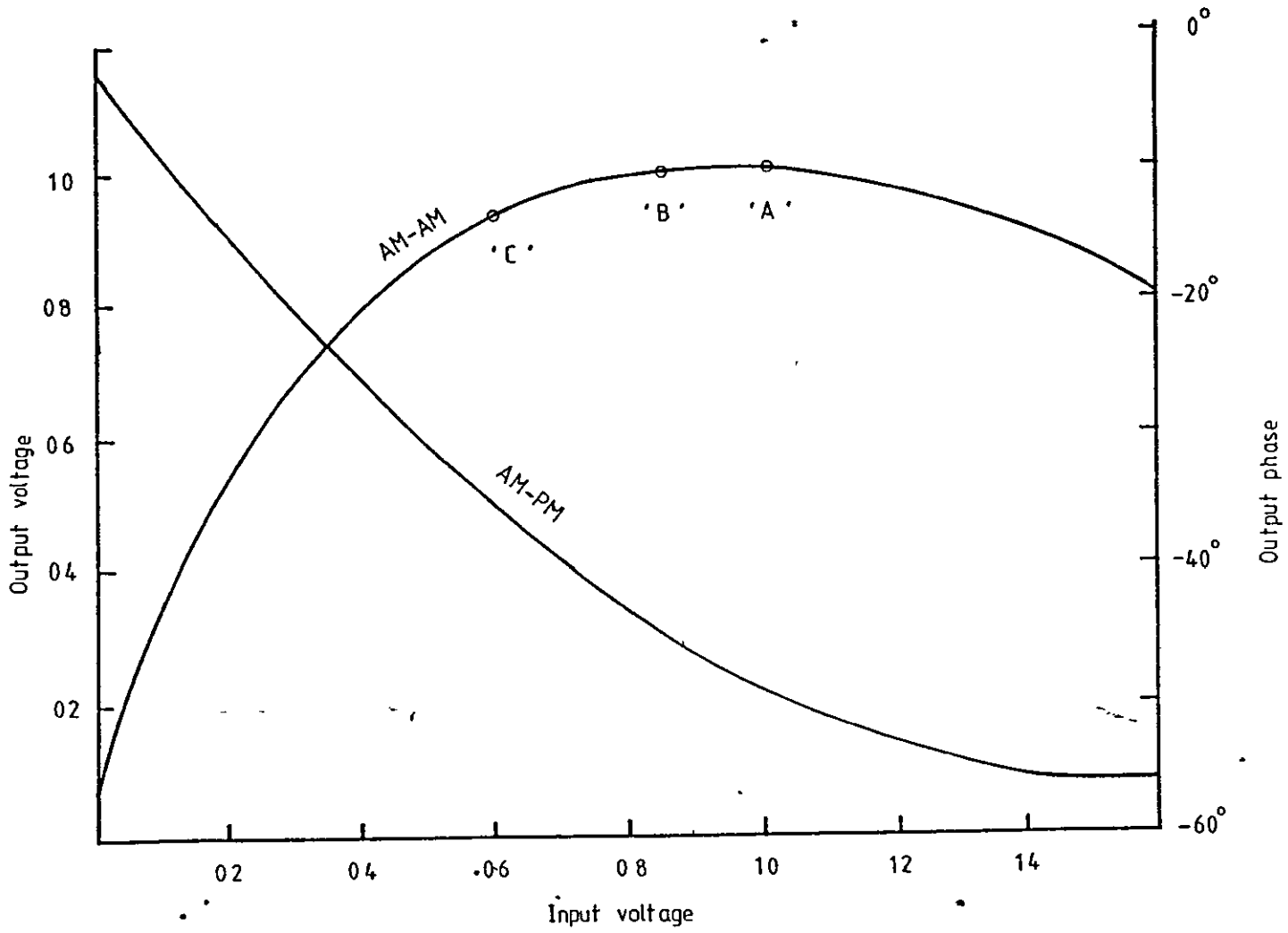


Figure 2.12 Assumed HPA characteristics.

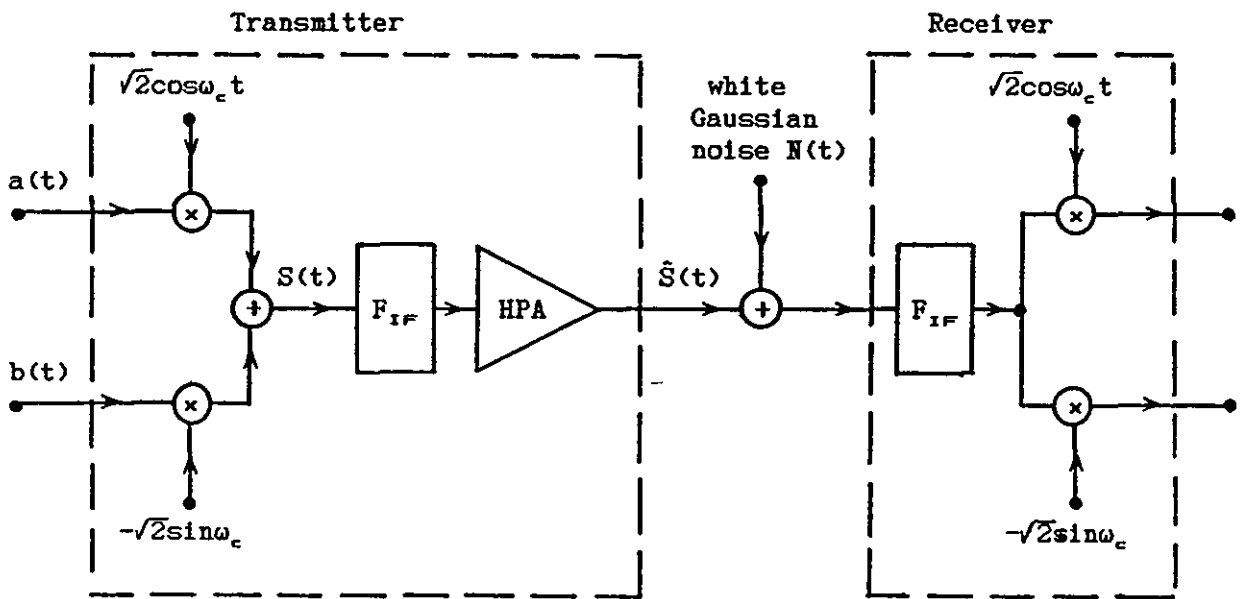


Figure 2.13a Model of a quadrature modulation system over a nonlinear satellite channel. F_{IF} , IF filter.

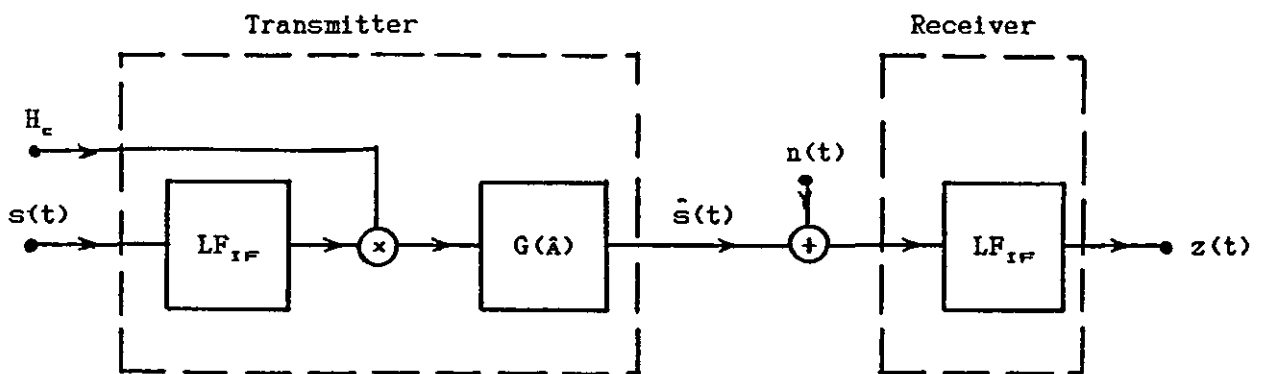


Figure 2.13b The equivalent baseband model of the system shown in Fig. 2.13a. LF_{IF} is the baseband equivalent model of the IF filter F_{IF} .

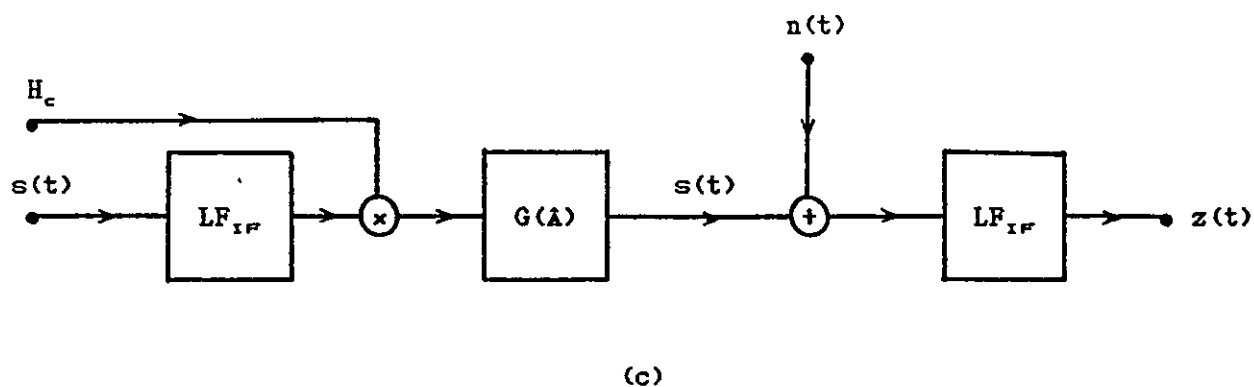
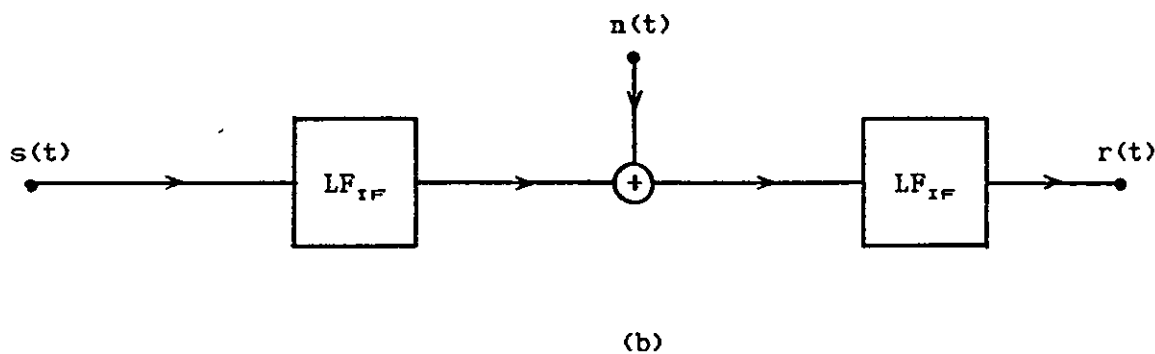
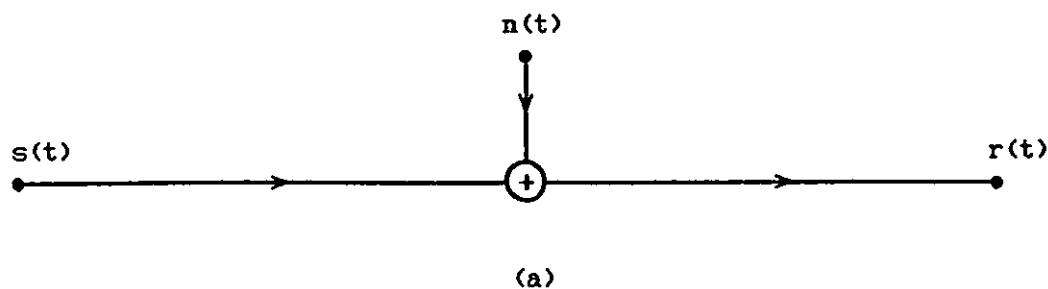


Figure 2.14 Baseband equivalent models of the bandpass channels. a) A linear and memoryless channel. b) A linear and bandlimited channel. c) A nonlinear and bandlimited channel.

The power of individual modulated signal is different. The variation is due to the different power from the earth stations and the different free space losses from different geographic locations.

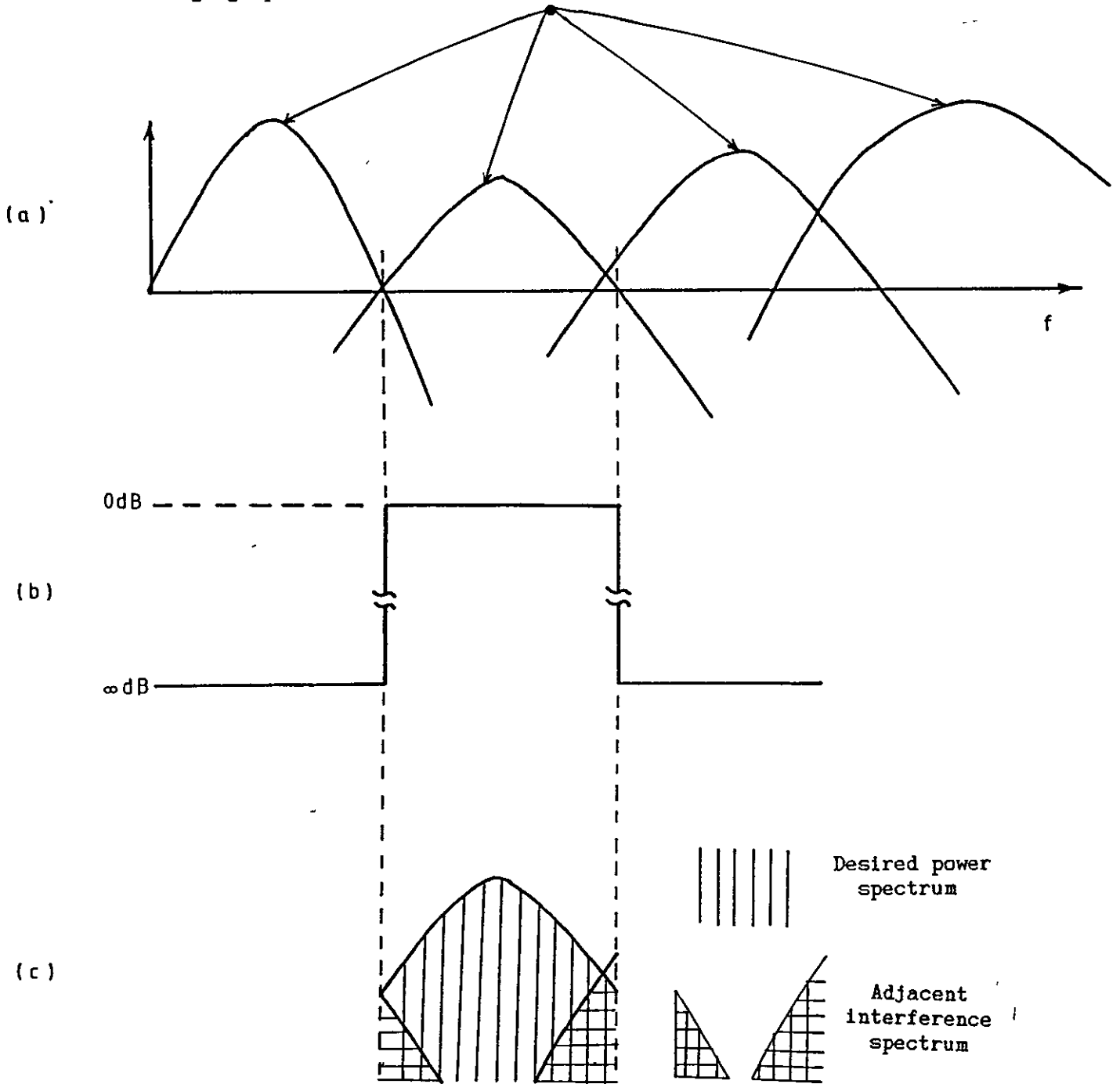


Figure 2.15 ACI. The cause of the ACI is insufficient transmitter channel filtering. a) Power spectral density displayed at the input of a received earth station. b) Ideal brick-wall bandpass filter for the desired signal. c) Power spectral density of the desired and interfering signals.

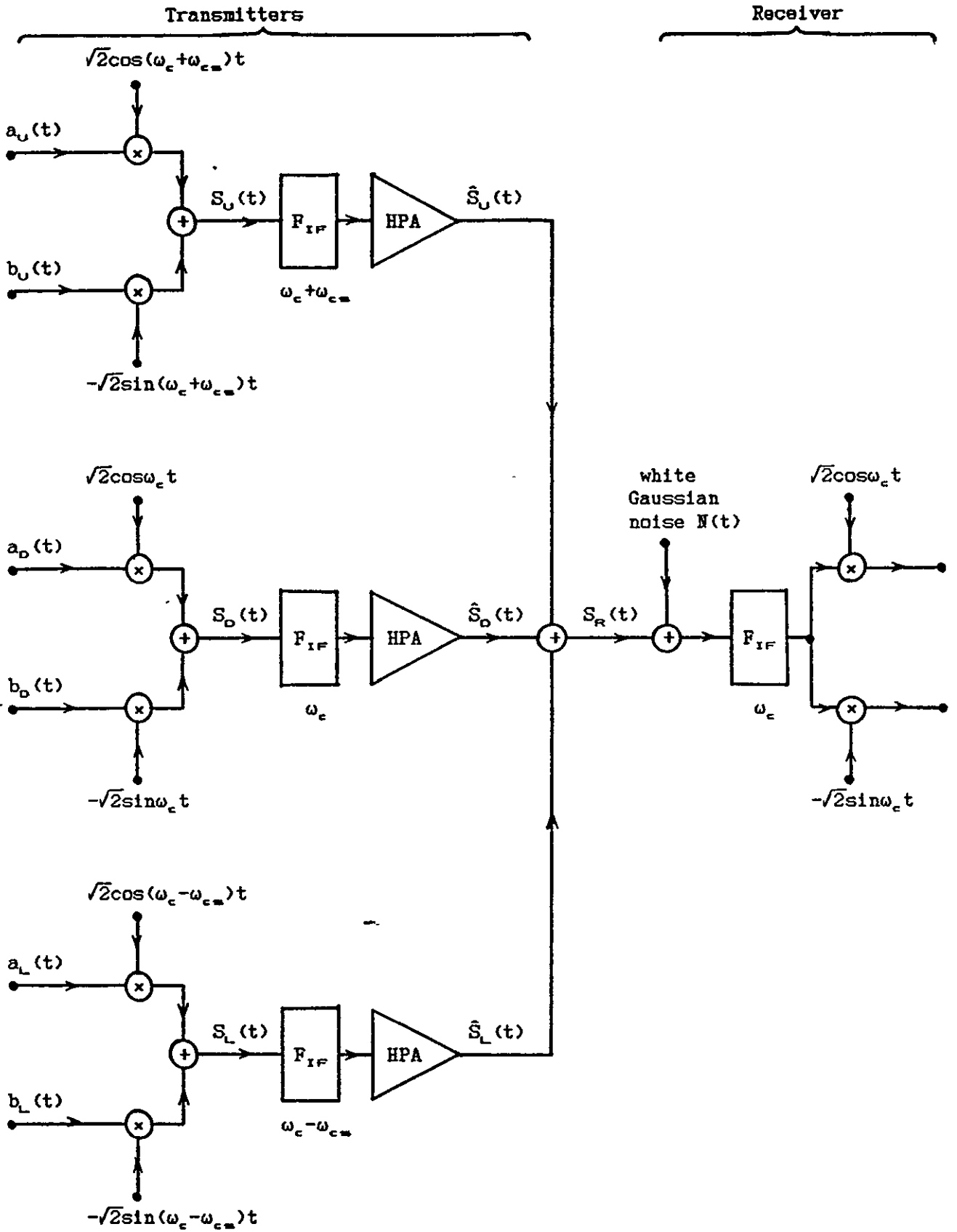


Figure 2.16 Model of a quadrature modulation system with a nonlinear satellite channel in an ACI environment. F_{IF} is the IF filter.

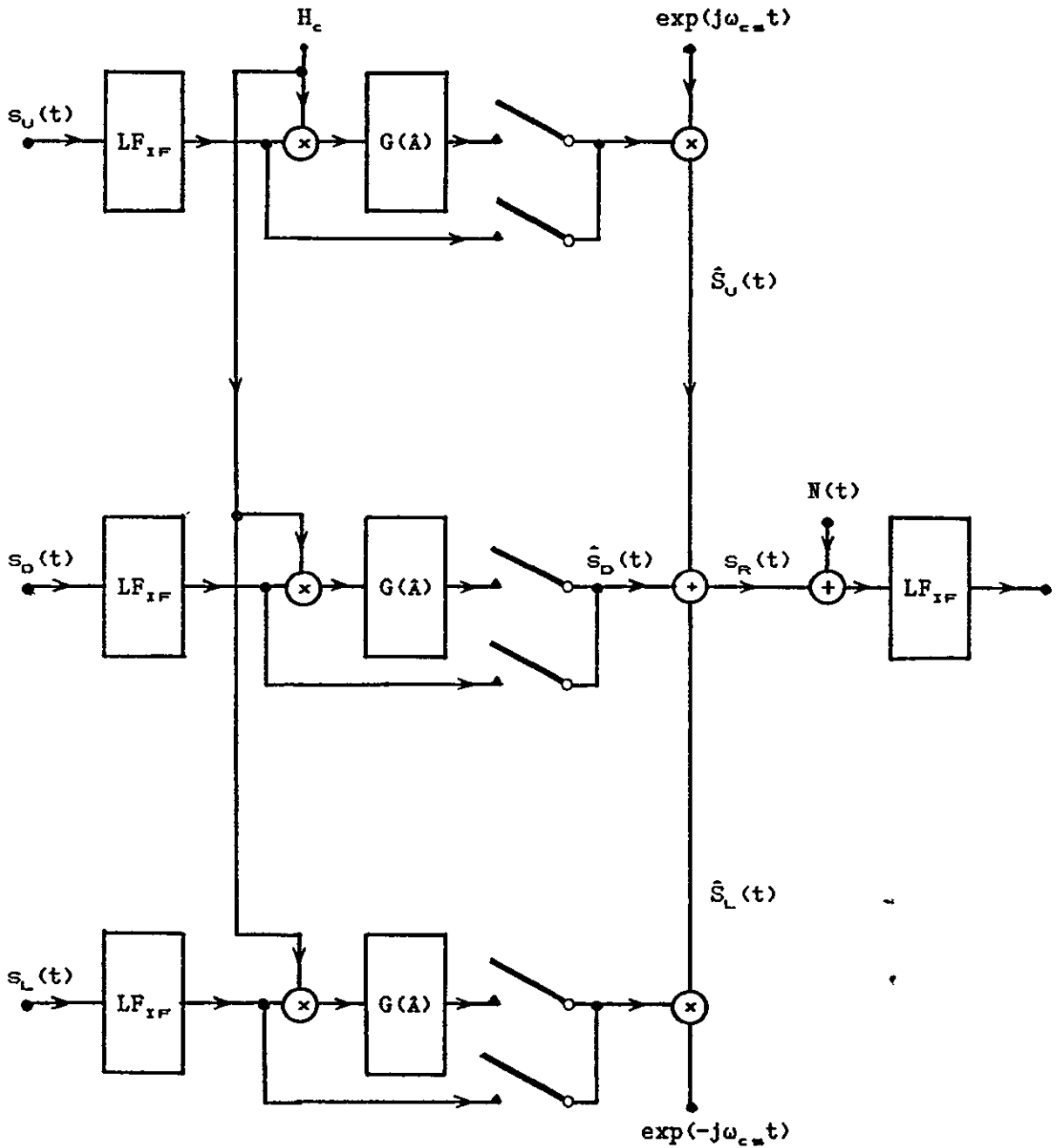


Figure 2.17 Baseband equivalent model of the system shown in Fig. 2.16. LF_{IF} is the baseband equivalent model of the IF filter F_{IF} . The switches determine whether the HPAs are operating in the linear or nonlinear mode.

CHAPTER 3

COHERENT QUATERNARY PHASE-SHIFT KEYING (QPSK) AND DIFFERENTIALLY ENCODED COHERENT QUATERNARY PHASE-SHIFT KEYING (DEQPSK) SYSTEMS OVER A LINEAR OR NONLINEAR SATELLITE CHANNEL

3.1 Description of coherent QPSK and DEQPSK systems

3.1.1 QPSK systems

In QPSK systems the modulated signal has four distinct states. These states are generated by a unique mapping scheme of consecutive pairs of bits into symbols. The symbol interval has a two-bit duration. The four possible pairs of bits are frequently mapped in accordance with the Gray code. An important property of this code is that adjacent symbols differ by only one bit (Fig. 3.2). In transmission systems corrupted by noise and interference, the most frequent errors are introduced by making decision error between adjacent states. In this case, the Gray code assures that a single symbol error corresponds to a single bit error.

A rectangular baseband modulating waveform is usually used to describe QPSK systems. However, it is not a practical waveform, so that a rounded baseband modulating waveform is used here to describe the QPSK systems instead.

A block diagram of a conventional QPSK system is shown in Fig. 3.1. The information to be transmitted is carried by the sequence of binary data-symbols $\{\alpha_L\}$. Each data symbol therefore carries one bit of information. The S/P (serial-to-parallel) converter converts the sequence $\{\alpha_L\}$ into two sequences of binary symbols $\{u_i^{(1)}\}$ and $\{u_i^{(2)}\}$, where $u_i^{(j)} = 0$ or 1 for $j=1, 2$. The relationship between the input data sequence $\{\alpha_L\}$ and the two binary sequences $\{u_i^{(1)}\}$ and $\{u_i^{(2)}\}$ is shown in Fig. 3.2. The Gray coder, in Fig. 3.1 codes these two sequences of symbols according to Table 3.1, and gives two output sequences $\{q_i^{(1)}\}$ and $\{q_i^{(2)}\}$, where $q_i^{(j)} = \pm 1$ for

$j=1, 2$. These two sequences are converted into the corresponding sequences of impulses $\{\sum_i q_i^{(1)} \delta(t-iT)\}$ and $\{\sum_i q_i^{(2)} \delta(t-iT)\}$, which are fed into the modulation filter and hence to produce two baseband modulating waveforms

$$a(t) = \sum_i q_i^{(1)} h_c(t-iT) \quad 3.1.1a$$

and

$$b(t) = \sum_i q_i^{(2)} h_c(t-iT) \quad 3.1.1b$$

where $h_c(t)$ is the impulse response of the modulation filter with the transfer function of $H_c(f)$. $a(t)$ and $b(t)$ are called the inphase and quadrature baseband signals, respectively. These two baseband signals are quadrature modulated, as described in Section 2.6, and then added linearly to give the QPSK signal

$$S(t) = \sqrt{2}a(t)\cos\omega_c t - \sqrt{2}b(t)\sin\omega_c t \quad 3.1.2$$

with ω_c the carrier frequency in rad/s. The resultant signal is fed into the bandpass transmission channel. Assume that the bandpass transmission channel introduces no attenuation, delay or distortion, but adds a Gaussian noise waveform, $N(t)$, to the transmitted signal. So at the receiver, the signal input to the demodulation filter is

$$r(t) = \sqrt{2}[a(t)\cos\omega_c t - b(t)\sin\omega_c t] + N(t) \quad 3.1.3$$

where $N(t)$ is a sample function of a Gaussian random process with zero mean and a two-sided power spectral density of $\frac{1}{2}N_0$ over the signal frequency band. Assume that the bandwidth of $N(t)$ is small compared with ω_c , so it can be expanded [1] into

$$N(t) = N_c(t)\cos\omega_c t - N_s(t)\sin\omega_c t \quad 3.1.4$$

where $N_c(t)$ and $N_s(t)$ are sample functions of Gaussian random processes

with zero mean and a two-sided power spectral density twice that of $N(t)$ (Appendix A7). Hence Eqn. 3.1.3 can be written as

$$r(t) = [\sqrt{2}a(t) + N_c(t)]\cos\omega_c t - [\sqrt{2}b(t) + N_s(t)]\sin\omega_c t \quad 3.1.5$$

Since the inphase and quadrature signal components are orthogonal [9],[10], the receiver is able to demodulate them independently to each other. The inphase and quadrature data signal components plus noise just prior to the demodulation filter are

$$\begin{aligned} r(t)\sqrt{2}\cos\omega_c t &= \{[\sqrt{2}a(t) + N_c(t)]\cos\omega_c t - [\sqrt{2}b(t) + N_s(t)]\sin\omega_c t\}\sqrt{2}\cos\omega_c t \\ &= [\sqrt{2}a(t) + N_c(t)]\sqrt{\frac{1}{2}}(1 + \cos 2\omega_c t) - [\sqrt{2}b(t) + N_s(t)]\sqrt{\frac{1}{2}}\sin 2\omega_c t \\ &= a(t) + \sqrt{\frac{1}{2}}N_c(t) + [a(t) + \sqrt{\frac{1}{2}}N_c(t)]\cos 2\omega_c t - [b(t) + \sqrt{\frac{1}{2}}N_s(t)]\sin 2\omega_c t \\ &= a(t) + \sqrt{\frac{1}{2}}N_c(t) + \text{h.f.c.} \end{aligned} \quad 3.1.6a$$

and

$$\begin{aligned} -r(t)\sqrt{2}\sin\omega_c t &= -\{[\sqrt{2}a(t) + N_c(t)]\cos\omega_c t - [\sqrt{2}b(t) + N_s(t)]\sin\omega_c t\}\sqrt{2}\sin\omega_c t \\ &= -[a(t) + \sqrt{\frac{1}{2}}N_c(t)]\sin 2\omega_c t + [\sqrt{2}b(t) + N_s(t)]\sqrt{\frac{1}{2}}(1 - \cos 2\omega_c t) \\ &= -[a(t) + \sqrt{\frac{1}{2}}N_c(t)]\sin 2\omega_c t + b(t) + \sqrt{\frac{1}{2}}N_s(t) - [b(t) + \sqrt{\frac{1}{2}}N_s(t)]\cos 2\omega_c t \\ &= b(t) + \sqrt{\frac{1}{2}}N_s(t) + \text{h.f.c.} \end{aligned} \quad 3.1.6b$$

respectively, where h.f.c. means the high frequency components. The demodulation filter blocks the h.f.c. in the signals and produces the wanted noisy inphase and quadrature baseband signal components, $a(t) + \sqrt{\frac{1}{2}}N_c(t)$ and $b(t) + \sqrt{\frac{1}{2}}N_s(t)$, respectively. When comparing with the inphase and quadrature baseband components of the signals in Eqn. 3.1.5, it can be seen that the demodulation process has reduced both the signal and noise powers by the same factor of $\sqrt{\frac{1}{2}}$ and so retained the signal/noise power ratio.

At the demodulation filter output, the inphase and quadrature baseband signal components are

$$r^{(1)}(t) = \sum_i q_i^{(1)} h(t-iT) + v^{(1)}(t) \quad 3.1.7a$$

and

$$r^{(2)}(t) = \sum_i q_i^{(2)} h(t-iT) + v^{(2)}(t) \quad 3.1.7b$$

respectively, where $h(t)$ is the inverse Fourier transform of $H(f)$ which is the transfer function of the modulation and demodulation filters in cascade. $v^{(1)}(t)$ and $v^{(2)}(t)$ are filtered Gaussian noise waveforms. Bearing in mind that the bandpass transmission channel introduces no attenuation, delay or distortion.

Assume that the modulation and demodulation filters have the same characteristics, i.e., $H_c(f) = H_r(f)$ in Fig. 3.1, and the combined transfer function, $H(f) = H_c(f)H_r(f)$, is a sinusoidal rolloff frequency response (Eqn. 2.2.3) with a linear phase characteristic, such that $h(0) = 1$ and $h(iT) = 0$, for all values of the integer i other than $i=0$. The signals $r^{(1)}(t)$ and $r^{(2)}(t)$ have no ISI at the time instants (iT) . Assume also that the receiver provides the ideal required timing signal, so that the two baseband waveforms, $r^{(1)}(t)$ and $r^{(2)}(t)$, at the demodulation filter output, are sampled at the time instants (iT) , to give two sequences of sample values $\{r_i^{(1)}\}$ and $\{r_i^{(2)}\}$ which are fed into the detector. Since there is no ISI at the sampling instants (iT) , which implies that $r_i^{(1)}$ and $r_i^{(2)}$ depend only on $q_i^{(1)}$ and $q_i^{(2)}$, respectively, but not any $\{q_j^{(1)}\}$ and $\{q_j^{(2)}\}$ for $j \neq i$. The resultant operation of the channel is to add to the input symbols $q_i^{(1)}$ and $q_i^{(2)}$ the noise components $v_i^{(1)}$ and $v_i^{(2)}$, respectively, to give at its output the samples, at time $t=iT$,

$$r_i^{(1)} = q_i^{(1)} + v_i^{(1)} \quad 3.1.8a$$

and

$$r_i^{(2)} = q_i^{(2)} + v_i^{(2)} \quad 3.1.8b$$

where $v_i^{(1)}$ and $v_i^{(2)}$ are sample values of Gaussian random variables with

zero mean and fixed variance σ^2 , the $\{v_i^{(1)}\}$ and $\{v_i^{(2)}\}$ being statistically independent and independent also of the $\{\alpha_L\}$.

It is shown, in Section 2.2, that under these assumed conditions, the optimum detection process for the $\{r_i^{(1)}\}$ and $\{r_i^{(2)}\}$ is by comparing each of them with a decision threshold of zero, therefore two separate threshold detectors are used to detect these two sequences of sample values $\{r_i^{(1)}\}$ and $\{r_i^{(2)}\}$, according to Table 3.3. The detected symbols are Gray decoded to produce the sequences $\{\hat{u}_i^{(1)}\}$ and $\{\hat{u}_i^{(2)}\}$. The sequence of decoded binary data symbols $\{\hat{\alpha}_L\}$ is obtained by using a P/S (parallel-to-serial) converter. In the absence of noise, the $\{\hat{\alpha}_L\}$ are the same as the $\{\alpha_L\}$.

In the absence of noise, Eqn. 3.1.8 becomes

$$r_i^{(1)} = q_i^{(1)} = \pm 1 \quad 3.1.9a$$

and

$$r_i^{(2)} = q_i^{(2)} = \pm 1 \quad 3.1.9b$$

The four possible received signal vectors are shown in Fig. 3.3. The signal points are said to represent a signal constellation. It can be seen that QPSK signals have 4 distinct phases, $\pm\pi/4$ and $\pm 3\pi/4$ radians.

3.1.2 DEQPSK systems

In the coherent QPSK system just described, each pair of binary symbols, $(u_i^{(1)} u_i^{(2)})$, is Gray coded linearly to one of the four possible symbols and then transmitted. At the receiver, one of the 4 possible phases, $\pm\pi/4$ and $\pm 3\pi/4$ radians, is received (Fig. 3.3) at the input of the detector. They are detected and Gray decoded linearly to obtain the corresponding pair of binary symbols (Table 3.3). However at the receiver, most carrier recovery circuits will introduce a fourfold ambiguity. This means that the carrier may shift the received signal vector (Fig. 3.3) by a phase of 0, $\pi/2$, π , or $3\pi/2$. To resolve this ambiguity, differential encoding is commonly used.

Differential encoding encodes the pair of binary symbols, $(u_i^{(1)}, u_i^{(2)})$, so that the phase change rather than the absolute phase carries the data, thus eliminating the need for a reference phase at the receiver. A block diagram of a conventional DEQPSK system is shown in Fig. 3.4. Each pair of binary symbols $(u_i^{(1)}, u_i^{(2)})$, at time $t=iT$ seconds, represents a 2-bit binary value. In generation of a differential encoded pair of binary symbols, $(d_i^{(1)}, d_i^{(2)})$, i.e., $d_i^{(j)}=0$ or 1 for $j=1,2$, the 2-bit binary value of the present pair of symbols, $(u_i^{(1)}, u_i^{(2)})$, is added to the 2-bit binary value of the previous differential encoded pair of symbols, $(d_{i-1}^{(1)}, d_{i-1}^{(2)})$, to form the present differential encoded pair of binary symbols, $(d_i^{(1)}, d_i^{(2)})$. This process produces two sequences $\{d_i^{(1)}\}$ and $\{d_i^{(2)}\}$ which are Gray coded (Table 3.1) to give two output sequences $\{q_i^{(1)}\}$ and $\{q_i^{(2)}\}$, where $q_i^{(j)}=\pm 1$ for $j=1,2$. Since each pair of the transmitted symbols represents a possible phase value received at the detector (Eqn. 3.1.9), this process actually produces the transmitted symbols which are the phase changes, rather than the absolute phases, of the data symbols to be received at the detector. The sampling, filtering and modulation processes following this are exactly the same as they are described in the QPSK system.

Assume that the transmission channel is same as the one used in the QPSK system described before. Assume also that the receiver provides the ideal required timing signal, so that the baseband signal components at the demodulator output are sampled, at the time instants (iT) , to give two sequences $\{r_i^{(1)}\}$ and $\{r_i^{(2)}\}$ which are threshold detected and Gray decoded to produce two binary sequences $\{\hat{d}_i^{(1)}, \hat{d}_i^{(2)}\}$. At the time instants (iT) , each pair of symbols $(\hat{d}_i^{(1)}, \hat{d}_i^{(2)})$ represents a 2-bit binary value. The differential decoded pair of binary symbols, $(\hat{u}_i^{(1)}, \hat{u}_i^{(2)})$ is obtained by subtracting from the binary values of the present pair of symbols $(\hat{d}_i^{(1)}, \hat{d}_i^{(2)})$ the binary values of the previous pair, $(\hat{d}_{i-1}^{(1)}, \hat{d}_{i-1}^{(2)})$, and the difference is expressed modulo-4. (An arbitrary initial pair of binary symbols may be assumed). The sequence of the binary-data symbols $\{\hat{\alpha}_i\}$ is obtained using a P/S (parallel-to-serial) converter.

3.2 Error probability performances of coherent QPSK and DQPSK signals

3.2.1 QPSK signal

In Section 2.2, it is shown that, the optimum filtering arrangement of a baseband data-transmission system is the filtering which is shared equally between the transmitter and the receiver filters and with a sinusoidal rolloff frequency response. Under these conditions and if binary antipodal signals are used, the bit error probability is given by $Q(\sqrt{2E_b/N_0})$ (Eqn. 2.2.15), where $2E_b/N_0$ is the ratio of the average transmitted energy per bit to the two-sided noise power spectral density at the input to the receiver.

The QPSK system, described in Section 3.1.1, has the filtering shared equally between the transmitter and receiver filters and with a sinusoidal rolloff frequency response, and so is the optimum filtering arrangement for baseband data transmission. However since the demodulation process does not alter the signal/noise power ratio (Section 3.1.1), the filtering arrangement is also optimum for a bandpass data transmission system; the inphase and quadrature channels, each carrying binary antipodal signals, are orthogonal and they can be demodulated independently of each other, so each of the two channels can be treated independently; hence, the bit error probability of each of the inphase and quadrature channels should also be equal to $Q(\sqrt{2E_b/N_0})$.

Denoting the bit error probability in the inphase channel as P_{e1} and in the quadrature channel as P_{eq} , the symbol error probability is therefore

$$\begin{aligned} P_{es} &= 1 - (1 - P_{e1})(1 - P_{eq}) \\ &= P_{e1} + P_{eq} - P_{e1}P_{eq} \end{aligned} \quad 3.2.1$$

Since $P_{e1} = P_{eq}$, and they are typical small quantities ($<10^{-2}$) in practice, a good approximation for the overall symbol error probability is

$$P_{es} \approx P_{e1} + P_{eq} = 2P_{e1} = 2P_{eq} \quad 3.2.2$$

The bit error probability of an individual channel is

$$P_{b1} = P_{eb1} = Q(\sqrt{2E_b/N_0}) \quad 3.2.3$$

so the symbol error probability is

$$P_{es} = 2P_{eb1} = 2Q(\sqrt{2E_b/N_0}) \quad 3.2.4$$

The Gray-coded and non-Gray-coded cases are shown in Table 3.2. In the Gray-coded constellation case, adjacent symbols differs by only one bit, whereas in the non-Gray-coded case, the adjacent symbols differ by one or by two bits. With AGWN, by far the most likely error in the detection of a symbol is that which involves the crossing of the nearest decision threshold. Thus the bit error rate of an ideal Gray-coded QPSK system approximately equals to one-half of its symbol error rate, i.e.,

$$P_e = \frac{1}{2}P_{es} = Q(\sqrt{2E_b/N_0}) \quad 3.2.5$$

A more vigorous analysis of the P_e and P_{es} relationship is presented in [2].

3.2.2 DEQPSK signal

In a differentially encoded coherent QPSK system (DEQPSK), the differential decoding process at the receiver is carried out after the detection process. During differential decoding, error multiplication by a factor of 2 occurs. Thus the bit error rate of the Gray-coded DEQPSK signal is (Eqn. 3.2.5)

$$P_{e(\text{DEQPSK})} = 2P_{e(\text{QPSK})} = 2Q(\sqrt{2E_b/N_0}) \quad 3.2.6$$

Equations 3.2.5 and 3.2.6 are the theoretical error-rate performances of the QPSK and DEQPSK systems transmitting signals over an optimum data-transmission channel where only AWGN is added. In any practical satellite links, there are many other factors, such as HPA distortion, ACI, etc.,

which affect the performances of the systems. Since these factors are too difficult to use mathematical expressions to analyse, their effects on error-rate performances require complex computer simulations. Because computer simulations are more easily carried out on the baseband models with the use of a digital computer, the baseband equivalent models of the different systems are modelled digitally as described in the following sections.

3.3 Baseband equivalent model of DEQPSK system, with a linear or a nonlinear satellite channel, for computer simulation

The DEQPSK system considered here operates at a speed of 64, 128, 256 or 512 kbit/s over a satellite link. Since DEQPSK signals use a quadrature modulation technique (Section 2.6), the system can be greatly simplified by assigning real values to the signal in one of the two parallel channels (that associated with $\sqrt{2}\cos\omega_c t$) and imaginary values to the signals in the other channel (that associated with $-\sqrt{2}\sin\omega_c t$), and then considering the linear modulator, the transmitter IF filter, the HPA, the receiver IF filter and the linear demodulator, as a baseband transmission path carrying complex-valued signals (Section 2.6). The resultant baseband equivalent model of the DEQPSK system, with a linear and memoryless, a linear and bandlimited, or a nonlinear and bandlimited satellite channel, for computer simulation, is shown in Fig. 3.5. The information to be transmitted is carried by the sequence of binary data-symbols $\{\alpha_i\}$, where the $\{\alpha_i\}$ are taken to be statistically independent and equally likely to be either 0 or 1. The encoded symbols $\{q_i\}$ are obtained from the $\{\alpha_i\}$, by the encoder, after being differentially encoded and Gray-code (Section 3.1.2). The i^{th} symbol has the value $q_i = \pm 1 \pm j$, where $j = \sqrt{-1}$, the $\{q_i\}$, of course, being statistically independent and equally likely to have any of the four possible values. Each q_i is a quaternary signal element. The sequence $\{q_i\}$ is used to form the sequence of impulses $\{q_i \delta(t - iT)\}$, at the input of the modulation filter. The signal waveform

• at the output of the filter is the complex-valued baseband signal

$$u(t) = \sum_i q_i h_e(t-iT) \quad 3.3.1$$

where $h_e(t)$ is the impulse response of the modulation filter, and at any given value of t , is real (Section 2.4.1).

Since a digital computer is used to do the simulation tests, the transmission system is modelled digitally for simulation. The continuous waveforms in the system are modelled as discrete waveforms. So the complex-valued waveform $u(t)$ is sampled, at the time instants $\{mT_m\}$ (8 times per symbol), where $T=8T_m$, to give the sequence $\{u_m\}$, where $u_m=u(mT_m)$ has a complex value. The $\{u_m\}$ are then fed to a baseband equivalent model of one of the bandpass channels. Three different bandpass channels, as shown in Fig. 2.14, are considered here. They are (a) linear and memoryless, (b) linear and bandlimited and, (c) nonlinear and bandlimited channels (Section 2.6).

(a) Linear and memoryless channel

This channel does not distort the signal, but only adds the Gaussian noise samples to the signal samples. So at time $t=mT_m$, the signal sample at the channel output is

$$w_m = u_m + n_m \quad 3.3.2$$

where w_m , u_m and n_m all have complex values. The real and imaginary parts of all noise samples are taken to be statistically independent Gaussian random variables with zero mean and fixed variance σ^2 (which will be discussed later).

(b) Linear and bandlimited channel

Over this channel, the signal is filtered by the baseband equivalent model of the transmitter IF filter. The sampled impulse responses of the baseband equivalent models of the transmitter and receiver IF filters,

sampled at $1/T_s$ samples per second, are given by the $(g+1)$ -component vector

$$F = [f_0 \ f_1 \ f_2 \ \dots \ f_g] \quad 3.3.3$$

where the $\{f_m\}$, for $0 \leq m \leq g$, have real valued components, as shown in Table 2.2, and $f_m = f(mT_s)$. The signal at the output of the filter is sampled at the time instants $\{mT_s\}$. So at time $t = mT_s$, the signal sample is

$$e_m = \sum_{n=0}^g u_{m-n} f_n \quad 3.3.4$$

where e_m has a complex value. After adding the noise component, the sample becomes

$$y_m = e_m + n_m \quad 3.3.5$$

where y_m also has a complex value. The sequence of $\{y_m\}$ is fed into the receiver IF filter which is modelled as a digital filter, with a sampling rate $1/T_s$ samples per second, and which produces at the output, at time $t = mT_s$, the sample

$$w_m = \sum_{n=0}^g y_{m-n} f_n \quad 3.3.6$$

where w_m has a complex value.

(c) Nonlinear and bandlimited channel

Over this channel, the $\{u_m\}$ are first filtered by the transmitter IF filter, as described in (b), to produce at its output, at time $t = mT_s$, the signal sample (Eqn. 3.3.4)

$$e_m = \sum_{n=0}^g u_{m-n} f_n \quad 3.3.7$$

where e_m has a complex value, which is then nonlinearly distorted by the

HPA. After adding the noise sample, the sample at the input of the receiver IF filter becomes (Eqn. 2.5.30)

$$z_m = e_m H_c G(\hat{\lambda}_m) + n_m \quad 3.3.8$$

where z_m , e_m and n_m all have complex values, $G(\hat{\lambda}_m)$ is the conversion function of the baseband equivalent model of the HPA, H_c is the HPA backoff factor, and $\hat{\lambda}_m$ is the one of the values $\{\lambda_n\}$ (Table 2.3) closest to the input signal envelope $|e_m H_c|$ (Section 2.5). The $\{z_m\}$ are fed into the receiver IF filter, at time $t = mT_s$, which produces the signal sample

$$w_m = \sum_{h=0}^m z_{m-h} f_h \quad 3.3.9$$

In all these three cases, the sampled signal $\{w_m\}$ (given by Eqn. 3.3.2, 3.3.6 and 3.3.9) from the baseband equivalent models of the bandpass channels are filtered by the demodulation filter. The sampled impulse response of the demodulator filter, sampled at the rate of $1/T_s$ samples per second, is given by the $(n+1)$ -component vector

$$P = [p_0 \ p_1 \ p_2 \ \dots \ p_n] \quad 3.3.10$$

where the $\{p_m\}$, for $0 \leq m \leq n$, have real-valued components (Table 2.1), and $p_m = p(mT_s)$. Thus, at time $t = mT_s$, the signal sample at the output of the demodulation filter is

$$r_m = \sum_{h=0}^m w_{m-h} p_h \quad 3.3.11$$

where r_m has a complex value. Assume that receiver provides the required ideal timing signal. So that the sequence $\{r_m\}$ is sampled once per symbol, at the time instants $\{iT\}$, to give the sequence $\{r_i\}$ which are detected and then decoded into the sequence of binary data-symbols $\{\hat{\alpha}_i\}$.

Since the bit-energy-to-noise power spectral density ratio at the input to the receiver is always used for comparison of performances of different systems, it is now to determine the two-sided power spectral density at the input to the receiver under the assumed conditions. The noise samples $\{n_m\}$ in Eqns. 3.3.2, 3.3.5 and 3.3.8 are assumed to have variance σ^2 . It is shown in Appendix A8 that, under these assumed conditions, the two-sided noise power spectral density at the input to the receiver is (Eqn. A8.10 or A8.11)

$$\frac{N_0}{2} = \frac{\sigma^2 T}{k} \quad 3.3.12$$

where k/T is the sampling rate used in the simulation tests. Equation 3.3.12 relates the two-sided noise power spectral density to the sampling rate used in the simulation tests. The sampling rate must be greater than twice the signal bandwidth to prevent aliasing.

To calculate $2E_b/N_0$ value, i.e., signal/noise power ratio or bit energy-to-noise power spectral density ratio value, in a simulation test, the average energy per sample of the transmitted signal is first measured (bearing in mind that the channel introduces no attenuation) by transmitting a few thousand symbols and using the equation (Eqn. A8.15)

$$\text{Average energy/sample} \quad P_m = \frac{1}{kL} \sum_{m=1}^{kL} |s_m|^2 \quad 3.3.13$$

where k : number of samples taken per T seconds in the simulation test
(i.e., $k=8$ for the present case),

L : number of transmitted symbols in the test,

and $|s_m|$: amplitude of the m^{th} sample in the transmitted signal, i.e., $|u_m|$, $|e_m|$, or $|e_m H_c G(\hat{A}_m)|$, as can be seen in Eqns. 3.3.2, 3.3.4 and 3.3.8, respectively, depending on which of the bandpass channels is used.

The value of the noise variance σ^2 for any required value of $2E_b/N_0$, under the assumed conditions, is then computed using the equation (Eqn. A8.21)

$$\sigma^2 = \frac{N_0 P_m k}{4E_b} \quad 3.3.14$$

The Gaussian random number generator in the computer is used to generate the inphase and quadrature noise samples with zero mean and fixed variance σ^2 .

After computing the value of σ^2 for the required value of $2E_b/N_0$, the test is then carried out again with a large number of symbols to find the probability of error, P_e , at the given value of $2E_b/N_0$. At the end of the test, the value of P_m (average energy per sample) is computed again, and the value of $2E_b/N_0$ are checked using the equation (Eqn. A8.20)

$$\frac{2E_b}{N_0} = \frac{P_m k}{2\sigma^2} \quad 3.3.15$$

to make sure it has the correct value.

Therefore, all the simulation tests, discussed in this thesis, are carried out in the sampled time domain by generating large numbers of binary data-symbols, encoding them, convolving them with the sampled impulse responses of the various filters in the baseband equivalent model, detecting and decoding them. The sampling rate is 8 samples per symbol.

It is shown in Appendix 8 that, when a continuous waveform is sampled at $1/T_s$ samples per second to produce the sampled signal, the latter must be scaled by the sampling interval T_s , in order to have the same signal energy level. However, the scaling factor is, for convenience, omitted here. This does not affect the signal/noise power ratio of the systems tested, because the signal and noise energy levels are measured at the same point, thus the scaling factors cancel each other.

3.4 Baseband equivalent model of DEQPSK system, with a linear or nonlinear satellite channel and in an ACI environment, for computer simulation

The baseband equivalent model of a quadrature modulation system, with a linear or nonlinear satellite channel and in an ACI environment, is described in Section 2.6. Here the baseband equivalent model of the DEQPSK system in an ACI environment for computer simulation is shown in Fig. 3.6, where there are three identical transmitters separated in frequency with a channel spacing of ω_{c_m} rad/s. One of them is for the desired channel, and the other two are for the upper and lower adjacent channels. These three transmitters could operate the HPAs either in the linear or nonlinear mode. $F_T(f)$ is the resultant transfer function of the modulation filter in cascade with the baseband equivalent model of the transmitter IF filter. The way to generate the equivalent baseband signals from the transmitters is exactly the same as that used for a single channel described in the last section. The data, of course, in each of the these three transmitters are statistically independent. As before, the system is modelled digitally for computer simulation.

The equivalent baseband transmitted signals, for the upper channel, desired channel and lower channel, with respect to the desired channel, are (Eqns. 2.6.11c, d and g)

$$\hat{s}_U(t) = [\hat{a}_U(t) + j\hat{b}_U(t)] \exp(j\omega_{c_m} t) \quad 3.4.1a$$

$$\hat{s}_D(t) = [\hat{a}_D(t) + j\hat{b}_D(t)] \quad 3.4.1b$$

and
$$\hat{s}_L(t) = [\hat{a}_L(t) + j\hat{b}_L(t)] \exp(-j\omega_{c_m} t) \quad 3.4.1c$$

as are shown in Section 2.6, where $\hat{a}_U(t) + j\hat{b}_U(t)$, $\hat{a}_D(t) + j\hat{b}_D(t)$, and $\hat{a}_L(t) + j\hat{b}_L(t)$, are the equivalent baseband signals with respect to the corresponding channels, and $j = \sqrt{-1}$. (Note that since the transmitters could operate the respective HPAs either in the linear or nonlinear mode, the signals could either or not be nonlinearly distorted by the HPAs.) The

signals are sampled at $1/T_m$ samples per second, at the time instants (mT_m) . (It should be noted that, since the adjacent channels are present, the sampling rate used in the tests must be high enough to prevent aliasing occurring in the upper channel.) At time $t=mT_m$, the signal samples are

$$\hat{s}_{U,m} = [\hat{a}_{U,m} + j\hat{b}_{U,m}] \exp(j\omega_{c_u}mT_m) \quad 3.4.2a$$

$$\hat{s}_{D,m} = [\hat{a}_{D,m} + j\hat{b}_{D,m}] \quad 3.4.2b$$

and
$$\hat{s}_{L,m} = [\hat{a}_{L,m} + j\hat{b}_{L,m}] \exp(-j\omega_{c_l}mT_m) \quad 3.4.2c$$

respectively, where $\hat{s}_{U,m} = \hat{s}_U(mT_m)$, $\hat{s}_{D,m} = \hat{s}_D(mT_m)$ and $\hat{s}_{L,m} = \hat{s}_L(mT_m)$. Thus after adding the noise component n_m at time $t=mT_m$, the signal sample at the input of the desired channel receiver is

$$\hat{s}_{R,m} = \hat{s}_{U,m} + \hat{s}_{D,m} + \hat{s}_{L,m} + n_m \quad 3.4.3$$

The real and imaginary parts of all noise samples are taken to be statistically independent Gaussian random variables with zero mean and fixed variance σ^2 given by Eqn. 3.3.14.

The sampled impulse responses of the baseband equivalent model of the receiver IF filter and of the modulation filter, sampled at the rate of $1/T_m$ samples per second, are given by the $(g+1)$ -component vector

$$F = [f_0 \quad f_1 \quad f_2 \quad \dots \quad f_g] \quad 3.4.4$$

and the $(n+1)$ -component vector

$$P = [p_0 \quad p_1 \quad p_2 \quad \dots \quad p_n] \quad 3.4.5$$

respectively, where $f_m = f(mT_m)$ and $p_m = p(mT_m)$. The delay in transmission is neglected here. Thus, at time $t=mT_m$, the sample value of the received

signal into the detector, is

$$r_m = \sum_{n=0}^N w_{m-n} p_n \quad 3.4.6$$

where

$$w_m = \sum_{n=0}^N \hat{s}_{r,m-n} f_n \quad 3.4.7$$

Assume that the receiver provides the required ideal timing signal, so that the sequence $\{r_m\}$ is sampled once per symbol, at the time instants $\{iT\}$, to give the sequence $\{r_i\}$, which are detected and Gray decoded into the sequence of detected binary data-symbols $\{\hat{\alpha}_i\}$.

3.5 Power spectra of QPSK and DEQPSK signals

In the QPSK system described in Section 3.1.1, the lowpass filtering is shared equally between the transmitter and receiver filters and with a sinusoidal rolloff frequency response. If the input data are random and equiprobable, the power spectra of the inphase and quadrature baseband signals at the modulation filter output have the same shape as the transfer function of the modulation filter. The modulation process, (i.e., multiplying the inphase and quadrature baseband signals by the carrier signal components $\sqrt{2}\cos\omega_c t$ and $-\sqrt{2}\sin\omega_c t$, respectively,) shifts the spectra by ω_c rad/s in the frequency domain from baseband to bandpass. When these signals are added linearly in the time domain to form the QPSK signal, the shapes of the individual spectra are not altered (this can be seen from the linearity property of Fourier transform). So if the bandpass channel is linear and memoryless (i.e., it does not distort the signals) and the carrier frequency is high enough to prevent aliasing, the power spectrum of the transmitted bandpass signal (i.e., the sum of the inphase and quadrature signals) has the shape same as the baseband signal power spectra which are shaped solely by the modulation filter.

The differential encoding process in DEQPSK systems does not alter the shapes of the spectra, so if the same transmitter filtering is used, DEQPSK signals will have the same signal power spectra as those of QPSK signals.

3.6 Spectral estimation of QPSK and DEQPSK signals by computer simulation

3.6.1 Basic principle on spectral estimation [3]

A good method of estimating the power spectral density of a modulated signal is by computer simulation. This method is quite straightforward and general. A pseudorandom data sequence is generated, and the modulation process is produced digitally. Since the signal has a certain bandwidth, the sampling rate must be high enough in order to prevent aliasing. Suppose there are k samples and the DFT (Discrete Fourier Transform) of sampled signal is $X_k(f)$. The power spectrum of the latter is estimated as [3]

$$S(f) = \frac{1}{k} |X_k(f)|^2 \quad 3.6.1$$

The shape of the spectrum is concerned here, so the factor $1/k$ can be neglected. Provided the sequence is suitably long and random, $S(f)$ will approach the exact signal spectrum. In order to get a good smooth estimation, it is need to average over a number of data sequence of several hundred symbols. Even so, considerable spectral variance remains, and small bias may remain. The variance can be reduced by a smoothing window, e.g., Turkey or Bartlett, though this will increase the bias and spectrum resolution [4],[5],[6]

3.6.2 Baseband equivalent model for spectral estimation

The baseband equivalent model, used for spectral estimation of the transmitted QPSK signal, is shown in Fig. 3.7. The spectra of the sampled

signals are estimated at three different points along the transmission path. They are at the outputs of the

- (a) modulation filter,
- (b) transmitter IF filter, and
- (c) HPA,

which are marked as points 'A', 'B' and 'C', respectively, in Fig. 3.7. Point 'A' is used to estimate the spectrum of the sampled signal shaped solely by the modulation filter. Point 'B' is used to estimate the spectrum of the sampled signal shaped by the overall transmitter filtering, for systems operating over a linear satellite channel. Whereas point 'C' is used to estimate the spectral spreading of the sampled signal caused by the HPA, for systems operating over a nonlinear satellite channel. The spectral estimation methods for these sampled signals are described as follows.

(a) To estimate the spectrum at point 'A', a sequence of L quaternary data-symbols $\{q_i\}$ are generated where $q_i = \pm 1 \pm j$ and $j = \sqrt{-1}$. The $\{q_i\}$ being statistically independent and equally likely to have any of the four possible values. The sequence $\{q_i\}$ is sampled at the time instants $\{iT\}$ and used to form the sequence of impulses $\{\sum_i q_i \delta(t - iT)\}$ which are fed into the modulation filter. The signal at the filter output is the complex-valued waveform

$$u(t) = \sum_i^L q_i h_i(t - iT) \quad 3.6.2$$

with $h_i(t)$ the impulse response of the modulation filter. The waveform $u(t)$ is sampled, at the time instants $\{mT_m\}$ (8 times per symbol), where $T_m = T/8$ and T is the symbol duration, to give the signal sequence $\{u_m\}$, with $u_m = u(mT_m)$.

(b) To estimate the signal spectrum of the sampled signal at point 'B' in Fig. 3.7, the sample values $\{u_m\}$ obtained in (a) are further filtered

by the baseband equivalent model of the transmitter IF filter. The sampled impulse response of the baseband equivalent model of the transmitter IF filter, sampled at the rate of $1/T_m$ samples per second, is given by the $(g+1)$ -component vector

$$F = [f_0 \quad f_1 \quad f_2 \quad \dots \quad f_g] \quad 3.6.3$$

where the $\{f_m\}$, for $0 \leq m \leq g$, have real-valued components (Table 2.2), so that at time $t = mT_m$, the signal sample at the IF filter output is

$$e_m = \sum_{n=0}^g u_{m-n} f_n \quad 3.6.4$$

(c) To estimate the spectral spreading of the sampled signal at point 'C', the sample values $\{e_m\}$ obtained in (b) are nonlinearly distorted by the HPA, so that at time $t = mT_m$, the signal sample at the output of the HPA is (Eqn. 2.5.30)

$$z_m = e_m H_c G(\hat{\lambda}_m) \quad 3.6.5$$

where $G(\hat{\lambda}_m)$ is the conversion function of the baseband equivalent model of the HPA, $\hat{\lambda}_m$ is the one of the $\{\lambda_m\}$ (Table 2.3) closest to the input signal envelope $|H_c e_m|$ (Section 2.5).

The FFT (Fast Fourier Transform) routine in the computer is used to evaluate the Fourier transform. Since the routine runs faster if the number of samples is a power of 2 (NAGF computer manual), the number of elements, in the resultant sequences $\{u_m\}$, $\{e_m\}$ and $\{z_m\}$, is arranged to be $2^{10} = 1024$. A Turkey window (i.e., a raised cosine pulse) is used to reduce the variance [4],[5],[6]. Since the $\{u_m\}$, $\{e_m\}$ and $\{z_m\}$ have complex values, the amplitude spectra of the real and imaginary components of these signals, representing the spectra of the inphase and quadrature signals, respectively, are computed separately by means of FFT and then

added to form the amplitude spectrum of the QPSK signal. The 1024 samples are reduced to 128 samples by averaging every 8 consecutive samples. In order to obtain a good estimate of the amplitude spectrum of the sampled signal, the same procedure is repeated for 100 different sequence of data-symbols $\{q_i\}$ and then averaged. The signal power spectral density of the sampled signal in dB is then obtained by taking the function $20\log_{10}(\cdot)$ on each of these 128 sample values.

Since if the same filtering are used, DEQPSK signals have the same spectra as those of QPSK signals. There is no need to estimate the DEQPSK signal spectra.

3.7 Simulation results and discussion

Computer simulation tests have been carried out to assess the error-rate performances of the different systems, using DEQPSK signals, with the equipment filters and HPA described in Section 2. The simulation models and methods are described in Sections 3.3, 3.4 and 3.6. In all simulation tests, it is assumed that the receiver provides the required ideal carrier and timing signals, and the data-transmission systems are optimised by sharing the overall filtering equally between the transmitter and receiver filters.

3.7.1 Performances of DEQPSK signals, with different truncation lengths of the sampled impulse responses of the modulation and demodulation filters, over a linear and memoryless bandpass channel.

This section studies the minimum truncation length of the sampled impulse responses of the modulation and demodulation filters (Section 2.4.1) required to approximate to the theoretical ideal error-rate performances of the signals in the practical region, i.e., $P_e = 10^{-3} - 10^{-4}$. The simulation model used to evaluate the error-rate performance is shown in Fig. 3.5, where the linear and memoryless channel is used (i.e., with Switches 'A' closed). Different truncation lengths of

the sampled impulse responses for different values of β are used as the sampled impulse responses of the modulation and demodulation filters. The effects of different values of β on the performance are shown in Fig. 3.8.

With $\beta=25\%$, Fig. 3.8a shows that, the minimum truncation length of the sampled impulse responses required for the modulation and demodulation filters to approximate to the theoretical ideal error-rate performance, at $P_e < 10^{-4}$, is $8T$. With $\beta=50\%$ and 75% , the results in Figs. 3.8b and 3.8c show that, the required minimum truncation length to approximate to the theoretical ideal error-rate performance at $P_e > 10^{-4}$ is $4T$. Whereas, with $\beta=100\%$, Fig. 3.8 shows that the required minimum truncation length is $2T$.

Table 3.4 shows the degradations in tolerance to noise of the DEQPSK signals with different truncation lengths, at $P_e=10^{-4}$, in comparison with that of an ideal DEQPSK system. These degradations are due to ISI caused by not using a long enough truncation length of the sampled impulse responses of the modulation and demodulation filters, and they can be reduced by using longer truncation lengths. It can be seen, in Fig. 3.8, that these degradations get larger at low error rates where ISI is the dominated factor causing errors.

The results indicate that the minimum truncation lengths of the sampled impulse responses of the modulation and demodulation filters, with $\beta=100\%$, 75% , 50% and 25% required to approximate to the theoretical ideal error-rate performance at $P_e=10^{-4}$ are $2T$, $4T$, $4T$ and $8T$, respectively.

3.7.2 Performances of DEQPSK signals over a linear and bandlimited bandpass channel

In any practical satellite system, the signal from the modulator at the transmitter is always further bandlimited by the IF filter before being up-converted to a microwave frequency, and at the receiver, a receiver IF filter, having the same characteristics as the transmitter IF filter, is always used to select the lower sideband of the desired downconverted

signal. Since these IF filters are narrowband to suppress ACI, they may also introduce ISI into the signal. This section studies the degradation in tolerance to noise caused by the bandlimited effects of the IF filters.

The simulation model used to evaluate the error-rate performance is shown in Fig. 3.5, where the linear and bandlimited channel is used (i.e., with Switches 'B' closed). The minimum truncation lengths of the sampled impulse responses of the modulation and demodulation filters obtained from the previous section are used here, i.e., the truncation lengths of $2T$, $4T$, $4T$ and $8T$ are used in the sampled impulse responses of the modulation and demodulation filters with $\beta=100\%$, 75% , 50% and 25% , respectively. The results are shown in Fig. 3.9, which suggest that with $\beta=75\%$, 50% , and 25% , there is no degradation in tolerance to noise over the region $P_e \gg 10^{-4}$, due to ISI caused by the IF filtering, whereas with $\beta=100\%$, the signal has very little degradation in tolerance to noise at $P_e \gg 10^{-4}$ because of its relatively wide bandwidth. This degradation, caused by ISI, is not obvious at high error rates because the errors are dominated by noise, while at lower error rates, the errors are dominated by ISI and so the degradation increases. Fig. 3.9 shows that, in the practical region of P_e , i.e., $P_e=10^{-4} - 10^{-3}$, the IF filters introduce a relatively low level of ISI.

3.7.3 Performances of DEQPSK signals with different truncation lengths of the sampled impulse responses of the modulation and demodulation filters, over a linear and bandlimited bandpass channel and in an ACI environment

ISI is a less serious effect than ACI, since the effects of the former (when present) can be greatly reduced through the modification of the detector, e.g. using a Viterbi detector [8], whereas the latter appears as additive noise in the performance of the system. This section studies the minimum truncation lengths of the sampled impulse responses of the modulation and demodulation filters required to bandlimit the signals over a linear bandpass channel and in an ACI environment.

In Section 3.7.1, it is shown that, over a linear and memoryless bandpass channel, the longer the truncation length of the sampled impulse responses of the modulation and demodulation filters, the better is the approximation of the signal to the theoretical ideal error-rate performance. In Section 3.7.2, it is shown that, over a linear and bandlimited bandpass channel, the minimum truncation lengths of the sampled impulse responses of the modulation and demodulation filters with $\beta=100\%$, 75% , 50% and 25% , required to approximate to the theoretical ideal error-rate performance of the signals, at $P_e \geq 10^{-4}$, are to be $2T$, $4T$, $4T$ and $8T$, respectively. Now in an ACI environment, these minimum truncation lengths may not be good enough because the longer the truncation length, the more tightly bandlimited are the signals. These effects can easily be seen by means of spectral estimation on the sampled signal at the output of the modulation filter. The model used to estimate the spectra of the sampled signal is shown in Fig. 3.7, where the spectrum of the sampled signal at point 'A' is studied. Different truncation lengths of the sampled impulse responses of the modulation filter, with $\beta=100\%$, 75% , 50% and 25% , are used. The results are shown in Fig. 3.10, which indicate that a longer truncation length can suppress more out of band radiation.

The simulation model, used to evaluate the error-rate performance of DEQPSK signal, over a linear bandlimited bandpass channel and in an ACI environment, is shown in Fig. 3.6, where the linear and bandlimited bandpass channel is used (i.e., with Switches 'B' closed) with the channel spacing $f_{c_m} = 5R/4$ Hz (where R is the symbol rate). Different truncation lengths of the sampled impulse responses of the modulation and demodulation filters, with $\beta=100\%$, 75% , 50% and 25% , are used in order to test if a longer truncation length of the sampled impulse responses would further bandlimit the transmitted signal spectra (hence suppress more ACI). The results of the simulation tests on the error-rate performances are shown in Fig. 3.11.

The results show that, with $\beta=100\%$ and truncation lengths $2T$ and $4T$ for the sampled impulse responses, the signals have the same degradation in tolerance to noise of about 1.8 dB at $P_e=10^{-4}$. This means that no improvement in performance can be obtained by using a truncation length of $4T$, instead of $2T$. Thus the truncation length of $2T$ is long enough to bandlimit the signal adequately. This DEQPSK signal, with $\beta=100\%$ and a truncation length of $2T$, is known here as signal 1A.

With $\beta=75\%$ and truncation lengths of $4T$ and $6T$ in the sampled impulse responses, the signals have the same degradation in tolerance to noise of about 1.2 dB at $P_e=10^{-4}$. For the same reason as that described in the previous paragraph, the truncation length of $4T$ is long enough to bandlimit the signal. This signal, with $\beta=75\%$ and a truncation length of $4T$, is known here as signal 2A.

With $\beta=50\%$, signals with truncation lengths of $4T$ and $6T$ have the same degradation in tolerance to noise of about 0.3 dB, at $P_e=10^{-4}$, so the truncation length of $4T$ is long enough. This DEQPSK signal, with $\beta=50\%$ and a truncation length of $4T$, is known here as signal 3A.

With $\beta=25\%$ the signals with truncation lengths of $8T$ and $10T$ have no degradation in tolerance to noise at $P_e \geq 10^{-4}$, so the truncation length of $8T$ is enough. This DEQPSK signal, with the truncation length of $8T$, is known here as signal 4A.

The degradations in tolerance to noise of the signals, at $P_e=10^{-4}$, with $f_{c_s}=5R/4$ Hz and $5.5R/4$ Hz, in comparison with that of an ideal DEQPSK system, are shown in Table 3.5

ACI arises from the spillover of signal power (or energy) from an adjacent channel, so it can be reduced by increasing the channel spacing f_{c_s} . With f_{c_s} increased to $5.5R/4$ Hz, the error-rate performances of signals 1A, 2A, 3A and 4A are shown Fig. 3.11b. It can be seen that, by increasing f_{c_s} to $5.5R/4$ Hz, the degradations in tolerance to noise caused

by ACI for signals 2A and 3A have been removed, but for signal 1A, the degradation has decreased from 1.8 dB to 0.5 dB at $P_e=10^{-4}$. Simulation tests have also been carried out for signal 4A with $f_{c_m}=4.5R/4$ Hz, and the results suggest that there is still no degradation at $P_e \geq 10^{-4}$. This is because signal 4A is a relatively narrowband signal.

Since ACI arises from overlapping of the signal power spectra of adjacent channels onto the wanted channel, it may provide some insight into the degradation in tolerance to noise by studying the transmitted signal power spectra of signals 1A, 2A, 3A and 4A over a linear and bandlimited channel. The model for spectral estimation is shown in Fig. 3.7, where the transmitted signal power spectrum at the output of the IF filter (i.e., marked as Point 'B' in the figure) is estimated. The estimated transmitted signal spectra of signals 1A, 2A, 3A and 4A, in an ACI environment, are shown in Figs. 3.12a, b, c and d.

In Fig. 3.12d it can be seen that, for signal 4A with $f_{c_m}=4.5R/4$ Hz, the transmitter IF filter has suppressed ACI to -15 dB, but computer simulation results have shown that, under these conditions, ACI does not cause any degradation in tolerance to noise to signal 4A at $P_e \geq 10^{-4}$, hence it can be said that ACI below -15 dB has an insignificant effect on the error-rate performance at $P_e \geq 10^{-4}$. Figure 3.12c shows that, with $f_{c_m}=5R/4$ Hz, ACI above -15 dB is small for signal 3A; and so it causes insignificant degradation at $P_e \geq 10^{-4}$, as is shown in Fig. 3.11a. Figures 3.12a and b show that, with $f_{c_m}=5R/4$ Hz, ACI above -15 dB is relatively larger for signals 1A and 2A, and so these cause the degradations in tolerance to noise of about 1.8 dB and 1.2 dB to signals 1A and 2A, respectively, at $P_e=10^{-4}$, as can be seen in Fig. 3.11.

Figures 3.12b and c also show that, with f_{c_m} increased to $5.5R/4$ Hz, signals 2A and 3A have no ACI above -15 dB and so they have no degradation in tolerance to noise at $P_e \geq 10^{-4}$, but for signal 1A (Fig. 3.12a), there is

a small amount of ACI above -15 dB which therefore has caused a small degradation in tolerance to noise at $P_{\text{e}}=10^{-4}$ to the signal. All these results show that, for DEQPSK signals, ACI below -15 dB has an insignificant effect on the performance, at $P_{\text{e}} \geq 10^{-4}$.

From the above results, it can be concluded that, with the preferred IF filters, the channel spacings for signals 1A, 2A, 3A and 4A must be $5.5R/4$, $5.5R/4$, $5R/4$ and $4.5R/4$ Hz, respectively, in order to limit the degradation in tolerance to noise to, say ≤ 0.5 dB, at $P_{\text{e}}=10^{-4}$. It is obvious that, since the channel is linear and so does not spread the spectra, narrowband signals (or the signals with smaller value of β) can achieve a better bandwidth efficiency, at the expense of a slight increase in equipment complexity (because a narrowband signal requires a longer truncation length of the sampled impulse responses of the modulation and demodulation filters to approximate to the theoretical ideal signal spectrum). It should be noted that the results obtained in this section are applied to the linear satellite channels which have the HPAs and TWTAs operating in the linear modes.

3.7.4 Performances of signals 1A, 2A, 3A and 4A over a nonlinear and bandlimited bandpass channel

For the present application, the HPA at the earth station is operating in the nonlinear mode for high power efficiency. This introduces AM-AM and AM-PM conversion effects of the transmitted signal. These effects degrade the tolerance to noise of the system, for the following two reasons (Section 2.5).

- 1) The signal is nonlinearly distorted.
- 2) Spectral restoration (known as spectral spreading) increases the ACI.

When the signal is nonlinearly distorted, the receiver filters no longer match the received signal, and inevitably degrade the performance.

The simulation model, used to evaluate the effects of nonlinear distortion on the error-rate performance, is shown in Fig. 3.5, where the nonlinear and bandlimited bandpass channel is used (i.e., with Switches 'C' closed). The error-rate performances for signals 1A, 2A, 3A and 4A (see Section 3.7.3 for the definitions) transmitted over the nonlinear and bandlimited channel, are shown in Figs. 3.13a, b and c, respectively. The HPA here operates at 0, 0.2 or 0.68 dB output backoff (see Section 2.5 for the reasons behind the use of these three backoff values).

With the HPA operating at 0 dB OBO (output backoff), Fig. 3.13a shows that, of these signals, signal 4A suffers the largest degradation in tolerance to noise (about 1.6 dB at $P_e=10^{-4}$) because of its relatively narrow bandwidth, which causes more severe fluctuations in the timing waveform (Fig. 2.8), thus more nonlinear distortion is caused by the HPA.

With the HPA operating at 0.2 dB OBO (i.e., slightly below saturation), Fig. 3.13b shows that the degradations in tolerance to noise of signals 1A, 2A and 3A remain the same as those with 0dB HPA OBO, at $P_e \geq 10^{-4}$, whereas signal 4A has reduced the degradation to about 1.1 dB (i.e., a 0.5 dB improvement is achieved).

Figure 3.13c shows that, with the HPA OBO value further increased to 0.68 dB, the degradations in tolerance to noise of signals 1A, 2A and 3A, at $P_e \geq 10^{-4}$ still remain the same as those with the HPA operating at 0 dB OBO, and the further improvement in error-rate performance of signal 4A is insignificant.

The degradations in tolerance to noise of the signals, at $P_e=10^{-4}$, are given in Table 3.6. It can be seen that, with the HPA operating at 0, 0.2 or 0.68 dB OBO, the P_e degradations of signals 1A, 2A and 3A, due to the nonlinear distortion effects, are insignificant (≤ 0.6 dB), at $P_e \geq 10^{-4}$. Whereas, for signal 4A with 0 dB HPA OBO, the degradation in tolerance to noise is about 1.6 dB, at $P_e=10^{-4}$, which can be reduced to about 1.1 dB by increasing the HPA OBO value from 0 dB to 0.2 dB. However, a further increase in the HPA OBO value does not give any significant improvement.

3.7.5 Performances of signals 1A, 2A, 3A and 4A over a nonlinear and bandlimited bandpass channel and in an ACI environment

Since the HPA has the characteristics (Fig. 2.12) of a soft limiter, a bandlimited signal with a nonconstant envelope fed through the HPA will suffer in spectrum spreading and increased ACI. These effects can be observed by means of spectrum estimation on the transmitted signal at the HPA output at the earth station. The model for spectrum estimation is shown in Fig. 3.7, where the spectrum of the sampled signal at the HPA output is studied. With the use of signals 1A, 2A, 3A and 4A (see Section 3.7.3 for the definitions), the estimated spectra are shown in Figs. 3.14a, b, c and d, respectively, and they indicate that the HPA has caused significant spectral spreading in the transmitted signals, and little improvement can be achieved by increasing the HPA OBO value from 0 dB to 0.68 dB.

Spectral spreading increases ACI, so inevitably it will cause a degradation in tolerance to noise in the transmission systems. The simulation model, used to evaluate the spectral spreading effects on the error-rate performances of signals 1A, 2A, 3A and 4A in an ACI environment, is shown in Fig. 3.6, where the nonlinear and bandlimited bandpass channel is used (i.e., with Switches 'A' closed). With the channel spacing $f_{cs} = 5R/4$ Hz (where R is the symbol rate), the error-rate performances of the signals with the HPA operating at 0, 0.2 and 0.68 dB OBO, are shown in Figs 3.15a,b and c, respectively.

With the HPA operating at 0 dB HPA OBO, Figure 3.15a shows that, of these signals, signal 2A has the best performance with a degradation of about 2.8 dB degradation at $P_e = 10^{-4}$, in comparison with that of an ideal DEQPSK system, whereas signal 4A has the worst performance.

With the HPA OBO value increased from 0 dB to 0.2 dB, Figure 3.15b shows that signal 3A has the best performance with a degradation of about

1.8 dB at $P_e=10^{-4}$, in comparison with that of an ideal DEQPSK system. It can be seen that signal 4A has the largest improvement in performance. The reason is that the nonlinear distortion effects have been reduced significantly (see the previous section), but not the spectrum spreading.

With the HPA OBO value further increased to 0.68 dB, Fig. 3.15c shows that the error-rate performances of signals 1A, 2A and 3A are about the same as in the cases of 0.2 dB HPA OBO, and signal 4A has reduced the degradation in tolerance to noise from 2.4 to 1.8 dB, at $P_e=10^{-4}$. Thus very little further improvement is obtained, and the penalty for this is about 0.5 dB HPA output power reduction caused by operating the HPA about 0.5 dB below its full power.

The degradations in tolerance to noise of the signals, at $P_e=10^{-4}$, at different HPA OBO values, in comparison with that of an ideal DEQPSK system, are shown in Table 3.7a. It can be seen that, for the present filters, HPA and channel spacing $f_{c_s}=5R/4$ Hz, the most cost effective arrangement is to use signal 3A and to operate the HPA slightly (say, e.g. 0.2dB) below saturation. The degradation in tolerance to noise is about 1.8 dB, at $P_e=10^{-4}$, in comparison with that of an ideal DEQPSK system. A better power efficiency cannot be obtained by increasing the HPA OBO value to 0.68dB.

With the channel spacing f_{c_s} increased to $5.5R/4$ Hz, the error-rate performances of the signals are shown in Figs. 3.16a, b, c and d. The degradations in tolerance to noise of the signals with different HPA OBO values at $P_e=10^{-4}$, in comparison with that of an ideal DEQPSK system, are shown in Table 3.7b. When the results in Table 3.7b are compared with those in Table 3.7a, it can be seen that the improvements in tolerance to noise, obtained by increasing the channel spacing from $5R/4$ to $5.5R/4$ Hz, are in the range 0.1-0.7 dB. The largest improvement is achieved by signal 1A at 0.2 and 0.68 dB HPA OBO. That is because signal 1A is a relatively

wideband signal with less envelope fluctuations, and so it suffers less from nonlinear distortion, thus the increased channel spacing has more effects on it.

These results have shown that, under these assumed conditions, for the present filters and HPA, with $f_{c_m}=5.5R/4$ Hz, the most cost effective arrangement is to use signal 1A (which requires less hardware complexity than those of signal 2A and 3A) and to operate the HPA slightly (say, e.g. 0.2 dB) below saturation. The degradation in tolerance to noise is about 1.7 dB, at $P_e=10^{-4}$, in comparison with that of an ideal DEQPSK system.

When comparing the case with $f_{c_m}=5R/4$ Hz against that with $f_{c_m}=5.5R/4$ Hz, it can be seen that no significant improvement ($\ll 0.7$ dB at $P_e=10^{-4}$) can be obtained by increasing the channel spacing from $5R/4$ to $5.5R/4$ Hz. This is because the spectra of the adjacent channels, that have been spread by the HPAs, are so wide that they extend across the whole desired channel bandwidth (Fig. 3.14), and ACI in the desired channel is not significantly reduced until a substantial increase in channel spacing has been achieved, as can be seen in Fig. 3.14. Hence, for reasons of bandwidth efficiency, $f_{c_m}=5R/4$ Hz is the most cost effective.

REFERENCES

- [1] Taub, H. and Schilling, D.C., *Principles of Communication Systems*, pp.235-281, McGraw-Hill (1971)
- [2] Linsey, W.C. and Simon, M.K., *Telecommunication Systems Engineering*, Prentice-Hall, Englewood Cliffs, N.J. (1973)
- [3] Wilson, S.G. and Gaus, R., "Power Spectra of Multi-h Phase Codes", *IEEE Trans. on Commun.*, vol. COM-29, pp.250-256, March 1981
- [4] Schwartz, M. and Shaw, L., *Signal Processing: discrete spectra analysis, detection and estimation*, Ch.3, McGraw-Hill (1975)
- [5] Oppenheim, A.V. and Schafer, R.W., *Digital Signal Processing*, Ch.11, Prentice-Hall, Englewood Cliffs, NJ
- [6] Papoulis, A., *Signal Analysis*, Ch. 12, McGraw-Hill (1971)
- [7] Nyquist, H., "Certain Topics in Telegraph Transmission Theory", *AIEEE Trans.* 47, pp.617-644 (1928)
- [8] Clark, A.P., *Advanced Data-Transmission Systems*, Pentech Press, London (1976)
- [9] Clark, A.P., *Principles of Digital Data Transmission*, Pentech Press, London (1976)
- [10] Schwartz, M., *Information Transmission, Modulation, and Noise*, 2nd Ed. McGraw-Hill Kogakusha, Tokyo (1970)

$u_i^{(1)}$	$u_i^{(2)}$	$q_i^{(1)}$	$q_i^{(2)}$
0	0	+1	+1
0	1	+1	-1
1	0	-1	+1
1	1	-1	-1

Table 3.1 Gray coding.

Input data		Gray coded		Non-Gray decod	
$u_i^{(1)}$	$u_i^{(2)}$	$q_i^{(1)}$	$q_i^{(2)}$	$q_i^{(1)}$	$q_i^{(2)}$
0	0	+1	+1	+1	+1
0	1	+1	-1	-1	-1
1	0	-1	+1	+1	-1
1	1	-1	-1	-1	+1

Table 3.2 Comparison of Gray coded and non-Gray coded.

Received sample values		Detected sample values		Gray decoded values	
$r_i^{(1)}$	$r_i^{(2)}$	$\hat{r}_i^{(1)}$	$\hat{r}_i^{(2)}$	$u_i^{(1)}$	$u_i^{(2)}$
>0	>0	+1	+1	0	0
>0	<0	+1	-1	0	1
<0	>0	-1	+1	1	0
<0	<0	-1	-1	1	1

Table 3.3 Threshold detection and Gray decoding.

$\beta =$	Truncation length of			
	2T	4T	4T	8T
25%	4.0	1.2	0.2	0
50%	0.4	0	0	0
75%	0.2	0		
100%	0			

Table 3.4 Degradations in tolerance to noise of DEQPSK signals, with different truncation lengths of the sampled impulse responses (Table 2.1) of the modulation and demodulation filters, with $B=100\%$, 75% , 50% and 25% , at $P_e=10^{-4}$, expressed in dB, measured in comparison with that of an ideal DEQPSK system (from Fig. 3.8):

$f_{c_m} =$ (in Hz)	Signal			
	1A	2A	3A	4A
5R/4	1.9	1.2	0.3	0
5.5R/4	0.6	0	0	0

Table 3.5 Degradations in tolerance to noise of signals 1A, 2A, 3A and 4A, over a linear channel and in an ACI environment, with the channel spacings $f_{c_m}=5R/4$ Hz and $5.5R/4$ Hz, at $P_e=10^{-4}$, expressed in dB, measured in comparison with that of an ideal DEQPSK system (from Fig. 3.11).

HPA OBO (in dB)	Signal			
	1A	2A	3A	4A
0	0.5	0.5	0.5	1.6
0.2	0.5	0.5	0.5	1.1
0.68	0.4	0.4	0.4	0.9

Table 3.6 Degradations in tolerance to noise of signals 1A, 2A, 3A, 4A, over a nonlinear and bandlimited channel, with the HPA operating at 0, 0.2, 0.68 dB OBO and in a non-ACI environment, at $P_e=10^{-4}$, expressed in dB, measured in comparison with that of an ideal DEQPSK system (from Fig. 3.13).

HPA OBO (in dB)	Signal			
	1A	2A	3A	4A
0	3.1	2.8	3.1	4.9
0.2	2.4	2.0	1.8	2.4
0.68	2.3	2.0	1.6	1.8

(a)

HPA OBO (in dB)	Signal			
	1A	2A	3A	4A
0	2.8	2.8	2.8	4.5
0.2	1.7	1.7	1.7	2.1
0.68	1.6	1.6	1.6	1.8

(b)

Table 3.7 Degradations in tolerance to noise of signals 1A, 2A, 3A, 4A, over a nonlinear and bandlimited channel, with the HPA operating at 0, 0.2, 0.68 dB OBO and in an ACI environment, with the channel spacing (a) $f_{c_m} = 5R/4$ Hz and, (b) $f_{c_m} = 5.5R/4$, at $P_e = 10^{-4}$, expressed in dB, measured in comparison with that of an ideal DEQPSK system (from Figs. 3.15 and 3.16).

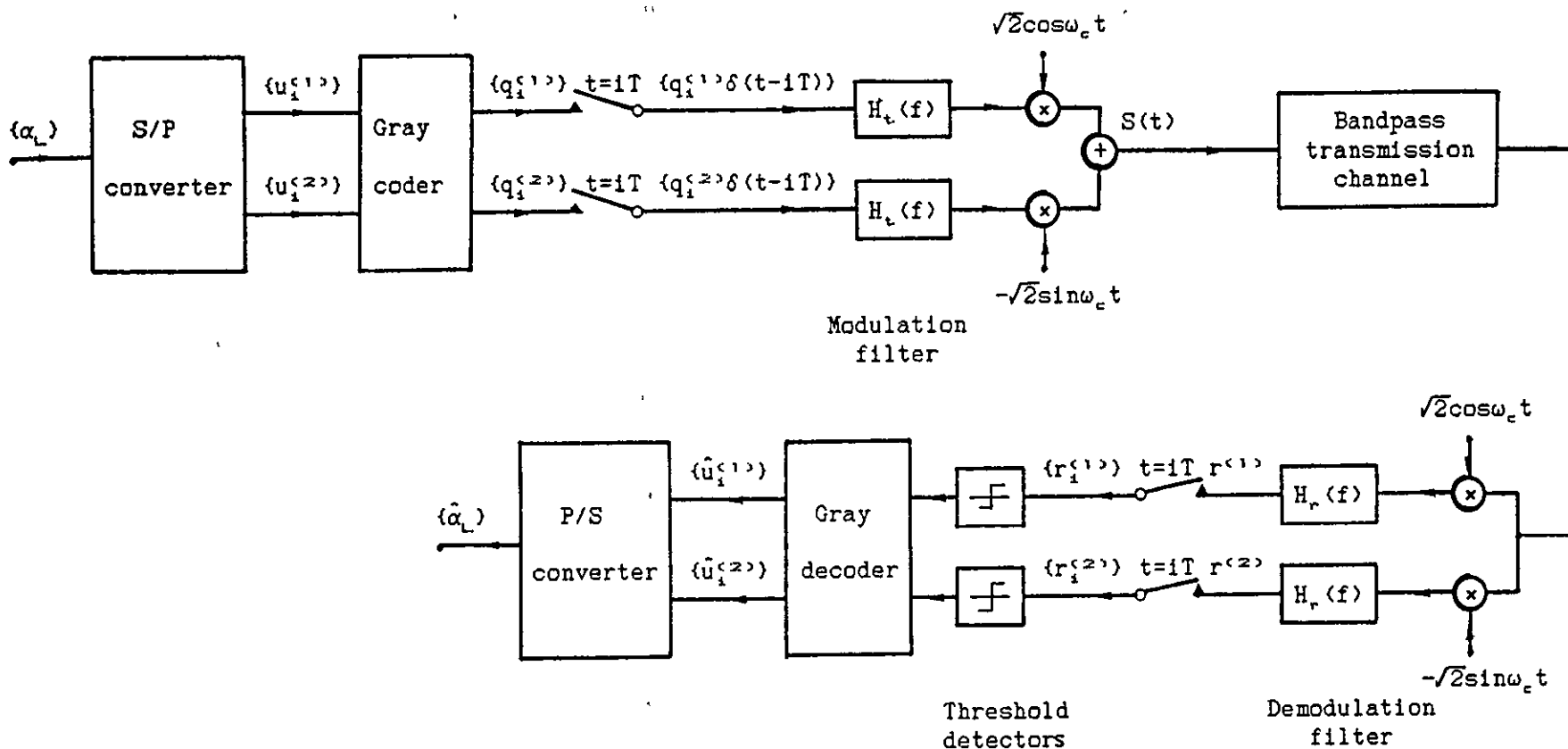


Figure 3.1 Block diagram of a conventional QPSK system representation. S/P and P/S mean serial-to-parallel and parallel-to-serial converters, respectively.

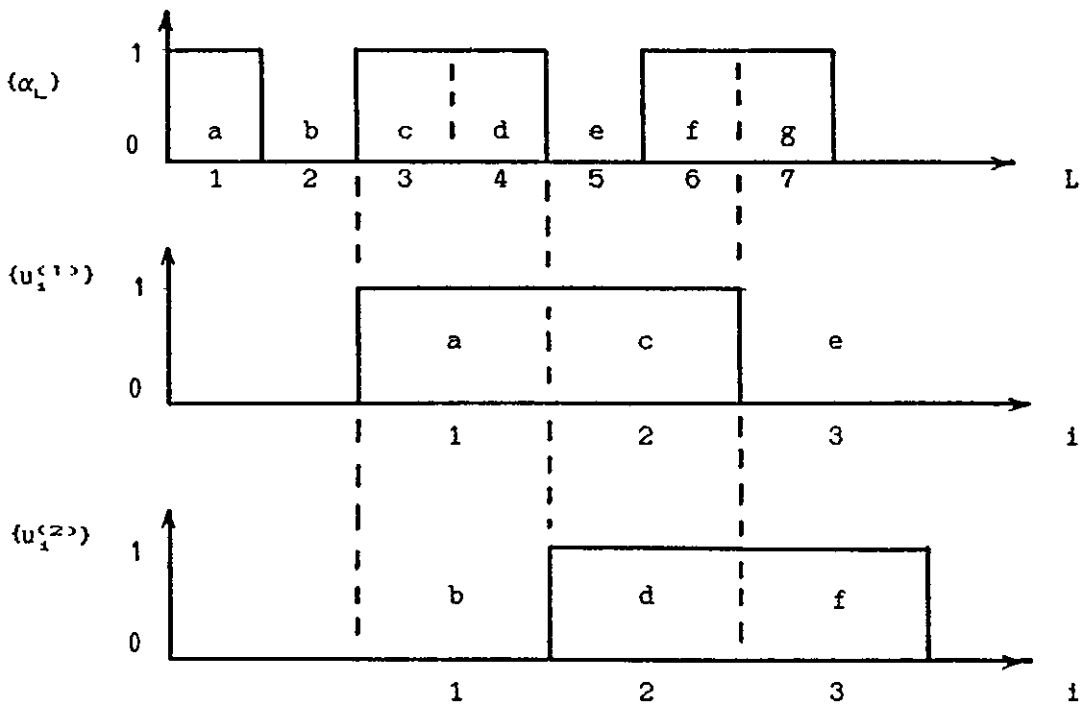


Figure 3.2 Relationship between input data sequence $\{\alpha_L\}$ and the two binary sequences $\{u_i^{(1)}\}$ and $\{u_i^{(2)}\}$.

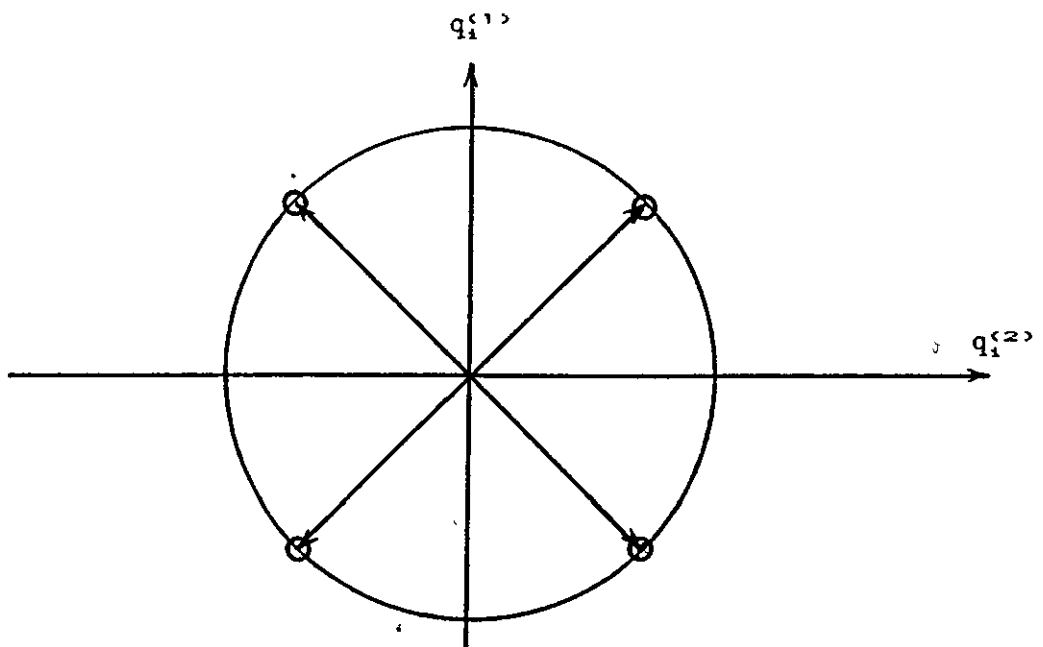


Figure 3.3 QPSK (or DEQPSK) signal constellation (possible received signal vectors).

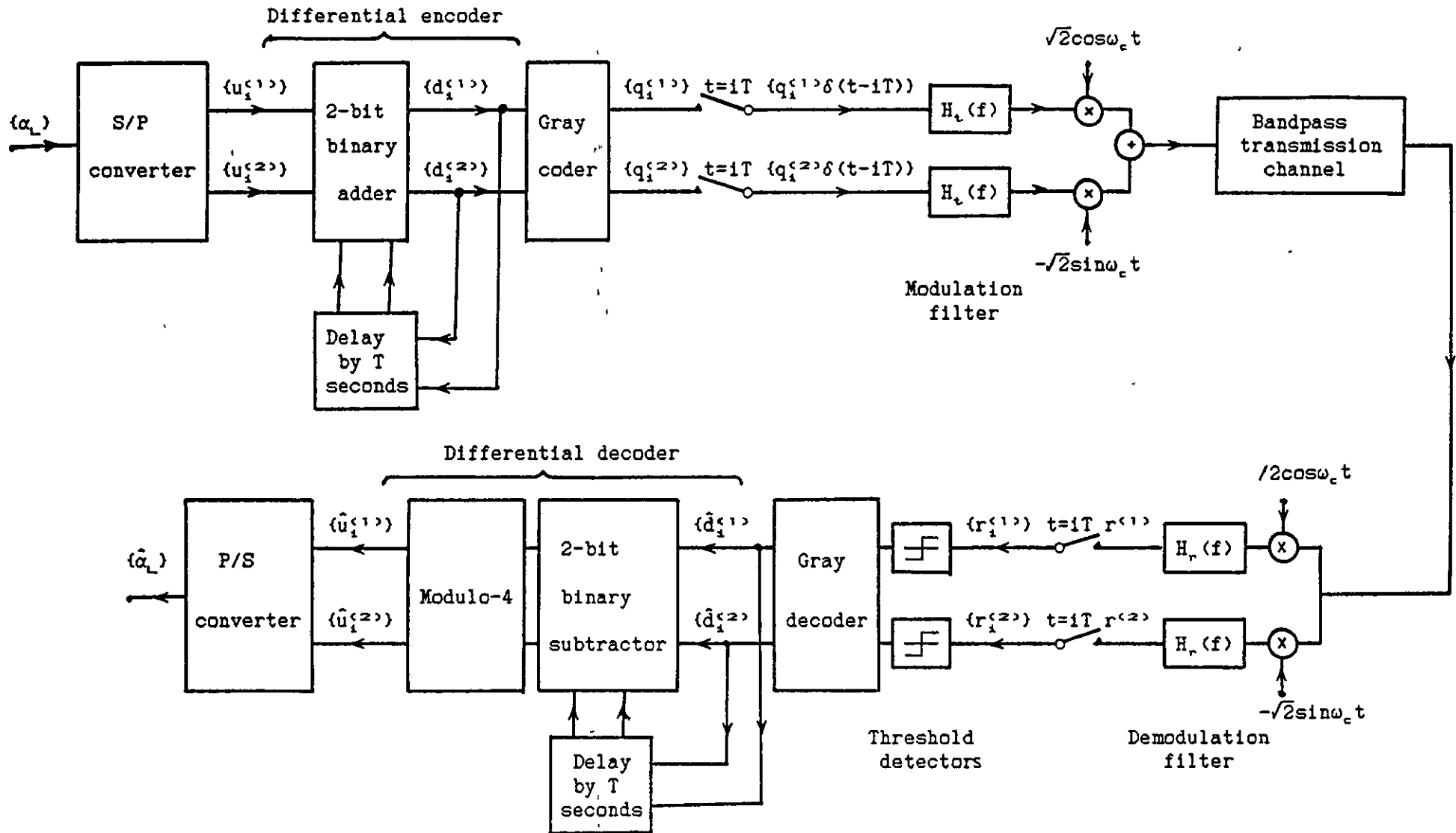


Figure 3.4 Block diagram of a conventional DEQPSK system representation. S/P and P/S mean serial-to-parallel converter and parallel-to-serial converters, respectively.

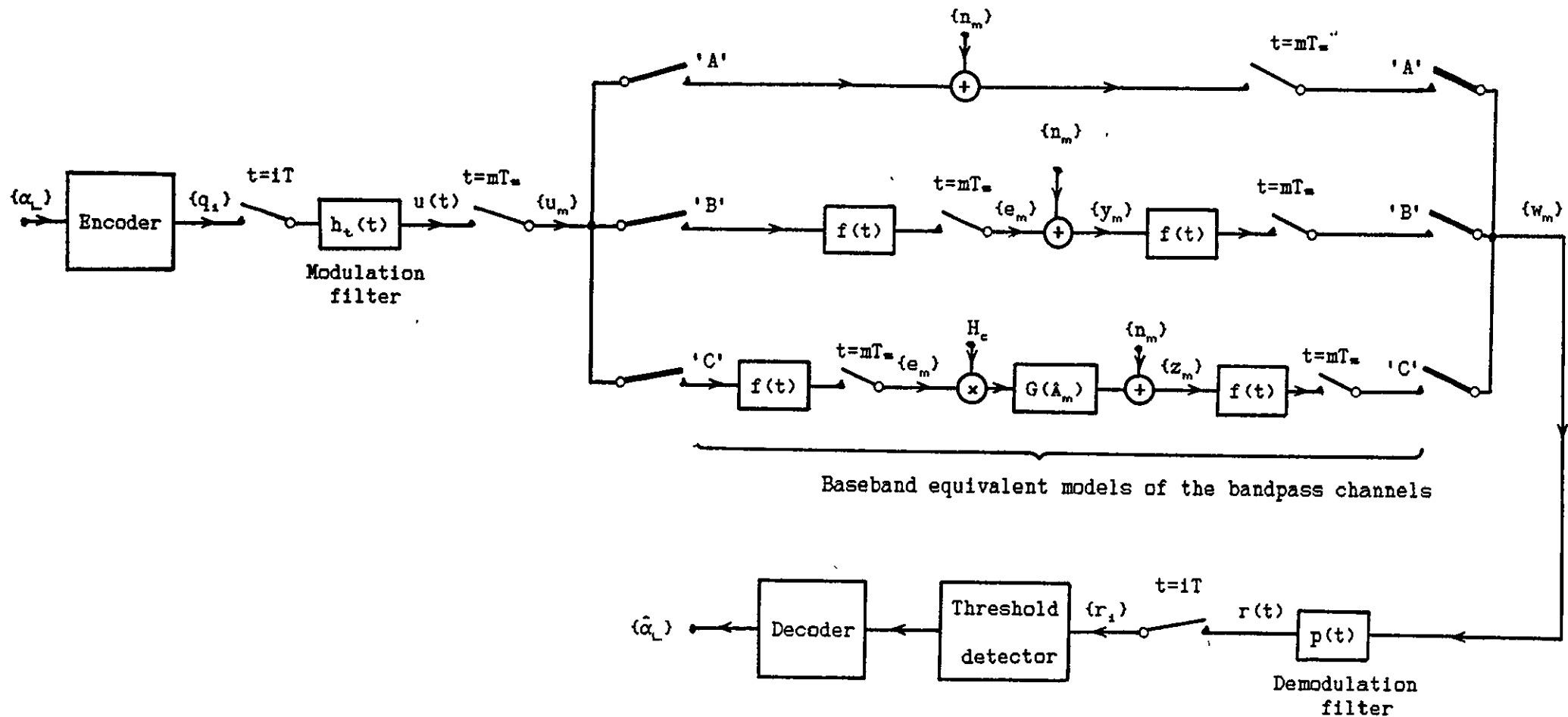


Figure 3.5 Baseband equivalent model of the DEQPSK system, with a linear and memoryless, a linear and bandlimited, or a nonlinear and bandlimited satellite channel, for computer simulation. $f(t)$ is impulse response of the baseband model of the IF filter. Switches 'A', 'B' and 'C' are for the linear and memoryless, the linear and bandlimited, and the nonlinear and bandlimited channels, respectively.

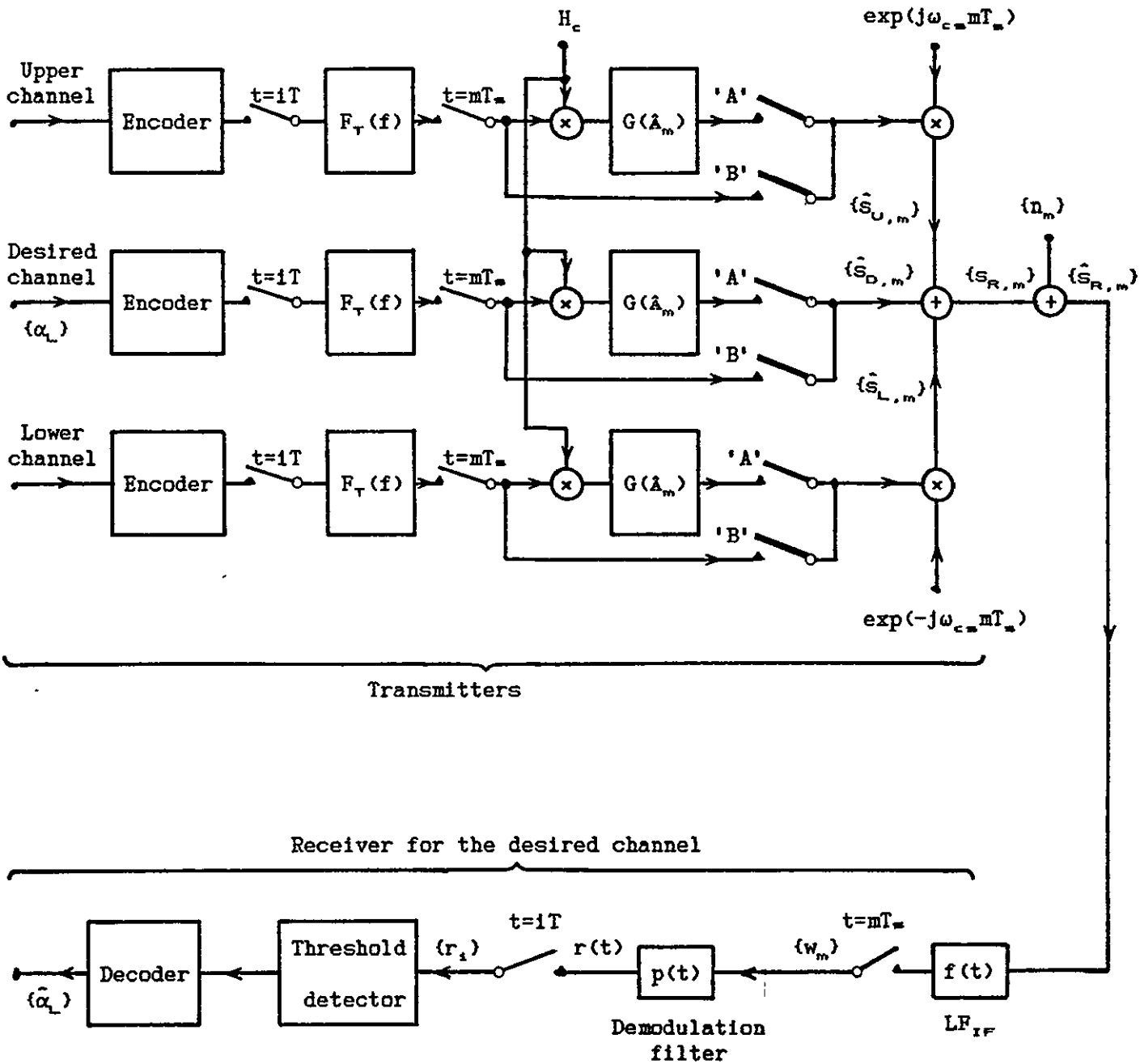


Figure 3.6 Baseband equivalent model of the DEQPSK system, with a linear and bandlimited or a nonlinear and bandlimited satellite channel and in an ACI environment, for computer simulation. $F_T(f)$ is the resultant transfer function of the baseband equivalent model of the IF filter in cascade with the modulation filter. LF_{IF} means the baseband equivalent model of the IF filter. Switches 'A' and 'B' are for the nonlinear and bandlimited channel and the linear and bandlimited channel, respectively.

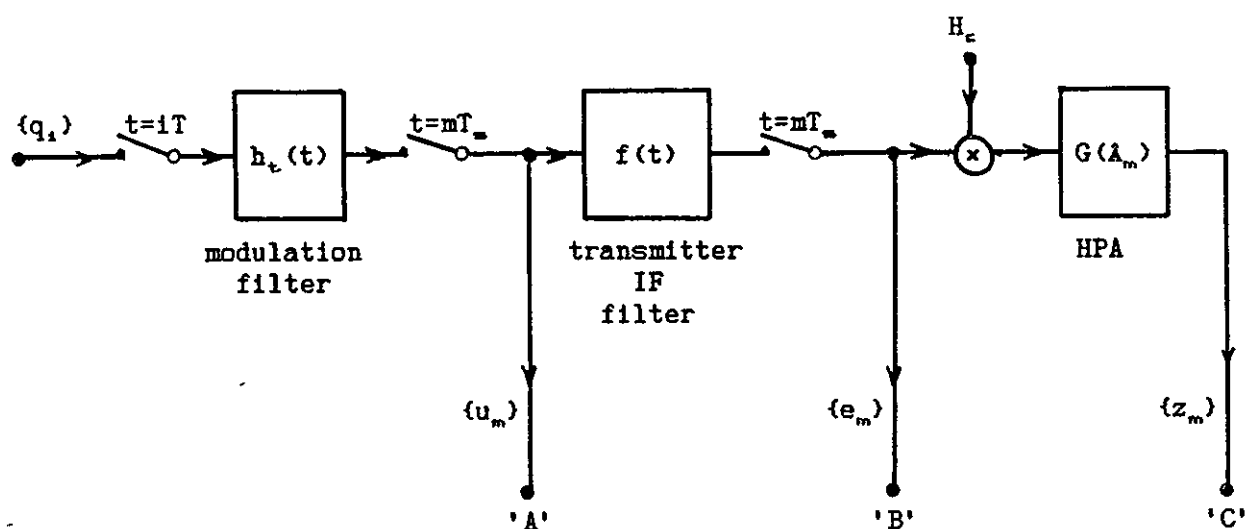


Figure 3.7 Baseband equivalent model for spectral estimation of DEQPSK signals at different points along the transmission path. $f(t)$ is the impulse response of the baseband equivalent model of the IF filter.

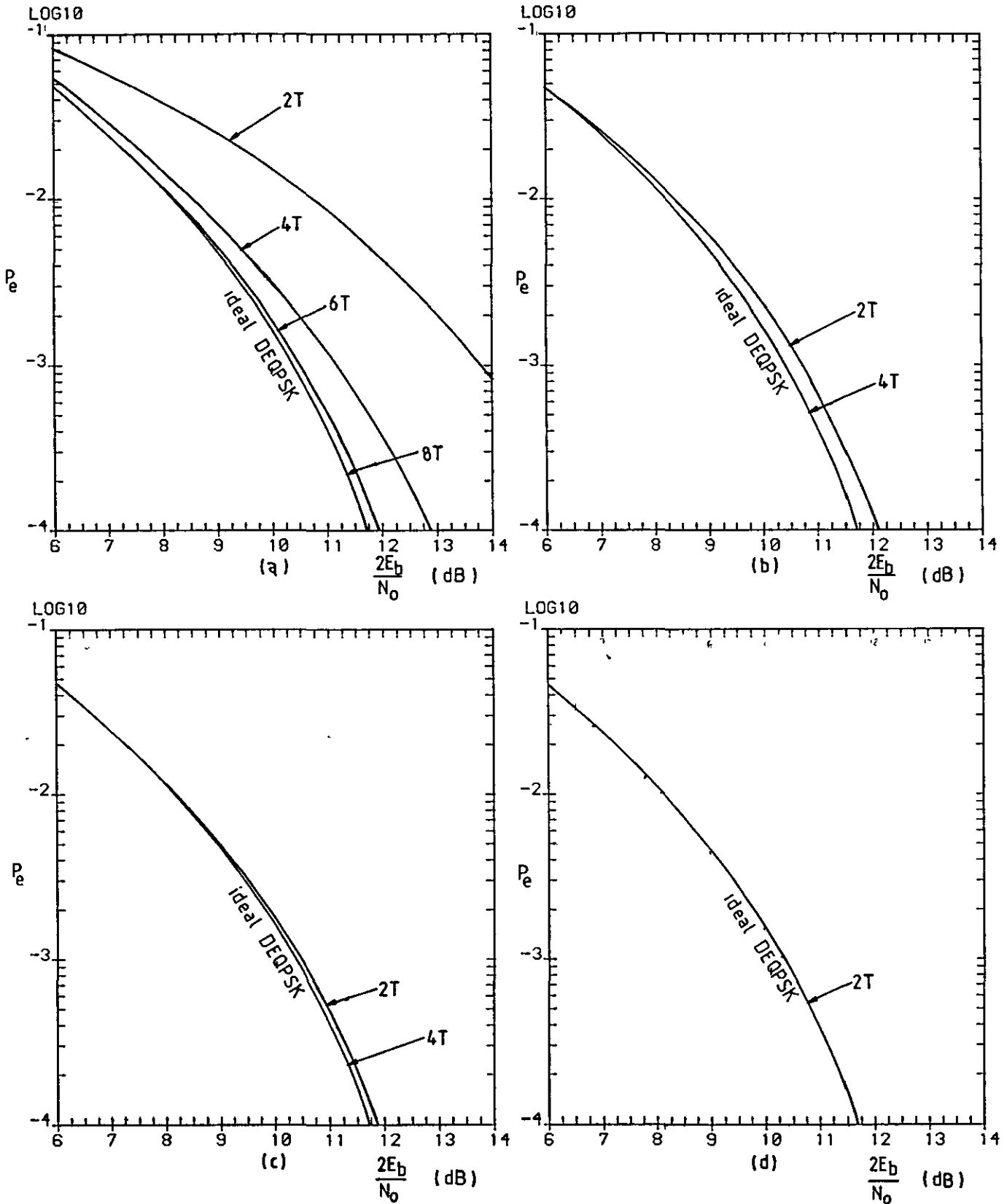


Figure 3.8 Error-rate performances of DEQPSK signals for different truncation lengths of the sampled impulse responses (Table 2.1) of the modulation and demodulation filters with β (a) =25%, (b) =50%, (c) =75% and, (d) =100%.

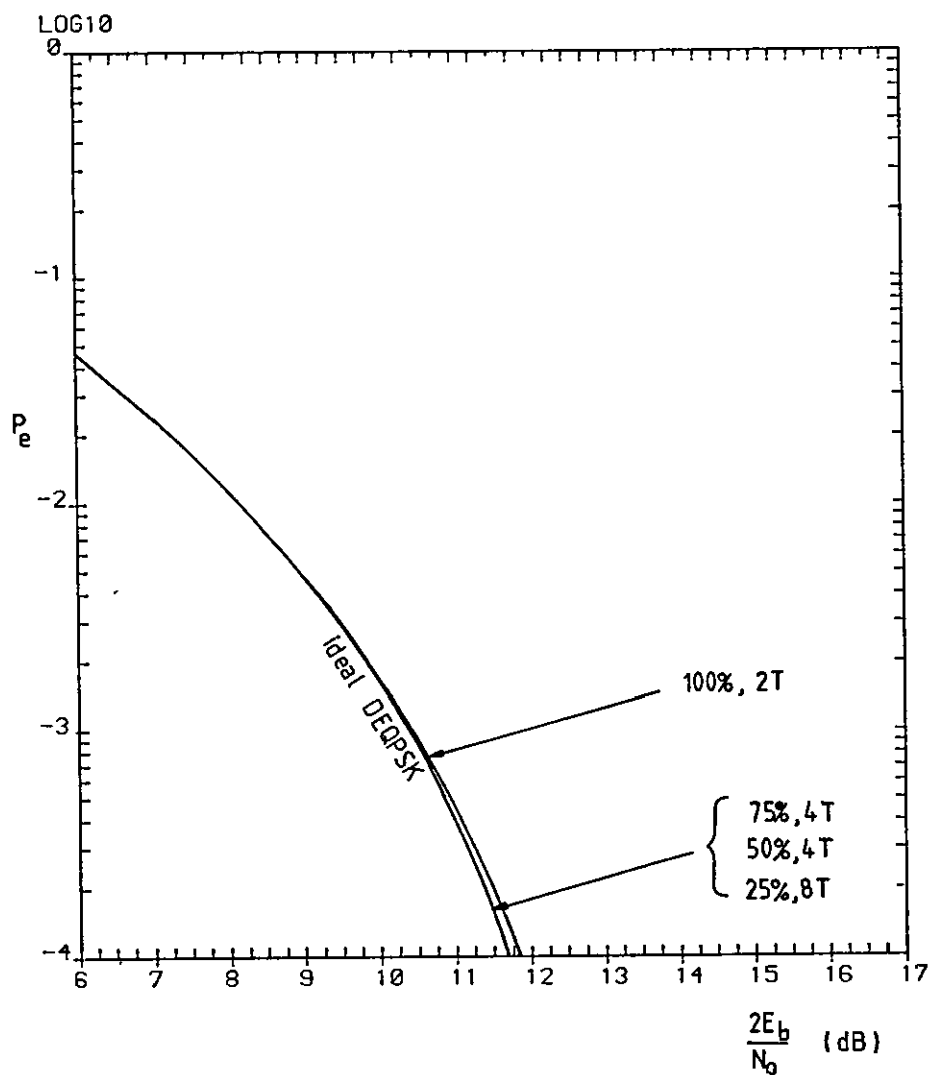
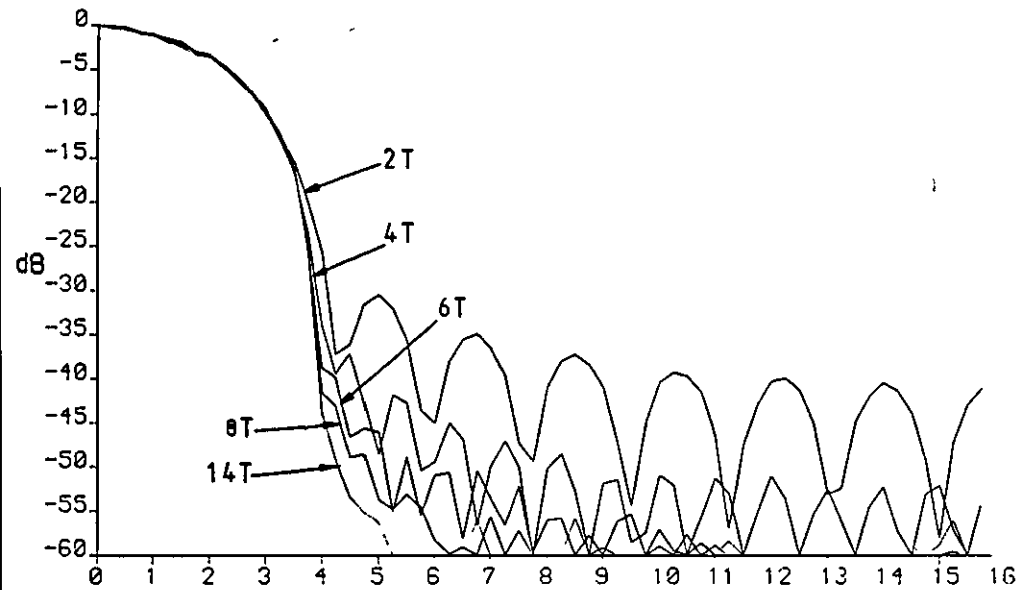
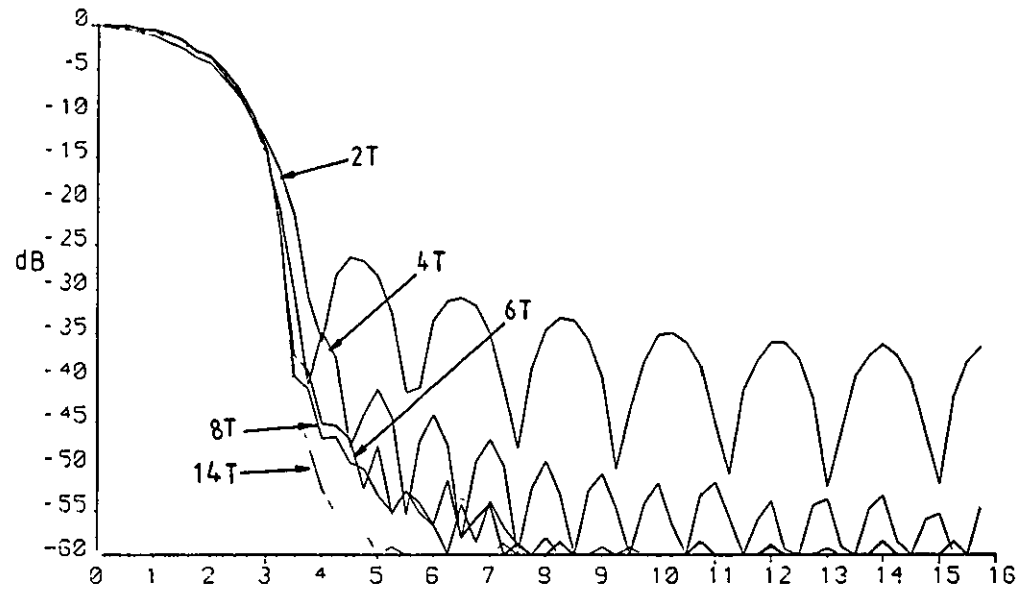


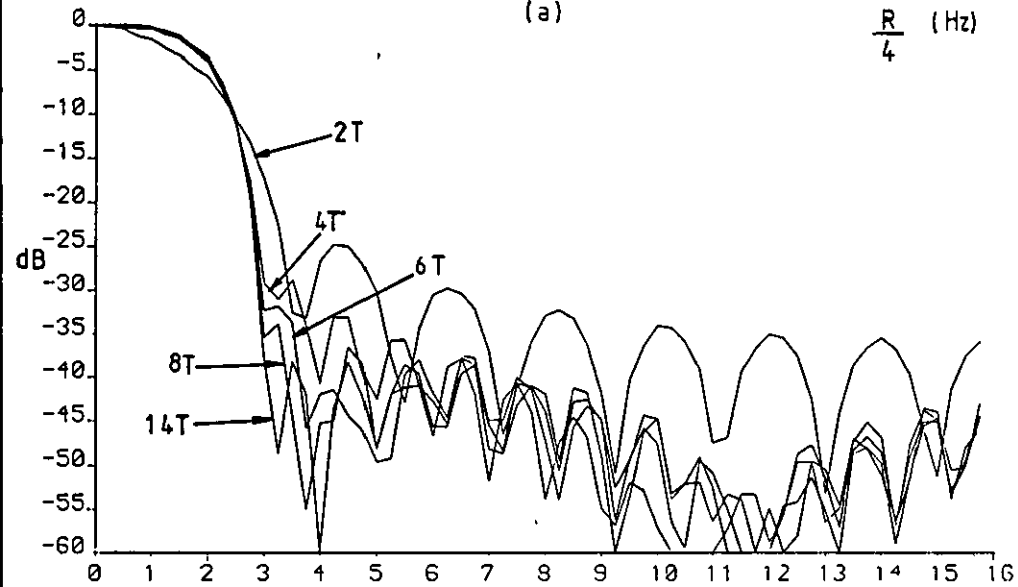
Figure 3.9 Error-rate performances of DEQPSK signals over a linear and bandlimited bandpass channel. The truncation lengths of 2T, 4T, 4T and 8T are used in the sampled impulse responses of the modulation and demodulation filters with $\beta=100\%$, 75%, 50% and 25%, respectively.



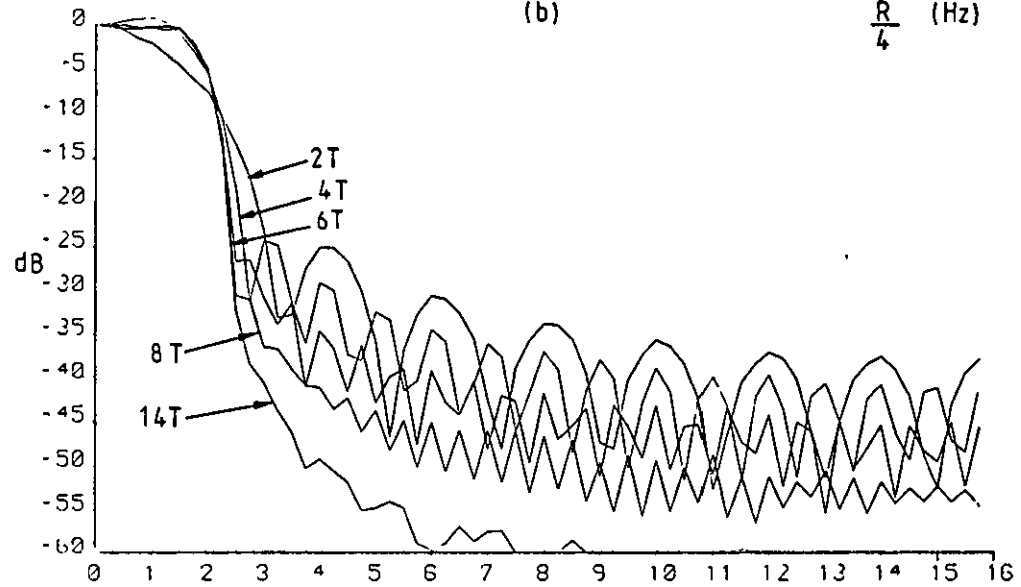
(a)

 $\frac{R}{4}$ (Hz)

(b)

 $\frac{R}{4}$ (Hz)

(c)

 $\frac{R}{4}$ (Hz)

(d)

 $\frac{R}{4}$ (Hz)

Figure 3.10 Power spectral densities of the baseband DEQPSK signals for different truncation lengths of the sampled impulse responses of the modulation filters with β (a) = 100%, (b) = 75%, (c) = 50% and (d) = 25%.

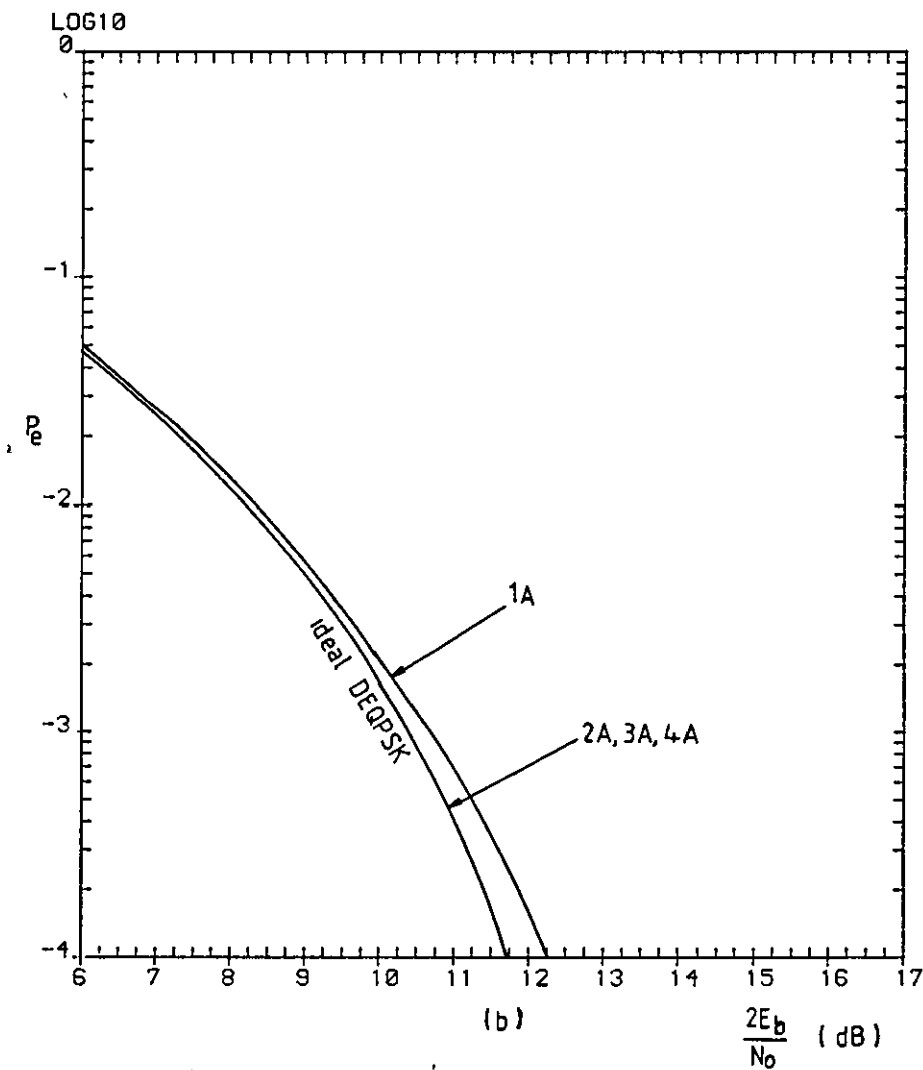
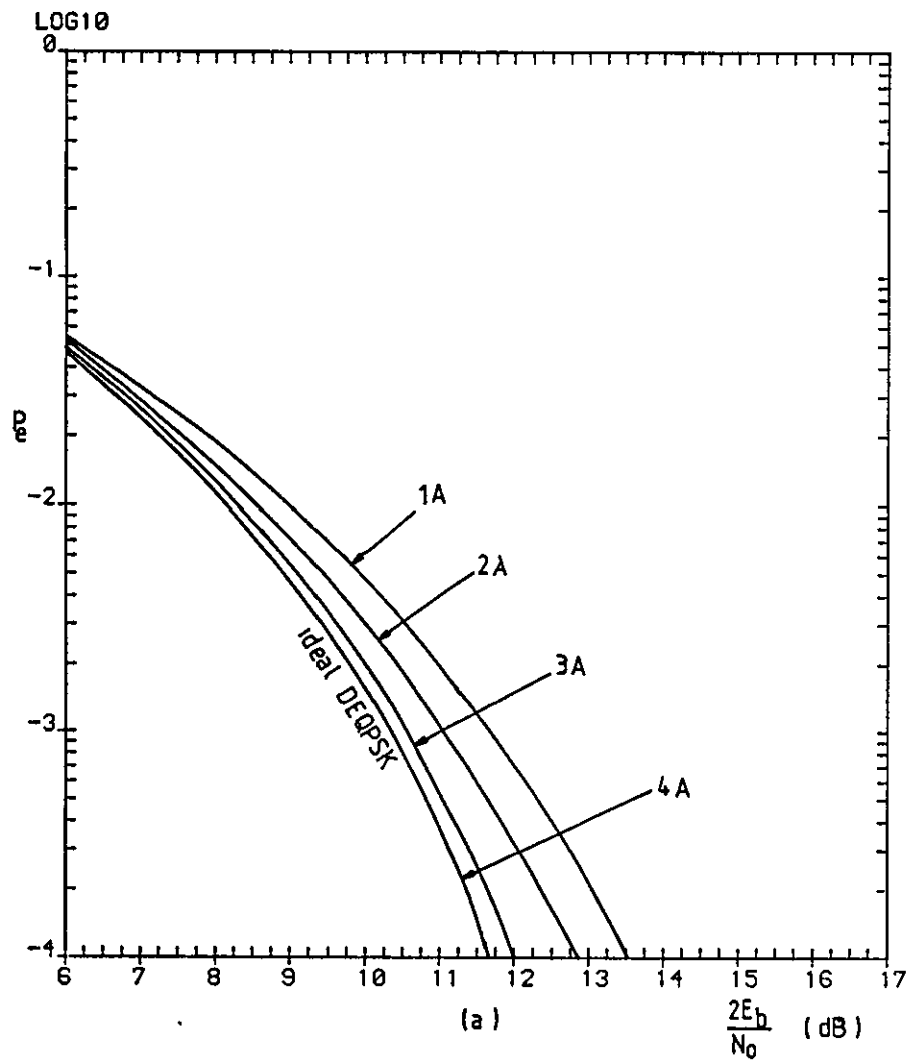


Figure 3.11 Error-rate performances of signals 1A, 2A, 3A and 4A over a linear channel and in an ACI environment, with the channel spacing $f_c =$ (a) $=5R/4$ Hz and (b) $=5.5R/4$ Hz.

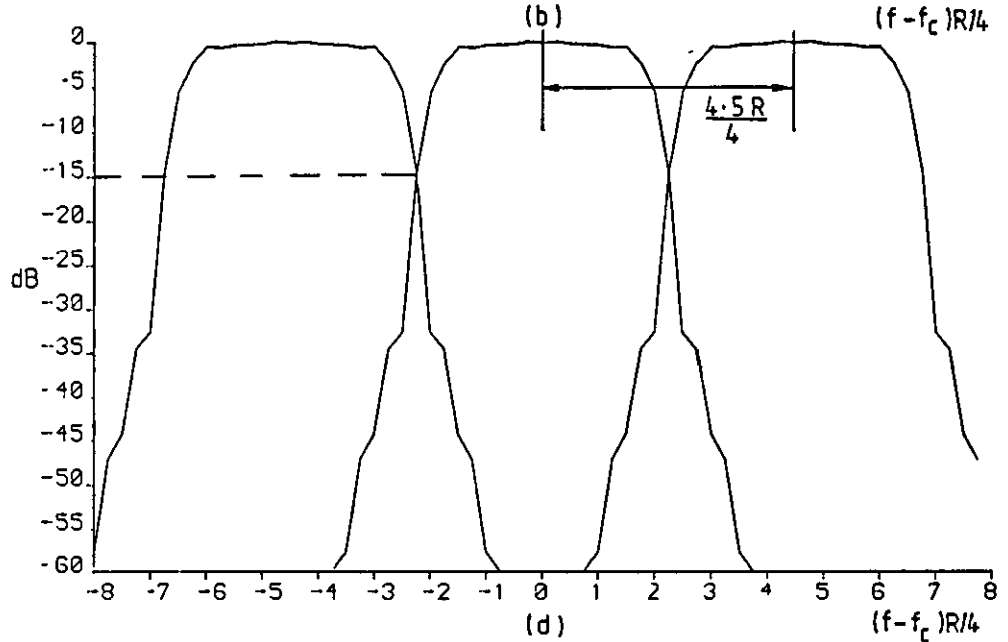
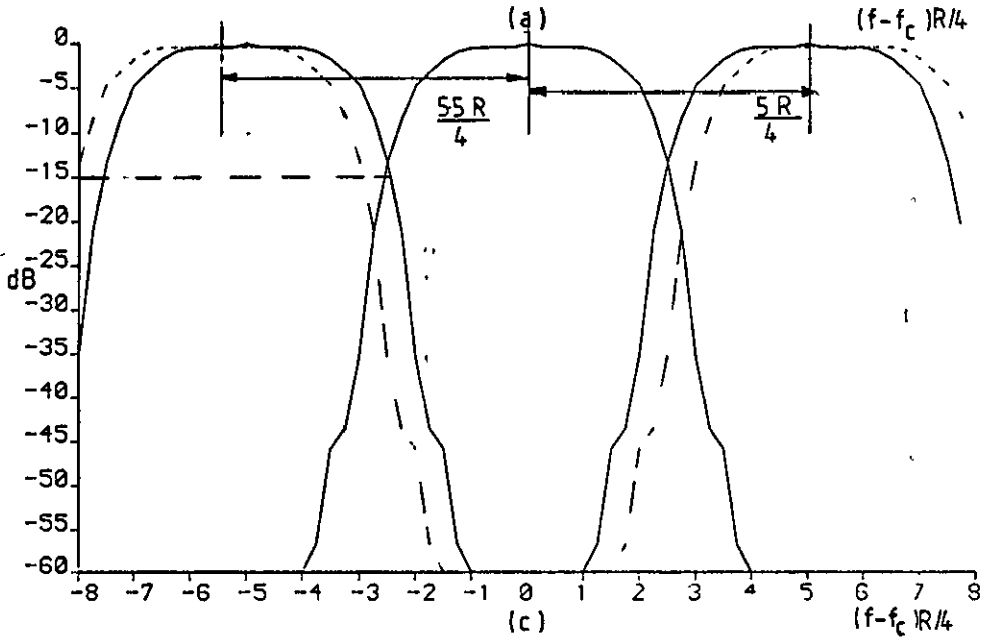
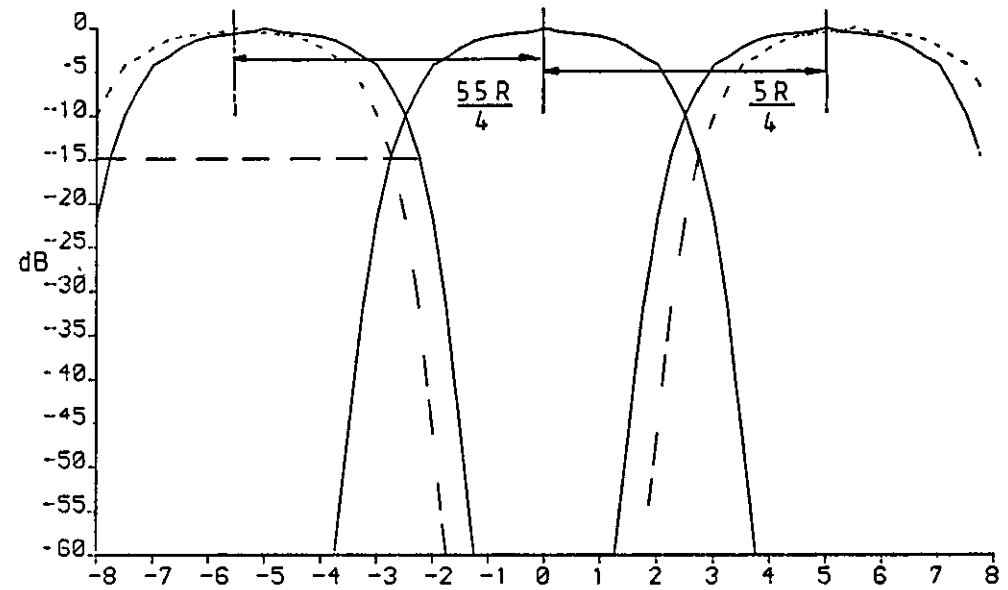
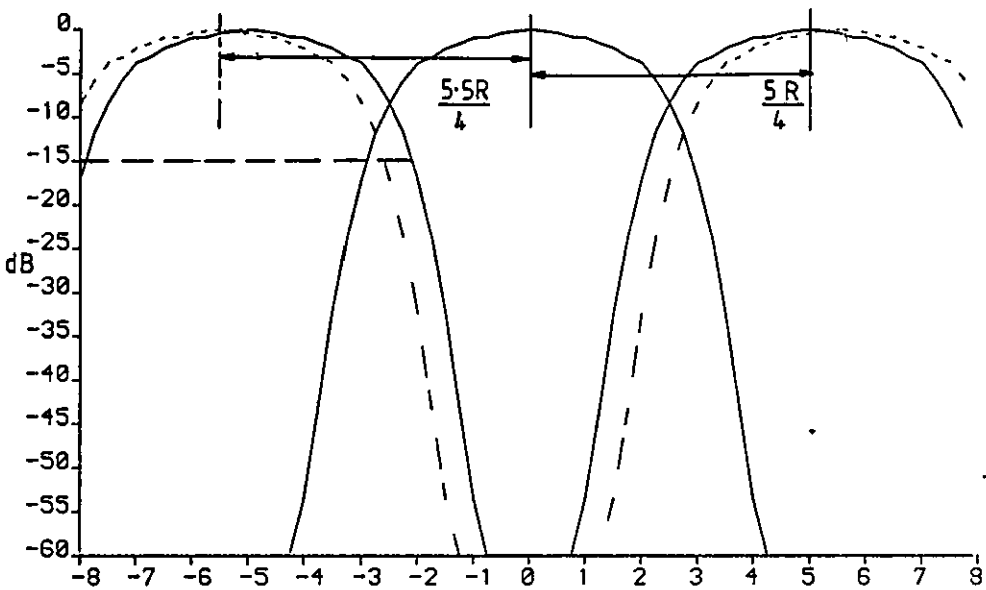


Figure 3.12 Transmitted spectral power densities of signals (a) 1A, (b) 2A, (c) 3A and (d) 4A in different ACI environments.

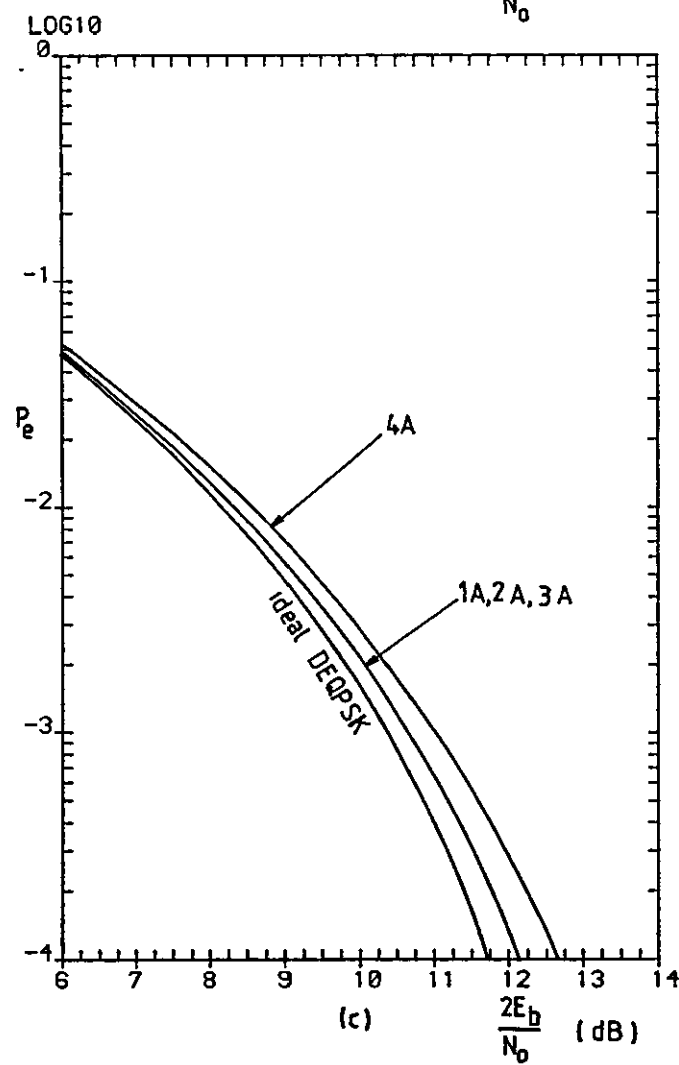
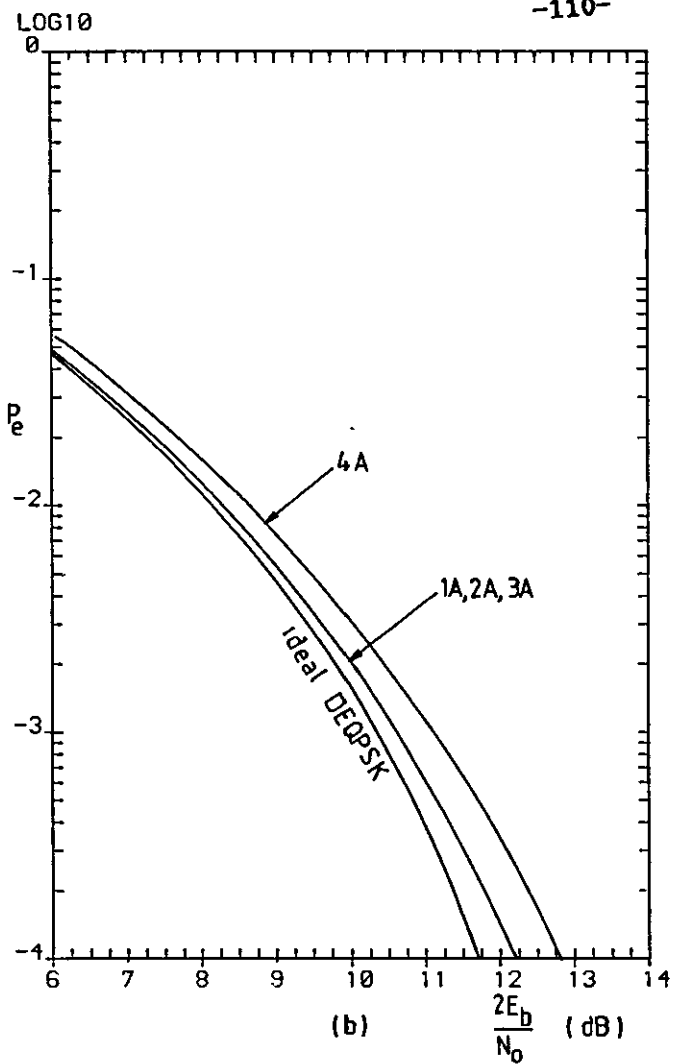
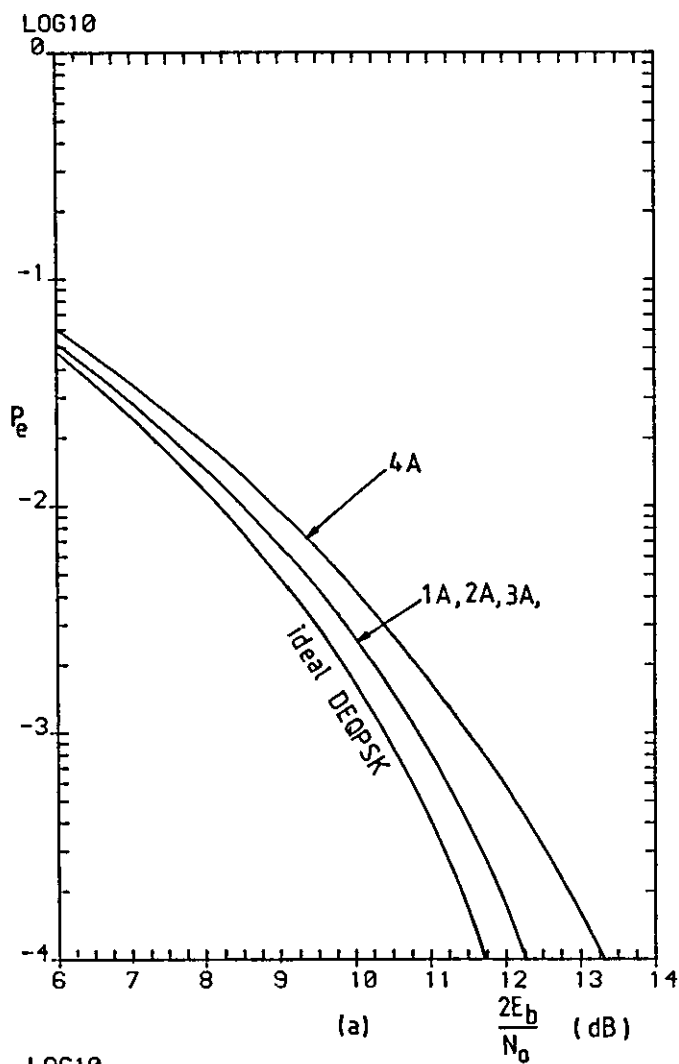


Figure 3.13 Error-rate performances of signals 1A, 2A, 3A and 4A, over a nonlinear and bandlimited channel, with the HPA operating at (a) 0 dB, (b) 0.2 dB and, (c) 0.68 dB OBO, respectively, and in a non-ACI environment.

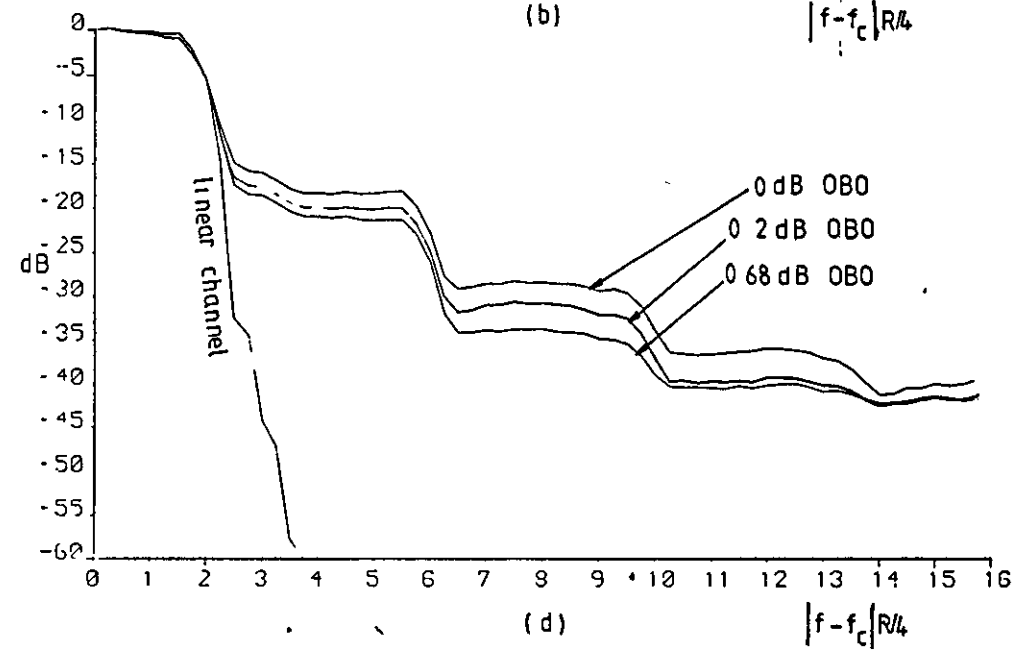
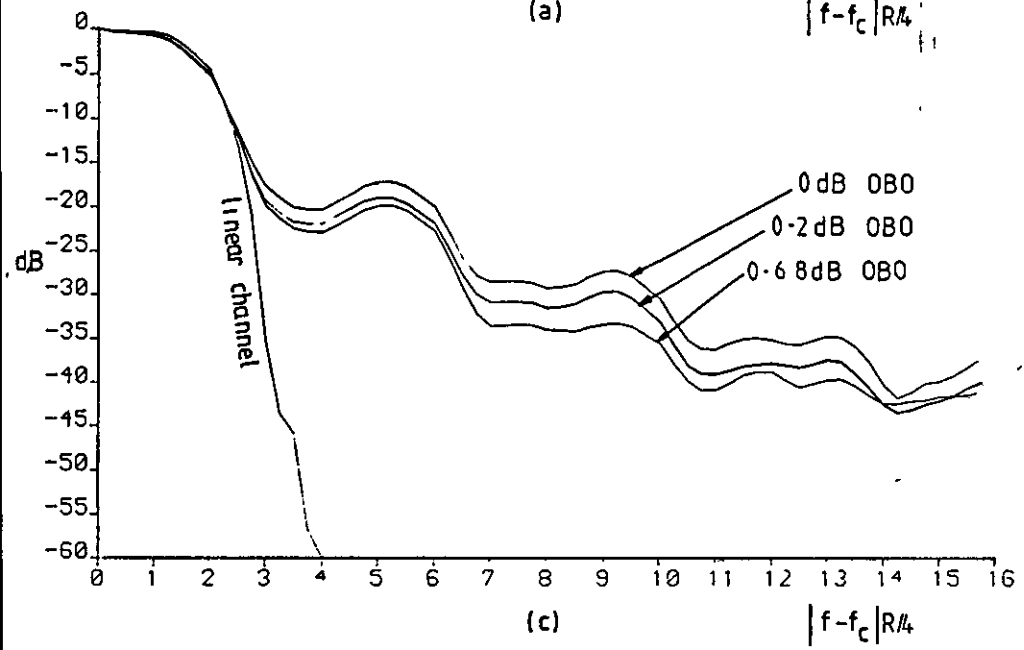
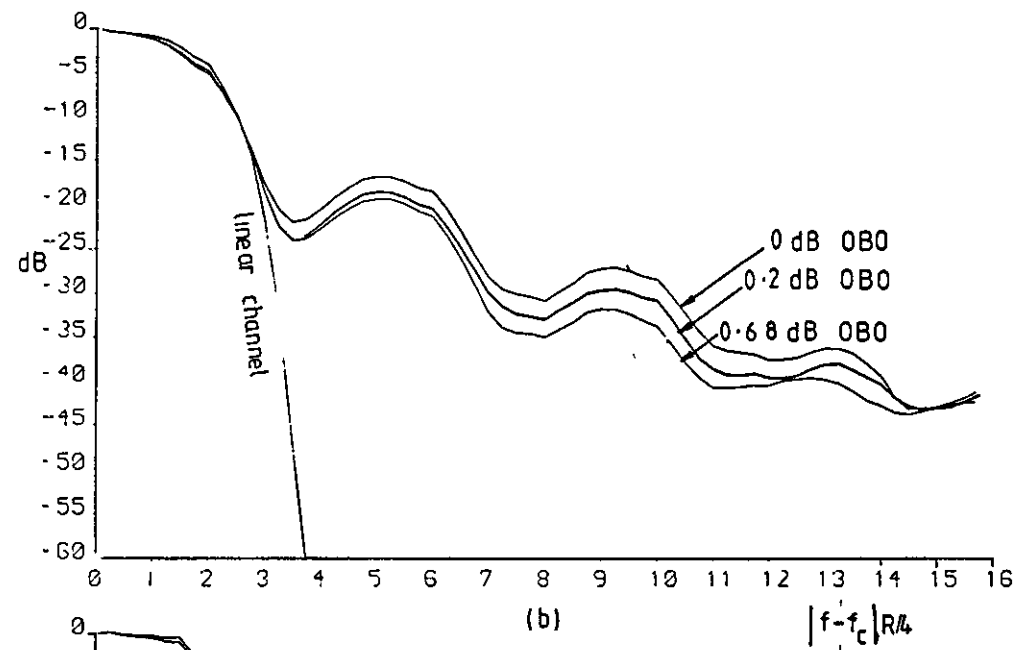
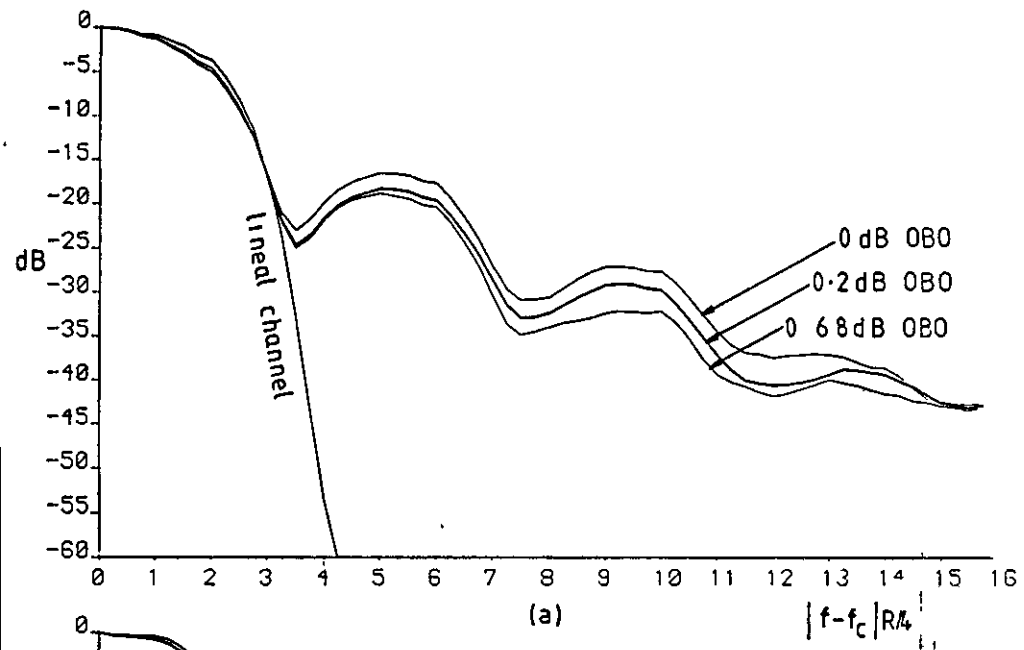


Figure 3.14 Power spectral densities of signals (a) 1A, (b) 2A, (c) 3A and, (d) 4A at the output of the HPA. The transmitted signal spectral power density over a linear channel are also shown for comparison.

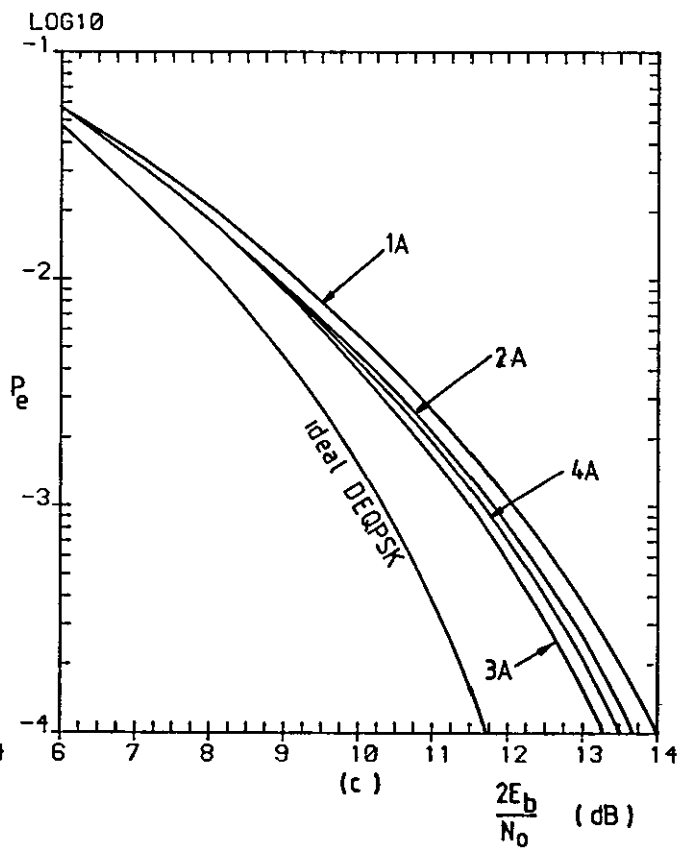
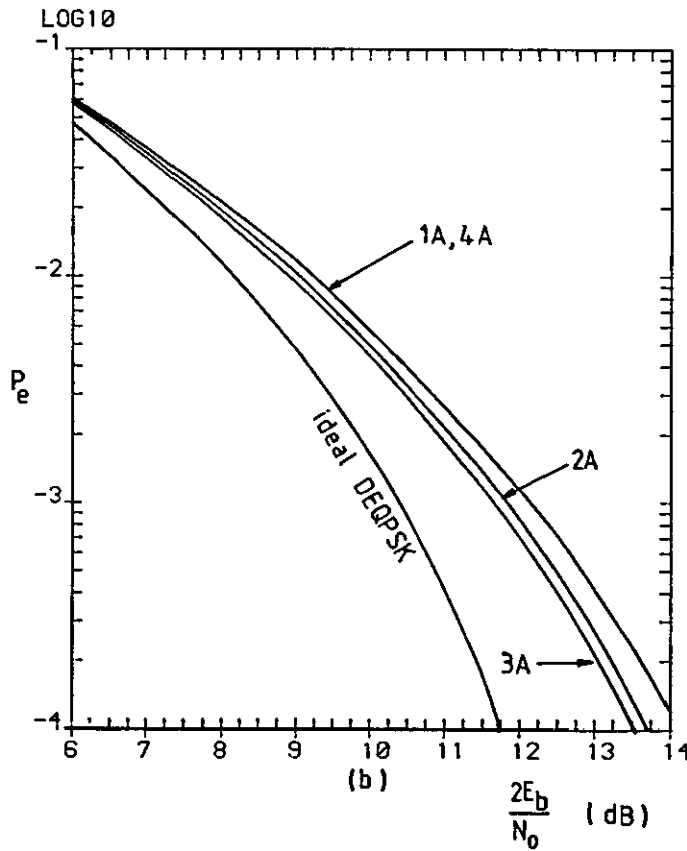
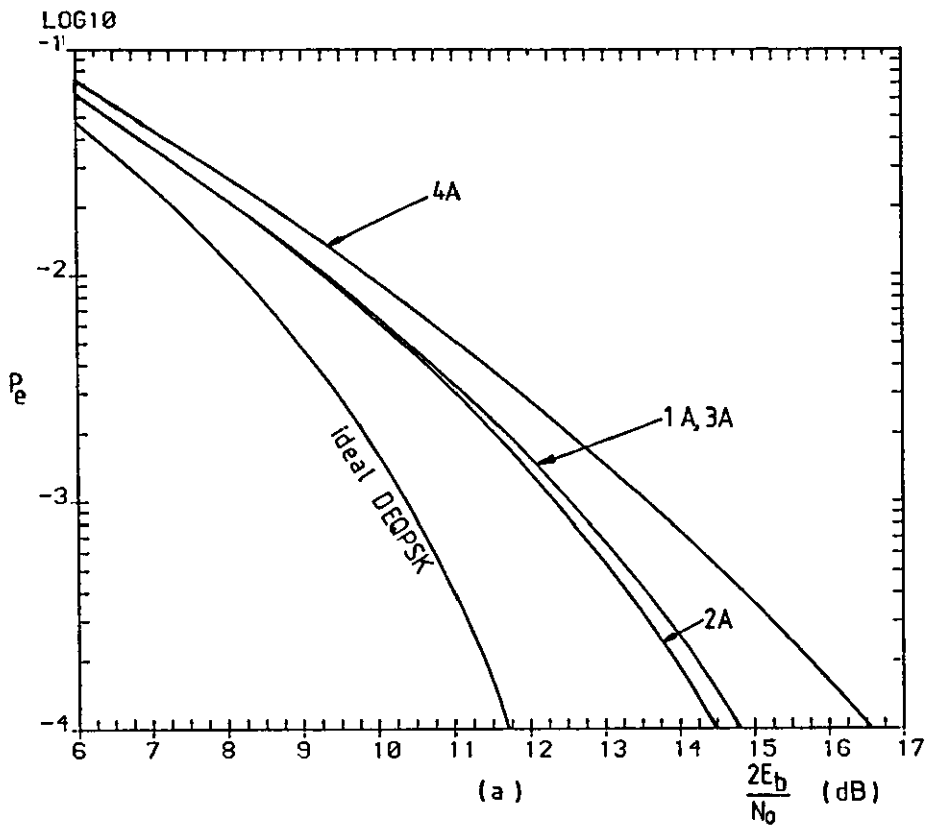


Figure 3.15 Error-rate performances of signals 1A, 2A, 3A and 4A, over a nonlinear channel, with the HPA operating at (a) 0, (b) 0.2 and (c) 0.68 dB CBO and in an ACI environment with the channel spacing $f_{ca} = 5R/4$ Hz.

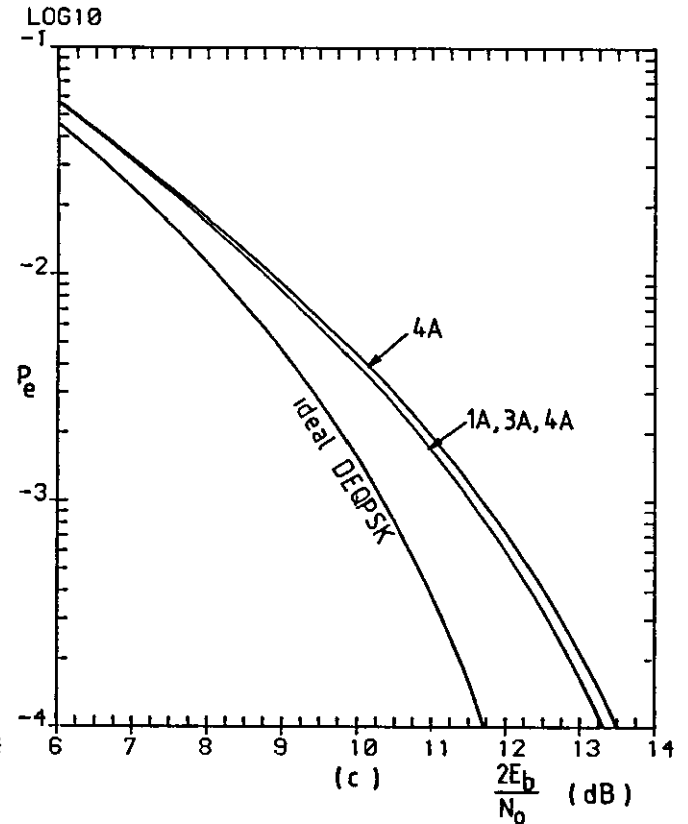
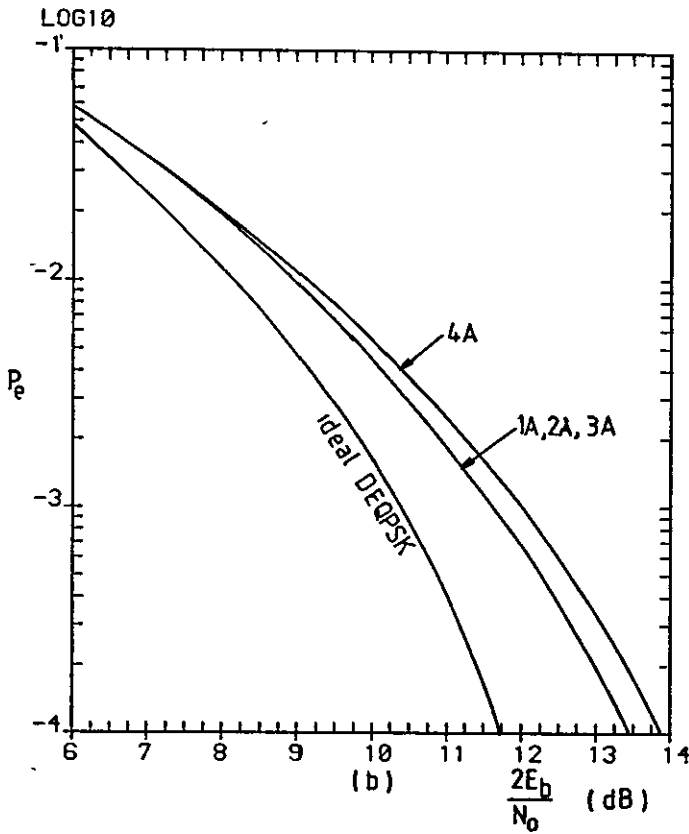
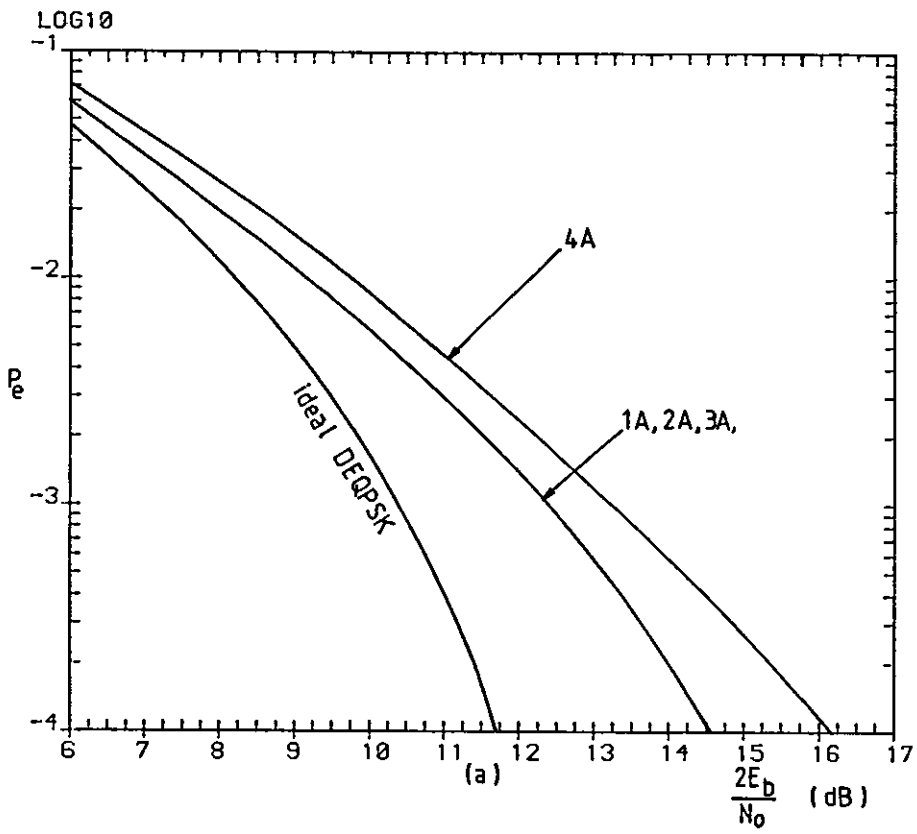


Figure 3.16 Error-rate performances of signals 1A, 2A, 3A and 4A, over a nonlinear channel, with the HPA operating at (a) 0, (b) 0.2 and (c) 0.68 dB OBO and in an ACI environment with the channel spacing $f_{ca} = 5.5R/4$ Hz.

CHAPTER 4

CONVOLUTIONALLY ENCODED COHERENT 8 PHASE-SHIFT KEYING (CE8PSK) SYSTEM [1],[2] OVER A LINEAR OR NONLINEAR SATELLITE CHANNEL

4.1 Introduction

Differentially encoded coherent quaternary phase-shift keying (DEQPSK) is currently the prevalent modulation technique proposed for digital satellite communications. When the information bit rate is limited by power considerations, forward-error-correction (FEC) coding may be used to decrease the power requirement necessary to achieve a desired tolerance to noise. The coded redundancy needed for error correction represents a bandwidth sacrifice in that the ratio of required bandwidth to information bit rate is increased by the use of FEC coding. Hence, the tradeoff is reduced bandwidth efficiency for increasing power efficiency.

Since modulation and FEC coding are intimately related, bandwidth and power can be utilized more effectively by combining these two functions. Correlative phase-shift keying (CORPSK) [3] is an example of this, and is sometimes referred to as coded trellis signalling. For M-ary PSK communications, the signal trellis is a phase trellis, and the unified signalling technique is categorized as coded phase modulation (CPM). Convolutionally encoded 8 phase-shift keying (CE8PSK) [1],[2] is an example of the latter. With CPM, the number M of phase positions may be increased to provide the redundancy for FEC coding without sacrificing bandwidth efficiency. With CE8PSK techniques, the phase is constrained to allow only four possible phase changes during each symbol interval.

4.1.1 Convolutional encoding [4],[5],[6],[7]

A convolutional encoder is shown in Fig. 4.1. It consists of a K-stage shift register, n modulo-2 adders, a commutator, and a set of connections between the K-stage shift register and the n modulo-2 adders. The input

data to the encoder is shifted into and along the shift register, k bits at a time. The outputs of the modulo-2 adders, determined by the connections to the shift register, are then sampled in turn by the commutator to produce n output bits. Consequently, the code rate is defined as k/n . The parameter K is called the constraint length of the convolutional code.

4.1.2 Convolutional FEC codes of rate 2/3 for 8PSK signal

Coding gain is the reduction in signal/noise power ratio required for providing a specified error-rate performance. It is used as the main performance measure for FEC coding. In the case of CE8PSK signals, coding gain can be expressed relative to the signal/noise power ratio requirement of an uncoded QPSK signal. As $P_e \rightarrow 0$ at high signal/noise power ratio, the reduction in required signal/noise power ratio is referred to as the asymptotic coding gain. The coding gain for practical values of P_e (e.g., at $P_e=10^{-3}$) is smaller than the asymptotic value.

Table 4.1 lists the two best codes discovered [1],[2] so far with 4 and 6-bits memory for CE8PSK signals, with asymptotic coding gains of 4.1 dB and 5 dB, respectively, for an AWGN channel. Hui et al [2] carried out a computer simulation study to evaluate the performances of these two codes over an AWGN channel using Viterbi-algorithm decoding. The results, as shown in Fig. 4.2, show that Code 2 gains the advantage of only 0.5 dB in tolerance to AWGN over Code 1, for practical values of P_e (i.e., $P_e=10^{-3} - 10^{-4}$). Since Code 1 requires 16 vectors of storage in the Viterbi decoder, whereas Code 2 requires 64 vectors, Code 1 is more cost effective and so is studied in this thesis.

4.2 Description of a convolutionally encoded coherent 8PSK (CE8PSK) system

The block diagram of a convolutionally encoded coherent 8PSK system is shown in Fig. 4.3. The information to be transmitted is carried by the

sequence of binary data-symbols $\{\alpha_n\}$. Each data symbol therefore carries one bit of information. The S/P (serial-to-parallel) converter converts the sequence $\{\alpha_n\}$ into two sequences of binary symbols $\{u_i^{(1)}\}$ and $\{u_i^{(2)}\}$, where $u_i^{(j)} = 0$ or 1 for $j=1,2$. The relationship between the input data sequence $\{\alpha_n\}$ and the binary sequences $\{u_i^{(1)}\}$ and $\{u_i^{(2)}\}$ is exactly the same as that in the case of the QPSK system described in Section 3.1.1 (Figure 3.2). The two sequences $\{u_i^{(1)}\}$ and $\{u_i^{(2)}\}$ are input to the convolutional encoder in pairs with a code rate $2/3$.

The representation of the code generator for Code 1 is shown in Fig. 4.4, which consists of a pair of sub-generators. One of the pair, associated with the input sequence $\{u_i^{(1)}\}$, has been labelled G1, while the other one, associated with the input sequence $\{u_i^{(2)}\}$, has been labelled as G2. There are three pairs of binary symbols $(u_{i-2}^{(1)}, u_{i-2}^{(2)})$, $(u_{i-1}^{(1)}, u_{i-1}^{(2)})$ and $(u_i^{(1)}, u_i^{(2)})$ used in the generator at the time $t=iT$, and each pair associated with one or more of the outputs $\{e_i^{(j)}\}$, where $j=1,2,3$. Let the pair of sub-generators G1 and G2 each have a K-stage shift register ($K=3$ for Code 1), so the code generator has a memory of $(K-1)$ symbols and the code has a constraint length of K symbols. The generator pairs are defined as follows.

$$G^{(1),j} = [g_1^{(1),j} \ g_2^{(1),j} \ g_3^{(1),j} \ \dots \ g_K^{(1),j}] \quad 4.2.1a$$

and
$$G^{(2),j} = [g_1^{(2),j} \ g_2^{(2),j} \ g_3^{(2),j} \ \dots \ g_K^{(2),j}] \quad 4.2.1b$$

specify the connection between a stage of the shift register and the j^{th} modulo-2 adder, both of which are associated with output $e_i^{(j)}$ at time $t=iT$. For the present case, there are 3 modulo-2 adders, so $j=1, 2$ or 3 . The component $g_n^{(1),j}$ is equal to 1 if the j^{th} modulo-2 adder is connected to stage n of the shift register in G1, otherwise, it is equal to 0. Again the component $g_n^{(2),j}$ is equal to 1 if the j^{th} modulo-2 adder is connected

to stage h of the shift register in G2, otherwise, it is equal to 0. The encoder determines the following quantities $(e_i^{(j)})$, for $j=1, 2, 3$.

$$e_i^{(j)} = \sum_{n=1}^K u_{i-n+1}^{(1)} g_n^{(1),j} + \sum_{n=1}^K u_{i-n+1}^{(2)} g_n^{(2),j} \quad 4.2.2$$

where the summations are modulo 2 so that $e_i^{(j)}=0$ or 1. Hence, the sequences $\{u_i^{(1)}\}$ and $\{u_i^{(2)}\}$ are encoded to give a sequence (e_i) , where e_i is a 3-component vector. At time $t=iT$, e_i has one of eight possible values given by

$$e_i = [e_i^{(1)} \quad e_i^{(2)} \quad e_i^{(3)}] \quad 4.2.4$$

where $e_i^{(j)}=1$ or 0 for $j=1, 2, 3$.

The Gray encoder, in Fig. 4.3, encodes each of the vectors in (e_i) according to Table 4.2, and gives two output sequences $\{q_i^{(1)}\}$ and $\{q_i^{(2)}\}$, where $q_i^{(j)}=\pm 0.924$ or ± 0.383 for $j=1,2$. These two sequences are used to form the corresponding sequences of impulses $\{\sum_i q_i^{(1)} \delta(t-iT)\}$ and $\{\sum_i q_i^{(2)} \delta(t-iT)\}$, at the input of the modulation filter, and hence to produce two baseband modulating waveforms

$$a(t) = \sum_i q_i^{(1)} h_t(t-iT) \quad 4.2.4a$$

and
$$b(t) = \sum_i q_i^{(2)} h_t(t-iT) \quad 4.2.4b$$

where $h_t(t)$ is the impulse response of the modulation filter with the transfer function of $H_t(f)$. $a(t)$ and $b(t)$ are called the inphase and quadrature baseband signals. These signals are then quadrature modulated, as described in Section 2.6, and added linearly to give the convolutionally encoded 8PSK (CE8PSK) signal

$$S(t) = \sqrt{2}a(t)\cos\omega_c t - \sqrt{2}b(t)\sin\omega_c t \quad 4.2.5$$

with ω_c the carrier frequency in rad/s. The resultant signal is then fed into the bandpass transmission channel. Assume that the bandpass transmission channel introduces no attenuation, delay or distortion, but

that it adds a Gaussian noise waveform, $N(t)$, to the transmitted signal, so that the channel is exactly the same as the one used in the QPSK system described in Section 3.1.1. At the input of the demodulator, the signal is

$$r(t) = \sqrt{2}[a(t)\cos\omega_c t - b(t)\sin\omega_c t] + N(t) \quad 4.2.6$$

where $N(t)$ is a sample function of a Gaussian random process with zero mean and a two-sided power spectral density of $\frac{1}{2}N_0$ over the signal frequency band. Assume that the bandwidth of $N(t)$ is small compared with its carrier frequency ω_c rad/s, so Eqn. 4.2.6 can be written [8] as

$$r(t) = [\sqrt{2}a(t)+N_c(t)]\cos\omega_c t - [\sqrt{2}b(t)+N_s(t)]\sin\omega_c t \quad 4.2.7$$

as can be seen from Eqn. 3.1.4, where $N_c(t)$ and $N_s(t)$ are sample functions of Gaussian random processes, with zero mean and a two-sided power spectral density twice that of $N(t)$ (Appendix A7).

It is shown, in Section 3.1.1, that under these conditions, the inphase and quadrature baseband signal components plus noise, at the demodulation filter output, are (Eqns. 3.1.7a and b)

$$r^{(1)}(t) = \sum_i q_i^{(1)}h(t-iT) + v^{(1)}(t) \quad 4.2.8a$$

and
$$r^{(2)}(t) = \sum_i q_i^{(2)}h(t-iT) + v^{(2)}(t) \quad 4.2.8b$$

respectively, where $h(t)$ is the inverse Fourier transform of $H(f)$, which is the transfer function of the modulation and demodulation filters in cascade. Also $v^{(1)}(t)$ and $v^{(2)}(t)$ are filtered Gaussian noise waveforms. Bear in mind that the bandpass channel introduces no attenuation, delay or distortion.

Assume that the modulation and demodulation filters have the same characteristics, and the combined transfer function is a sinusoidal rolloff frequency response (Eqn. 2.2.3) with a linear phase characteristic, so that $h(0)=1$ and $h(iT)=0$, for all values of the integer i other than $i=0$. The signals $r^{(1)}(t)$ and $r^{(2)}(t)$ have no ISI at the time

instants $\{iT\}$. Assume also that the receiver provides the ideal required timing signal, so the two baseband waveforms, $r^{(1)}(t)$ and $r^{(2)}(t)$, at the demodulation filter output are sampled at the time instants $\{iT\}$, to give two sequences of sample values $\{r_i^{(1)}\}$ and $\{r_i^{(2)}\}$ to the decoder. At time $t=iT$, the samples are (Eqn. 3.1.8)

$$r_i^{(1)} = q_i^{(1)} + v_i^{(1)} \quad 4.2.9a$$

and
$$r_i^{(2)} = q_i^{(2)} + v_i^{(2)} \quad 4.2.9b$$

where $v_i^{(1)}$ and $v_i^{(2)}$ are sample values of Gaussian random variables with zero mean and fixed variance σ^2 , the $\{v_i^{(1)}\}$ and $\{v_i^{(2)}\}$ being statistically independent and independent also of the $\{\alpha_L\}$.

The received samples $\{r_i^{(1)}\}$ and $\{r_i^{(2)}\}$ are fed to the decoder which produces at its output the sequence of symbols $\{\hat{\alpha}_L\}$ which forms the sequence of decoded data symbols. In the absence of noise, the $\{\hat{\alpha}_L\}$ are the same as the $\{\alpha_L\}$. The aim of the decoder is to generate the sequence $\{\hat{\alpha}_L\}$ such that the corresponding sequences $\{q_i^{(1)}\}$ and $\{q_i^{(2)}\}$, which would have been transmitted in response to the given $\{\alpha_L\}$ at the transmitter input, are at the minimum resultant (total) unitary distance from the received sequences $\{r_i^{(1)}\}$ and $\{r_i^{(2)}\}$ [9].

In the absence of noise, Eqn. 4.2.9 becomes

$$r_i^{(1)} = q_i^{(1)} = \pm 0.924 \text{ or } \pm 0.383 \quad 4.2.10a$$

and
$$r_i^{(2)} = q_i^{(2)} = \pm 0.924 \text{ or } \pm 0.383 \quad 4.2.10b$$

The eight possible received signals vectors (signal constellation) are shown in Fig. 4.5. It can be seen that CE8PSK signals have eight distinct possible phases, $\pm\pi/8$, $\pm 3\pi/8$, $\pm 5\pi/8$ and $\pm 7\pi/8$ radians

4.3 Baseband equivalent model of CE8PSK system, with a linear or nonlinear satellite channel, for computer simulation

The CE8PSK system considered here operates at a speed of 64, 128, 256 or 512 kbit/s over a satellite link. Since CE8PSK signals use a quadrature modulation technique, the system can be greatly simplified by assigning real values to the signals in one of the two parallel channels (that associated with $\sqrt{2}\cos\omega_c t$) and imaginary values to the signals in the other channel, and then considering the linear modulator, the transmitter IF filter, the HPA, the receiver IF filter and the linear demodulator, as a baseband transmission path carrying complex-valued signals. The resultant system is shown in Fig. 4.6. The information to be transmitted is carried by the sequence of binary data-symbols $\{\alpha_n\}$, where the $\{\alpha_n\}$ are taken to be statistically independent and equally likely to have the possible values of 0 or 1. The encoded symbols $\{q_n\}$ are obtained from the $\{\alpha_n\}$, by the encoder, after being S/P converted, convolutionally encoded and then Gray encoded (Section 4.2). The i^{th} symbol has the value

$$q_i = (\pm 0.924 \pm j0.383) \text{ or } (\pm 0.383 \pm j0.924) \quad 4.3.1$$

where $j = \sqrt{-1}$, the $\{q_i\}$, of course, being statistically independent and equally likely to have any of the eight possible values. The sequence $\{q_i\}$ is used to form the corresponding sequence of impulses $\{\sum_i q_i \delta(t-iT)\}$ at the input of the modulation filter. The signal waveform at the output of the modulation filter is the complex-valued baseband signal

$$u(t) = \sum_i q_i h_c(t-iT) \quad 4.3.2$$

where $h_c(t)$ is the impulse response of the modulation filter and, at any given value of t , is real (Section 2.4.1).

Similar to the system described in Section 3.3, the system is modelled digitally for computer simulation. The continuous waveforms are modelled as discrete waveforms. The waveform $u(t)$ is sampled 8 samples per symbol,

at the time instants $\{mT_m\}$, where $T=8T_m$, to give the sequence $\{u_m\}$, where $u_m = u(mT_m)$. The $\{u_m\}$ are then fed to a baseband equivalent model of one of the bandpass channels, as shown in Fig. 4.6. As with the DEQPSK systems described in Section 3.3, three different bandpass channels are considered here. They are (a) linear and memoryless bandpass, (b) linear and bandlimited bandpass and, (c) nonlinear and bandlimited bandpass channels (Section 2.6). For the description of the processing of the samples $\{u_m\}$ in the baseband equivalent model of these three channels and for the calculation of $2E_b/N_0$ in the simulation tests, see Section 3.3.

The sampled signal $\{w_m\}$ (given by Eqn 3.3.2, 3.3.6 or 3.3.9, depending on which channel is used), from the baseband equivalent model of any one of the bandpass channels, are filtered by the demodulation filter. The sampled impulse response of the demodulation filter, sampled at the rate of $1/T_m$ samples per second, is given by the $(n+1)$ -component vector

$$P = [p_0 \quad p_1 \quad p_2 \quad \dots \quad p_n] \quad 4.3.3$$

where the $\{p_m\}$, for $0 \leq m \leq n$, have real-valued components (Table 2.1), and $p_m = p(mT_m)$. Thus, at time $t = mT_m$, the signal sample at the filter output is

$$r_m = \sum_{n=0}^n w_{m-n} p_n \quad 4.3.4$$

where r_m has a complex value.

Assume that the receiver provides the required ideal timing signal, so the signal is sampled once per symbol, at the time instants $\{iT\}$, to give the sequence $\{r_i\}$, where r_i has a complex value. The $\{r_i\}$ are fed to the decoder which produces at its output the sequence of symbols $\{\hat{\alpha}_i\}$ which form the sequence of decoded binary-data symbols. These decoded symbols $\{\hat{\alpha}_i\}$, having the minimum probability of being incorrect, form the possible sequence of data symbols at the input to the transmitter for which there is minimum mean-square difference (minimum unitary distance squared) [10] between the corresponding received sequence of $\{q_i\}$ in the absence of

noise and the samples $\{r_i\}$ actually received [11]. Thus, under these conditions, minimum-distance decoding minimises the probability of error in decoding the received signal. In the absence of noise, the $\{\hat{\alpha}_L\}$ are the same as the $\{\alpha_L\}$ at the input to the encoder at the transmitter.

When the $\{r_i\}$ are fed to the decoder, the decoder forms and stores a set of $m=2^L$ vectors (sequences) $\{X_L\}$, where

$$X_L = [x_1 \quad x_2 \quad x_3 \quad \dots \quad x_L] \quad 4.3.5$$

and $x_h=0$ or 1 , for $h=1, 2, \dots, L$. x_h here represents a possible value of α_h . For each stored vector X_L the decoder forms the vector

$$Y_i = [y_1 \quad y_2 \quad y_3 \quad \dots \quad y_i] \quad 4.3.6$$

where $i=L/2$ (because a coded-symbol is transmitted for each pair of data symbols). The $\{y_h\}$, for $h=1, 2, \dots, i$, have complex values, and Y_i would have been transmitted in place of the sequence of the $\{q_i\}$ had the vector X_L been fed to the encoder at the transmitter in place of the vector

$$\alpha_L = [\alpha_1 \quad \alpha_2 \quad \alpha_3 \quad \dots \quad \alpha_L] \quad 4.3.7$$

that was actually sent. The ISI introduced by the channel is neglected in the decoding process in order to reduce the equipment complexity of the decoder. (This assumption is valid because the IF filters only introduce a low level of ISI, as is shown in Section 3.7.2.) The decoder then forms and stores together with each X_L , the corresponding distance measure

$$C_i = c_1 + c_2 + c_3 + \dots + c_i \quad 4.3.8$$

where for $h=1, 2, \dots, i$, $c_h=|r_h-y_h|^2$. $|r_h-y_h|$ is the absolute value of the complex value (r_h-y_h) . C_i is the square of the unitary distance between the corresponding sequences (vectors) $\{r_i\}$ and $\{y_i\}$. Whether the square of the unitary distance or the unitary distance itself is used, does not affect the basic operation of the system, so that this distance measure will be considered simply as the distance [8]. The m vectors with the minimum distances, subject to any constraints that may be applied to the possible values of some of the $\{x_h\}$.

In practice, each time a new set of m distances $\{C_i\}$ are stored, together with the corresponding m vectors $\{X_L\}$, the values of the smallest distance is subtracted from each C_i , thus setting the smallest C_i to zero. This prevents overflow in the stored values of the $\{C_i\}$, which would otherwise inevitably occur during the reception of a long message. However, to avoid unnecessarily complicating the description of the Viterbi-algorithm decoder, this modification will be neglected. Furthermore, although the distance C_i is that between the $\{r_i\}$ and the $\{y_i\}$, it will, for simplicity, be referred to as the distance of the corresponding X_L .

Ideally, no firm decision is reached as to the value of any α_n until the whole sequence $\{r_i\}$ has been received, when all $\{\alpha_n\}$ are decoded simultaneously from the received $\{r_i\}$, the decoded values $\{\hat{\alpha}_L\}$ being the values of the $\{x_n\}$ in the stored vector X_L having the smallest distance C_i . In practice, as much delay as possible is introduced before decoding (reaching a firm decision on) the value of any α_n , and now $(\hat{\alpha}_{L-2n+1}, \hat{\alpha}_{L-2n+2})$ taken as the values of (x_{L-2n+1}, x_{L-2n+2}) , respectively, in the stored vector X_L having the smallest distance C_i . The integer n is, preferably, several times greater than K (the constraint length of the code) in order to avoid a significant increase in the error probability due to taking firm decisions on the $\{\alpha_n\}$ before the whole message is received [12]. In the determination of $(\hat{\alpha}_{L-2n+1}, \hat{\alpha}_{L-2n+2})$ the decoder does not need to consider the values of $x_{L-2n}, x_{L-2n-1}, \dots$. Thus, instead of storing m L -component vectors $\{X_L\}$, the decoder stores the corresponding $2n$ -component vector $\{Z_L\}$, where

$$Z_L = [x_{L-2n+1} \quad x_{L-2n+2} \quad x_{L-2n+3} \quad \dots \quad x_L] \quad 4.3.9$$

so that Z_L is formed by the last $2n$ components of the corresponding vector X_L . The distance C_i of this vector X_L is now said to be the distance of Z_L .

4.4 Viterbi-algorithm decoder for CE8PSK signals

In the Viterbi-algorithm decoder the receiver holds in store the $m=4^{k-1}$ vectors $\{Z_L\}$ with the minimum distances corresponding to the 4^{k-1} different possible combinations of values of $x_{L-2k+3}, x_{L-2k+4}, \dots, x_L$. Thus each stored vector Z_L forms the last $2n$ components of the vector X_L that minimises C_i subject to the constraint that $x_{L-2k+3}, x_{L-2k+4}, \dots, x_L$ have the given values. It is assumed for convenience here that $L > K$. Associated with each stored vector Z_L is stored the corresponding C_i . The decoded binary data-symbols $(\tilde{\alpha}_{L-2n+3}, \tilde{\alpha}_{L-2n+4})$ are taken to be the values of (x_{L-2n+3}, x_{L-2n+4}) , respectively, in the vector Z_L associated with the smallest C_i . Following the receipt of the sample r_{i+1} , each of the stored vectors $\{Z_L\}$ forms a common part of 4 vectors $\{X_{L+2}\}$, having the four possible values of (x_{L+1}, x_{L+2}) . Each of these 4 possible vectors is associated with the corresponding distance

$$C_{i+1} = C_i + c_{i+1} \quad 4.4.1$$

where

$$c_{i+1} = |r_{i+1} - y_{i+1}|^2 \quad 4.4.2$$

and C_i is the distance of the original vector Z_L . For each of the 4^{k-1} possible combinations of values $x_{L-2k+5}, x_{L-2k+6}, \dots, x_{L+1}, x_{L+2}$, the decoder now selects the vector Z_{L+2} having the smallest C_{i+1} and stores both Z_{L+2} and C_{i+1} . $(\tilde{\alpha}_{L-2n+3}, \tilde{\alpha}_{L-2n+4})$ are taken to be the values of (x_{L-2n+3}, x_{L-2n+4}) , respectively, in the stored vector Z_{L+2} associated with the smallest C_{i+1} , and the process continues in this way.

r_{i+1} and y_{i+1} in Eqn. 4.4.2 are complex-valued and so it requires two operations of squaring or multiplication to determine each value of c_{i+1} (i.e., the unitary distance of two complex numbers). There are 4 different values of c_{i+1} to be computed for each of the m vectors $\{Z_L\}$. So that it requires altogether $8m$ operations of squaring or multiplication to determine all the possible values $\{c_{i+1}\}$. However, y_{i+1} , in Eqn. 4.4.2, has only 8 different values because it is one of the possible received

complex-valued samples (Fig. 4.5). Thus, of these $4m$ values of c_{i+1} , many have the same values. There are only 8 possible values of c_{i+1} , and each of them requires 2 operations of squaring or multiplication to determine. Therefore, following the receipt of the sample r_{i+1} , the decoder has to carry out 16 operations of squaring or multiplication to compute the 8 different values of c_{i+1} , which are used to form the $4m$ values $\{C_{i+1}\}$.

A good starting up procedure at the beginning of a transmission is to send a known sequence of $\{\alpha_L\}$, immediately correct synchronization has been achieved at the receiver, and then to set one of the m stored vectors $\{Z_L\}$ in the decoder to the correct sequence and its associated C_i to zero. The remaining vectors $\{Z_L\}$ may be set to any values, and their associated $\{C_i\}$ are all set to some very high value. After a few decoding operations, that is after a few received samples $\{r_i\}$, all the stored vectors $\{Z_L\}$ will have been derived from the original correct vector. It is not, in fact, absolutely necessary that this vector be correct, so that when the decoder has no prior knowledge of the transmitted $\{\alpha_L\}$, the vector Z_L associated with zero may be selected arbitrarily. Correct operation will now be achieved after an initial burst of errors. However, it is absolutely necessary that the receiver provides the required carrier signal with no ambiguity at the beginning of the transmission in order to decode the CE8PSK signal, otherwise, if the recovered carrier has a phase shift of $h\pi/4$, where $h=1, 2, 3, 4, 5, 6, \text{ or } 7$, then the decoder is not able to decode the receiving signal, i.e., catastrophic failure occurs. (This problem is discussed in Chapter 5.)

It can be seen that the processing of 4^K vectors and 4^K values of distances, following by the storage of 4^{K-1} $2n$ -component vectors $\{Z_L\}$ and

4^{K-1} values $\{C_i\}$, are involved in the decoding of each received pair of data $(\alpha_{L+1}, \alpha_{L+2})$. In the present case, $K=3$, it requires 16 vectors which expand into 64 vectors (i.e., each vector expands 4 ways, for 4 possible values of (x_{L+1}, x_{L+2})) to form a Viterbi-algorithm decoder at the receiver. In receiving each sample r_{i+1} , the decoder carries out two operations of squaring or multiplication to determine a value of c_{i+1} (Eqn. 4.4.2). Since there are eight possible values of y_{i+1} , the decoder has to carry out altogether 16 operations of squaring or multiplication to compute the 8 different values of c_{i+1} , which are used to form the 64 values $\{C_{i+1}\}$

4.5 Baseband equivalent model of CE8PSK system, with a linear or nonlinear satellite channel and in an ACI environment, for computer simulation

The baseband equivalent model of a quadrature modulation system, with a linear or nonlinear satellite channel in an ACI environment, is described in Section 2.6. Here the baseband equivalent model of the CE8PSK system, in an ACI environment, for computer simulation, is shown in Fig. 4.7, where there are three identical transmitters separated in frequency with a channel spacing of ω_{c_m} rad/s. This model is similar to the one shown in Fig. 3.6 (see the description in Section 3.4). $F_T(f)$ is the resultant transfer function of the modulation filter in cascade with the baseband equivalent model of the transmitter IF filter. The way to generate the equivalent baseband signals from the transmitters is exactly the same as that used for a single channel described in Section 4.3. The data, of course, in each of these three transmitters are statistically independent. As before, the system is modelled digitally for computer simulation.

The baseband equivalent of the transmitted signals from the upper, desired and lower channels with respect to the desired channel, are (Eqns. 2.6.11c, d and g)

$$\hat{s}_U(t) = [\hat{a}_U(t) + j\hat{b}_U(t)] \exp(j\omega_{c_u}t) \quad 4.5.1a$$

$$\hat{s}_D(t) = [\hat{a}_D(t) + j\hat{b}_D(t)] \quad 4.5.1b$$

and
$$\hat{s}_L(t) = [\hat{a}_L(t) + j\hat{b}_L(t)] \exp(-j\omega_{c_u}t) \quad 4.5.1c$$

as are shown in Section 2.6, where $\hat{a}_U(t)+j\hat{b}_U(t)$, $\hat{a}_D(t)+j\hat{b}_D(t)$ and $\hat{a}_L(t)+j\hat{b}_L(t)$ are the equivalent baseband signals with respect to the corresponding channels, and $j=\sqrt{-1}$. (Note that since the HPAs could be operating either in the linear or nonlinear mode, the signals could either or not be nonlinearly distorted, by the HPAs.) The signals are sampled at $1/T_s$ samples per second, at the time instants (mT_s) . At time $t=mT_s$, the signal samples are

$$\hat{s}_{U,m} = [\hat{a}_{U,m} + j\hat{b}_{U,m}] \exp(j\omega_{c_u}mT_s) \quad 4.5.2a$$

$$\hat{s}_{D,m} = [\hat{a}_{D,m} + j\hat{b}_{D,m}] \quad 4.5.2b$$

and
$$\hat{s}_{L,m} = [\hat{a}_{L,m} + j\hat{b}_{L,m}] \exp(-j\omega_{c_u}mT_s) \quad 4.5.2c$$

respectively, where $\hat{s}_{U,m}=\hat{s}_U(mT_s)$, $\hat{s}_{D,m}=\hat{s}_D(mT_s)$ and $\hat{s}_{L,m}=\hat{s}_L(mT_s)$. Thus, after adding the noise sample n_m , at time $t=mT_s$, the signal sample at the input of the desired channel receiver is

$$\hat{s}_{R,m} = \hat{s}_{U,m} + \hat{s}_{D,m} + \hat{s}_{L,m} + n_m \quad 4.5.3$$

The real and imaginary parts of all noise samples $\{n_m\}$ are taken to be statistically independent Gaussian random variables with zero mean and variance σ^2 . (See Eqn. 3.3.14 for the required value of σ to be used in simulation.)

The sampled impulse responses of the baseband equivalent model of the receiver IF filter and of the modulation filter, sampled at the rate of $1/T_m$ samples per second, are given by the $(g+1)$ -component vector

$$F = [f_0 \quad f_1 \quad f_2 \quad \dots \quad f_g] \quad 4.5.4$$

and the $(n+1)$ -component vector

$$P = [p_0 \quad p_1 \quad p_2 \quad \dots \quad p_n] \quad 4.5.5$$

respectively, where $f_m = f(mT_m)$ and $p_m = p(mT_m)$. The delay in transmission is neglected here. Thus, at time $t = mT_m$, the sample value of the received signal at the input of the detector is

$$r_m = \sum_{h=0}^n w_{m-h} p_h \quad 4.5.6$$

where

$$w_m = \sum_{h=0}^g s_{R, m-h} f_h \quad 4.5.7$$

Assume that the receiver provides the required ideal timing signal, so (r_m) is sampled once per symbol, at the time instants (iT) , to give the sequence of samples (r_i) which are fed to the Viterbi decoder (Section 4.4) which produces at its output the sequence of binary data-symbol $(\hat{\alpha}_L)$.

4.6 Performances of CE8PSK signals

An analysis method generally applicable to the derivation of the error probability for convolutional codes is not available. Most authors use lower and upper bounds for the error probability as performance criteria.

In the presence of AWGN the probability of detecting a modulated signal $m_2(t)$ when a modulated $m_1(t)$ has been sent, is given by (Appendix A9)

$$P_E = Q\left(\frac{d_{1,2}}{\sqrt{2N_0}} \right) \quad 4.6.1$$

where N_0 is the two-sided noise spectral density and $d_{1,2}$ is the Euclidean

distance between the modulated signals $m_j(t)$ and $m_i(t)$ given by

$$d_{i,j}^2 = \int_t [m_i(t) - m_j(t)]^2 dt \quad 4.6.2$$

It is well known that for low probability of error this probability is almost completely determined by the minimum Euclidean distance d_{min} between two signals corresponding to different values of the data symbols [13],[14],[15]. Hence, at a large signal/noise power ratio, the symbol error rate probability of a CE8PSK signal can be written as

$$P_e \approx Q\left(\sqrt{\frac{d_{min}^2}{2N_0}}\right) \quad 4.6.3$$

where d_{min} here is the minimum Euclidean distance between any two received signals corresponding to different data-symbol values. Thus the symbol error rate probability P_e is asymptotically determined by the minimum Euclidean distance d_{min} .

The coding gain of CE8PSK signals can be expressed as the tolerance to noise relative to that of an uncoded QPSK signal. At large signal/noise power ratio, the reduction in required signal/noise power ratio is referred to as the asymptotic coding gain, which is completely determined by the minimum Euclidean distance, as can be seen in Eqn. 4.6.3. So, if an uncoded QPSK signal has a minimum Euclidean distance of d_0 , then the asymptotic coding gain for a CE8PSK signal is equal to the square of the ratio of the minimum Euclidean distance, d_{min} of CE8PSK signal to d_0 , i.e., d_{min}^2/d_0^2 . (Note that both QPSK and CE8PSK signals carry 2 information bits per symbol.)

For the CE8PSK signal considered in this thesis (i.e., using Code 1 in Table 4.1), the value d_{min}^2/d_0^2 of the signal has been found to be 2.586 [2], and so the asymptotic coding gain is 4.1 dB. In many cases, the performance in the nonasymptotic region (e.g. $P_e=10^{-3}$ - 10^{-4}) is more important, so computer simulation tests are usually used to evaluate the

performances of CE8PSK signals. For the present case, the performance of the CE8PSK signal, using Code 1 shown in Table 4.2, over an AWGN channel, has been evaluated by computer simulation [1] and is shown in Fig. 4.2. This indicates that a coding gain of 2.6 dB, relative to an uncoded QPSK signal, can be obtained at $P_e=10^{-4}$. At sufficiently low error rates the coding gain would approach the asymptotic value.

4.7 Power spectra of CE8PSK signals

As with QPSK or DEQPSK signals, CE8PSK signals carry two information bits per symbol. If the same transmitter filtering is used, CE8PSK signals have the same signal spectra as those of QPSK or DEQPSK signals (Section 3.5).

4.7.1 Spectral estimation of CE8PSK signals by computer simulation

The basic principle of spectral estimation is described briefly in Section 3.6.1. The baseband equivalent model, used for spectral estimation of the transmitted CE8PSK signal, is shown in Fig. 4.8, which is very similar to that for QPSK spectral estimation shown in Fig. 3.7. The only difference is the encoder which convolutionally and Gray encodes the input data $\{\alpha_L\}$. As with QPSK signals, the spectra of the sampled signals are estimated at three different points along the transmission path. They are at the outputs of the

- (a) modulation filter
- (b) IF filter, and
- (c) HPA,

which are marked as points 'D', 'E' and 'F', respectively, in Fig. 4.8. The method of spectral estimation for the three sampled signals are described as follows.

- (a) To estimate the spectrum at point 'D', a sequence of L binary data-symbols $\{\alpha_L\}$ is generated, where $\{\alpha_L\}$ are taken to be statistically independent and equally likely to have value of 0 or 1. The encoded

symbols $\{q_i\}$ are obtained from $\{\alpha_i\}$, by the encoder, after being S/P (serial-to-parallel) converted, convolutionally encoded and then Gray encoded (Section 4.2). The i^{th} symbol has the value

$$q_i = (\pm 0.924 \pm j0.383) \text{ or } (\pm 0.383 \pm j0.924) \quad 4.7.1$$

where $j = \sqrt{-1}$, the $\{q_i\}$ being statistically independent and equally likely to have any of the eight possible values. The sequence $\{q_i\}$ is used to form the sequence of impulses $\{\sum_i q_i \delta(t-iT)\}$ which are fed into the modulation filter. The signal at the filter output is the complex-valued waveform

$$u(t) = \sum_i q_i h_t(t-iT) \quad 4.7.2$$

where $h_t(t)$ is the impulse response of the modulation filter. The waveform $u(t)$ is sampled, at the time instants $\{mT_m\}$ (8 samples per symbol), where $T_m = T/8$ and T is the symbol duration, to give the sequence $\{u_m\}$, with $u_m = u(mT_m)$

(c) and (b) For the description of spectral estimation at points 'E' and 'F', see the description of spectral estimation at points 'B' and 'C', respectively, in Section 3.6.2.

The procedures (a), (b) and (c) are exactly the same as for the corresponding QPSK signal spectral estimation described in Section 3.6.2.

4.8 Distance measures for minimum-distance decoding of CE8PSK signals

In the CE8PSK system described in Section 4.2, the binary symbols in the original data signal are statistically independent and equally likely to be either 0 or 1. The decoding process that minimises the probability of error in the decoding of the whole received sequence selects the possible sequence of data symbols fed to the encoder at the transmitter that maximises that corresponding conditional probability density function of the received signal [11]. The received signal is sampled once per

received encoded symbol and the decoding operation is carried out on the resultant sample values. In the presence of additive Gaussian noise, giving noise samples that are statistically independent Gaussian random variables with zero mean and fixed variance (referred to here as 'white' Gaussian noise), the decoded message having the minimum probability of being incorrect, is the possible sequence of data symbols at the input to the encoder at the transmitter for which there is the minimum unitary distance between the corresponding received sequence of samples in the absence of noise and the samples actually received [11]. Thus, under these conditions, minimum-distance decoding, using the unitary distance, minimises the probability of error in decoding the received signal. The minimum-distance decoding of CE8PSK signal can be achieved in practice by means of the Viterbi-algorithm [11] which is described in Section 4.4.

Let the $(i+1)$ sample values r_1 to r_i used for decoding of $\{\alpha_L\}$, Eqn. 4.3.7 in Section 4.2, be given by the i -component row vector

$$R_i = [r_1 \ r_2 \ r_3 \ \dots \ r_i] \quad 4.8.1$$

where the $\{r_h\}$, for $h=1, 2, \dots, i$, have complex values. R_i is the vector formed by the received samples. The Viterbi decoder forms and stores a set of $m=2^L$ vectors (sequences) $\{X_L\}$, where

$$X_L = [x_1 \ x_2 \ x_3 \ \dots \ x_L] \quad 4.8.2$$

and $x_h=0$ or 1 , for $h=1, 2, \dots, L$. x_h here represents a possible value of α_h . For each stored vector X_L the decoder forms the vector

$$Y_i = [y_1 \ y_2 \ y_3 \ \dots \ y_i] \quad 4.8.3$$

where $i=L/2$, $\{y_h\}$, for $h=1, 2, \dots, i$, have complex values, and Y_i would have been transmitted in place of the sequence of the $\{q_i\}$ (the

convolutionally encoded symbols), had the vector X_L been fed to the encoder at the transmitter in place of the vector

$$\alpha_L = [\alpha_1 \ \alpha_2 \ \alpha_3 \ \dots \ \alpha_L] \quad 4.8.4$$

that was actually sent. The decoder forms and stores together with each X_L , the corresponding distance (Eqn. 4.3.8)

$$C_i = c_1 + c_2 + c_3 + \dots + c_i \quad 4.8.5$$

$$= \sum_{n=1}^i c_n \quad 4.8.6$$

where, for $h=1, 2, \dots, i$, $c_h = |r_h - y_h|^2$ if the square of the unitary distance [10] is used as the distance measure.

The maximum likelihood sequence of possible data symbols, determined from the received vector R_i , is given by the possible vector X_L associated with the smallest value of C_i , which is the square of the unitary distance [10] between the vectors R_i and Y_i . As mentioned in Section 4.3, whether the square of the unitary distance or the unitary distance itself is used, does not affect the basic operation of the system, so that the square of the unitary distance will be considered simply as the distance. Since the encoded data symbols $\{q_i\}$ are statistically independent and equally likely to have any of their 8 possible values, the maximum likelihood vector X_L is the most likely to be correct, given the received vector R_i [10],[16].

In the Viterbi-algorithm decoder (Section 4.4), several estimates of the sequence of data symbols so far received are determined upon the receipt of each sample r_{i+1} , and each estimate is associated with the corresponding (square of the) unitary distance. In receiving each sample r_{i+1} , the decoder carries out two operations of squaring or multiplication to determine one of the 8 possible values of c_{i+1} . So that altogether there 16 operations of squaring or multiplication to be done. Details of the process are given in Section 4.4. A useful reduction in complexity of

maximum-likelihood decoding can be achieved by using a different distance measure, instead of the unitary distance.

Six distance measures are studied here. The equations satisfied by them are given in Table 4.3. For the distance measure D, the distance c_n between the complex values r_n and y_n , is given by the difference between their phase angles. It involves no operation of squaring or multiplication, but requires the use of a look-up table. This means that less signal processing is required and, for the same equipment complexity, better accuracy can be achieved because the phase angle is real-valued.

4.8.1 Distance measure A

Consider the h^{th} components in the vectors R_1 and Y_1 which are

$$r_n = r_{a,n} + jr_{b,n} \quad 4.8.7$$

and
$$y_n = y_{a,n} + jy_{b,n} \quad 4.8.8$$

respectively, where $j = \sqrt{-1}$. For $h=1$ to l , $r_{a,n}$ and $y_{a,n}$ are the real parts, and $r_{b,n}$ and $y_{b,n}$ are the imaginary parts of the complex values r_n and y_n , respectively. r_n and y_n can be written, in the polar coordinate, as

$$r_n = |r_n| (\cos \Omega_n + j \sin \Omega_n) \quad 4.8.9$$

and
$$y_n = |y_n| (\cos \phi_n + j \sin \phi_n) \quad 4.8.10$$

respectively, where

$$|r_n| = (r_{a,n}^2 + r_{b,n}^2)^{1/2} \quad 4.8.11$$

$$|y_n| = (y_{a,n}^2 + y_{b,n}^2)^{1/2} \quad 4.8.12$$

$$\Omega_n = \tan^{-1} \left(\frac{r_{b,n}}{r_{a,n}} \right) \quad 4.8.13$$

and
$$\phi_n = \tan^{-1} \left(\frac{y_{b,n}}{y_{a,n}} \right) \quad 4.8.14$$

$|r_n|$ and $|y_n|$ are the absolute values of the complex values r_n and y_n , respectively, and Ω_n and ϕ_n are the phase angles of the complex values r_n

and y_n , respectively. The square of the unitary distance between r_n and y_n is (Eqns. 4.8.9 and 4.8.10)

$$\begin{aligned}
 c_n &= |r_n - y_n|^2 && 4.8.15 \\
 &= (|r_n|\cos\Omega_n - |y_n|\cos\phi_n)^2 + (|r_n|\sin\Omega_n - |y_n|\sin\phi_n)^2 \\
 &= |r_n|^2\cos^2\Omega_n + |y_n|^2\cos^2\phi_n + |r_n|^2\sin^2\Omega_n + |y_n|^2\sin^2\phi_n \\
 &\quad - 2|r_n||y_n|(\cos\Omega_n\cos\phi_n + \sin\Omega_n\sin\phi_n) \\
 &= |r_n|^2 + |y_n|^2 - 2|r_n||y_n|\cos(\Omega_n - \phi_n) && 4.8.16
 \end{aligned}$$

Hence from Eqns. 4.8.6 and 4.8.16, the square of the unitary distance between the vectors R_i and Y_i is

$$\begin{aligned}
 C_i &= \sum_{n=1}^i c_n \\
 &= \sum_{n=1}^i [|r_n|^2 + |y_n|^2 - 2|r_n||y_n|\cos(\Omega_n - \phi_n)] \\
 &= \sum_{n=1}^i [|r_n|^2 + |y_n|^2] - 2 \sum_{n=1}^i [|r_n||y_n|\cos(\Omega_n - \phi_n)] && 4.8.17
 \end{aligned}$$

Since, under the assumed conditions, the possible received samples, $\{y_n\}$, for $n=1, 2, \dots, i$, lie on a circle in the two-dimensional complex-number plane (see the CE8PSK signal constellation in Fig. 4.5), the values of $|y_n|$, for $n=1, 2, \dots, i$, are constant and equal to the radius of the circle, bearing in mind that the ISI introduced by the channel has been neglected. Thus the term $\sum_{n=1}^i [|r_n|^2 + |y_n|^2]$, in Eqn. 4.8.17, is a constant common to all the distances $\{C_i\}$. Since the decoder is concerned only with the relative distances, not their actual values, this common term can be neglected, without affecting the decoding performance, and Equation 4.8.17 is reduced to

$$C_i = -2|y_n| \sum_{n=1}^i |r_n| \cos(\Omega_n - \phi_n) \quad 4.8.18$$

The factor $2|y_n|$, outside the summation term is, in fact, a scaling factor

common to all $\{C_i\}$. Again since the decoder is concerned only with the relative distances, this common factor can be set to unity without affecting the decoding performance, and Equation 4.8.18 is reduced further to

$$C_i = - \sum_{n=1}^i [|r_n| \cos(\Omega_n - \phi_n)] \quad 4.8.19$$

$$= \sum_{n=1}^i c_n \quad 4.8.20$$

where now
$$c_n = -|r_n| \cos(\Omega_n - \phi_n) \quad 4.8.21$$

is used. This is known here as the distance measure A. Although this distance is not the actual square of the unitary distance, when used by the Viterbi decoder, it is equivalent to the square of the unitary distance and so leads to the optimum decoding performance. This is because the distance measure, as given by Eqn 4.8.21, is derived from the square of the unitary distance measure, as given by Eqn 4.8.15.

Using the distance measure A, as given by Eqn. 4.8.21, five modified distance measures are derived.

4.8.2 Distance measure B

From Eqn. 4.8.21, the distance measure A is represented by the equation

$$c_n = -|r_n| \cos(\Omega_n - \phi_n)$$

where $|r_n|$ is the amplitude of the n^{th} component in the vector R_i and gives the amplitude information to the decoder. If the amplitude information is removed, the equation becomes

$$c_n = -\cos(\Omega_n - \phi_n) \quad 4.8.22$$

This is known here as the distance measure B. From Eqns. 4.8.6 and 4.8.22, the distance between the vectors R_i and Y_i , using the distance measure B, is

$$C_i = - \sum_{n=1}^i \cos(\Omega_n - \phi_n) \quad 4.8.23$$

4.8.3 Distance measure C

Using the cosine series [17,p43]

$$\cos(x) = 1 - \frac{x^2}{2!} + \frac{x^4}{4!} - \frac{x^6}{6!} + \dots \quad 4.8.24$$

Equation 4.8.22 can be written as

$$\begin{aligned} c_n &= -\cos(\Omega_n - \phi_n) \\ &= -1 + \frac{(\Omega_n - \phi_n)^2}{2!} - \frac{(\Omega_n - \phi_n)^4}{4!} + \dots \end{aligned} \quad 4.8.25$$

$$\text{and so } 1 - \cos(\Omega_n - \phi_n) = \frac{(\Omega_n - \phi_n)^2}{2!} - \frac{(\Omega_n - \phi_n)^4}{4!} + \dots \quad 4.8.26$$

When used in the Viterbi decoder the distance measures, using $-\cos(\Omega_n - \phi_n)$ and $1 - \cos(\Omega_n - \phi_n)$, will give the same decoding performance because the decoder is concerned with the relative distances, not the actual distances. Ω_n and ϕ_n are the phase angles computed by taking the function $\tan^{-1}(\cdot)$ of the complex values r_n and y_n , respectively, (Eqns. 4.8.13 and 4.8.14), so $|\Omega_n| < \pi$, $|\phi_n| < \pi$, and $|\Omega_n - \phi_n| < 2\pi$. The function of $1 - \cos(\Omega_n - \phi_n)$, for $|\Omega_n - \phi_n| < 2\pi$, is shown in Fig. 4.9. Note that the function $1 - \cos(\Omega_n - \phi_n)$ is symmetrical around $(\Omega_n - \phi_n) = 2\pi$ for positive values of $(\Omega_n - \phi_n)$, and is symmetrical around $(\Omega_n - \phi_n) = -\pi$ for negative values of $(\Omega_n - \phi_n)$. In Eqn. 4.8.26, if the first term is used as an approximation for the true value of $1 - \cos(\Omega_n - \phi_n)$, it becomes

$$1 - \cos(\Omega_n - \phi_n) \approx \frac{(\gamma_n)^2}{2!} \quad 4.8.27$$

$$\text{Here } \gamma_n = \begin{cases} |\Omega_n - \phi_n|, & \text{for } |\Omega_n - \phi_n| < \pi \\ 2\pi - |\Omega_n - \phi_n|, & \text{for } |\Omega_n - \phi_n| > \pi \end{cases} \quad 4.8.28$$

are the conditions to make the function $(\gamma_n)^2/2!$ symmetrical around $(\Omega_n - \phi_n) = \pi$ for positive values of $(\Omega_n - \phi_n)$ and around $(\Omega_n - \phi_n) = -\pi$ for

negative values of $(\Omega_n - \phi_n)$. Now if the decoder uses

$$c_n = \frac{(\gamma_n)^2}{2!} \tag{4.8.29}$$

as the distance measure, since the decoder is concerned with the relative distances, not the actual values, the factor $1/2!$ in Eqn. 4.8.29 can be neglected without affecting the performance of the decoding process, hence Eqn. 4.8.29 becomes

$$c_n = \gamma_n^2 \tag{4.8.30}$$

This is known here as the distance measure C. From Eqns. 4.8.6 and 4.8.30, the distance between R_1 and Y_1 , using the distance measure C, is

$$C_1 = \sum_{n=1}^1 \gamma_n^2 \tag{4.8.31}$$

where γ_n is given by Eqn. 4.8.28.

4.8.4 Distance measure D

The distance measure C is derived from the distance measure B by using the approximation (Eqn. 4.8.27)

$$1 - \cos(\Omega_n - \phi_n) \approx \frac{(\gamma_n)^2}{2!} \tag{4.8.32}$$

where

$$\gamma_n = \begin{cases} |\Omega_n - \phi_n|, & \text{for } |\Omega_n - \phi_n| \leq \pi \\ 2\pi - |\Omega_n - \phi_n|, & \text{for } |\Omega_n - \phi_n| > \pi \end{cases} \tag{4.8.33}$$

The function $1 - \cos(\Omega_n - \phi_n)$ is shown on in Fig. 4.10. It can be seen that the function can also be approximated graphically by the piecewise linear function

$$1 - \cos(\Omega_n - \phi_n) \approx \frac{2\gamma_n}{\pi} \tag{4.8.34}$$

where the properties of γ_n given by Eqn. 4.8.33, are used to make the piecewise linear function, $2\gamma_n/\pi$, symmetrical around $\gamma_n = \pm\pi$ for $|\Omega_n - \phi_n| \leq 2\pi$. For the reason that the decoder is concerned only with relative distances, and not with their actual values, the common factor $2/\pi$ in Eqn. 4.8.34 can

be set to unity without affecting the decoding performance and the decoder can use

$$c_n = \gamma_n \quad 4.8.35$$

as the distance measure, bearing in mind that $\gamma_n > 0$. This is known here as the distance measure D. From Eqns. 4.8.6 and 4.8.35, the distance between the R_i and Y_i , using the distance measure D, is

$$C_i = \sum_{n=1}^i \gamma_n \quad 4.8.36$$

with γ_n given by Eqn. 4.8.33 (or 4.8.28). This is also the phase distance between the two vectors R_i and Y_i .

Equations. 4.8.22, 4.8.30 and 4.8.25, satisfying the distance measures B, C and D, respectively, are shown in Fig. 4.11, where they have all been normalised to 1 at $\gamma_n = \pm\pi$.

4.8.5 Distance measure E

In the distance measure C (Eqn. 4.8.30), the square of the phase difference (distance) is used to approximate to the function $1 - \cos(\Omega_n - \phi_n)$, where the amplitude information $|r_n|$ is neglected. Here, if the amplitude information $|r_n|$ is re-introduced into the distance measure C, Eqn. 4.8.30 becomes

$$c_n = |r_n| \gamma_n^2 \quad 4.8.37$$

This is here known as the distance measure E, with $|r_n|$ the absolute value (or envelope) of r_n given by Eqn. 4.8.11. From Eqns. 4.8.6 and 4.8.37, the distance between the vectors R_i and Y_i using the distance measure E, is

$$C_i = \sum_{n=1}^i |r_n| \gamma_n^2 \quad 4.8.38$$

4.8.6 Distance measure F

Similarly, if the amplitude information $|r_n|$ is re-introduced to the

distance measure D, Eqn. 4.8.35 becomes

$$c_n = |r_n| Y_n \tag{4.8.39}$$

This is known here as the distance measure F. From Eqns. 4.8.6 and 4.8.39 the distance between the vectors R_i and Y_i , using the distance measure F, is

$$C_i = \sum_{n=1}^i |r_n| Y_n \tag{4.8.40}$$

The equations, satisfied by the different measures just described, are shown in Table 4.3. Note that; when used in the Viterbi decoder, the distance measure A is equivalent to the unitary distance measure. Clearly, the decoder that accepts as the decoded sequence $(\hat{\alpha}_L)$ that giving the minimum unitary distance between the corresponding (\hat{q}_i) and the received (r_i) , minimizes the probability of error in the decoding of the (α_L) from the (r_i) , so the distance measure A gives the optimum performance. The use of any of the other five distance measures therefore necessarily gives a higher probability of error in the decoding of the received sequence. The most computationally simple distance measure is the distance measure D because it involves no operation of squaring or multiplication.

With the distance measure D, following the receipt of r_{i+1} , the Viterbi decoder now computes each of the $4m$ values of c_{i+1} using the equation (Eqn. 4.8.33)

$$c_{i+1} = \begin{cases} |\Omega_{i+1} - \phi_{i+1}|, & \text{for } |\Omega_{i+1} - \phi_{i+1}| \leq \pi \\ 2\pi - |\Omega_{i+1} - \phi_{i+1}|, & \text{for } |\Omega_{i+1} - \phi_{i+1}| > \pi \end{cases} \tag{4.8.41}$$

where Ω_{i+1} and ϕ_{i+1} are real-valued. The decoder carries out the operations of subtraction, instead of squaring or multiplication. However, ϕ_{i+1} in Eqn. 4.8.41 has only 8 possible values because it is one of the 8 possible received phase angles. So, of these $4m$ values of c_{i+1} , many have the same values. In fact, there are only 8 different values of c_{i+1} , and each requires either 1 or 2 operations of subtractions to determine.

4.9 Simulation results and discussion

Computer simulation tests have been carried out to assess the error-rate performances of the different systems, using CE8PSK signals with the equipment filters and HPA whose characteristics are shown in Sections 2.4 and 2.5. The simulation models and methods used to obtain the results in this section are described in Sections 4.3, 4.4 and 4.5. In all simulation tests, it is assumed that the receiver provides the required ideal carrier and clock signals, the data-transmission systems are optimised by sharing the overall filtering equally between the transmitter and receiver filters, and the Viterbi decoder at the receiver uses 16 stored vectors with a delay of 32 symbols in decoding.

For DEQPSK signals, it is shown in Section 3.7.3 that, the minimum truncation lengths of the sampled impulse responses of the modulation and demodulation filters, with $\beta=100\%$, 75%, 50% and 25%, required to approximate to the theoretical ideal error-rate performance at $P_e > 10^{-4}$, are $2T$, $4T$, $4T$ and $8T$, respectively, and they are denoted as signals 1A, 2A, 3A and 4A, respectively. Now for CE8PSK signals, the same wave shapes of the modulating signals are used in the simulation tests, but they are known here as signals 1B, 2B, 3B and 4B, instead of signals 1A, 2A, 3A and 4A, respectively. Thus signals 1B, 2B, 3B and 4B apply to CE8PSK signals, with $\beta=100\%$, 75%, 50% and 25%, and with truncation lengths of the sampled impulse responses of $2T$, $4T$, $4T$ and $8T$, respectively.

4.9.1 Performances of signals 1B, 2B, 3B and 4B over a linear and bandlimited bandpass channel

The model used to evaluate the error-rate performance is shown in Fig. 4.6, where the linear and bandlimited channel was used (i.e., with Switches 'B' closed). The simulation results have suggested that, under the assumed conditions, signals 1B, 2B, 3B and 4B have no degradation in tolerance to noise at $P_e > 10^{-4}$, in comparison with that of an ideal CE8PSK system. When comparing the degradations of the CE8PSK signals with

those of the DEQPSK signals, under the same assumed conditions, as shown in Fig. 3.11 (which shows that signal 1A has a small degradation at $P_e=10^{-4}$), it can be seen that, CE8PSK signals suffer less further degradation in tolerance to noise, due to low level ISI, than DEQPSK signals.

4.9.2 Performances of signals 1B, 2B, 3B and 4B over a linear and bandlimited bandpass channel and in an ACI environment

The model used for the spectral estimation of CE8PSK signals is shown in Fig. 4.8, where the transmitted signal power spectra at the outputs of the modulation filter and IF filter were studied. The simulation results have suggested that, provided that the same transmitter filtering is used, signals 1B, 2B, 3B and 4B have exactly the same spectra as those of signals 1A, 2A, 3A and 4A (Figs. 3.10 and 3.12), respectively. So if the same transmitter filtering and channel spacing are used, the CE8PSK and DEQPSK systems should have the same level of ACI introduced into the desired channels.

The simulation model, used to evaluate the error-rate performances of signals 1B, 2B, 3B and 4B in an ACI environment, is shown in Fig. 4.7, where the linear and bandlimited bandpass channel is used (i.e., with Switches 'B' closed). The simulation results, with the channel spacing $f_{c.s.}=5R/4$ Hz (where R is the symbol rate), are shown in Fig. 4.12a, which indicate that signals 3B and 4B have little or no degradation in tolerance to noise at $P_e > 10^{-4}$, whereas signals 1B and 2B have the degradations of about 0.5 dB, and 1.1 dB, respectively, at $P_e=10^{-4}$, in comparison with that of an ideal CE8PSK system. The degradations of the signals at $P_e=10^{-4}$, measured in comparison with that of an ideal CE8PSK system, are shown in Table 4.4. Comparing with the degradations of the DEQPSK signals, under the same conditions (as shown in Table 3.5 which shows that signals 1A and 2A have the degradations of about 1.8 dB and 1.2

dB, respectively, at $P_e=10^{-4}$, it can be seen that, CE8PSK signals suffer less further degradation, due to ACI, than DEQPSK signals.

With the channel spacing f_{c_m} increased from $5R/4$ Hz to $5.5R/4$ Hz, the performances of signals 1B, 2B and 3B are shown in Fig. 4.12b, which indicates that the degradation in tolerance to noise of signal 1B has been nearly removed completely, at $P_e \geq 10^{-4}$. (See Table 3.5 for the comparison of the degradation with signal 1A under the same conditions).

4.9.3 Performances of signals 1B, 2B, 3B and 4B over a nonlinear and bandlimited bandpass channel

The reasons for the degradation in tolerance to noise caused by the HPA are described in Section 3.7.4. The model used to evaluate the effects of nonlinear distortion on error-rate performance is shown in Fig. 4.6, where the nonlinear and bandlimited bandpass channel is used (i.e., with Switches 'C' closed). The results for signals 1B, 2B, 3B and 4B, with the HPA operating at 0, 0.2 and 0.68 dB OBO, are shown in Figs. 4.13a, b and c, respectively.

At 0 dB HPA OBO (Fig. 4.13a), signals 1B, 2B and 3B suffer little degradations in tolerance to noise at $P_e \geq 10^{-4}$, while signal 4B, being a relatively narrowband signal, has a degradation of about 1 dB at $P_e=10^{-4}$, in comparison with that of an ideal CE8PSK system. (The reason for this is explained in Section 3.7.4.)

At 0.2 dB HPA OBO, (i.e., slightly backed-off below saturation), Fig. 4.14b shows that signals 1B, 2B and 3B have little improvements in performance, although signal 4B has reduced the degradation from 1dB to about 0.6 dB, at $P_e=10^{-4}$, in comparison with that with 0 dB HPA OBO.

With the HPA OBO value increased from 0.2 dB to 0.68 dB (Fig. 4.14c), the error-rate performances of signals 1B, 2B, 3B and 4B remain the same as those with 0.2 dB HPA OBO.

The degradations in tolerance to noise of the CE8PSK signals, at $P_e=10^{-4}$, with the HPA operating at 0, 0.2 and 0.68 dB OBO, measured in comparison with that of an ideal CE8PSK system, are shown in Table 4.5a. It can be seen that, with the HPA operating in the nonlinear mode at the earth station, the degradations in tolerance to noise of CE8PSK signals due to nonlinear distortion are insignificant. The worst case is when signal 4B is used with the HPA operating at 0 dB OBO, and the degradation is about 1 dB at $P_e=10^{-4}$, in comparison with that of an ideal CE8PSK system. In all the other cases, the degradations are in the range 0.4-0.7 dB at $P_e=10^{-4}$. Hence, with the HPA operating at 0, 0.2 and 0.68 dB OBO, the error-rate performances for the CE8PSK signals, when transmitted over the nonlinear and bandlimited bandpass channel are about the same.

Table 4.5b (reproduced from Table 3.6) shows the degradations in tolerance to noise of DEQPSK signals, under the same assumed conditions. It can be seen that the nonlinear distortion effects on degradations of all the CE8PSK and DEQPSK signals tested are about the same. However when the HPA is operating at 0 dB OBO, signal 4B has a degradation of about 1 dB at $P_e=10^{-4}$, while signal 4A loses 1.6 dB.

4.9.4 Performances of signals 1B, 2B, 3B and 4B over a nonlinear and bandlimited bandpass channel and in an ACI environment

In Section 3.7.4, it is mentioned that the degradations in tolerance to noise caused by the HPA are due to nonlinear distortion and increased ACI created by spectral restoration. The effects on performance of spectral restoration will now be studied. It is shown in Section 3.7.5, that the increased ACI can be observed by means of spectral estimation on the transmitted signal, at the output of the HPA at the earth station. The model used for spectral estimation is shown in Fig. 4.8, where the spectrum at point 'F' was studied. The simulation

results have shown that, with the HPA operating at 0, 0.2 and 0.68 dB, the transmitted spectra of signals 1B, 2B, 3B and 4B at the output of the HPA, are exactly the same as those of signals 1A, 2A, 3A and 4A shown in Fig. 3.14. So, if the same transmitter filters, HPA and channel spacing are used, both CE8PSK and DEQPSK signals will have the same level of ACI introduced into the desired channel.

Since the HPA causes significant spectral spreading of the signals (Fig. 3.14), it is obvious that the degradation in tolerance to noise is bound to occur. The simulation model, used to evaluate the error-rate performance of CE8PSK signals in an ACI environment, is shown in Fig. 4.7, where the nonlinear and bandlimited bandpass channel is used (i.e., with Switches 'B' closed). Results of computer simulation tests are shown in Fig. 4.14a, b and c, for the case where the HPA operating at 0, 0.2 and 0.68 dB OBO and the channel spacing is $f_{c_s}=5R/4$ Hz.

At 0 dB OBO (Fig. 4.14a), signals 1B, 2B and 3B have degradations of about 1.8 dB, while signal 4B loses about 2.3 dB at $P_s=10^{-4}$, in comparison with that of an ideal CE8PSK system.

With the HPA OBO increased from 0 dB to 0.2 dB (Fig. 4.14b), signals 1B, 2B, 3B and 4B have degradations of about 1 dB at $P_s=10^{-4}$, in comparison with that of an ideal CE8PSK system. So the performances of signals 1B, 2B and 3B are improved by 0.5 dB, while that of signal 4B is improved by about 1 dB at $P_s=10^{-4}$.

With the HPA OBO value increased further from 0.2 to 0.68 dB (Fig. 4.14c), the error-rate performances of signals 1B, 2B, 3B and 4B remain unchanged.

Table 4.6a shows the degradations in tolerance to noise of the signals at $P_s=10^{-4}$, measured in comparison with that of an ideal CE8PSK system. It can be seen that, for the preferred IF filters, HPA and with the channel spacing $f_{c_s}=5R/4$ Hz, the most cost effective arrangement is to use signal

1B (less hardware complexity than those of signals 2B and 3B) and to operate the HPA slightly backed off (say, e.g., 0.2 dB) below saturation. The degradation is about 1 dB at $P_{av}=10^{-4}$, in comparison with that of an ideal CE8PSK system. A better power efficiency cannot be obtained by increasing the HPA OBO value further.

With the channel spacing f_{ca} increased from $5R/4$ Hz to $5.5R/4$ Hz, the error-rate performances are as shown in Figs. 4.15a, b and c. The degradations in tolerance to noise of the signals at $P_{av}=10^{-4}$, with different HPA OBO values, measured in comparison with that of an ideal CE8PSK system, are shown in Table 4.6b. Comparing the degradations in Table 4.6a with those in Table 4.6b, it can be seen that the improvements in performances obtained by increasing the channel spacing from $5R/4$ Hz to $5.5R/4$ Hz are in the range 0 - 0.4 dB.

Comparing the degradations in tolerance to noise with those of the DEQPSK signals (Table 3.7) under the same assumed conditions, it can be seen that, CE8PSK signals suffer less further degradation in tolerance to noise, due to ACI, than DEQPSK signals. This is also seen in Section 4.9.2.

4.9.5 Performances given by the distance measure A - F in decoding CE8PSK signals over a linear and bandlimited channel

The distance measures A - F used in this section are described in Section 4.8 and the equations satisfied by the distance measures are shown in Table 4.3. The simulation model used to evaluate the error-rate performances of CE8PSK signals is shown in Fig. 4.6, where the linear and bandlimited channel is used (i.e., with Switches 'B' closed). The Viterbi decoder operating with the distance measures A - F are used in the tests. The simulation results suggest that, the performances are independent of the shapes of the baseband signal used for the particular shapes tested. That is, for the given distance measure (A, B, C, D, E or F), the

performances of signals 1B, 2B, 3B and 4B remain the same, thus the performance is dependent on the distance measures used, but not on the particular shape of the baseband waveform tested. The error-rate performances given by the distance measures A - F, are shown in Fig. 4.16, which indicates that the distance measures, when listed in the order of their relative tolerances to noise and starting with the best, are A or E, F, B or D, and C. The distance measure E gives the same performance as distance measure A (which is equivalent to the unitary distance measure when used in the decoder), and the distance measures B and D also give the same error-rate performance, at $P_e \gg 10^{-4}$. It can be seen in Fig. 4.16 that the degradations in tolerance to noise given by the distance measures B - F, when measured relative to the optimum distance measure, are in the range 0 - 0.6 dB. Thus, if it is not critically important that the decoder achieves the very best performance, the distance measure D achieves a good compromise between performance and complexity.

REFERENCES

- [1] Lebowitz, S.H. and Rhodes, S.A., "Performance of 8PSK Signaling for Satellite Communications", *IEEE Int. Conf. on Commun.*, pp.47.4.1-47.4.8 (1981)
- [2] Hui, J. and Fang, R.J.F., "Convolutional Code and Signal Waveform Design for Band-Limited Satellite Channels", *IEEE Int. Conf. on Commun.*, pp.47.5.1-47.5.9 (1981)
- [3] Muilwijk, D., "Correlative Phase Shift Keying - A Class of Constant Envelope Modulation Techniques", *IEEE Trans. on Commun.*, vol. COM-29, pp.226-236, March 1981
- [4] Feher, K., *Digital Communicayions: Satellite/Earth Station Engineering*, Prentice-Hall, Englewood Cliffs, NJ (1983)
- [5] Proakis, J., *Digital Communications*, McGraw-Hill (1983)
- [6] Bhargava, U.K., Hacocun, D., Matyas, R. and Nuspl, P.P., *Digital Communications by Satellite*, John Wiley & Sons (1982)
- [7] Viterbi, A.J. and Omura, J.K., *Principle of Digital Communication and coding*, McGraw-Hill (1979)
- [8] Taub, H. and Schilling, D.C., *Principles of Communication Systems*, pp.235-281, McGraw-Hill (1971)
- [9] Clark, A.P., "Minimum-distance decoding of binary convolutional codes", *Computer and Digital Techniques*, vol. 1, pp. 190-196, Oct. 1978
- [10] Clark, A.P., *Advanced Data-Transmission Systems*, Pentech Press, London (1977)
- [11] Viterbi, A.J., "Convolutional Codes and Their Performance in Communication Systems", *IEEE Trans. on Commun.*, vol. COM-19, pp.751-772, 1971
- [12] Hemati, F. and Costello, D.J., "Truncation Error Probability in Viterbi Decoding", *ibid.*, COM-25, pp.530-532, 1977
- [13] Wozencraft, J.M. and Jacobs, I.M., *Principles of Communication Engineering*, John Wiley & Sons, N.Y. (1967)
- [14] Aulin, I., "CPM-An Efficient Constant Amplitude Modulation Scheme", *International Journal of Satellite Communications*, April 1984
- [15] Aulin, I., "CPM-The Effect of Filtering and Hard Limiting", *International Journal of Satellite Communications*, April 1984
- [16] Clark, A.P., "Distance Measures for Near-Maximum-Likelihood Detection Processes", *IEE Proc.*, Vol. 128, Pt.E., No. 3, May 1981
- [17] Ledermann, W., *Complex number*, ELBS (1977)

Code	Code memory (K-1) bit	Sub-generator codes		j	Asymptotic gain gains (dB)
		$G^{(1),j}$	$G^{(2),j}$		
1	4	0 1 0	1 0 1	1	4.1
		1 1 1	0 0 1	2	
		0 0 0	0 1 0	3	
2	6	0 1 1 0	1 0 1 1	1	5
		1 1 0 1	1 0 0 1	2	
		0 0 0 0	1 1 0 0	3	

Table 4.1 Rate 2/3 binary codes for CE8PSK signals.

Octal symbol	Phase (degrees)	Magnitude of quadrature components	
		$q_i^{(1)}$	$q_i^{(2)}$
$e_i^{(1)} e_i^{(2)} e_i^{(3)}$			
0 0 0	+ 22.5	+0.924	+0.383
0 0 1	+ 67.5	+0.383	+0.924
0 1 0	+112.5	-0.383	+0.924
0 1 1	+157.5	-0.924	+0.383
1 0 0	-157.5	-0.924	-0.383
1 0 1	-112.5	-0.383	-0.924
1 1 0	- 67.5	+0.383	-0.924
1 1 1	- 22.5	+0.924	-0.383

Table 4.2 Gray encoding for CE8PSK signals.

Distance measure	Equation
A	$c_n = - r_n \cos \gamma_n$
B	$c_n = -\cos \gamma_n$
C	$c_n = \gamma_n^2$
D	$c_n = \gamma_n$
E	$c_n = r_n \gamma_n^2$
F	$c_n = r_n \gamma_n$

where $\gamma_n = \Omega_n - \phi_n$

where $\gamma_n = \begin{cases} |\Omega_n - \phi_n|, & \text{for } |\Omega_n - \phi_n| \leq \pi \\ 2\pi - |\Omega_n - \phi_n|, & \text{for } |\Omega_n - \phi_n| > \pi \end{cases}$

Table 4.3 Equations for different distance measures. $|r_n|$, Ω_n and ϕ_n are given by Equations 4.8.11, 4.8.13 and 4.8.14, respectively.

$f_{c_m} =$ (in Hz)	Signal			
	1B	2B	3B	4B
5R/4	1.1	0.5	0.2	0
5.5R/4	0.2	0	0	0

Table 4.4 Degradations in tolerance to noise of signals 1B, 2B, 3B and 4B, over a linear and bandlimited channel and in an ACI environment, with the channel spacings $f_{c_m} = 5R/4$ Hz and $5.5R/4$ Hz, at $P_e = 10^{-4}$, expressed in dB, in comparison with that of an ideal CDE8PSK system (from Fig. 4.12).

HPA OBO (in dB)	Signal			
	1B	2B	3B	4B
0	0.5	0.5	0.7	1.
0.2	0.4	0.4	0.4	0.6
0.68	0.4	0.4	0.4	0.6

(a)

HPA OBO (in dB)	Signal			
	1A	2A	3A	4A
0	0.5	0.5	0.5	1.6
0.2	0.5	0.5	0.5	1.1
0.68	0.4	0.4	0.4	0.9

(b)

Table 4.5 Degradations in tolerance to noise of signals (a) 1B, 2B, 3B and 4B , and (b) 1A, 2A, 3A and 4A, over a nonlinear and bandlimited channel, with the HPA operating at 0, 0.2 and 0.68 dB OBO and in an non-ACI environment, at $P_e=10^{-4}$, expressed in dB, measured in comparison with those of the corresponding ideal systems (from Fig. 4.13).

HPA OBO (in dB)	Signal			
	1B	2B	3B	4B
0	1.8	1.8	1.8	2.3
0.2	1.3	1.1	1	1.3
0.68	1.3	1.1	1	1.3

(a)

HPA OBO (in dB)	Signal			
	1B	2B	3B	4B
0	1.7	1.7	1.7	2.3
0.2	1.2	1.1	1.1	1.4
0.68	0.9	0.9	0.9	1.2

(b)

Table 4.6 Degradations in tolerance to noise of signals 1B, 2B, 3B, 4B, over a nonlinear and bandlimited channel, with the HPA operating at 0, 0.2 and 0.68 dB OBO and in an ACI environment, with channel spacing (a) $f_{c_s}=5R/4$ Hz and, (b) $f_{c_s}=5.5R/4$ Hz, at $P_e=10^{-4}$, expressed in dB, measured in comparison with that of an ideal CE8PSK system (from Figs. 4.14 and 4.15).

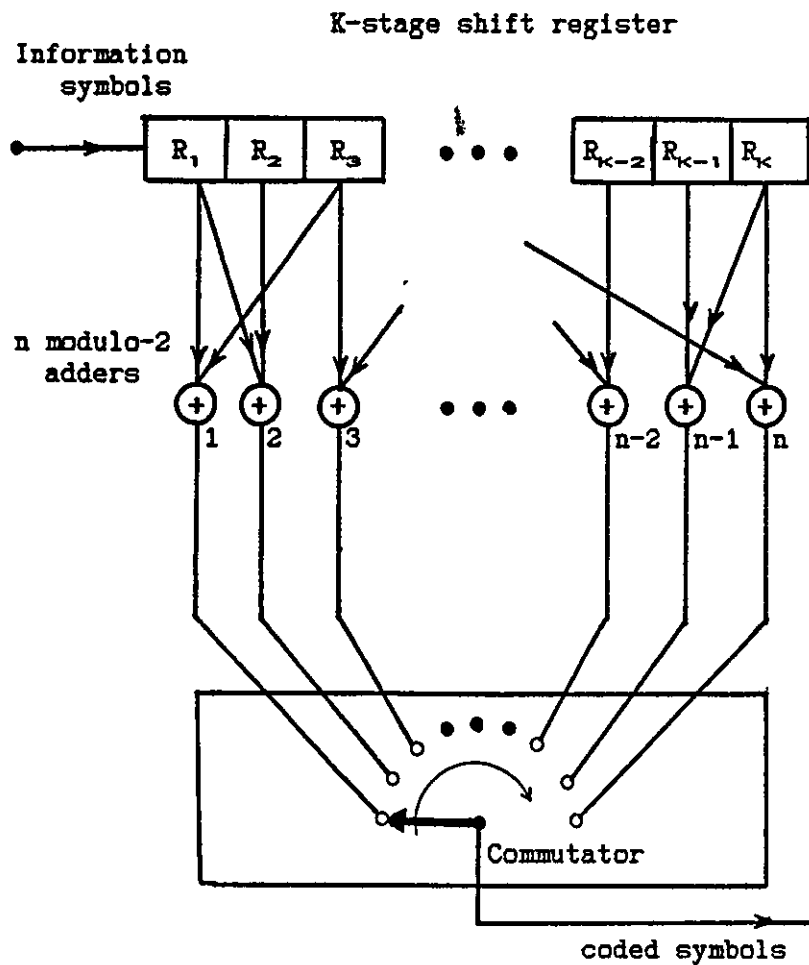


Figure 4.1 General convolutional encoder.

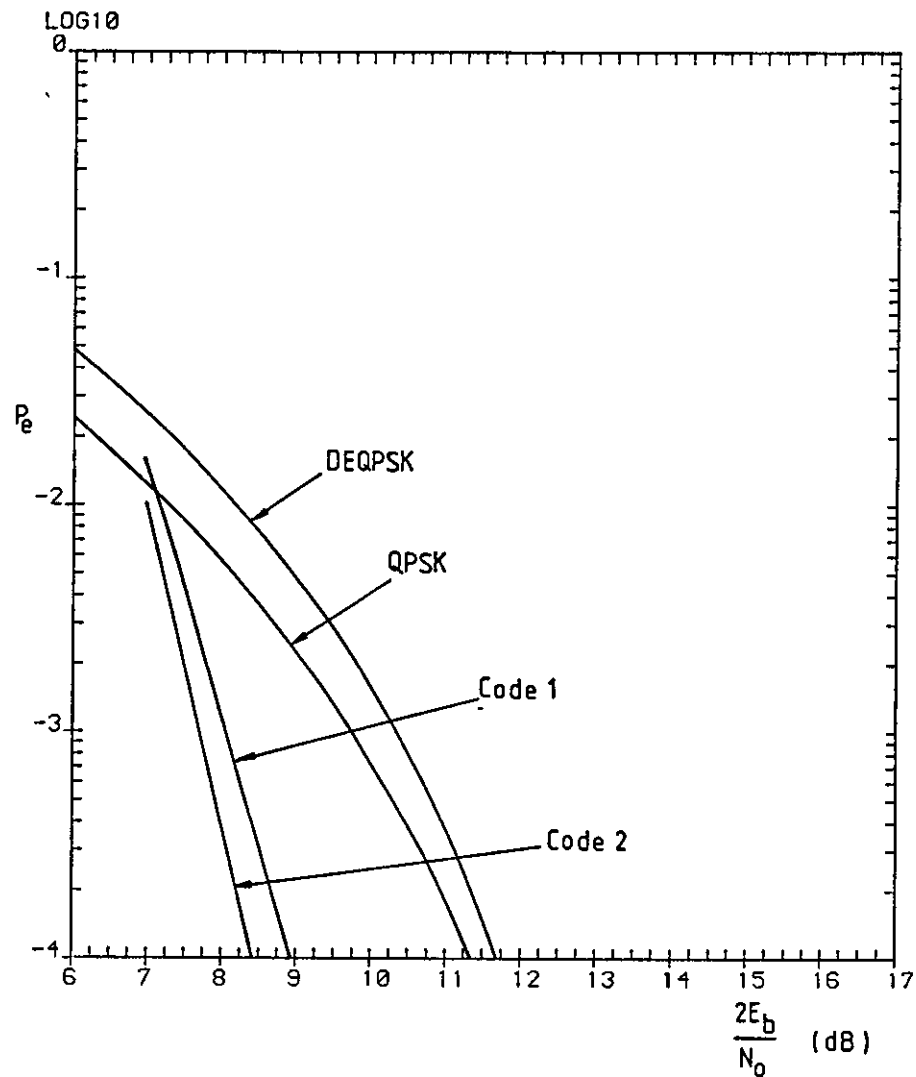


Figure 4.2 Error-rate performances of Codes 1 and 2 in Table 4.1 over an AWGN channel using Viterbi decoding.

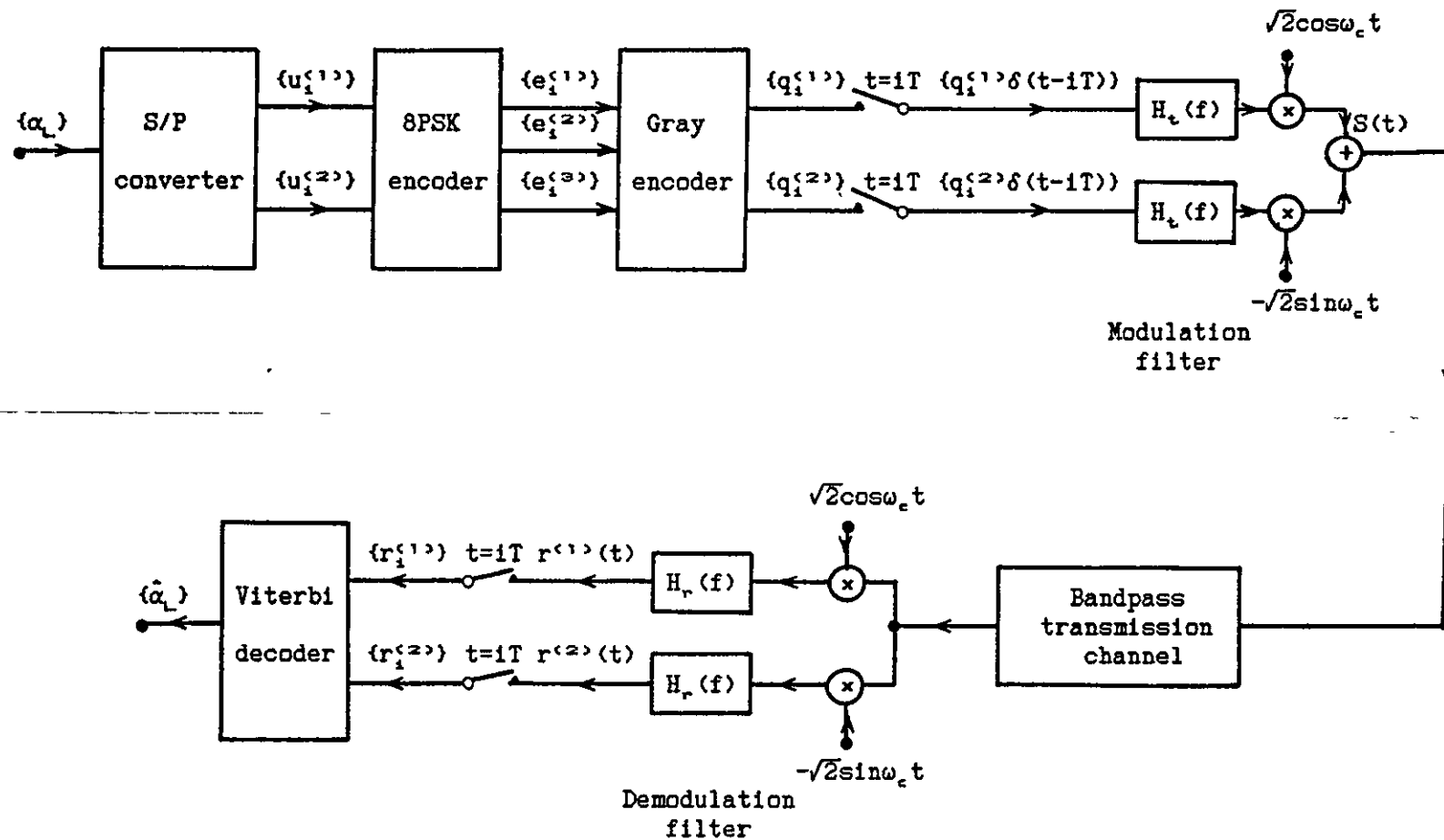


Figure 4.3 Block diagram of a convolutional encoder 8PSK (CE8PSK) system representation. S/P means serial-to-parallel.

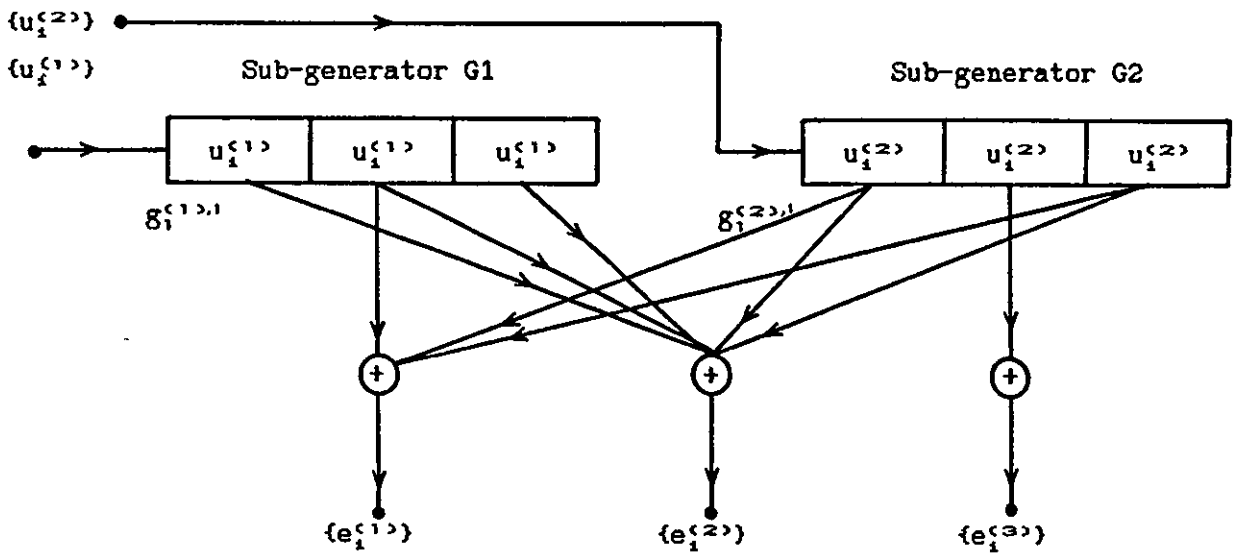


Figure 4.4 Encoder configuration for Code 1.

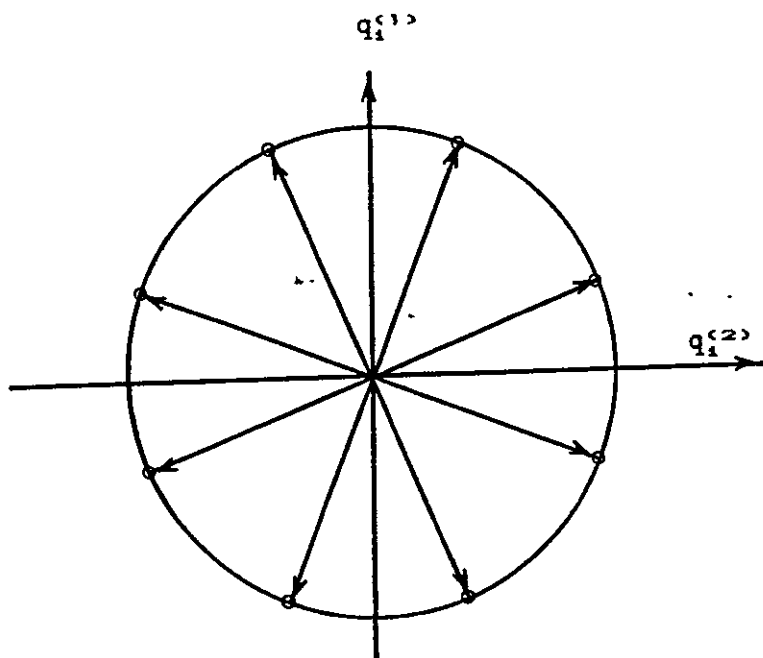


Figure 4.5 CRPSK signal constellation (possible received signal vectors).

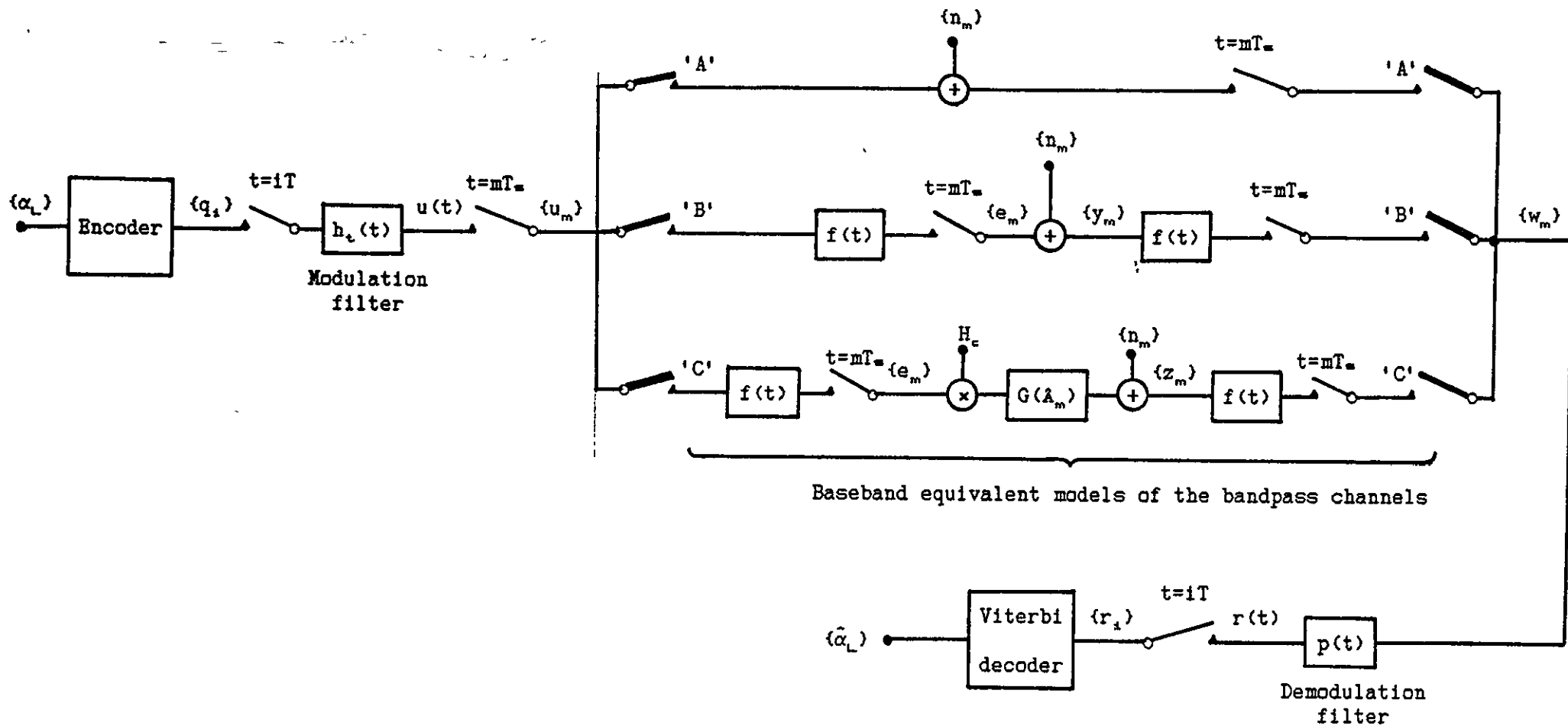


Figure 4.6 Baseband equivalent model of the CE8PSK system, with a linear and memoryless, a linear and bandlimited, or a nonlinear and bandlimited satellite channel, for computer simulation. $f(t)$ is impulse response of the baseband model of the IF filter. Switches 'A', 'B' and 'C' are for the linear and memoryless, the linear and bandlimited, and the nonlinear and bandlimited channels, respectively.

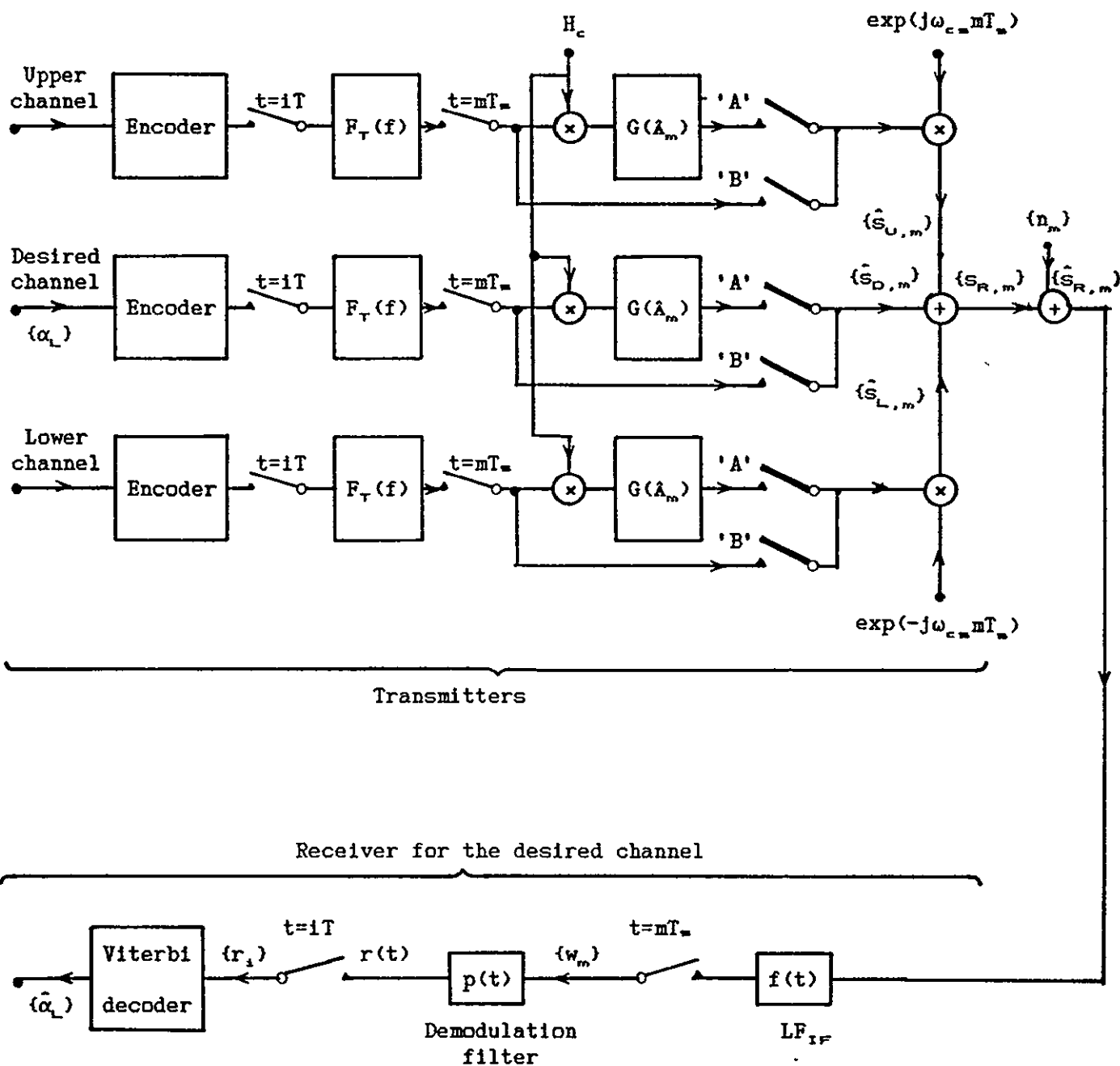


Figure 4.7 Baseband equivalent model of the CBPSK system, with a linear and bandlimited or a nonlinear and bandlimited satellite channel and in an ACI environment, for computer simulation. $F_T(f)$ is the resultant transfer function of the baseband equivalent model of the IF filter in cascade with the modulation filter. LF_{IF} means the baseband equivalent model of the IF filter. Switches 'A' and 'B' are for the nonlinear and bandlimited channel, and the linear and bandlimited channel, respectively.

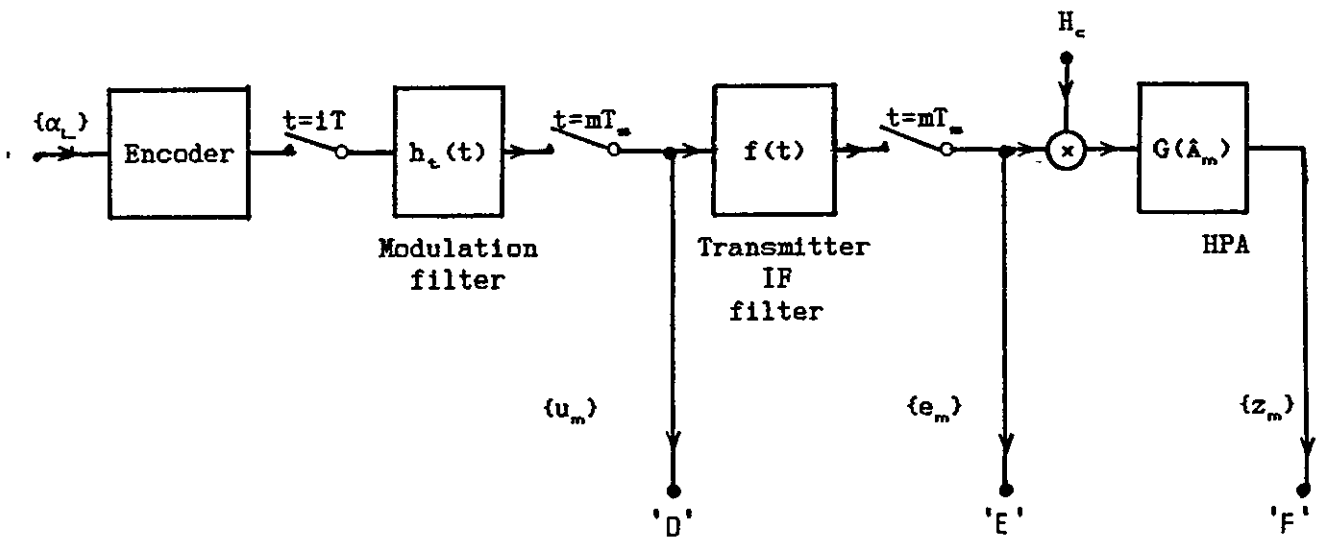


Figure 4.8 Baseband equivalent model for spectral estimation of CE8PSK signals at different points along the transmission path. $f(t)$ is the impulse response of the baseband equivalent model of the IF filter.

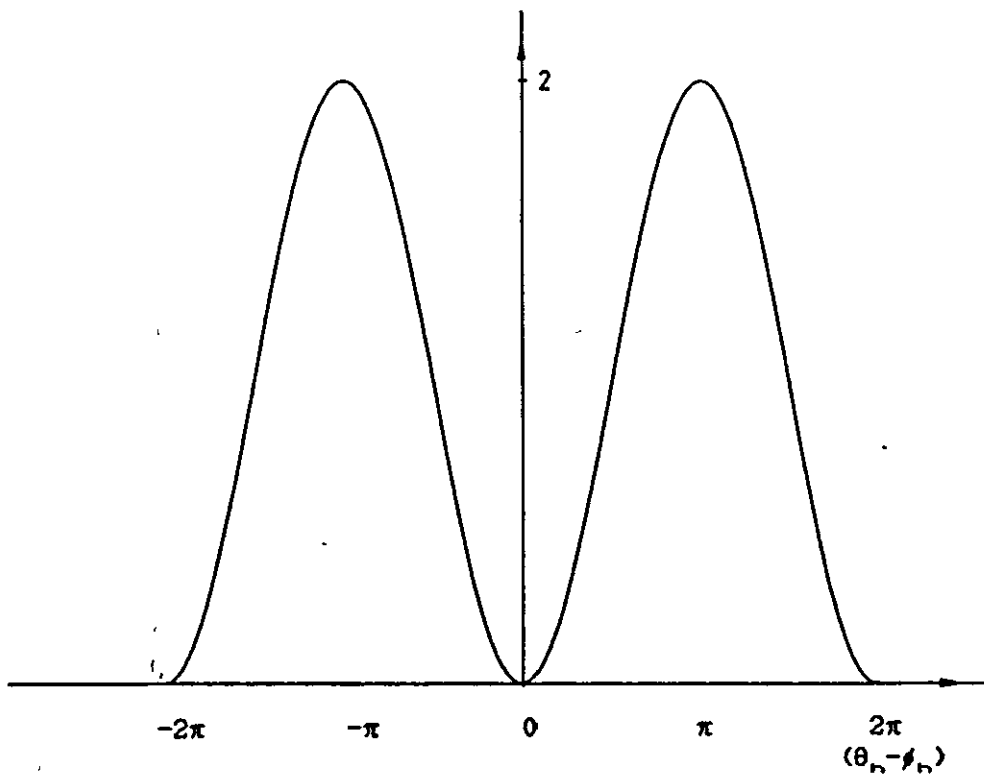


Figure 4.9 $1 - \cos(\theta_n - \phi_n)$ versus $(\theta_n - \phi_n)$.

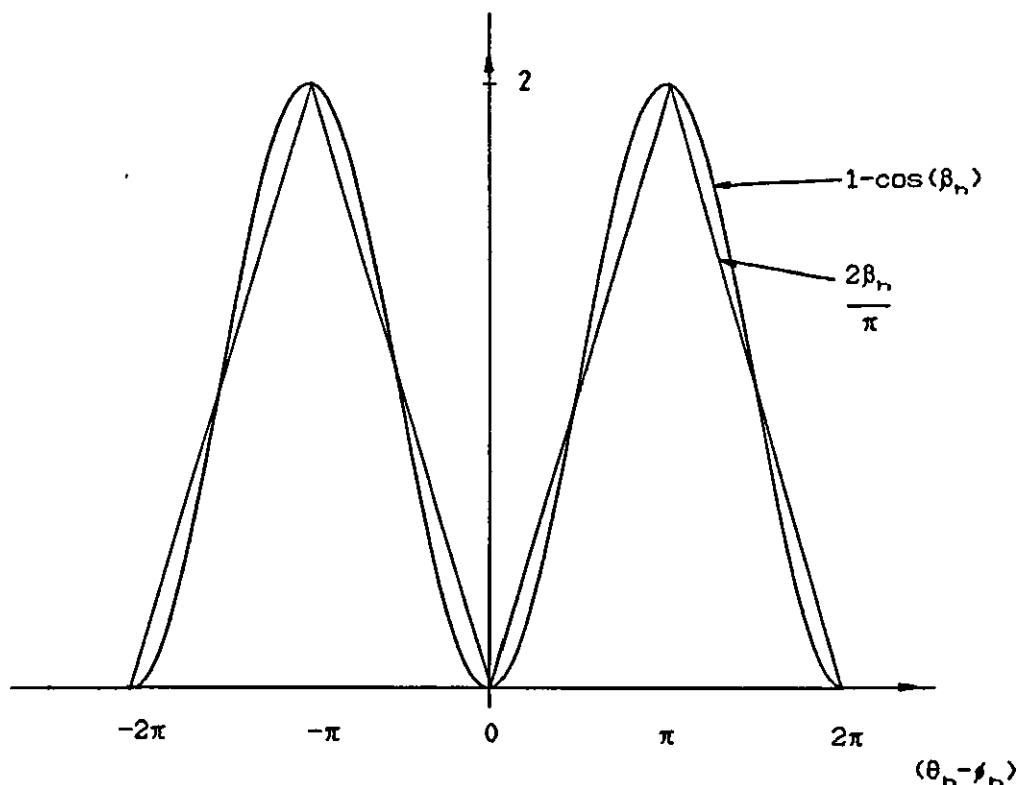


Figure 4.10 Piecewise linear approximation for the function $1-\cos(\theta_n-\phi_n)$.

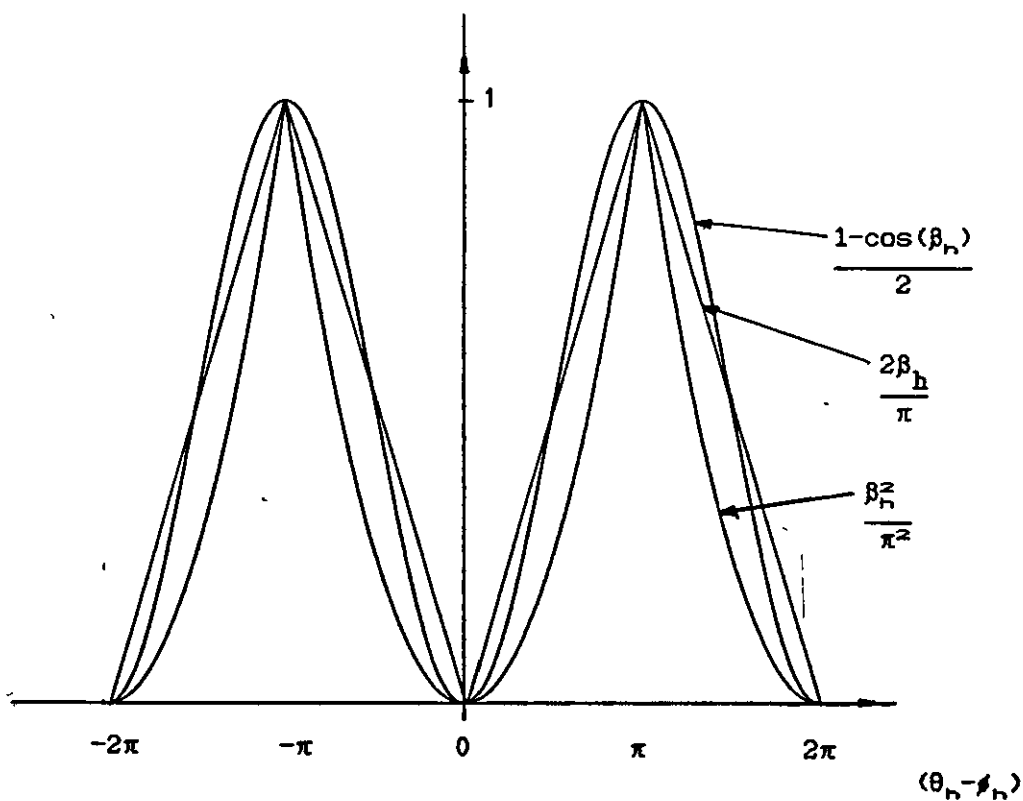


Figure 4.11 The functions for the distance measures B, C and D.

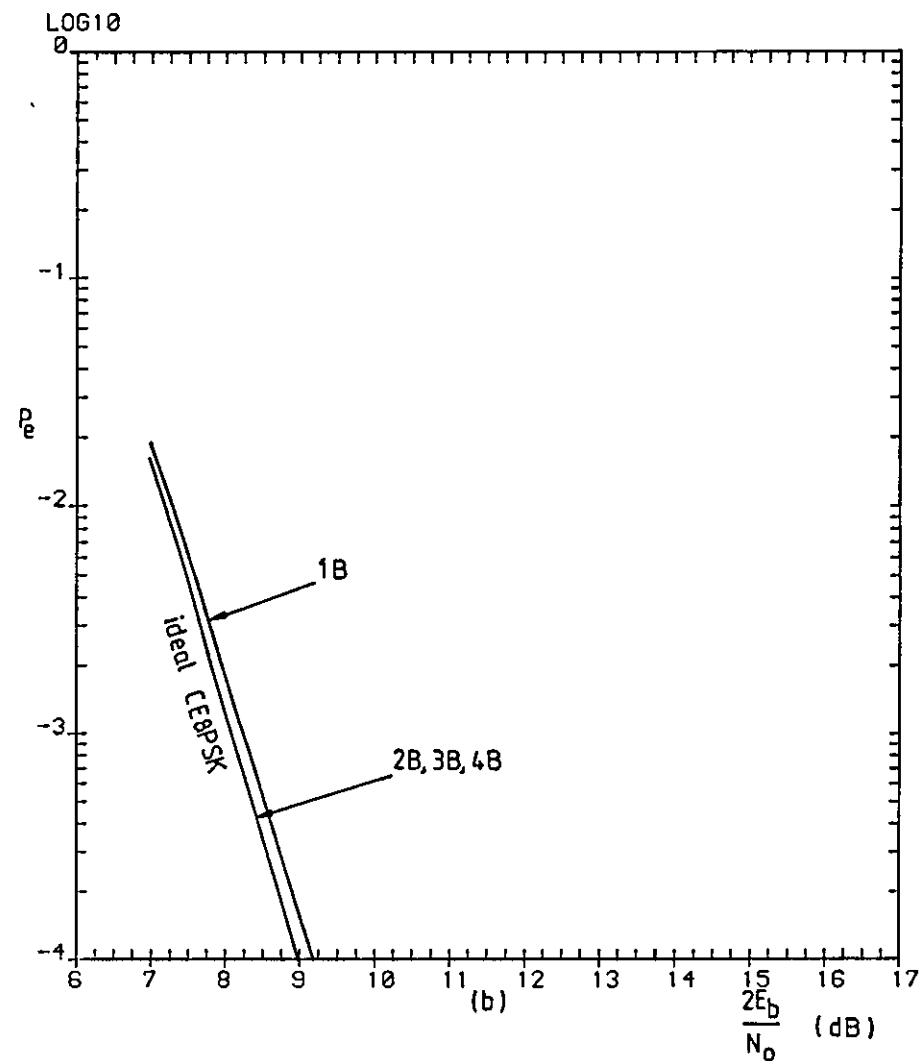
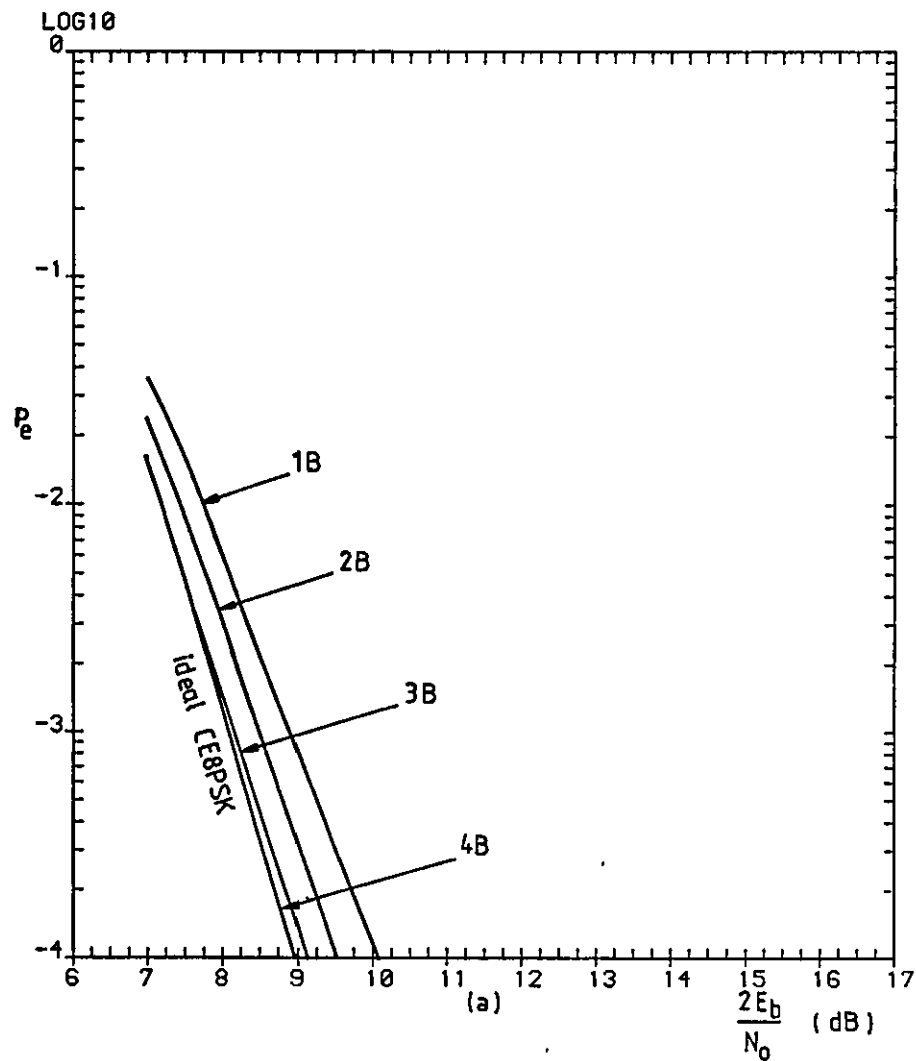


Figure 4.12 Error-rate performances of signals 1B, 2B, 3B and 4B over a linear channel and in an ACI environment, with the channel spacing $f_c =$ (a) $=5R/4$ Hz and, (b) $=5.5R/4$ Hz.

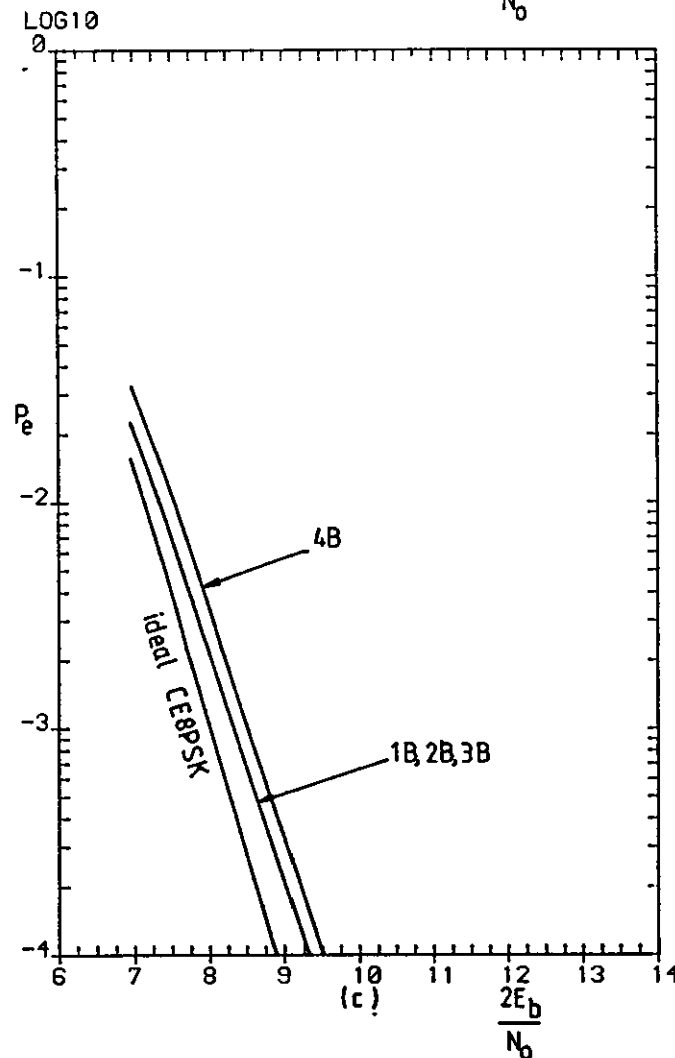
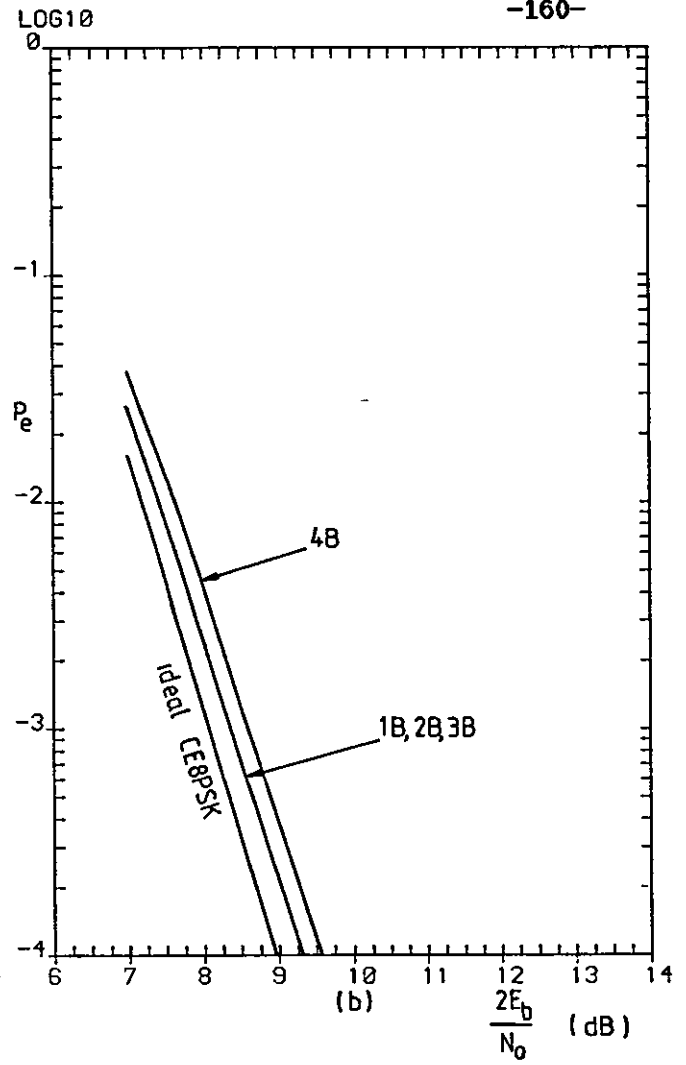
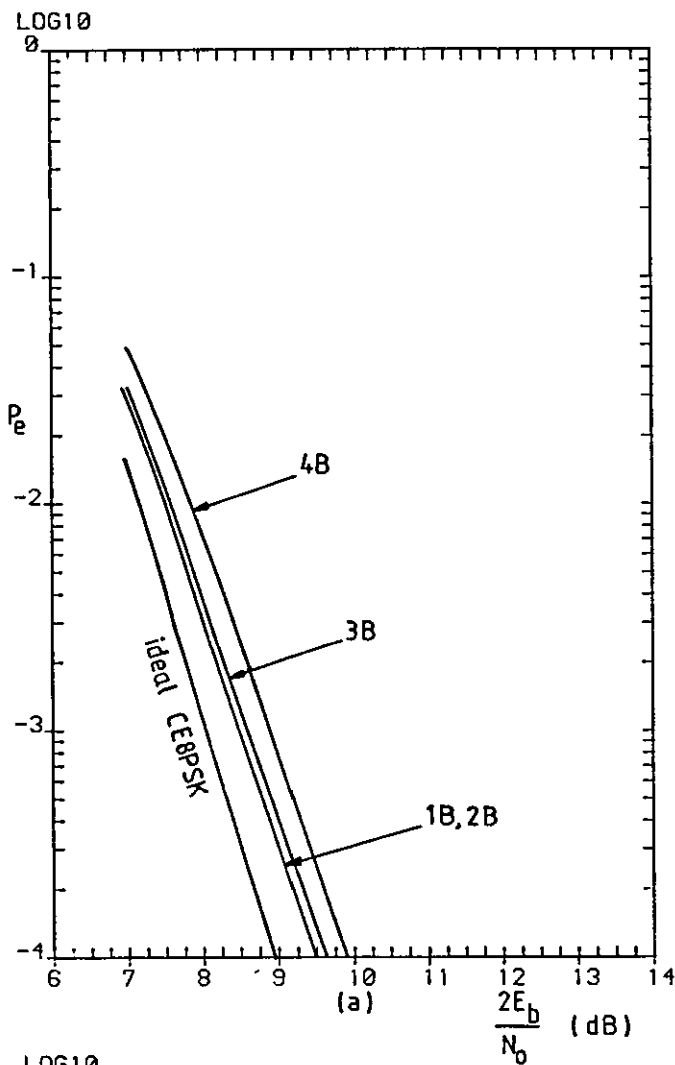


Figure 4.13 Error-rate performances of signals 1B, 2B, 3B and 4B over a nonlinear and bandlimited channel, with the HPA operating at (a) 0 dB, (b) 0.2 dB and, (c) 0.68 dB OBO, respectively, and in a non-ACI environment.

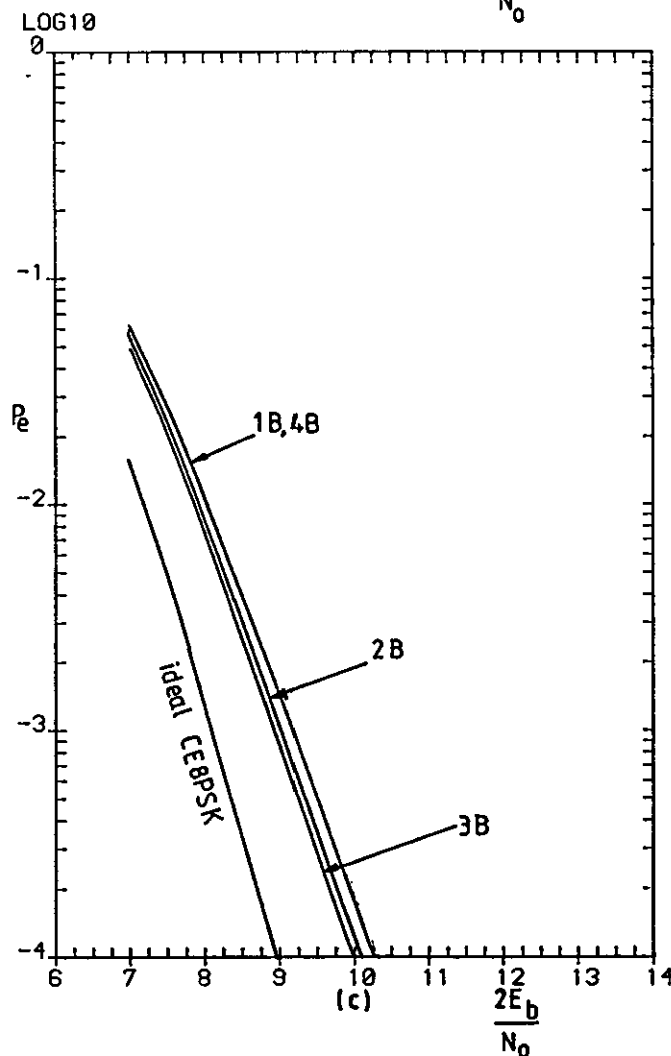
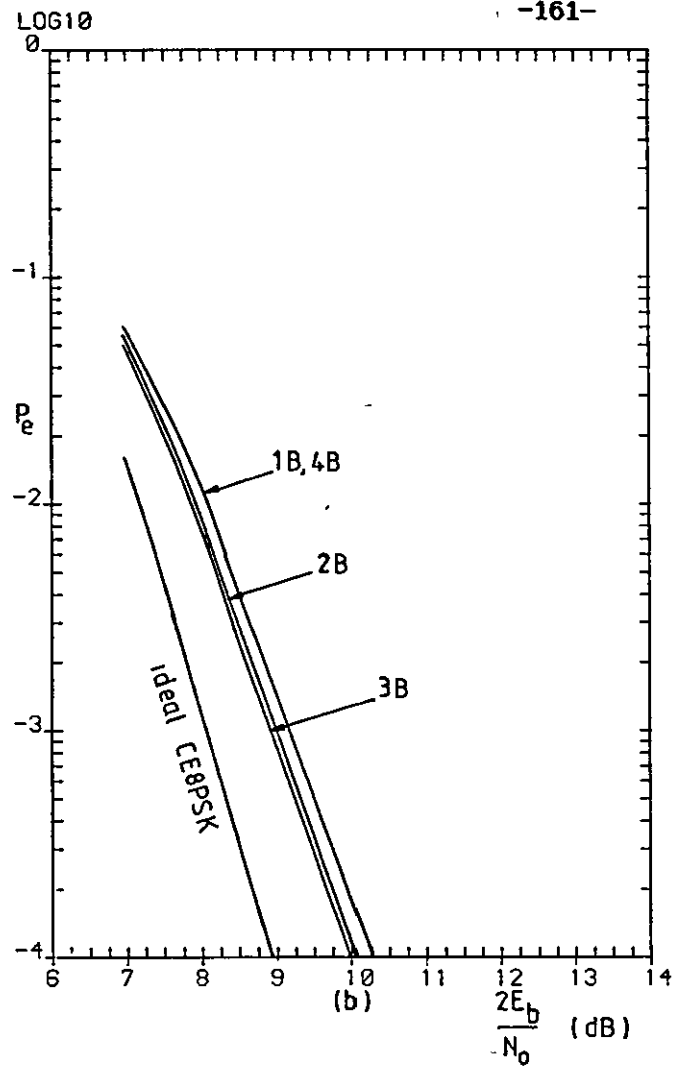
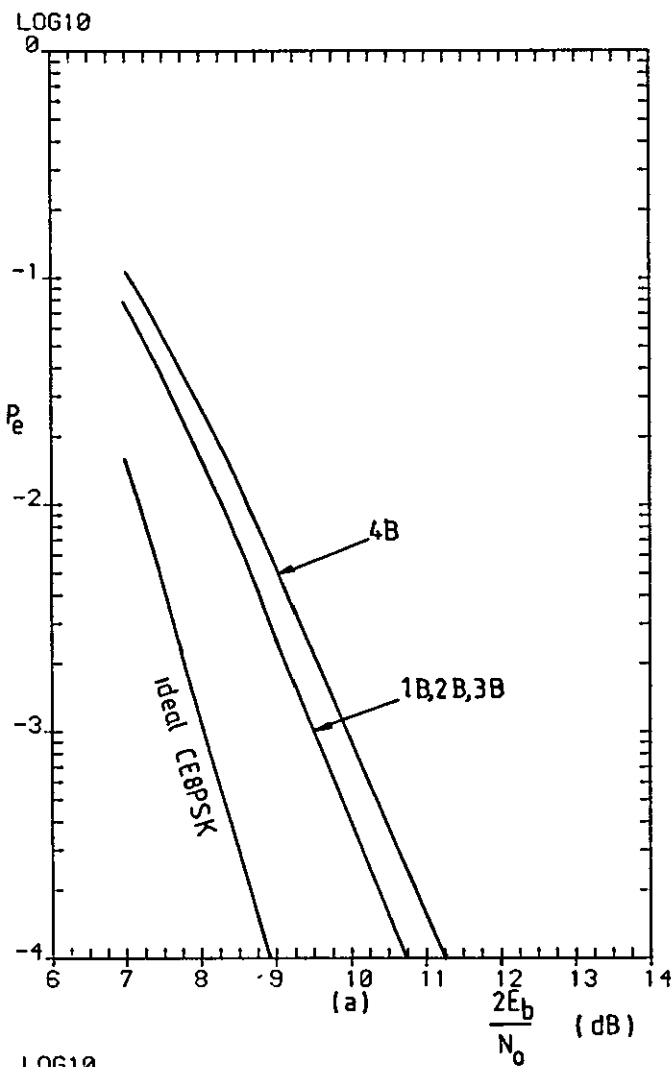


Figure 4.14 Error-rate performances of signals 1B, 2B, 3B and 4B over a nonlinear and bandlimited channel, with the HPA operating at (a) 0 dB, (b) 0.2 dB and, (c) 0.68 dB OBO, respectively, and in an ACI environment with the channel spacing $f_{c_s} = 5R/4$ Hz.

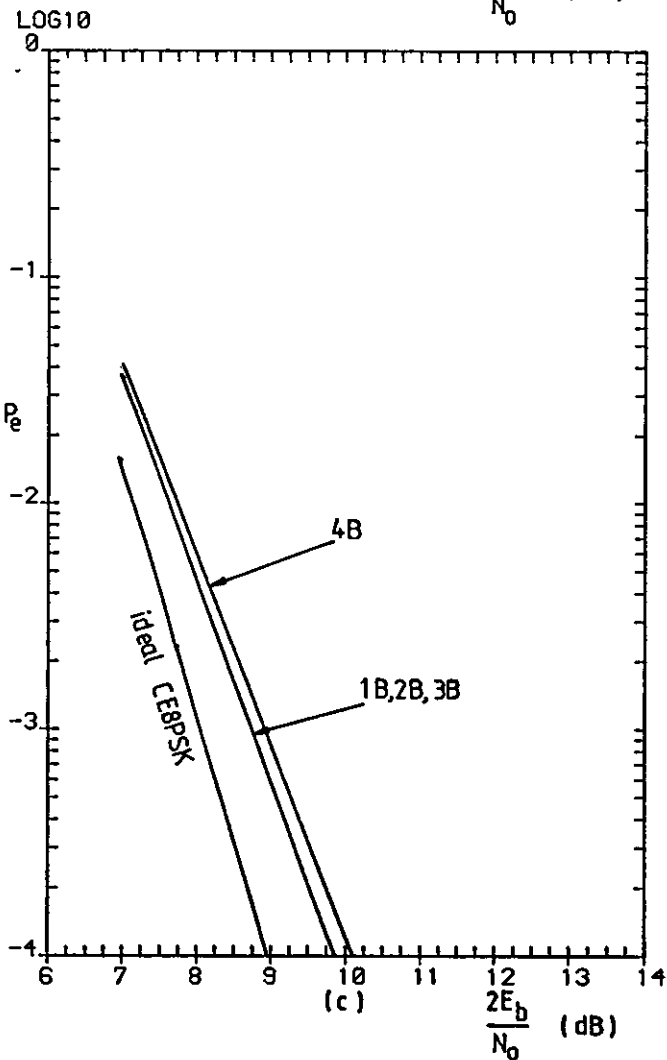
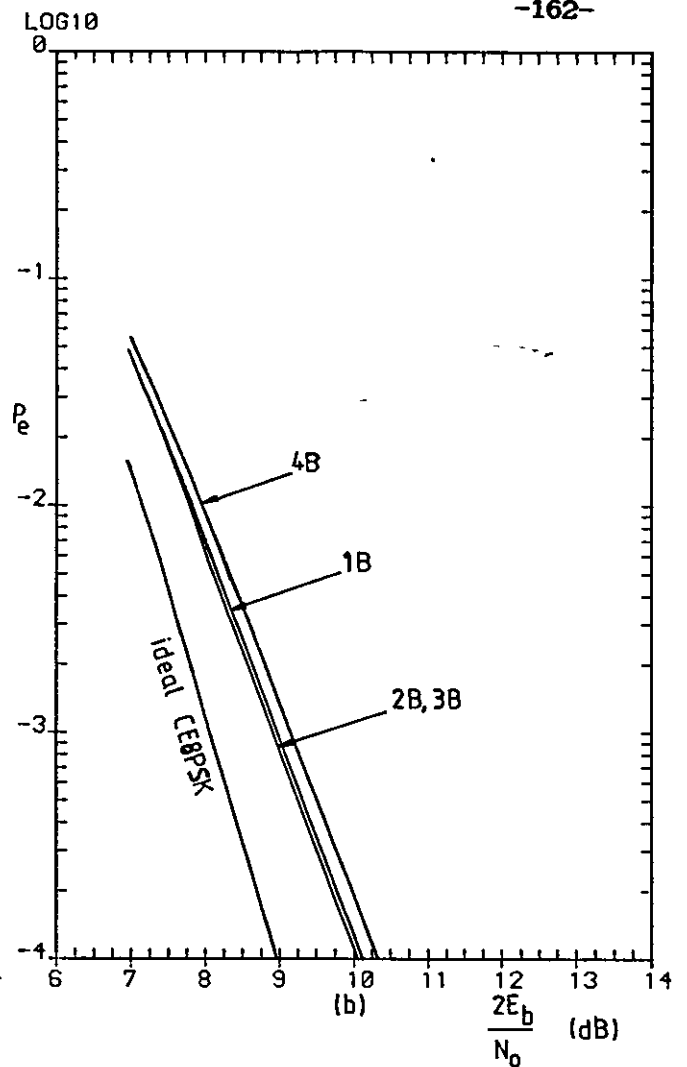
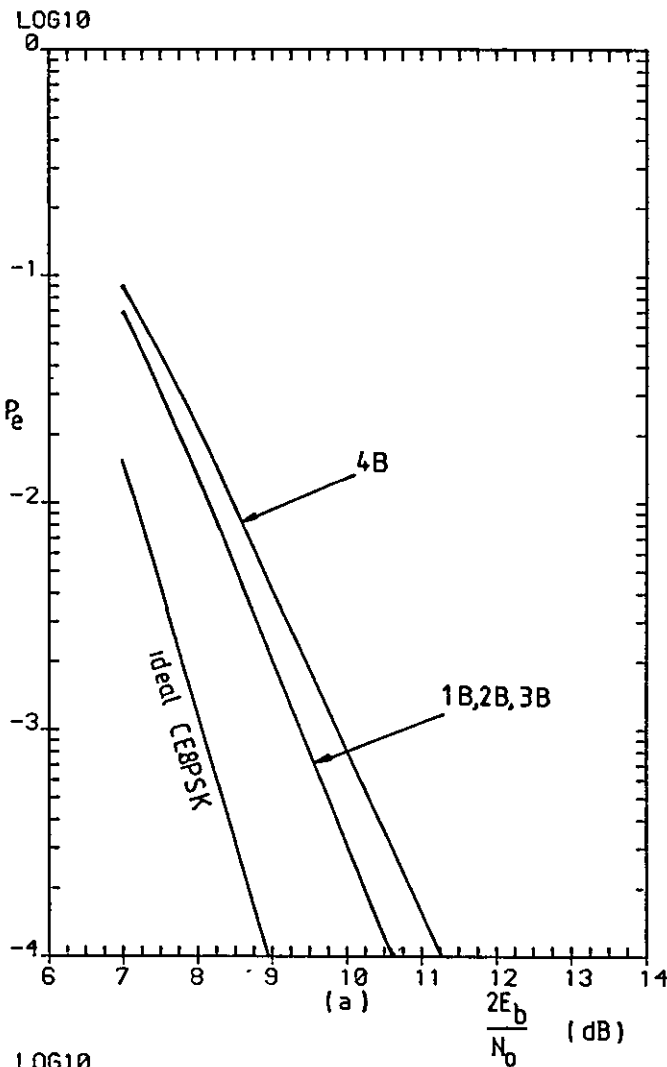


Figure 4.15 Error-rate performances of signals 1B, 2B, 3B and 4B over a nonlinear and bandlimited channel, with the HPA operating at (a) 0 dB, (b) 0.2 dB and, (c) 0.68 dB OBO, respectively, and in an ACI environment with the channel spacing $f_{c,m} = 5.5R/4$ Hz.

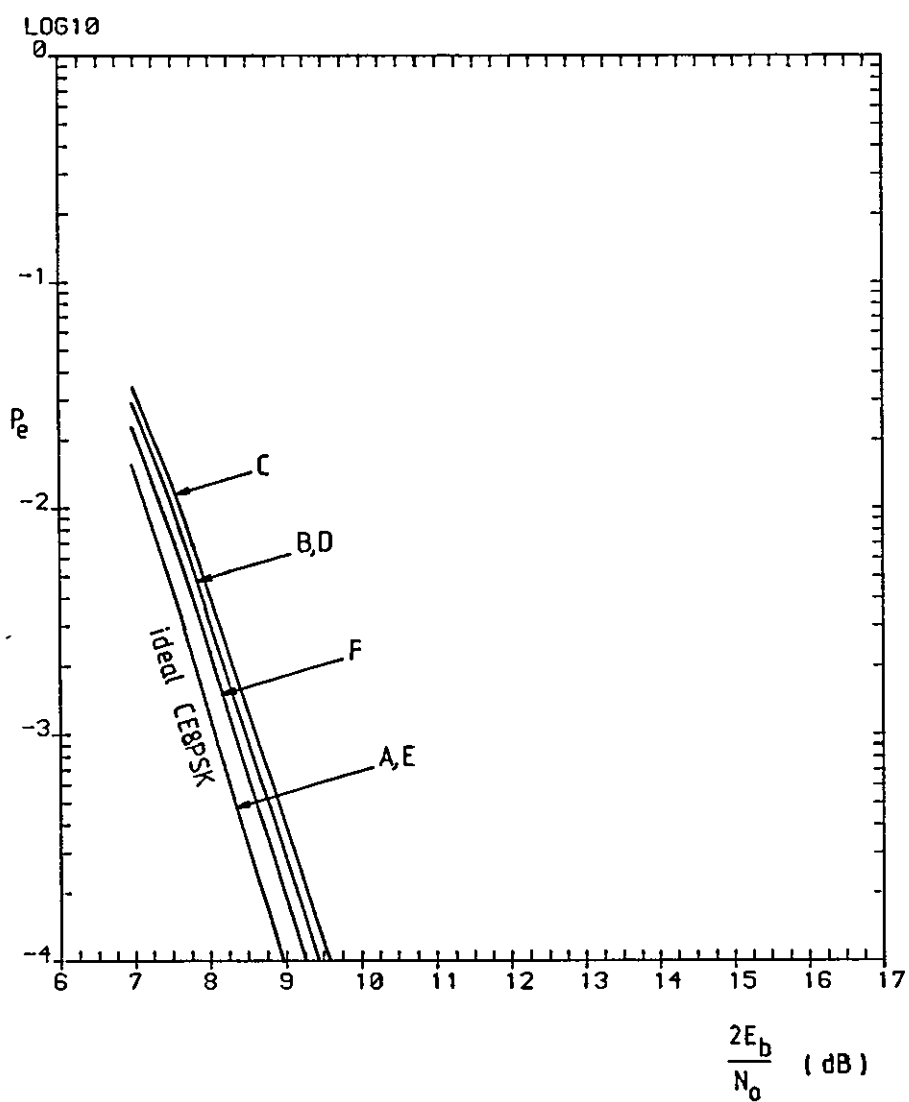


Figure 4.16 Error-rate performances of the CB8PSK signal given by the distance measures A - F.

CHAPTER 5

BASEBAND PREDISTORTION TECHNIQUE AND CONVOLUTIONALLY AND DIFFERENTIALLY ENCODED COHERENT 8 PHASE-SHIFT KEYING (CDE8PSK) TECHNIQUE

5.1 Baseband predistortion technique

5.1.1 Introduction

At present, HPA, TWT and FET (Field Effect Transistor) amplifiers are generally used for high power microwave amplification. The linearity of FET amplifier is somewhat superior to that of HPA and TWT, as its nonlinear effects are considered negligible with reasonable output backoff. However, the maximum FET amplifier output is currently only about 1-4 W in 2-8 GHz [1]. The HPA and TWTA are used exclusively in high power amplifiers, for high capacity satellite transmission. For the present project, although the satellite TWTA is assumed to be operating in the linear mode, the HPA at the earth station distorts the pulse shape, which results in a reduction in tolerance to noise of the system. In addition, it causes spectral spreading which increases ACI, which in turn further degrades the performance. These effects are shown in Sections 3.7.5 and 4.9.4. Hence, without nonlinear compensation, efficient high capacity digital transmission can only be achieved by operating with a large backoff.

Predistortion is one of the best of the many methods of nonlinear compensation [2],[3],[4]. Using this technique, inverse distortion is added to the HPA input to cancel HPA nonlinear distortion. Because of the high microwave power, most predistortion circuit realizations have been achieved by predistortion of the microwave signal. This thesis presents a scheme [5] which compensates for the nonlinear effects of the HPA by predistorting the baseband signal prior to modulation, as opposed to

correcting the distortion after modulation. It is assumed that the characteristics and the operating point of the HPA are known. The circuit realization advantages of the baseband predistorter are greatest in low data rate applications because the component costs are much smaller than the equivalent microwave realization.

5.1.2 Description of the baseband predistorter

From Section 2.5.2, for a modulation signal (Eqn. 2.5.1)

$$S(t) = \sqrt{2}a(t)\cos\omega_c t - \sqrt{2}b(t)\sin\omega_c t \quad 5.1.1$$

with the equivalent baseband signal represented (Appendix A6) as the complex-valued signal (Eqn. 2.5.19)

$$s(t) = a(t) + jb(t) \quad 5.1.2$$

where $j=\sqrt{-1}$, input to the HPA, the equivalent baseband signal at the HPA output, with the use of the HPA backoff factor H_c , is given by (Eqns. 2.5.21, 2.5.20 and 2.5.17)

$$z(t) = s(t)H_c G(\hat{\lambda}) \quad 5.1.3$$

$$= [a(t) + jb(t)]H_c [G_p(\hat{\lambda}) + jG_q(\hat{\lambda})] \quad 5.1.4$$

where $G(\hat{\lambda}) = [G_p(\hat{\lambda}) + jG_q(\hat{\lambda})] \quad 5.1.5$

is the conversion function of the HPA and is dependent on the envelope $\hat{\lambda}$. $\hat{\lambda}$ is a short-hand notation for

$$\hat{\lambda}(t) = H_c [a^2(t) + b^2(t)]^{1/2} \quad 5.1.6$$

from Eqn. 2.5.18.

The baseband predistorter, described here, adds inverse distortion to the inphase and quadrature components, $a(t)$ and $b(t)$, of the modulation signal, $S(t)$, to cancel HPA nonlinear distortion. Note that $a(t)$ and $b(t)$ are the inphase and quadrature modulated waveforms, respectively, so that

predistortion is carried out on the baseband signal. The baseband predistorter consists of two circuits, as shown in Fig. 5.1: the envelope predistortion circuit and the phase predistortion circuit. The former predistorts the (inphase and quadrature) components of the signal equally; however, this does not change the signal phase, while the latter in cascade with the envelope predistortion circuit predistorts the phase of the signal, yet, does not affect the amplitude of the envelope.

Figure 5.1 shows a block diagram of the baseband predistorter. It has two major parts:

- (1) A circuit that predistorts the amplitude of the baseband signal $s(t)$. It is a hardware realization of the operation

$$[a(t) + jb(t)]|D(E)|$$

where $|D(E)|$ is the predistorter amplitude conversion function, whose value is dependent on the signal envelope E . E is a short-hand notation for

$$E(t) = [a^2(t) + b^2(t)]^{1/2} \tag{5.1.7}$$

- (2) A circuit that predistorts the phase angle of the complex-valued baseband signal $s(t)$ (Eqn. 5.1.2). It is a hardware realization of the operation

$$[a(t) + jb(t)]\{\cos[f(E)] + j\sin[f(E)]\}$$

where $f(E)$ is the predistorter phase conversion function, whose value is dependent on E .

In fact, these two operations can be combined by using a single circuit with a hardware realization given by

$$x(t) = [a(t) + jb(t)]|D(E)|\{\cos[f(E)] + j\sin[f(E)]\} \tag{5.1.8}$$

$$= [a(t) + jb(t)]\{|D(E)|\cos[f(E)] + j|D(E)|\sin[f(E)]\} \tag{5.1.9}$$

$$= [a(t) + jb(t)]\{D_p(E) + jD_q(E)\} \tag{5.1.10}$$

$$\text{with } D_p(E) = |D(E)|\cos[f(E)] \quad 5.1.11a$$

$$\text{and } D_q(E) = |D(E)|\sin[f(E)] \quad 5.1.11b$$

where $x(t)$ is the predistorted baseband (modulating) signal, and $D_p(E)$ and $D_q(E)$ are the inphase and quadrature conversion functions, respectively, of the predistorter. A lookup table may be used to supply these multiplicative factors, $D_p(E)$ and $D_q(E)$, (which will be derived later in this section,) to apply to each of the baseband signal components, for any given value of E , as shown in Fig. 5.2b. These values are calculated such that they cancel as much as possible the nonlinear effects of the HPA.

5.1.3 Modelling of the baseband predistorter

Let $D(E) = D_p(E) + jD_q(E)$, where $j = \sqrt{-1}$. Then Eqn. 5.1.10 becomes

$$x(t) = [a(t) + jb(t)]D(E) \quad 5.1.12$$

where $D(E)$ represents the conversion function of the predistorter. The equivalent model of the predistorter is shown in Fig. 5.3a, where the predistorter is represented by the conversion function $D(E)$. Since the value of $D(E)$ is dependent on the input signal envelope $E(t)$, it can be varied by multiplying $E(t)$ by a constant factor P_c (as in the case of the HPA) to give the signal envelope (Eqn. 5.1.7)

$$\hat{E}(t) = P_c [a(t)^2 + b^2(t)]^{1/2} \quad 5.1.13$$

This is equivalent to shifting the operating point along the predistorter transfer characteristics by using the value of P_c , so that P_c can be used to locate the operating point at the required backoff value. P_c is called the predistorter backoff factor. Hence, with the use of the predistorter backoff factor, the signal from the predistorter output, for an input signal of

$$u(t) = a(t) + jb(t) \quad 5.1.14$$

is given by (Eqns. 5.1.10 and 5.1.12)

$$x(t) = [a(t) + jb(t)]P_c[D_p(\hat{E}) + jD_q(\hat{E})] \quad 5.1.15$$

$$= [a(t) + jb(t)]P_c D(\hat{E}) \quad 5.1.16$$

$$= u(t)P_c D(\hat{E}) \quad 5.1.17$$

In practice, the analog baseband signal components, $a(t)$ and $b(t)$, are generated by using a pair of digital filters and then an D/A conversion process (Section 2.4.1). Thus predistortion can be carried out digitally on the baseband signal, before the D/A conversion process. Samples of $D(\hat{E})$ which provide sufficient resolution can be stored in a lookup table (Fig. 5.2), and used to determine the required output signal samples. The samples are obtained as follows.

(1) The predistorter AM-AM characteristic is obtained by graphically inverting the HPA AM-AM characteristic, so that the input of the HPA AM-AM characteristic becomes the output of the predistorter AM-AM characteristic. This is illustrated in Fig. 5.4b. Since the predistorter cannot cancel the nonlinear effect of the HPA over the region above saturation, no attempt is made to invert this region. To represent the predistorter AM-AM characteristic by, say h discrete values of $|D(\hat{E})|$, the predistorter voltage transfer characteristic is quantized into regular intervals of δ volts, along the input axis. The values of $|D(\delta_m)|$, where $\delta_m = m\delta$, for $m=1, 2, \dots, h$, are then obtained using the predistorter AM-AM characteristic and the equation

$$|D(\delta_m)| = \frac{\text{Output voltage for an input value of } m\delta \text{ volts}}{m\delta \text{ volts}} \quad 5.1.18$$

This is the AM-AM conversion function of the predistorter.

(2) The predistorter AM-PM characteristic is the negative of the phase rotation introduced by the HPA. Hence by drawing horizontal lines from the predistorter AM-AM characteristic to the HPA AM-PM characteristic, the predistorter AM-PM characteristic can be obtained by taking the negative sign of the corresponding HPA AM-PM values. For example, the negative phase rotation marked as point 'C' on the predistorter AM-PM characteristic is shown by the path 'C' on Fig. 5.4. The complete predistorter AM-PM characteristic is shown in Fig. 5.4b. The quadrature components, $D_p(\delta_m)$ and $D_q(\delta_m)$, of the predistorter characteristic function, for $m=1, 2, \dots, h$, are then obtained using the predistorter phase characteristic and $|D(\delta_m)|$ with the following two equations

$$D_p(\delta_m) = |D(\delta_m)| \cos[f(\delta_m)] \quad 5.1.19a$$

and
$$D_q(\delta_m) = |D(\delta_m)| \sin[f(\delta_m)] \quad 5.1.19b$$

where $f(\delta_m)$ is the AM-PM conversion function of the predistorter and $|D(\delta_m)|$, for $m=1, 2, \dots, h$, have been obtained in (1).

(3) The values of $D_p(\delta_m)$ and $D_q(\delta_m)$, for $m=1, 2, \dots, h$, are then taken as real and imaginary values, respectively, such that

$$D(\delta_m) = D_p(\delta_m) + jD_q(\delta_m) \quad 5.1.20$$

Hence, the conversion function of the predistorter, $\{D(\delta_m)\}$, are obtained.

Since the modulation filter is digital, consider time $t=iT_m$, where $1/T_m$ is the sampling rate. The digital baseband signal, at the filter output, at time iT_m , is given by (Eqn. 5.1.14)

$$u_i = a_i + jb_i \quad 5.1.21$$

where $a_i = a(iT_m)$ and $b_i = b(iT_m)$. So from Eqns. 5.1.17, 5.1.16 and 5.1.15,

the signal sample from the predistorter output, at time $t=iT_u$, is

$$x_i = u_i P_c D(\hat{e}) \quad 5.1.22$$

$$= (a_i + jb_i) P_c D(\hat{e}_i) \quad 5.1.23$$

$$= (a_i + jb_i) P_c [D_p(\hat{e}_i) + jD_q(\hat{e}_i)] \quad 5.1.24$$

$$= [P_c a_i D_p(\hat{e}_i) - P_c b_i D_q(\hat{e}_i)] + j[P_c a_i D_q(\hat{e}_i) + P_c b_i D_p(\hat{e}_i)] \quad 5.1.25$$

where now \hat{e}_i is a quantized value which may not be equal to, but is at least close to, the signal envelope $|u_i P_c|$ at the predistorter input. Equation 5.1.25 shows that, it is possible to achieve a considerable reduction in equipment complexity by combining the operation of modulation filtering and predistortion in a single lookup table.

The model shown in Fig. 5.3b is used to assess the performance of the predistorter, in computer simulation tests. The values of $\{D(\delta_n)\}$, for $n=1, 2, \dots, 32$, obtained by quantizing the predistorter characteristics (Fig. 5.4b) into regular intervals along the input axis and using Eqns. 5.1.18, 5.1.19 and 5.1.20, are shown in Table 5.1.

From Fig. 5.4b, it can be seen that the predistorter introduces nonlinear AM-AM and AM-PM conversion effects. This results in spectral spreading of a signal with a nonconstant envelope, as is seen from the results shown in Section 5.3.1. However, the predistorted signal, at the output of the predistorter, must not be bandlimited if it is used to cancel HPA nonlinear distortion. This is because the high frequency components in the signal, generated in the predistortion process, are needed to cancel the nonlinear distortion of the HPA. Results of computer simulation tests suggest that, if the predistorted signal is bandlimited by the transmitter IF filter F_{IF} , then it ceases to cancel the nonlinear distortion introduced by the HPA. Thus the predistorted signal must not be bandlimited before feeding it into the HPA.

Predistortion is carried out on the sampled baseband signal, whereas the HPA is operating on a continuous bandpass signal. However, as mentioned before, a D/A conversion process is used at the output of the predistorter to obtain the required shape of the analog modulating baseband waveforms, and so a pair of post D/A lowpass filters has to be used to reject spurious signals (Section 2.4.3). It is assumed here that, in all the transmission system models which use the predistorter, the post D/A filters have a rectangular frequency response and a linear phase characteristic over the predistorted signal bandwidth. Clearly, the predistorted signal has a bandwidth of half of the digital sampling rate, i.e., $1/2T_s$. These filters do not distort the signal and so are not included in the simulation models.

5.1.4 Model of the predistorter in cascade with the HPA, used for computer simulation

The baseband equivalent model of the HPA is shown in Fig. 2.11c and discussed in Section 2.5. Here the model of the predistorter in cascade with the HPA, used for computer simulation, is shown in Fig. 5.5. The signal sample value, at the input to the predistorter, at time $t=iT_s$, is (Eqn. 5.1.21)

$$u_i = a_i + jb_i$$

From Eqn 5.1.22, the output signal sample from the predistorter, at time $t=iT_s$, is

$$x_i = u_i P_c D(\hat{e}_i) \quad 5.1.26$$

where x_i and $D(\hat{e}_i)$ have complex values. $D(\hat{e}_i)$ is the conversion function of the predistorter, and \hat{e}_i is a quantized value which may not be equal, but is at least close to the input signal envelope $|u_i P_c|$ (the absolute value of $u_i P_c$). P_c is the predistorter backoff factor used to locate the required operating point on the predistorter characteristics. The predistorted signal sample x_i is then backed off by the HPA backoff factor

H_c and fed into the HPA, which gives at its output the signal sample, at time $t=iT_s$,

$$v_i = x_i H_c G(\hat{A}_i) \quad 5.1.27$$

Hence, from Eqns. 5.1.26 and 5.1.27,

$$v_i = u_i P_c D(\hat{e}_i) H_c G(\hat{A}_i) \quad 5.1.28$$

where v_i and $G(\hat{A}_i)$ have complex values. $G(\hat{A}_i)$ is the conversion function of the HPA, \hat{A}_i is a quantized value which may not be equal, but is at least close to the input signal envelope $|u_i P_c D(\hat{e}_i) H_c|$, and H_c is the HPA backoff factor used to locate the required operating point on the HPA characteristics.

5.1.5 Backoff factor of the baseband predistorter

When using predistortion, inverse distortion is added to the HPA input to cancel HPA nonlinear distortion. The distortion varies as the operating point (output power) of the HPA is varied, and so the predistorter must be backed off at a suitable operating point in order to obtain the optimum performance (i.e., optimum cancellation of nonlinear distortion).

Figure 5.6 shows how the HPA AM-AM conversion effect on a signal is cancelled by using the predistorter. It can be seen that, when an input signal with a sinusoidal envelope is fed into the predistorter, the envelope of the signal at its output is amplitude distorted, but if the predistorted signal is fed into the HPA backed off at the right operating point, the original envelope is recovered. Figure 5.6 shows that, when the signal with an average voltage of BX volts is fed into the predistorter, the average output voltage is not BY volts, but BZ volts. This is caused by the nonlinear AM-AM conversion effect of the predistorter. So when the predistorted signal is fed into the HPA, it should be backed off at BZ volts, instead of BY volts, in order to obtain the optimum cancellation of nonlinear distortion, because the average voltage into the HPA is now BZ volts.

Since the AM-AM conversion effect of the predistorter is nonlinear, the optimum operating point for compensating for the nonlinear effects of the HPA operating at a given backoff value cannot be found directly or simply from the predistorter characteristics. Computer simulation tests were, in fact, used to find this. Extensive computer simulation tests, which take into account ACI, have been carried out and the results suggest that 0.68 and 1.16 dB IBO (Input Backoff) of the predistorter are the optimum values (i.e., give the best error-rate performances) for the HPA operating at 0.2 and 0.68 dB OBO, respectively. Since the predistorter can only cancel the HPA nonlinear effects occurring below saturation, when predistortion is used, the HPA should be operating below saturation. Thus in all the transmission systems which use the predistorter described in this thesis, the HPA is operating either at 0.2 or 0.68 dB OBO with the predistorter operating at 0.68 or 1.16 dB IBO, respectively.

5.1.6 Baseband equivalent model of DEQPSK or CE8PSK system (or CDE8PSK system) with the use of the predistorter

Since the predistorted signal at the predistorter output must not be bandlimited in order to cancel HPA nonlinear distortion (Section 5.1.3), the transmitter IF filter F_{IF} cannot be used. In order to maintain the equal sharing of the overall filtering between the transmitter and receiver filters (as has been assumed in all the transmission systems discussed so far), the modulation filter should now have the characteristics of the baseband equivalent model of the receiver IF filter in cascade with the demodulation filter. In practice, since this filter is digital, it is not difficult to realize. So in all the transmission system models with the use of the predistortion technique described in this thesis, the above filter arrangement is assumed. Hence the equal sharing of the overall filtering between the transmitter and receiver filters is maintained.

The baseband equivalent model of a DEQPSK or CE8PSK system (or CDE8PSK system described later), with the use of the predistorter in an ACI environment, is shown in Fig. 5.7. (The model is modified from the model shown in Fig. 3.6 or 4.7.) For DEQPSK systems, the transmitters have a differential and Gray encoder, and the receiver has a threshold detector, a Gray and differential decoder. Whereas for CE8PSK systems, the transmitters have a convolutional and Gray encoder, and the receiver has a Viterbi decoder. The simulation methods are exactly as described in Sections 3.3 and 3.4 (and 4.5 for CE8PSK signal), except that with e_m in Eqn. 3.3.8 replaced by x_m (Eqn. 5.1.26)

$$x_m = u_m P_c D(\hat{e}_m) \quad 5.1.29$$

Thus Eqn. 3.3.8 becomes

$$z_m = u_m P_c D(\hat{e}_m) H_c G(\hat{\lambda}_m) + n_m \quad 5.1.30$$

where z_m , u_m , $D(\hat{e}_m)$, $G(H_c)$ and n_m all have complex values. \hat{e}_m and $\hat{\lambda}_m$ are the quantized values which are closest to the corresponding input signal envelopes $|u_m P_c|$ and $|u_m P_c D(\hat{e}_m) H_c|$, respectively.

5.2 Convolutionally and differentially encoded 8 phase-shift keying (CDE8PSK) technique

5.2.1 Description of a CDE8PSK system

In any modulation technique, if the information is transmitted in N different phases, there is an N -fold ambiguity in the data recovery. The ambiguity is not a defect of the carrier recovery circuit, but is inherent to suppressed-carrier, phase-shift keying [6]. It can only be resolved by special encoding or other information carried in the message.

In QPSK signals (Section 3.1.1), since the information is carried in 4 different phases, the carrier recovery circuit has a fourfold ambiguity, and so differential encoding is used to resolve the ambiguity. In the CE8PSK system described in Section 4.2, each pair of data bits, together

with the previous two pairs of data bits, are used to determine one of the eight possible carrier phases by means of the convolutional encoder. So when carrier is recovered, there is an eight-fold ambiguity. A simulation test has been carried out for the CE8PSK signal and the result suggests that if the recovered carrier has a wrong reference phase, the decoder is not able to decode the received signal, i.e., catastrophic failure results. So, before designing the carrier recovery circuit (which is discussed in Chapter 7), the eight-fold ambiguity in carrier recovery must be resolved first.

The simplest method of resolving the ambiguity is to send a training sequence of data, at the start of any transmission, to locate the phase of the reference carrier. The advantage of the method is that no special coding is required. However, the disadvantage is that, during the transmission, if there is a sudden phase change or fading in the signal, the carrier may lose the reference phase and catastrophic failure results.

Another method to resolve the ambiguity is to use a differential encoding technique. In the DEQPSK system described in Section 3.1.2, the differential encoder at the transmitter encodes each pair of binary symbols, so that the phase change rather than the absolute phase carries the data, thus eliminating the need for a reference phase at the receiver. The same principle, in fact, can be applied to CE8PSK signals which then become convolutionally and differentially encoded 8PSK (CDE8PSK) signals. The block diagram of a CDE8PSK system is shown in Fig. 5.8. The information to be transmitted is carried by the sequence of binary data-symbols $\{\alpha_n\}$. The $\{\alpha_n\}$, after being serial-to-parallel converted and convolutionally encoded (Section 4.2), produce a sequence of $\{e_i\}$, where e_i is a 3-component vector. At time $t=iT$, e_i has one of 8 possible values given by (Eqn. 4.2.4 in Section 4.2)

$$e_i = [e_i^{(1)} \quad e_i^{(2)} \quad e_i^{(3)}] \tag{5.2.1}$$

where $e_i^{(j)} = 0$ or 1, for $j=1, 2, 3$. Each vector e_i represents a 3-bit binary

sequence. In the generation of a differential encoded vector d_1 , where d_1 is also a 3-component vector with 8 possible values given by

$$d_1 = [d_1^{(1)} \quad d_1^{(2)} \quad d_1^{(3)}] \quad 5.2.2$$

where $d_1^{(j)} = 1$ or 0 , for $j=1, 2, 3$, the present vector, e_1 , is added to the previous differential encoded vector, d_{1-1} , to form the present differential encoded vector d_1 . This process produces a sequence $\{d_1\}$. Each vector of the sequence $\{d_1\}$ is then Gray encoded, according to Table 5.2 (which is similar to Table 4.2), to give two output sequences $\{q_1^{(1)}\}$ and $\{q_1^{(2)}\}$ where $q_1^{(j)} = \pm 0.924$ or ± 0.383 , for $j=1, 2$. The sampling, filtering and modulation processes, etc., following this are exactly the same as described in the CE8PSK system in Section 4.2.

Assume that, in Fig. 5.8, the bandpass transmission channel introduces no attenuation, delay or distortion, but that it adds a Gaussian noise waveform, $N(t)$, to the transmitted signal, so that the channel is exactly the same as the one used in the QPSK or CE8PSK systems described in Sections 3.1.1 or 4.2, respectively. At the input of the demodulator, the signal is (Eqn. 4.2.6)

$$r(t) = \sqrt{2}[a(t)\cos\omega_c t - b(t)\sin\omega_c t] + N(t) \quad 5.2.3$$

where $N(t)$ is a sample function of a Gaussian random process with zero mean and a two-sided power spectral density of $\frac{1}{2}N_0$ over the signal frequency band. Assume that the bandwidth of $N(t)$ is small compared with its carrier frequency ω_c rad/s, so Eqn. 5.2.3 can be written [7] as

$$r(t) = [\sqrt{2}a(t) + N_c(t)]\cos\omega_c t - [\sqrt{2}b(t) + N_s(t)]\sin\omega_c t \quad 5.2.4$$

as can be seen from Eqn. 3.1.4, where $N_c(t)$ and $N_s(t)$ are sample functions of Gaussian random processes, with zero mean and a two-sided power spectral density twice that of $N(t)$ (Appendix A7).

It has been shown, in Section 3.1.1, that under these conditions, the inphase and quadrature baseband signal components, at the demodulation filter output, are (Eqn. 3.1.7 or 4.2.8)

$$r^{(1)}(t) = \sum_i q_i^{(1)} h(t-iT) + v^{(1)}(t) \quad 5.2.5a$$

and
$$r^{(2)}(t) = \sum_i q_i^{(2)} h(t-iT) + v^{(2)}(t) \quad 5.2.5b$$

respectively, where $h(t)$ is the inverse Fourier transform of $H(f)$ which is the transfer function of the modulation and demodulation filters in cascade. $v^{(1)}(t)$ and $v^{(2)}(t)$ are filtered Gaussian noise waveforms. Bearing in mind that the bandpass channel introduces no attenuation, delay or distortion.

Assume that, in Fig. 5.8, the modulation and demodulation filters have the same characteristics, and the combined transfer function is a sinusoidal rolloff amplitude characteristic (Eqn 2.2.3) with a linear phase characteristic, so that $h(0)=1$ and $h(iT)=0$, for all values of the integer i other than $i=0$. The signals $r^{(1)}(t)$ and $r^{(2)}(t)$ have no ISI at the time instants $\{iT\}$. Assume also that the receiver provides the ideal required timing signal, so the two baseband waveforms, $r^{(1)}(t)$ and $r^{(2)}(t)$, at the demodulation filter output are sampled at the time instants $\{iT\}$, to give two sequences of sample values $\{r_i^{(1)}\}$ and $\{r_i^{(2)}\}$ to the decoder. At time $t=iT$, the samples are (Eqn. 3.1.8)

$$r_i^{(1)} = q_i^{(1)} + v_i^{(1)} \quad 5.2.6a$$

and
$$r_i^{(2)} = q_i^{(2)} + v_i^{(2)} \quad 5.2.6b$$

where $v_i^{(1)}$ and $v_i^{(2)}$ are sample values of Gaussian random variables with zero mean and fixed variance σ^2 , the $\{v_i^{(1)}\}$ and $\{v_i^{(2)}\}$ being statistically independent and independent also of the $\{\alpha_i\}$.

The received samples $\{r_i^{(1)}\}$ and $\{r_i^{(2)}\}$ are fed to the decoder which produces at its output the sequence of symbols $\{\hat{\alpha}_i\}$ which forms the

sequence of decoded data symbols. In the absence of noise, the $\{\hat{\alpha}_L\}$ are the same as the $\{\alpha_L\}$. The aim of the decoder is to generate the sequence $\{\hat{\alpha}_L\}$ such that the corresponding sequences $\{q_i^{(1)}\}$ and $\{q_i^{(2)}\}$, which would have been transmitted in response to the given $\{\alpha_L\}$ at the transmitter input, are at the minimum unitary (total) distance from the received sequences $\{r_i^{(1)}\}$ and $\{r_i^{(2)}\}$ [8].

5.2.2 Baseband equivalent model of CDE8PSK system, with a linear or nonlinear satellite channel, for computer simulation

The CDE8PSK system here operates at a speed of 64, 128, 256 or 512 kbit/s over a satellite link. Since CDE8PSK signals, as for CE8PSK signals, use a quadrature modulation technique, the system can be greatly simplified by assigning real values to the signals in one of the two parallel channels (that associated with $\sqrt{2}\cos\omega_c t$) and imaginary values to the signals in the other channel, and then considering the linear modulator, the transmitter IF filter, the HPA, the receiver IF filter and the linear demodulator, as a baseband transmission path carrying complex-valued signals, as is done for the CE8PSK system shown in Section 4.3. In fact, apart from the differentially encoding process used at the transmitter and the decoding process used at the receiver, a CDE8PSK system is exactly the same as a CE8PSK system, thus the model shown in Fig. 4.6 is used here to describe the CDE8PSK system over a linear or nonlinear channel (see the description shown in Section 4.3). The information to be transmitted is carried by the sequence of binary data-symbols $\{\alpha_L\}$, where the $\{\alpha_L\}$ have the possible values 0 or 1. The coded symbols $\{q_i\}$ are obtained from the $\{\alpha_L\}$, by the convolutional and Gray encoder (Section 5.2.1). The i^{th} symbol has the value

$$q_i = (\pm 0.924 \pm j0.383) \text{ or } (\pm 0.383 \pm j0.924) \quad 5.2.7$$

where $j = \sqrt{-1}$, the $\{q_i\}$, of course, being statistically independent and

equally likely to have any of the eight possible values. The $\{q_i\}$ are used to form the sequence of impulses $\{\sum_i q_i \delta(t-iT)\}$ at the input of the modulation filter. The signal waveform at the output of the modulation filter is the complex-valued baseband signal

$$u(t) = \sum_i q_i h_t(t-iT) \quad 5.2.8$$

where $h_t(t)$ is the impulse response of the modulation filter and, at any given value of time t , is real (Section 2.4.1). Similar to the DEQPSK and CE8PSK system shown in Section 3.3 or 4.3, respectively, the system is modelled digitally. The continuous waveforms in the system are modelled as discrete waveforms.

The waveform $u(t)$ is sampled 8 times per symbol, at the time instants $\{mT_m\}$, where $T=8T_m$, to give the sequence $\{u_m\}$, where $u_m=u(mT_m)$. The $\{u_m\}$ are then fed to a baseband equivalent model of one of the bandpass channels, as shown in Fig. 4.6.

For the description of the processing of the sampled signal $\{u_m\}$ in the baseband equivalent model of (a) a linear and memoryless bandpass channel, (b) a linear and bandlimited bandpass channel and, (c) a nonlinear and bandlimited bandpass channel, and for the calculation of $2E_b/N_0$ in the simulation tests, see Section 3.3.

The sampled signal $\{w_m\}$ (given by Eqn 3.3.2, 3.3.6 or 3.3.9, depending on which channel is used), are filtered by the demodulation filter. The sampled impulse response of the demodulation filter, sampled at the rate of $1/T_m$ samples per second, is given by the $(n+1)$ -component vector

$$P = [p_0 \quad p_1 \quad p_2 \quad \dots \quad p_n] \quad 5.2.9$$

where the $\{p_m\}$, for $0 \leq m \leq n$, have real-valued components (Table 2.1), and $p_m=p(mT_m)$. Thus at time $=mT_m$, the signal sample at the filter output is

$$r_m = \sum_{n=0}^n w_{m-n} p_n \quad 5.2.10$$

where r_m has a complex value.

Assume that the receiver provides the required ideal timing signal, so the sequence $\{r_m\}$ is sampled once per symbol, at the time instants $\{iT\}$, to give the sequence $\{r_i\}$, where r_i has a complex value. The $\{r_i\}$ are fed to the decoder which produces at its output the sequence of symbols $\{\hat{\alpha}_L\}$ which form the sequence of decoded binary-data symbols.

5.2.3 Suboptimum decoder for CDE8PSK signals

In the CDE8PSK system, the phase change carries the data, not the absolute phase, so the decoder is slightly different from the Viterbi-algorithm decoder used for CE8PSK signals.

When the $\{r_i\}$ are fed to the decoder, the decoder forms and stores a set of $m=2^L$ vectors (sequences) $\{X_L\}$, where

$$X_L = [x_1 \quad x_2 \quad x_3 \quad \dots \quad x_L] \quad 5.2.11$$

and $x_h=0$ or 1 , for $h=1, 2, \dots, L$. x_h here represents a possible value of α_h . For each stored vector X_L , the decoder forms eight different vectors

$$Y_1^{(j)} = [y_1^{(j)} \quad y_2^{(j)} \quad y_3^{(j)} \quad \dots \quad y_L^{(j)}] \quad 5.2.12$$

where $y_i^{(j)}$ is a possible value of r_i and $i=L/2$ (because a coded-symbol is transmitted for each pair of data symbols). The $\{y_h^{(j)}\}$, for $h=1, 2, \dots, L$, have complex values and are the possible values of the transmitted signal values. Since the transmitted signals phases are differentially encoded, the first component (i.e., the initial phase), $y_1^{(j)}$, for $j=1, 2, \dots, 8$, takes on 8 different possible values in the eight vectors. This takes into account the 8 possible initial reference phases. $Y_1^{(j)}$, for $j=1, 2, \dots, 8$, would have been transmitted in place of the sequence of the $\{q_i\}$ had the vector X_L been fed to the encoder at the transmitter in place of the vector

$$\alpha_L = [\alpha_1 \quad \alpha_2 \quad \alpha_3 \quad \dots \quad \alpha_L] \quad 5.2.13$$

that was actually sent, subject to the constraint that $y_1^{(j)}$ was the

initial phase. Clearly, since the transmitted signal phases are differentially encoded, the possible values of $y_2^{(j)}$, $y_3^{(j)}$, ..., $y_i^{(j)}$ in each of the 8 vectors, $\{Y_i^{(j)}\}$, depend on the first component (initial phase) of that vector. The ISI introduced by the channel is neglected in the decoding process in order to reduce the equipment complexity of the decoder. (This assumption is valid because the IF filters only introduce a low level of ISI, as is shown in Section 3.7.2.) The decoder forms and stores together with each X_L , the corresponding 8 possible distances

$$C_i^{(j)} = c_1^{(j)} + c_2^{(j)} + c_3^{(j)} + \dots + c_i^{(j)} \quad 5.2.14$$

where, for $h=1, 2, \dots, i$, $c_h^{(j)} = |r_h - y_h^{(j)}|^2$. $|r_h - y_h^{(j)}|$ is the absolute value of the complex value $(r_h - y_h^{(j)})$. Since, for $j=1, 2, \dots, 8$, there are 8 different vectors, $Y_i^{(j)}$, which form 8 different values of $C_i^{(j)}$, there are 8 possible distances associated with each X_L . This takes into account the 8 possible phase references (i.e., the eightfold phase ambiguity) caused by the carrier recovery circuit.

Ideally, no firm decision is reached as to the value of any α_n until the whole sequence $\{r_i\}$ has been received, when all $\{\alpha_n\}$ are decoded simultaneously from the received $\{r_i\}$, the decoded values $\{\hat{\alpha}_L\}$ being the values of the $\{x_n\}$ in the stored vector X_L having the smallest distance $C_i^{(j)}$. To reduce the equipment complexity, as for the Viterbi decoder, in the determination of $\{\hat{\alpha}_{L-2n+1}, \hat{\alpha}_{L-2n+2}\}$, the decoder does not consider the values of $x_{L-2n}, x_{L-2n-1}, \dots$. Thus, instead of storing m L -component vectors $\{X_L\}$, the decoder stores the corresponding $2n$ -component vector $\{Z_L\}$, where

$$Z_L = [x_{L-2n+1} \quad x_{L-2n+2} \quad x_{L-2n+3} \quad \dots \quad x_L] \quad 5.2.15$$

so that Z_L is formed by the last $2n$ components of the corresponding vector X_L . The distances $\{C_i^{(j)}\}$, for $j=1, 2, \dots, 8$, of this vector X_L are now said to be the distances of Z_L .

In practice, in the decoder the receiver holds in store $m=4^{K-1}$ (K is the constraint length of the code) vectors $\{Z_L\}$, with the minimum distance of $C_1^{(j)}$, for $j=1, 2, \dots, 8$, corresponding to the 4^{K-1} different possible combinations of values of $x_{L-2K+3}, x_{L-2K+4}, \dots, x_L$. Thus each stored vector Z_L forms the last $2n$ components of the vector X_L that minimises $C_1^{(j)}$, for $j=1, 2, \dots, 8$, subject to the constraint that $x_{L-2K+3}, x_{L-2K+4}, \dots, x_L$, have the given values, and $y_{1-K+1}^{(j)}$, for $j=1, 2, \dots, 8$, take on the 8 different possible values. It is assumed for convenience here that $L > 2K$. Associated with each stored vector Z_L are stored the corresponding $\{C_1^{(j)}\}$, for $j=1, 2, \dots, 8$. Therefore, there are altogether $8m$ different values of $C_1^{(j)}$. The decoded binary data-symbols $(\hat{\alpha}_{L-2n+1}, \hat{\alpha}_{L-2n+2})$ are taken to be the values of (x_{L-2n+1}, x_{L-2n+2}) , respectively, in the vector Z_L associated with the smallest $C_1^{(j)}$. Following the receipt of the sample r_{i+1} , each of the stored vectors $\{Z_L\}$ forms a common part of 4 vectors $\{X_{L+2}\}$, having the 4 possible values of (x_{L+1}, x_{L+2}) . Each of these 4 vectors is associated with 8 corresponding distances

$$C_{i+1}^{(j)} = C_1^{(j)} + c_{i+1}^{(j)} \quad 5.2.16$$

for $j=1, 2, \dots, 8$, where

$$c_{i+1}^{(j)} = |r_{i+1} - y_{i+1}^{(j)}|^2 \quad 5.2.17$$

and, for $j=1, 2, \dots, 8$, the $\{C_1^{(j)}\}$ are distances of the original vector Z_L , and the $\{y_{i+1}^{(j)}\}$ are complex values and have 8 possible received values. For each of the 4^{K-1} possible combinations of values, $x_{L-2K+5}, x_{L-2K+6}, \dots, x_{L+1}, x_{L+2}$, the decoder now selects the vector Z_{L+2} , having the smallest $C_{i+1}^{(j)}$ and then it stores the vector Z_{L+2} and the 8 smallest values $\{C_{i+1}^{(j)}\}$, for $j=1, 2, \dots, 8$. $(\hat{\alpha}_{L-2n+3}, \hat{\alpha}_{L-2n+4})$ are taken to be the values of (x_{L-2n+3}, x_{L-2n+4}) , respectively, in the stored vector Z_{L+2} associated with the smallest $C_{i+1}^{(j)}$, and the process continues in this way.

r_{i+1} , and $y_{i+1}^{(j)}$ in Eqn. 5.2.17 are complex-valued and it requires two operations of squaring or multiplication to determine each of the 4 possible values of $c_{i+1}^{(j)}$ (i.e., the unitary distance of two complex numbers). Hence, for $j=1, 2, \dots, 8$, it requires 64 operations of squaring or multiplication to compute the 32 values of $c_{i+1}^{(j)}$ for each vector X_{L+2} . There are m vectors Z_L , so it requires altogether $64m$ operations of squaring or multiplication. However, $y_{i+1}^{(j)}$, in Eqn. 5.2.7, has only 8 possible values because it is one of the 8 possible received complex-valued samples. Thus, of these $32m$ values of $c_{i+1}^{(j)}$, many have the same values. There are only 8 different values of $c_{i+1}^{(j)}$, and each of them requires 2 operations of squaring or multiplication to determine. Therefore, following the receipt of the sample r_{i+1} , the decoder has to carry out only 16 operations of squaring or multiplication to compute the 8 different values of c_{i+1} , which are used to form the $32m$ values $\{C_{i+1}\}$.

The starting up procedure can be exactly the same as that for decoding CE8PSK signals (Section 4.4). However, now it is not necessary that the receiver provides the required carrier signal with no ambiguity, as it is required for decoding CE8PSK signals. If the recovered carrier has a phase shift of $h\pi/4$, where $h=1, 2, \dots, \text{ or } 7$, because the signal is differentially encoded, the decoder is still able to decode the received signal, although with an initial burst of errors (about 4 to 9 bits).

It can be seen that the processing of 4^K vectors and 8×4^K values of distances, followed by the storage of 4^{K-1} $2n$ -component vectors $\{Z_L\}$ and $8 \times 4^{K-1}$ values $\{C_{i+1}^{(j)}\}$, are involved in the decoding of each received pair of data $(\alpha_{L+1}, \alpha_{L+2})$. For the present, $K=3$, it requires 16 vectors which expand into 64 vectors to form the decoder, and each vector is now associated with eight different distances, i.e., a total of 128 distances. These 128 distances expand into 512 distances on the expansion of the vectors. (Each distance expands 4 ways, since there are 4 possible values

of (x_{1+1}, x_{1+2}) . The decoder must store 4^{K-1} $2n$ -component vectors and so requires the same amount of storage as for CE8PSK signals, but it requires 512 distances, instead of 64 in each decoding process

Although the decoder resolves the 8-fold ambiguity in carrier recovery of CDE8PSK signals, because the differential encoder at the transmitter is a feedback loop, it is only a suboptimum decoder and not a true Viterbi decoder for the signal.

Having done this, it is discovered that a true Viterbi decoder can be designed to resolve the 8-fold ambiguity in carrier recovery of CE8PSK signals. This is described briefly in Section 8.1.

5.2.4 Performance of CDE8PSK signal

For DEQPSK signals, the differential decoding process is performed after signal detection. If one symbol is in error, the decoder output will tend to have double symbol errors because 2 symbols are compared for each output symbol. Thus the bit error rate of the Gray encoded DEQPSK signal is twice as much as Gray encoded QPSK signal.

For CDE8PSK signals, the convolutional and differential encoding processes are carried out simultaneously in the decoder. If one symbol is in error, the decoder output will tend to have two, three or four symbol errors, because each symbol is correlated with three other symbols. The performance of the CDE8PSK signal, using Code 1 (Table 4.2), over an AWGN channel, and with the suboptimum decoder used with a delay of 32 symbols in decoding, has been evaluated by computer simulation. The result, as shown in Fig. 5.9, indicates that the difference between the performances of CE8PSK and CDE8PSK signals increases as P_e increases. This cannot be caused by the correlation property of the transmitted symbols. If it were, the difference would have decreased as P_e increased. However, this is expected because the decoder is no longer the true Viterbi decoder

5.3 Simulation results and discussion

Computer simulation tests have been carried out to assess the error-rate performances of the different systems, with the use of the predistorter, using DEQPSK, CE8PSK and CDE8PSK signals, with the preferred equipment filters and HPA. In all simulation tests, it is assumed that the receiver provides the ideal required carrier and timing signals, and the data-transmission systems are optimized by sharing the overall filtering equally between the transmitter and receiver. In the cases of CE8PSK and CDE8PSK signals, the decoder uses 16 stored vectors with a delay of 32 symbols in decoding.

5.3.1 Reductions in spectral spreading

Computer simulation tests have been carried out to estimate the spectra of CDE8PSK signals, over the linear and memoryless channel and the linear and bandlimited channel. The results suggest that, with the use of the same transmitter filtering, CDE8PSK signals have the same spectra as those of DEQPSK and CE8PSK signals (Fig. 3.14). This is expected because the differential encoding process does not alter the signal spectra.

Computer simulation tests have also been carried out to estimate the signal spectra at the output of the HPA for different types of signals. The results show that, if the same transmitting filtering are used, DEQPSK, CE8PSK and CDE8PSK signals all have the similar shapes of signal spectra. With the use of the predistorter prior to the HPA, the power spectra of DEQPSK, CE8PSK and CDE8PSK signals at the output of the HPA, with and without the predistorter, and at the output of the predistorter, over the nonlinear channel, were estimated. The results suggest that, with the same modulation filter, the predistorter has the same effect on all the signals, i.e., DEQPSK, CE8PSK and CDE8PSK signals all have the similar spectra. So, under the same conditions, DEQPSK, CE8PSK and CDE8PSK systems have the same level of ACI in the desired channel. With the HPA operating at 0.2 and 0.68 dB OBO, the estimated signal power spectra of

signal 1A, 2A, 3A and 4A at the output of the HPA, with and without the use of the predistorter, are shown in Figs. 5.10 and 5.11, respectively. The estimated power signal spectra of the corresponding signals at the output of the predistorter are also shown in the same figures. The results show that, since the predistorter is a nonlinear device, it causes spectral spreading to the signals, but the consequent spectral spreading at the output of the HPA is significantly reduced. Comparing the power spectra at the output of the HPA, without the use of the predistorter, against the power spectra with the use of the predistorter, it can be seen that a significant reduction in spectral spreading at the HPA output has been achieved by the use of the predistorter. The transmitted signal power spectra, over a linear channel, are also shown in the same figures for comparison.

5.3.2 Performances of signals 1A, 2A, 3A and 4A

(A) with the use of the predistorter in a non ACI environment

The simulation model, used to evaluate the error-rate performances of DEQPSK signals, is shown in Fig. 5.7, with Switches 'A' open (so there is no ACI). The performances of signals 1A, 2A, 3A and 4A, with the HPA operating at 0.2 and 0.68 dB OBO, are shown in Figs. 5.12a and b, respectively.

It can be seen that, at 0.68 dB HPA OBO, signals 1A, 2A, 3A and 4A have insignificant degradations in tolerance to noise at $P_e > 10^{-4}$, in comparison with that of an ideal DEQPSK system. Thus the nonlinear effects introduced by the HPA on the signals have been almost completely removed by the predistorter. Table 5.3 shows the degradations in tolerance to noise of the signals at $P_e = 10^{-4}$, with the HPA operating at 0.2 and 0.68 dB OBO, measured in comparison with that of an ideal DEQPSK system. Comparing with the degradations in tolerance to noise of the signals under the same conditions, but without the use of the predistorter, as shown in Table 3.6, it can be seen that the predistorter has improved the performances by cancelling the nonlinear effects of the HPA.

(B) with the use of the predistorter in an ACI environment

The simulation model, used to evaluate the error-rate performance, is shown in Fig. 5.7, with Switches 'A' closed (so there is ACI from the upper and lower channels). The error-rate performances of signals 1A, 2A, 3A and 4A, with the channel spacing $f_{c_m} = 5R/4$ Hz and with the HPA operating at 0.2 and 0.68 dB OBO, are shown in Figs. 5.13a and b, respectively.

At 0.2 dB OBO (Fig. 5.13a), signal 3A has the best performance. Table 5.4 shows the degradations in tolerance to noise of the signals at $P_e = 10^{-4}$, measured in comparison with that of an ideal DEQPSK system. Comparing with the degradations of the corresponding signals, under the same conditions, but without the use of the predistorter, as shown in Table 3.7a, it can be seen that the predistorter has improved the performances of all signals. The largest improvements of about 2.4 dB and 4 dB, at $P_e = 10^{-4}$, are made by signals 3A and 4A, respectively. These improvements are expected since the spectral spreading (and ACI) have been reduced significantly by the predistorter, as can be seen in Figs. 5.10 and 5.11.

Figure 5.13b shows that very little improvement can be obtained by increasing the HPA OBO value from 0.2 dB to 0.68 dB. The penalty for this improvement is about 0.5 dB HPA output power reduction caused by operating the HPA about 0.5 dB below its full output power. Table 5.4 also shows the degradations in tolerance to noise of the signals at $P_e = 10^{-4}$, measured in comparison with that of an ideal DEQPSK system

Comparing the degradations of the signals in Table 5.4, with those obtained under the same conditions but with a linear channel, in Table 3.5, it can be seen that signals 1A and 2A have a slightly better performance over a nonlinear channel than those over a linear channel. The reason is that, after predistorting by the predistorter and distorting by

the HPA, the bandwidths of the main lobes of the signal spectra become narrower, hence ACI is reduced. This can be seen in Figs. 5.10a, 5.10b, 5.11a and 5.12b.

With $f_{c_s}=4.5R/4$ Hz, at 0.2 dB and 0.68 dB HPA OBO, the error-rate performances of signal 4A are shown by the dotted lines in Figs. 5.13a and b, respectively. They suggest degradations in tolerance to noise of about 0.9 dB and 0.7 dB, respectively, at $P_e=10^{-4}$, in comparison with that of an ideal DEQPSK system. Thus, under these assumed conditions, signal 4A can provide a better power-bandwidth efficiency.

From the above results, it can be concluded that, under the assumed conditions, for the preferred filters, predistorter and HPA, if it is not critically important that the modem achieves the very best available tolerance to noise, the most cost effective arrangement is to use signal 4A and to operate the HPA slightly below saturation (say 0.2 dB OBO) with $f_{c_s}=4.5/4$ Hz. The degradation in tolerance to noise is about 0.9 dB at $P_e=10^{-4}$, in comparison with that of an ideal DEQPSK system.

If the very best available tolerance to noise is required by the system, then the most cost effective arrangement is signal 3A, with $f_{c_s}=5R/4$ Hz and the HPA slightly below saturation (say 0.2 dB OBO). The degradation in tolerance to noise is about 0.7 dB, at $P_e=10^{-4}$, in comparison with that of an ideal DEQPSK system.

5.3.3 Performances of signals 1B, 2B, 3B and 4B with the use of the predistorter in an ACI environment

The results in Section 4.9.3 have shown that the nonlinear effects of the HPA on the error-rate performances of signals 1B, 2B, 3B and 4B are quite insignificant. Obviously, with the use of the predistorter, these effects will be further reduced, so there is no need to evaluate the degradations in tolerance to noise of signals 1B, 2B, 3B and 4B due to the nonlinear effects of the HPA.

To evaluate the error-rate performances of signals 1B, 2B, 3B and 4B with the use of the predistorter in an ACI environment, the same model as shown in Fig. 5.7 is used, with Switches 'A' closed. The performances of the signals, with the HPA operating at 0.2 and 0.68 dB OBO, the channel spacing $f_{c_s}=5R/4$ Hz and the unitary distance measure used in the Viterbi decoder, are shown in Figs. 5.14a and b.

At 0.2 dB HPA OBO (Fig. 5.14a), signals 3B and 4B provide the best performances. Table 5.5 shows the degradations in tolerance to noise of the signals at $P_e=10^{-4}$, measured in comparison with that of an ideal CE8PSK system. Comparing with the results without the use of the predistorter, as shown in Table 4.6a or Fig. 4.14, it can be seen that the predistorter has reduced the degradations, due to the HPA, of all the signals. These improvements in P_e degradations are expected since the spectral spreading (and ACI) have been reduced significantly (Section 5.3.1 and Figs. 5.10 and 5.11).

Figure 5.14b shows that very little improvement can be obtained by increasing the HPA OBO value from 0.2 dB to 0.68 dB. The penalty for this is about 0.5 dB HPA output power reduction. The degradations in tolerance to noise of the signals at $P_e=10^{-4}$, measured in comparison with that of an ideal CE8PSK system are shown in Table 5.5.

Now, if the degradations in Table 5.5 are compared with those in Table 5.4 obtained in the previous section, it can be seen that, under the same assumed conditions, the CE8PSK signals have smaller degradations than those of the DEQPSK signals. This is because, in an ACI environment, CE8PSK signals suffer less further degradation in tolerance to noise, due to ACI, than DEQPSK signals. This is also seen in Sections 4.9.4. and 4.9.2

At 0.2 dB and 0.68 dB HPA OBO, with $f_{c_s}=4.5/4$ Hz, the performances of signal 4B are shown by the dotted lines in Figs. 5.14a and b, respectively. They suggest degradations of about 0.8 dB and 0.3 dB, at

$P_e=10^{-4}$, in comparison with that of an ideal CE8PSK system. Thus signal 4B provides a better bandwidth efficiency.

From the above results, it can be concluded that, under the assumed conditions, for the preferred filters, predistorter and HPA, if it is not critically important that the modem achieves the very best available tolerance to noise, the most cost effective arrangement is to use signal 4B and to operate the HPA slightly below saturation (say 0.2 dB OBO), with $f_{c_m}=4.5R/4$ Hz. The degradation in tolerance to noise is about 0.8 dB at $P_e=10^{-4}$, in comparison with that of an ideal CE8PSK system.

If the very best available tolerance to noise is required by the system, then the most cost effective arrangement is signal 3B or 4B, with $f_{c_m}=5R/4$ Hz and the HPA slightly below saturation (say 0.2 dB OBO). the degradation in tolerance to noise is about 0.4 dB, at $P_e=10^{-4}$, in comparison with that of an ideal CE8PSK system.

5.3.4 Performances of CDE8PSK signals

(A) over a linear and bandlimited bandpass channel

To evaluate the error-rate performances of CDE8PSK signals, over a linear and bandlimited channel, the same model as shown in Fig. 4.6 is used, with Switches 'B' closed. Here the encoder at the transmitter carries out convolutional, differential and Gray encoding of the input data, as described in Section 5.2.1, while the decoder at the receiver is that described in Section 5.2.3. To avoid confusion, the CDE8PSK signals here are called signals 1C, 2C, 3C and 4C, instead of signals 1B, 2B, 3B and 4B, respectively. Thus signals 1C, 2C, 3C and 4C are referred to CE8PSK signals with $\beta=100\%$, 75%, 50% and 25%, and with truncation lengths of the sampled impulse responses of 2T, 4T, 4T and 8T, respectively. The results of the computer simulations suggest that, for signals 1C, 2C, 3C and 4C transmitting over the linear and bandlimited bandpass channel, there is no degradation in tolerance to noise at $P_e>10^{-4}$, in comparison with that of an ideal CDE8PSK system.

(B) with the use of the predistorter in an ACI environment

To evaluate the error-rate performances of CDE8PSK signals with the use of the predistorter in an ACI environment, the same model as shown in Fig. 5.7 is used, with Switches 'A' closed. The encoder at the transmitter now carries out convolutional, differential and Gray encoding of the input data, as described in Section 5.2.1, while the decoder at the receiver is that described in Section 5.2.3.

The error-rate performances of signals 1C, 2C, 3C and 4C, with the HPA operating at 0.2 dB and 0.68 dB OBO, the channel spacing $f_{c_m} = 5R/4$ Hz, and the unitary distance measure used in the decoder, are shown in Figs. 5.15a and b.

At 0.2 dB HPA OBO (Fig. 5.15a), signals 3C and 4C provide the best performances. Table 5.6 shows the degradations in tolerance to noise of the signals at $P_e = 10^{-4}$, measured in comparison with that of an ideal CE8PSK system. Figure 5.15b shows that very little improvement can be obtained by increasing the HPA OBO value from 0.2 dB to 0.68 dB. The penalty for this is about 0.5 dB HPA output power reduction, caused by operating the HPA about 0.5 dB below its full output power.

At 0.2 dB and 0.68 dB HPA OBO, with $f_{c_m} = 4.5R/4$ Hz, the error-rate performances of signal 4C are shown by the dotted lines in Figs. 5.15a and b, respectively, which suggest degradations of about 1.3 dB and 1 dB, at $P_e = 10^{-4}$, respectively. Thus signal 4C provides a better power-bandwidth efficiency than the other signals.

Comparing the results in Table 5.6 with those in Table 5.5, it can be seen that the differential encoding causes a degradation of about 0.7 dB, at $P_e = 10^{-4}$. This is expected because the decoder is no longer the optimum decoder, as described in Section 5.2.4.

If the very best available tolerance to noise is required by the system, the most cost effective arrangement is to use signals 3C or 4C, with $f_{c_m} = 5R/4$ Hz and to operate the HPA slightly below saturation (say

0.2 dB OBO). The degradation in tolerance to noise is about 1 dB at $P_e=10^{-4}$, in comparison with that of an ideal CE8PSK system.

From the above results, it can be concluded that, under the assumed conditions, for the preferred filters, predistorter and HPA, if it is not critically important that the modem achieves the very available tolerance to noise, the most cost effective arrangement is signal 4C, with $f_{c_m}=4.5R/4$ Hz and the HPA slightly below saturation (say 0.2 dB OBO). The degradation in tolerance to noise is about 1.3 dB at $P_e=10^{-4}$, in comparison with that of an ideal CE8PSK system.

Comparing the performance of signal 4C (Fig.5.15a), with that of signal 4A (Fig. 5.13a), with $f_{c_m}=4.5R/4$ Hz and the HPA operating at 0.2 dB OBO, it can be seen that, despite the degradation caused by using differential encoding, under the assumed conditions, signal 4C still gains an advantage of 2.4 dB, at $P_e=10^{-4}$, over signal 4A, and hence is worth considering.

REFERENCES

- [1] Microwave J., vol. 24, pp.29, 109, Nov. 1981
- [2] Namiki, J., "An Automatically Controlled Predistorter for Multilevel Quadrature Amplitude Modulation", *IEEE Trans. on Commun.*, vol. COM-31, NO. 5, pp.707-712, May 1983
- [3] Hecken, p. and Heidt, R.C., "Prediction Linearization of the AR-6A Transmitter", in *Conf. Rec., ICC'80*, pp.33.1.1-33.1.6
- [4] Gray, L.F., Alstyne, J.V. and Sadrin, W.A., "Application of Broadband Linearizer to Earth Station", in *Conf. Rec., ICC'80*, pp.33.4.1
- [5] Girard, H. and Feher, K., "A New Baseband Linearizer for More Efficient Utilization of Earth Station Amplifiers Used for QPSK Transmission", *IEEE Trans. on Selected Area in Commun.*, vol. SAC-1, NO. 1, pp.46-56, Jan. 1983
- [6] Gardner, F.M., *Phaselock Techniques*, 2nd Ed, John Wiley & Sons (1979)
- [7] Taub, H. and Schilling, D.C., *Principles of Communication Systems*, pp.235-281, McGraw-Hill (1971)
- [8] Clark, A.P., "Minimum-distance decoding of binary convolutional codes", *Computer and Digital Techniques*, vol. 1, NO. 4, pp.190-196, Oct. 1978
- [9] Clark, A.P., *Advanced Data-Transmission Systems*, Pentech Press, London (1976)
- [10] Viterbi, A.J., "Convolutional Codes and Their Performance in Communication Systems", *IEEE Trans. on Commun.*, vol. COM-19, pp.751-772, 1971
- [11] Hemati, F. and Costello, D.J., "Truncation Error Probability in Viterbi Decoding", *ibid.*, COM-25, pp.530-532, 1977

$m(\delta)$	$D(\delta_m)$ $= D_p(\delta_m) + jD_q(\delta_m)$		$m(\delta)$	$D(\delta_m)$ $= D_p(\delta_m) + jD_q(\delta_m)$	
1	0.280	-0.005	21	0.594	-0.544
2	0.280	-0.012	22	0.594	-0.544
3	0.280	-0.015	23	0.594	-0.544
4	0.285	-0.020	24	0.594	-0.544
5	0.309	-0.033	25	0.594	-0.544
6	0.309	-0.038	26	0.594	-0.544
7	0.319	-0.051	27	0.594	-0.544
8	0.341	-0.063	28	0.594	-0.544
9	0.357	-0.076	29	0.594	-0.544
10	0.358	-0.086	30	0.594	-0.544
11	0.386	-0.104	31	0.594	-0.544
12	0.399	-0.122	32	0.594	-0.544
13	0.418	-0.136			
14	0.432	-0.157			
15	0.453	-0.188			
16	0.468	-0.218			
17	0.492	-0.251			
18	0.504	-0.315			
19	0.574	-0.425			
20	0.594	-0.544			

Table 5.1 Sampled representation of the predistorter conversion function (or characteristics) shown in Fig. 5.4b.

3-bit binary sequence	Phase (degrees)	Magnitude of quadrature components	
		$q_i^{(1)}$	$q_i^{(2)}$
$d_i^{(1)} d_i^{(2)} d_i^{(3)}$			
0 0 0	+ 22.5	+0.924	+0.383
0 0 1	+ 67.5	+0.383	+0.924
0 1 0	+112.5	-0.383	+0.924
0 1 1	+157.5	-0.924	+0.383
1 0 0	-157.5	-0.924	-0.383
1 0 1	-112.5	-0.383	-0.924
1 1 0	- 67.5	+0.383	-0.924
1 1 1	- 22.5	+0.924	-0.383

Table 5.2 Gray encoding for CDE8PSK signals.

HPA OBO (in dB)	Signal			
	1A	2A	3A	4A
0.2	0.4	0.4	0.4	0.6
0.68	0.1	0.1	0.1	0.2

Table 5.3 Degradations in tolerance to noise of signals 1A, 2A, 3A and 4A, with the use of the predistorter, over a nonlinear and bandlimited channel, with the HPA operating at 0, 0.2 and 0.68 dB OBO and in an non-ACI environment, at $P_{av}=10^{-4}$ expressed in dB, measured in comparison with that of an ideal DEQPSK system (from Fig. 5.12).

HPA OBO (in dB)	Signal			
	1A	2A	3A	4A
0.2	1.7	1.1	0.7	0.9
0.68	1.7	1	0.5	0.4

Table 5.4 Degradations in tolerance to noise of signals 1A, 2A, 3A and 4A, with the use of the predistorter and the HPA operating at 0, 0.2 and 0.68 dB OBO and in an ACI environment with the channel spacing $f_{ca}=5R/4$ Hz, at $P_{av}=10^{-4}$ expressed in dB, measured in comparison with that of an ideal DEQPSK system (from Fig. 5.13).

HPA OBO (in dB)	Signal			
	1B	2B	3B	4B
0.2	0.9	0.7	0.4	0.4
0.68	1	0.6	0.2	0.1

Table 5.5 Degradations in tolerance to noise of signals 1B, 2B, 3B and 4B, 3A and 4A, with the use of the predistorter and the HPA operating at 0, 0.2 and 0.68 dB OBO and in an ACI environment with the channel spacing $f_{c_s}=5R/4$ Hz, at $P_s=10^{-4}$ expressed in dB, in measured comparison with that of an ideal DEQPSK system (from Fig. 5.14).

HPA OBO (in dB)	Signal			
	1C	2C	3C	4C
0.2	1.7	1.5	1	1
0.68	1.6	1.3	0.9	0.9

Table 5.6 Degradations in tolerance to noise of signals 1C, 2C, 3C, 4C, with the use of the predistorter and the HPA operating at 0, 0.2 and 0.68 dB OBO and in an ACI environment, with channel spacing $f_{c_s}=5R/4$ Hz, at $P_s=10^{-4}$ expressed in dB, measured in comparison with that of an ideal CE8PSK system (from Fig. 5.15).

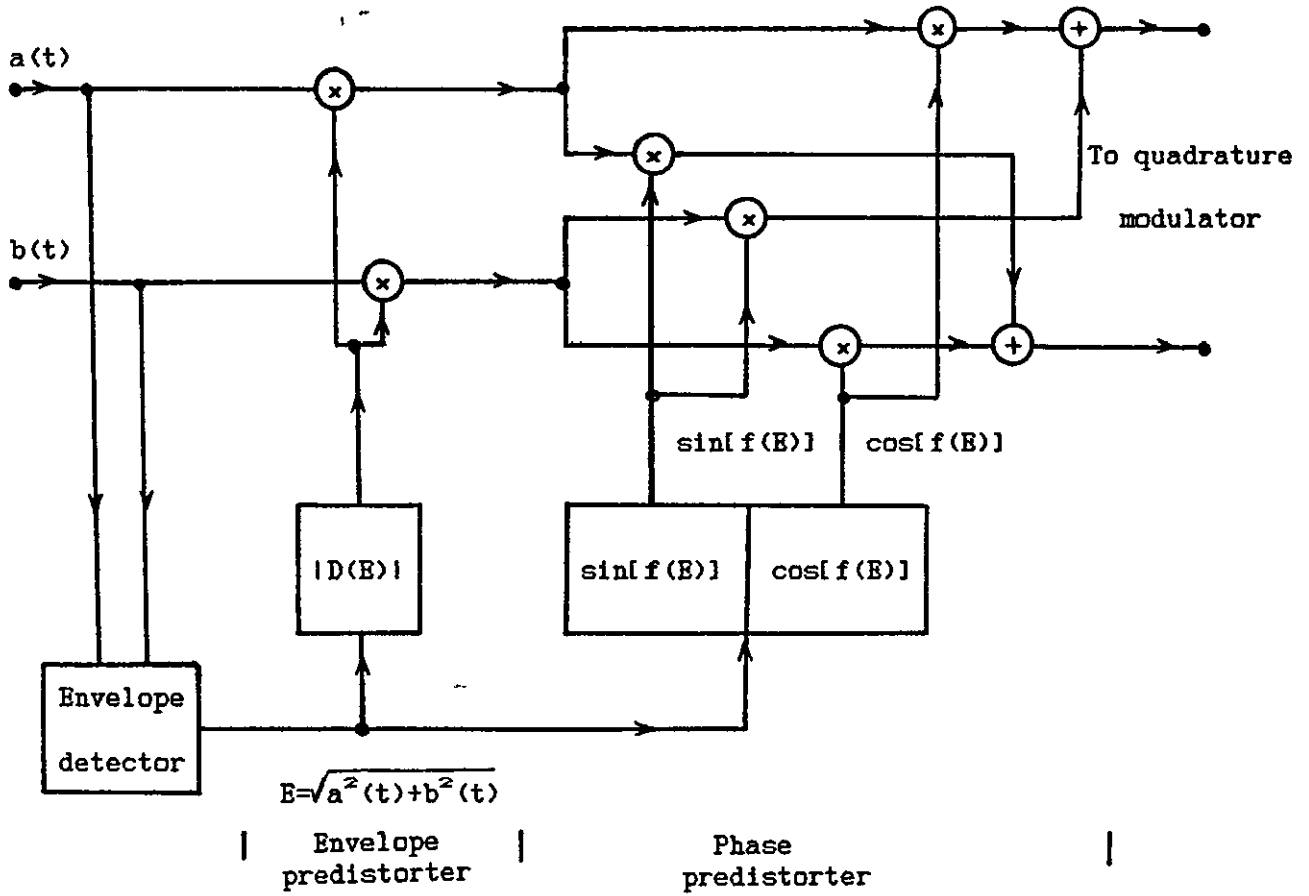


Figure 5.1 Baseband predistorter block diagram.

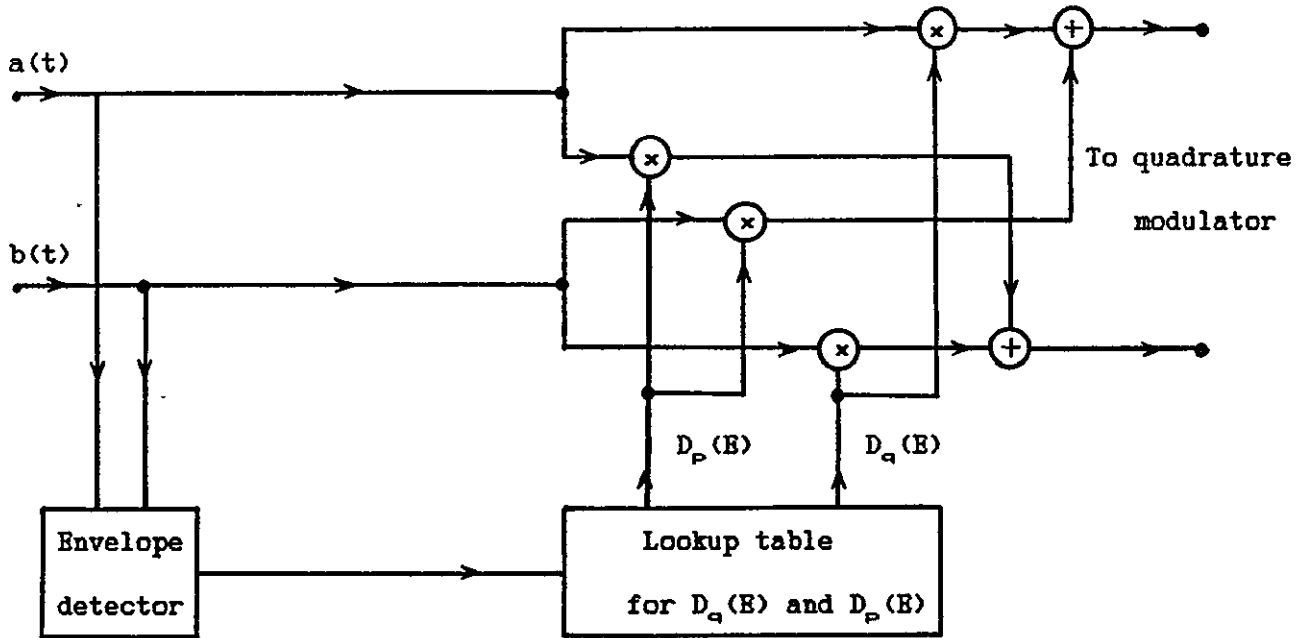
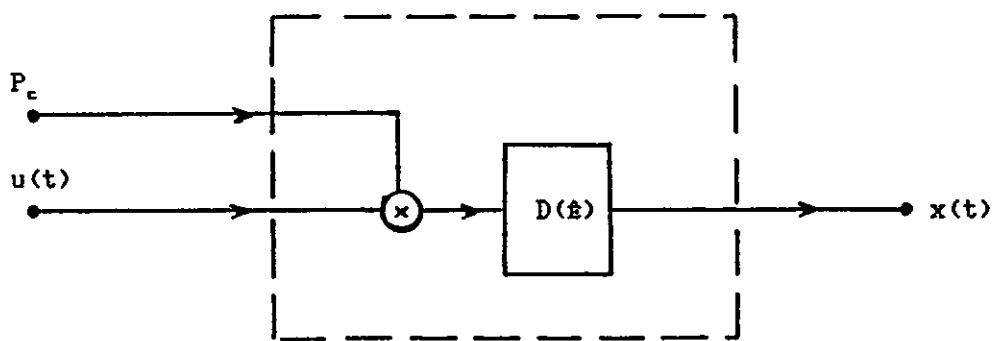
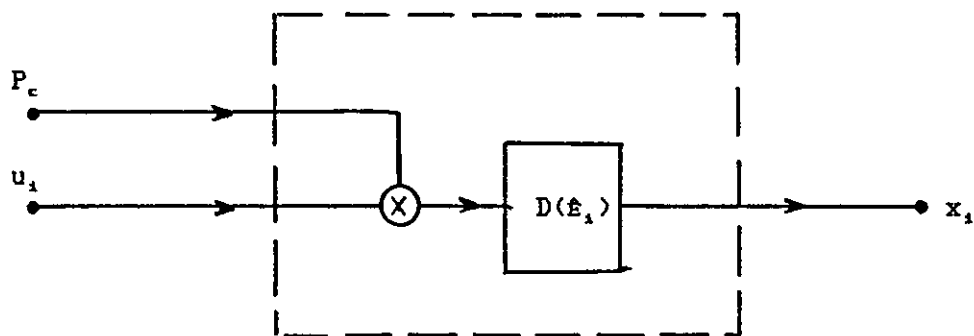


Figure 5.2 A simplified model of the one shown Fig. 5.1.



(a)



(b)

Figure 5.3 (a) Equivalent model of the predistorter. (b) Equivalent model of the predistorter for computer simulation.

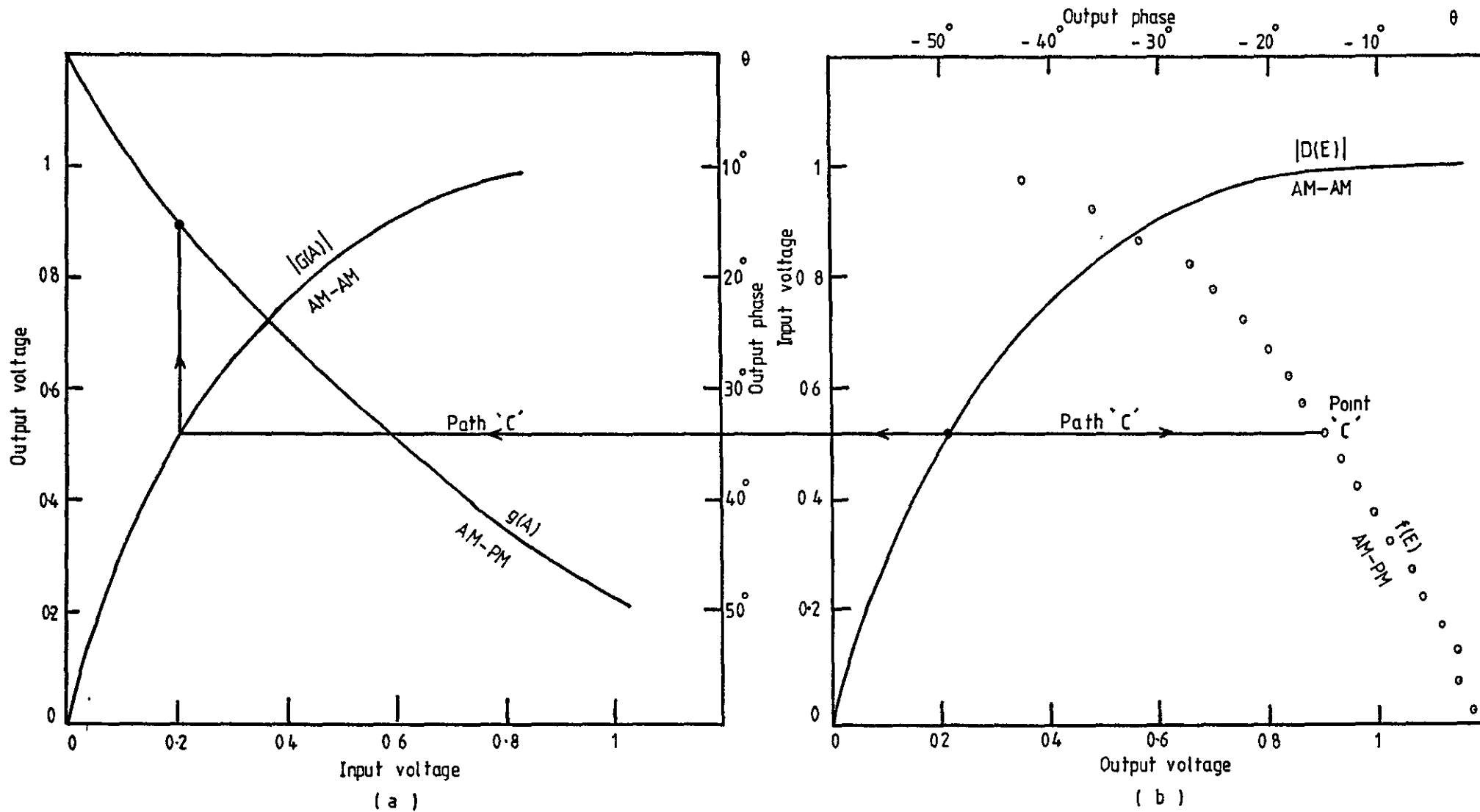


Figure 5.4 (a) HPA characteristics (Figure 2.12). (b) Predistorter characteristics.

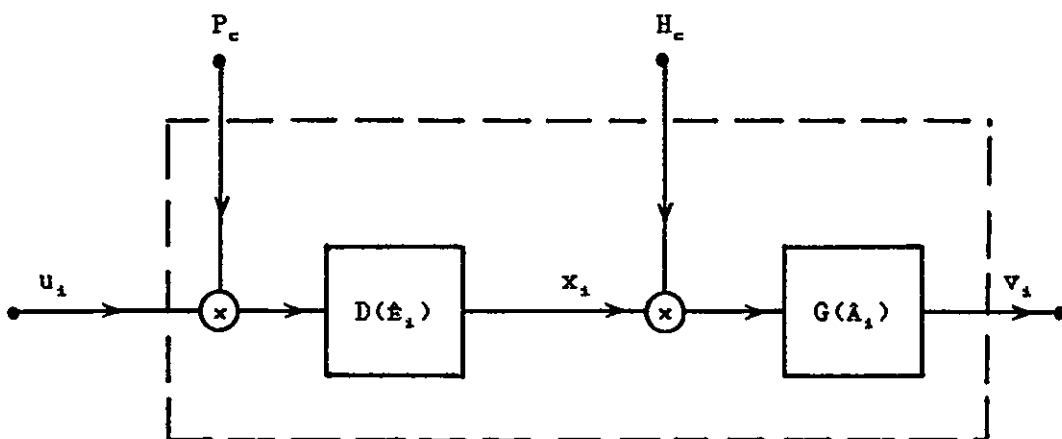


Figure 5.5 Baseband equivalent model of the predistorter in cascade with the HPA.

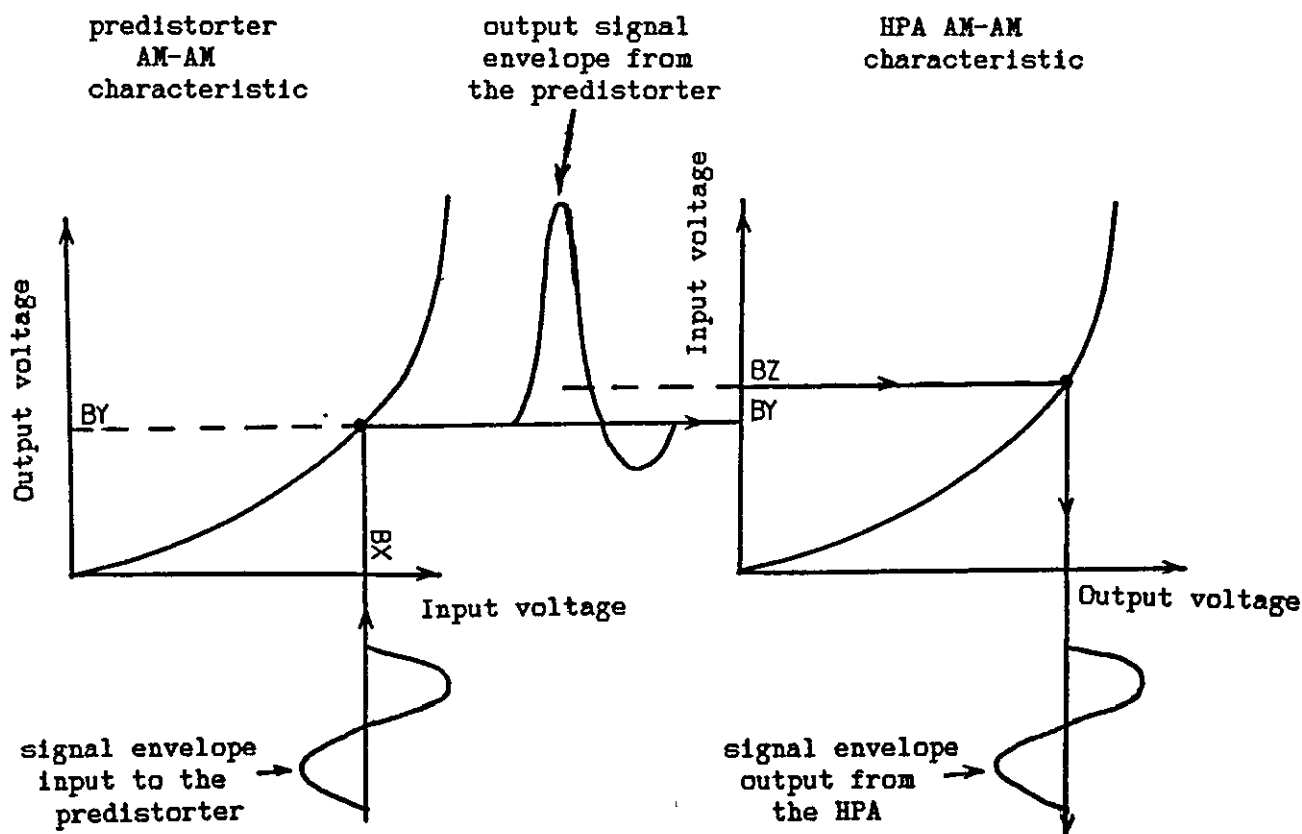


Figure 5.6 Diagram to show how the predistorter removes HPA amplitude distortion.

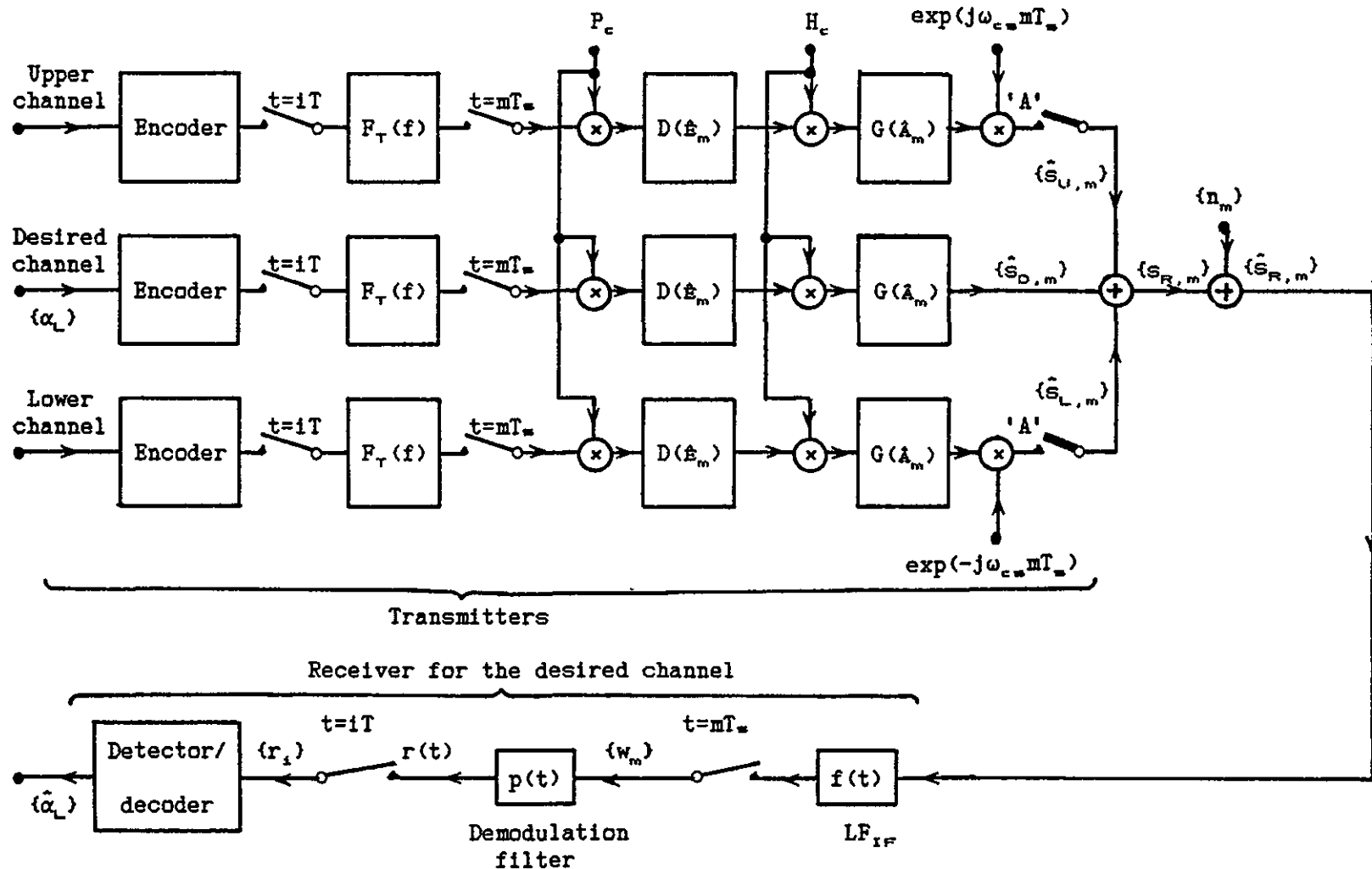


Figure 5.7 Baseband equivalent model of the DEQPSK or CE8PSK (or CDE8PSK) system, with the use of the predistorter and with a linear or a nonlinear satellite channel, for computer simulation. $F_T(f)$ is the resultant transfer function of the baseband equivalent model of the IF filter in cascade with the modulation filter. Switches 'A' determine whether the system is in an ACI or non-ACI environment.

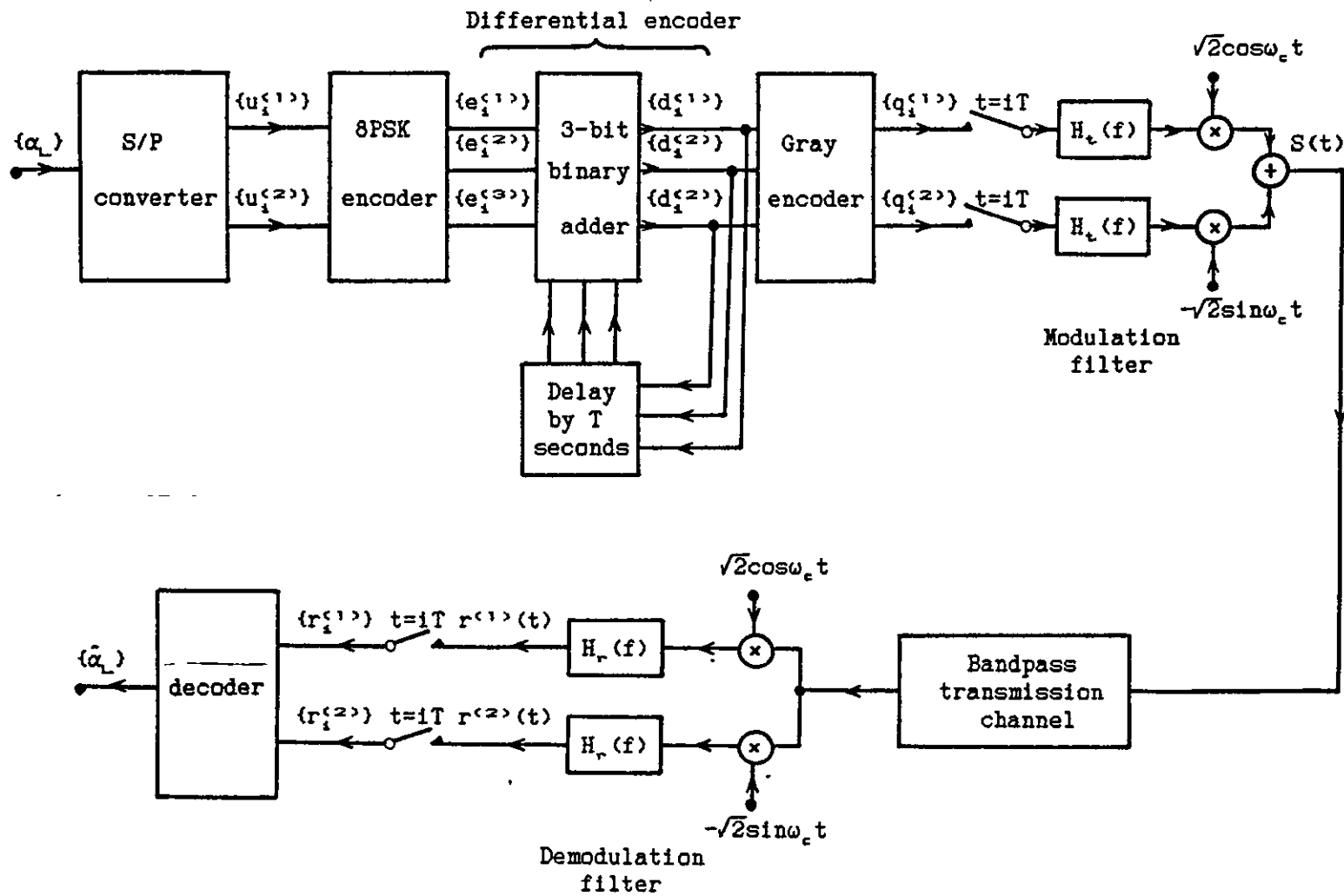


Figure 5.8 Block diagram of a convolutionally and differentially encoded 8PSK (CDE8PSK) system. S/P means serial-to-parallel.

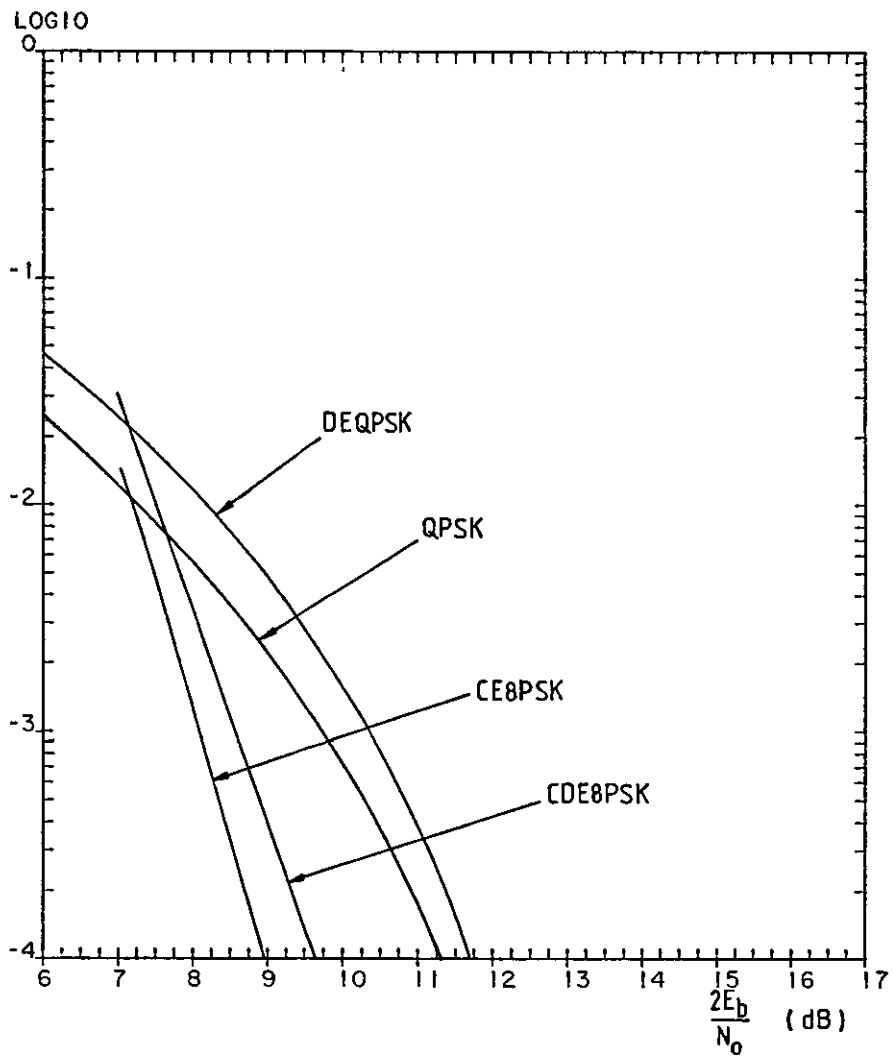


Figure 5.9
AWGN channel.

Error-rate performances of CE8PSK and CDE8PSK signals over an

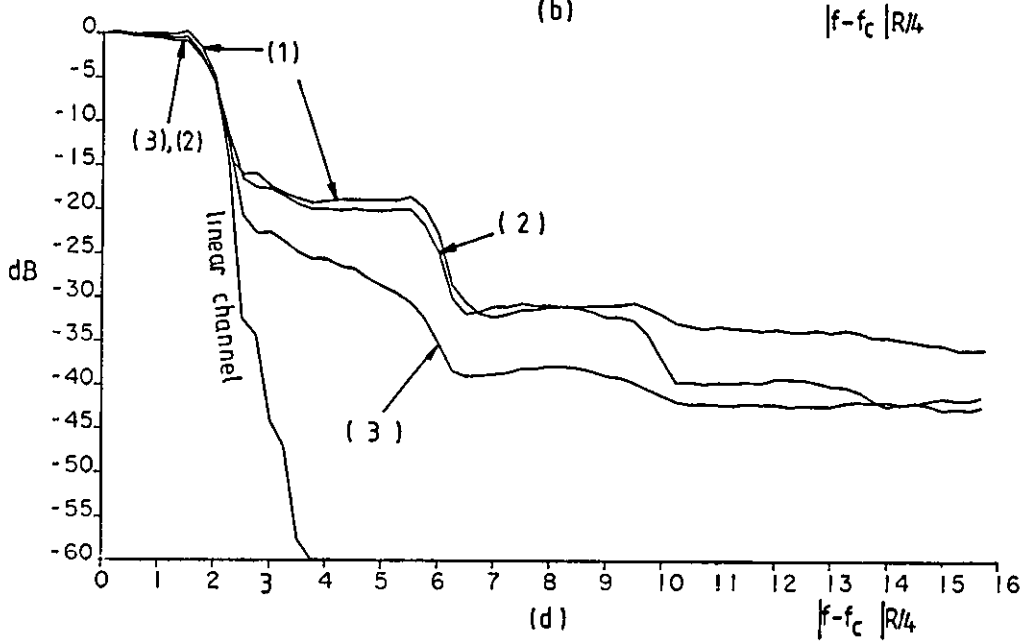
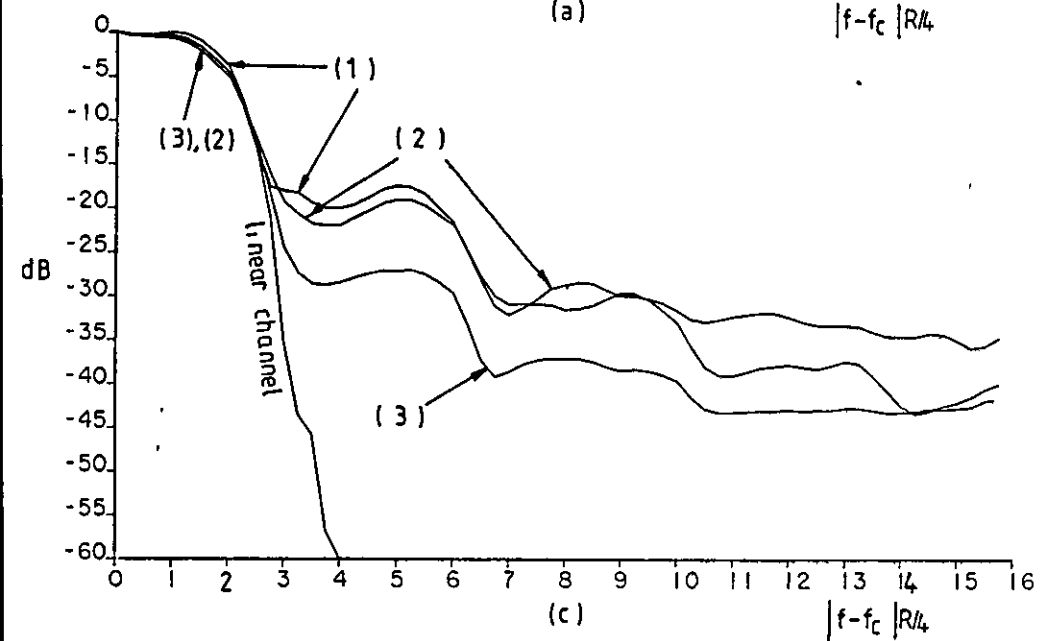
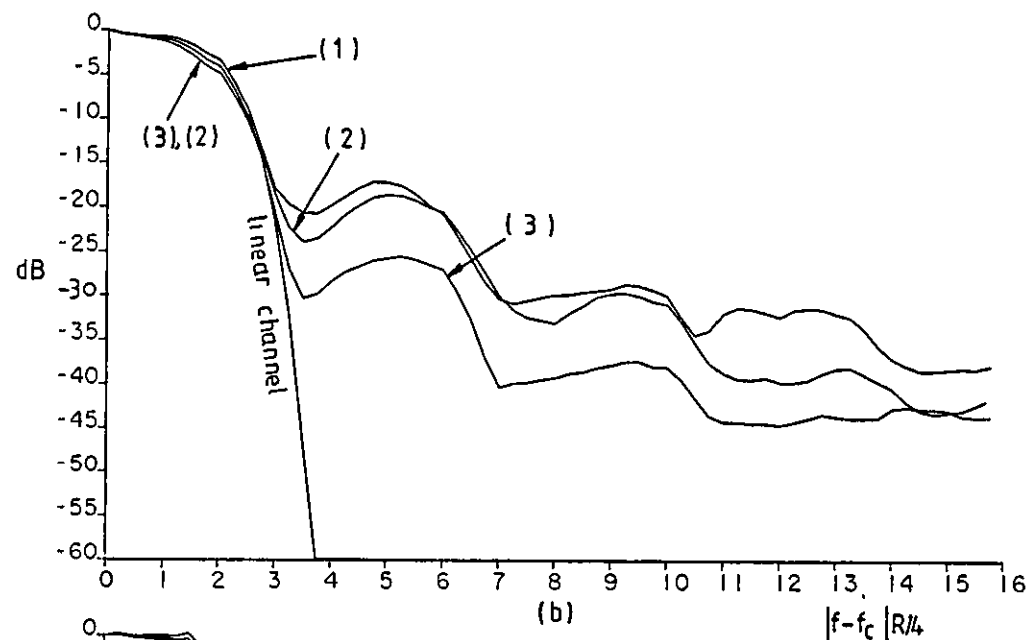
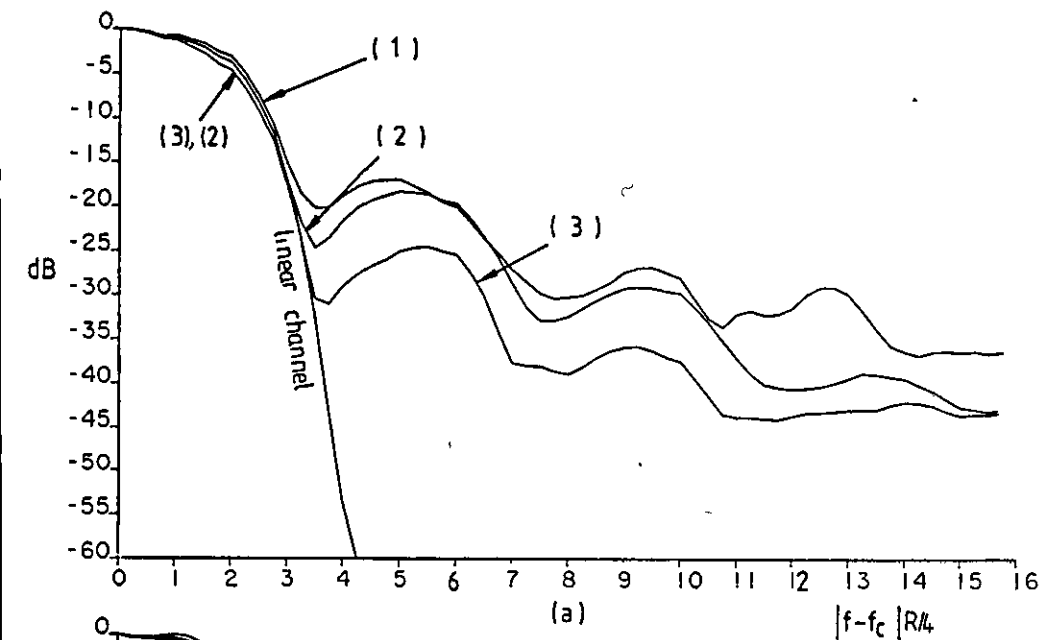


Figure 5.10 Power spectral densities of signals (a) 1A, (b) 2A, (c) 3A and, (d) 4A at the outputs of the (1): predistorter, (2): HPA without the predistorter and, (3): HPA with the predistorter, with the HPA and predistorter operating at 0.2 dB OBO and 0.68 dB IBO, respectively.

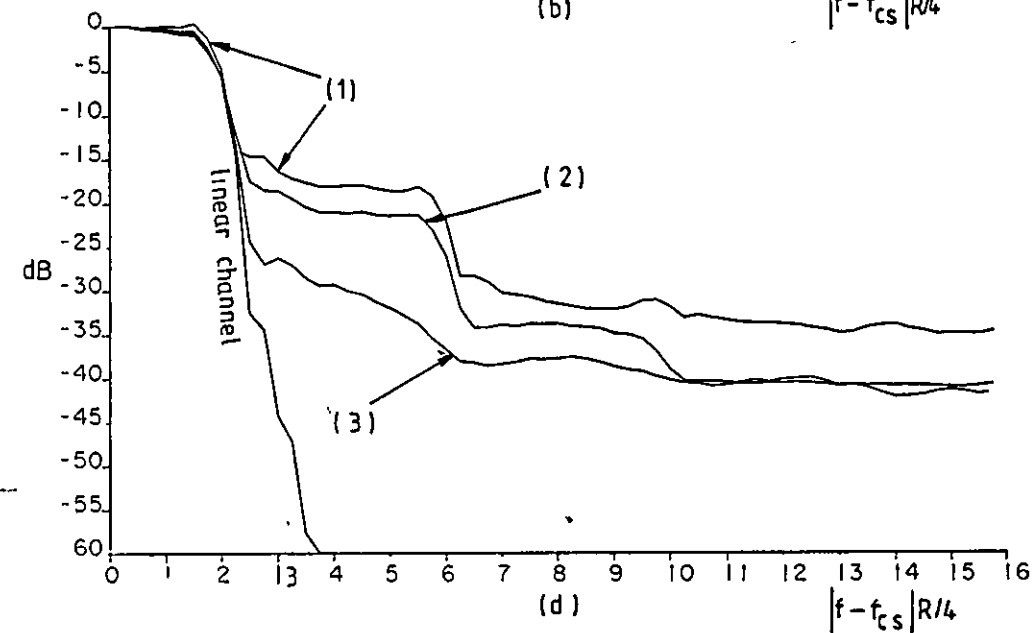
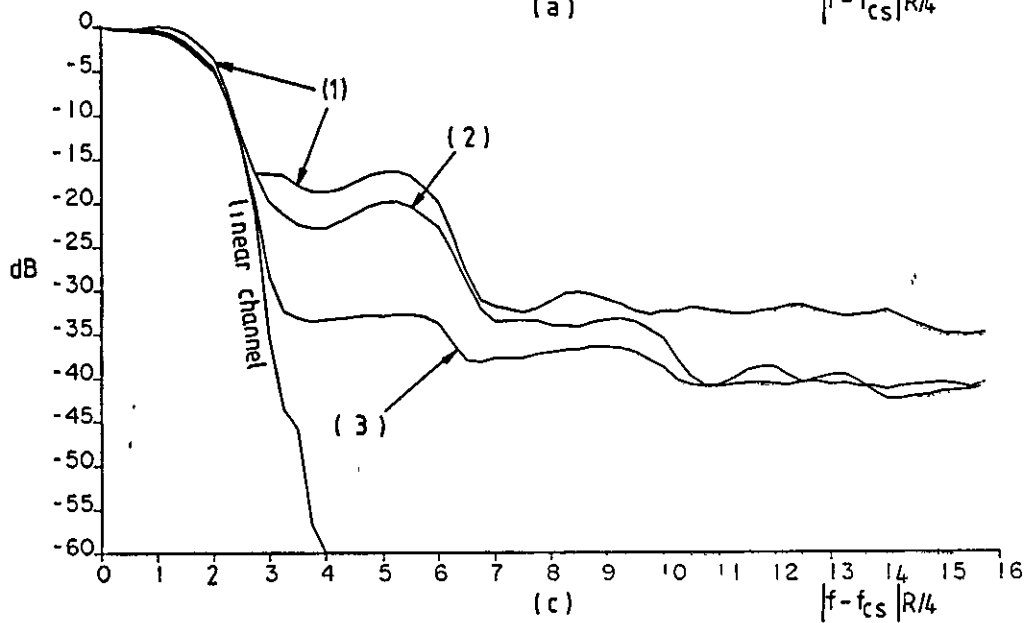
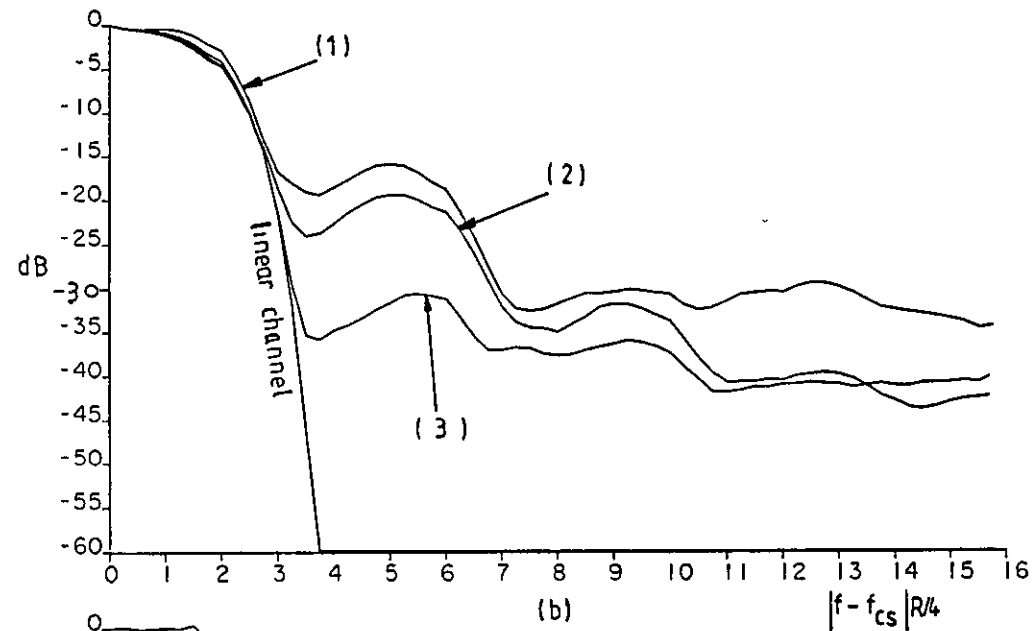
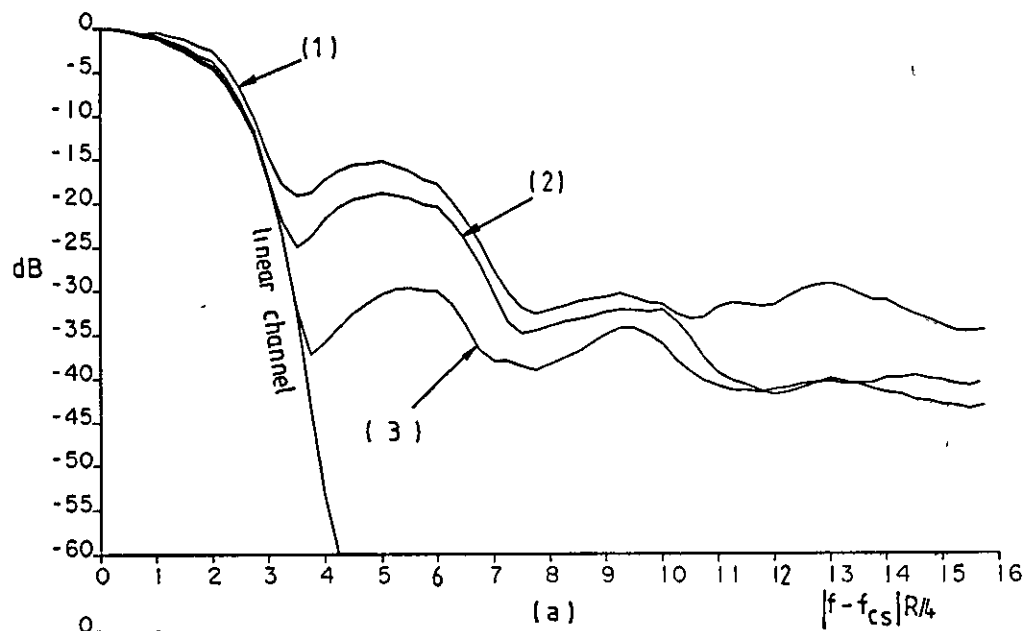


Figure 5.11 Power spectral densities of signals (a) 1A, (b) 2A, (c) 3A and, (d) 4A at the outputs of the (1): predistorter, (2): HPA without the predistorter and, (3): HPA with the predistorter, with the HPA and predistorter operating at 0.68 dB OBO and 1.16 dB IBO, respectively.

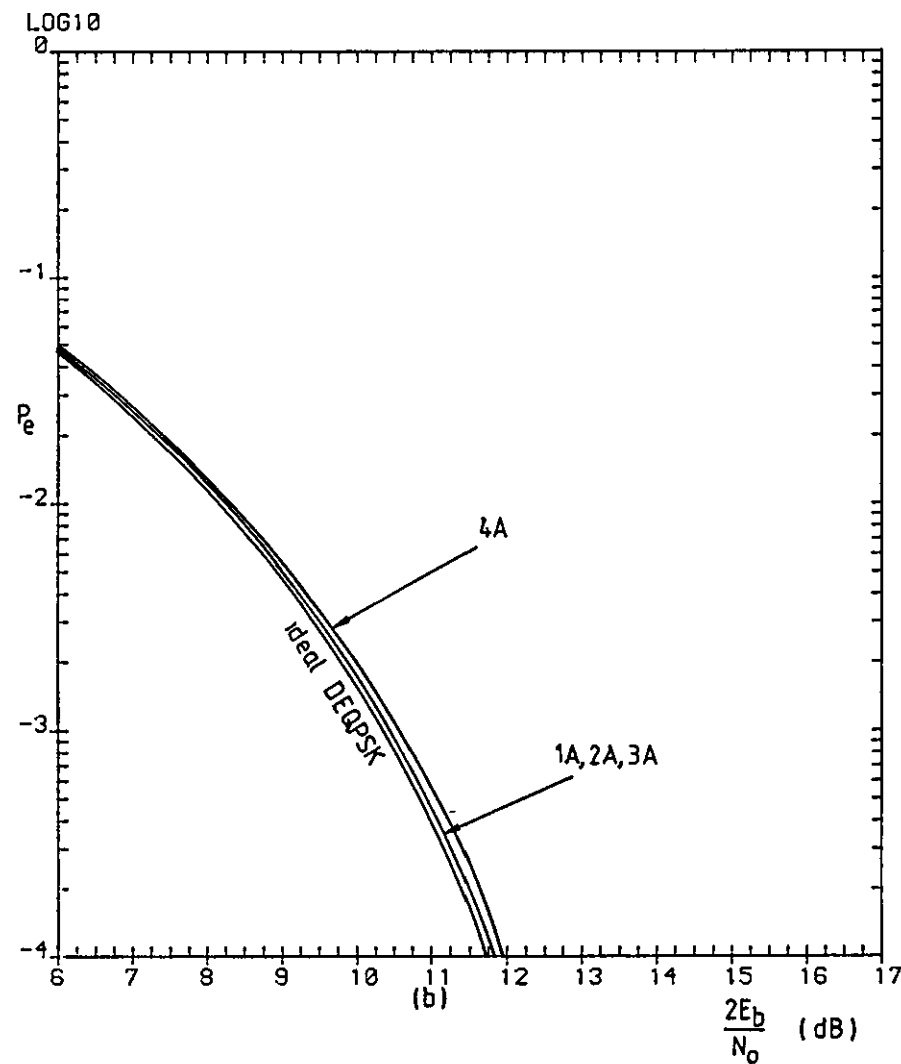
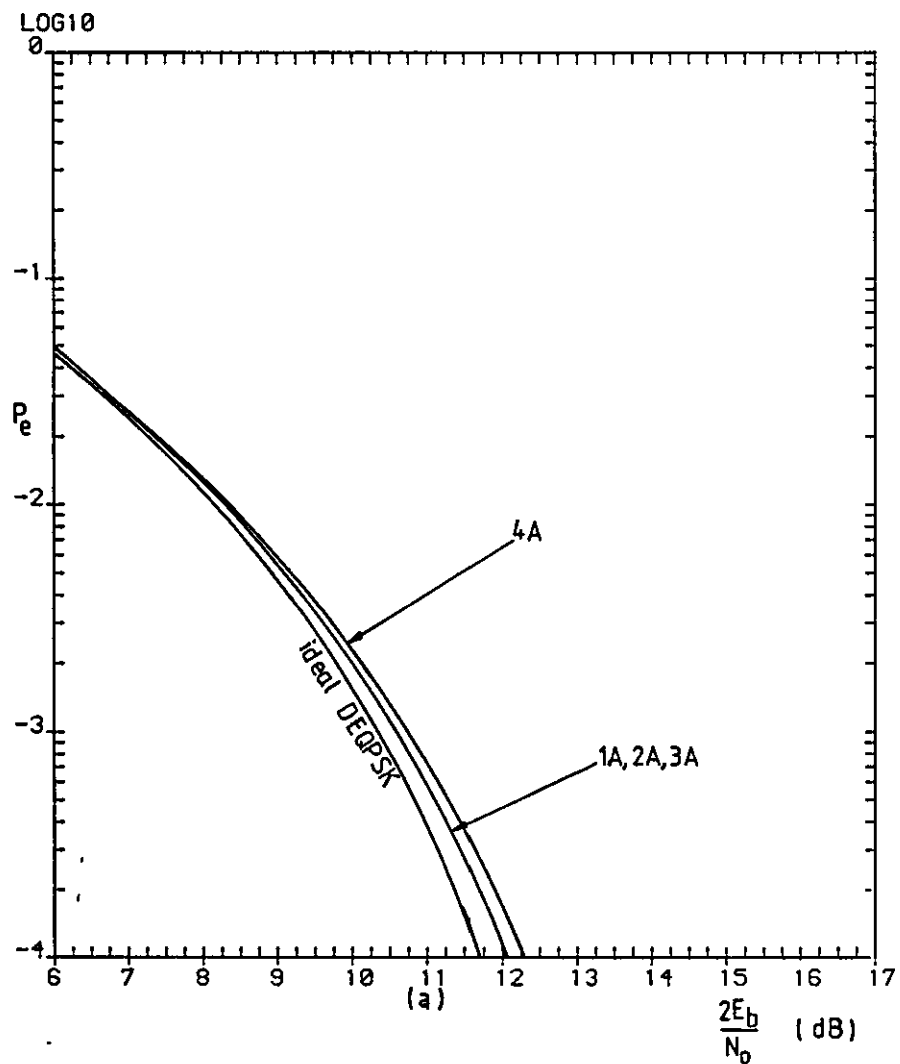


Figure 5.12 Error-rate performances of signals 1A, 2A, 3A and 4A, with the use of the predistorter, over a nonlinear and bandlimited channel, with the HPA operating at (a) 0.2 dB and, (b) 0.68 dB OBO, and in a *non-ACI* environment.

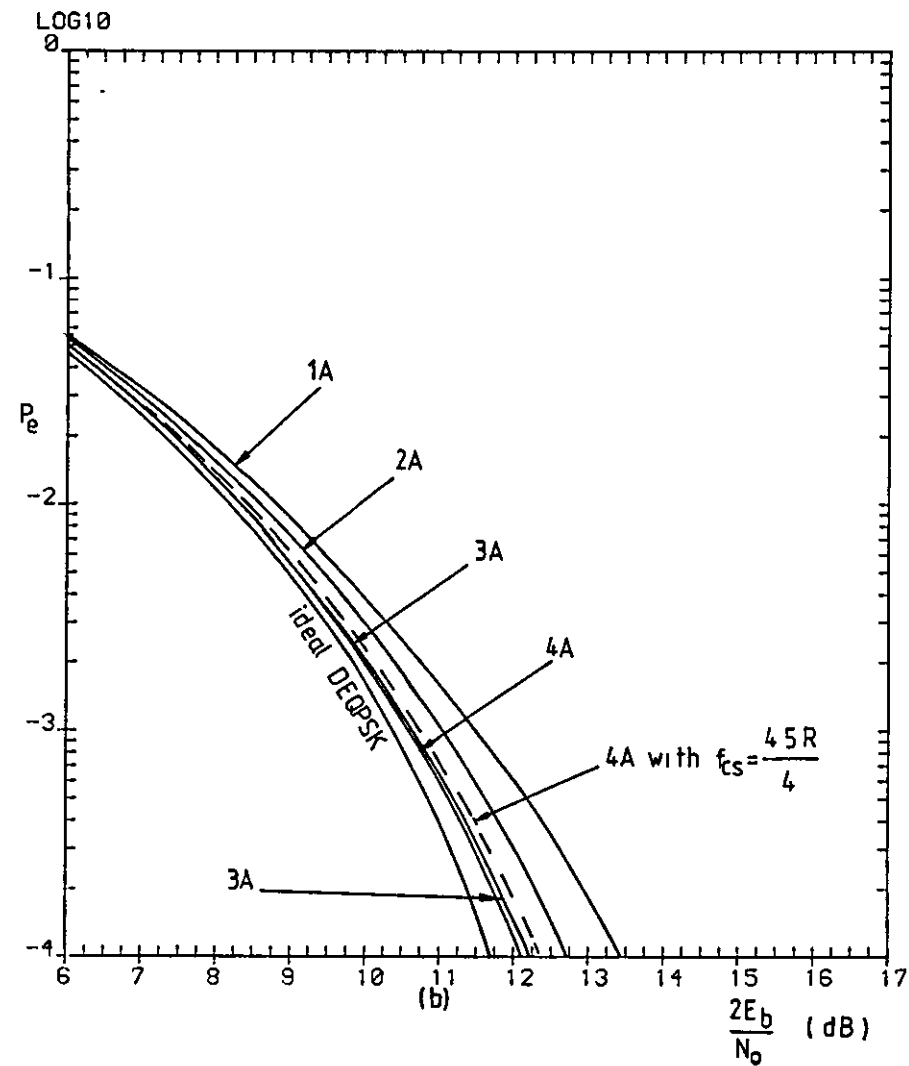
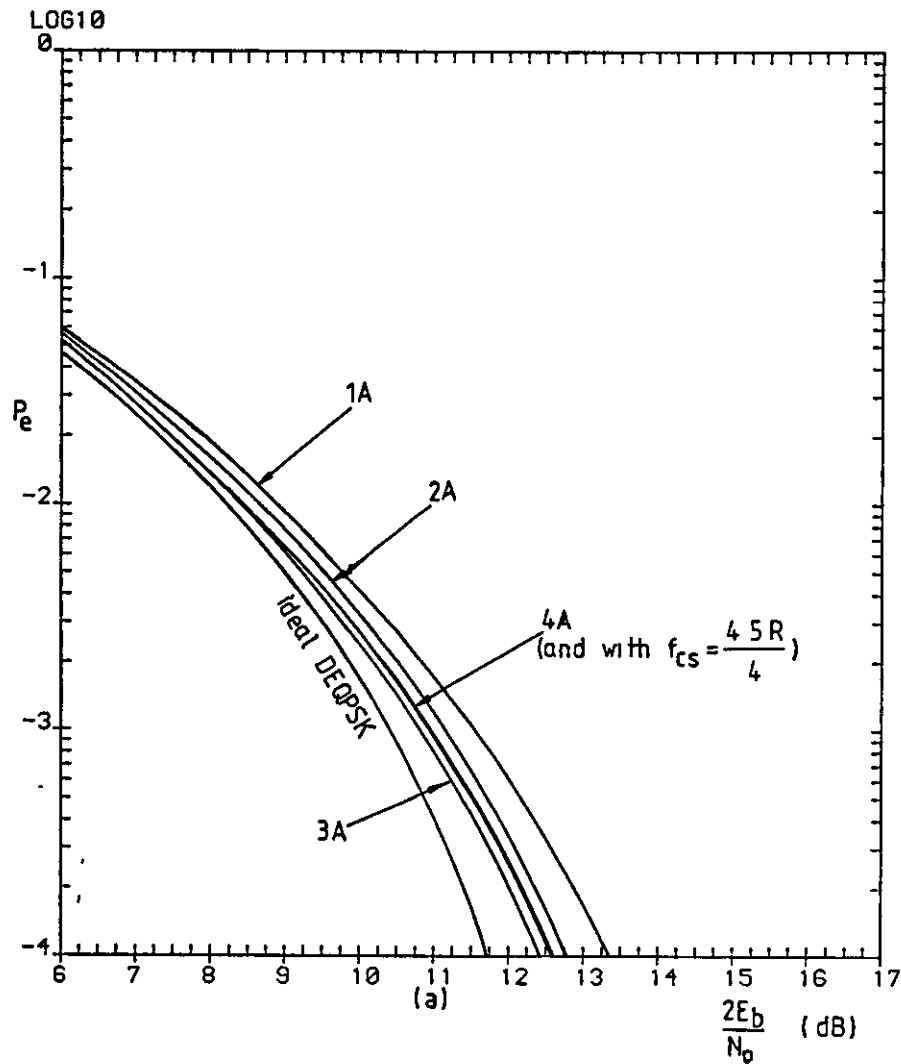


Figure 5.13 Error-rate performances of signals 1A, 2A, 3A and 4A, with the use of the predistorter and the HPA operating at (a) 0.2 dB and, (b) 0.68 dB OBO, over a nonlinear and bandlimited channel and in an ACI environment, and with the channel spacing $f_{cs} = 5R/4$ Hz.

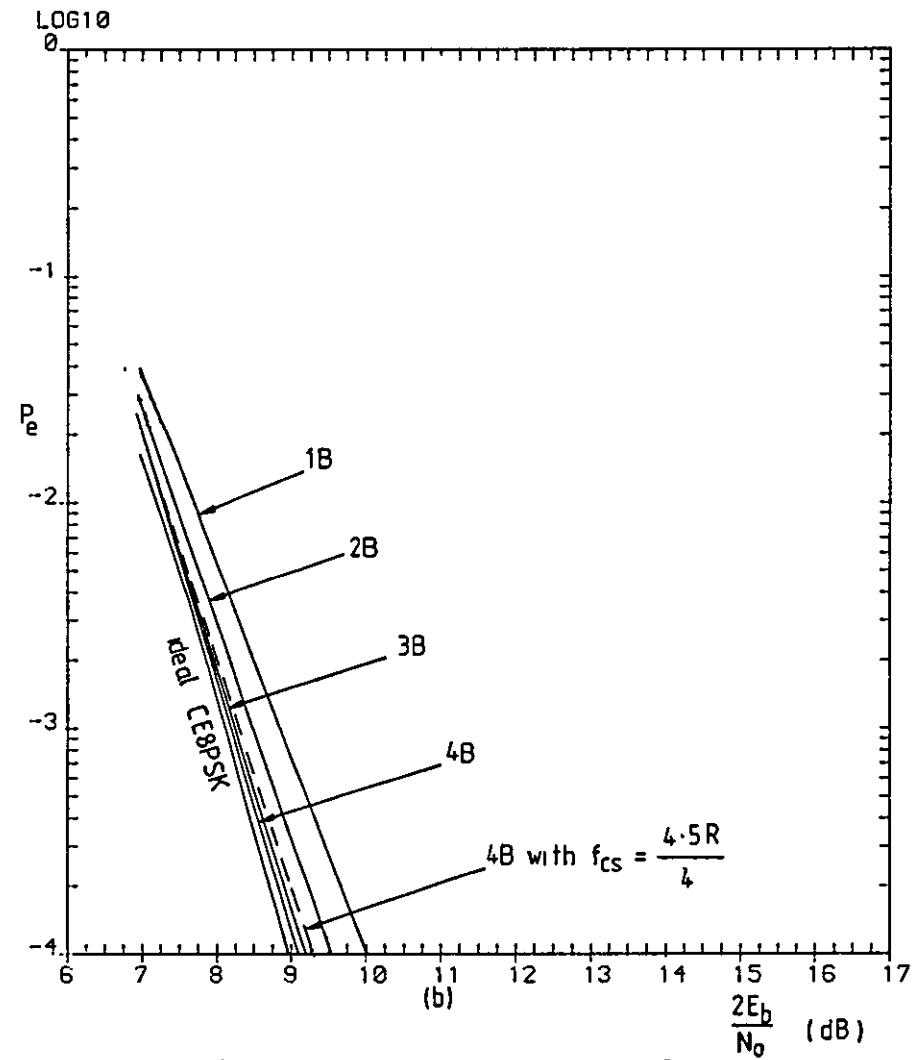
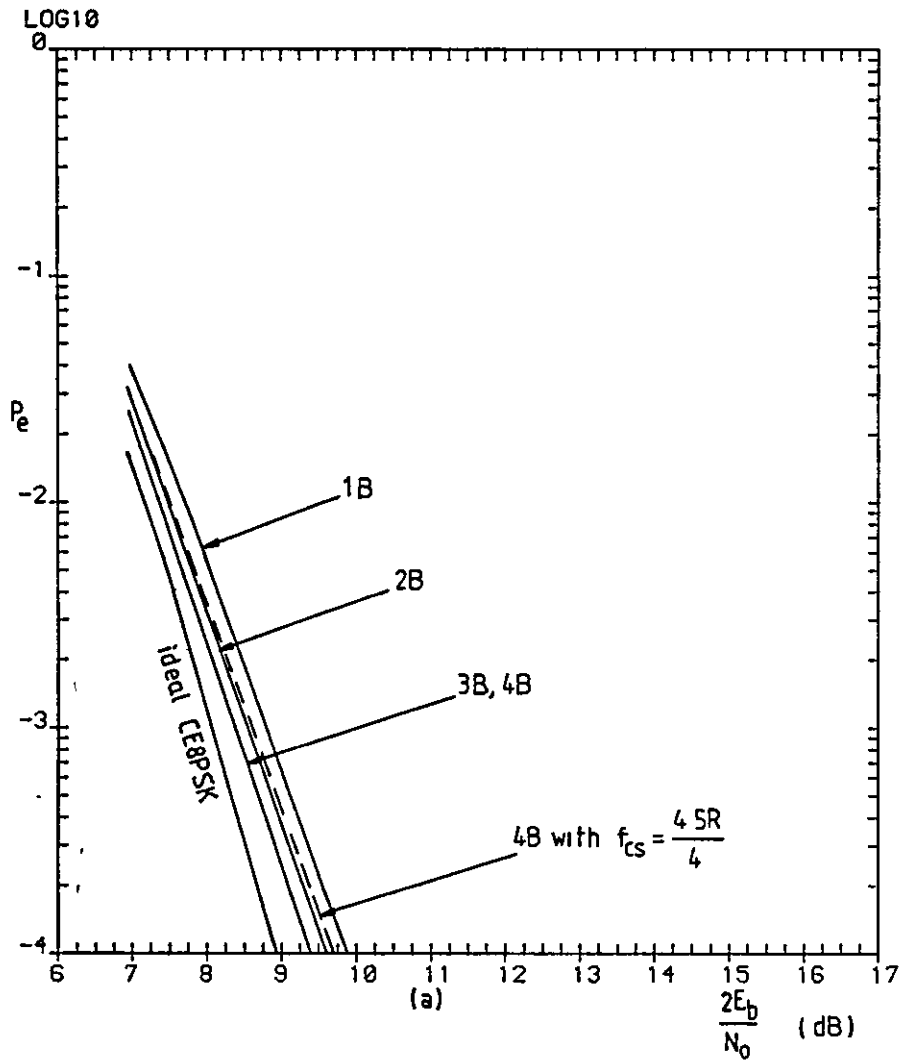


Figure 5.14 Error-rate performances of signals 1B, 2B, 3B and 4B, with the use of the predistorter and the HPA operating at (a) 0.2 dB and, (b) 0.68 dB OBO, over a nonlinear and bandlimited channel and in an ACI environment, and with the channel spacing $f_{cs} = 5R/4$ Hz.

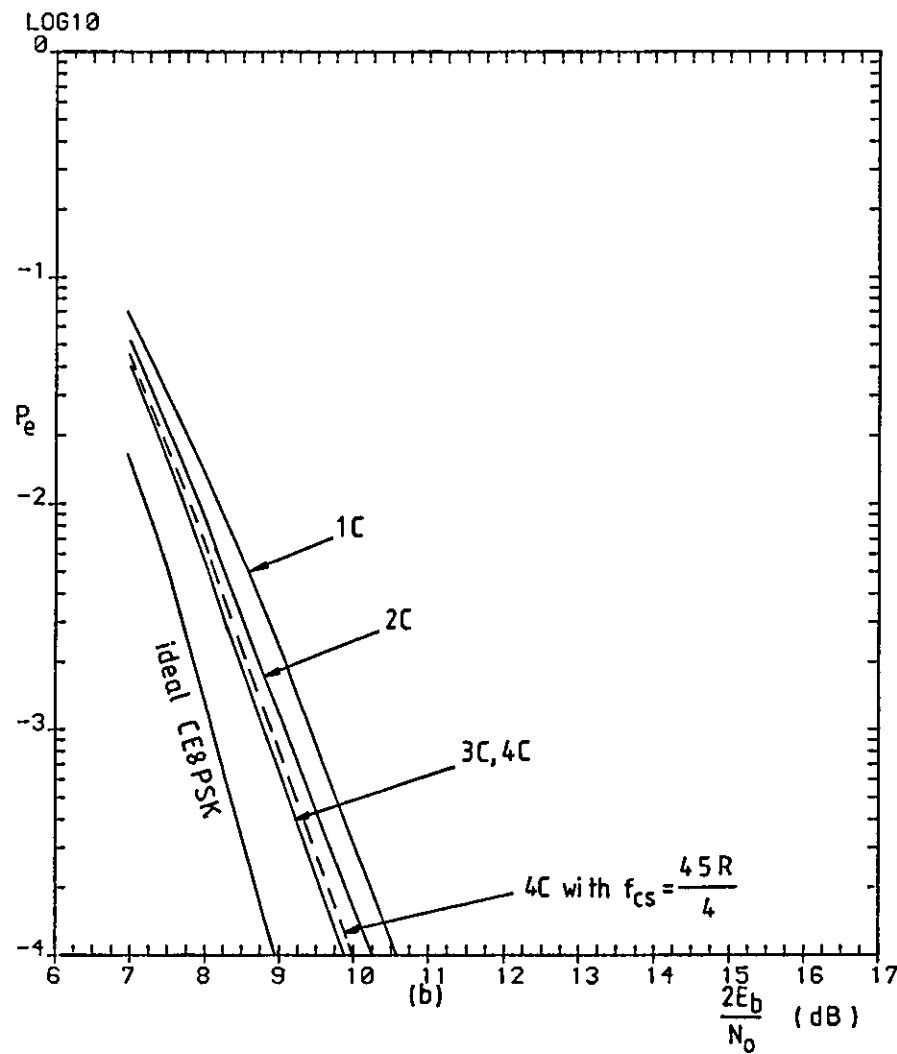
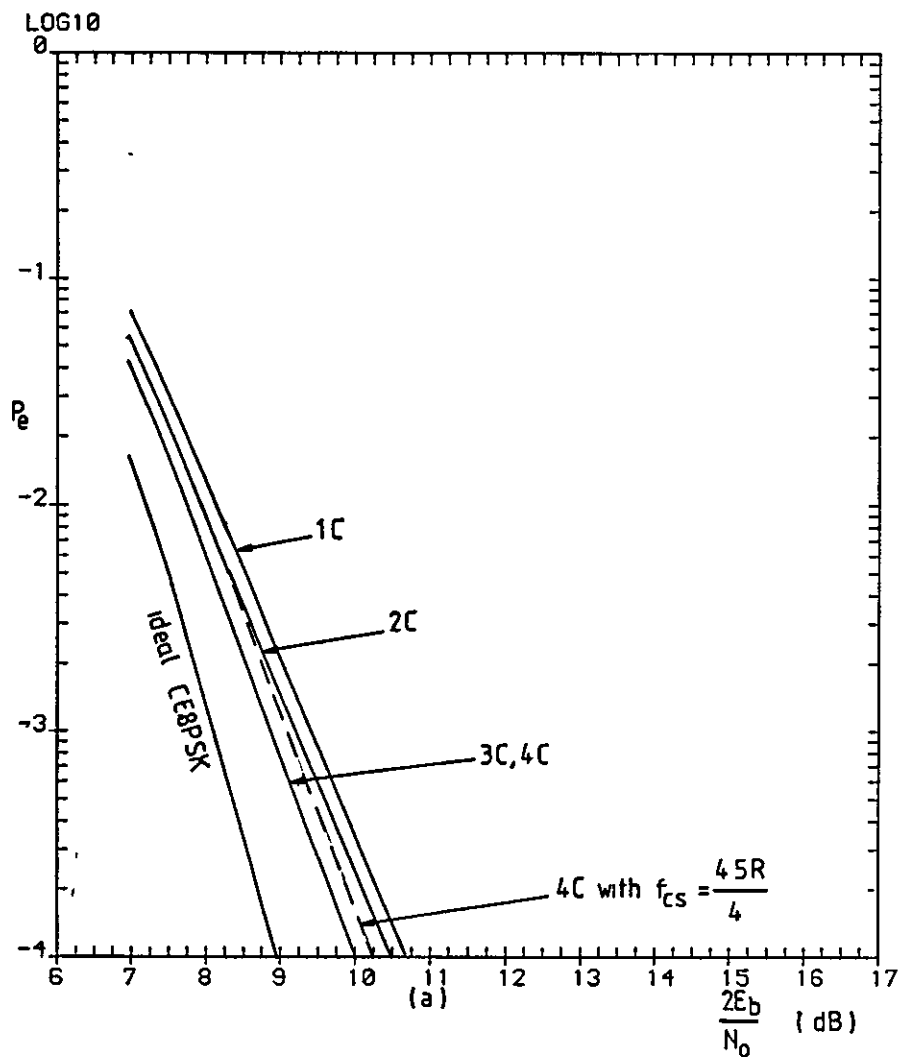


Figure 5.15 Error-rate performances of signals 1C, 2C, 3C and 4C, with the use of the predistorter, over a nonlinear and bandlimited channel, with the HPA operating at (a) 0.2 dB and, (b) 0.68 dB OBO and in a *non-ACI* environment.

CHAPTER 6

PHASE DEMODULATION

6.1 Phase detector

For CE8PSK signals, the results in Section 4.9.5 show that, using the distance measure D (i.e., using the phase angle of the received complex-valued signal as the distance measure), instead of the unitary distance measure (i.e., the optimum distance measure), in the Viterbi-algorithm decoder causes only about 0.5 dB degradation at $P_e=10^{-4}$. The PD (phase detector), presented here, measures the phase angle of the received complex-valued signal and feeds it into the decoder which uses the distance measure D . Since the distance measure D is an one-dimensional distance measure and if it is used, a useful reduction in equipment complexity can be achieved (Section 4.8), thus it leads to the potentially most cost-effective modem.

In the DEQPSK system described in Section 3.1, the threshold detection process is used by comparing each of the received samples, $r_i^{(1)}$ and $r_i^{(2)}$, with a decision threshold of zero. Now, if the received complex-valued signal is converted into its phase angle using the $\tan^{-1}(r_i^{(1)}/r_i^{(2)})$ function, then the resultant phase angle can also be detected for the data, using threshold detection by comparing it with the decision thresholds of 0 , $\pm\pi/2$ and $\pm\pi$ radians, according to Table 6.1. These two different threshold detection processes have the same tolerance to noise because they use exactly the same decision thresholds, but are represented in two different coordinate systems: one is in the Rectangular Cartesian Coordinate System, while the other one in the Polar Coordinate System. However, using the phase threshold-detector is equivalent to using the distance measure D to measure the phase distance of the received sample from each of the thresholds (possible received signal phase angles) and take the one with the minimum distance as the detected value. Thus, in

this thesis, the use of the distance measure D for DEQPSK signals will, for simplicity, be referred to as the phase threshold detection process.

The block diagram of a satellite earth station receiver is shown in Fig. 6.1, where the pre A/D conversion filters are used to remove the unwanted signal spectral components generated in the demodulation process, without distorting the wanted signals. The inphase and quadrature baseband waveforms are converted into digital signals by means of an A/D conversion process and are then fed into the demodulation filter (Section 2.4.4). The signal from the filter is sampled at the time instants $\{iT\}$, to give the inphase and quadrature sample sequences $\{A_i\}$ and $\{B_i\}$, respectively. Since $\{A_i\}$ and $\{B_i\}$ are digital samples, a lookup table can be used to extract the phase angles using the function $\tan^{-1}(B_i/A_i)$. So at time $t=iT$, the lookup table produces at its output the phase sample

$$\Omega_i = \tan^{-1}(B_i/A_i) \quad 6.1.1$$

The lookup table which realizes the function $\tan^{-1}(B_i/A_i)$ is known here as the digital tan phase detector (DTPD), which has a linear phase characteristic with a period of 2π .

6.2 Amplifier limiter

In the previous description, the demodulated signal, before being fed into the demodulation filter, is converted into digital signal by means of an A/D conversion process, so an automatic gain controlled (AGC) amplifier is always required to set the received signal to a predetermined level and so to ensure that the signal at the input to the A/D converter drives that device over its full range.

Now, if only the phase information of the signal is used (i.e., the amplitude information is neglected), provided that the received modulated-carrier signal has a constant or near-constant envelope, then little or no useful information carried by the phase of the signal is lost in the receiver by first slicing the receiving waveform at the output of the

receiver IF filter in an ideal amplifier limiter with the characteristic shown in Fig. 6.2, and then extracting the phase for subsequent use in the decoding/detecting process. (An ideal amplifier limiter gives a rectangular output waveform, obtained by taking a very narrow slice of the signal, about the value of zero, and amplifying the sliced signal to the required level.) The advantages of slicing the signal in an amplifier limiter are:-

- (1) no AGC amplifier is required because the received signal is set, to the predetermined level by the amplifier limiter,
- (2) the correct operation of the receiver is now independent of the received signal level, with the range of levels handled by the slicer, and
- (3) the signals at the input to the A/D converters can have a fixed range which is independent of the received signal level, but depend only on the output power of the amplifier limiter.

6.2.1 Analysis of slicing the received bandpass signal in an ideal amplifier limiter

To understand the slicing operation, it is necessary to study the characteristic of the assumed ideal limiter. Consider in Fig. 6.3, the received bandpass (DEQPSK, CE8PSK or CDE8PSK) signal. At the input of the limiter the signal is given by

$$S_1(t) = \sqrt{2}a_1(t)\cos\omega_c t - \sqrt{2}b_1(t)\sin\omega_c t \quad 6.2.1$$

$$= \sqrt{2}[a_1^2(t) + b_1^2(t)]\cos[\omega_c t + \Omega(t)] \quad 6.2.2$$

where $\Omega(t) = \tan^{-1}[b_1(t)/a_1(t)] \quad 6.2.3$

$\sqrt{2}a_1(t)$ and $\sqrt{2}b_1(t)$ are the inphase and quadrature baseband signal components, respectively. The signal has an envelope of

$$E(t) = \sqrt{2[a_1^2(t) + b_1^2(t)]} \quad 6.2.4$$

Since the amplifier limiter has a constant amplitude envelope versus time characteristic (Fig. 6.2) and as the memoryless infinite bandwidth amplifier limiter introduces in no change of signal phase, the signal at its output is

$$\hat{S}_o(t) = \sqrt{C} \text{sign}(\cos[\omega_c t + \Omega(t)]) \quad 6.2.5$$

where C is a constant dependent on the output power of the amplifier limiter. $\text{sign}(x)$ is 1 or -1 depending upon whether $x > 0$ or $x < 0$. $\hat{S}_o(t)$ is a rectangular waveform that preserves the locations of the zero crossings of the signal at the input. The zonal filter (Fig. 6.3) following the amplifier limiter is used to remove all harmonics and pass only the fundamental band output

$$S_o(t) = \sqrt{C} \cos[\omega_c t + \Omega(t)] \quad 6.2.6$$

$$= \sqrt{C} \cos\Omega(t)\cos\omega_c t - \sqrt{C} \sin\Omega(t)\sin\omega_c t \quad 6.2.7$$

The difference between the signals $\hat{S}_o(t)$ and $S_o(t)$ is that $\hat{S}_o(t)$ is a rectangular waveform whereas $S_o(t)$ is a rounded waveform, but both signals preserve the same signal phase. ($\hat{S}_o(t)$ and $S_o(t)$ are used in the phase demodulators A and B, respectively, described in Section 6.3.)

From Eqn. 6.2.3,

$$\cos\Omega(t) = \frac{a_1(t)}{\sqrt{a_1^2(t) + b_1^2(t)}} \quad 6.2.8a$$

and

$$\sin\Omega(t) = \frac{b_1(t)}{\sqrt{a_1^2(t) + b_1^2(t)}} \quad 6.2.8b$$

Thus, from Eqns. 6.2.7, and 6.2.8, $S_o(t)$ can be written as

$$S_o(t) = \frac{\sqrt{C}a_1(t)}{\sqrt{a_1^2(t) + b_1^2(t)}} \cos\omega_c t - \frac{\sqrt{C}b_1(t)}{\sqrt{a_1^2(t) + b_1^2(t)}} \sin\omega_c t \quad 6.2.9$$

Let

$$\sqrt{2}a_o(t) = \frac{\sqrt{C}a_i(t)}{\sqrt{a_i^2(t) + b_i^2(t)}} \quad 6.2.10a$$

and

$$\sqrt{2}b_o(t) = \frac{\sqrt{C}b_i(t)}{\sqrt{a_i^2(t) + b_i^2(t)}} \quad 6.2.10b$$

Then $\sqrt{2}a_o(t)$ and $\sqrt{2}b_o(t)$ are the inphase and quadrature baseband signal components of $S_o(t)$, respectively. Clearly, if the signal $S_i(t)$ at the input has a constant envelope, Eqn. 6.2.4 becomes

$$\sqrt{2a_i^2(t) + 2b_i^2(t)} = K \quad 6.2.11$$

where K is a constant, and

$$\sqrt{a_i^2(t) + b_i^2(t)} = K/\sqrt{2} \quad 6.2.12$$

so Equations 6.2.10a and 6.2.10b become

$$a_o(t) = \sqrt{C/K} a_i(t) \quad 6.2.13a$$

and

$$b_o(t) = \sqrt{C/K} b_i(t) \quad 6.2.13b$$

respectively. $\sqrt{C/K}$ is a constant, thus the inphase and quadrature baseband signal components of the received signal are not distorted by the amplifier limiter.

But, if $S_i(t)$ has a nonconstant envelope, Eqn. 6.2.11 becomes

$$\sqrt{2a_i^2(t) + 2b_i^2(t)} \neq K \quad 6.2.14$$

and so $a_o(t)$ and $b_o(t)$ become dependent on both baseband signal components, $a_i(t)$ and $b_i(t)$, of the received signal, as can be seen in Eqns. 6.2.10a and 6.2.10b. This interdependent influence of each baseband signal component by the other in quadrature is termed interphase crosstalk. Of course the smaller is the envelope fluctuations of the signal at the input, the less is the distortion and crosstalk in the signal from the output.

6.3 Optimum filter arrangement for using the amplifier limiter and distance measure D

All the data-transmission systems, considered so far, are optimized by sharing the overall filtering equally between the transmitter and receiver filters. The lowpass filtering is shared equally between modulation and demodulation filters and with a 100%, 75%, 50% or 25% sinusoidal rolloff frequency response. In Sections 3.7.2 and 4.9.1, the results suggest that the transmitter and receiver filters introduce a relatively low level of ISI, thus the overall filtering transfer functions of these data-transmission systems have, in fact, approximately a 100%, 75%, 50% or 25% sinusoidal rolloff frequency response.

Whenever an amplifier limiter is used at the receiver, it is absolutely essential to use matched-filtering and remove as much noise as possible at the input to the amplifier limiter. Otherwise there may be a serious degradation in signal-to-noise power ratio at the output of the amplifier limiter. This means that, at least, the receiver IF filter at the input of the amplifier limiter should be matched to the received data signal. Inevitably, therefore some distortion must be accepted in the demodulated waveforms. However, if the distance measure D is used, and since an ideal amplifier limiter does not change the phase of the signal, an optimum filter arrangement can still be obtained for this arrangement by completing the matched-filtering using the receiver IF filter, as shown in Fig. 6.3. In the system, the overall transmitter filtering is same as those of the systems considered before, but the the baseband equivalent model of the receiver IF filter has the transfer function of the baseband equivalent model of the transmitter IF filter in cascade with the modulation filter, so that the complete matched-filtering is done by the receiver IF filter alone. The ideal amplifier limiter slices the receiving signal but keeps the phase unchanged. It is assumed that the pre A/D filters, with wide bandwidths, does not further distort the phase of the

signal. Thus the system has the optimum filter arrangement for using the amplifier limiter and distance measure D because the complete matched-filtering process has been achieved before the slicing process. Although the amplifier limiter distorts the signal amplitude, this does not affect the decoding performance of the signal if the distance measure D is used.

This filter arrangement is optimum for using the amplifier limiter and distance measure D, and in this chapter, it will, for simplicity, be referred to as the optimum filter arrangement.

6.4 Phase demodulation of the amplifier limited signals

6.4.1 Phase demodulation of the amplifier limited signals

Having determined the optimum filter arrangement of the transmission system, using the amplifier limiter and the distance measuer D, it is required now to determine the phase demodulation process that extracts the phase from the received signal.

The two phase demodulators described here are modifications of a conventional ideal coherent demodulator, so that a reference carrier is required for the demodulation processes. It is assumed that the receiver provides the required ideal carrier signal. The data-transmission system with the use of an amplifier limiter and phase demodulation is shown in Fig. 6.3. The system can be used for DEQPSK, CE8PSK or CDE8PSK signals, depending on the encoder used at the transmitter and the detector/decoder used at the receiver. From Eqn. 6.2.1, the signal at the receiver IF filter output is given by

$$S_1(t) = \sqrt{2}a_1(t)\cos\omega_c t - \sqrt{2}b_1(t)\sin\omega_c t \quad 6.4.1$$

which is sliced in the ideal amplifier limiter. The signals at the outputs of the amplifier limiter and zonal filter are (Eqns. 6.2.5 and 6.2.6)

$$\hat{S}_o(t) = \sqrt{C} \text{sign}(\cos[\omega_c t + \Omega(t)]) \quad 6.4.2$$

and
$$S_o(t) = \sqrt{C} \cos[\omega_c t + \Omega(t)] \quad 6.4.3$$

respectively, where C is the constant dependent on the output power of the

amplifier limiter. These signals are ready for phase demodulation and $\Omega(t)$ is the phase required to be extracted.

A. Phase demodulator A - analysis

The phase demodulator A is used here in Fig. 6.3. The signals at the inputs of the inphase and quadrature pre A/D conversion filters are

$$S_o\sqrt{2}\cos\omega_c t = \sqrt{C} [\cos\Omega(t)\cos\omega_c t - \sin\Omega(t)\sin\omega_c t]\sqrt{2}\cos\omega_c t \quad 6.4.4$$

$$= \sqrt{C/2} \cos\Omega(t) + \text{h.f.c.} \quad 6.4.5$$

$$= A(t) + \text{h.f.c.} \quad 6.4.6$$

and

$$-S_o\sqrt{2}\sin\omega_c t = -\sqrt{C} [\cos\Omega(t)\cos\omega_c t - \sin\Omega(t)\sin\omega_c t]\sqrt{2}\sin\omega_c t \quad 6.4.7$$

$$= \sqrt{C/2} \sin\Omega(t) + \text{h.f.c.} \quad 6.4.8$$

$$= B(t) + \text{h.f.c.} \quad 6.4.9$$

respectively, where

$$A(t) = \sqrt{C/2} \cos\Omega(t) \quad 6.4.10$$

$$B(t) = \sqrt{C/2} \sin\Omega(t) \quad 6.4.11$$

and h.f.c. means the high frequency components. The pre A/D conversion filters block the high frequency components in the signals. Equations 6.4.10 and 6.4.11 show that the phase $\Omega(t)$ of the received complex-valued signal is determined uniquely by the baseband signal components $A(t)$ and $B(t)$. Also, since

$$A^2(t) + B^2(t) = [\sqrt{C/2} \sin\Omega(t)]^2 + [\sqrt{C/2} \cos\Omega(t)]^2 \quad 6.4.12$$

$$= C/2 \quad 6.4.13$$

is a constant, the received complex-valued signal at the output of the pre A/D filters is constrained to lie on the circle ABCD as shown in Fig. 6.4, where the value of $\sqrt{C/2}$ is dependent on the output level of the amplifier limiter. Assume that the receiver provides the ideal required timing signal, so that the signals $A(t)$ and $B(t)$ are sampled, at the time

instants (iT) , to give the sequences (A_i) and (B_i) where, at time $t=iT$

$$A_i = A(iT) = \sqrt{C/2} \cos[\Omega(iT)] = \sqrt{C/2} \cos\Omega_i \quad 6.4.14$$

and
$$B_i = B(iT) = \sqrt{C/2} \sin[\Omega(iT)] = \sqrt{C/2} \sin\Omega_i \quad 6.4.15$$

In the absence of noise and ISI, the possible received and demodulated DEQPSK, CE8PSK and CDE8PSK signals, at time $t=iT$, are shown in Fig. 6.4. The samples A_i and B_i are fed to the DTPD (digital tan phase detector; see Section 6.1), which produces at its output the phase angle

$$\Omega_i = \tan^{-1}(B_i/A_i) \quad 6.4.16$$

Since the maximum possible values of $|A_i|$ and $|B_i|$ in Eqns. 6.3.14 and 6.3.15 are $\sqrt{C/2}$, which is only dependent on the amplifier limiter output power, the A/D converters can be adjusted so that they are not overloaded.

The demodulator just described, using two multiplication processes as the demodulation process and the DTPD (digital tan phase detector; see Section 6.1) to extract the phase, is known here as phase demodulator A.

B. Phase demodulator B - analysis

The phase demodulator B is used here in Fig. 6.3. The rectangular signal $\tilde{S}_o(t)$ is passed through a half-wave rectifier (h.w.r.) to remove the negative parts of the signal. The reference signals are also sliced and then rectified to remove the negative parts of the signals. So all signals going into the EX-OR gates are rectangular waveforms with just two possible levels. Figure 6.5 shows the waveforms at the input and output of the EX-OR gate associated with $\sqrt{2}\cos\omega_c t$. It can be seen that $\hat{A}(t)$, which is the short-term d.c. component in $x(t)$, varies linearly with the phase angle (time delay) between the two input waveforms over the range 0 to π radians and also over the range π to 2π radians. Similarly for $\hat{B}(t)$ and the phase-shifted reference carrier. The pre A/D conversion filters, in Fig. 6.3, block the h.f.c. and produce the short term d.c.

signals $\hat{A}(t)$ and $\hat{B}(t)$ at the corresponding outputs. The d.c. component at the output of either of the A/D conversion filters versus the phase difference of the signals at the inputs is shown in Fig. 6.6a, where k is dependent on the output voltage of the EX-OR gate. If the d.c. components at the pre A/D conversion filter outputs are level shifted by $-k$ volts, Figure 6.6a becomes Figure 6.6b, which is the preferred arrangement. It can be seen that there is a piecewise linear relationship between $\hat{A}(t)$ and $\hat{B}(t)$, as shown in Fig. 6.7, and so the phase angle of the received complex-valued signal can be determined uniquely by and varies linearly with $\hat{A}(t)$ and $\hat{B}(t)$. With the system just described, the received complex-valued signal is constrained to lie on the square DEFG as shown in Fig. 6.7.

Assume that the receiver provides the ideal timing signal, so that the signals $\hat{A}(t)$ and $\hat{B}(t)$ are sampled, at the time instants $\{iT\}$, to give the sequences $\{\hat{A}_i\}$ and $\{\hat{B}_i\}$, where $\hat{A}_i = \hat{A}(iT)$ and $\hat{B}_i = \hat{B}(iT)$. In the absence of noise and ISI, the possible received and demodulated DEQPSK, CE8PSK and CDE8PSK signals are shown in Fig. 6.7. The samples \hat{A}_i and \hat{B}_i are fed into the DTPD (digital tan phase detector; see Section 6.1) to produce the phase sample angle

$$\Omega_i = \tan^{-1}(\hat{B}_i/\hat{A}_i) \quad 6.4.17$$

It should be noted that the lookup tables realizing Eqns. 6.4.16 and 6.4.17 are different because usually $B_i \neq \hat{B}_i$ and $A_i \neq \hat{A}_i$ for a given value of Ω_i .

Since the maximum possible values of $|\hat{A}_i|$ and $|\hat{B}_i|$ are k , which is only dependent on the output voltage of the EX-OR gates, the A/D converters can be adjusted so that they are not overloaded.

The demodulator just described, using two EX-OR gate operations as the demodulation process and DTPD (digital tan phase detector) to extract the phase, is known here as phase demodulator B.

6.4.2 Baseband equivalent model of the amplifier limiter in cascade with phase demodulator A or B, for computer simulation

A. Phase demodulator A

The equivalent baseband signals of $S_1(t)$ (Eqn. 6.2.1) at the input to the amplifier limiter and of $S_o(t)$ (Eqn. 6.2.9) from the output of the zonal-filter can be represented (Appendix A6) as the complex-valued signals

$$s_1(t) = a_1(t) + jb_1(t) \quad 6.4.18$$

$$\text{and } s_o(t) = \frac{\sqrt{C}a_1(t)}{\sqrt{2\sqrt{a_1^2(t)+b_1^2(t)}}} + j \frac{\sqrt{C}b_1(t)}{\sqrt{2\sqrt{a_1^2(t)+b_1^2(t)}}} \quad 6.4.19$$

respectively, where $j=\sqrt{-1}$. Since the value of \sqrt{C} is dependent on the amplifier limiter output power, which can be set to any positive real value without loss of generality, it is convenient to set $C=2$. Under this condition, from Eqns. 6.4.18 and 6.4.19, the baseband equivalent model of the amplifier limiter in cascade with the zonal-filter can be represented by the function

$$AL(t) = \frac{1}{\sqrt{a_1^2(t)+b_1^2(t)}} \quad 6.4.20$$

So for the signal $s_1(t)=a_1(t)+jb_1(t)$ at the input to the amplifier limiter, the signal from the output of the zonal-filter is

$$\begin{aligned} s_o(t) &= AL(t)s_1(t) \\ &= \frac{a_1(t)}{\sqrt{a_1^2(t)+b_1^2(t)}} + j \frac{b_1(t)}{\sqrt{a_1^2(t)+b_1^2(t)}} \end{aligned} \quad 6.4.21$$

The slicing process has retained the signal phase angle, but distorted the signal amplitude by setting its envelope to a predetermined level and the received complex-valued signal is therefore constrained to lie on a circle (Fig. 6.4). The linear demodulator (two multipliers) and pre A/D conversion filters do not further distort the signal, so that the

amplifier limiter, the zonal-filter, the linear demodulator and the pre A/D filters can be represented by the baseband equivalent model with the function

$$\text{PDMA}(t) = \frac{1}{\sqrt{a_1^2(t) + b_1^2(t)}} \quad 6.4.22$$

B. Phase demodulator B

Phase demodulator A is a linear device, but phase demodulator B is not. This can be seen by comparing the possible received complex-valued signals at the outputs of phase demodulators A and B, as shown in Figs. 6.4 and 6.7, respectively. The amplifier limiter distorts the signal amplitude at the input by constraining it to lie on the circle, while phase demodulator B further distorts the signal amplitude by constraining it to lie on the square. So for a complex-valued signal (Eqn. 6.4.18)

$$s_1(t) = a_1(t) + jb_1(t) \quad 6.4.23$$

at the input to the amplifier limiter in cascade with phase demodulator B, the signal from the pre A/D conversion filter output is

$$\hat{s}_o(t) = \frac{[a_1(t) + jb_1(t)]k}{|a_1(t)| + |b_1(t)|} \quad 6.4.24$$

as can be seen from Fig. 6.7. Since the value of k is dependent on the EX-OR gate output voltage, which can be set to any positive real value without loss of generality, it is convenient to set $k=1$. Under this condition, Eqn. 6.4.24 becomes

$$\hat{s}_o(t) = \frac{[a_1(t) + jb_1(t)]}{|a_1(t)| + |b_1(t)|} \quad 6.4.25$$

The demodulation process has also retained the signal phase angle, but distorted the signal amplitude. The received complex-valued is constrained to lie on a square in the complex-number plane (Fig. 6.7). The pre A/D

conversion filters do not distort the signal, so the amplifier limiter, the nonlinear demodulator (two EX-OR gates) and the pre A/D conversion filters can be represented by the baseband equivalent model with the function

$$\text{PDMB}(t) = \frac{1}{|a_1(t)| + |b_1(t)|} \quad 6.4.26$$

The functions PDMA(t) and PDMB(t) are modelled digitally for computer simulation. In the corresponding sampled signal, the functions given by Eqns.6.4.22 and 6.4.26, at time $t=mT_m$, can be written as

$$\text{PDMA}_m = \frac{1}{\sqrt{a_{1,m}^2 + b_{1,m}^2}} \quad 6.4.27$$

$$\text{PDMB}_m = \frac{1}{|a_{1,m}| + |b_{1,m}|} \quad 6.4.28$$

respectively, where $\text{PDMA}_m = \text{PDMA}(mT_m)$, $\text{PDMB}_m = \text{PDMB}(mT_m)$, $a_{1,m} = a_1(mT_m)$ and $b_{1,m} = b_1(mT_m)$. Equations 6.4.27 and 6.4.28 are used in computer simulation tests to assess the performance of the system.

Although phase demodulator B causes further signal distortion to the signal, while phase demodulator A does not, if the optimum filter arrangement and distance measure D is used, the phase demodulators have the same tolerance to noise. This is indicated in Fig. 6.8. R and R' are the complex-valued signal before and after slicing, and so R' has been constrained to lie on the circle. With phase demodulator A, the received signal remains at the same position, whereas, with phase demodulator B, the received signal is further distorted and so constrained to lie on the square and becomes R". The phase angle Ω_1 of these signals remain the same. Hence, under these conditions, if the distance measure D is used, the error-rate performance is independent of which of the phase demodulators is used.

6.5 Suboptimum filter arrangement for using the amplifier limiter and distance measure D

With the use of the distance measure D at the detector/decoder, the data-transmission system, as shown in Fig. 6.3, has the optimum filters for use with the amplifier limiter. However, the system is impractical because it is very difficult to design a narrowband analogue bandpass filter with the wanted frequency response. The system requires the receiver IF filter to have its baseband equivalent model the same as the resultant transfer function of the baseband equivalent model of the transmitter IF filter in cascade with the modulation filter.

A practical filter arrangement for a DEQPSK, CE8PSK or CDE8PSK system, using the amplifier limiter and the distance measure D, is shown in Fig. 6.9. In this arrangement, the receiver IF filter, having the same characteristics as the transmitter IF filter, matches the received data signal and removes as much noise as possible at the input to the amplifier limiter. Provided that the signal envelope is nearly constant, no severe signal distortion results, with no very serious reduction in tolerance to noise. The signal at the output of the receiver IF filter is sliced and then demodulated using phase demodulator A or B. At the outputs of the pre A/D conversion filters, the signal is sampled and fed into the demodulation filter.

It is required now to determine the characteristics of the demodulation filter that matches the baseband data signal as closely as possible. Since the signal has been nonlinearly distorted by the amplifier limiter and perhaps phase demodulator B, it may not be possible to find a filter exactly matching the baseband data signal.

Figure 6.10 shows the baseband equivalent model of the DEQPSK, CE8PSK or CDE8PSK system, with a linear and bandlimited channel. From Eqns. 6.4.22 and 6.4.26, the functions representing the baseband

equivalent models of the amplifier limiter in cascade with phase demodulator A or B are

$$\text{PDMA}(t) = \frac{1}{\sqrt{a_1^2(t) + b_1^2(t)}} \quad 6.5.1$$

and

$$\text{PDMB}(t) = \frac{1}{|a_1(t)| + |b_1(t)|} \quad 6.5.2$$

respectively, with $a_1(t)$ and $b_1(t)$ the inphase and quadrature baseband components of the signal at the input to the amplifier limiter.

With the use of phase demodulator A and if the signal at the input has a constant envelope, i.e., $a_1^2(t) + b_1^2(t)$ is a constant, the signal is not distorted. The demodulation filter which has the same characteristics as the modulation filter can be used to match the received baseband data signal.

However, with the phase demodulator B, even if the signal has a constant envelope so that the amplifier limiter does not distort the signal, the demodulator will. Inevitably, therefore some distortion must be accepted in the received baseband data signal.

For the DEQPSK, CE8PSK and CDE8PSK signals, the received bandpass signals have a nonconstant envelope due to the transmitter filtering. Inevitably, the amplifier limiter introduces nonlinear amplitude distortion into the signals, regardless of which of the phase demodulators is used. In this case, it may not be possible to design a demodulation filter which exactly matches the received baseband data signal.

Computer simulation tests, using the model shown in Fig. 6.10, have been carried out to find the received baseband data waveforms of DEQPSK, CE8PSK and CDE8PSK signals, over the linear and bandlimited channel, at the outputs of the receiver IF filter, and phase demodulators A and B. Figure 6.11 shows the results for CE8PSK signals. (Note that DEQPSK, CE8PSK and CDE8PSK signals have the same waveform shapes, provided that

the same transmitter filtering is used.) They show that, for a given transmitted signal and for either phase demodulator A or B, the shapes of the received baseband data waveforms are quite similar to each other. Hence, if the demodulation filter, which has the same characteristics as the modulation filter, is used, no very serious degradation in performance results, even though the demodulation filter may not exactly match the data waveforms. Figure 6.11 shows that the data waveforms, using phase demodulator B, have more spikes than those using phase demodulator A. Hence phase demodulator B should have a poorer performance than phase demodulator A.

This is a suboptimum filter arrangement for use with the amplifier limiter and distance measure D (because the demodulation filter does not exactly match the received signal), and, for simplicity, it will be referred to as the suboptimum filter arrangement.

6.6 Performances of DEQPSK and CE8PSK signals with the optimum filter arrangement, for the amplifier limiter, phase demodulators and distance measure D, over a linear bandpass channel

With the optimum filter arrangement, as shown in Fig. 6.3, the matched filtering is achieved by the receiver IF filter. For DEQPSK signals, the arrangement has the same error-rate performance as that using the conventional demodulator, independent of which of the phase demodulators is used (because they produce the same phase value for a given received complex-valued signal; see Fig. 6.9). However for CE8PSK signals, since the amplifier limiter nonlinearly distorts the signal envelope, even if the optimum distance measure (unitary distance measure) is used in the Viterbi decoder, a degradation in tolerance to noise is inevitable. (This is because the amplitude information is essential for the Viterbi-decoder to achieve the optimum decoding performance). However if the distance measure D is used with this filter arrangement, phase demodulators A and B

have the same effect on performance (because they produce the same phase value for a given signal, see Fig. 6.9). The degradation at $P_{av}=10^{-4}$ is about 0.5 dB (which is caused by the fact that the distance measure is suboptimum; see Section 4.9.5).

6.7 Discussion of the simulation results for DEQPSK, CE8PSK and CDE8PSK signals, with the use of the suboptimum filters for the amplifier limiter, phase demodulator A or B and distance measure D

The simulation model used to assess the error-rate performances of different signals, with the use of the suboptimum filters for the amplifier limiter, phase demodulator A or B and the distance measure D, over a linear and bandlimited satellite channel, is shown in Fig. 6.10.

Figure 6.12 shows the simulation model used to assess the performances of different signals with the use of the predistorter, HPA, the suboptimum arrangement for the amplifier limiter, and the phase demodulator A or B with a nonlinear and bandlimited satellite channel and in an ACI environment. The filter characteristics in these two models are same as those in Figs. 3.5 or 4.6.

These two simulation models (Figs. 6.10 and 6.11) can be used for DEQPSK, CE8PSK or CDE8PSK signals, depending on the encoder used at the transmitter and the detector/decoder used at the receiver. Computer simulation tests over these two models have been carried out to assess the effects of the amplifier limiter and the two phase demodulators on the performances. The results are shown and discussed in the following sections. In all simulation tests, it is assumed that the receiver provides the required ideal carrier and timing signals, and in the case of CE8PSK and CDE8PSK signals, the decoder uses 16 stored vectors with a 32-symbol delay in decoding.

6.7.1 Performances of signals 1A, 2A, 3A and 4A

A. Over a linear and bandlimited bandpass channel

The simulation model is shown in in Fig. 6.10. The error-rate performances of signals 1A, 2A, 3A and 4A are shown in Fig. 6.13, which shows that, after slicing, the phase demodulators A and B have similar error-rate performances. Signal 1A, with only about 0.5 dB degradation in tolerance to noise at $P_e=10^{-4}$, in comparison with that of an ideal system, has the best performance, which is independent of whether phase demodulator A or B is used. This is because signal 1A is a relatively wideband signal with less envelope fluctuations and hence less nonlinear distortion introduced by the amplifier limiter and phase demodulator, so the amplifier limiter and phase demodulators are better suited to wideband signals. The degradations in tolerance to noise of the signals, with the use of phase demodulators A and B, at $P_e=10^{-4}$, measured in comparison with that of an ideal DEQPSK system, are shown in Table 6.2.

B. With the use of the predistorter over a nonlinear bandpass channel and in an non-ACI environment

The simulation model used to evaluate the error-rate performances of signals 1A, 2A, 3A and 4A is shown in Fig. 6.12, with Switches 'A' open (so there is no ACI). The results, with the HPA operating at 0.2 dB and 0.68 dB OBO, and phase demodulator A or B used at the receiver, are shown in Fig. 6.14. It can be seen that, after slicing the signals, phase demodulators A and B have essentially the same error-rate performance. The results also show that signal 1A suffers the least degradation in tolerance to noise because of its reduced envelope fluctuations. Table 6.3 shows the degradations in tolerance to noise of the signals, with the use of the amplifier limiter and phase demodulator A or B, at $P_e > 10^{-4}$, measured in comparison with that of an ideal DEQPSK system. Comparing these results with the degradations in Table 5.3, it can be seen that the

slicing and phase demodulation processes have caused a further degradation 1.1-2.8 dB relative to the DEQPSK signals at $P_e=10^{-4}$.

C. With the use of the predistorter over a nonlinear bandpass channel and in an ACI environment

The simulation model used to evaluate the error-rate performances of signals 1A, 2A, 3A and 4A is shown in Fig. 6.12, with Switches 'A' closed (so there is ACI coming from the upper and lower adjacent channels). The results, with the HPA operating at 0.2 dB and 0.68 dB OBO, the channel spacing $f_{c_m}=5R/4$ Hz and with the use of phase demodulator A or B, are shown in Fig. 6.15. It can be seen that phase demodulators A and B have similar performances, at $P_e \geq 10^{-4}$. The results also show that for signals 4A with 0.68 dB HPA OBO, the phase demodulator A gains 1 dB over the phase demodulator B, at $P_e=10^{-4}$. This is because signal 4A is a relatively narrow band signal with more severe envelope fluctuations, so that more nonlinear distortion is caused by the amplifier limiter and phase demodulator. By comparing the results shown in Figs. 6.13 and 6.14 (or Tables 6.3 and 6.4), it can be seen that, with the use of the amplifier limiter and phase demodulator A or B, the degradations caused by ACI are larger than those with the use of the conventional demodulator (Fig. 5.13 or Table 5.14), which implies that the phase demodulators are more sensitive to ACI than the conventional demodulator. This is expected because ACI acts as noise in the wanted signal, and the wanted signal is nonlinearly distorted by the phase demodulator, so that the demodulator filter no longer matches the wanted data signal. Table 6.4 shows the degradations in tolerance to noise of the signals, at $P_e=10^{-4}$, using phase demodulator A or B, measured in comparison with that of an ideal DEQPSK system.

Although it is shown in Section 5.3.2 that, signal 4A provides the most effective arrangement, when the predistorter and conventional demodulator

are used, this is not the case when slicing and phase modulation are used. The results in Fig. 6.15 show that, for the assumed conditions, signal 3A provides the best performance.

From the results in this section, it can be concluded that, for the given filters, predistorter, HPA, amplifier limiter and phase demodulator A or B, the most effective arrangement is to use signal 3A with $f_{c_s}=5R/4$ Hz and HPA operating slightly below saturation, say 0.2 dB OBO. The degradation is about 2.8 - 3.3 dB, at $P_e=10^{-4}$, in comparison with that of an ideal DEQPSK system. When comparing this result with that using a conventional demodulator (Fig. 5.13 and Table 5.4), it can be seen that slicing and phase demodulation have caused a degradation of about 2.1-2.6 dB, at $P_e=10^{-4}$.

Of the two phase demodulators, phase demodulator B is more cost effective than phase demodulator A because of its simplicity in hardware implementation (no zonal-filter is required), but it involves a penalty in tolerance to noise, at $P_e=10^{-4}$, of 0.5 dB, relative to phase demodulator A.

6.7.2 Performances of signals 1B, 2B, 3B and 4B

A. With the use of different distance measures over a linear and bandlimited bandpass channel

The simulation model used to evaluate the error-rate performances is shown in Fig. 6.10. In the cases where the distance measure involves the envelope information (i.e., when the distance measures A, B or E is used), the DTPD (digital tan phase detector) is removed from the model and the decoder has the operation of computing the values of the envelope and phase of the received signal. The error-rate performances of signals 1B, 2B, 3B and 4B, with the use of different distance measures, are shown in Figs. 6.16 and 6.17. It can be seen that, with the use of the suboptimum filter arrangement, the degradations in tolerance to noise of signals 1B,

2B, 3B and 4B, with the use of the unitary distance measure (i.e., the distance measure A) or the distance measure E, are in the range 0.5-1.1 dB, in comparison with that of an ideal CE8PSK system. The results also show that, when the suboptimum distance measures B, C and D (Section 4.8) are used, the further degradations in tolerance to noise of the signals are in the range 0-0.5 dB, in comparison with that of the optimum distance measure. Thus the distance measure D achieves a good compromise between performance and complexity. The error-rate performances of CE8PSK signals with the use of the distance measure D is shown in Fig. 6.18, which indicate that, after slicing, phase demodulators A and B have a similar performance. Signal 1B, with about 0.9 dB P_e degradation at $P_e=10^{-4}$, in comparison with that of an ideal CE8PSK system, has the best performance (see Section 6.7.1 for the reason) and its performance is independent of whether phase demodulator A or B is used. Note that 0.5 dB of the degradation is due to using the distance measure D. Hence, if the distance measure D is used, the extra penalty for using the suboptimum filter arrangement (with the amplifier limiter) is only about 0.4 dB at $P_e=10^{-4}$. Table 6.5 shows the degradations in tolerance to noise of the signals at $P_e=10^{-4}$, with the uses of the amplifier limiter, phase demodulator A or B and the distance measure D, measured in comparison with that of an ideal CE8PSK system.

B. With the use of the predistorter and the distance measure D over a nonlinear bandpass channel in an ACI environment

The simulation model used to evaluate the error-rate performances of signals 1B, 2B, 3B and 4B is shown in Fig. 6.12, with Switches 'A' closed. The results, with the HPA operating at 0.2 dB and 0.68 dB OBO, the channel spacing $f_{c_s}=5R/4$ Hz and with phase demodulator A or B, are shown in Figs. 6.19 and 6.20. It can be seen that, after slicing the signal, phase demodulators A and B have similar performances, at $P_e \gg 10^{-4}$, for signals

1B, 2B, 3B and 4B. The P_e degradations of the signals at $P_e=10^{-4}$, measured in comparison with that of an ideal CE8PSK system, are shown in Table 6.6. Comparing Table 6.6 with Table 6.4, it can be seen that phase demodulators A and B have a smaller difference in performance for CE8PSK signals than for DEQPSK signals

In Section 5.3.3, it has been shown that signal 4B provides the most cost effective arrangement, when predistortion and conventional demodulation are used, but this is not the case when slicing and phase demodulation are used. With the HPA operating at 0.2 dB and 0.68 dB OBO, the performances of signal 4B, with phase demodulator B and $f_{c_m}=4.5R/4$ Hz, are shown by the dotted lines on Figs. 6.19b and 6.20b, respectively. It can be seen that, at 0.2 and 0.68 dB HPA OBO, this arrangement has degraded the performances of the signal by about 3.4 dB and 3.2 dB, at $P_e=10^{-4}$, in comparison with that of an ideal CE8PSK system. The performances are more than 1 dB worse than those of any of the signals with $f_{c_m}=5R/4$ Hz.

From the results shown in Figs. 6.19 and 6.20, it can be concluded that, for the given filters, predistorter and HPA, when the amplifier limiter, phase demodulator A or B and distance measure D are used, the most cost effective arrangement is signal 3B with $f_{c_m}=5R/4$ Hz, and with the HPA slightly below saturation, say 0.2 dB OBO. The degradation in tolerance to noise is about 1.6 dB, at $P_e=10^{-4}$, in comparison with that of an ideal CE8PSK system. This degradation is due to (1) the predistorter and HPA, (2) the amplifier limiter, (3) ACI, (4) the suboptimum distance measure D, (5) phase demodulator A or B, and (6) the suboptimum filters. When comparing with the degradation (2-2.6 dB) of signal 3A (a DEQPSK signal), under the assumed conditions, obtained in the previous section, it is obvious that the CE8PSK signal suffers less further degradation caused by using slicing and phase demodulation.

6.7.3 Performances of signals 1C, 2C, 3C and 4C

A. With the use of the distance measure D over a linear and bandlimited bandpass channel

The simulation model used to evaluate the error-rate performances of signals 1C, 2C, 3C and 4C are shown in Fig. 6.10. The results are shown in Fig. 6.21. As in the case of CE8PSK signals, CDE8PSK signals, after slicing the signal, phase demodulators A and B have a similar performance, at $P_e=10^{-4}$. The degradations in tolerance to noise of the signals, at $P_e=10^{-4}$, measured in comparison with that of an ideal CE8PSK system, are shown in Table 6.7. In Section 5.2.4, it is shown that the differential encoding in CDE8PSK signals causes a degradation in tolerance to noise of about 0.7 dB, at $P_e=10^{-4}$, in comparison with that of an ideal CE8PSK system. Hence when comparing the degradations in tolerance to noise shown in Table 6.7 with those shown in Table 6.5, it can be seen that differential encoding causes a degradation of about 0.7 dB, at $P_e=10^{-4}$, in all CDE8PSK signals.

B. With the use of the predistorter and the distance measure D over a nonlinear channel and in an ACI environment

The simulation model used to evaluate the error-rate performances of signals 1C, 2C, 3C and 4C is shown in Fig. 6.11, with switches 'A' closed. The results, with the HPA operating at 0.2 dB and 0.68 dB OBO, the channel spacing $f_{ca}=5R/4$ Hz and the use of phase demodulator A or B, are shown in Figs. 6.22 and 6.23. It can be seen that, after slicing the signal, phase demodulators A and B have a similar performance, at $P_e \geq 10^{-4}$, for signals 1C, 2C, 3C and 4C. The degradations in tolerance to noise of the signals at $P_e=10^{-4}$, measured in comparison with that of an ideal CE8PSK system, are shown in Table 6.8.

In Section 5.3.4, it is shown that signal 4C provides the most cost effective arrangement when predistortion and conventional demodulation are used, but this is not the case when slicing and phase demodulation are

used. With the HPA operating at 0.2 dB and 0.68 dB OBO, the performances of signals 4C, with the use of phase demodulator B and $f_{c_m}=4.5R/4$ Hz, are shown by the dotted lines in Figs. 6.8a and b, respectively. It can be seen that, at 0.2 and 0.68 dB HPA OBO, this arrangement introduces degradations of about 4.2 and 4.1 dB, at $P_e=10^{-4}$, in comparison with that of an ideal CE8PSK system. Their performances are more than 1 dB worse than that of any of the signals with $f_{c_m}=5R/4$ Hz.

From the results in this section, it can be concluded that, for the given filters, predistorter and HPA, with slicing, phase demodulator A or B and distance measure D, the most cost effective arrangement is to use signal 3C with $f_{c_m}=5R/4$ Hz and to operate the HPA slightly below saturation. The degradation in tolerance to noise is about 2.5 dB, at $P_e=10^{-4}$, in comparison with that of an ideal DE8PSK system. The degradation is due to (1) differential encoding, (2) the predistorter and HPA, (3) the amplifier limiter, (4) ACI, (5) the suboptimum distance measure D, (6) phase demodulator A or B, and (7) the suboptimum filters. Note that, under these conditions, Phase demodulators A and B have essentially the same performance, so that phase demodulator B is more cost effective because of its simplicity in hardware implementation (no zonal-filter is required).

When comparing the error-rate performance of signal 3C (Fig. 6.23) with that of signal 3A (Fig. 6.15), under the same conditions, it can be seen that signal 3C has an advantage of 2.6 dB at $P_e=10^{-4}$, over signal 3A. Hence, despite the degradation caused by using the suboptimum distance measure and differential encoding, signal 3C is still worth considering.

Received sample values		Received phase angle (in radian)	Phase threshold detected values	
$r_i^{(1)}$	$r_i^{(2)}$	$\Omega_i = \tan^{-1}(r_i^{(1)}/r_i^{(2)})$	$\hat{r}_i^{(1)}$	$\hat{r}_i^{(2)}$
>0	>0	$0 \leq \Omega_i < \pi/2$	+1	+1
>0	<0	$0 > \Omega_i \geq -\pi/2$	+1	-1
<0	>0	$\pi/2 \leq \Omega_i < \pi$	-1	+1
<0	<0	$-\pi/2 > \Omega_i \geq -\pi$	-1	-1

Table 6.1 Phase threshold detection.

Phase demodulator	Signal			
	1A	2A	3A	4A
A	0.5	0.9	1.1	1.8
B	0.5	0.9	1.2	2.2

Table 6.2 Degradations in tolerance to noise of signals 1A, 2A, 3A and 4A, over a linear and limited channel, with the use of the suboptimum filters, the amplifier limiter and phase demodulator A or B, at $P_e=10^{-4}$, expressed in dB, measured in comparison with that of an ideal DEQPSK system (from Fig. 6.13).

HPA OBO (in dB)	Signal				Phase demodulator
	1A	2A	3A	4A	
0.2	1.5	1.6	1.9	2.8	A
0.2	1.5	1.6	2	3.3	B
0.68	1.1	1.5	2	2.6	A
0.68	1.1	1.5	2	2.9	B

Table 6.3 Degradations in tolerance to noise of signals 1A, 2A, 3A and 4A, over a nonlinear and bandlimited channel, with the use of the suboptimum filters, the predistorter, the HPA operating at 0.2 or 0.68 dB OBO, the amplifier limiter and phase demodulator A or B and in a non-ACI environment, at $P_e=10^{-4}$, expressed in dB, measured in comparison with that of an ideal DEQPSK system (from Fig. 6.14).

HPA OBO (in dB)	Signal				Phase demodulator
	1A	2A	3A	4A	
0.2	3.3	2.8	2.8	4	A
0.2	3.3	3.3	3.3	4.8	B
0.68	3.3	3	2.4	3.3	A
0.68	3.3	3	2.7	4.2	B

Table 6.4 Degradations in tolerance to noise of Signals 1A, 2A, 3A and 4A, over a nonlinear and bandlimited channel, with the use of the suboptimum filters, the predistorter, the HPA operating at 0.2 or 0.68 dB OBO, the amplifier limiter and phase demodulators A or B and in an ACI environment with $f_{ca}=5R/4$ Hz, at $P_n=10^{-4}$, expressed in dB, measured in comparison with that of an ideal DEQPSK system (from Fig. 6.15).

Phase demodulator	Signal			
	1B	2B	3B	4B
A	0.9	1.1	1.2	1.5
B	0.9	1.1	1.3	1.6

Table 6.5 Degradations in tolerance to noise of Signals 1B, 2B, 3B and 4B, over a linear and limited channel, with the use of the suboptimum filters, the amplifier limiter, phase demodulator A or B and the distance measure D, at $P_n=10^{-4}$, expressed in dB, measured in comparison with that of an ideal CE8PSK system (from Fig. 6.18).

HPA OBO (in dB)	Signal				Phase demodulator
	1B	2B	3B	4B	
0.2	2	1.8	1.6	2	A
0.2	2.3	1.9	1.6	2.3	B
0.68	2	1.7	1.5	1.7	A
0.68	2.2	1.8	1.6	2	B

Table 6.6 Degradations in tolerance to noise of Signals 1B, 2B, 3B and 4B, over a nonlinear and limited channel, with the use of the suboptimum filters, the predistorter, the HPA operating at 0.2 or 0.68 dB OBO, the amplifier limiter, phase demodulator A or B and the distance measure D and in an ACI environment, with $f_{ca}=5R/4$ Hz, at $P_n=10^{-4}$, expressed in dB, measured in comparison with that of an ideal CE8PSK system (from Figs. 6.19 and 6.20).

Phase demodulator	Signal			
	1C	2C	3C	4C
A	1.5	1.7	1.8	2.2
B	1.5	1.7	1.9	2.4

Table 6.7 Degradations in tolerance to noise of Signals 1C, 2C, 3C and 4C, over a linear and limited channel, with the use of the suboptimum filters, the amplifier limiter, phase demodulator A or B and distance measure D, at $P_e=10^{-4}$, expressed in dB, measured in comparison with that of an ideal CE8PSK system (from Fig. 6.21).

HPA OBO (in dB)	Signal				Phase demodulator
	1C	2C	3C	4C	
0.2	2.9	2.6	2.5	2.9	A
0.2	3	2.7	2.6	3	B
0.68	3	2.6	2.4	2.6	A
0.68	3.1	2.6	2.4	2.9	B

Table 6.8 Degradations in tolerance to noise of Signals 1C, 2C, 3C, 4C, over a nonlinear and limited channel, with the use of the the suboptimum filters, the predistorter, the HPA operating at 0.2 or 0.68 dB OBO, the amplifier limiter, phase demodulator A or B and the distance measure D and in an ACI environment, with $f_{ca}=5R/4$ Hz, at $P_e=10^{-4}$, expressed in dB, measured in comparison with that of an ideal CE8PSK system (from Figs. 6.22 and 6.23).

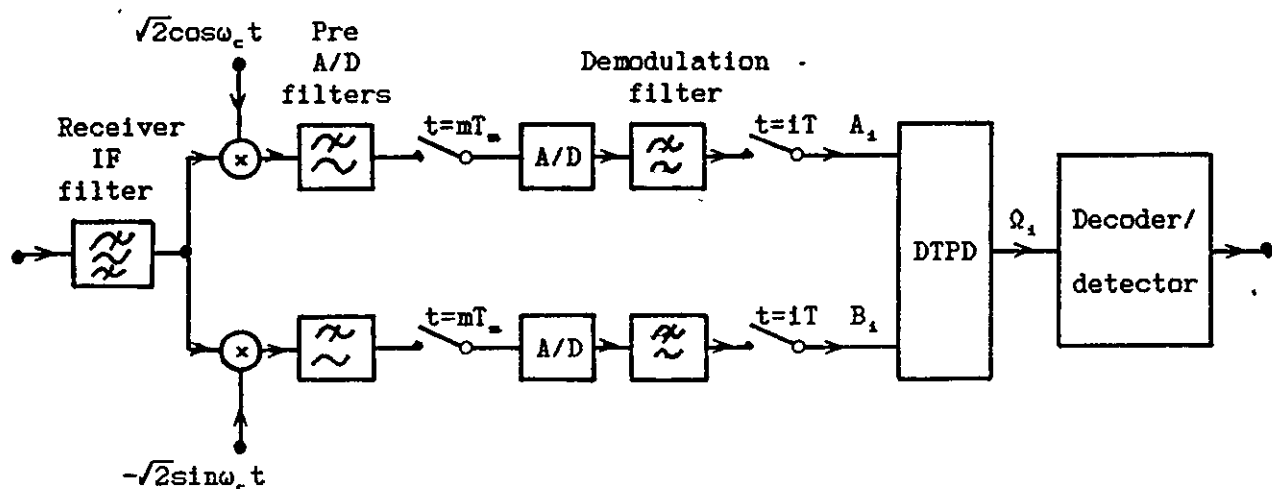


Figure 6.1 Block diagram of a satellite earth station receiver with the use of a DTPD (digital tan phase detector).

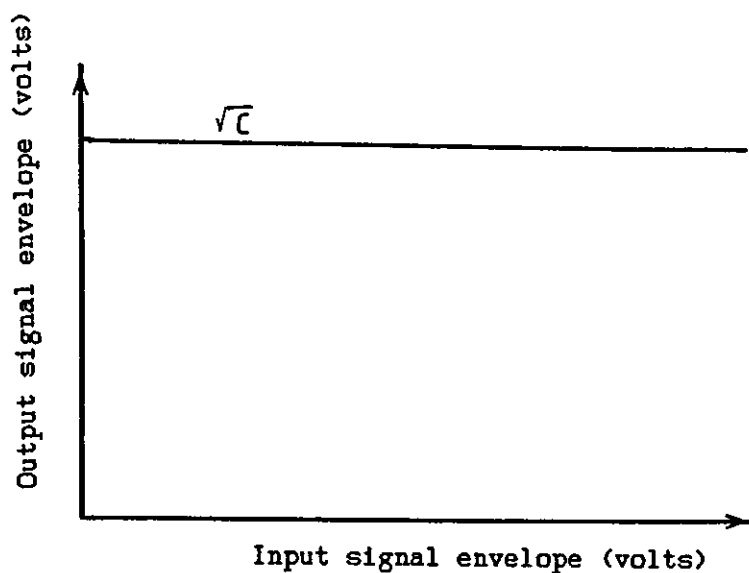


Figure 6.2 Characteristic of an ideal amplifier limiter.

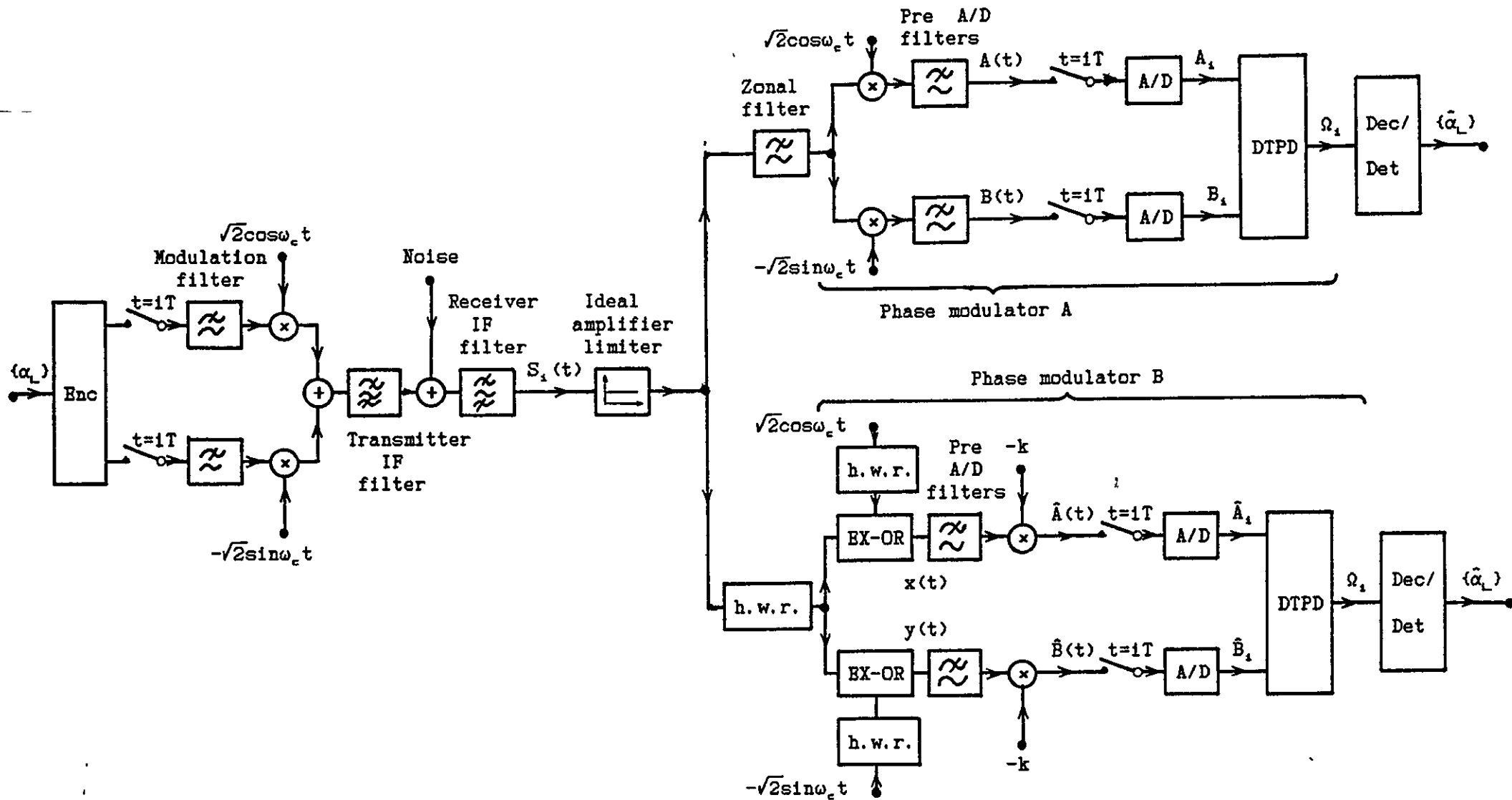


Figure 6.3 Optimum filter arrangement of the DEQPSK, CE8PSK or CDE8PSK system for using the amplifier limiter and phase demodulators A and B. The D/Cs and post-D/A filters at the transmitter are not shown. The baseband equivalent model of the receiver IF filter has the same characteristics as the baseband equivalent model of the transmitter IF filter in cascade with the modulation filter. h.w.r. means half-wave rectifier, Enc means encoder, Dec/det means decoder or detector, and DTPD means digital tan phase detector.

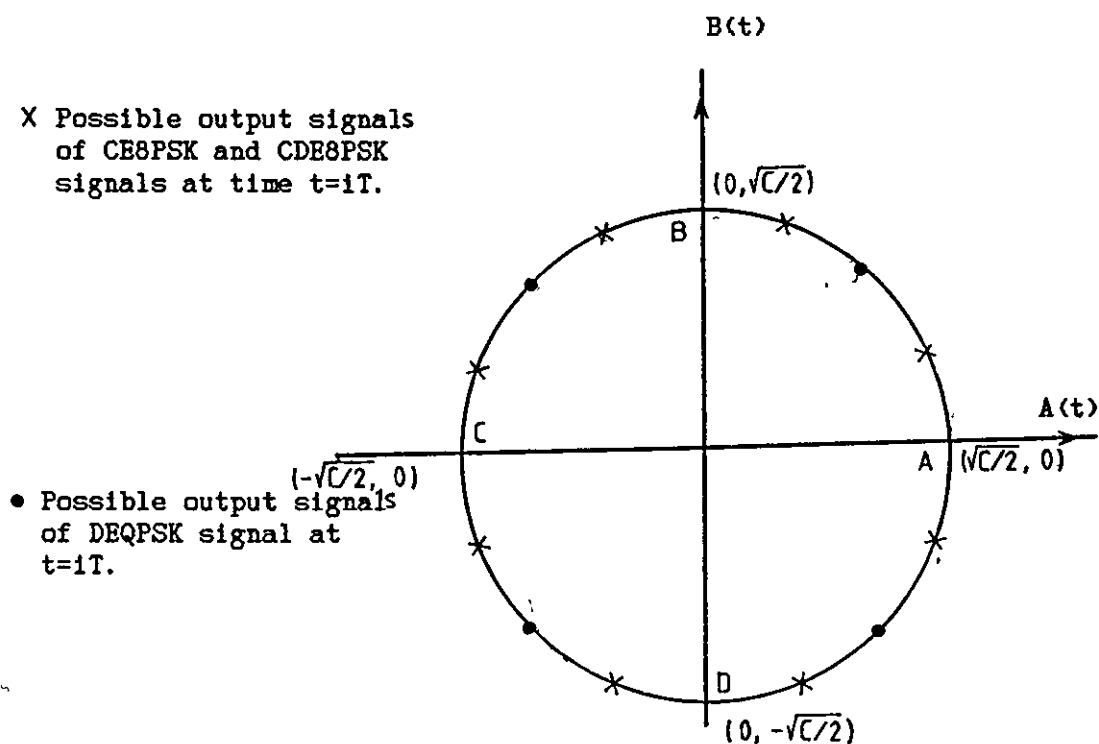


Figure 6.4 Possible output signals when using the amplifier limiter and phase demodulator A.

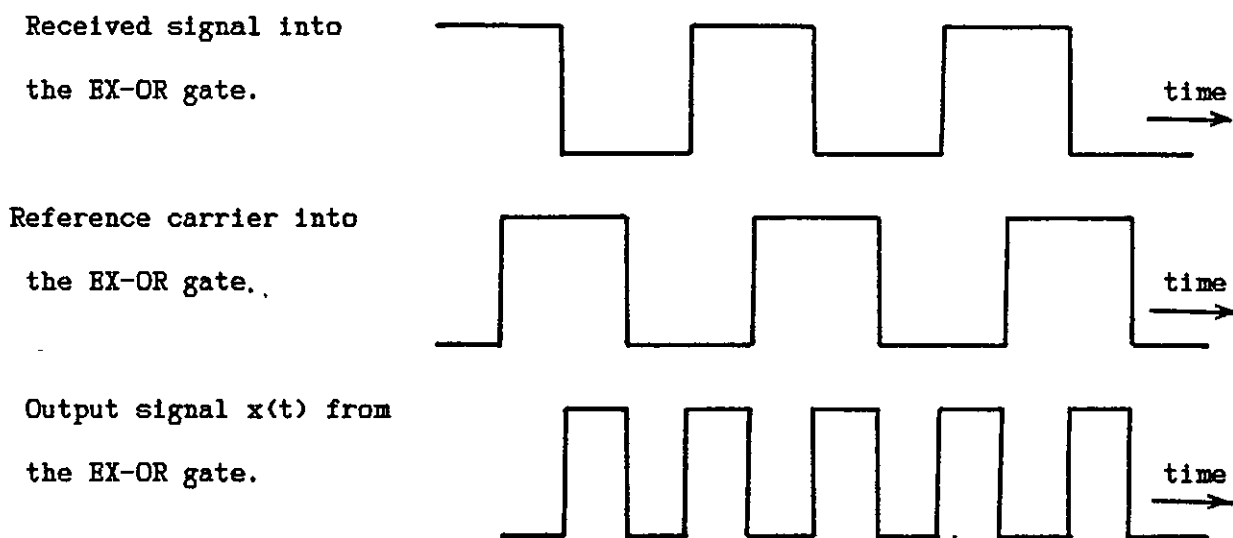


Figure 6.5 Signal waveforms at the input and output of the EX-OR gate.

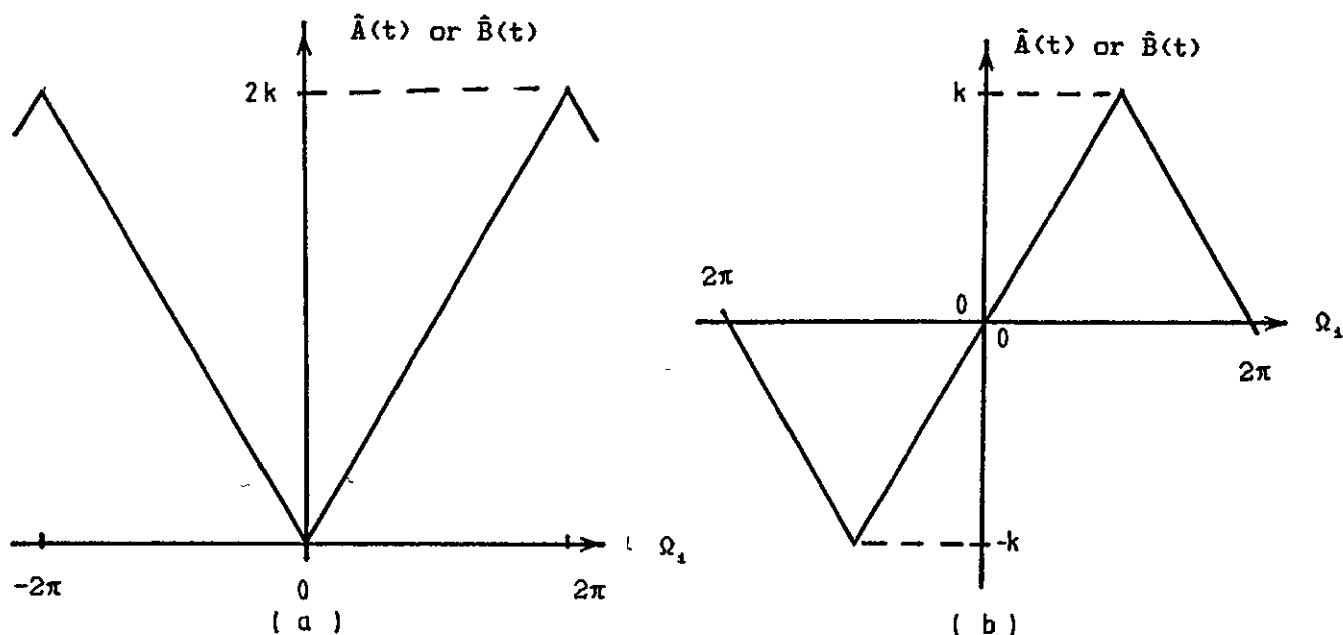


Figure 6.6 Characteristics of the EX-OR gate. (a) before and, (b) after the output short-term d.c. signals $\hat{A}(t)$ and $\hat{B}(t)$ have been level shifted by $-k$ volts. Ω_1 is the phase angle between the input waveforms.

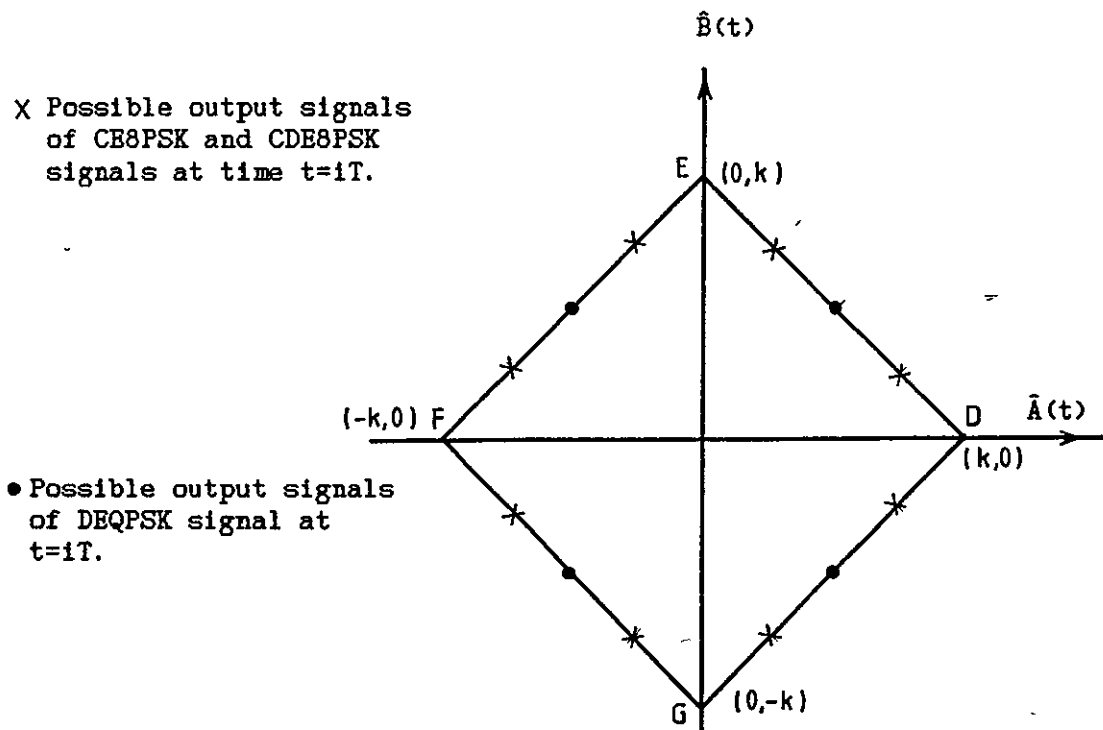


Figure 6.7 Possible output signals when using the amplifier limiter and phase demodulator B.

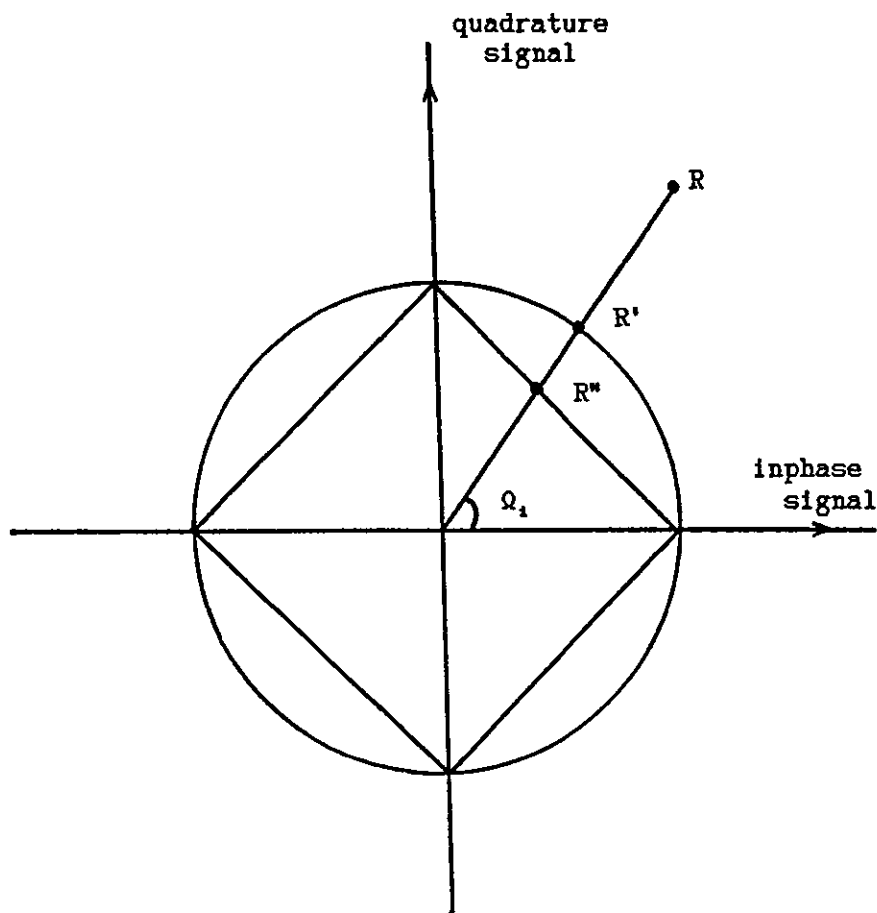


Figure 6.8 Received complex-valued signal after slicing and phase demodulation. After slicing, R' is constrained to lie on the circle. With phase demodulator A, the signal remains at the same position, whereas, with phase demodulator B, the signal is further distorted and constrained to lie on the square and becomes R'' . The angles Ω_1 of these complex-valued signals are the same.

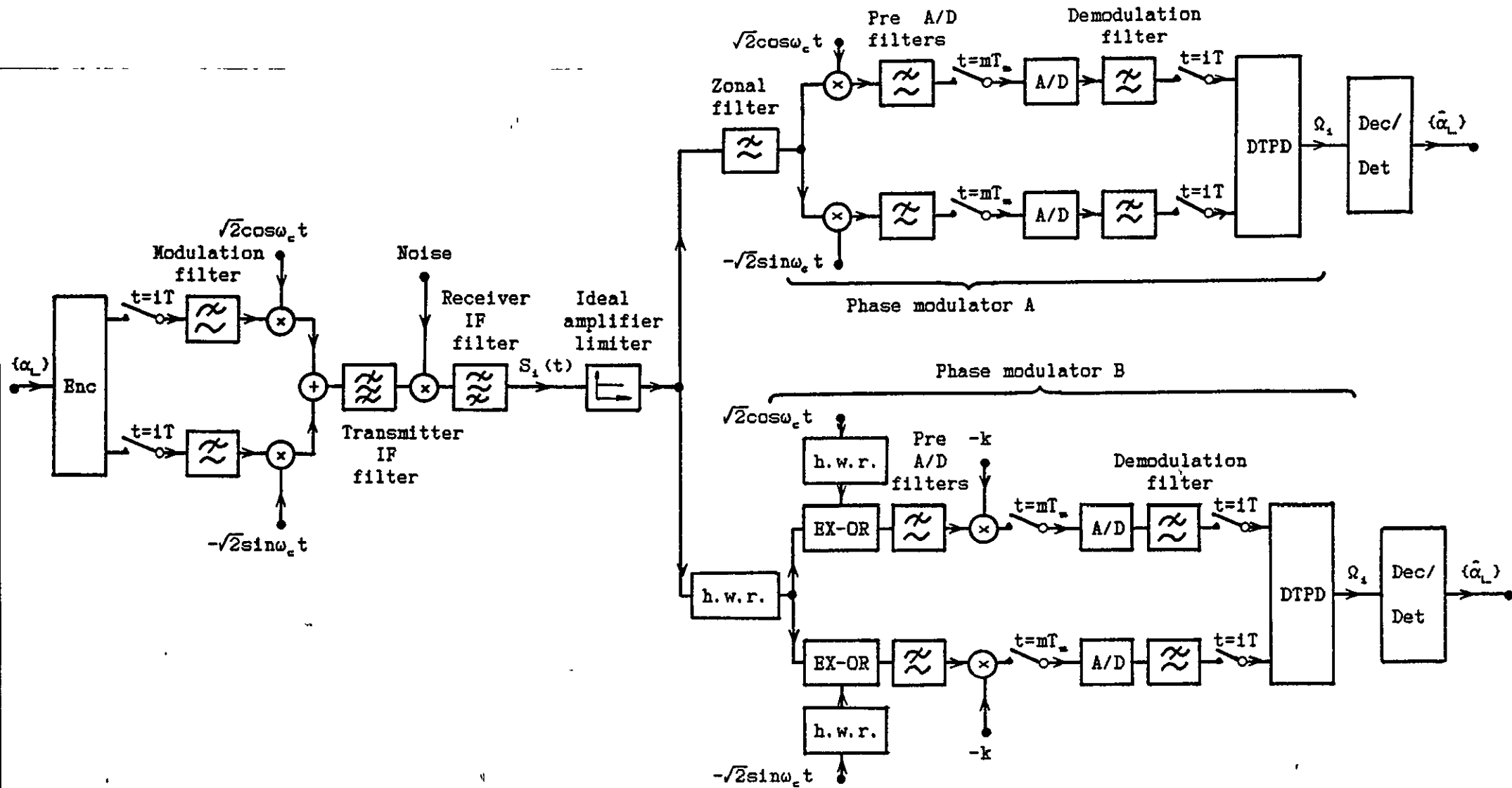


Figure 6.9 Suboptimum filter arrangement of the DEQPSK, CE8PSK or CDE8PSK system for using the amplifier limiter and phase demodulators A and B. The receiver IF filter has the same characteristics as the transmitter IF filter. The D/Cs and post-D/A filters at the transmitter are not shown. h.w.r. means half-wave rectifier, Enc means encoder, Dec/det means decoder or detector, and DTPD means digital tan phase detector.

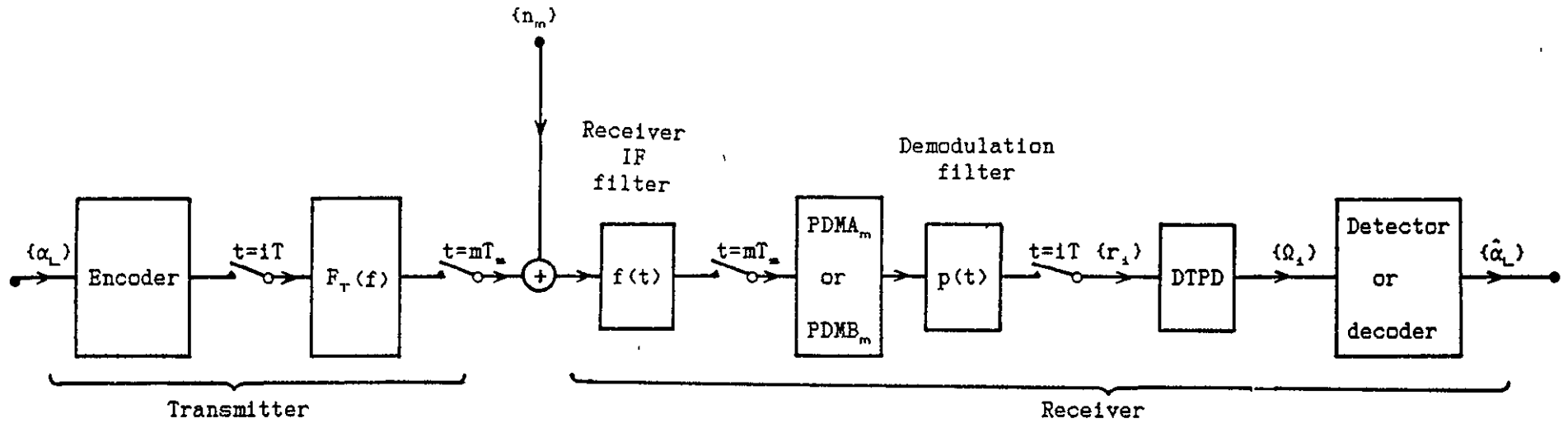


Figure 6.10 Baseband equivalent model of the DEQPSK, CE8PSK or CDE8PSK system, transmitting signal over a linear and bandlimited satellite channel, with the use of the suboptimum filters for the amplifier limiter, phase demodulator A or B and the distance measure D, for computer simulation $F_T(f)$ is the resultant transfer function of the baseband equivalent of the transmitter IF filter in cascade with the modulation filter.

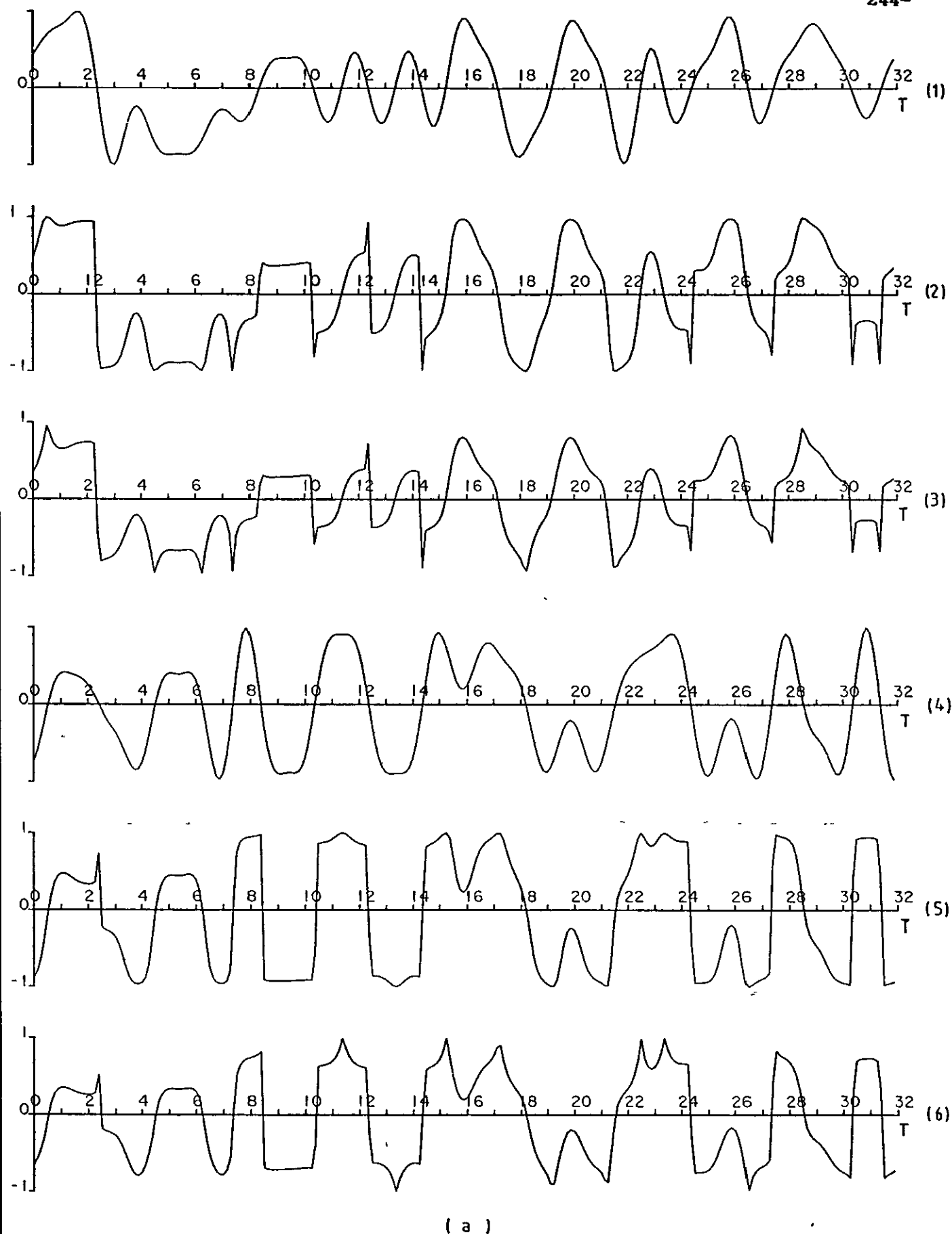
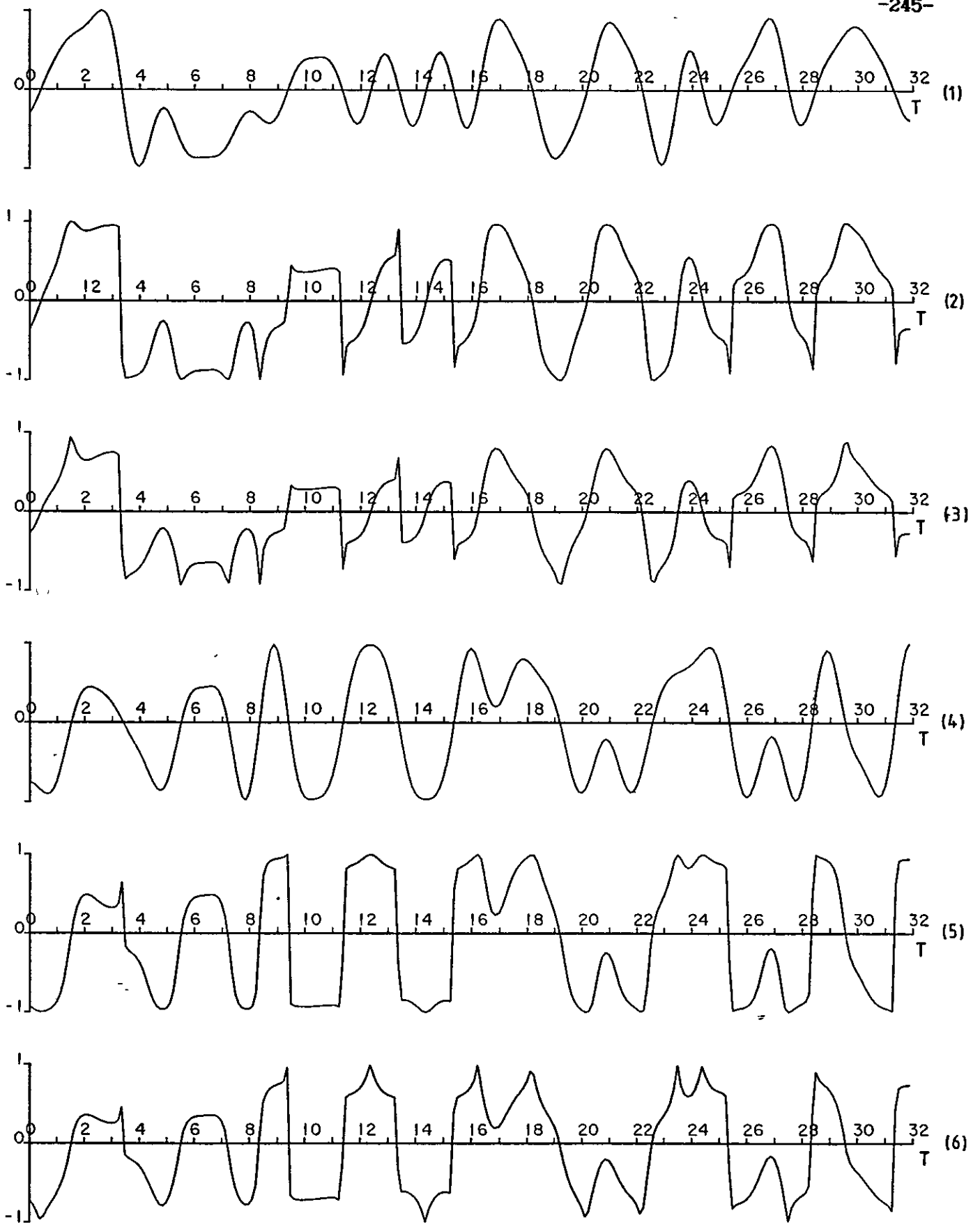
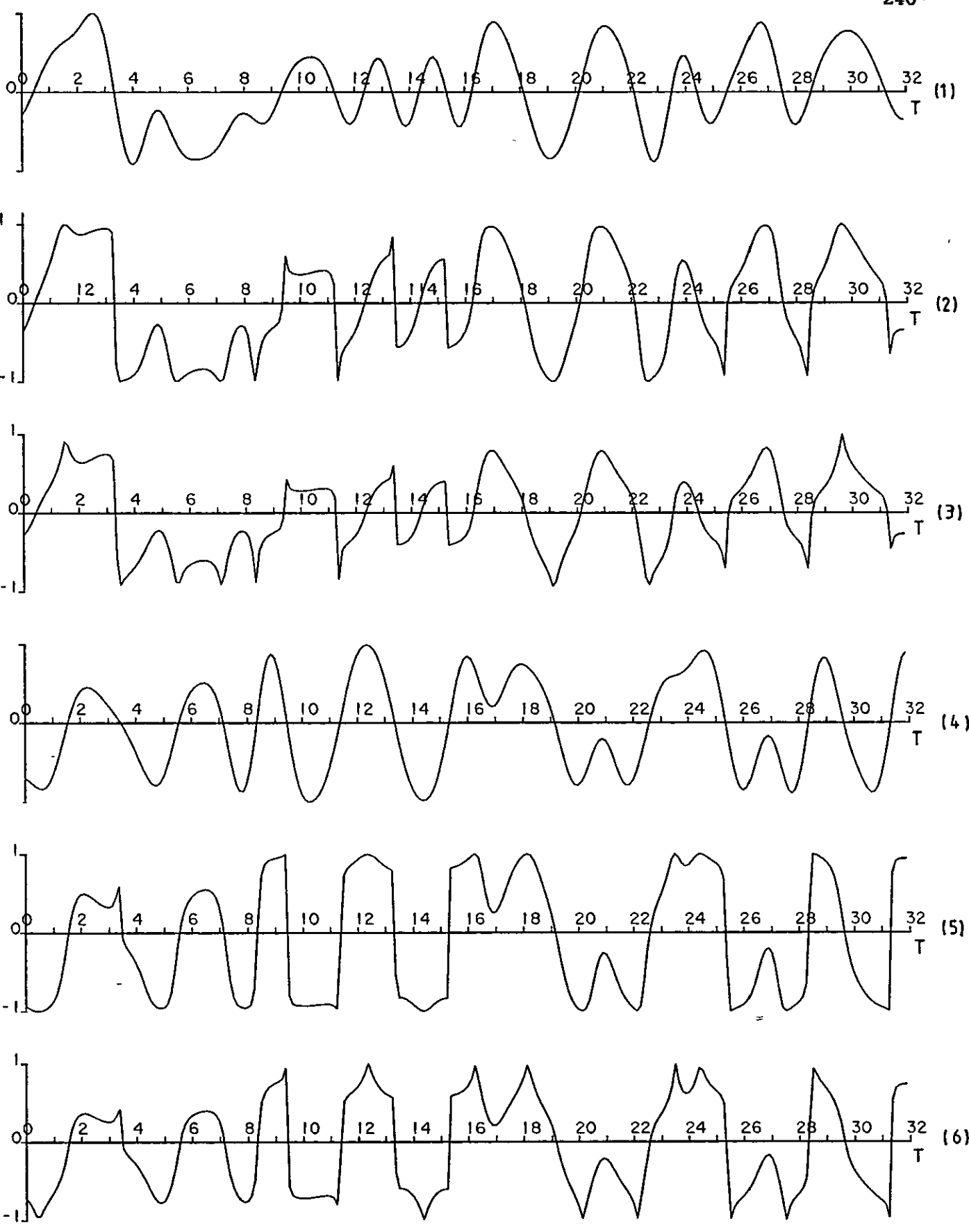


Figure 6.11 The received baseband data waveforms of signals (a) 1B, (b) 2B, (c) 3B and, (d) 4B (CE8PSK signals) over a linear channel, at the outputs of the receiver IF filter, phase demodulators A and B. (1), (2) and (3) are the inphase baseband waveforms at the outputs of the receiver IF filter, phase demodulator A, and phase demodulator B, respectively (4), (5) and (6) are the quadrature baseband waveforms at the outputs of the receiver IF filter, phase demodulator A, and phase demodulator B, respectively.



(b)

Figure 6.11 (Continue)



(c)

Figure 6.11 (Continue)

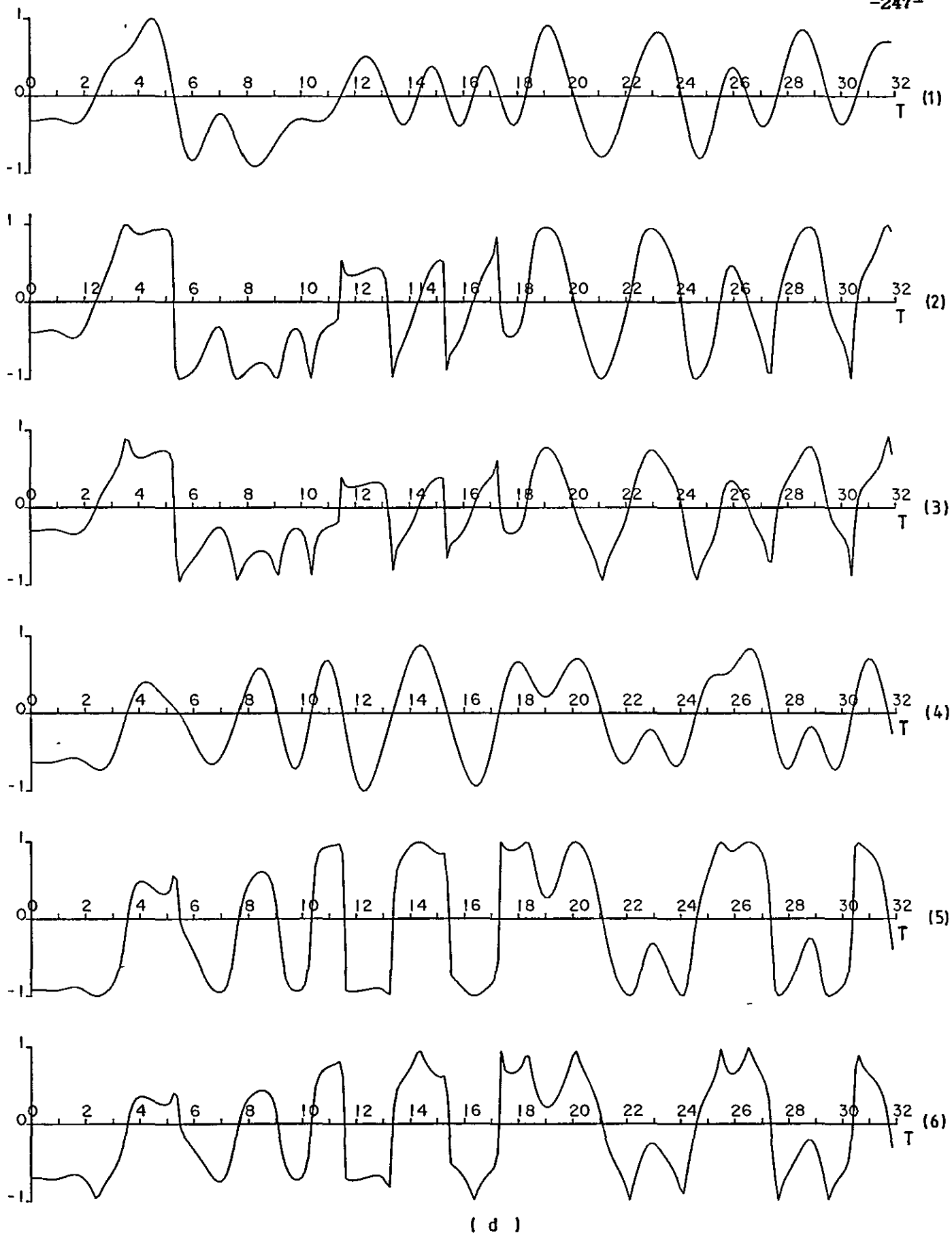


Figure 6.11 (Continue)

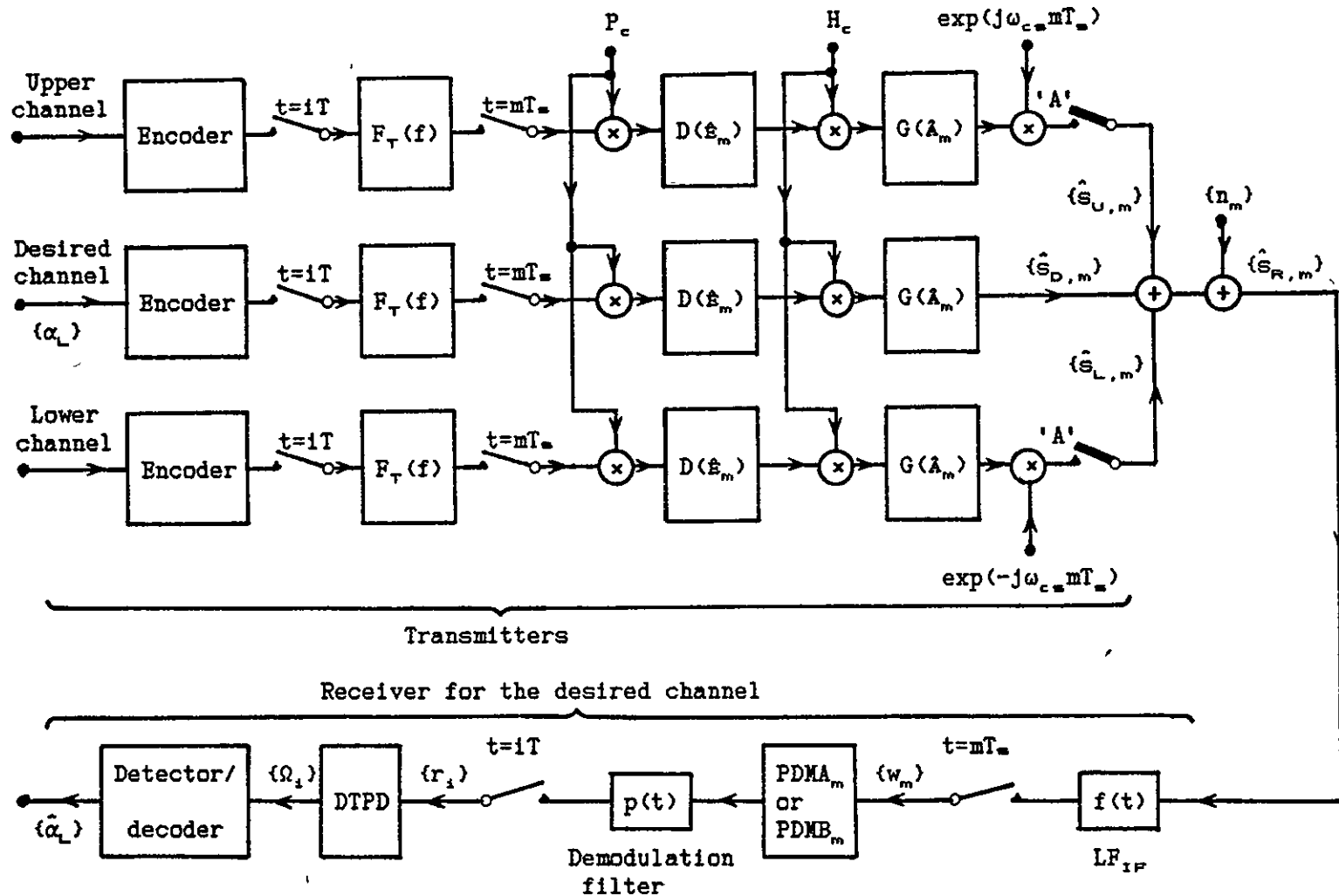


Figure 6.12 Baseband equivalent model of the DEQPSK, CE8PSK or CDE8PSK system, with the use of the suboptimum filters, the predistorter, the amplifier limiter, phase demodulator A or B and the distance measure D, for computer simulation. $F_T(f)$ is the resultant transfer function of the baseband equivalent model of the IF filter in cascade with the modulation filter. LF_{IF} means the baseband equivalent model of the IF filter. Switches 'A' determine whether the system is in an ACI environment.

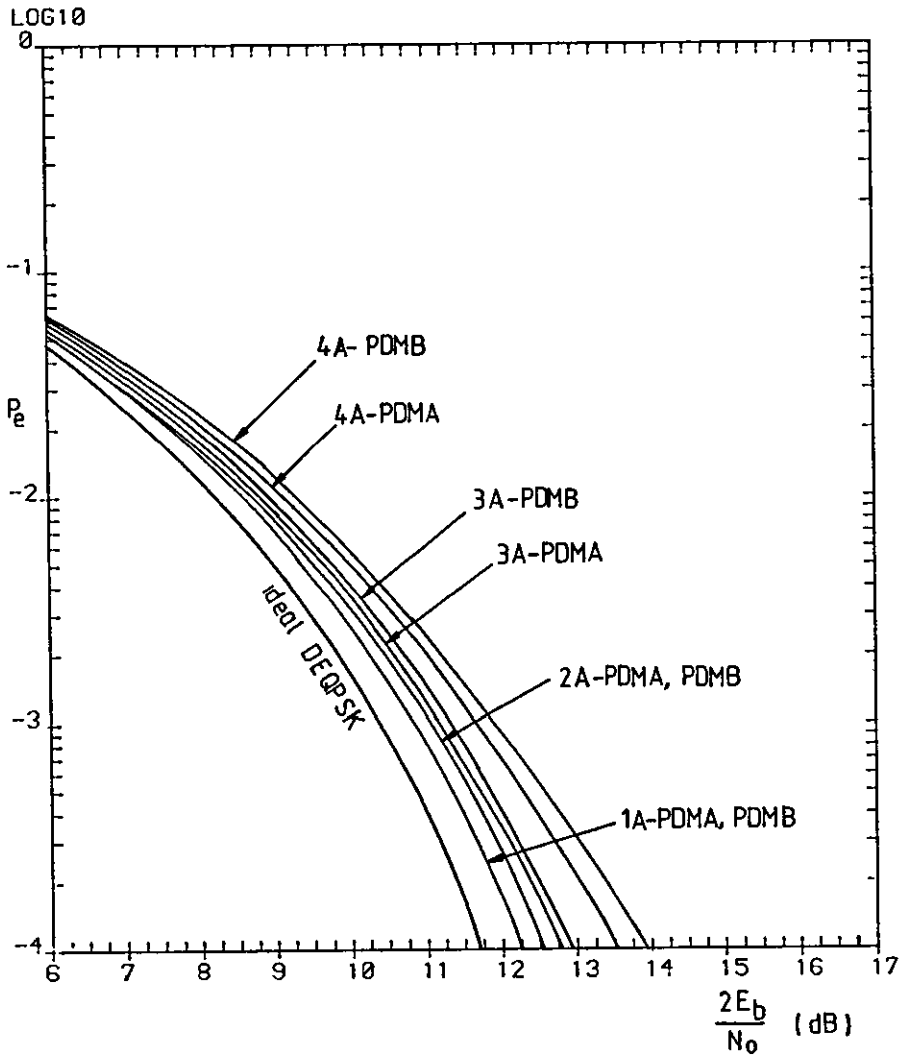


Figure 6.13 Error-rate performances of signals 1A, 2A, 3A and 4A, over a linear channel, with the use of the suboptimum filters, the amplifier limiter and phase demodulators A and B. PDMA and PDMB mean phase demodulator A and phase demodulator B, respectively.

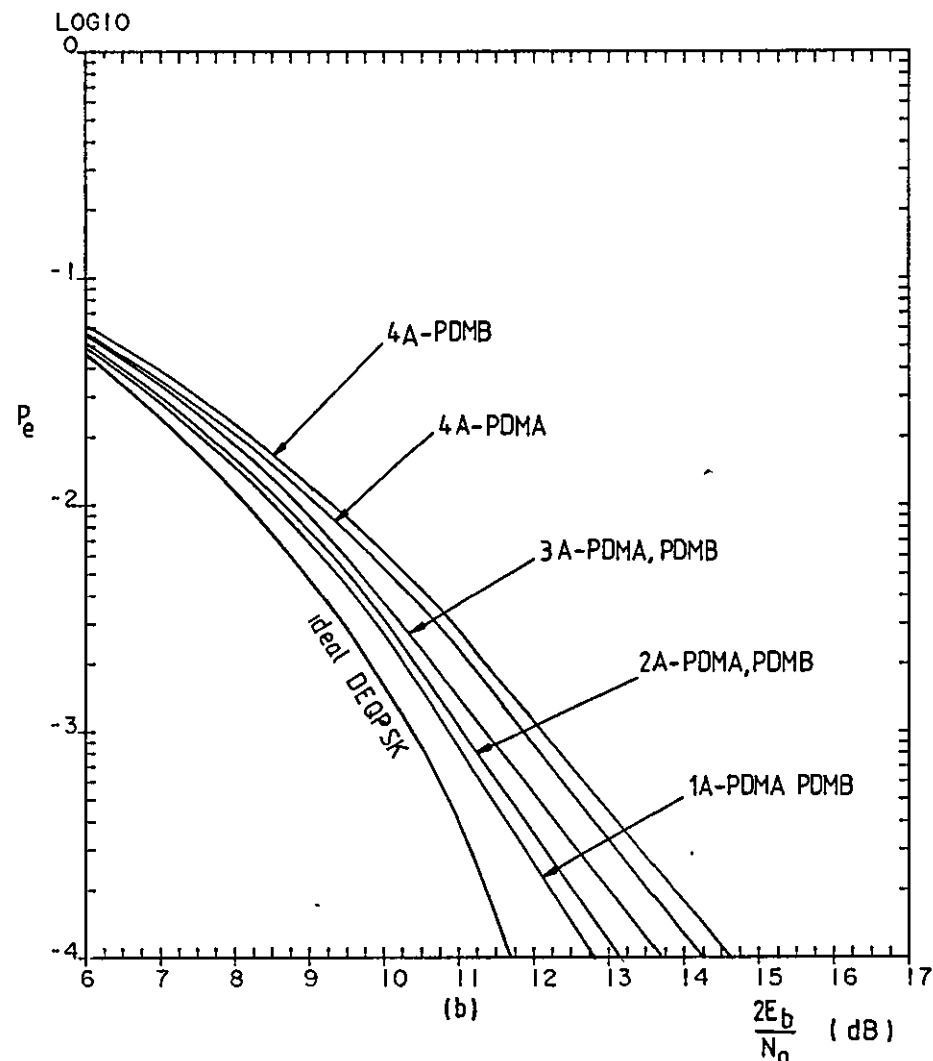
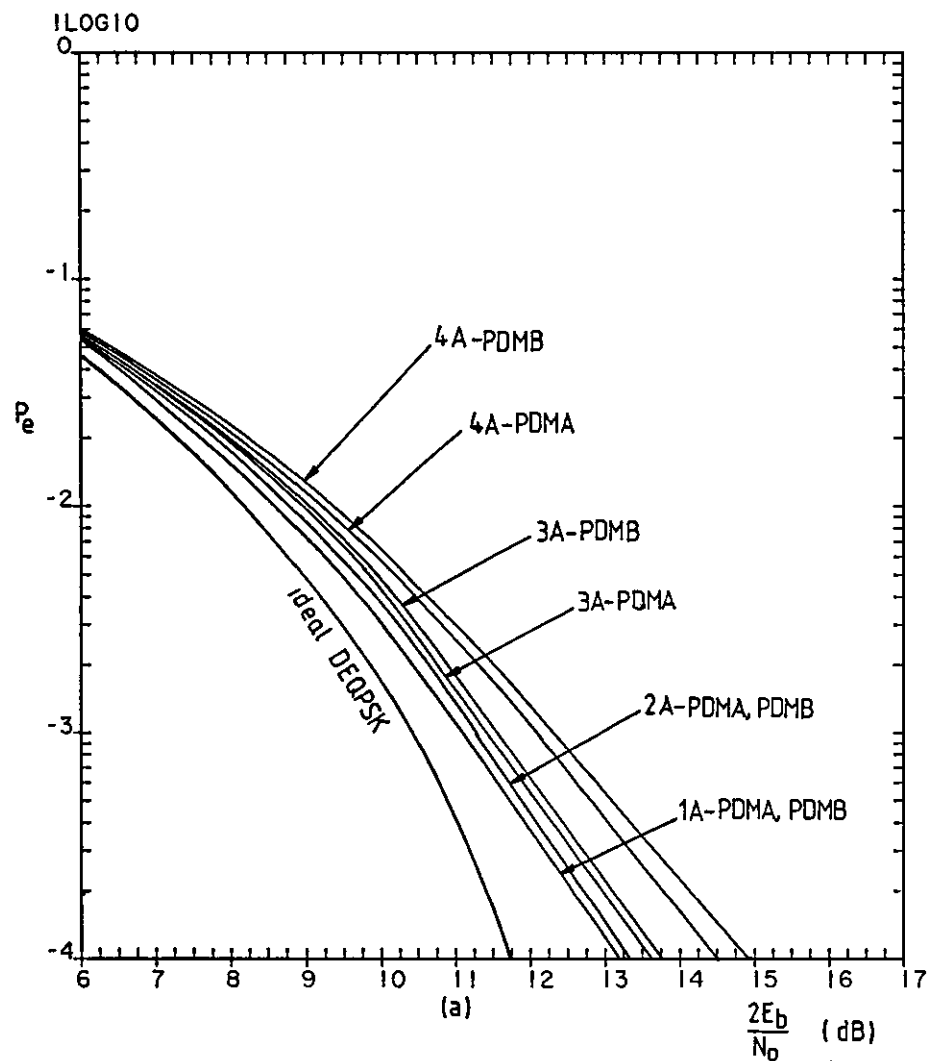


Figure 6.14 Error-rate performances of signals 1A, 2A, 3A and 4A, over a nonlinear and bandlimited channel, with the use of the suboptimum filters, the predistorter, the HPA operating at (a) 0.2 dB and, (b) 0.68 dB OBO, the amplifier limiter and phase demodulators A and B and in a non-ACI environment. PDMA and PDMB mean phase demodulator A and phase demodulator B, respectively.

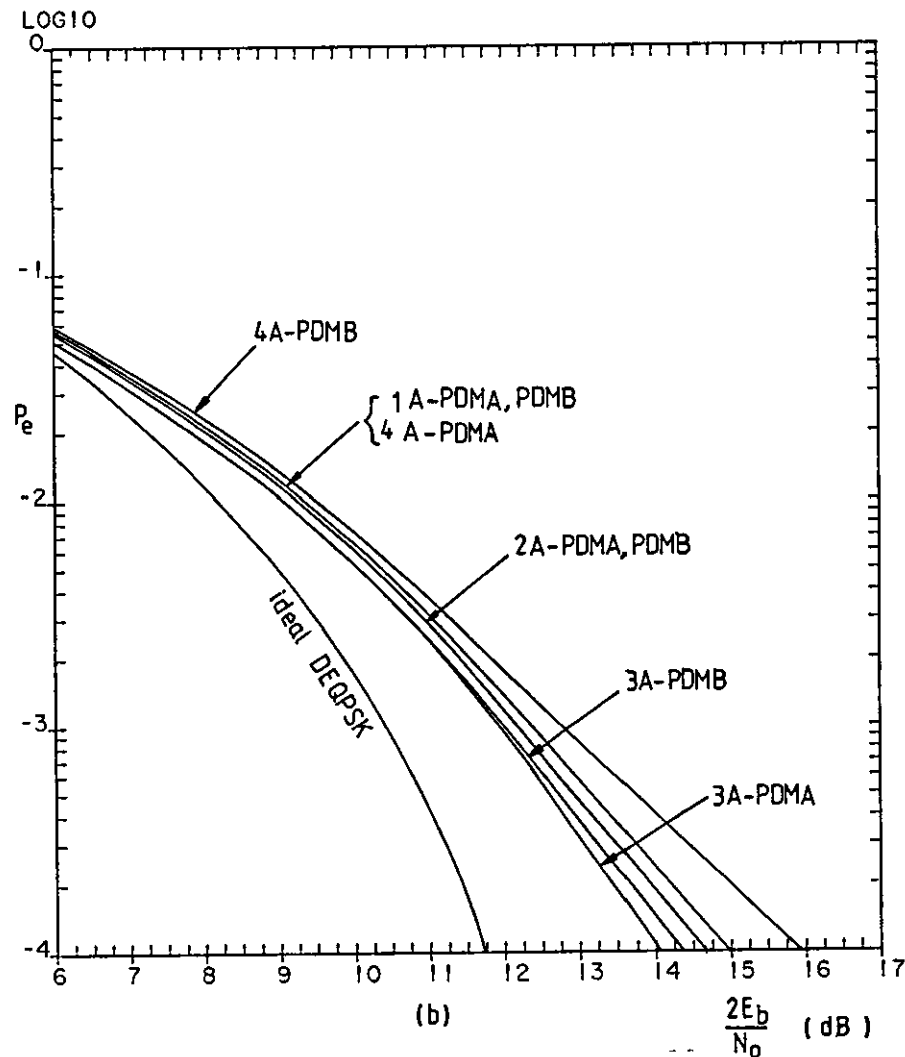
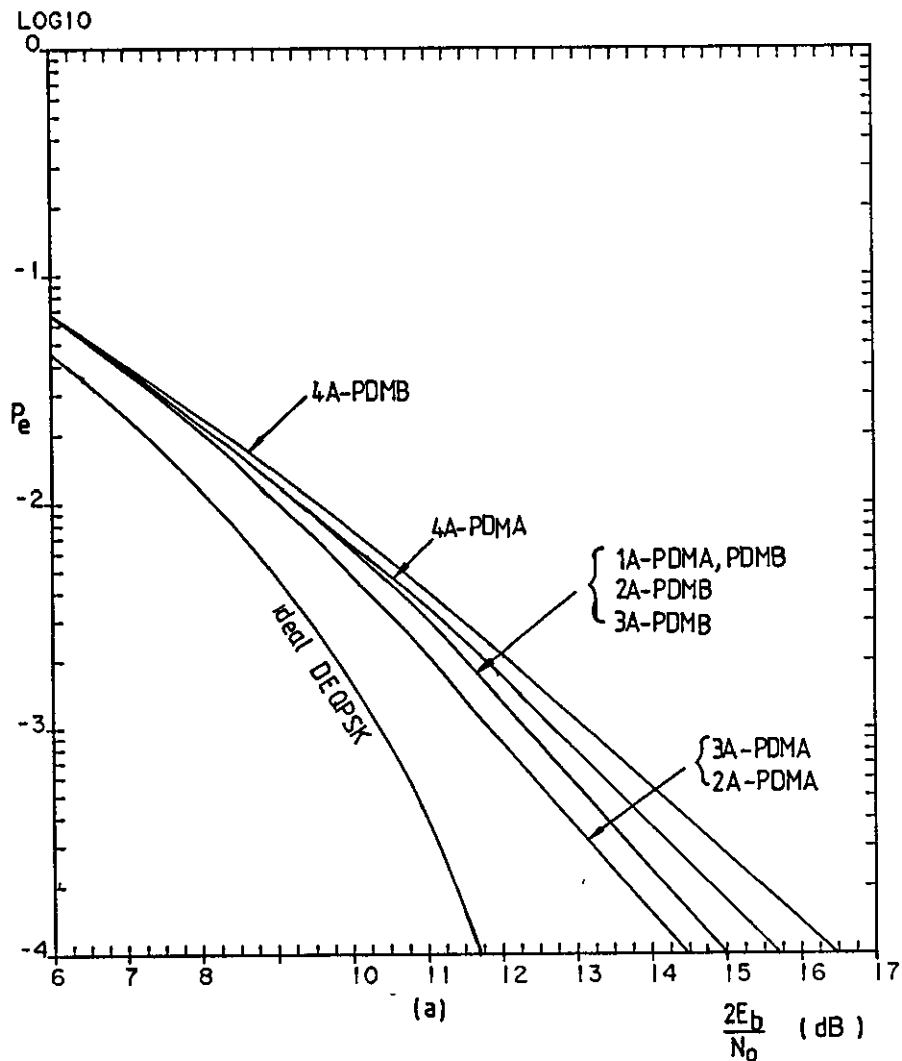


Figure 6.15 Error-rate performances of signals 1A, 2A, 3A and 4A, over a nonlinear and bandlimited channel, with the use of the suboptimum filters, the predistorter, the HPA operating at (a) 0.2 dB and, (b) 0.68 dB OBO, the amplifier limiter and phase demodulators A or B and in an ACI environment with $f_{c_{max}}=5R/4$ Hz. PDMA and PDMB mean phase demodulator A and phase demodulator B, respectively.

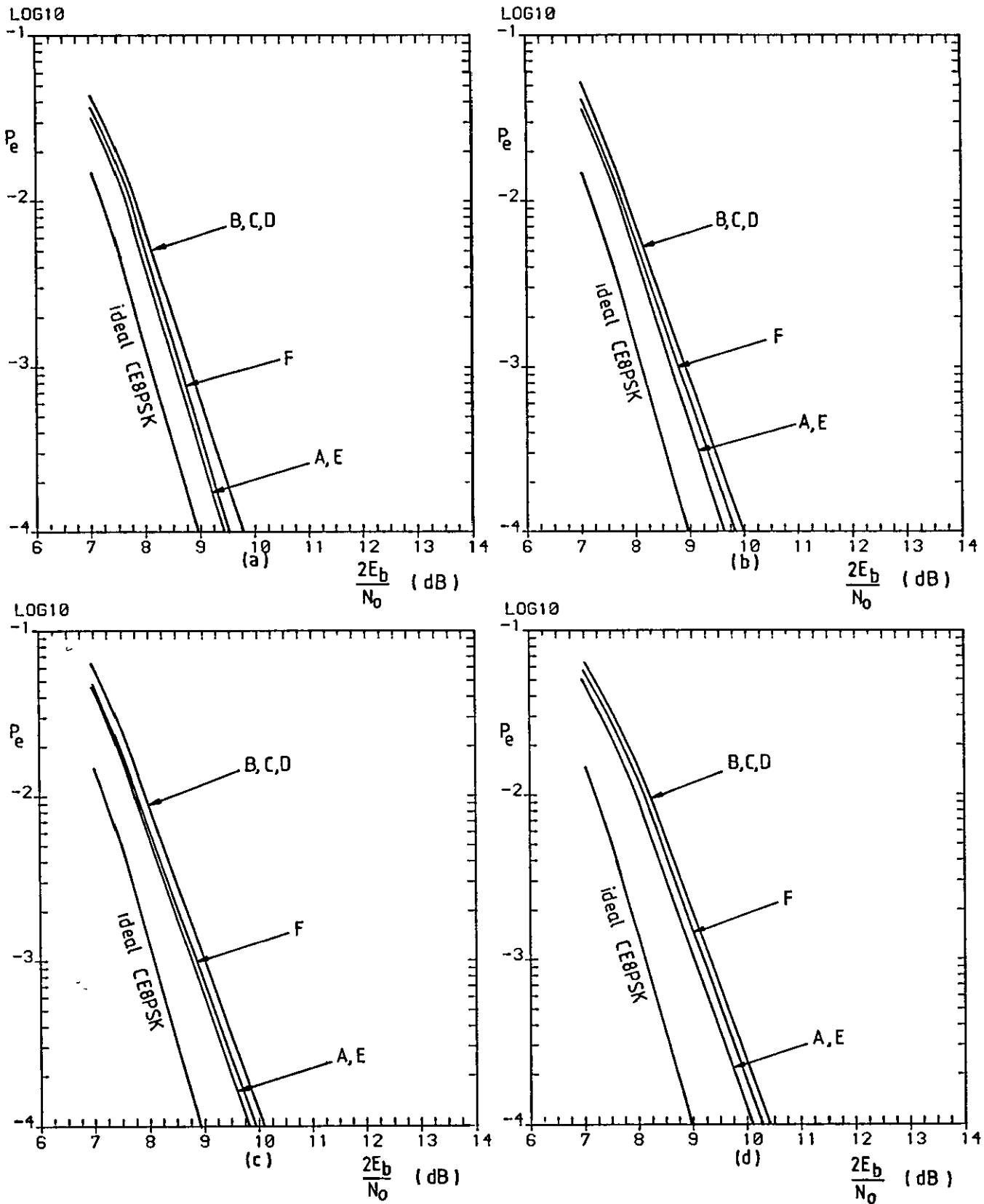


Figure 6.16 Error-rate performances of signals (a) 1B, (b) 2B, (c) 3B and, (d) 4B, over a linear and bandlimited channel, with the use of the suboptimum filters, the amplifier limiter and phase demodulators A, given by different distance measures.

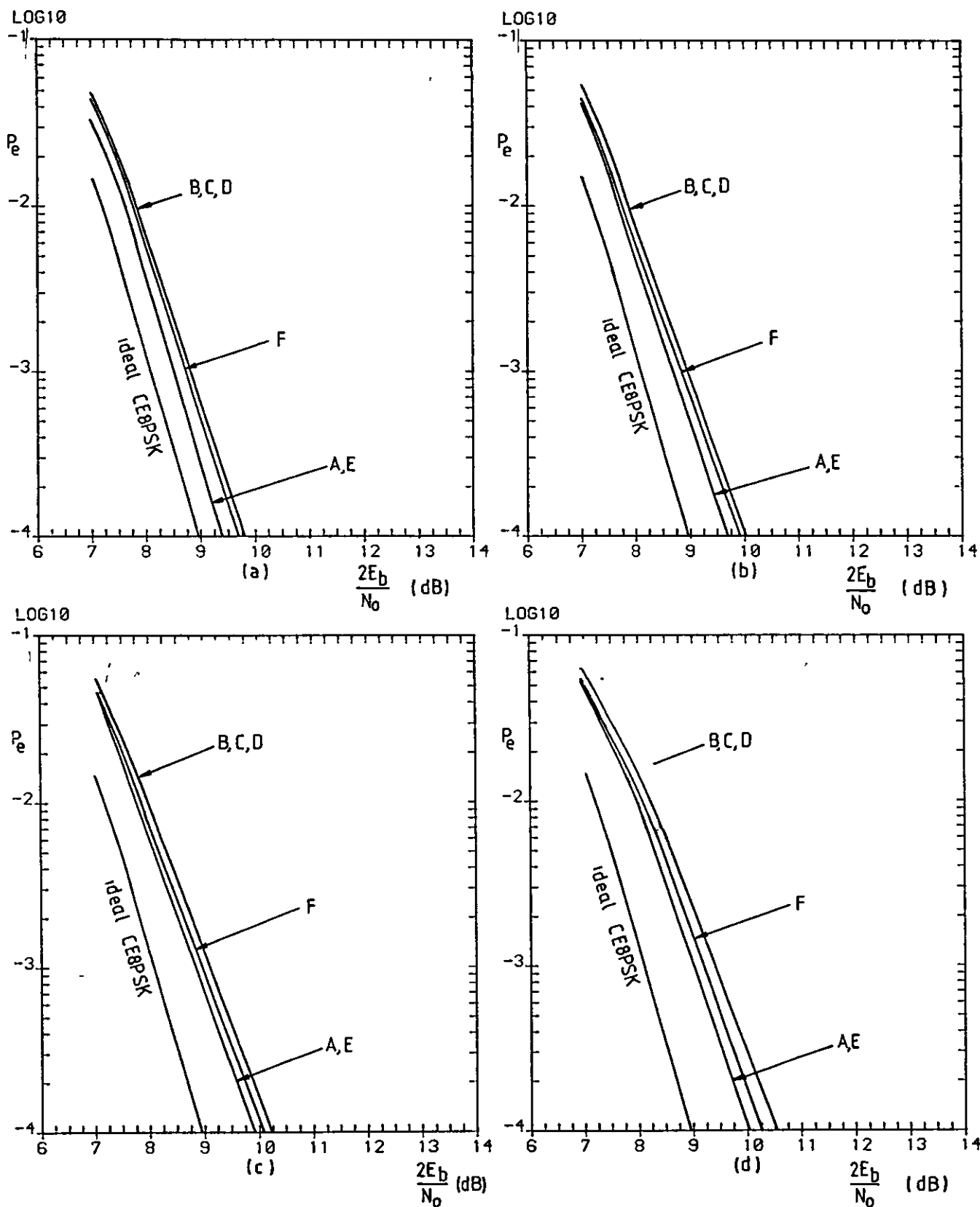


Figure 6.17 Error-rate performances of signals (a) 1B, (b) 2B, (c) 3B and, (d) 4B, over a linear and bandlimited channel, with the use of the suboptimum filters, the amplifier limiter and phase demodulators B, given by different distance measures.

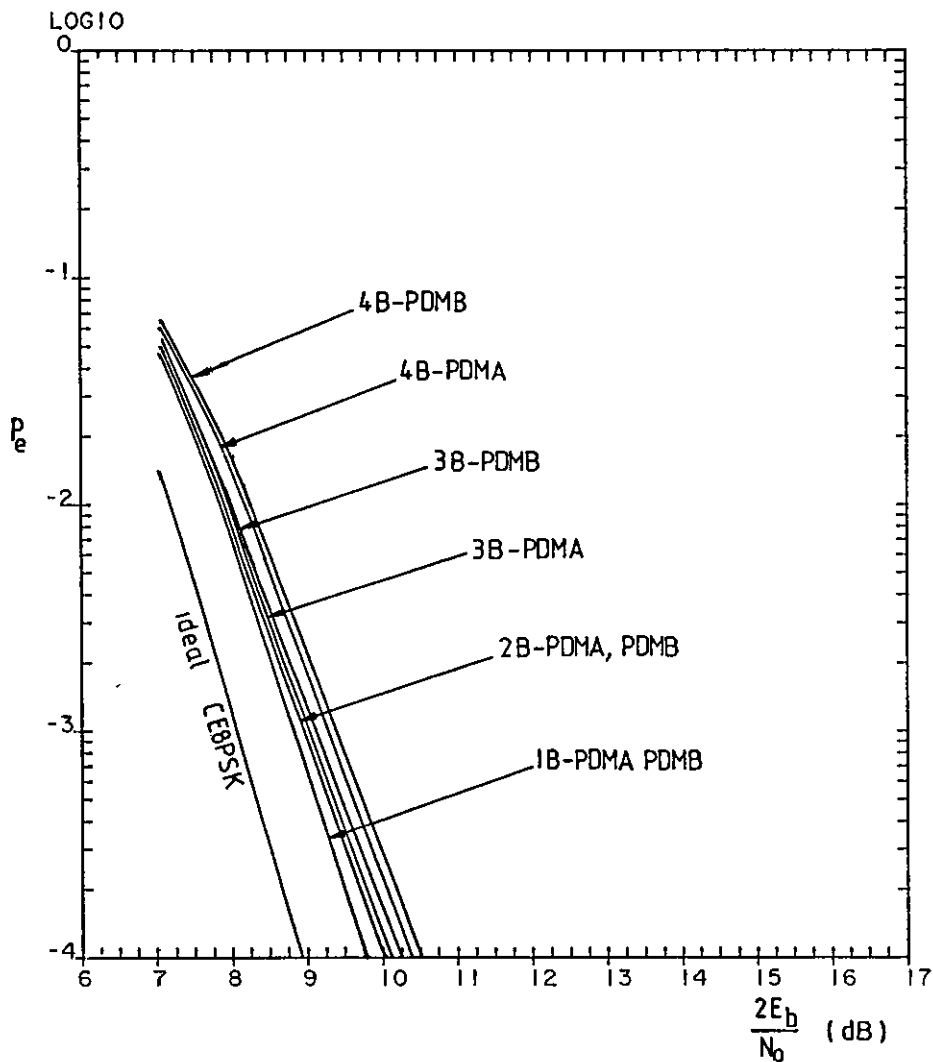


Figure 6.18 Error-rate performances of signals 1B, 2B, 3B and 4B, over a linear channel, with the use of the suboptimum filters, the amplifier limiter and phase demodulators A and B. PDMA and PDMB mean phase demodulator A and phase demodulator B, respectively.

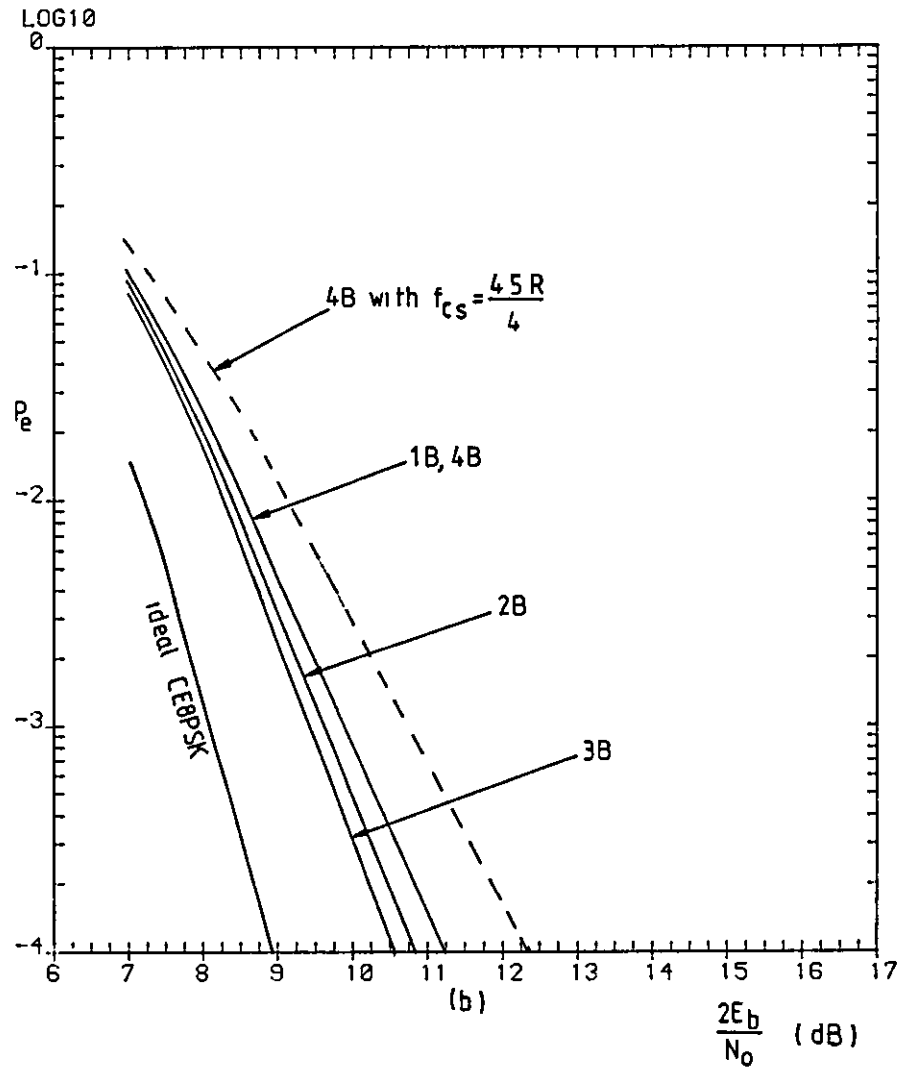
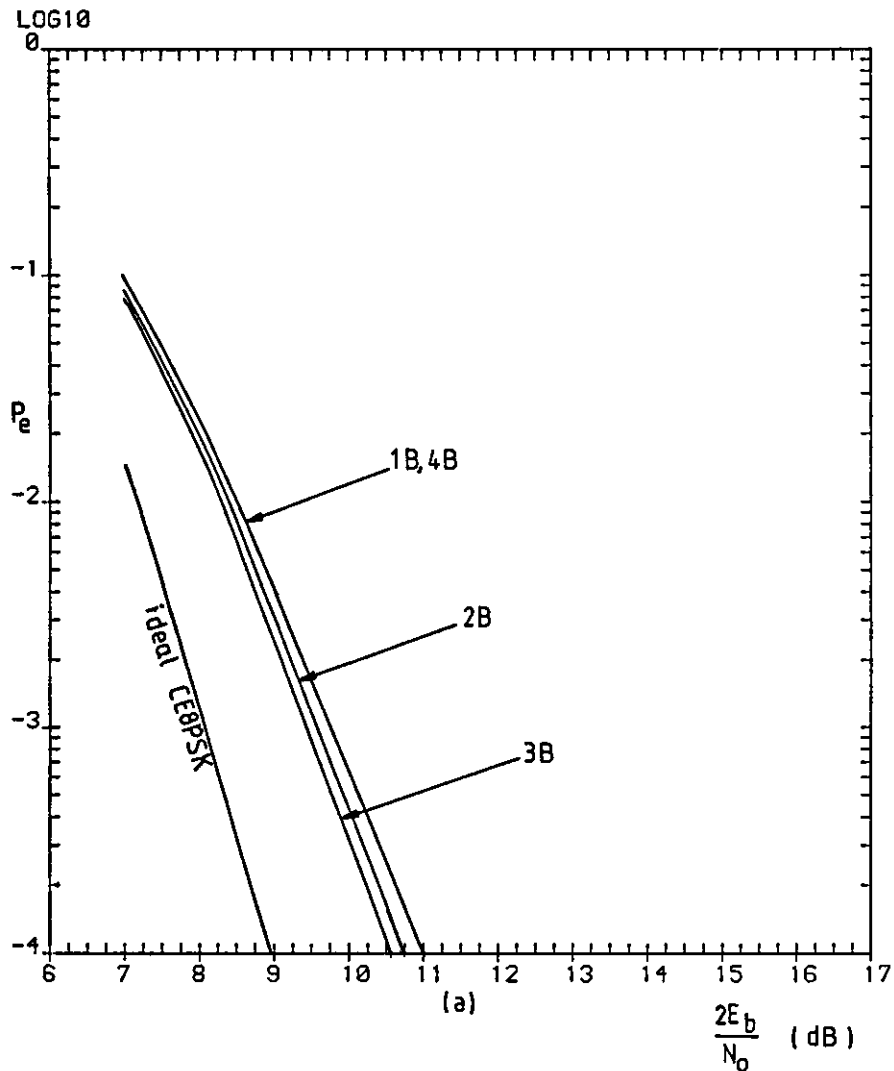


Figure 6.19 Error-rate performances of signals 1B, 2B, 3B and 4B, over a nonlinear and bandlimited channel, with the use of the suboptimum filters, the predistorter, the HPA operating at 0.2 dB OBO, the amplifier limiter and phase demodulators (a) A and, (b) B and in an ACI environment, with $f_{cs} = 5R/4$ Hz.

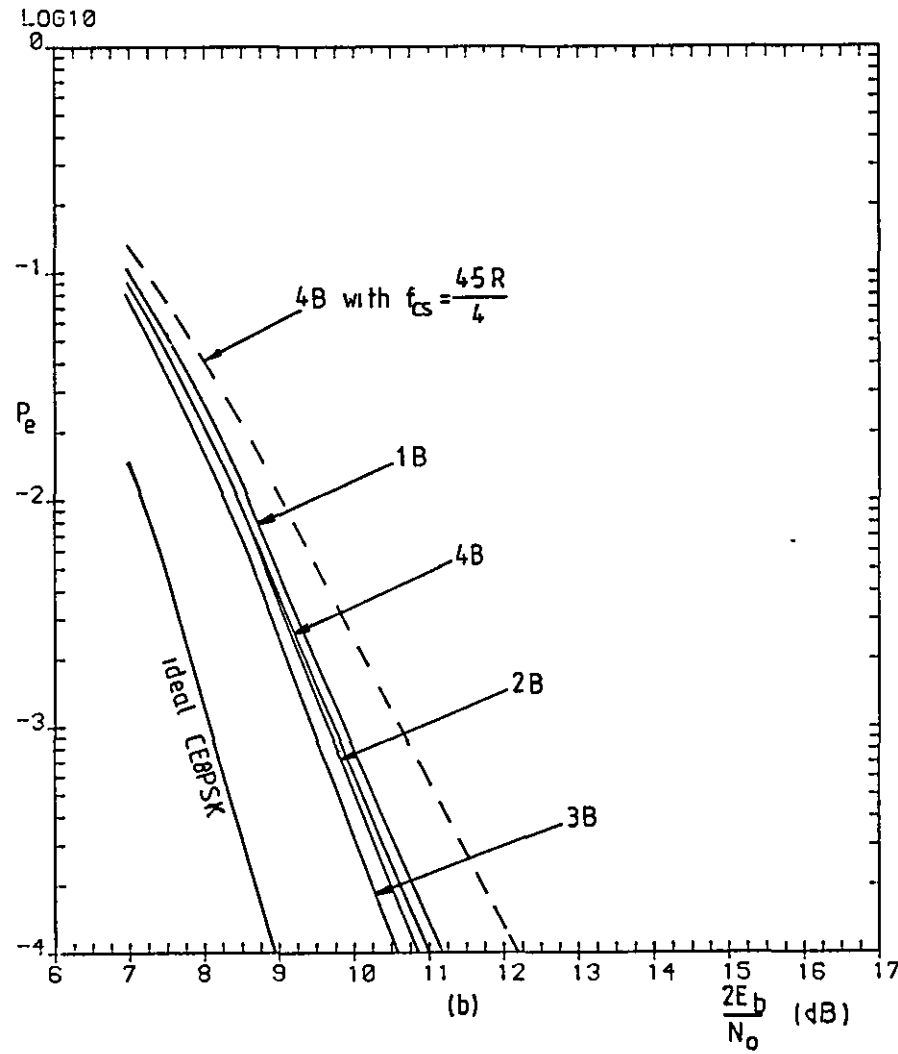
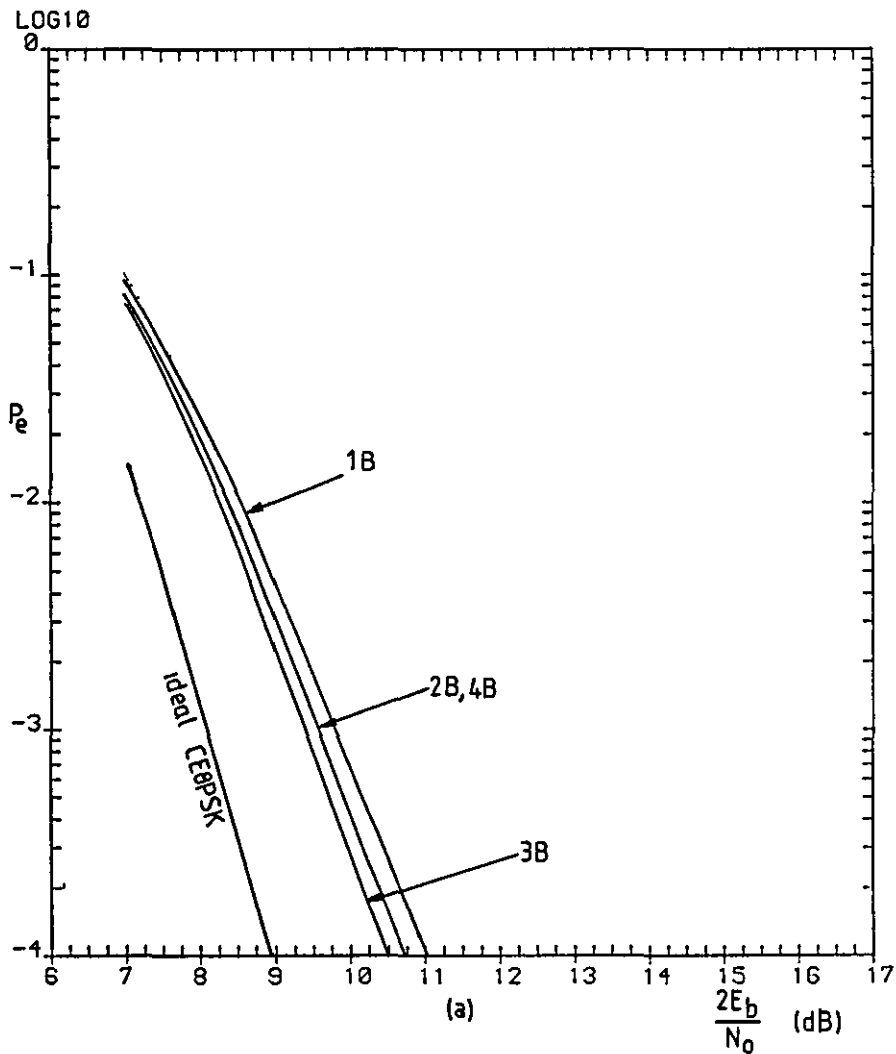


Figure 6.20 Error-rate performances of signals 1B, 2B, 3B and 4B, over a nonlinear and bandlimited channel, with the use of the suboptimum filters, the predistorter, the HPA operating at 0.68 dB OBO, the amplifier limiter and phase demodulators (a) A and, (b) B and in an ACI environment, with $f_{cs} = 5R/4$ Hz.

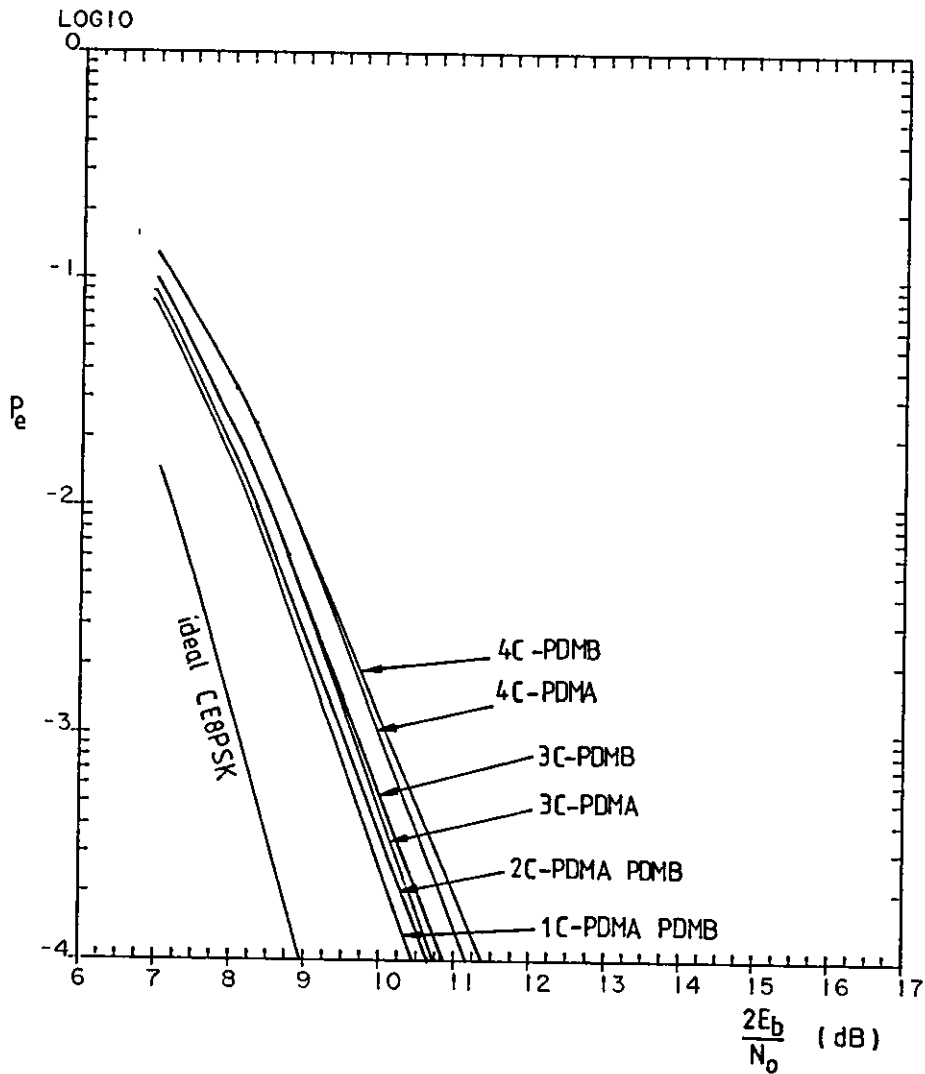


Figure 6.21 Error-rate performances of signals 1C, 2C, 3C and 4C, over a linear channel, with the use of the suboptimum filters, the amplifier limiter and phase demodulators A and B. PDMA and PDMB mean phase demodulator A and phase demodulator B, respectively.

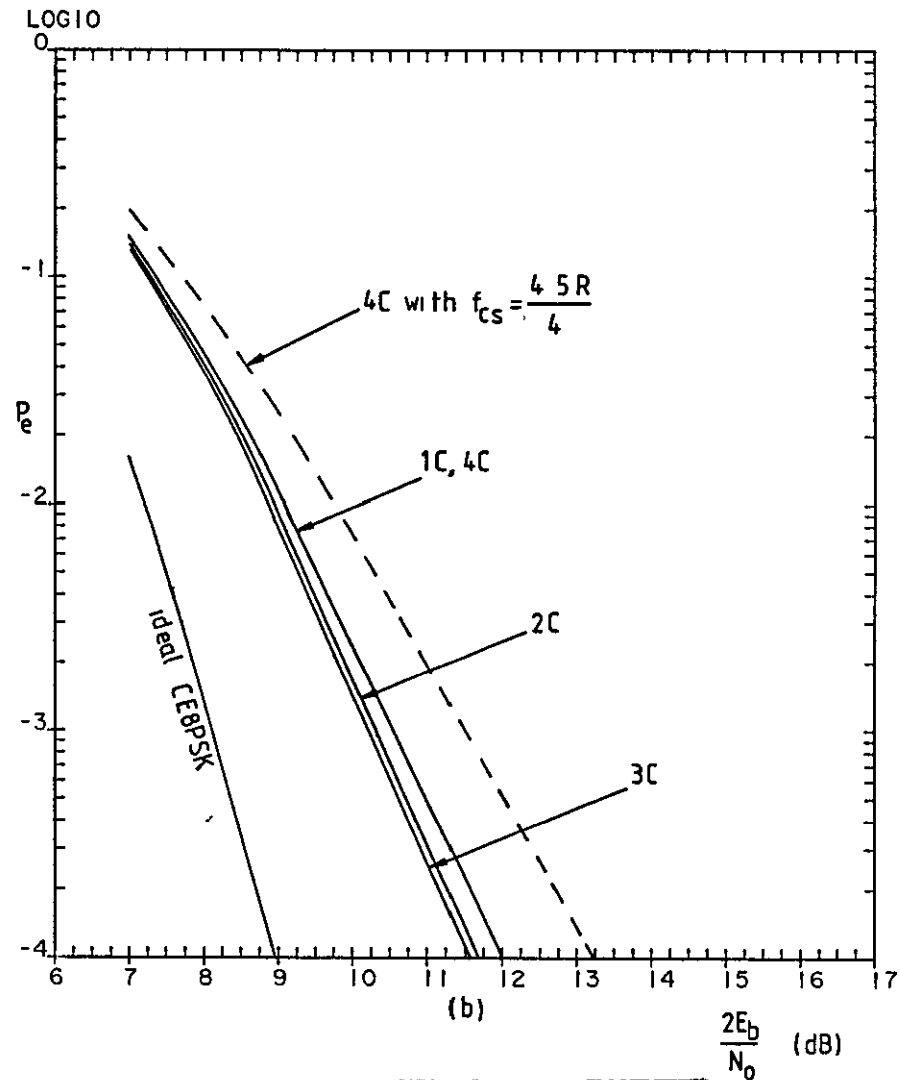
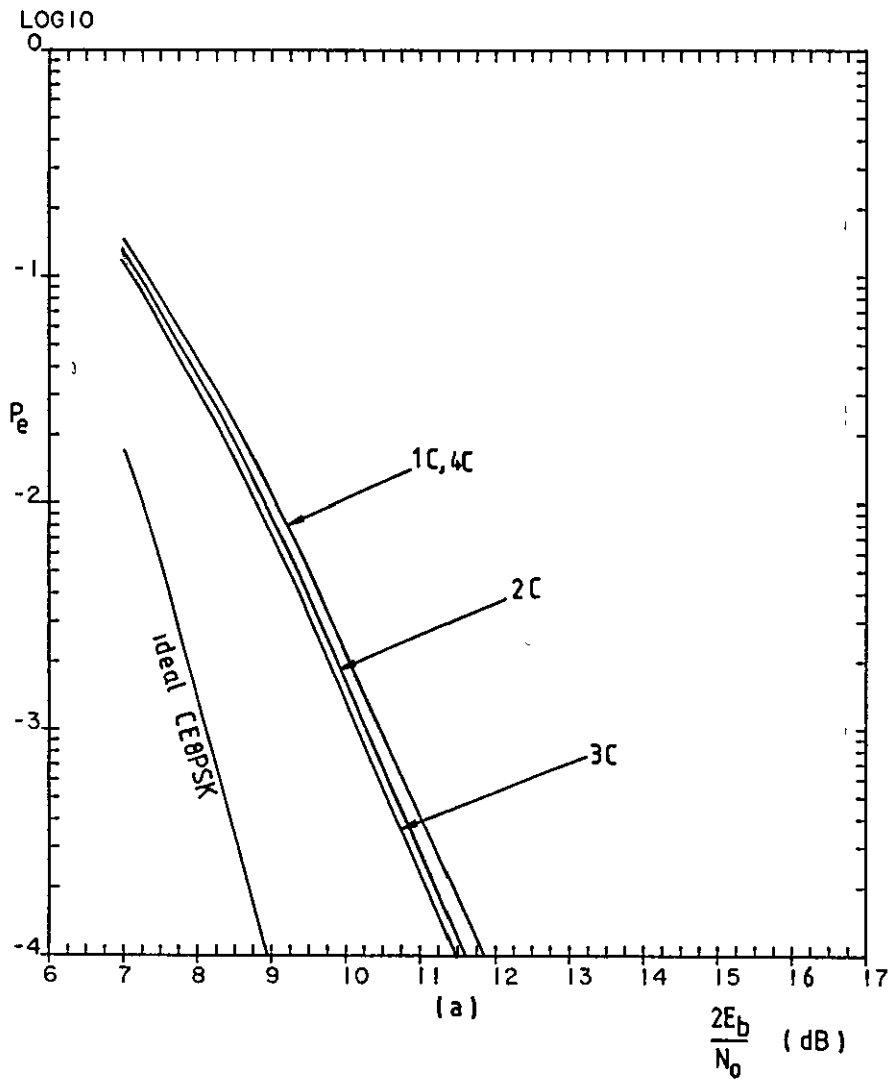


Figure 6.22 Error-rate performances of signals 1C, 2C, 3C and 4C, over a nonlinear and bandlimited channel, with the use of the suboptimum filters, the predistorter, the HPA operating at 0.2 dB OBO, the amplifier limiter and phase demodulators (a) A and, (b) B and in an ACI environment, with $f_{cs} = 5R/4$ Hz.

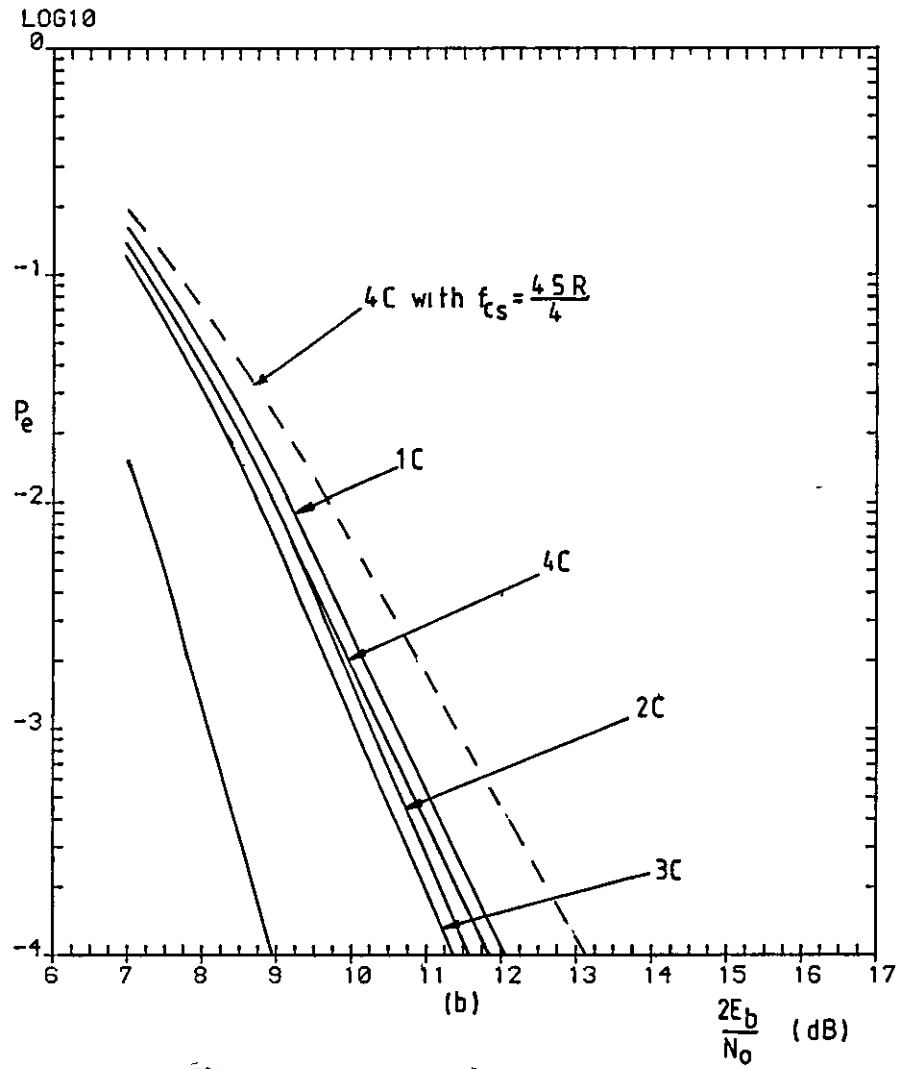
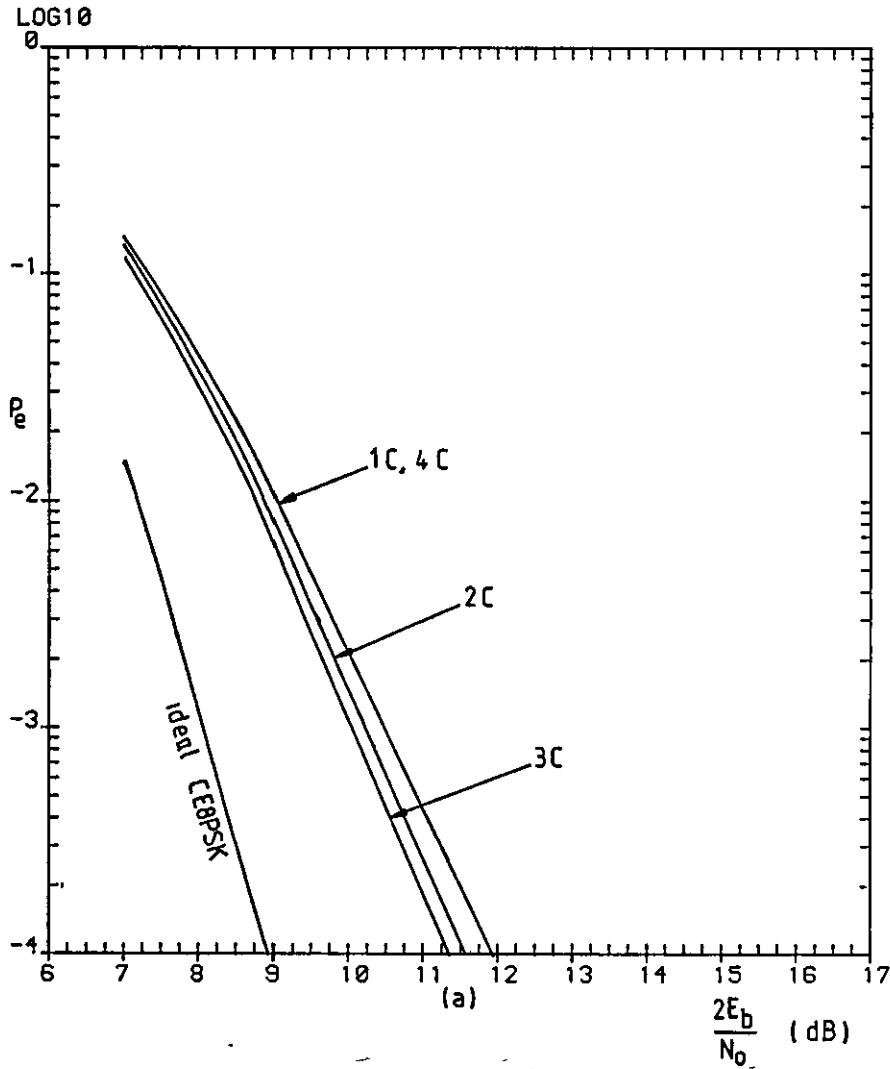


Figure 6.23 Error-rate performances of signals 1C, 2C, 3C and 4C, over a nonlinear and bandlimited channel, with the use of the suboptimum filters, the predistorter, the HPA operating at 0.68 dB OBO, the amplifier limiter and phase demodulators (a) A and, (b) B and in an ACI environment with $f_{c_s} = 5R/4$ Hz.

CHAPTER 7

CARRIER RECOVERY

7.1 Introduction

Previous discussion on the demodulation process assumed that the receiver provides the required ideal carrier and timing signals. In this section, carrier-recovery techniques are studied with emphasis on applications to DEQPSK and CDE8PSK signals.

In satellite communications, carrier recovery for coherent demodulation can be classified according to application: continuous or burst transmission. When transmission is continuous, e.g. in FDMA systems, the carrier acquisition time (i.e., time to recover the carrier) need not be rapid. However, in TDMA systems, a succession of short-duration bursts emanating from a number of different stations is presented to the demodulator. Each burst has its own independent carrier phase and consequently a rapid carrier acquisition time is required. For the present mobile system, although an FDMA system is assumed, a rapid carrier acquisition time is still required in order for the modem to recover the data after a sudden signal fade due to passing under an obstacle, e.g. a flyover, a bridge, etc., above the vehicle.

To recover the carrier at the receiver, phase-locked loops (PLLs) are commonly used. There has been a tremendous amount of work done in this area. There are books [1],[2],[3],[4] which cover the analysis and design of the PLL in one way or the other. In the early development of the PLL, the work was primarily for analog phase-locked loops (APLLs). However, with increasing emphasis on digital circuitry, because of its decreasing cost, increased reliability and smaller size, there have been efforts to develop digital phase locked loops (DPLLs).

A PLL (APLL or DPLL) is a device which tries to track the phase of the incoming signal. It is realized by a phase detector (PD), a loop filter,

and a voltage-controlled oscillator (VCO) (see Fig. A11.1a in Appendix A11.1). The PD compares the phase of the input signal with that of the VCO and produces an error voltage which is a sinusoidal function (triangular and sawtooth are also possible, though sinusoidal is the most common one) of the error signal. This error signal is filtered and applied to the VCO whose output frequency moves in a direction so as to reduce the phase difference of the input signal and output of the VCO. When the loop is "locked", the short-term frequency of the VCO is exactly or very nearly equal to the average frequency of the input signal.

DEQPSK and CDE8PSK signals use quadrature modulation (Sections 2.6, 3.1.1 and 5.2.1), in which the modulated waves consists of the sum of two double sideband suppressed carrier components. Since the carrier is absent from the signal, a conventional APLL or DPLL (Appendices A11.1 and A11.2) will fail to track, and carrier regeneration is required. Generating a reference carrier from a suppressed carrier signal can be achieved in a number of ways, including the M^{th} power method, the Costas loop and the decision-feedback loop (Appendices A11.3, A11.4 and A11.5). In the M^{th} power loop (Appendix A11.3), the carrier of the M -ary phase signal is generated by raising the signal to the power M (using an M^{th} power device), and a PLL is used to track the M^{th} harmonic component. Frequency division by M of the PLL output yields the required carrier reference. One of the disadvantages of the loop is that, in some situations where IF multiplication is not practical, e.g., a CDE8PSK signal with 70 MHz IF frequency, it would require an 8^{th} power loop in which the PLL would have to track the 560 MHz frequency component, so that a Costas loop may be used (Appendix A11.4).

The decision-feedback loop (Appendix A11.5) is a modification of the Costas loop. In the case of the demodulation of BPSK signals, it has been shown [4] that the decision-feedback loop provides an improved performance

relative to the squaring loop (i.e., with $M=2$ in the M^{th} power loop). But apart from the difficulties in hardware implementation, similar to the other methods mentioned before, it also suffers from the "hangup" phenomenon [5] (Appendix A11.2).

In this thesis, a modified-decision feedback loop (MDFL) is presented to recover the carrier signal for DEQPSK signals. The loop employs a digital control oscillator (DCO), instead of a VCO. This is because the phase error signal used to control the phase of the carrier signal from the oscillator is digital, while the high frequency carrier signal from the oscillator cannot be digital and so must be analog. The loop does not suffer from the "hangup" phenomenon. Computer simulation tests on the MDFL have been carried out for CDE8PSK signals, but unfortunately the results have suggested that the MDFL has a poor performance. Therefore a decision-directed loop (DDL) is used instead. These two loops are described in the following sections.

7.2 Carrier recovery loops for DEQPSK and CDE8PSK signals

The DEQPSK signal receiver with the use of the MDFL and the CDE8PSK signal receiver with the use of the DDL are shown in Figs. 7.1 and 7.2, respectively. In order to avoid complicating the description of these two loops, the DEQPSK and CDE8PSK systems shown in Sections 3.2.1 and 5.2.1, respectively, are assumed here, so that the overall channel transfer functions of the systems have a sinusoidal rolloff frequency response and a linear phase characteristic over the bandwidth. Assume that the receivers in these two systems provide their required ideal timing (but not carrier) signals which are needed in using the MDFL and DDL. Also assume that the distance measure D is used at the receivers. (For the description of generating the signals at the transmitters, see Sections 3.2.1 and 5.2.1.)

In both systems, the signals at the inputs of the receivers are given by

$$r(t) = [\sqrt{2}a(t) + N_c(t)] \cos[\omega_c t + \theta(t)] - [\sqrt{2}b(t) + N_s(t)] \sin[\omega_c t + \theta(t)] \quad 7.2.1$$

with $N_s(t)$ and $N_c(t)$ as defined in Eqn. 3.1.5 or 5.2.3, and $\theta(t)$ is an arbitrary phase angle.

Let the inphase and quadrature reference signals from the digital controlled oscillator (DCO) be $\sqrt{2} \cos[\omega_c t + \hat{\theta}(t)]$ and $-\sqrt{2} \sin[\omega_c t + \hat{\theta}(t)]$, respectively, with $\hat{\theta}(t)$ the estimate of $\theta(t)$. The inphase and quadrature data signal components plus noise just prior to the demodulation filter are

$$\begin{aligned} & r(t) \cos[\omega_c t + \hat{\theta}(t)] \\ &= [a(t) + \sqrt{\frac{1}{2}} N_c(t) \{ \cos[2\omega_c t + \theta(t) + \hat{\theta}(t)] + \cos[\theta(t) - \hat{\theta}(t)] \}] \\ &\quad - [b(t) + \sqrt{\frac{1}{2}} N_s(t) \{ \sin[2\omega_c t + \theta(t) + \hat{\theta}(t)] + \sin[\theta(t) - \hat{\theta}(t)] \}] \\ &= [a(t) + \sqrt{\frac{1}{2}} N_c(t)] \cos[\theta(t) - \hat{\theta}(t)] \\ &\quad - [b(t) + \sqrt{\frac{1}{2}} N_s(t)] \sin[\theta(t) - \hat{\theta}(t)] + \text{h.f.c.} \\ &= [a(t) + \sqrt{\frac{1}{2}} N_c(t)] \cos \epsilon(t) \\ &\quad - [b(t) + \sqrt{\frac{1}{2}} N_s(t)] \sin \epsilon(t) + \text{h.f.c.} \end{aligned} \quad 7.2.2a$$

$$\begin{aligned} \text{and } & -r(t) \sin[\omega_c t + \hat{\theta}(t)] \\ &= -[a(t) + \sqrt{\frac{1}{2}} N_c(t) \{ \sin[2\omega_c t + \theta(t) + \hat{\theta}(t)] - \sin[\theta(t) - \hat{\theta}(t)] \}] \\ &\quad - [b(t) + \sqrt{\frac{1}{2}} N_s(t) \{ \cos[2\omega_c t + \theta(t) + \hat{\theta}(t)] - \cos[\theta(t) - \hat{\theta}(t)] \}] \\ &= [a(t) + \sqrt{\frac{1}{2}} N_c(t)] \sin[\theta(t) - \hat{\theta}(t)] \\ &\quad + [b(t) + \sqrt{\frac{1}{2}} N_s(t)] \cos[\theta(t) - \hat{\theta}(t)] + \text{h.f.c.} \\ &= [a(t) + \sqrt{\frac{1}{2}} N_c(t)] \sin \epsilon(t) \\ &\quad + [b(t) + \sqrt{\frac{1}{2}} N_s(t)] \cos \epsilon(t) + \text{h.f.c.} \end{aligned} \quad 7.2.2b$$

respectively, with the phase error signal

$$\epsilon(t) = \theta(t) - \hat{\theta}(t) \quad 7.2.3$$

The term h.f.c. means the high frequency components. The demodulation

filter blocks the high frequency components in the signals and produces the inphase and quadrature baseband signal components

$$r^{(1)}(t) = [a(t) + \sqrt{\frac{1}{2}N_c}(t)]\cos\epsilon(t) - [b(t) + \sqrt{\frac{1}{2}N_m}(t)]\sin\epsilon(t) \quad 7.2.4a$$

$$\text{and } r^{(2)}(t) = [a(t) + \sqrt{\frac{1}{2}N_c}(t)]\sin\epsilon(t) + [b(t) + \sqrt{\frac{1}{2}N_m}(t)]\cos\epsilon(t) \quad 7.2.4b$$

respectively. Let $\sqrt{\frac{1}{2}N_c}(t) = n_c(t)$ and $\sqrt{\frac{1}{2}N_m}(t) = n_m(t)$. Then $n_c(t)$ and $n_m(t)$ are the sample functions of Gaussian random processes with zero mean and a two-sided power spectral density of $\frac{1}{2}N_0$ over the bandwidth of the baseband data signals $a(t)$ and $b(t)$, respectively (Appendix A7.1). Equation 7.2.4 becomes

$$r^{(1)}(t) = [a(t) + n_c(t)]\cos\epsilon(t) - [b(t) + n_m(t)]\sin\epsilon(t) \quad 7.2.5a$$

$$\text{and } r^{(2)}(t) = [a(t) + n_c(t)]\sin\epsilon(t) + [b(t) + n_m(t)]\cos\epsilon(t) \quad 7.2.5b$$

respectively. Assume that the bandwidth of the demodulation filter is much greater than the frequency offset, so that the distortion introduced by the demodulation filter is negligible. Thus the inphase and quadrature baseband signal components at the demodulator filter output can be written as (Eqn. 3.1.7)

$$r^{(1)}(t) = [\sum_i q_i^{(1)} h(t-iT) + v^{(1)}(t)] \cos\epsilon(t) - [\sum_i q_i^{(2)} h(t-iT) + v^{(2)}(t)] \sin\epsilon(t) \quad 7.2.6a$$

$$\text{and } r^{(2)}(t) = [\sum_i q_i^{(1)} h(t-iT) + v^{(1)}(t)] \sin\epsilon(t) + [\sum_i q_i^{(2)} h(t-iT) + v^{(2)}(t)] \cos\epsilon(t) \quad 7.2.6b$$

respectively, where $h(t)$ is the inverse Fourier transform of the transfer function of the overall channel; $v^{(1)}(t)$ and $v^{(2)}(t)$ are filtered Gaussian noise waveforms. $q_i^{(1)}$ and $q_i^{(2)}$ are the transmitted symbols whose values are depending on whether a DEQPSK or CDE8PSK signal is used (Section 3.1 or 4.2). Since the transfer function of the overall channel is a sinusoidal rolloff frequency response with a linear phase characteristic

(Section 3.1), so that $h(0)=1$ and $h(iT)=0$, for all integer i other than $i=0$. The signals $r^{(1)}(t)$ and $r^{(2)}(t)$, at the demodulator output, are sampled, at the time instants (iT) . Since the demodulation filter is a pair of digital baseband filters (Section 2.4.1), it introduces a delay of NT seconds (this is the delay to make the filters realisable and is half the value of the truncation length of the sampled impulse responses of the modulation and demodulation filters). N is dependent on the lengths of the sampled impulse responses of the digital filters. For examples, signals 1A and 1C have $N=1$, signals 2A, 2C 3A and 3C have $N=2$, while signals 4A and 4C have $N=4$. So, at time $t=iT$, the signal samples at the output of the demodulation filter are

$$r_i^{(1)}(t) = [q_{i-N}^{(1)} + v_{i-N}^{(1)}] \cos \epsilon_{i-N} - [q_{i-N}^{(2)} + v_{i-N}^{(2)}] \sin \epsilon_{i-N} \quad 7.2.7a$$

$$\text{and } r_i^{(2)}(t) = [q_{i-N}^{(1)} + v_{i-N}^{(1)}] \sin \epsilon_{i-N} + [q_{i-N}^{(2)} + v_{i-N}^{(2)}] \cos \epsilon_{i-N} \quad 7.2.7b$$

$\epsilon_{i-N} = \epsilon[(i-N)T]$ and $v_{i-N}^{(j)} = v^{(j)}[(i-N)T]$, for $j=1, 2$, are the phase error and noise signal samples, respectively, received at time $t=(i-N)T$. These two samples are fed into the DTPD (digital tan phase detector; see Section 6.1), at time $t=iT$, which produces at its output the sample of the phase angle given by

$$\begin{aligned} \Omega_{i-N} &= \tan^{-1} (r_i^{(2)} / r_i^{(1)}) \\ &= \tan^{-1} \left[\frac{(q_{i-N}^{(1)} + v_{i-N}^{(1)}) \sin \epsilon_{i-N} + (q_{i-N}^{(2)} + v_{i-N}^{(2)}) \cos \epsilon_{i-N}}{(q_{i-N}^{(1)} + v_{i-N}^{(1)}) \cos \epsilon_{i-N} - (q_{i-N}^{(2)} + v_{i-N}^{(2)}) \sin \epsilon_{i-N}} \right] \quad 7.2.9 \end{aligned}$$

$$\begin{aligned} &= \tan^{-1} \left[\frac{\tan \epsilon_{i-N} + \left(\frac{q_{i-N}^{(2)} + v_{i-N}^{(2)}}{q_{i-N}^{(1)} + v_{i-N}^{(1)}} \right)}{1 - \left(\frac{q_{i-N}^{(2)} + v_{i-N}^{(2)}}{q_{i-N}^{(1)} + v_{i-N}^{(1)}} \right) \tan \epsilon_{i-N}} \right] \quad 7.2.10 \end{aligned}$$

which is then fed to the detector/decoder. This is the phase angle of the received signal, with noise and with (frequency and phase) offsets at time $t=(i-N)T$ seconds. Thus, at time $t=iT$ seconds, the received samples $r_i^{(1)}$ and $r_i^{(2)}$ carry the symbols which were transmitted at time $t=(i-N)T$

seconds, bearing in mind that the transmission path introduces no delay. Under noise free conditions, i.e., when $v_{i-N}^{(1)} = v_{i-N}^{(2)} = 0$ in Eqn. 7.2.10, the phase angle becomes

$$\Omega_{i-N} = \tan^{-1} \left[\frac{\tan \epsilon_{i-N} + \left(\frac{q_{i-N}^{(2)}}{q_{i-N}^{(1)}} \right)}{1 - \left(\frac{q_{i-N}^{(2)}}{q_{i-N}^{(1)}} \right) \tan \epsilon_{i-N}} \right] \quad 7.2.11$$

but $q_{i-N}^{(2)} / q_{i-N}^{(1)} = \tan \psi_{i-N}$ 7.2.12

where ψ_{i-N} is the phase angle received at time $t=(i-N)T$ in the absence of noise and of (phase and frequency) offsets, and is called the data phase angle. So, from Eqns. 7.2.11 and 7.2.12, the received phase angle, at time $t=iT$, can be written as

$$\Omega_{i-N} = \tan^{-1} \left[\frac{\tan \epsilon_{i-N} + \tan \psi_{i-N}}{1 - \tan \psi_{i-N} \tan \epsilon_{i-N}} \right] \quad 7.2.13$$

$$= \tan^{-1} [\tan(\epsilon_{i-N} + \psi_{i-N})] \quad 7.2.14$$

$$= \epsilon_{i-N} + \psi_{i-N} \quad 7.2.15$$

so the error in the phase angle, at time $t=iT$, can be written as

$$\epsilon_{i-N} = \Omega_{i-N} - \psi_{i-N} \quad 7.2.16$$

$$= \theta_{i-N} - \hat{\theta}_{i-N} \quad 7.2.17$$

as can be seen from Eqn. 7.2.3, where $\theta_{i-N} = \theta[(i-N)T]$ and $\hat{\theta}_{i-N} = \hat{\theta}[(i-N)T]$.

7.2.1 Modified-decision feedback loop (MDFL) - for DEQPSK signals

In the MDFL of the DEQPSK receiver shown in Fig. 7.1a, the phase error ϵ_{i-N} , given by Eqn. 7.2.16, is estimated, filtered and then used to control the phase of the DCO signal. The data phase angle, ψ_{i-N} , transmitted at time $t=(i-N)T$ (Eqn. 7.2.12), is estimated, at time $t=iT$, using phase threshold estimation of the received phase angle Ω_{i-N} , according to Table 7.1, so that $\hat{\psi}_{i-N}$, the estimate of ψ_{i-N} , has 4 possible values $\pm\pi/4$ and $\pm3\pi/4$ radians. Even in the absence of noise and ISI, the

estimated phase angle $\hat{\psi}_{i-N}$ may not be equal to the transmitted phase angle ψ_{i-N} . This is because $\hat{\psi}_{i-N}$ might have been rotated from ψ_{i-N} to another quadrant by the (carrier) phase error ϵ_{i-N} if $|\epsilon_{i-N}| > \pi/4$. See Eqn. 7.2.15 which gives the received phase angle under noise free conditions. So in this case, the estimated phase angle is

$$\hat{\psi}_{i-N} = \psi_{i-N} \pm 0, \pm \pi/2 \text{ or } \pm \pi \quad 7.2.18$$

or
$$\hat{\psi}_{i-N} = \psi_{i-N} \pm k\pi/2 \quad 7.2.19$$

for $k=0, 1$ or 2 , depending on the value of ϵ_{i-N} .

From Eqns. 7.2.16 and 7.2.19, the actual phase error is

$$\epsilon_{i-N} = \Omega_{i-N} - \hat{\psi}_{i-N} \pm k\pi/2 \quad 7.2.20$$

so that
$$(\epsilon_{i-N} \pm k\pi/2) = \Omega_{i-N} - \hat{\psi}_{i-N} \quad 7.2.21$$

The estimate of the phase error, from Eqn, 7.2.21, can be written as

$$\hat{\epsilon}_{i-N} = \epsilon_{i-N} \pm k\pi/2 \quad 7.2.22$$

$$= \Omega_{i-N} - \hat{\psi}_{i-N} \quad 7.2.23$$

where $\hat{\psi}_{i-N}$ has one of the values $\pm\pi/4$ and $\pm 3\pi/4$, and is obtained from the phase threshold-estimator (Table 7.1). The received phase angle Ω_{i-N} is obtained from the DTPD (digital tan phase detector) using the equation

$$\Omega_{i-N} = \tan^{-1} (r_i^{(2)} / r_i^{(1)}) \quad 7.2.24$$

Clearly, Ω_{i-N} and $\hat{\psi}_{i-N}$ always lie on the same quadrant, so that $\hat{\epsilon}_{i-N}$ lies in the range $-\pi/4$ to $\pi/4$ radians and has an ambiguity of $\pm k\pi/2$. Differential encoding is therefore required to resolve the ambiguity. With the system just described, the characteristic of the PD has a sawtooth shape with a period of $\pm\pi/4$.

The estimated phase error $\hat{\epsilon}_{i-N}$, in Eqn. 7.2.23, is filtered by $F(z)$ to give the phase error signal, for the duration $iT \leq t < (i+1)T$,

$$e_i = F(z)\hat{\epsilon}_{i-N} \quad 7.2.25$$

which is used to control the phase of the DCO whose transfer function is

given by γ/s . Thus, the phase of the DCO signal, for the duration $iT \leq t < (i+1)T$, is

$$\hat{\theta}(s) = \frac{\gamma}{s} e_i \tag{7.2.26}$$

where $\hat{\theta}(s)$ is in Laplace notation, i.e., $\hat{\theta}(s) = \mathcal{L}\{\hat{\theta}(t)\}$, γ is the DCO gain factor, and e_i is constant for the duration $iT \leq t < (i+1)T$.

For the purpose of computer simulation, the system is modelled digitally. The signal at the DCO output is sampled at the time instants (mT_m) , at a rate of $1/T_m$ samples per second, where $T = 8T_m$. γ/s is the transfer function of the DCO, expressed as a Laplace transform. $1/s$ in the s -plane is mapped into the z -plane [6] and becomes $1/(1-z^{-1})$, where z^{-1} represents a delay of one sample period. The signal phase angle from the DCO is

$$\hat{\theta}_{m/i-N} = \frac{1}{1-z^{-1}} e_i \gamma \tag{7.2.27}$$

$$= \frac{1}{1-z^{-1}} \gamma F(z) \tilde{e}_{i-N} \tag{7.2.28}$$

for $iT < mT_m < (i+1)T$, where $\hat{\theta}_{m/i-N}$ is the predicted phase $\hat{\theta}$ at time $t = mT_m$, determined from the received information at time $t = (i-N)T$, to give a phase error ϵ_{i-N} . In order to obtain a zero static phase error (resulting phase error) for an initial frequency error (Appendix A11.2), a second order loop filter with the transfer function (Eqn. A11.2.18)

$$F(z) = 1 + \mu z / (z-1) \tag{7.2.29}$$

is used, where μ is a constant. The baseband equivalent model of the DEQPSK signal receiver, used for computer simulation, is shown in Fig. 7.1b, where the DCO gain factor has been combined with the filter $F(z)$ and the function $\exp[-j(\cdot)]$ is used to convert the phase angles into complex-valued signals.

7.2.2 Decision-directed loop (DDL) - for CDE8PSK signals

In the MDFL, the detected phase angle $\hat{\psi}_{1-N}$ is used with the received phase angle Ω_{1-N} to estimate the phase error $\hat{\epsilon}_{1-N}$. Clearly, the tolerance to noise of the detector has an important effect on the tracking performance of the MDFL. In the DEQPSK system, the phase threshold detection process (Section 6.1 and Table 6.1) is the optimum detection process for detecting $\hat{\psi}_{1-N}$ from Ω_{1-N} (Table 7.1), in the presence of AWGN. Since it is optimum, in the sense that it minimises the probability of error in $\hat{\psi}_{1-N}$, it is also optimum for phase estimation using in the MDFL.

For CDE8PSK signals, the threshold detection process is not the optimum detection process, because the transmitted symbols are convolutionally and differentially encoded. If a threshold detector is used, i.e., ignoring the convolutional and differential encoding of the transmitted symbols, CDE8PSK signals become simple 8PSK signals which have a degradation in tolerance to additive white Gaussian noise of about 3.5 dB at $P_e=10^{-3}$, in comparison with that of an ideal QPSK system, at a given bandwidth [7], so that the MDFL cannot be used for CDE8PSK signals. In fact, computer simulation tests have shown that, even in the absence of noise and ISI, the MDFL cannot be used for the CDE8PSK signals (i.e., signals 1C, 2C, 3C and 4C) over a nonlinear channel. This is because the adjacent points in the signal constellation (Fig. 4.5) are so close that, if a threshold detection process is used, the AM-AM and AM-PM conversion effects of the HPA will themselves cause errors in detection.

For CDE8PSK signals (Section 5.2), since the suboptimum decoder is used as the decoding process, the loop can make use of the decoded value from the decoder to estimate the carrier phase. This is called Decision Directed Carrier Phase Estimation [8] and the loop is called the decision-directed loop (DDL), as shown in Fig. 7.2. The only difference between the MDFL and DDL is in the carrier phase estimation processes. In the MDFL, at time $t=iT$, the detected signal phase angle $\hat{\psi}_{1-N}$ is obtained from the phase threshold-detector and then compared with the received signal phase

angle Ω_{i-N} to estimate the phase error $\hat{\epsilon}_{i-N}$ (Eqn. 7.2.23). Whereas in the DDL, the decoded signal phase angle is obtained from a more sophisticated decoder and then compared with the received signal phase angle to estimate the phase error (Fig. 7.2a).

In CDE8PSK signals, the changes in phase carry the data information, not the absolute phases. In the decoder the receiver holds in store the $m=4^{K-1}$ (K: constraint length of the code) $2n$ -component vectors $\{Z_L\}$, where (Eqn 5.2.15)

$$Z_L = [x_{L-2n+1} \quad x_{L-2n+2} \quad x_{L-2n+3} \quad \dots \quad x_L] \quad 7.2.30$$

with the minimum distances of $\{C_i^{(j)}\}$, for $j=1, 2, \dots, 8$, corresponding to the 4^{K-1} different possible combinations of values of $x_{L-2K+3}, x_{L-2K+4}, \dots, x_L$ (Section 5.2.3). Thus each stored vector Z_L forms the last $2n$ components of the vector X_L (Eqn. 5.2.11) that minimises $C_i^{(j)}$, for $j=1, 2, \dots, 8$, subject to the constraint that $x_{L-2K+3}, x_{L-2K+4}, \dots, x_L$ have the given values, and $\theta_{i-K+1}^{(j)}$ (i.e., the phase angle of the complex value $y_{i-K+1}^{(j)}$, used in Section 5.2), for $j=1, 2, \dots, 8$, takes on the 8 different possible values. Associated with each stored vector Z_L are stored the corresponding $\{C_i^{(j)}\}$, for $j=1, 2, \dots, 8$. There are altogether $8m$ different values of $C_i^{(j)}$.

Following the receipt of the phase angle Ω_{i+1-N} at time $t=(i+1)T$ (assuming the distance measure D is used), each of the stored vectors $\{Z_L\}$ forms a common part of 4 vectors $\{X_{L+2}\}$, having the 4 possible values of (x_{L+1}, x_{L+2}) . Each of these 4 vectors is associated with 8 corresponding distances (Eqn. 5.2.16)

$$C_{i+1}^{(j)} = C_i^{(j)} + c_{i+1}^{(j)} \quad 7.2.31$$

for $j=1, 2, \dots, 8$, where (similar to Eqn. 5.2.17)

$$c_{i+1} = \begin{cases} |\Omega_{i+1-N} + \theta_{i+1}^{(j)}| & , \text{for } |\Omega_{i+1-N} + \theta_{i+1}^{(j)}| \leq \pi \\ 2\pi - |\Omega_{i+1-N} + \theta_{i+1}^{(j)}| & , \text{for } |\Omega_{i+1-N} + \theta_{i+1}^{(j)}| > \pi \end{cases} \quad 7.2.32$$

as can be seen from Eqn. 4.8.41. N is the delay caused by the demodulation

filter. The $\{\phi_{i+1}^{(j)}\}$, for $j=1, 2, \dots, 8$, have real values that are all different, and each of them represents a possible phase angle, which would have been transmitted at time $t=(i+1)T$. For each of the 4^{K-1} possible combinations of values of $x_{L-2K+5}, x_{L-2K+6}, x_{L-2K+7}, \dots, x_{L+1}, x_{L+2}$, the decoder now selects the vector Z_{L+2} having the smallest $C_{i+1}^{(j)}$, and stores Z_{L+2} and the 8 smallest values $C_{i+1}^{(j)}$, for $j=1, 2, \dots, 8$. $(\hat{\alpha}_{L-2n+3}, \hat{\alpha}_{L-2n+4})$ are taken to be the values of (x_{L-2n+3}, x_{L-2n+4}) , respectively, in the stored vector Z_{L+2} associated with the smallest $C_{i+1}^{(j)}$, hence there is a delay of $(n-1)T$ seconds in decoding. The signal phase angle $\Omega_{i+2-N-n}$, received at time $t=(i+2-n)T$ seconds is estimated at time $t=(i+1)T$, as $\hat{\psi}_{i+2-N-n}$ by convolutional and differential encoding of the components in Z_{L+2} , subject to the constraint that $\phi_{i+1}^{(j)}$, with the smallest $C_{i+1}^{(j)}$, has been received at time $t=(i+1)T$ seconds. This operation is carried out by the phase estimator. $\hat{\psi}_{i+2-N-n}$ has 8 possible values $\pm\pi/8, \pm3\pi/8, \pm5\pi/8$ and $\pm7\pi/8$. However, even in the absence of noise and ISI, the estimated phase angle $\hat{\psi}_{i+2-N-n}$ may not be equal to the transmitted phase angle $\psi_{i+2-N-n}$. This is because $\hat{\psi}_{i+2-N-n}$ might have been rotated through an angle of \dots from $\psi_{i+2-N-n}$ by the (carrier) phase error $\epsilon_{i+2-N-n}$ if $|\epsilon_{i+2-N-n}| > \pi/8$. See Eqn. 7.2.15 which gives the received phase under noise free conditions. Thus

$$\hat{\psi}_{i+2-N-n} = \psi_{i+2-N-n} \pm 0, \pm\pi/4, \pm2\pi/4, \pm3\pi/4 \text{ or } \pm\pi \quad 7.2.33$$

$$\text{or} \quad \hat{\psi}_{i+2-N-n} = \psi_{i+2-N-n} \pm k\pi/4 \quad 7.2.34$$

with $k=0, 1, 2, 3$ or 4 , depending on the value of $\epsilon_{i+2-N-n}$. From Eqn. 7.2.16, the phase error received at time $t=(i+2-n)T$ is

$$\epsilon_{i+2-N-n} = \Omega_{i+2-N-n} - \psi_{i+2-N-n} \quad 7.2.35$$

and so from Eqns. 7.2.34 and 7.2.35, the phase error can be written as

$$\epsilon_{i+2-N-n} = \Omega_{i+2-N-n} - \hat{\psi}_{i+2-N-n} \pm k\pi/4 \quad 7.2.35$$

$$\text{so that} \quad (\epsilon_{i+2-N-n} \pm k\pi/4) = \Omega_{i+2-N-n} - \hat{\psi}_{i+2-N-n} \quad 7.2.37$$

The estimate of the phase error, from Eqn. 7.2.37, can be written as

$$\hat{\epsilon}_{i+2-N-n} = \epsilon_{i+2-N-n} \pm k\pi/4 \quad 7.2.38$$

$$= \Omega_{i+2-N-n} - \hat{\psi}_{i+2-N-n} \quad 7.2.39$$

Differential encoding is therefore required to resolve the ambiguity of $\pm k\pi/4$. $\hat{\psi}_{i+2-N-n}$ is obtained by convolutional and differential encoding the components in the stored vector Z_{L+2} associated with the smallest $C_{i+1}^{(j)}$, subject to the constraint that $C_{i+1}^{(j)}$ was received. $\hat{\psi}_{i+2-N-n}$ and $\Omega_{i+2-N-n}$ may not lie in the same quadrant, and so $\hat{\epsilon}_{i+2-N-n}$ ranges from -360° to 360° . As far as the data recovery is concerned, the phase error $\hat{\epsilon}_{i+2-N-n}=359^\circ$ is same as $\hat{\epsilon}_{i+2-N-n}=-1^\circ$, but $\hat{\epsilon}_{i+2-N-n}=-1^\circ$ leads to a faster acquisition than that of $\hat{\epsilon}_{i+2-N-n}=359^\circ$. The loop is more rapid in acquisition if the following two conditions are imposed upon Eqn. 7.2.39.

$$\hat{\epsilon}_{i+2-N-n} = \begin{cases} \Omega_{i+2-N-n} - \hat{\psi}_{i+2-N-n}, & \text{for } |\Omega_{i+2-N-n} - \hat{\psi}_{i+2-N-n}| < \pi \\ |\Omega_{i+2-N-n} - \hat{\psi}_{i+2-N-n}| - 2\pi, & \text{for } |\Omega_{i+2-N-n} - \hat{\psi}_{i+2-N-n}| > \pi \end{cases} \quad 7.2.40$$

where $\hat{\epsilon}_{i+2-N-n}$ now is constrained to lie in the range $-\pi$ to π radians. The

received phase angle $\Omega_{i+2-N-n}$ is obtained from the DTPD. (Eqn. 7.2.24) with

a delay of nT seconds and the estimated phase angle $\hat{\psi}_{i+2-N-n}$ is obtained from the phase estimator. The PD characteristics of the loop are time-varying because the transmitted symbols are convolutionally and differentially encoded and the estimated phase angle is dependent on the convolutional code used and the previous decoded symbols.

Since the phase angle received at time $t=(i+2-n)T$ is estimated at time $t=(i+1)T$, there is a delay of $(n-1)T$ seconds in phase estimation. This $(n-1)T$ seconds delay, caused by the decoder, increases the loop bandwidth and may cause instability and a substantial performance loss compared with the case where there is no delay. Thus the loop gain may have to be reduced to give an acceptable performance. Increasing the value of the loop gain may increase the acquisition time, so that a compromise must be

reached [7]. One method to remove the (n-1)T delay caused by the decoder is to use the early decoding process which is as follows.

Following the receipt of the sample Ω_{i+1-N} at time $t=(i+1)T$, each of the stored vectors $\{Z_L\}$ forms a common part of 4 vectors $\{X_{L+2}\}$, having the 4 possible values of (x_{L+1}, x_{L+2}) . Each of these 4 vectors is associated with 8 corresponding distances (Eqns. 7.2.31 and 7.2.32)

$$C_{i+1}^{(j)} = C_i^{(j)} + c_{i+1}^{(j)} \tag{7.2.41}$$

for $j=1, 2, \dots, 8$, where

$$c_{i+1}^{(j)} = \begin{cases} |\Omega_{i+1-N} + \phi_{i+1}^{(j)}| & , \text{for } |\Omega_{i+1-N} + \phi_{i+1}^{(j)}| \leq \pi \\ 2\pi - |\Omega_{i+1-N} + \phi_{i+1}^{(j)}| & , \text{for } |\Omega_{i+1-N} + \phi_{i+1}^{(j)}| > \pi \end{cases} \tag{7.2.42}$$

where, for $j=1, 2, \dots, 8$, the $\{\phi_{i+1}^{(j)}\}$ have real values that are all different and each represents a possible phase angle, which would have been transmitted at time $t=(i+1-N)T$ seconds. For each of the 4^{K-1} possible combinations of values of $x_{L-2K+5}, x_{L-2K+6}, \dots, x_{L+1}, x_{L+2}$, the decoder selects the phase angle $\phi_{i+1}^{(j)}$, having the smallest $C_{i+1}^{(j)}$. The received signal phase angle Ω_{i+1-N} is estimated as $\hat{\psi}_{i+1-N}$ by setting $\hat{\psi}_{i+1-N} = \phi_{i+1}^{(j)}$, subject to the constraint that $\phi_{i+1}^{(j)}$, with the smallest $C_{i+1}^{(j)}$, was decoded. From Eqn. 7.2.40, the estimated phase error, at time $t=(i+1)T$, is

$$\hat{\epsilon}_{i+1-N} = \begin{cases} \Omega_{i+1-N} - \hat{\psi}_{i+1-N} & , \text{for } |\Omega_{i+1-N} - \hat{\psi}_{i+1-N}| \leq \pi \\ |\Omega_{i+1-N} - \hat{\psi}_{i+1-N}| - 2\pi & , \text{for } |\Omega_{i+1-N} - \hat{\psi}_{i+1-N}| > \pi \end{cases} \tag{7.2.43}$$

Using the early decoding process, the phase angle received at time $t=(i+1-N)T$ is estimated at time $t=(i+1)T$. There is a delay of NT seconds (as for the threshold detection process) which is caused by the demodulation filter. The delay introduced by the decoder is therefore removed. Since the distance measure D is used, the hardware implementation is greatly simplified. This is because $\hat{\epsilon}_{i+1-N}$ is, in fact, the incremental distance computed by the decoder, as can be seen by comparing Eqns. 7.2.42 to 5.2.17.

As in the MDFL, the estimated phase error $\hat{\epsilon}_{i+1-N}$ (Fig. 7.2a), in Eqn. 7.2.43, is filtered by $F(z)$ to give the phase error signal, for the duration $(i+1)T < t < (i+2)T$ (Eqn. 7.2.25)

$$e_{i+1} = F(z)\hat{\epsilon}_{i+1-N} \quad 7.2.44$$

In computer simulation tests, the signal at the DCO output is sampled at the time instants $\{mT_m\}$, at the rate of $1/T_m$ samples per second, where $T=8T_m$. The phase angle from the DCO is (Eqns. 7.2.27 and 7.2.28)

$$\hat{\theta}_{m/i+1-N} = \frac{1}{1-z^{-1}} e_{i+1} \gamma \quad 7.2.45$$

$$= \frac{1}{1-z^{-1}} \gamma F(z)\hat{\epsilon}_{i+1-N} \quad 7.2.46$$

for $(i+1)T < mT_m < (i+2)T$, where γ is the DCO gain factor, $F(z)$ is the filter transfer function, and $\hat{\theta}_{m/i+1-N}$ is the predicted phase angle θ at time $t=mT_m$ derived from received information at time $t=(i+1-N)T$ seconds, to give a phase error $\hat{\epsilon}_{i+1-N}$. The baseband equivalent model of the DDL at the CDE8PSK receiver, with the use of the early decoding process, phase demodulator B and a second order loop filter, for computer simulation, is shown in Fig. 7.2b, where the DCO gain factor γ has been combined with the filter $F(z)$.

7.2.3 Acquisition

When a loop commences operation in an unlocked condition, it must be brought into lock either by its own action or with the help of auxiliary circuits. The process of bringing a loop into lock is called acquisition. If the loop acquires lock by itself, the process is called self-acquisition and if it is assisted by auxiliary circuits, the process is called aided acquisition [1].

A. Phase and frequency acquisition

Phase is usually self-acquired. Under noise free conditions, the wider the loop bandwidth, the less is the acquisition time. However, when noise

is present, the loop bandwidth must be reduced in order to provide a stable loop, although this may increase the acquisition time [1].

Acquisition of frequency is ordinarily more difficult, is slower, and is more difficult to design than is phase acquisition. Self-acquisition of frequency is known as frequency pull-in or simply pull-in. Pull-in tends to be slow and often unreliable, so that a number of aided frequency-acquisition techniques have been devised, including frequency sweeping, frequency discrimination, and bandwidth widening methods [1].

B. Pull-in limits of the MDFL and DDL

If the initial frequency error is large enough, the loops cannot pull in. The largest frequencies for which the loops can pull into lock are called the pull-in limits and are denoted by Δf_p .

Suppose a frequency offset of Δf_p Hz with an initial phase error $\pi/8 - \theta_0$, where $\theta_0 < \pi/4$, causes a phase error $\hat{\epsilon}(t)$, as shown in Fig. 7.3a. The estimated phase error $\hat{\epsilon}(t)$, using the MDFL (with a sawtooth characteristic), is shown by the solid line. If $\hat{\epsilon}(t)$ is sampled at the time instants (iT) , the sample values are $\theta_0 + \pi/8$, $\theta_0 - \pi/8$, $\theta_0 + \pi/8$, ..., and so are oscillating between 2 values. The average value of $\hat{\epsilon}(t)$ is θ_0 which is the initial phase error. If the loop reaches the steady-state, θ_0 is removed by the loop, but the phase error oscillates between $\pi/8$, $-\pi/8$, with a period of $2T$ seconds. This is the same for the case with an initial phase of $\pi/8 + \theta_0$, where $\theta_0 > \pi/4$, as shown in Fig. 7.3b. Under these conditions, the average phase error is zero and so the loop fails to track the frequency offset Δf_p Hz. This occurs when

$$2\pi|\Delta f_p| = \frac{\pi}{4T} \tag{7.2.47}$$

$$|\Delta f_p| = 0.125/T \tag{7.2.48}$$

so $\Delta f_p = \pm 0.125R$ 7.2.49

with $R=1/T$ the symbol rate. This is the pull-in limit of the MDFL. For

R=32, 64, 128 and 256 kbaud/s, the pull-in limits are 4, 8, 16 and 32 kHz, respectively. It can be shown that, for an M-ary phase keying (MPSK) signal, the phase error characteristic, using the MDFL, is a sawtooth with a period of π/M . Thus Eqn. 7.2.47 becomes

$$2\pi|\Delta f_p| = \frac{\pi}{MT} \tag{7.2.50}$$

and the pull-in limit is

$$\Delta f_p = \pm R/2M \tag{7.2.51}$$

Hence for BPSK and 8PSK signals, i.e., M=2 and 8, the pull-in limits are $\pm 0.25R$ and $\pm 0.0625R$, respectively. In deriving the pull-in limits, the effects of the delay in estimation of the phase, the noise and loop bandwidth have been neglected. Of course, these effects reduce the pull-in limits, as is shown in Section 7.4.3.

It is difficult to determine the pull-in limit of the DDL for CDE8PSK signal because the transmitted symbols are correlated.

C. Extended-pull-in-limit method for the MDFL and DDL

The pull-in limits of the MDFL and DDL can be extended using a sequence of training symbols. That is, at the beginning of a transmission, the transmitter sends a sequence of symbols representing π radians phase reversals in the DEQPSK or CDE8PSK signal. So, for the DEQPSK signal with no noise, the samples received at the input of the detector, at time $t=(i-1)T$ and iT , are

$$\Omega_{i-N-1}^+ = \epsilon_{i-N-1} + \psi_{i-N-1} \tag{7.2.52}$$

and
$$\Omega_{i-N}^+ = \epsilon_{i-N} + \psi_{i-N} \tag{7.2.53}$$

respectively, as can be seen from Eqn. 7.2.15. Ω_{i-N-1}^+ and Ω_{i-N}^+ are the received phase angles measured in an anticlockwise direction on the polar coordinate system, i.e., $\Omega^+=\Omega$ for $0 \leq \Omega < \pi$ and $\Omega^+=\Omega+2\pi$ for $\Omega < 0$. ψ_{i-N-1} and

ψ_{i-N} are the data phase angles transmitted at time $t=(i-N-1)T$ and $(i-N)T$, respectively, and ϵ_{i-N-1} and ϵ_{i-N} are the phase errors caused by the carrier. The difference of the two received phase angles is

$$\Omega_{i-N-1}^+ - \Omega_{i-N}^+ = \epsilon_{i-N-1} - \epsilon_{i-N} + \psi_{i-N-1} - \psi_{i-N} \quad 7.2.54$$

but $|\psi_{i-N} - \psi_{i-N-1}| = \pi$ because of the phase reversal between adjacent symbols, so, after removing the phase angle $|\psi_{i-N} - \psi_{i-N-1}|$, the phase difference in T seconds is

$$\Delta\epsilon_{i-N} = \begin{cases} \Omega_{i-N}^+ - \Omega_{i-N-1}^+ - \pi, & \text{for } \Omega_{i-N}^+ - \Omega_{i-N-1}^+ \geq 0 \\ \Omega_{i-N}^+ - \Omega_{i-N-1}^+ + \pi, & \text{for } \Omega_{i-N}^+ - \Omega_{i-N-1}^+ < 0 \end{cases} \quad 7.2.55$$

Since frequency is the derivative of phase, $\Delta\epsilon_{i-N}$ contains the frequency offset information and can be used to remove the frequency offset, but not the phase offset. Thus, if this method is used, frequency lock is followed by phase lock. It should be noted that the value of $\Delta\epsilon_{i-N}$ is non-data aided because it is derived only from the phase angles of the received signals. Hence the method is independent of whether a DEQPSK or CDE8PSK signal is used.

In Eqn 7.2.55, since $0 \leq \Omega_{i-N}^+ \leq 2\pi$ and $0 \leq \Omega_{i-N-1}^+ \leq 2\pi$, it follows that $|\Omega_{i-N}^+ - \Omega_{i-N-1}^+| \leq 2\pi$ and $|\Delta\epsilon_{i-N}| \leq \pi$, as can be seen from the equation. The maximum value of $|\Delta\epsilon_{i-N}|$ is

$$|\Delta\epsilon_{i-N}|_{\max} = 2\pi|\Delta f_p|T = \pi \quad 7.2.56$$

where Δf_p is the pull-in limit of the method and can be written as

$$|\Delta f_p| = R/2 \quad 7.2.57$$

or
$$\Delta f_p = \pm R/2 \quad 7.2.58$$

where R is the symbol rate. For $R=32, 64, 128$ and 256 kbaud/s, the pull-in limits, using this method, are $16, 32, 64$ and 128 kHz/s (compared to $4, 8, 16$ and 32 kHz when using the MDFL), respectively. In deriving Eqn. 7.2.58, the effects of the delay in the estimation of $\Delta\epsilon_{i-N}$, the noise and

bandwidth of the loop have all been neglected. Of course, these effects reduce the pull-in limit, as is shown in Section 7.4.3. Since the method is only used for frequency acquisition, it is referred to here as the extended-pull-in-limit method.

When using this method, the training symbols, used at the beginning of transmission, are for tracking the frequency offset. If sudden signal fade occurs during transmission, provided that, when the signal returns, the frequency offset is not too large for self-acquisition of the MDFL/DDL, the MDFL/DDL can still track the frequency and phase offsets without the need of the training symbols, but of course with a burst of errors.

D. Variable-Bandwidth method

Two general principles that apply to any carrier recovery loop are as follows [1].

- 1) To minimize the output phase jitter due to external noise, the loop bandwidth should be made as narrow as possible.
- 2) To obtain the best tracking and acquisition properties, the loop bandwidth should be made as wide as possible.

These principles are directly opposed to one another; an improvement in one can come only at the expense of a degradation in the other. In order to satisfy both these principles, a variable-bandwidth method can be used. Since the speed of acquisition is improved by widening the loop bandwidth [1], the loop can be designed to have a large bandwidth for rapid acquisition at the beginning of a transmission and a much narrow bandwidth for good tracking in the presence of noise. It should be apparent that an increase of bandwidth can be successful only if the signal/noise power ratio is sufficiently large. If the bandwidth is too large, the loop will be unstable and acquisition is unlikely to be achieved.

In the MDFL and DDL, the loop gain μ and the DCO gain γ control the bandwidth of the loops, so that the variable-bandwidth method can easily be realized by using different values of γ and μ before and after acquisition is achieved.

7.3 Frequency and phase offsets

The movement of the satellite changes the frequencies of signals reaching it and transmitted back to earth. This is called the Doppler-shift effect. One of the advantages of using geosynchronous orbits is that the Doppler shift is negligible. Satellites in elliptical orbits, because of the motion of the satellite relative to the earth stations, can introduce significantly different Doppler shifts for different earth stations. These cause different frequency offsets. Apart from the Doppler shifts, the earth station transmitter oscillators and the satellite translation oscillator can also introduce frequency offsets.

The frequency offsets caused by these factors degrade the performance and increase the complexity of the modem. They are more critical for lower data rate modem. For example, a modulation bandwidth of 32 kHz is comparable to a frequency offset of 20 kHz. The performance of the system can be expected to be unacceptable because of the narrow band receiver IF filter which will remove a large amount of the wanted signal energy and introduce significant ISI into the signal.

7.3.1 Modelling of frequency and phase offsets of a quadrature modulation system with a nonlinear channel and in an ACI environment

The model of a quadrature modulation system with frequency and phase offsets and in an ACI environment, is shown in Fig. 7.4. The signals at the transmitter outputs of the upper, desired and lower channels are .

$$\begin{aligned} S_u(t) &= \sqrt{2}a_u(t)\cos[\omega_c t + \omega_{c_u} t + \theta_u(t)] \\ &\quad - \sqrt{2}b_u(t)\sin[\omega_c t + \omega_{c_u} t + \theta_u(t)] \end{aligned} \quad 7.3.1a$$

$$\begin{aligned} S_o(t) &= \sqrt{2}a_o(t)\cos[\omega_c t + \theta_o(t)] \\ &\quad - \sqrt{2}b_o(t)\sin[\omega_c t + \theta_o(t)] \end{aligned} \quad 7.3.1b$$

and

$$\begin{aligned} S_l(t) &= \sqrt{2}a_l(t)\cos[\omega_c t - \omega_{c_l} t + \theta_l(t)] \\ &\quad - \sqrt{2}b_l(t)\sin[\omega_c t - \omega_{c_l} t + \theta_l(t)] \end{aligned} \quad 7.3.1c$$

respectively. Assume that the signals have been predistorted by the

respective predistorters and amplified by the respective HPAs, so that $a_U(t)$ and $b_U(t)$, $a_D(t)$ and $b_D(t)$ and $a_L(t)$ and $b_L(t)$ are the nonlinearly distorted inphase and quadrature baseband signal components in the upper, desired and lower channels, respectively. ω_c is the carrier frequency in rad/s in the desired channel, ω_{c_m} is the channel spacing in rad/s, and $\theta_U(t)$, $\theta_D(t)$ and $\theta_L(t)$ are any arbitrary phase angles.

Assume that the inphase and quadrature signal components of the ACI from the adjacent channels affect the inphase and quadrature signal components, respectively, equally for the desired channel all the time, so that $\theta_U(t)=\theta_L(t)=\theta_D(t)$. Equation 7.3.1 becomes

$$\begin{aligned} S_U(t) = & \sqrt{2}a_U(t)\cos[\omega_c t + \omega_{c_m} t + \theta_D(t)] \\ & - \sqrt{2}b_U(t)\sin[\omega_c t + \omega_{c_m} t + \theta_D(t)] \end{aligned} \quad 7.3.2a$$

$$\begin{aligned} S_D(t) = & \sqrt{2}a_D(t)\cos[\omega_c t + \theta_D(t)] \\ & - \sqrt{2}b_D(t)\sin[\omega_c t + \theta_D(t)] \end{aligned} \quad 7.3.2b$$

and

$$\begin{aligned} S_L(t) = & \sqrt{2}a_L(t)\cos[\omega_c t - \omega_{c_m} t + \theta_D(t)] \\ & - \sqrt{2}b_L(t)\sin[\omega_c t - \omega_{c_m} t + \theta_D(t)] \end{aligned} \quad 7.3.2c$$

respectively. The phase and frequency offsets are caused by the discrepancies of the phase and frequency of the received signal carrier and those of the reference carrier at the receiver. Let $\Delta\omega$ be the frequency offset in rad/s and θ_m be the phase offset in radians, then the resultant offset in radians is $\Delta\omega t + \theta_m$. So after adding the offsets to the signal (Fig. 7.4), the signal become (Eqn. 7.3.2)

$$\begin{aligned} \hat{S}_U(t) = & \sqrt{2}a_U(t)\cos[(\omega_c + \omega_{c_m} + \Delta\omega)t + \theta_m] \\ & - \sqrt{2}b_U(t)\sin[(\omega_c + \omega_{c_m} + \Delta\omega)t + \theta_m] \end{aligned} \quad 7.3.3a$$

$$\begin{aligned} \hat{S}_D(t) = & \sqrt{2}a_D(t)\cos[(\omega_c + \Delta\omega)t + \theta_m] \\ & - \sqrt{2}b_D(t)\sin[(\omega_c + \Delta\omega)t + \theta_m] \end{aligned} \quad 7.3.3b$$

and

$$\begin{aligned} \hat{S}_L(t) = & \sqrt{2}a_L(t)\cos[(\omega_c - \omega_{c_m} + \Delta\omega)t + \theta_m] \\ & - \sqrt{2}b_L(t)\sin[(\omega_c - \omega_{c_m} + \Delta\omega)t + \theta_m] \end{aligned} \quad 7.3.3c$$

respectively, where the phase $\theta_D(t)$, in Eqn. 7.3.2, has been included in

$\Delta\omega t + \theta_{\pm}$. These can be written as

$$\begin{aligned}\hat{S}_U(t) &= \sqrt{2}\{a_U(t)\cos[(\omega_{c_m} + \Delta\omega)t + \theta_{\pm}] - b_U(t)\sin[(\omega_{c_m} + \Delta\omega)t + \theta_{\pm}]\}\cos\omega_c t \\ &\quad - \sqrt{2}\{a_U(t)\sin[(\omega_{c_m} + \Delta\omega)t + \theta_{\pm}] + b_U(t)\cos[(\omega_{c_m} + \Delta\omega)t + \theta_{\pm}]\}\sin\omega_c t\end{aligned}\quad 7.3.4a$$

$$\begin{aligned}\hat{S}_D(t) &= \sqrt{2}\{a_D(t)\cos[\Delta\omega t + \theta_{\pm}] - b_D(t)\sin[\Delta\omega t + \theta_{\pm}]\}\cos\omega_c t \\ &\quad - \sqrt{2}\{a_D(t)\sin[\Delta\omega t + \theta_{\pm}] + b_D(t)\cos[\Delta\omega t + \theta_{\pm}]\}\sin\omega_c t\end{aligned}\quad 7.3.4b$$

and

$$\begin{aligned}\hat{S}_L(t) &= \sqrt{2}\{a_L(t)\cos[(\omega_{c_m} + \Delta\omega)t - \theta_{\pm}] + b_L(t)\sin[(\omega_{c_m} - \Delta\omega)t - \theta_{\pm}]\}\cos\omega_c t \\ &\quad - \sqrt{2}\{a_L(t)\cos[(\omega_{c_m} - \Delta\omega)t - \theta_{\pm}] - b_L(t)\sin[(\omega_{c_m} - \Delta\omega)t - \theta_{\pm}]\}\sin\omega_c t\end{aligned}\quad 7.3.4c$$

respectively. The equivalent baseband signals, with respect to the desired channel, can be represented (Appendix A6) as the complex-valued signals

$$\begin{aligned}\hat{S}_U(t) &= \{a_U(t)\cos[(\omega_{c_m} + \Delta\omega)t + \theta_{\pm}] - b_U(t)\sin[(\omega_{c_m} + \Delta\omega)t + \theta_{\pm}]\} \\ &\quad + j\{a_U(t)\sin[(\omega_{c_m} + \Delta\omega)t + \theta_{\pm}] + b_U(t)\cos[(\omega_{c_m} + \Delta\omega)t + \theta_{\pm}]\}\end{aligned}\quad 7.3.5a$$

$$\begin{aligned}\hat{S}_D(t) &= \{a_D(t)\cos[\Delta\omega t + \theta_{\pm}] - b_D(t)\sin[\Delta\omega t + \theta_{\pm}]\} \\ &\quad + j\{a_D(t)\sin[\Delta\omega t + \theta_{\pm}] + b_D(t)\cos[\Delta\omega t + \theta_{\pm}]\}\end{aligned}\quad 7.3.5a$$

$$\begin{aligned}\text{and } \hat{S}_L(t) &= \{a_L(t)\cos[(\omega_{c_m} - \Delta\omega)t - \theta_{\pm}] + b_L(t)\sin[(\omega_{c_m} - \Delta\omega)t - \theta_{\pm}]\} \\ &\quad + j\{a_L(t)\cos[(\omega_{c_m} - \Delta\omega)t - \theta_{\pm}] - b_L(t)\sin[(\omega_{c_m} - \Delta\omega)t - \theta_{\pm}]\}\end{aligned}\quad 7.3.5c$$

respectively. These can be simplified into

$$\begin{aligned}\hat{S}_U(t) &= [a_U(t) + jb_U(t)] \{\cos[(\omega_{c_m} + \Delta\omega)t + \theta_{\pm}] + jsin[(\omega_{c_m} + \Delta\omega)t + \theta_{\pm}]\} \\ &= [a_U(t) + jb_U(t)] \exp\{j[(\omega_{c_m} + \Delta\omega)t + \theta_{\pm}]\}\end{aligned}\quad 7.3.6a$$

$$\begin{aligned}\hat{S}_D(t) &= [a_D(t) + jb_D(t)] \{\cos[\Delta\omega t + \theta_{\pm}] + jsin[\Delta\omega t + \theta_{\pm}]\} \\ &= [a_D(t) + jb_D(t)] \exp\{j[\Delta\omega t + \theta_{\pm}]\}\end{aligned}\quad 7.3.6b$$

$$\begin{aligned}\text{and } \hat{S}_L(t) &= [a_L(t) + jb_L(t)] \{\cos[(\omega_{c_m} - \Delta\omega)t - \theta_{\pm}] - jsin[(\omega_{c_m} - \Delta\omega)t - \theta_{\pm}]\} \\ &= [a_L(t) + jb_L(t)] \exp\{-j[(\omega_{c_m} - \Delta\omega)t - \theta_{\pm}]\}\end{aligned}\quad 7.3.6c$$

respectively, where $a_U(t) + jb_U(t)$, $a_D(t) + jb_D(t)$, and $a_L(t) + jb_L(t)$ are the equivalent baseband transmitted signals of the upper, desired and lower channels, respectively, without offsets. The resultant equivalent baseband

signal (i.e., the sum of the signals in Eqn. 7.3.6), with respect to the desired channel is

$$s_R(t) = \hat{s}_U(t) + \hat{s}_O(t) + \hat{s}_L(t) \quad 7.3.7$$

The baseband equivalent model of the system can be simplified by assigning, in each of the three channels, real values to the signals in one of the two parallel channels (that associated with $\sqrt{2}\cos(\cdot)$), and imaginary values to the signals in the other channel, and then considering the transmission path as a baseband transmission path carrying complex-valued signals.

For the description of the baseband equivalent of the noise $N(t)$, see Section 2.6.

7.3.2 Equivalent baseband model of the DEQPSK or CDE8PSK system, with the use of the MDFL or DDL, for computer simulation

The baseband equivalent model of the DEQPSK or CDE8PSK system with the use of the predistorter, the amplifier limiter, phase demodulator B and the MDFL or DDL and in an ACI environment, for computer simulation tests, is shown in Fig. 7.5. For a DEQPSK system, the encoder differentially and Gray encodes the data symbols at the input. The receiver contains a threshold detector, Gray decoder and the MDFL. For a CDE8PSK system, the encoder convolutionally, differentially and Gray encodes the data symbols, and the decoder and DDL are used at the receiver.

The description of the upper and lower of the adjacent channels in the DEQPSK or CDE8PSK system, are given in Section 3.2.4 or 5.2.1, respectively. The equivalent baseband signals at the output of the transmitter, from the upper, desired and lower channels, are (Eqn. 7.3.6)

$$\hat{s}_U(t) = [a_U(t) + jb_U(t)] \exp\{j[(\omega_{c_m} + \Delta\omega)t + \theta_m]\} \quad 7.3.8a$$

$$\hat{s}_O(t) = [a_O(t) + jb_O(t)] \exp\{j[\Delta\omega t + \theta_m]\} \quad 7.3.8b$$

... and
$$\hat{s}_L(t) = [a_L(t) + jb_L(t)] \exp\{-j[(\omega_{c_m} - \Delta\omega)t - \theta_m]\} \quad 7.3.8c$$

The signals $a_U(t) + jb_U(t)$, $a_O(t) + jb_O(t)$ and $a_L(t) + jb_L(t)$ are defined in

Eqn. 7.3.6, $\Delta\omega$ and θ_m are defined in Eqn. 7.3.3, and ω_{c_m} is the channel spacing in rad/s. The system is modelled digitally for computer simulation, so the signals are sampled at the time instants (mT_m) (where $1/T_m$ is the sampling rate used in the simulation tests). Thus at time $t=mT_m$, the signal samples are

$$\hat{s}_{U,m} = [a_{U,m} + jb_{U,m}] \exp\{j[(\omega_{c_m} + \Delta\omega)mT_m + \theta_m]\} \quad 7.3.9a$$

$$\hat{s}_{D,m} = [a_{D,m} + jb_{D,m}] \exp\{j[\Delta\omega mT_m + \theta_m]\} \quad 7.3.9b$$

and
$$\hat{s}_{L,m} = [a_{L,m} + jb_{L,m}] \exp\{-j[(\omega_{c_m} - \Delta\omega)mT_m - \theta_m]\} \quad 7.3.9c$$

respectively, where $\hat{s}_{U,m} = \hat{s}_U(mT_m)$, $\hat{s}_{D,m} = \hat{s}_D(mT_m)$, $\hat{s}_{L,m} = \hat{s}_L(mT_m)$, $a_{U,m} = a_U(mT_m)$, $a_{D,m} = a_D(mT_m)$, $a_{L,m} = a_L(mT_m)$, $b_{U,m} = b_U(mT_m)$, $b_{D,m} = b_D(mT_m)$, and $b_{L,m} = b_L(mT_m)$.

The signal sample at the input of the desired channel receiver, at time $t=mT_m$, is

$$\hat{s}_{R,m} = s_{R,m} + n_m \quad 7.3.10a$$

$$= \hat{s}_{U,m} + \hat{s}_{D,m} + \hat{s}_{L,m} + n_m \quad 7.3.10b$$

where $s_{R,m} = s_R(mT_m)$ (Eqn. 7.3.1). The real and imaginary parts of all noise samples $\{n_m\}$ are taken to be statistically independent Gaussian variable with zero mean and fixed variance σ^2 .

The sampled impulse responses of the baseband equivalent model of the receiver IF filter and of the demodulation filter, sampled at the rate of $1/T_m$ samples per second, are given by the $(g+1)$ -component vector

$$F = [f_0 \quad f_1 \quad f_2 \quad \dots \quad f_g] \quad 7.3.11$$

and the $(n+1)$ -component vector

$$P = [p_0 \quad p_1 \quad p_2 \quad \dots \quad p_n] \quad 7.3.12$$

respectively, where $f_m = f(mT_m)$ and $p_m = p(mT_m)$. Assume that the transmission

path introduces no delay. The signal sample at the output of the receiver IF filter, at time $t=mT_s$, is

$$e_m = \sum_{n=0}^{\infty} \hat{s}_{r, m-n} f_n \quad 7.3.13$$

whose phase angle is corrected by the signal from the MDFL or DDL to give the signal

$$e_m = e_m \exp(-j\hat{\theta}_{m/i-N}) \quad 7.3.14$$

$$= \left[\sum_{n=0}^{\infty} \hat{s}_{r, m-n} f_n \right] \exp(-j\hat{\theta}_{m/i-N}) \quad 7.3.15$$

for $iT < mT_s \leq (i+1)T$, where $\hat{\theta}_{m/i-N}$ (Eqn. 7.2.28) is the predicted phase $\hat{\theta}$ at time $t=mT_s$ derived from the received information at time $t=(i-N)T$. The sample \hat{e}_m is fed to the amplifier limiter in cascade with phase demodulator B to give (Eqn 6.4.28)

$$\hat{e}_m = \frac{\hat{e}_m}{|\text{Re}(\hat{e}_m)| + |\text{Im}(\hat{e}_m)|} \quad 7.3.16$$

where $\text{Re}(\cdot)$ and $\text{Im}(\cdot)$ are the real and imaginary parts of (\cdot) , respectively. The signal is then filtered by the demodulation filter. At time $t=mT_s$, the signal sample at the output of the demodulation filter is

$$r_m = \sum_{n=0}^n \hat{e}_{m-n} p_n \quad 7.3.17$$

where r_m has a complex value.

Assume that the receiver provides the required ideal timing signal, so that the signal is sampled once per symbol, at the time instants (iT) , to give the sequence of samples (r_i) which are fed to the DTPD (digital tan phase detector). At time $t=iT$, the DTPD produces the phase angle Ω_{i-N} at its output which is then fed to the detector/decoder to produce the phase estimate $\hat{\theta}_{i-N}$, as described in Sections 7.2.1 and 7.2.2. The phase error

estimate $\hat{\epsilon}_{1-N}$ is then computed using Eqns. 7.2.22 or 7.2.41, depending on whether the MDFL or DDL is used. $\hat{\epsilon}_{1-N}$ is filtered by $F(z)$ and used to control the phase of the DCO output, so that the phase angle from the DCO, at time $t=mT_s$, is

$$\hat{\theta}_{m/1-N} = \frac{1}{1-z^{-1}} \gamma F(z) \hat{\epsilon}_{1-N}, \quad \text{for } iT < mT_s < (i+1)T \quad 7.3.18$$

as can be seen in Eqn. 7.2.46, where γ is the DCO gain factor.

7.4 Simulation results and discussion

It is shown in Sections 6.7.1 and 6.7.3 that, for the preferred filters, predistorter, HPA, amplifier limiter and phase demodulator, the most cost effective arrangement is to use signal 3A or 3C (depending upon whether the DEQPSK or CDE8PSK signal is used), with $f_{c_s}=5R/4$ Hz and to operate the HPA slightly, say 0.2 dB OBO, below saturation. So in this section, this arrangement is used for studying the carrier recovery techniques. Phase demodulator B is used at the receiver because it is more cost effective than phase demodulator A. The relationship between μ and γ , where μ is the loop filter constant and γ is the DCO gain, is maintained at $\mu/\gamma=1/2$ (Eqn. A11.2.29), so that there is only one variable in the MDFL and DDL to be optimised. (Optimising two separate variables would take too much computing time.)

The DEQPSK and CDE8PSK systems, considered so far, operate at a speed of 64, 128, 256 or 512 kbit/s, but here, for convenience, the systems considered here are assumed to be operating at a speed of 64 kbit/s.

7.4.1 Performances of DEQPSK and CDE8PSK signals with different frequency offsets in an ACI environment

It is not possible to estimate the maximum frequency offset of the satellite transmission system without knowing the actual satellite orbit, the uplink and downlink frequencies, the tolerance of the transmitter local oscillator and the satellite frequency translator (Section 7.3).

Since these factors are not specified in this project, the maximum frequency offsets which the DEQPSK and CDE8PSK systems can tolerate are evaluated by means of computer simulation.

The simulation model used to evaluate the effects of frequency offset on the error-rate performances of these two systems is shown in Fig. 7.5. At the beginning of every transmission, the MDFL or DDL (depending upon whether the DEQPSK or CDE8PSK signal is used), is used to track the carrier signal. After the steady state has been reached, the loop is then opened so that it does not affect the reference carrier signal at the receiver of the desired channel. With the channel spacing $f_{c_m} = 5R/4$ Hz = 40 kHz (where $R = 32$ kHz is assumed) and 0.2 dB HPA OBO, the error-rate performances of the DEQPSK signals, with different values of the frequency offset, Δf , are shown in Figs. 7.6 and 7.7.

Tables 7.2a and 7.3a show the degradations in tolerance to noise of the DEQPSK signals, at $P_e = 10^{-4}$, with different values of Δf , measured in comparison with those with $\Delta f = 0$. The results indicate that, the signals with wider bandwidths suffer larger degradations in tolerance to noise than those with narrower bandwidths. This is to be expected, because the larger the bandwidth of the signal, the more severe is the distortion introduced by the receiver IF filter due to a frequency offset. Tables 7.2b and 7.3b show the degradations in tolerance to noise of the DEQPSK and CDE8PSK, respectively, at $P_e = 10^{-4}$, with different frequency offsets, measured in comparison with those of the corresponding ideal systems.

Table 7.2 indicates that, although signal 4A has the narrowest bandwidth of the DEQPSK signals and so suffers least from frequency offsets, it is degraded more severely by the amplifier limiter and phase demodulator B. Thus with $\Delta f \leq 4$ kHz, signal 3A gives the best performance of the DEQPSK signals, and so it achieves the best compromise between distortion caused by frequency offsets and distortion caused by the amplifier limiter and phase demodulator B.

Table 7.3 shows that, of the CDE8PSK signals, signal 4C suffers least from frequency offsets, but it is degraded more severely by the amplifier limiter and phase demodulator B. With $\Delta f \leq 3$ kHz, Table 7.3b shows that signal 3C achieves the best compromise between distortion caused by frequency offset and distortion caused by the amplifier limiter and phase demodulator B. Thus it gives the best performance of the CDE8PSK signals. However with $\Delta f = 4$ kHz, signal 4C has a better performance than signal 4C. This is because as Δf gets larger, the distortion caused by a frequency offset has a greater effect than the distortion caused by the amplifier limiter and phase demodulator B. Although Table 7.2b shows that with $\Delta f = 4$ kHz, signal 4C is superior to signal 3C, it is inferior when $\Delta f = 3$ kHz, however, the difference is negligible. Since signal 3C is simply to implement, it is more cost effective.

When comparing the degradations in tolerance in Table 7.2a with those in Table 7.3a, it can be seen that, in the presence of AWGN, CDE8PSK signals have a better tolerance to frequency offsets than DEQPSK signals.

It is not possible to optimise the loops without knowing the maximum possible frequency offset which will occur in the systems. Tables 7.2a and 7.3a show that, when $\Delta f \geq 4$ kHz, signals 3A and 3C are degraded by more than 2 dB, at $P_e = 10^{-4}$, measured in comparison with the corresponding cases where $\Delta f = 0$, so in this thesis, $\Delta f_{max} = 4$ kHz is assumed (arbitrarily) to be the maximum possible value of frequency offset which will occur in the systems. Of course, for systems operating at 128, 256 and 512 kbit/s, the respective assumed values of Δf_{max} are 8, 16 and 32 kHz, respectively.

7.4.2 Steady-state performances of the MDFL and DDL

Since in the presence of ACI and noise, signals 3A and 3C give the best compromise between distortion caused by frequency offsets and distortion caused by the amplifier limiter and phase demodulator B, they are used in this section to study the steady-state performances of the MDFL and DDL, respectively.

The computer simulation model, used to assess the steady-state performances of the loops, is shown in Fig. 7.5. With $\Delta f = 0$ Hz, $f_{c_m} = 5R/4 = 40$ kHz, $\mu/\gamma = 1/2$ (Eqn. A11.2.29), and the HPA operating at 0.2 dB OBO, the steady-state performances of the MDFL and DDL in the DEQPSK and CDE8PSK systems, respectively, with different values of γ and μ , are shown in Fig. 7.8. It can be seen that the smaller the values of γ and μ , the better is the performance, because the narrower is the loop bandwidth [8]. Since the DDL is data-aided and the error bursts in the CDE8PSK signal occur relatively more often at high error-rates, Figure 7.8b shows that the DDL causes larger degradations in tolerance to noise at high error-rate. However, it improves at low error-rates. This effect is less obvious for the MDFL in the DEQPSK system, as can be seen in Figure 7.8a, because the detected symbols are not correlated. The degradations in tolerance to noise of signals 3A and 3C, with different values of γ and μ used in the loops, at $P_e = 10^{-4}$, measured in comparison with those using an ideal carrier recovery loop, are shown in Tables 7.4.

Although, with narrower loop bandwidths, the MDFL and DDL can provide better steady-state performances, the acquisition time may be slow, so it is not possible to determine the optimum values γ and μ of the loops without knowing their transient responses.

7.4.3 Transient responses of the MDFL and DDL

Self frequency acquisition

In Section 7.2.3, it is shown that the pull-in limit for the MDFL is $\Delta f_p = \pm 4$ kHz (Eqn. 7.2.49), but in deriving this pull-in limit, the effects of the delay in phase estimation, noise and the loop bandwidth, are neglected. In practice, all these effects are present, and it is difficult to analyse them theoretically, so that computer simulation tests must be used.

The computer simulation model shown in Fig. 7.5 is used to assess the pull-in limits of the MDFL and DDL under different conditions. With the

use of the MDFL, in the absence of phase and frequency offsets, signals 1A, 2A, 3A and 4A are used with $2E_b/N_0=13$ dB. This is because with $2E_b/N_0=13$ dB the error-rates are in the practical region of $10^{-4} - 10^{-3}$, (Fig. 7.6c). Increasing values of γ and μ are tried in the MDFL until the system becomes unstable. Clearly, the largest values of γ and μ which do not cause the system to be unstable are the values which have the largest pull-in limits for the signal. This is the largest bandwidth which the loop can have without causing the system to become unstable. Since signals 1A, 2A, 3A and 4A introduce different delays in phase estimation, they have different largest values of γ and μ and so they have different pull-in limits, as shown in Table 7.5a. Then, with the use of the DEQPSK signals (i.e., signals 1A, 2A, 3A and 4A) and the respective largest values of γ and μ , increasing values of frequency offset are then applied until the system becomes unstable. The largest frequency offset from which the loop can acquire lock gives the pull-in limit. Results are shown in Table 7.5 which indicate that the effects of the delay in phase estimation, noise and ACI, etc., have reduced the pull-in-limit of the MDFL from the value of 4 kHz. The results also indicate that signals 1A and 4A, with $N=1$ and 4, have the largest and smallest pull-in limits, respectively, as expected.

Then, with frequency offsets set to the pull-in limits, the minimum values of γ and μ which can still acquire lock are found, as shown in Table 7.5. Of course, these values of γ and μ increase the acquisition time relative to the maximum values of γ and μ , due to the narrower loop bandwidths.

The maximum values of γ and μ are noise dependent because they determine the loop bandwidth. If the loop bandwidth is too wide, the system becomes unstable. Obviously, at higher signal/noise power ratio, larger values of γ and μ can be used, leading to a larger pull-in-limit and a smaller acquisition time. However, the smallest values of γ and μ

are not noise dependent, but are determined by the fact that the MDFL (or DDL) is data-aided and if it does not pull in fast enough, most of the data will be wrongly detected and cannot not be used to aid the loop to acquire lock. Thus if values of γ and μ smaller than the minimum were used, the loop would not acquire lock.

Similar procedures are carried out for the CDE8PSK signals with the DDL at $2E_b/N_0=11$ dB, because with $2E_b/N_0=11$ dB, the error-rates are in the practical region of 10^{-4} - 10^{-3} (Fig. 7.7c). The results are given in Table 7.5b.

Aided frequency acquisition

From Table 7.5, it can be seen that the largest pull-in-limits which signals 3A and 3C can have are 700 Hz. This is less than the assumed maximum possible frequency offset of 4 kHz in the systems (Section 7.4.1), so aided frequency techniques have to be used.

The variable-bandwidth method (Section 7.2.3) is one of the aided frequency techniques. So when using signal 3C in a CDE8PSK system, if the possible maximum frequency offset in the system is less than 700 Hz, $\gamma=0.08$ and $\mu=0.04$ can be used to acquire lock (Table 7.5), and smaller values of γ and μ can be used after acquisition. Similar for the DEQPSK system with the use of signal 3A, where $\gamma=0.08$ and $\mu=0.04$ can be used for faster acquisition and smaller values of γ and μ can be used after acquisition. It should be apparent that an increase of bandwidth can be useful only if the signal/noise power ratio is sufficiently large. If the bandwidth is too large, the loop becomes unstable and acquisition is unlikely to be achieved. However, with the use of this aided frequency technique, the pull-in limits of the MDFL and DDL still do not reach 4 kHz, so the extended-pull-in-limit method (Section 7.2.3) must be used instead.

The extended-pull-in-limit method is non-data-aided, so that signals 3A and 3C have the same pull-in limit. Computer simulation tests, using the model shown in Fig. 7.5 and the extended-pull-in-limit method with $\mu=0.1$ and $\gamma=0.05$, have been carried out. The results suggest that, at $2E_b/N_0=12.5$ dB, the pull-in limit can be extended up to 13 kHz. The results also suggest increasing μ above 0.1 and γ above 0.05 will cause the system to become unstable. Thus $\mu=0.1$ and $\gamma=0.05$ are the optimum values for the extended-pull-in-limit method, in the sense that it leads to the most rapid frequency acquisition.

A series of two hundred tests have been carried out to assess the transient responses of the extended-pull-in-limit method with $\mu=0.1$ and $\gamma=0.05$ for signals 3A and 3C at $2E_b/N_0=13$ and 12.5 dB, respectively. With these values of signal/noise power ratio, the error-rates are in the practical region of 10^{-4} - 10^{-9} (Figs. 7.6c and 7.7c). The frequency offset is taken as 4 kHz and the initial phase error is uniformly distributed in the range $-\pi < \theta < \pi$. The results show that, with the use of the extended-pull-in-limit method, the loops can acquire lock with any resultant carrier phase. This is to be expected because the method can only be used to acquire frequency lock but not phase lock. The latter has to be acquired later by the MDFL or DDL. Results of forty tests are given in Figs. 7.9 and 7.10. Since the extended-pull-in-limit method requires training symbols at the beginning of transmission, it is important to know its acquisition time. The results of four hundred tests have indicated that, in the worst case, steady state could be reached 160 symbol intervals after the occurrence of a frequency jump. It seems that the extended-pull-in-limit method with $\mu=0.1$ and $\gamma=0.05$ can be used at the beginning of transmission over 160 symbols before switching to the MDFL or DDL for continuous (steady state) operation.

It is not possible to determine the optimum values of γ and μ of the loops without knowing the possible maximum frequency offset caused by a sudden signal fade. Of course, the smaller the values of μ and γ , the better is the performance (Fig. 7.8). However, if μ and γ are too small, the loops cannot track the frequency offset caused by a sudden signal fade. So the optimum values of μ and γ can be specified only if the maximum frequency offset is specified.

Figure 7.8a shows that, for $\gamma < 0.03$ and $\mu < 0.015$ in the MDFL, there is a reduction of less than 1 dB in tolerance to noise of signal 3A, at $P_e = 10^{-4}$, measured in comparison with that using an ideal carrier recovery loop. However Table 7.5 shows that, with $\gamma = 0.03$ and $\mu = 0.015$, the pull-in limit for signal 3A is only 700 Hz. Thus if $\Delta f \leq 700$ Hz, the MDFL can be used without requiring any aided frequency acquisition technique to acquire lock. A series of two hundred tests has been carried out to find the transient response of the MDFL at $2E_b/N_0 = 13$ dB. With $2E_b/N_0 = 13$ dB, the error-rate is in the practical region, i.e., $P_e = 10^{-4} - 10^{-3}$ (Fig. 7.6c). The frequency offset is taken to be 750 Hz and the initial phase error is uniformly distributed in the range $-\pi \leq \theta \leq \pi$. The results indicate that the MDFL can acquire lock in one of 4 stable positions, as expected. No "hangup" occurred in the tests. Results of fifty tests are shown in Fig. 7.11.

Figure 7.8b shows that any values of $\gamma = 0.01$ and $\mu = 0.005$ used in the DDL, there is a reduction of less than 1 dB in tolerance to noise of signal 3C, at $P_e = 10^{-4}$, relative to the corresponding system using an ideal carrier loop. Simulation tests show that with $\gamma = 0.01$ and $\mu = 0.005$, the pull-in limit of signal 3C is reduced to 200 Hz. A series of two hundred tests have been carried out to find the transient response of the DDL at $2E_b/N_0 = 11$ dB. With $2E_b/N_0 = 11$ dB, the error-rate is in the practical region of $10^{-4} - 10^{-3}$ (Fig. 7.7c). The frequency offset Δf is taken as 200 Hz and the initial phase error is uniformly distributed in the range $-\pi \leq \theta \leq \pi$. The

results indicate that the DDL can acquire lock in one of 8 stable position, as expected. No "hangup" occurred in the tests. Results of fifty tests are shown in Fig. 7.12.

It seems that, if the frequency offsets caused by a sudden signal fade are less than 700 and 200 Hz in the DEQPSK and CDE8PSK systems, respectively, then the extended-pull-in-limit method with $\mu=0.1$ and $\gamma=0.005$ can be used at the beginning of transmission over 160 symbols before switching to the MDFL with $\mu=0.03$ and $\gamma=0.015$ or the DDL with $\mu=0.01$ and $\gamma=0.005$ for continuous tracking. Of course, if the frequency offsets caused by sudden signal fade are larger than 700 and 200 Hz, then larger values of μ and γ have to be used in the MDFL and DDL which, inevitably, will cause larger degradations in tolerance to noise. On the other hand, if the possible frequency offsets are less than the given values, then smaller values of μ and γ can be used which, of course, cause smaller degradations in tolerance to noise. This is why the optimum values of μ and γ cannot be specified unless the possible frequency offset is known.

Simulation tests have been carried out for signal 3A, with the extended-pull-in-limit method used with $\mu=0.1$ and $\gamma=0.05$ at the beginning of transmission over 120 symbols before switching to the MDFL with $\mu=0.03$ and $\gamma=0.015$ for continuous operation. The results are shown in Fig. 7.13. Simulation tests have also been carried out for signal 3C, with the extended-pull-in-limit method used with $\mu=0.1$ and $\gamma=0.05$ at the beginning of transmission over 160 symbols before switching to the DDL with $\mu=0.01$ and $\gamma=0.005$ for continuous operation. The results are shown in Fig. 7.14. Since the MDFL has a larger pull-in limit, it requires 120 training symbols, instead of 160 symbols, at the beginning of transmission.

Although the optimum values of μ and γ depend on the possible frequency offset, the values $\mu=0.1$ and $\gamma=0.05$ used in the extended-pull-in-limit method are always optimum because they leads to the fastest frequency acquisition time.

Phase acquisition

As mentioned in Section 7.2.3, phase is usually self acquired, so it is less critical and is studied here. The simulation model shown in Fig. 7.5 is also used to study the phase acquisition of the MDFL and DDL. A series of two hundred tests has been carried out for signal 3A at $2E_b/N_0=13$ dB. With $2E_b/N_0=13$ dB, the error-rate is in the practical region of $10^{-4} - 10^{-3}$ (Fig. 7.6c). The MDFL is used here with $\mu=0.03$ and $\gamma=0.015$. Also $\Delta f=0$ and the initial phase error is uniformly distributed in the range $-\pi \leq \theta < \pi$. The results indicate that the MDFL can acquire lock in one of 4 stable positions. No "hangup" occurred in the tests. Results of fifty tests are shown in Fig. 7.15. The same procedures have been carried out for signal 3C with $2E_b/N_0=11$ dB with the uses of the DDL with $\mu=0.01$ and $\gamma=0.005$. The results indicate that the DDL can acquire lock in one of the 8 stable positions. No "hangup" occurred in the tests. Results of fifty tests are shown in Fig. 7.16. It can be seen from these results that, since the loops can acquire lock in different stable positions, the acquisition time is rapid (less than 10 symbols).

7.4.4 Steady-state performances of the MDFL and DDL, in the presence of frequency offset

The simulation model shown in Fig. 7.5 is used to assess the steady-state performances of the loops, in the presence of frequency offset. Simulation tests have been carried out for signal 3A. with $f_c=5R/4=40$ kHz, $\mu=0.03$ and $\gamma=0.015$ in the MDFL, and the HPA operating at 0.2 dB OBO. The extend-pull-in-limit method is used here with $\mu=0.1$ and $\gamma=0.005$ at the beginning of transmission over the first 120 symbols before switching to the MDFL. The error-rate performances of signal 3A with frequency offsets of 2 and 4 kHz, are shown in Fig. 7.17. The same procedures have been carried out for signal 3C, with $\mu=0.01$ and $\gamma=0.005$ in the DDL instead. The error-rate performances are also shown in Fig. 7.17. It can be seen that, under the assumed conditions, with $\Delta f=2$ kHz and

4 kHz, despite the degradations caused by using differential encoding and the suboptimum distance measure, signal 3C still gains the advantages of 4dB and 5dB, respectively, over signal 3A, hence the CDE8PSK signal, signal 3C, is more cost effective.

REFERENCES

- [1] Gardner, F.M., *Phaselock Techniques*, 2nd Ed. John Wiley & Sons (1979)
- [2] Viterbi, A.J., *Principles of Coherent Communication*, McGraw-Hill (1966)
- [3] Stiffler, J.J., *Theory of Synchronous Communications*, Prentice-Hall, Englewood Cliffs, N.J. (1973)
- [4] Linsey, W.C. and Simon, M.K, *Telecommunication Systems Engineering*, Prentice-Hall, Englewood Cliffs, N.J. (1973)
- [5] Gardner, F.M., "Hang-up in Phase-Lock Loop", *IEEE Trans. on Commun.*, Vol. COM-25, NO.10 Oct. 1977
- [6] Lynn, .P.A., *An introduction to The Analysis and Processing of Signals*, 2nd Ed.
- [7] Bhargava, U.K., Haccoun, D., Matyas, R. and Muspl, P.P, *Digital Communications by Satellite*, John Wiley & Sons (1981)
- [8] Harvey, J.D., *Synchronisation Techniques*, Internal report, Loughborough University of Technology

Received sample values		Received phase values	Detected phase value
$r_{i-m}^{(1)}$	$r_{i-m}^{(2)}$	$\Omega_{i-m} = \tan^{-1}(r_{i-m}^{(1)}/r_{i-m}^{(2)})$	\hat{Y}_{i-m}
>0	>0	$0 \leq \Omega_i < \pi/2$	$\pi/4$
>0	<0	$0 > \Omega_i \geq -\pi/2$	$-\pi/4$
<0	>0	$\pi/2 \leq \Omega_i < \pi$	$3\pi/4$
<0	<0	$-\pi/2 > \Omega_i \geq -\pi$	$-3\pi/4$

Table 7.1 Phase threshold estimation for Ω_{i-m} used in the MFDL.

Frequency offsets (Hz)	Signal			
	1A	2A	3A	4A
2 k	1.2	0.5	0.2	0
4 k	4.1	4.1	2.2	2.2

(a)

Frequency offsets (Hz)	Signal			
	1A	2A	3A	4A
0 k	3.3	3.3	3.3	4.8
2 k	4.5	3.8	3.5	4.8
4 k	7.4	7.4	5.5	7

(b)

Table 7.2 Degradations in tolerance to noise of signals 1A, 2A, 3A and 4A, due to different frequency offsets, over a nonlinear and limited channel, with the use of the suboptimum filters, the predistorter, the HPA operating at 0.2 dB OBO, the amplifier limiter and phase demodulator B and in an ACI environment with $f_{c_m} = 5R/4$ Hz, at $P_s = 10^{-4}$, expressed in dB, (a) measured in comparison with those of corresponding cases without frequency offset and, (b) measured in comparison with that of an ideal DEQPSK system (from Fig. 7.6).

Frequency offsets (Hz)	Signal			
	1C	2C	3C	4C
2 k	0.5	0.5	0.4	0.1
3 k	1.4	1.3	0.9	0.5
4 k	2.3	2.4	2.1	1.5

(b)

Frequency offsets (Hz)	Signal			
	1C	2C	3C	4C
0 k	3	2.7	2.6	3
2 k	3.5	3.2	3	3.1
3 k	4.4	4	3.7	3.8
4 k	5.3	5.1	4.7	4.5

(b)

Table 7.3 Degradations in tolerance to noise of signals 1C, 2C, 3C and 4C, due to different frequency offsets, over a nonlinear and limited channel, with the use of the suboptimum filters, the predistorter, the HPA operating at 0.2 dB OBO, the amplifier limiter and phase demodulator B, and in an ACI environment with $f_{c_m} = 5R/4$ Hz, at $P_n = 10^{-4}$, expressed in dB, (a) measured in comparison with those of the corresponding cases without frequency offset and, (b) measured in comparison with that of an ideal DEQPSK system (from Fig. 7.7).

Signal	$\mu=$	$\gamma=$	Degradation in tolerance to noise
3A	0.02	0.01	0.5
	0.03	0.015	1
	0.04	0.02	1.6
	0.05	0.025	2.6
3C	0.005	0.0025	0.4
	0.008	0.004	0.6
	0.01	0.005	0.7
	0.02	0.01	1.7
	0.03	0.015	3

Table 7.4 Degradations in tolerance to noise of signals 3A and 3C, with different values of μ and γ used in the MDFL and DDL, respectively, over a nonlinear channel, with the use of the amplifier limiter, the predistorter, the HPA operating at 0.2 dB OBO, phase demodulator B and the suboptimum filters and in an ACI environment with $f_{c_{-}}=5R/4$ Hz, at $P_{-}=10^{-4}$, expressed in dB, measured in comparison with those using an ideal carrier recovery loop (from Fig. 7.8).

Signal	largest values of		smallest values of		Pull-in-limit (Hz)
	μ	γ	μ	γ	
1A	0.1	0.05	0.09	0.045	1500
2A	0.08	0.04	0.03	0.015	700
3A	0.08	0.04	0.03	0.015	700
4A	0.04	0.02	0.02	0.01	300
1C	0.01	0.05	0.1	0.05	1000
2C	0.08	0.04	0.08	0.04	700
3C	0.08	0.04	0.08	0.04	700
4C	0.04	0.02	0.02	0.01	300

Table 7.5 The pull-in-limits of the MDFL and DDL for the DEQPSK and CDE8PSK signals, at $2E_b/N_0 = 13$ and 11 dB, respectively, over a nonlinear channel, with the use of the predistorter, the HPA operating at 0.2 dB OBO, the amplifier limiter, phase demodulator B and the suboptimum filters and in an ACI environment with $f_{c_m} = 5R/4$ Hz.

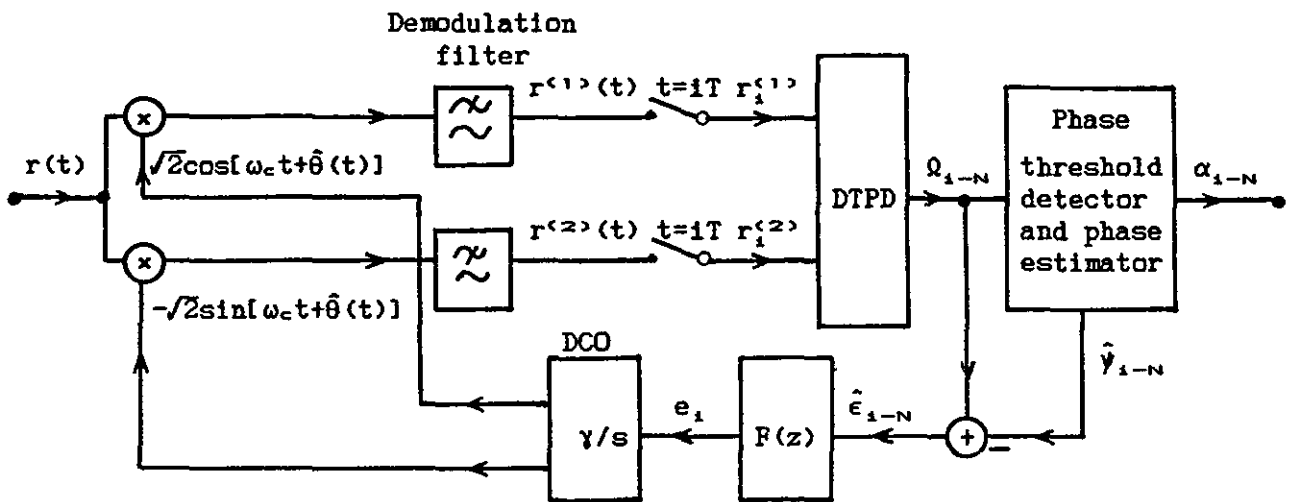


Figure 7.1a DEQPSK signal receiver with the use of the MDL.

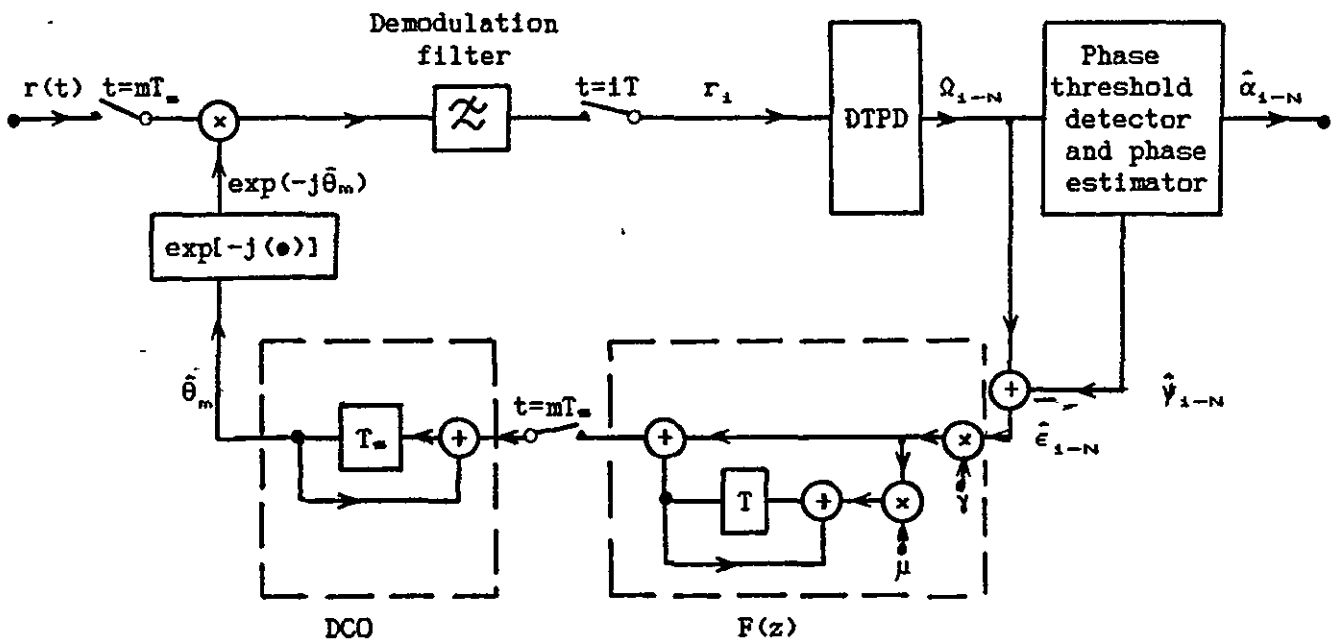


Figure 7.1b Baseband equivalent model of the DEQPSK signal receiver shown in Figure 7.1a.

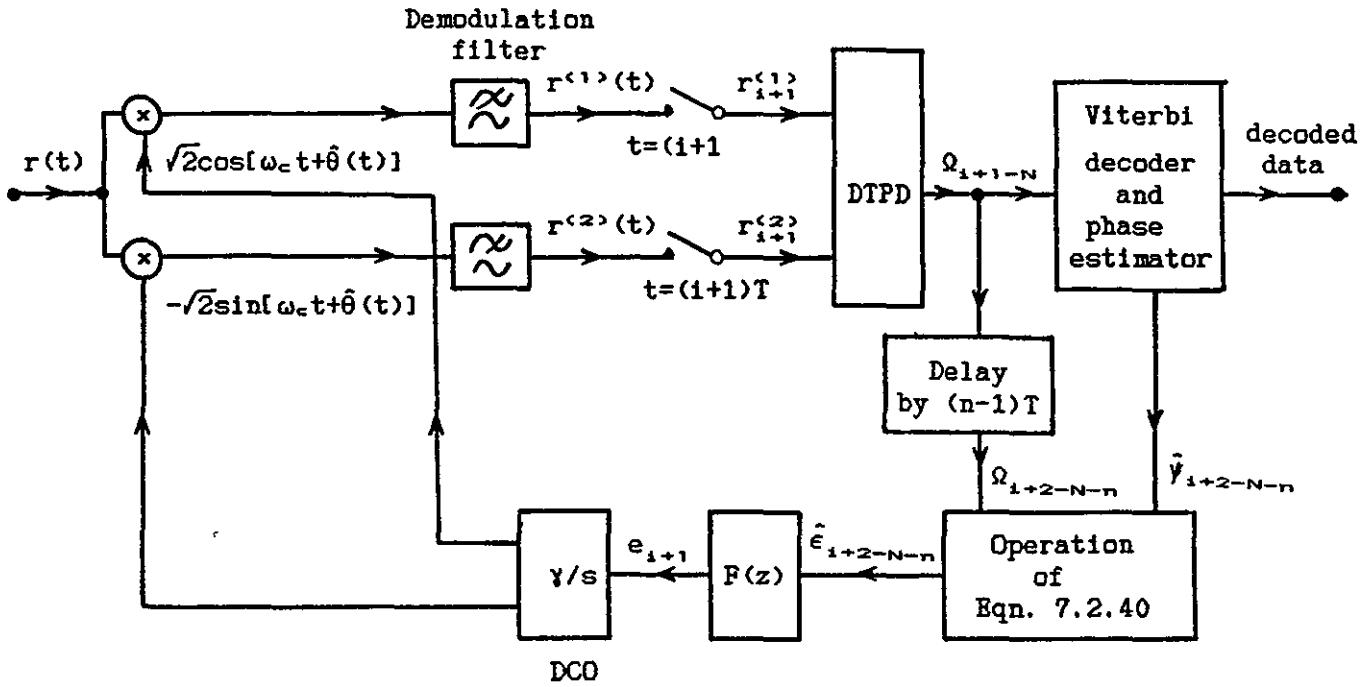


Figure 7.2a CE8PSK signal receiver with the use of the DDL.

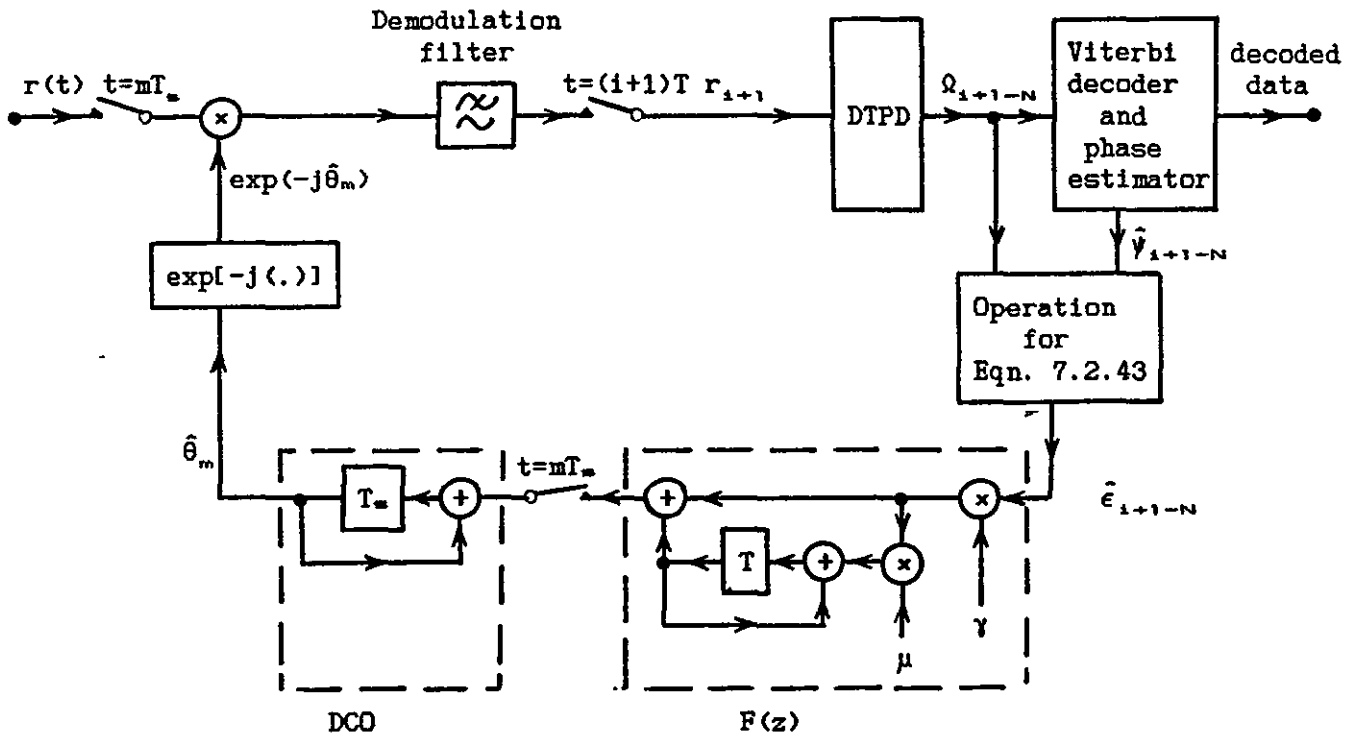


Figure 7.2b Baseband equivalent model of the CE8PSK signal receiver (with the use of early decoding) shown in Figure 7.2a.

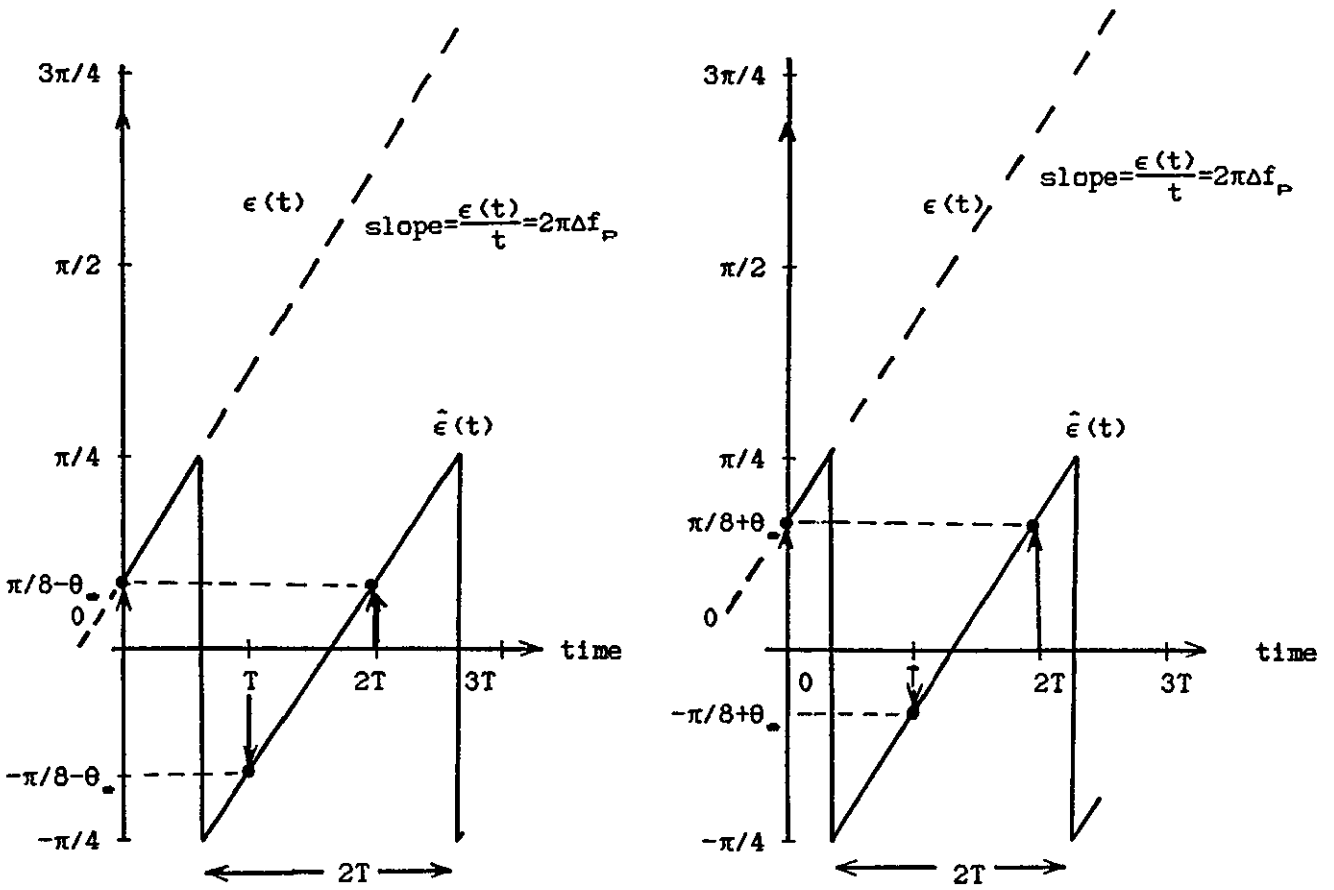


Figure 7.3 Phase errors caused by the pull-in limit of the MDFL with the initial phase errors of (a) $\pi/8 - \theta$ and (b), $\pi/8 + \theta$.

Frequency and phase offsets

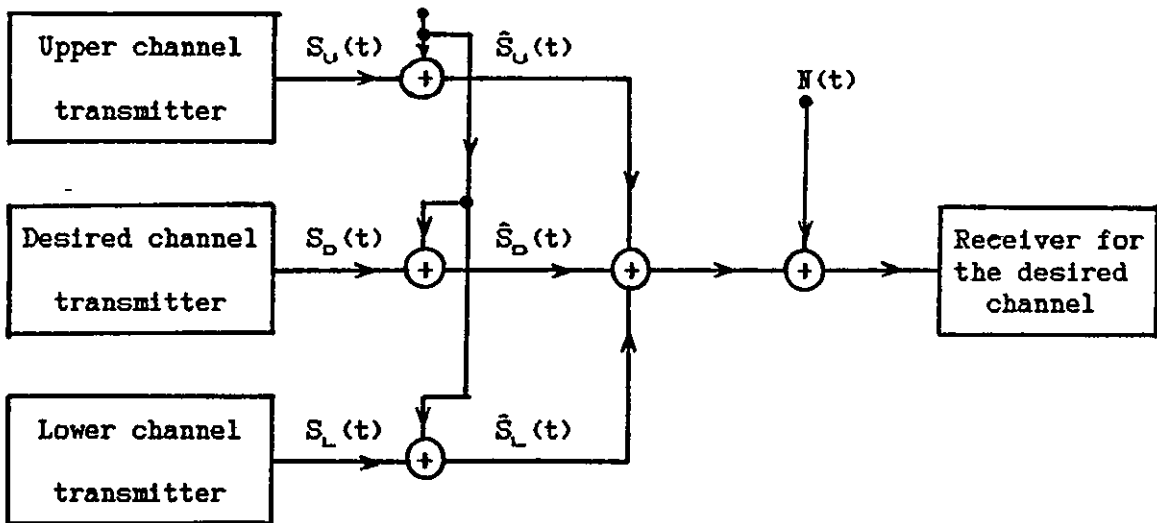


Figure 7.4 Model of a quadrature modulation system with frequency and phase offsets and in an ACI environment.

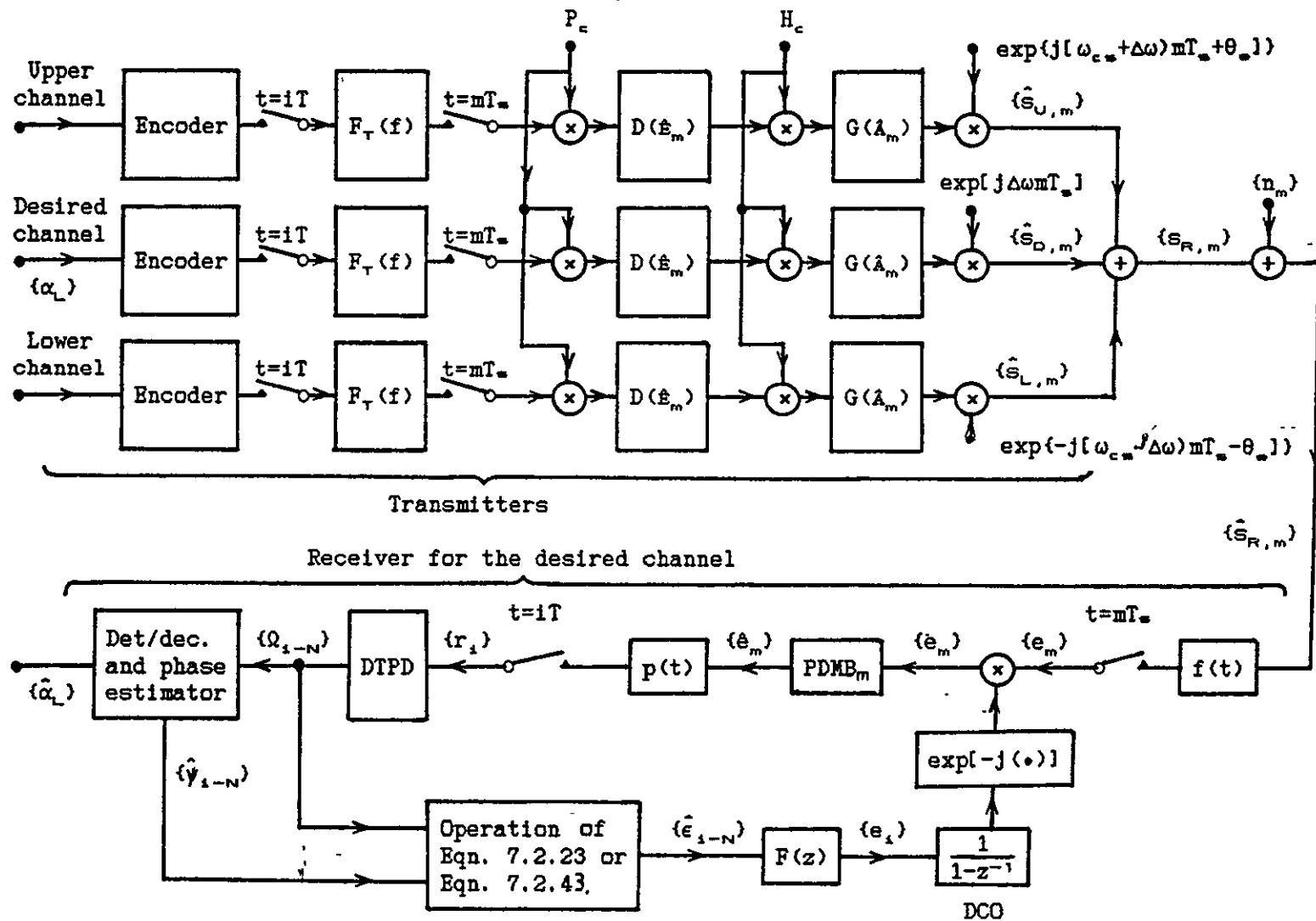


Figure 7.5 Baseband equivalent model of the DEQPSK or CDE8PSK system, with the use of the MDFL or DDL, respectively, and with a nonlinear and bandlimited satellite channel and in an ACI environment, for computer simulation. The suboptimum filters, the predistorer, the amplifier limiter, phase demodulator B and the distance measure D are assumed. The operation of Eqn. 7.2.23 or 7.2.43 is for the MDFL or DDL, respectively. $F_T(f)$ is the resultant transfer function of the baseband equivalent model of the transmitter IF filter in cascade with the modulation filter. Det/dec means detector or decoder.

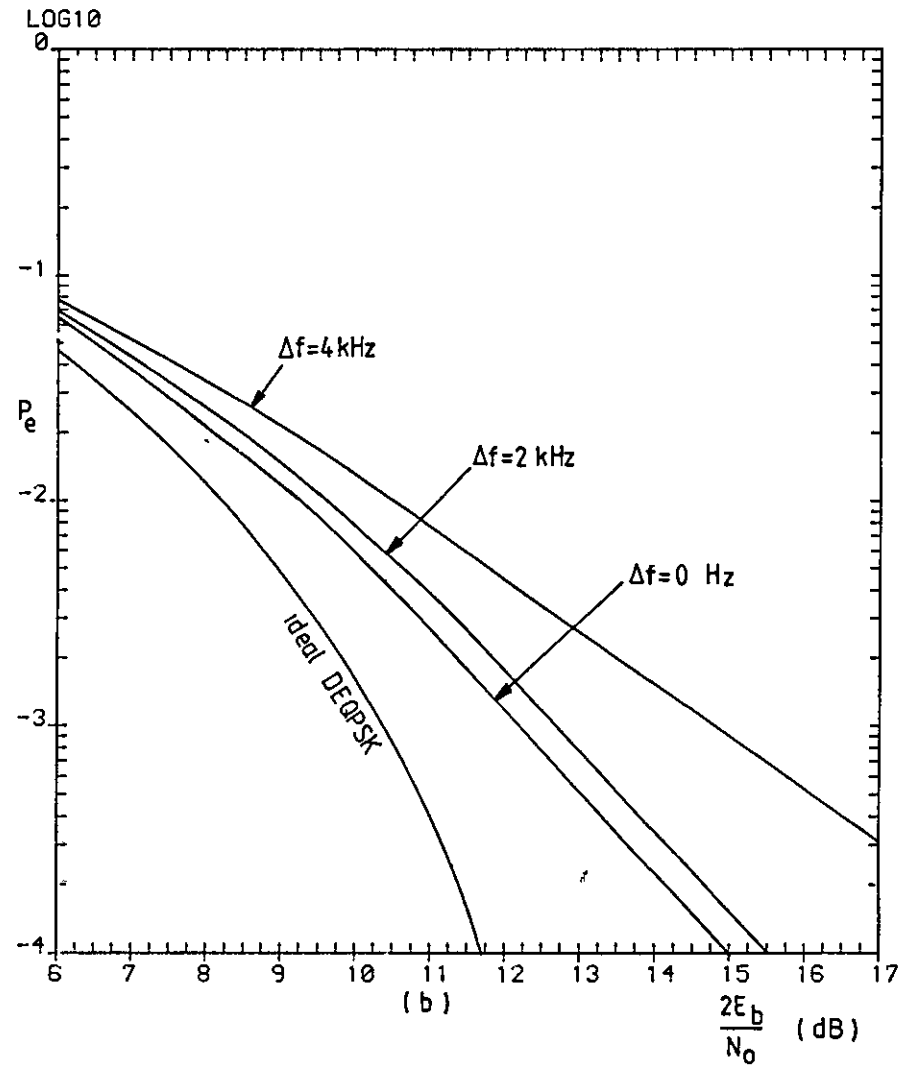
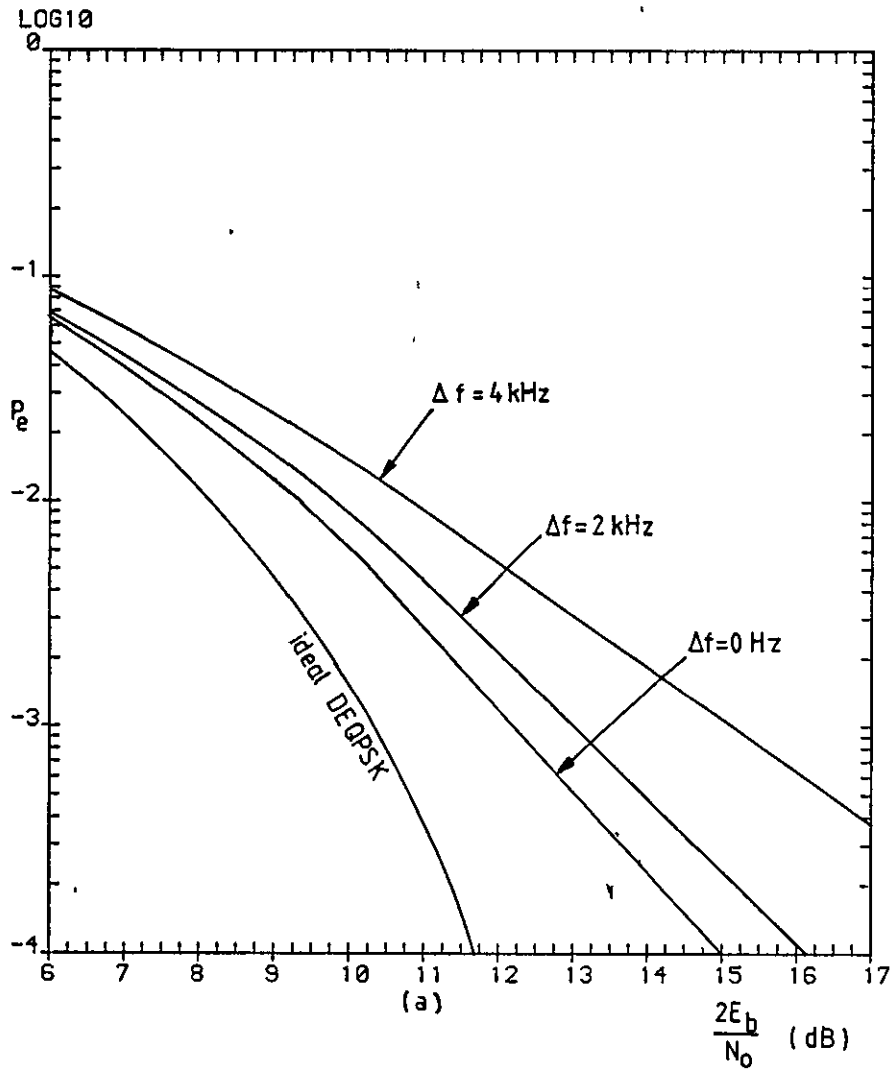


Figure 7.6 Error-rate performances of signals a) 1A, b) 2A, c) 3A and d) 4A, with different frequency offsets and with the use of the suboptimum filters, the predistorter, the HPA operating at 0.2 dB OBO, the amplifier limiter and phase demodulator B and in an ACI environment with $f_{c_{int}} = 5R/4$ Hz.

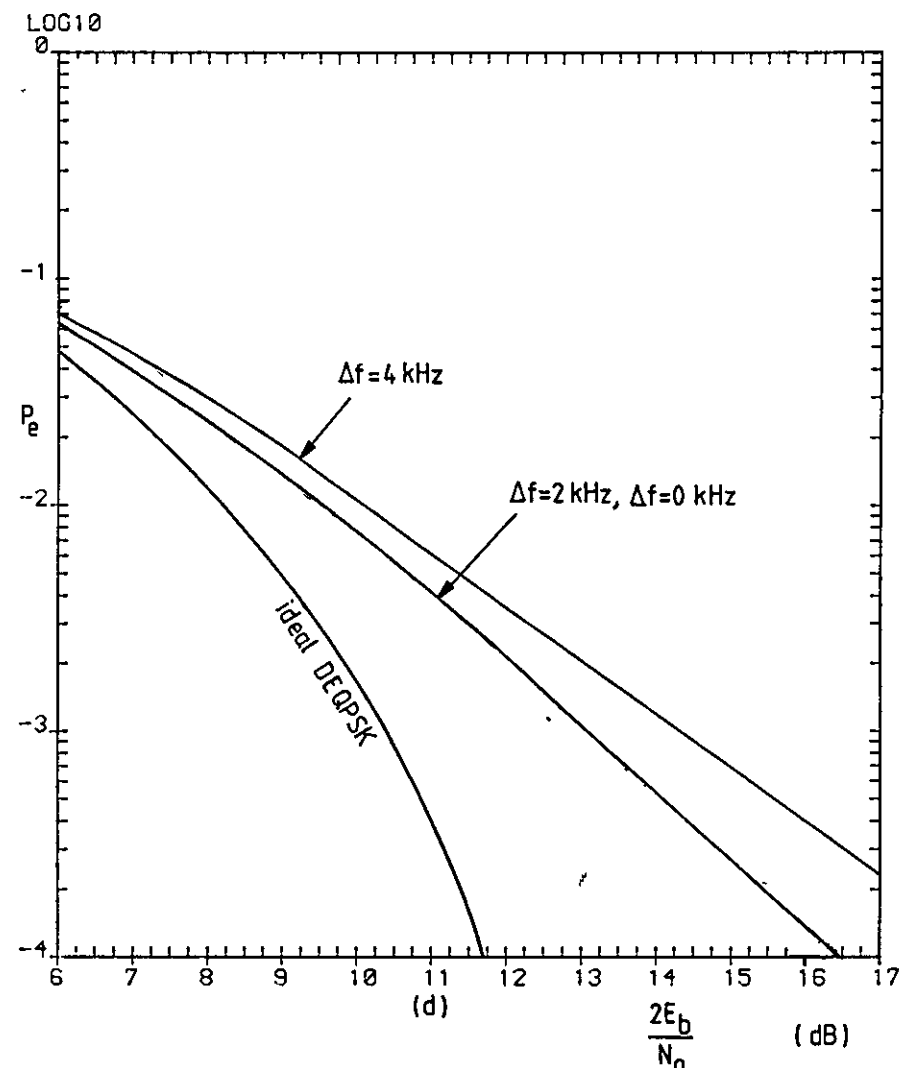
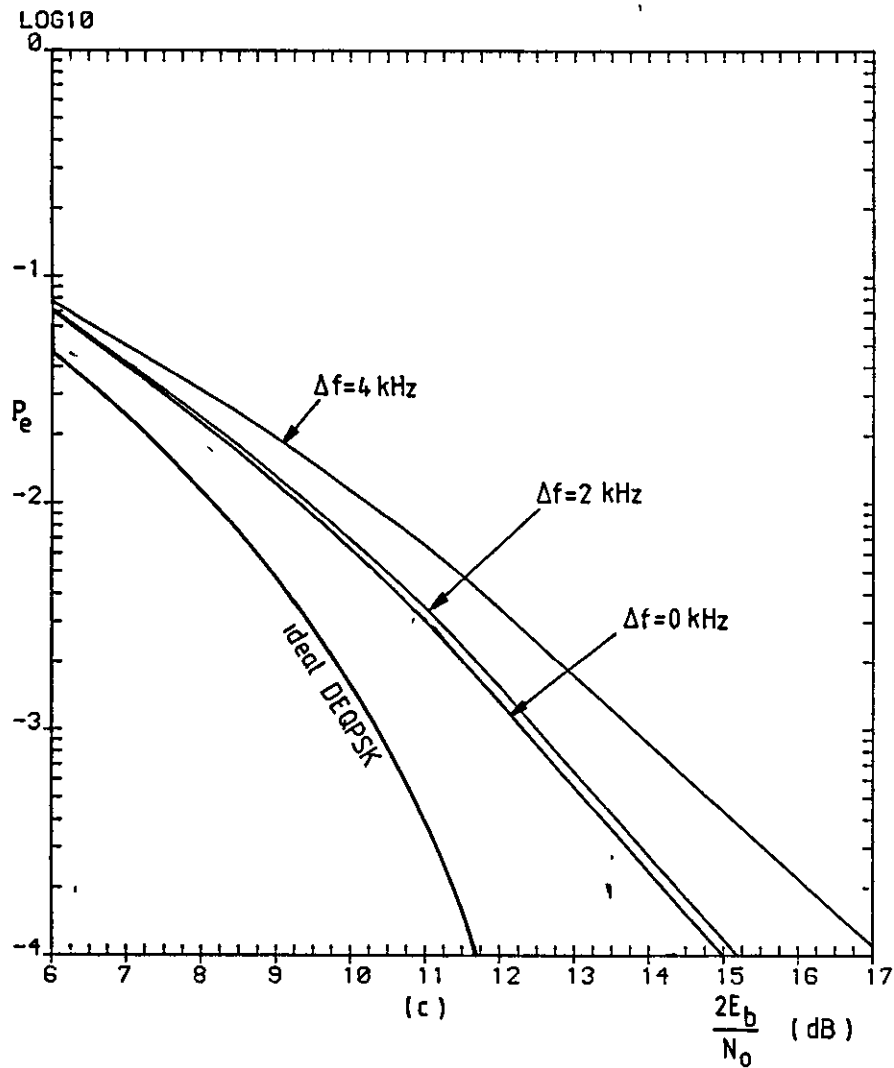


Figure 7.6

(continue).

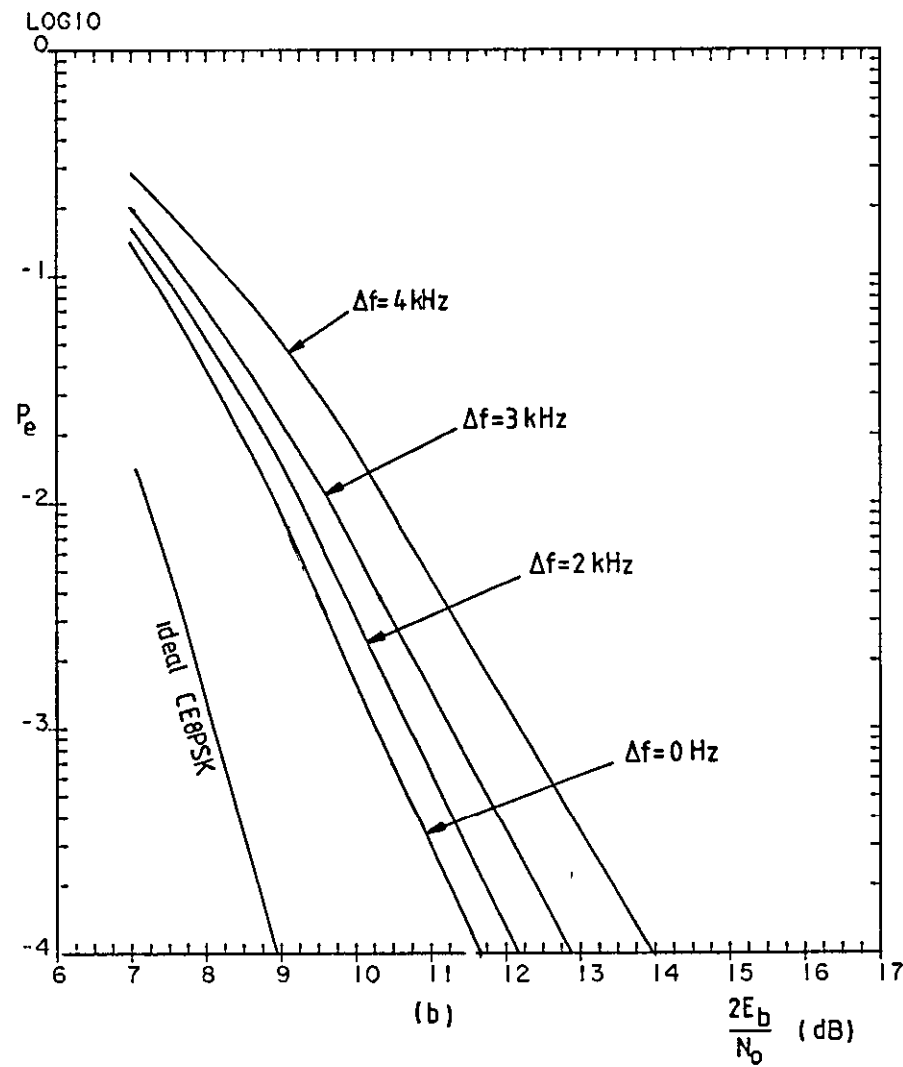
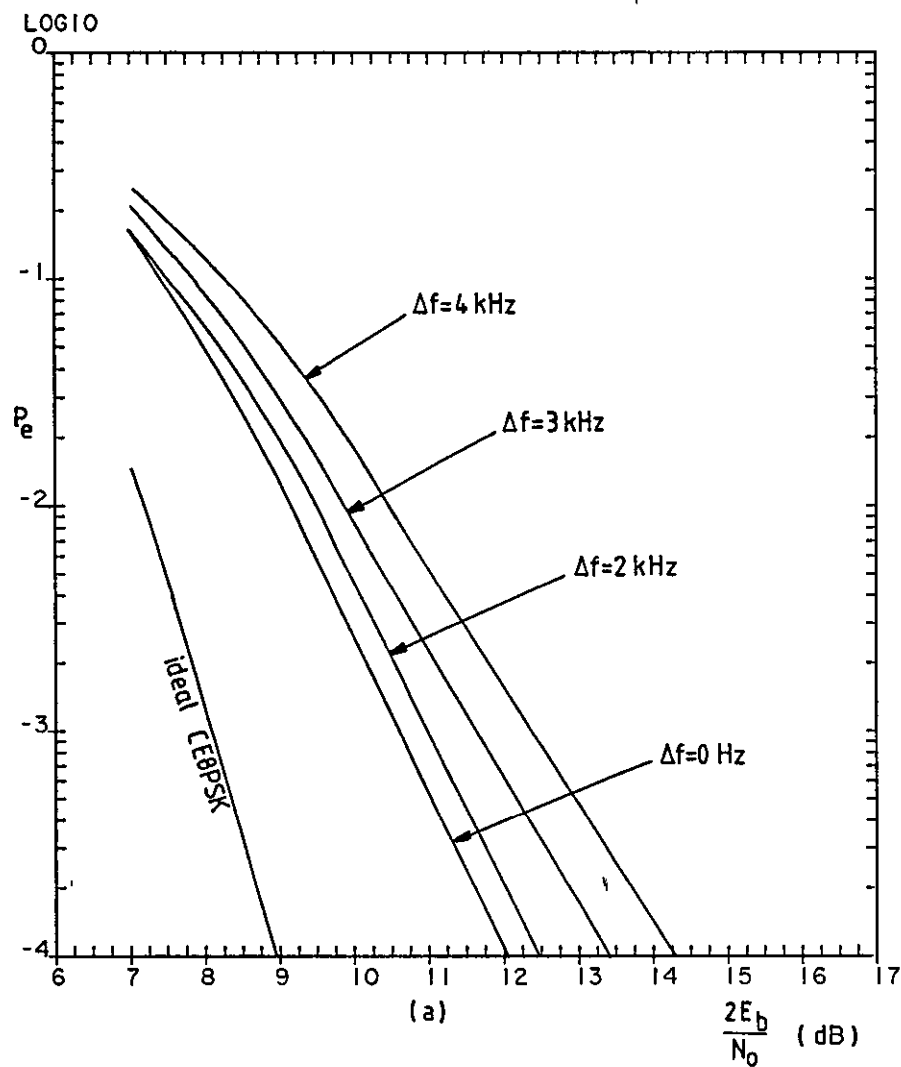


Figure 7.7 Error-rate performances of signals a) 1C, b) 2C, c) 3C and d) 4C, with different frequency offsets and with the use of the suboptimum filters, the predistorter, the HPA operating at 0.2 dB OBO, the amplifier limiter and phase demodulator B and in an ACI environment with $f_{ca} = 5R/4$ Hz.

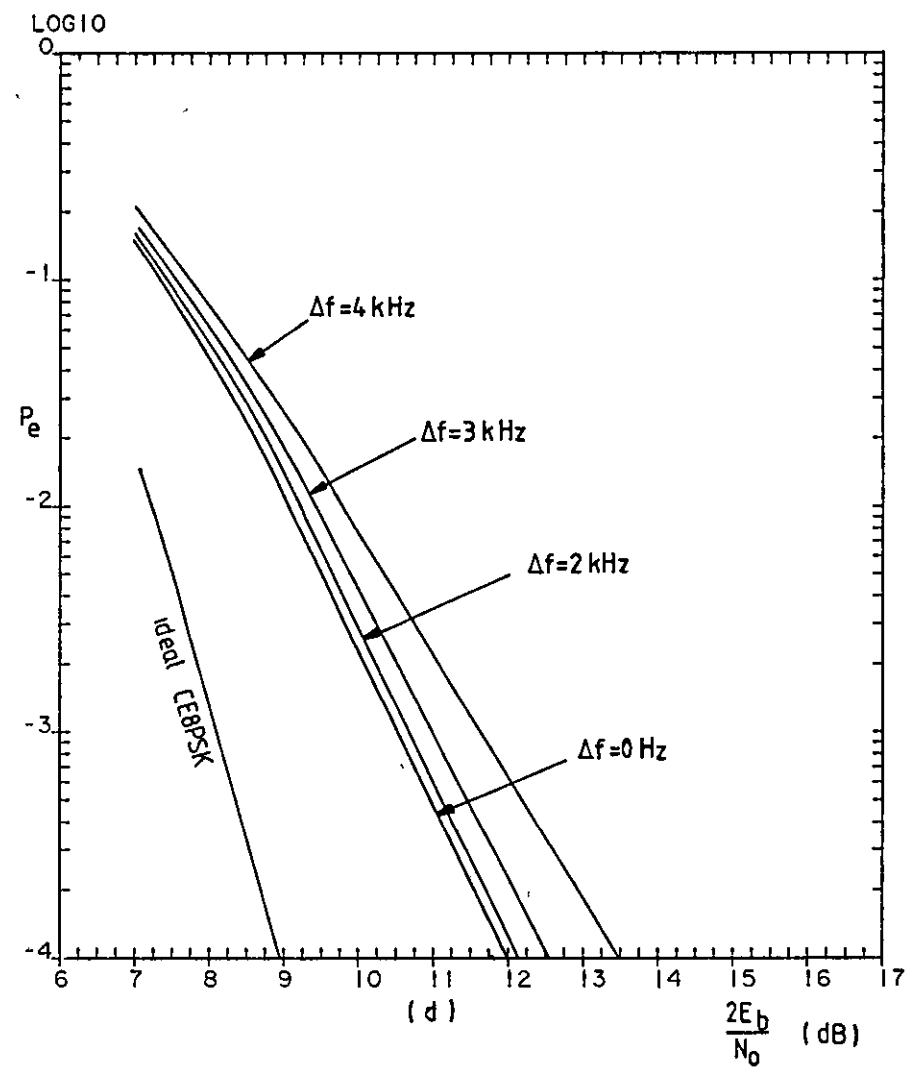
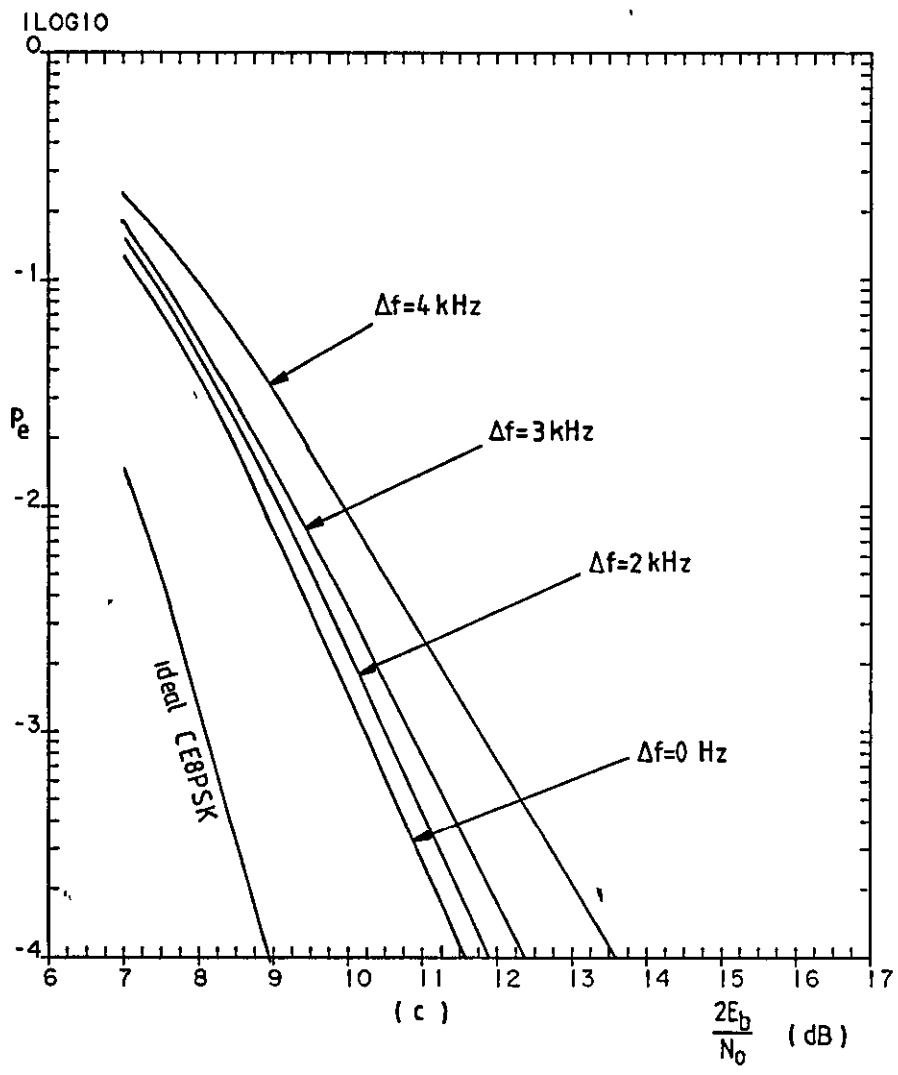


Figure 7.7 (continue).

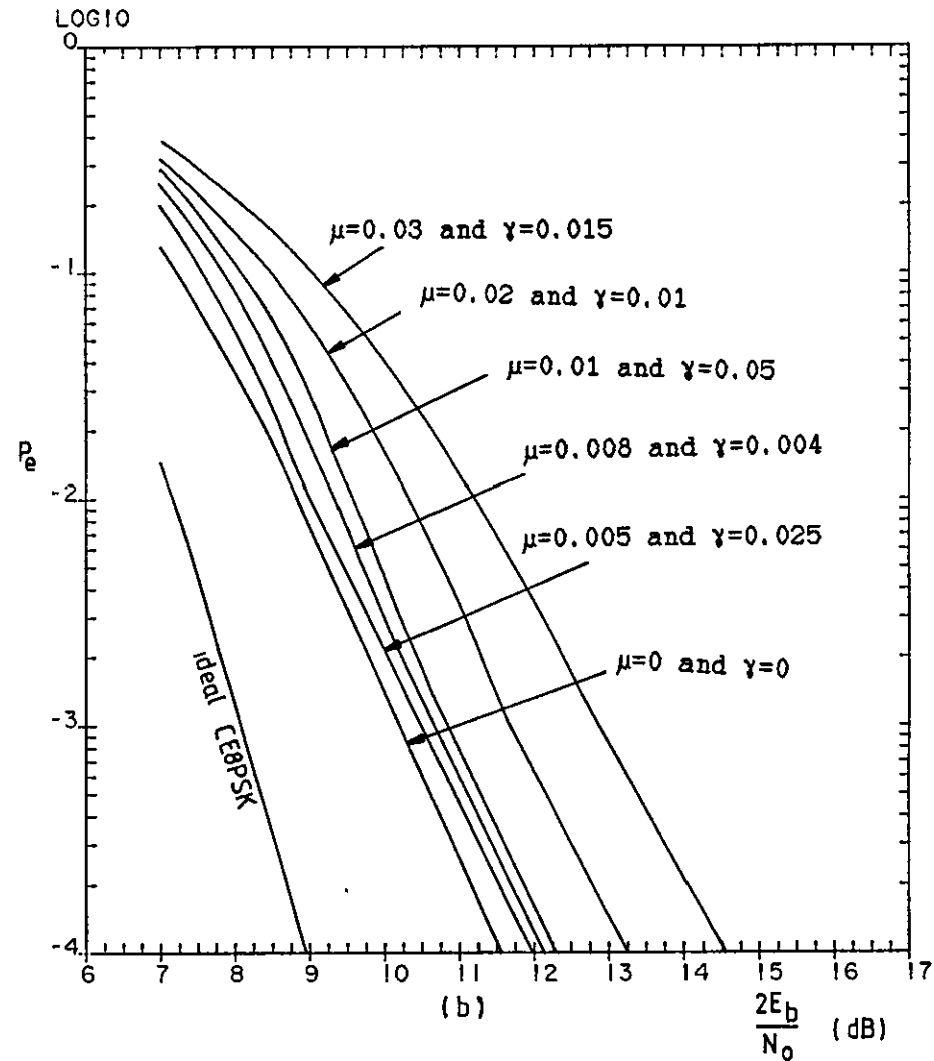
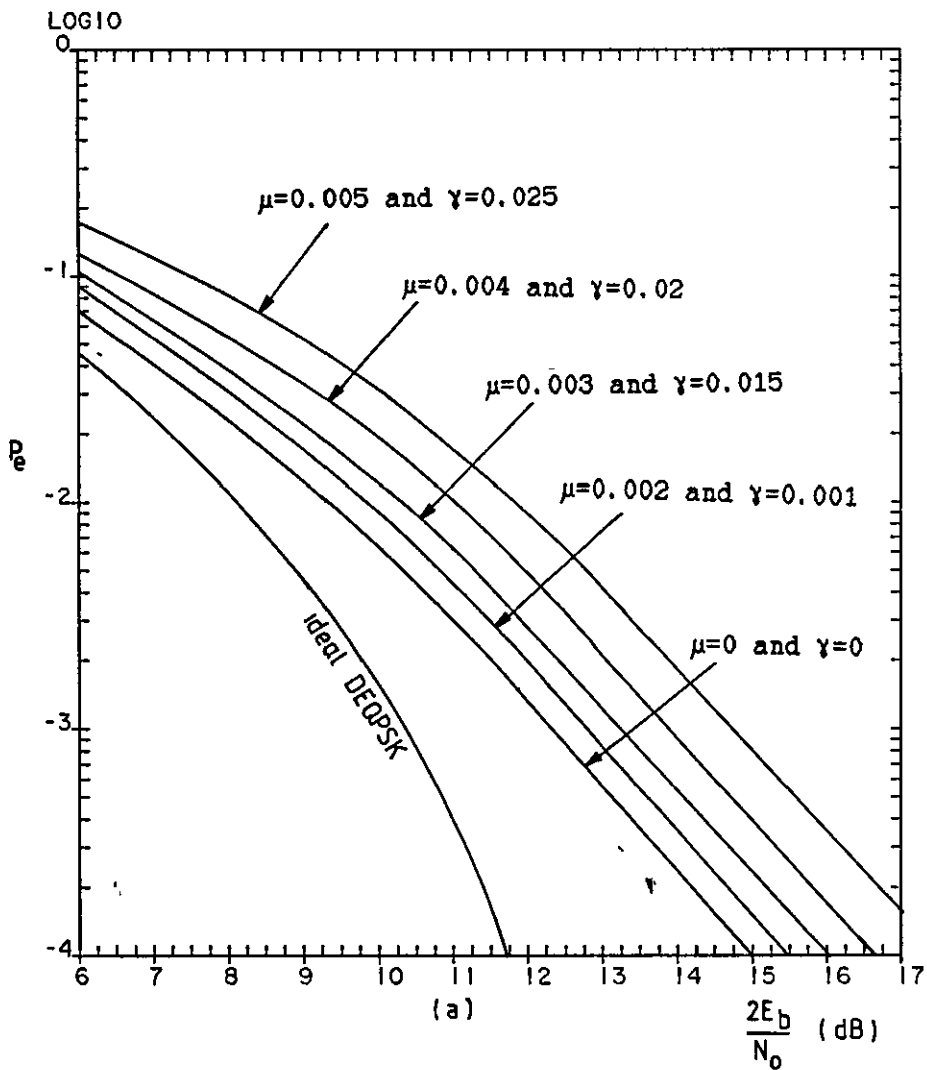


Figure 7.8 Error-rate performances of signals a) 3A and, b) 3C, with different values of μ and γ used in the MDFL and DDL, respectively, and with the use of the suboptimum filters, the predistorter, the HPA operating at 0.2 dB OBO, the amplifier limiter and phase demodulator B and in an ACI environment with $f_{c,ac} = 5R/4$ Hz.

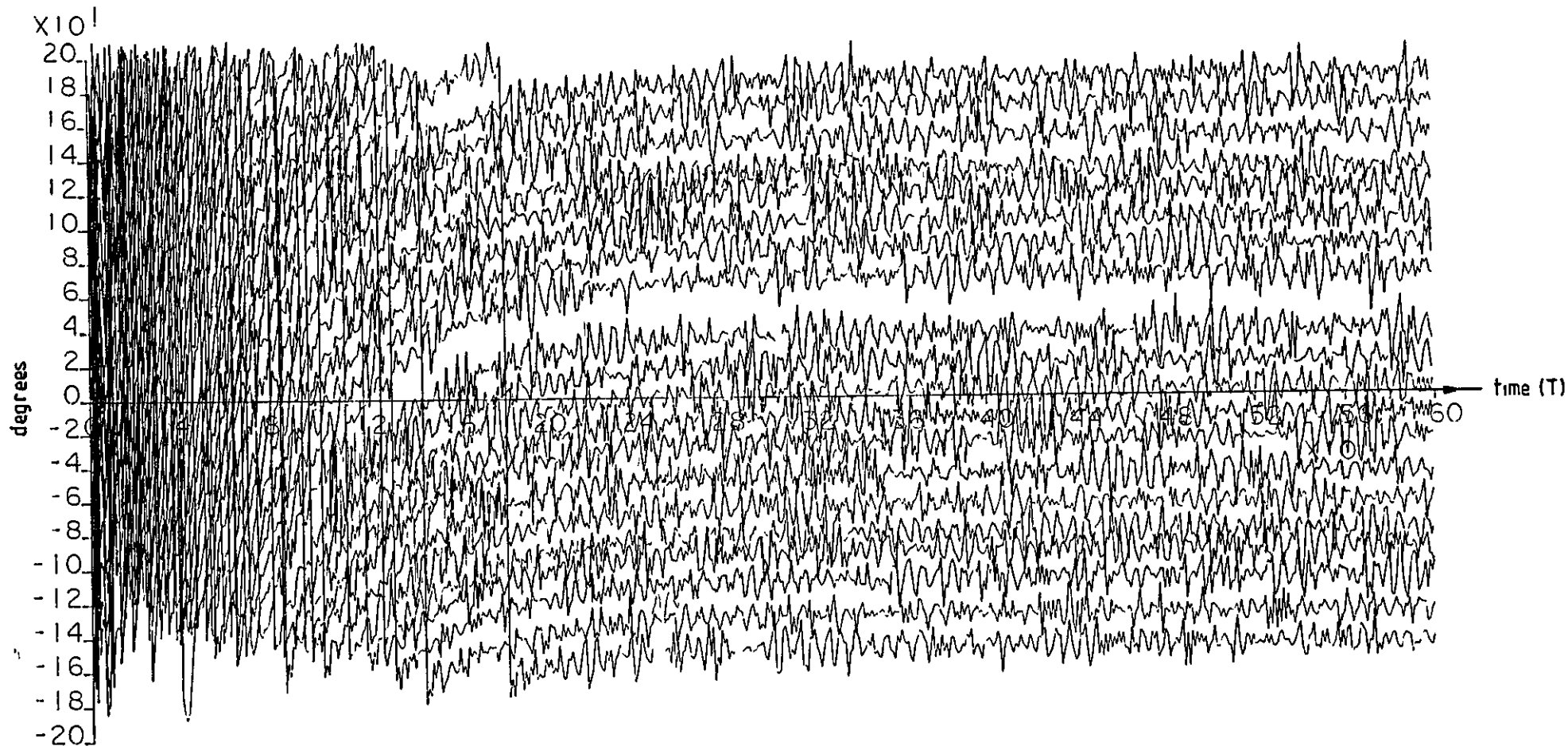


Figure 7.9 Results of twenty tests on the transient response of the extended-pull-in-limit method with $\mu=0.1$ and $\gamma=0.05$. The frequency offset is taken as 4 kHz and the initial phase error is uniformly distributed in the range $-\pi \leq \theta < \pi$. Signal 3A, at $2E_b/N_0=13$ dB, is used with the suboptimum filters, the predistorter, the HPA operating at 0.2 dB OBO, the amplifier limiter and phase demodulator B and in an ACI environment with $f_{ca}=5R/4$ Hz.

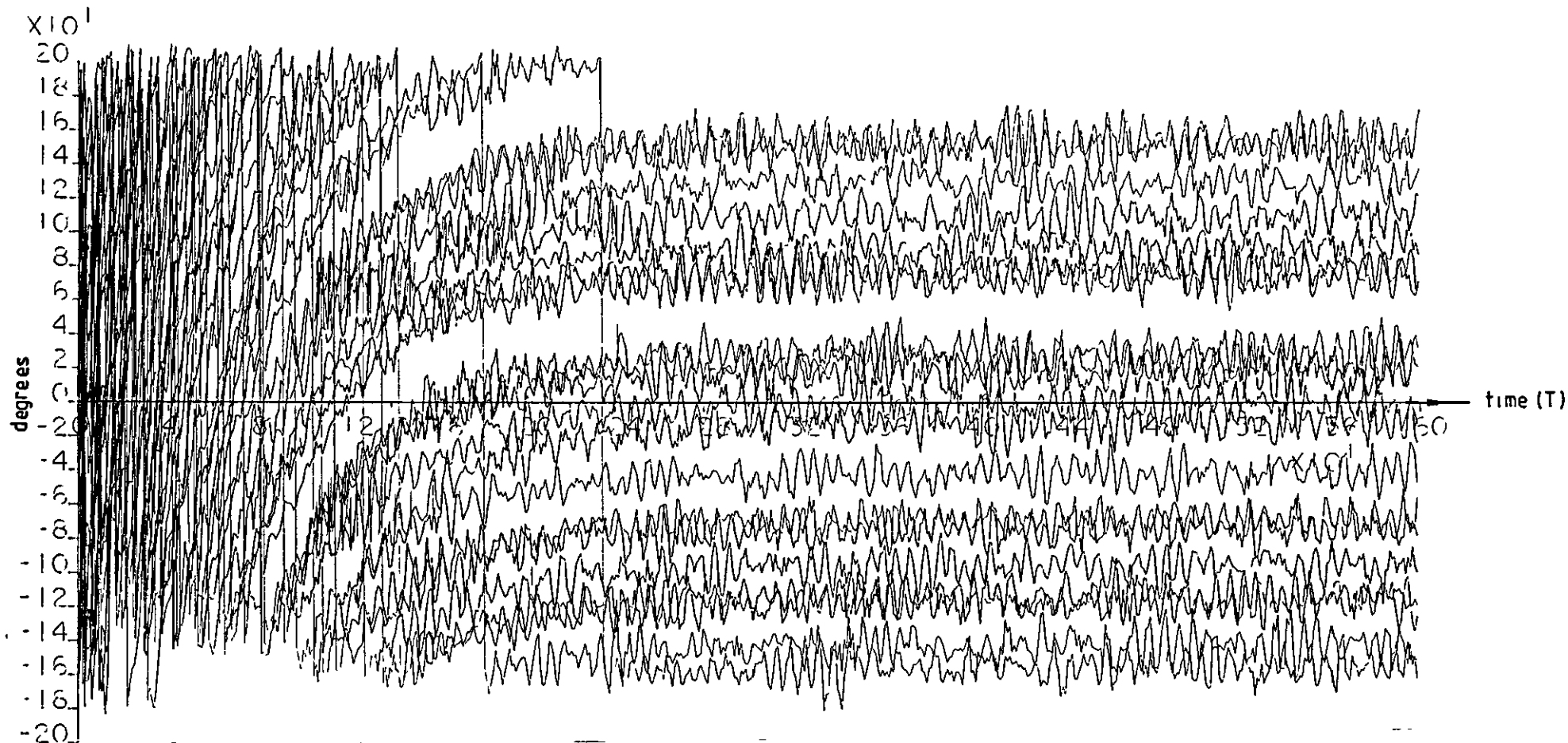


Figure 7.10 Results of twenty tests on the transient response of the extended-pull-in-limit method with $\mu=0.1$ and $\gamma=0.05$. The frequency offset is taken as 4 kHz and the initial phase error is uniformly distributed in the range $-\pi \leq \theta < \pi$. Signal 3C, at $2E_b/N_0=12.5$ dB, is used with the suboptimum filters, the predistorter, the HPA operating at 0.2 dB OBO, the amplifier limiter and phase demodulator B and in an ACI environment with $f_{ca}=5R/4$ Hz.

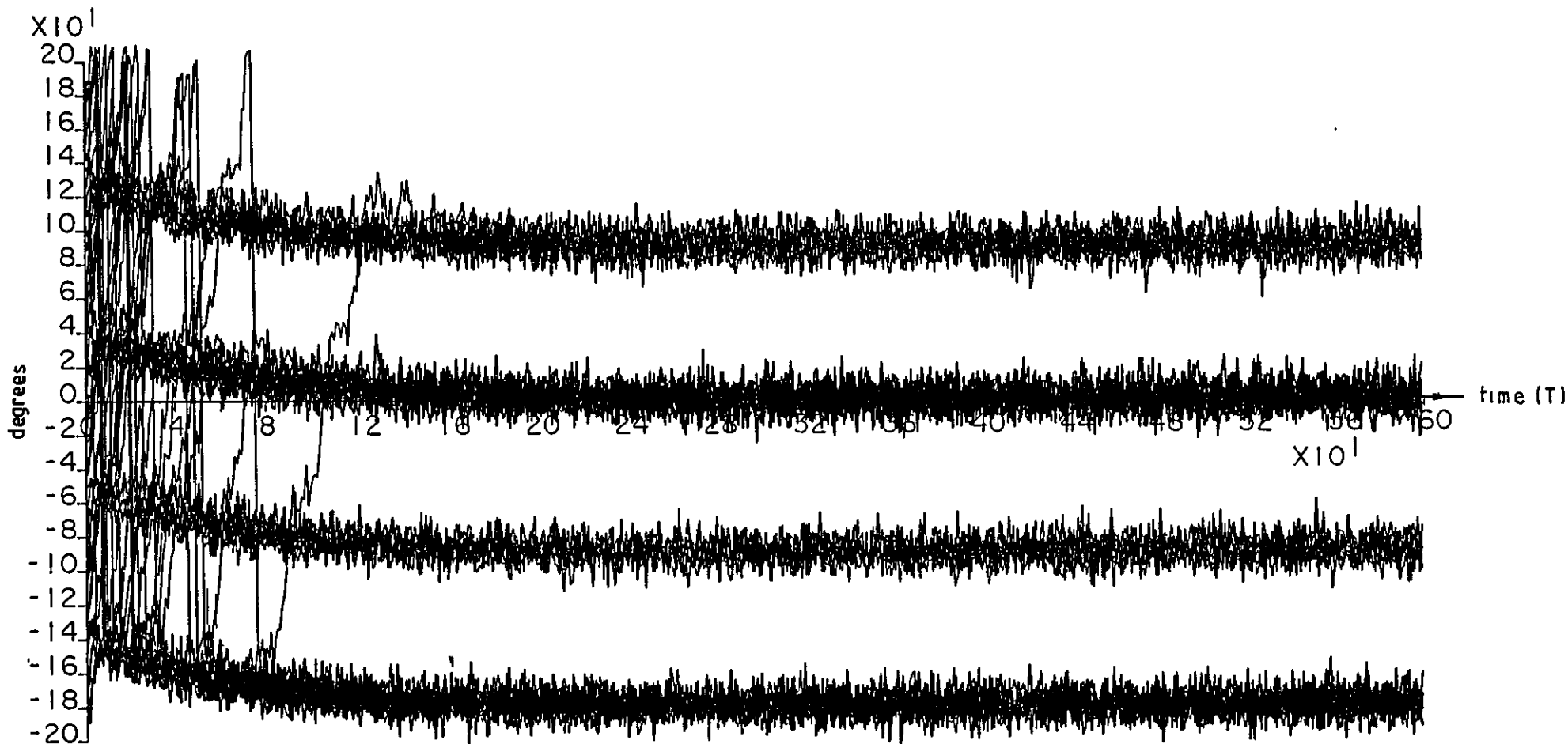


Figure 7.11 Results of fifty tests on the transient response of the MDFL with $\mu=0.03$ and $\gamma=0.015$. The frequency offset is taken as 700 Hz and the initial phase error is uniformly distributed in the range $-\pi \leq \theta < \pi$. Signal 3A, at $2E_b/N_0=13$ dB, is used with the suboptimum filters, the predistorter, the HPA operating at 0.2 dB OBO, the amplifier limiter and phase demodulator B and in an ACI environment with $f_{ca}=5R/4$ Hz.

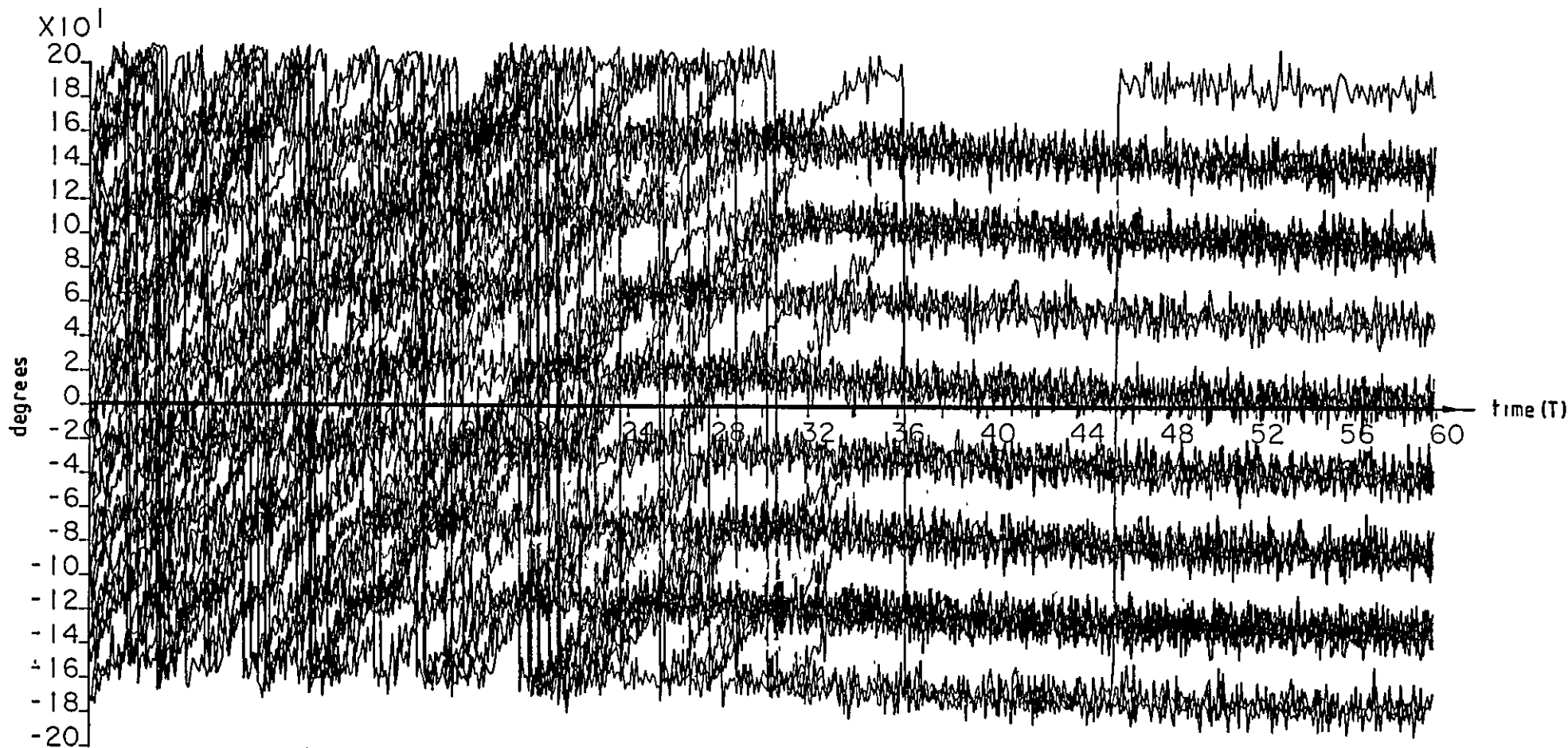


Figure 7.12 Results of fifty tests on the transient response of the DDL with $\mu=0.01$ and $\gamma=0.005$. The frequency offset is taken as 200 Hz and the initial phase error is uniformly distributed in the range $-\pi < \theta < \pi$. Signal 3C, at $2E_b/N_0=11$ dB, is used with the suboptimum filters, the predistorter, the HPA operating at 0.2 dB OBO, the amplifier limiter and phase demodulator B, and in an ACI environment with $f_{c_m}=5R/4$ Hz.

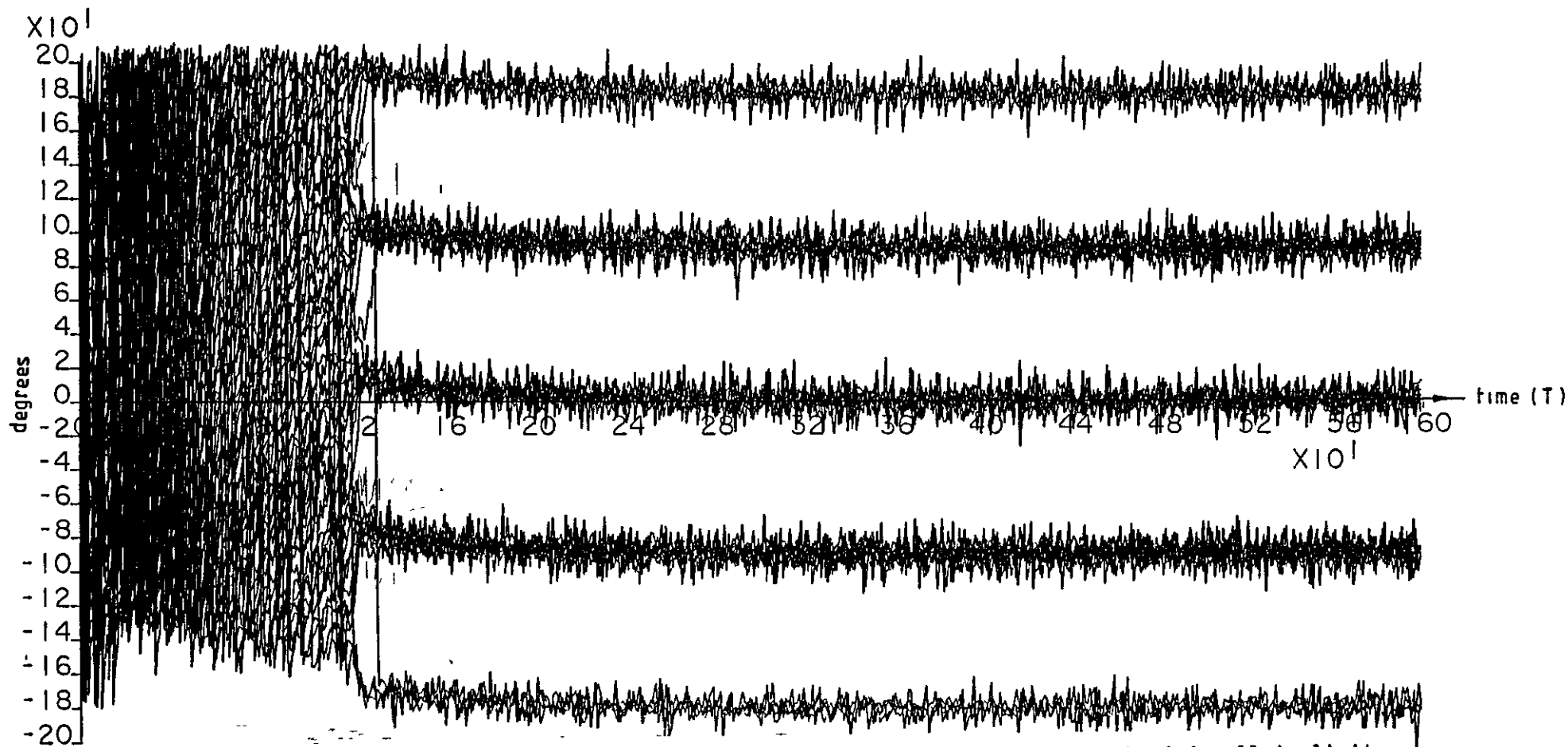


Figure 7.13 Results of fifty tests on the transient response of the extended-pull-in-limit method with $\mu=0.1$ and $\gamma=0.05$ and MDFL with $\mu=0.03$ and $\gamma=0.015$. The extended-pull-in-limit method is used at the beginning of transmission over 120 symbols before switching to the MDFL. The frequency offset is taken as 4 kHz and the initial phase error is uniformly distributed in the range $-\pi/8$ to $\pi/8$. Signal 3A, at $2E_b/N_0=13$ dB, is used with the suboptimum filters, the predistorter, the HPA operating at 0.2 dB OBO, the amplifier limiter and phase demodulator B and in an ACI environment with $f_{ca}=5R/4$ Hz.

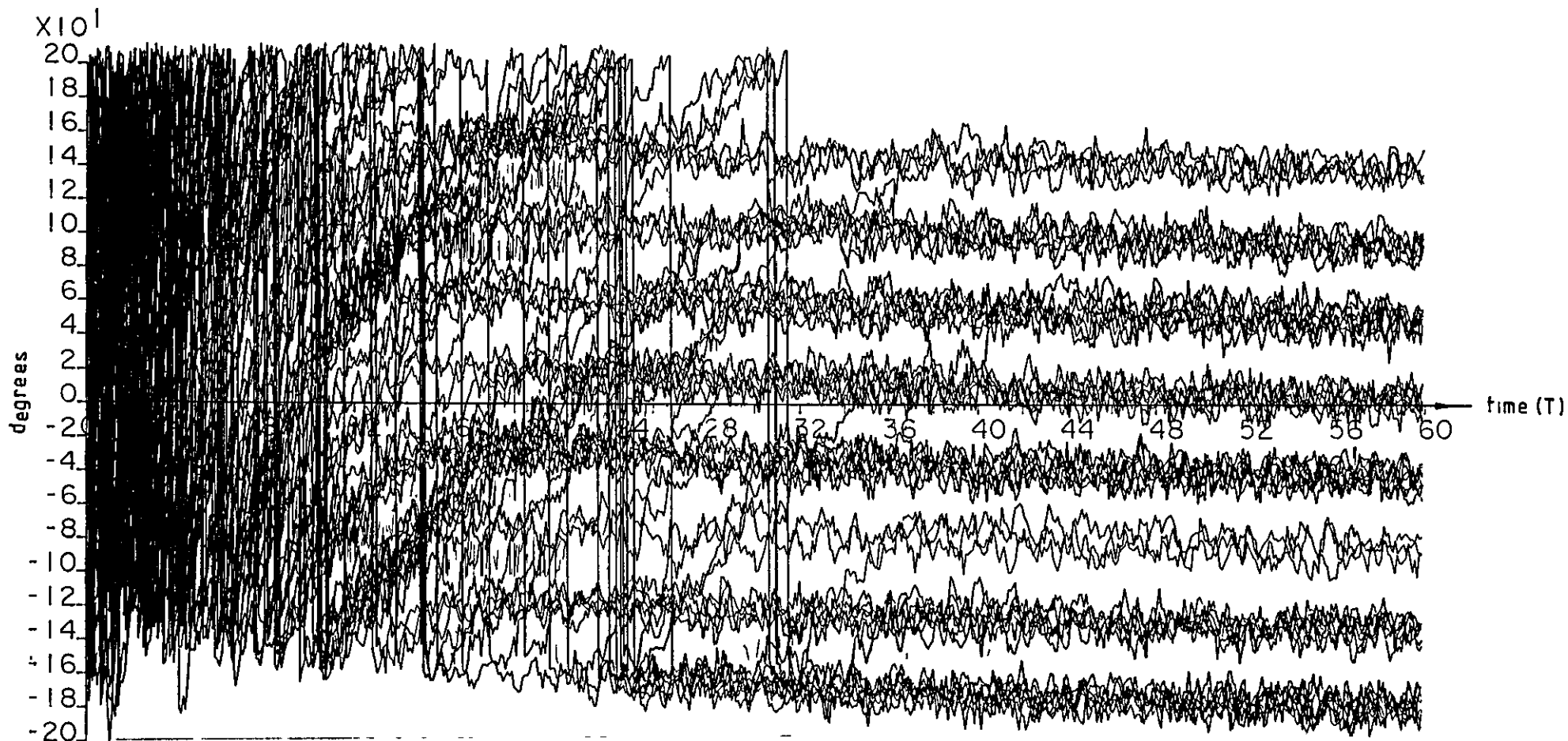


Figure 7.14 Results of fifty tests on the transient response of the extended-pull-in-limit method with $\mu=0.1$ and $\gamma=0.05$ and DDL with $\mu=0.01$ and $\gamma=0.005$. The extended-pull-in-limit method is used at the beginning of transmission over 160 symbols before switching to the DDL. The frequency offset is taken as 4 kHz and the initial phase error is uniformly distributed in the range $-\pi \leq \theta < \pi$. Signal 3C, at $2E_b/N_0=12.5$ dB, is used with the suboptimum filters, the predistorter, the HPA operating at 0.2 dB OBO, the amplifier limiter and phase demodulator B and in an ACI environment with $f_{c_{max}}=5R/4$ Hz.

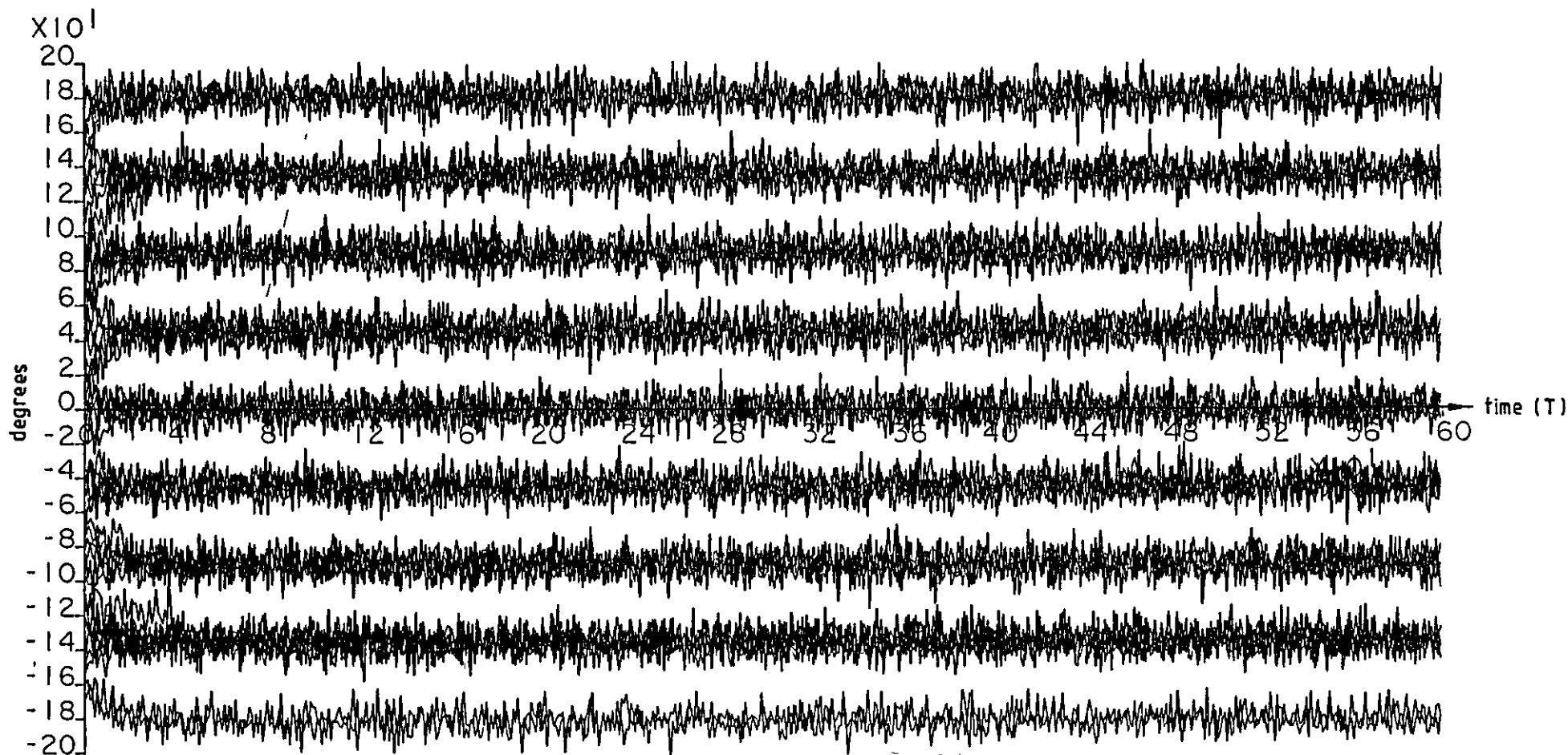


Figure 7.15 Results of fifty tests on the transient response of the MDFL with $\mu=0.03$ and $\gamma=0.015$. The frequency offset is taken as zero and the initial phase error is uniformly distributed in the range $-\pi \leq \theta \leq \pi$. Signal 3A, at $2E_b/N_0=13$ dB, is used with the suboptimum filters, the predistorter, the HPA operating at 0.2 dB OBO, the amplifier limiter and phase demodulator B and in an ACI environment with $f_{c_{\text{max}}}=5R/4$ Hz.

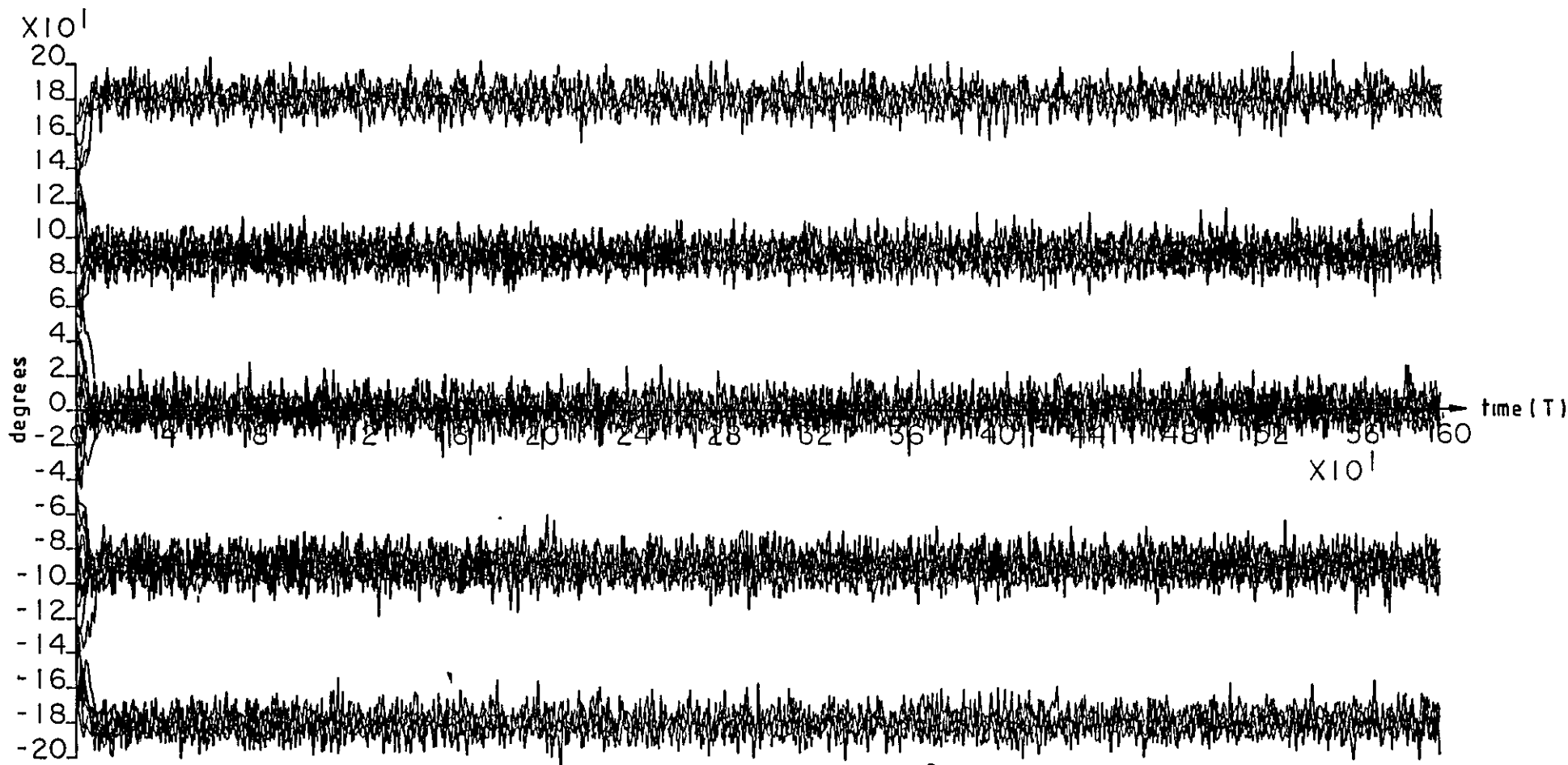


Figure 7.16 Results of fifty tests on the transient response of the DDL with $\mu=0.01$ and $\gamma=0.005$. The frequency offset is taken as zero and the initial phase error is uniformly distributed in the range $-\pi < \theta < \pi$. Signal 3C, at $2E_b/N_0=11$ dB, is used with the suboptimum filters, the predistorter, the HPA operating at 0.2 dB OBO, the amplifier limiter and phase demodulator B and in an ACI environment with $f_{c_m}=5R/4$ Hz.

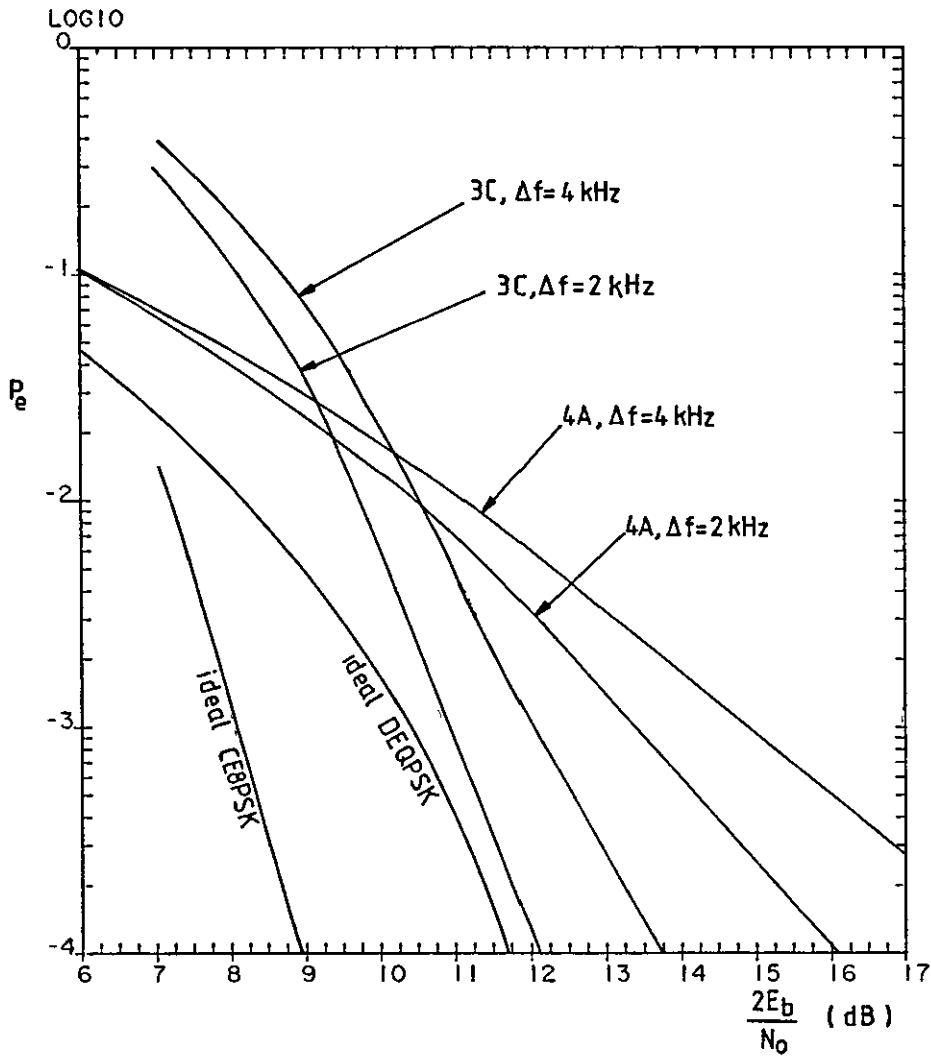


Figure 7.17 Error-rate performances of signals 3A and 3C, with $\mu=0.03$ and $\gamma=0.015$ in the MDPL and $\mu=0.01$ and $\gamma=0.005$ in the DDL, respectively. The frequency offset is taken as 2 or 4 kHz with the use of the suboptimum filters, the predistorter, the HPA operating at 0.2 dB OBO, the amplifier limiter and phase demodulator B and in an ACI environment with $f_{ca}=5R/4$ Hz.

CHAPTER 8

COMMENTS ON THE RESEARCH PROJECT

8.1 Possible further investigations

The thesis contains various results of data-transmission systems using DEQPSK, CE8PSK and CDE8PSK signals under different assumed conditions. The following is a list of the possible objectives worth further investigating

(1) An investigation into the feasibility of timing recovery, since the MDFL and DDL described in the thesis require the timing signal for operation.

(2) CDE8PSK signals require 512 costs for decoding each received symbol. Further investigation is worth studying to reduce the equipment complexity of the decoder.

(3) The baseband predistorter is found to be very promising for using with phase-shift keying signals which have a low-spectral efficiency. The predistortion technique, used with high-spectral efficient modulation techniques, e.g., 16-ary quadrature amplitude modulation technique, requires investigation.

(4) The baseband predistortion technique is based on the assumption that the characteristics of the HPA is known. Investigation of the technique into the hardware experiment requires to be studied.

(5) In the transmission systems described in the thesis, it is assumed that the TWTA on the satellite is operating in the linear mode. Further investigation is required to study the performance of the system if the TWTA is also operating in a nonlinear mode. This is essential for TDMA systems.

(6) In the thesis, the predistortion technique is used for a single nonlinearity. Predistortion of two nonlinearities in cascade is worth studying, as for the case described in (5).

(7) Although the decoder in Section 5.2.3 can be used to resolve the 8-fold ambiguity in recovering the reference carrier from CDE8PSK signals, it is only an suboptimum decoder. This is because the differential encoding at the transmitter is a feedback loop, so the decoder is not a true Viterbi decoder.

Having done the suboptimum, it is discovered that a true Viterbi decoder can be designed to resolve the 8-fold ambiguity in recovering the reference carrier from CE8PSK signals. Note that, since CE8PSK signals do not have a differential encoder (feedback loop) at the transmitter, a true Viterbi decoder is possible to be designed.

The true Viterbi-algorithm decoder for CE8PSK signals is described in Section 4.4, where the receiver is assumed to provide the required ideal carrier signal with a correct phase. This means that, at the receiver, the decoder assumes that the recovered carrier has the same phase as the received signal. If the recovered carrier has a wrong reference phase, the decoder is not able to decode the received signal, i.e., catastrophic failure results.

To resolve the 8-fold ambiguity, the decoder at the receiver has 8 similar Viterbi-algorithm decoders. Each of them is same as the one described in Section 4.4. They assume the reference carrier has a phase shift of $h\pi/4$, for $h=0, 1, 2, 3, 4, 5, 6$ and 7 . If the reference carrier has a phase shift of $\pi/4$, where $h=1, 2, 3, 4, 5, 6$ or 7 , one of the 8 Viterbi decoders will have the correct assumed phase and will be able to decode the received signal correctly.

A good starting up procedure at the beginning of a transmission is to set all $\{C_1\}$ to zero. After a few decoding operations, the Viterbi decoder with the assumed phase same as that of the received signal, will have the minimum values of $\{C_1\}$. Whereas the others will have very large values of $\{C_1\}$. If there is no sudden phase change during the transmission, only one of the 8 Viterbi decoders is used in decoding the received signal.

If there is a sudden phase shift of $h\pi/4$, where $h=1, 2, 3, 4, 5, 6$ or 7 occurred during the transmission, the rate of increase of C_1 will suddenly be very high. Thus the decoder can measure the rate of increase of C_1 to check whether a sudden phase shift has occurred. If it does occur, the decoder resets all (C_i) to zeros. Hence the one, with the assumed carrier phase same as the new phase of the received signal, will start in operation. This method has been developed and tested at Loughborough University, but further studied is required with CE8PSK signals.

8.2 Conclusions

Several shapes of modulating waveforms and different values of channel spacing have been tested for data-transmission systems, using DEQPSK and CE8PSK signals, over a nonlinear satellite channel and in an ACI environment. The results indicate that the most cost effective arrangement is to use signals 3A or 3B (depending upon whether a DEQPSK or a CE8PSK signal is used), with the HPA operating slightly below saturation and with the channel spacing of $5R/4$ Hz. Bandwidth and power efficiency cannot be improved by increasing the HPA OBO value or the channel spacing.

A method of predistorting the baseband signal has been described in the thesis, and the results of the tests show that a better bandwidth and power efficiency can be achieved by using the baseband predistorter. The results of the the investigation indicate that, with the use of the predistorter, the most cost effective arrangement is signals 4A or 4B (depending upon whether a DEQPSK or CE8PSK signal is used), with the HPA operating slightly below saturation and with the channel spacing of $4.5R/4$ Hz.

Several different distance measures have been developed to reduce the equipment complexity of the decoder for CE8PSK signals. The distance measure D is considered to be the most promising one. The results show that, when using the distance measure D for decoding the CE8PSK signals, the degradation is only about 0.5 dB at $P_e=10^{-4}$, relative to the unitary distance measure.

The catastrophic failure of CE8PSK signals, caused by a wrong reference carrier phase recovered at the receiver, has been prevented by using a differential encoding technique which has been described in the thesis. The penalty for this is about 0.7 dB at $P_e=10^{-4}$.

Slicing and phase demodulation is considered to be a viable technique for reduction in equipment complexity of the modem. This has been investigated in the thesis. The results are very promising. Two phase

demodulators have been developed for use after the amplifier limiting process. They are phase demodulators A and B. These two phase demodulators have similar performances. The results of the investigation show that, with the uses of the predistorter, amplifier limiter, phase demodulator A or B, the most cost effective arrangement is to use signal 3A, 3B or 3C (depending upon whether a DEQPSK, CB8PSK or CDE8PSK signal is used), with the HPA operating slightly below saturation and with the channel spacing of $5R/4$ Hz.

Finally, two data-aided loops for recovering a reference carrier in the DEQPSK and CDE8PSK systems have been developed. They are the MDFL and DDL. These two loops have limited pull-in-limits, so that a method to extend the pull-in limits of these two loops, using a training sequence at the beginning of transmission, has been designed to enable the loops to track a frequency offset of up to $13R/32$ Hz. In the presence of frequency offset, the most cost effective signal is signals 3A or 3C, depending upon whether a DEQPSK or CDE8PSK signal is used. The signal can tolerate frequency offsets of up to $4R/32$ Hz, with a degradation of about 2 dB, at $P_e=10^{-4}$, relative to the case with no frequency offset. The results also show that, with the use of the designed carrier recovery loops, Signal 3C is much better than signal 3A.

Appendix A1

MATCHED-FILTER DETECTION I 11

Consider an arbitrary signal waveform $s(t)$, with a duration of T seconds, such that $s(t)$ is zero for $t > 0$ and $t < T$. This signal waveform is received in the presence of AWGN (additive white Gaussian noise) $w(t)$ having zero means and a two-sided power spectral density $\frac{1}{2}N_0$ over all positive and negative frequencies. Thus the received signal is

$$r(t) = s(t) + w(t) \quad \text{A1.1}$$

The received signal $r(t)$ is fed to a linear filter whose transfer function is $H(f)$ and impulse response $h(t)$. The signal and noise waveforms at the filter output are $s_0(t)$ and $w_0(t)$, respectively, as shown in Fig. A1.1.

The problem is to determine the filter characteristics which maximise the signal/noise power ratio at the output of the linear filter at time $t=T$.

The output signal/noise power at time $t=T$ is

$$\text{SNR}_0 = \frac{s_0^2(T)}{E[w_0^2(T)]} \quad \text{A1.2}$$

where, this is, of course, the ratio of the instantaneous signal power to the expected noise power.

If the spectrum (Fourier transform) of $s(t)$ is $G(f)$, then

$$G(f) = \int_{-\infty}^{\infty} s(t)\exp(-j2\pi ft)dt \quad \text{A1.3}$$

and

$$s(t) = \int_{-\infty}^{\infty} G(f)\exp(j2\pi ft)df \quad \text{A1.4}$$

where f is the frequency in Hz and $j = \sqrt{-1}$.

The spectrum of $s_o(t)$ is $G(f)H(f)$, and

$$s_o(t) = \int_{-\infty}^{\infty} G(f)H(f)\exp(j2\pi ft)df \quad A1.5$$

The magnitude of the output signal $s_o(t)$ at time $t=T$ is

$$|s_o(T)|^2 = \left| \int_{-\infty}^{\infty} G(f)H(f)\exp(-j2\pi fT)df \right|^2 \quad A1.6$$

The power spectral density of $w_o(t)$ is

$$\frac{1}{2}N_o |H(f)|^2$$

and the expected power level of $w_o(t)$ is

$$N = \frac{1}{2}N_o \int_{-\infty}^{\infty} |H(f)|^2 df \quad A1.7$$

Thus the ratio of instantaneous signal power to expected noise power, at the output of the linear filter at time $t=T$ seconds, is

$$SNR_o = \frac{\left| \int_{-\infty}^{\infty} H(f)G(f)\exp(j2\pi fT)df \right|^2}{\frac{1}{2}N_o \int_{-\infty}^{\infty} |H(f)|^2 df} \quad A1.8$$

By the Schwartz Inequality [2]

$$\left| \int_{-\infty}^{\infty} U(f)V(f)df \right|^2 \leq \int_{-\infty}^{\infty} |U(f)|^2 df \int_{-\infty}^{\infty} |V(f)|^2 df \quad A1.9$$

where $U(f)$ and $V(f)$ may be any finite complex functions of f .

Equality holds in Eqn. A1.9 when

$$U(f) = cV^*(f) \quad A1.10$$

for any real constant c . $V^*(f)$ is the complex conjugate of $V(f)$.

In Eqn. A1.9 substitute $H(f)$ for $U(f)$ and $G(f)\exp(j2\pi fT)$ for $V(f)$, so that

$$\begin{aligned} \left| \int_{-\infty}^{\infty} H(f)G(f)\exp(j2\pi fT)df \right|^2 &\leq \int_{-\infty}^{\infty} |H(f)|^2 df \int_{-\infty}^{\infty} |G(f)\exp(j2\pi fT)|^2 df \\ &= \int_{-\infty}^{\infty} |H(f)|^2 df \int_{-\infty}^{\infty} |G(f)|^2 df \end{aligned} \quad \text{A1.11}$$

From Eqn. A1.8 and A1.11, the maximum of signal/noise power is given by

$$\text{SNR}_{O(\text{max})} = \frac{\int_{-\infty}^{\infty} |H(f)|^2 df \int_{-\infty}^{\infty} |G(f)|^2 df}{\frac{1}{2}N_0 \int_{-\infty}^{\infty} |H(f)|^2 df} \quad \text{A1.12}$$

$$= \frac{1}{\frac{1}{2}N_0} \int_{-\infty}^{\infty} |G(f)|^2 df \quad \text{A1.13}$$

From Parseval's theorem [2],

$$\int_{-\infty}^{\infty} |G(f)|^2 df = \int_{-\infty}^{\infty} s^2(t) dt = E \quad \text{A1.14}$$

where E is the total signal energy of the signal waveform $s(t)$.

Thus
$$\text{SNR}_{O(\text{max})} = \frac{E}{\frac{1}{2}N_0} \quad \text{A1.15}$$

From Eqn. A1.10, the signal/noise power ratio has its maximum value when

$$\begin{aligned} H(f) &= c[G(f)\exp(j2\pi fT)]^* \\ &= cG^*(f)\exp(-j2\pi fT) \\ &= cG(-f)\exp(-j2\pi fT) \end{aligned} \quad \text{A1.16}$$

$$\begin{aligned}
 \text{and} \quad h(t) &= \int_{-\infty}^{\infty} H(f) \exp(j2\pi ft) df \\
 &= c \int_{-\infty}^{\infty} G(-f) \exp[-j2\pi f(T-t)] df \\
 &= cs(T-t)
 \end{aligned} \tag{A1.17}$$

$$\text{so that} \quad H(f) = cG^*(f) \exp(-j2\pi fT) \tag{A1.18}$$

$$h(t) = cs(T-t) \tag{A1.19}$$

From Eqns. A1.13 and A1.18, the signal power at the output of the linear filter at $t=T$, under the assumed conditions of $SNR_{o(max)}$, is

$$\begin{aligned}
 \int_{-\infty}^{\infty} |H(f)|^2 df \int_{-\infty}^{\infty} |G(f)|^2 df &= c^2 \int_{-\infty}^{\infty} |G(f)|^2 df \int_{-\infty}^{\infty} |G(f)|^2 df \\
 &= c^2 E^2
 \end{aligned} \tag{A1.20}$$

Also the average noise power at the output of the linear filter is

$$N = \int_{-\infty}^{\infty} \frac{1}{2} N_o |H(f)|^2 df = \frac{1}{2} N_o c^2 \int_{-\infty}^{\infty} |G(f)|^2 df = \frac{1}{2} N_o c^2 E \tag{A1.21}$$

The filter satisfying Eqns. A1.18 and A1.19 is said to be matched to the received signal $s(t)$ and is known as a matched filter [3],[4].

Since $s(t)=0$, for $t < 0$ and $t > T$,

then $h(t)=0$, for $t < 0$ and $t > T$.

so that $h(t)$ is physically realisable.

Suppose now that the received signal is $ks(t)$ where $s(t)$ is known at the receiver but k is an unknown real number, whose value it is required to estimate as accurately as possible at the receiver. If the signal $ks(t)$ is fed to the matched filter given by Eqn. A1.19, then in the absence of

noise, the output signal at time $t=T$ is the convolution of $ks(t)$ and $h(t)$, and is

$$\begin{aligned} \int_{-\infty}^{\infty} ks(t)h(T-t)dt &= \int_0^T ks(t)h(T-t)dt \\ &= \int_0^T ks(t)cs(t)dt \\ &= kc \int_0^T s^2(t)dt \\ &= kcE \end{aligned} \tag{A1.22}$$

from Eqns. A1.14 and A1.19. E is the energy of $s(t)$, not of $ks(t)$.

When $ks(t)$ is received in the presence of AWGN $w(t)$, the input signal to the matched filter becomes

$$r(t) = ks(t) + w(t) \tag{A1.23}$$

and the output signal from the matched filter at time $t=T$ is now

$$\begin{aligned} r_o(t) &= \int_0^T r(t)h(T-t)dt = \int_0^T [ks(t)+w(t)]cs(t)dt \\ &= kc \int_0^T s^2(t)dt + c \int_0^T w(t)s(t)dt \\ &= kcE + w_o \end{aligned} \tag{A1.24}$$

where $w_o = c \int_0^T w(t)s(t)dt$ A1.25

w_o is a sample value of a Gaussian random variable with zero mean.

Equation A1.24 shows that

$$r_o = c \int_0^T r(t)s(t)dt \tag{A1.26}$$

so that r_o could alternatively be obtained by multiplying $r(t)$ by $cs(t)$

and integrating the product over the time interval 0 to T. This operation is performed by the appropriate correlation receiver, which is therefore equivalent to the matched filter.

In order to estimate k, assuming a prior knowledge of c and E at the receiver, r_o is multiplied by $1/cE$ to give

$$\frac{r_o}{cE} = k + \frac{w_o}{cE} \tag{A1.27}$$

r_o/cE is the estimate of k given by the matched filter. w_o/cE is the error in this estimate and is introduced by the Gaussian noise. The matched filter maximises the ratio of instantaneous signal power to average noise power in the estimate of k.

Suppose now that k is equally likely to have one of two values k_1 and k_2 , where $k_2 > k_1$, and where k_1 and k_2 are both known at the receiver. $ks(t)$ is here a binary signal element.

It can be seen from Eqn. A1.27 that in the absence of noise

$$\frac{r_o}{cE} = k \quad \text{where } k = k_1 \text{ or } k_2 \tag{A1.28}$$

so that k is now given exactly by the value of r_o/cE . However, when $ks(t)$ is received together with the noise waveform $w(t)$, r_o/cE will not normally have the correct value k_1 or k_2 .

To detect the value of k with the minimum probability of error, r_o/cE is now compared with a threshold level of $\frac{1}{2}(k_1+k_2)$, which lies half way between k_1 and k_2 .

When $r_o < \frac{1}{2}cE(k_1+k_2)$, k is detected as k_1 ,
 and when $r_o > \frac{1}{2}cE(k_1+k_2)$, k is detected as k_2 .

It can be shown that this arrangement minimizes the probability of error under the assumed conditions [5].

The probability of error in a detection process may be determined as follows. From Eqn. A1.24

$$r_o = kcE + w_o$$

where
$$w_o = c \int_0^T w(t)s(t)dt \quad A1.29$$

From Eqn. A1.21, w_o is sample value of a Gaussian random variable with zero mean and variance

$$\eta^2 = \frac{1}{2}N_o c^2 E \quad A1.30$$

Thus
$$r_o/cE = k + w_o/cE \quad A1.31$$

where w_o/cE is a sample value of a Gaussian random variable with zero mean and variance

$$\sigma^2 = \eta^2/c^2 E^2 = \frac{1}{2}N_o/E \quad A1.32$$

When k_1 is received, k is wrongly detected if

$$r_o/cE > \frac{1}{2}(k_1 + k_2)$$

or
$$w_o/cE > d$$

where
$$d = \frac{1}{2}(k_1 + k_2) \quad A1.33$$

so that the probability of error is

$$\begin{aligned} P_{e1} &= \int_d^\infty \frac{1}{\sqrt{2\pi\sigma^2}} \exp\left(-\frac{w^2}{2\sigma^2}\right) dw = \int_{d/\sigma}^\infty \frac{1}{\sqrt{2\pi}} \exp\left(-\frac{w^2}{2}\right) dw \\ &= Q\left(\frac{d}{\sigma}\right) \end{aligned} \quad A1.34$$

where
$$Q(y) = \int_y^\infty \frac{1}{\sqrt{2\pi}} \exp\left(-\frac{w^2}{2}\right) dw \quad A1.35$$

is called the Q-function.

When k_2 is received, k is wrongly detected if

$$r_o/cE < \frac{1}{2}(k_1 + k_2)$$

or

$$w_o/cE < -d$$

so that the probability of error is

$$\begin{aligned} P_{e2} &= \int_{-\infty}^{-d} \frac{1}{\sqrt{2\pi\sigma^2}} \exp\left(\frac{-w^2}{2\sigma^2}\right) dw = \int_d^{\infty} \frac{1}{\sqrt{2\pi\sigma^2}} \exp\left(\frac{-w^2}{2\sigma^2}\right) dw \\ &= Q\left(\frac{d}{\sigma}\right) \end{aligned} \quad \text{A1.36}$$

Clearly, the probability of error is the same, whether k_1 or k_2 is received, and is

$$P_e = P_{e1} = P_{e2} = Q\left(\frac{d}{\sigma}\right) = Q\left(\frac{d}{\sqrt{\frac{1}{2}N_o/E}}\right) = Q\left(\sqrt{\frac{d^2 E}{\frac{1}{2}N_o}}\right) \quad \text{A1.37}$$

It can be seen from Eqn. A1.37 that the error probability is independent of the shape of the signal waveform, and is dependent only on d , E and N_o .

It has been shown that the matched filter maximizes the signal/noise power at its output, so that for given values of k_1 and k_2 and therefore for a given value of d , it minimizes the average noise power at its output.

In a situation such as that considered here, where the wanted signal k is equally likely to have one of two values k_1 and k_2 , and is received in the presence of a zero-mean Gaussian random variable, the detection process that minimizes the probability of error compares the received signal (in this case $r_o/cE = k + w_o/cE$) with a threshold level half way between the two possible values k_1 and k_2 of the wanted signal. The wanted signal k is now detected as k_1 or k_2 depending upon whether the received signal lies below or above the threshold, that is depending upon whether the received signal is nearer to k_1 or k_2 , respectively.

The combination of the matched filter and the following detection process in which the output from the matched filter is compared with the appropriate threshold level, is an arrangement of matched filter detection. This is the optimum detection process for the wanted signal, under the assumed conditions, and it minimizes the probability of error in a detection process.

The average energy of the two waveforms $k_1s(t)$ and $k_2s(t)$ is

$$\frac{1}{2}(k_1 + k_2)^2E = \frac{1}{2}(k_1 - k_2)^2E + \frac{1}{2}(k_1 + k_2)^2E \quad A1.38$$

where E is the energy of $s(t)$. For any given values of k_1 , $-k_2$ and E , the average of the two signal waveforms has a minimum value of d^2E when $k_1 = k_2 = -d$. But from Eqn. A1.37, the probability of error is dependent only on d , E and N_0 , so that for a given probability of error and given values of d , and E , the average signal/noise power ratio at the input to the matched-filter has its minimum value when $k_1 = -k_2 = -d$. In other words, the tolerance to AWGN is maximized under these conditions.

When $k_1 = -d$ and $k_2 = d$

the optimum decision threshold is zero, so that k is detected as k_1 when $r_0 < 0$, and k is detected as k_2 when $r_0 > 0$.

The probability of error in the detection of k is now

$$Q\left(\frac{d}{\sigma}\right) = Q\left(\sqrt{\frac{d^2E}{\frac{1}{2}N_0}}\right) = Q\left(\sqrt{\frac{E_d}{\frac{1}{2}N_0}}\right) \quad A1.39$$

where E_d is the energy of each signal waveform $k_1s(t)$ and $k_2s(t)$. The error probability is a function only of the signal/noise power ratio at the input to the matched filter, and has its minimum value for any given signal/noise ratio.

This is clearly the optimum combination of signal design and detection process for a binary-coded signal, where the two binary values are equally likely and the signal is received in the presence of AWGN. Any waveform of

duration T seconds may be used for the transmitted signal-element, so long as it has the required energy and so long as the waveform corresponding to one of the two binary values is the negative of that corresponding to the other binary value. Such a signal is known as a binary antipodal signal-element.

Since a decision threshold of zero is used for the detection of the binary value, the receiver requires no prior knowledge of the values of k_1 and k_2 other than that k_1 is negative and k_2 is positive. In other words, the receiver requires no prior knowledge of the received signal level in order to achieve optimum detection of the element binary value.

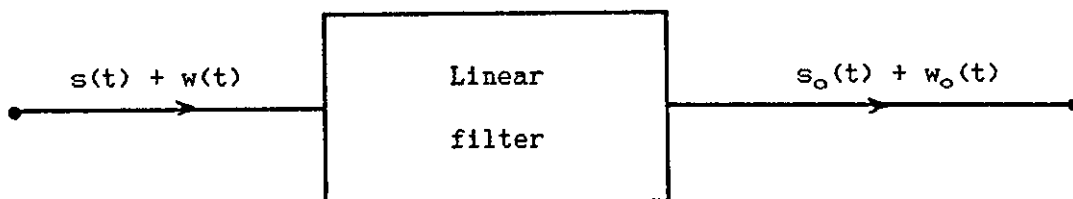


Figure A1.1 Linear filtering of $r(t)$.

APPENDIX A2

IMPULSE RESPONSES OF THE TRANSFER FUNCTIONS GIVING A RECTANGULAR SPECTRUM AND A SINUSOIDAL ROLLOFF SPECTRUM

A2.1 Rectangular spectrum

The transfer function giving a rectangular spectrum is

$$H(f) = \begin{cases} T, & -\frac{1}{2T} < f < \frac{1}{2T} \\ 0, & \text{elsewhere} \end{cases} \quad \text{A2.1}$$

as shown in Fig. 2.3a in Section 2.2.1.

The impulse response of the transfer function is

$$\begin{aligned} h(t) &= \int_{-\infty}^{\infty} H(f) \exp(j2\pi ft) df = \int_{-1/2T}^{1/2T} T \exp(j2\pi ft) df \\ &= T \left[\frac{\exp(j2\pi ft)}{j2\pi f} \right]_{-1/2T}^{1/2T} = \frac{\exp(j\pi t/T) - \exp(-j\pi t/T)}{j2\pi t/T} \\ &= \frac{\sin(\pi t/T)}{\pi t/T} \end{aligned} \quad \text{A2.2}$$

as shown in Fig. 2.3b in Section 2.2.1

A2.2 Sinusoidal rolloff spectrum

The transfer function of a sinusoidal rolloff spectrum is

$$H(f) = \begin{cases} T & , 0 \leq |f| < \frac{(1-\beta)}{2T} \\ \frac{T}{2} \left[1 - \sin \frac{\pi T}{\beta} \left(|f| - \frac{1}{2T} \right) \right] & , \frac{(1-\beta)}{2T} \leq |f| \leq \frac{(1+\beta)}{2T} \\ 0 & , \text{elsewhere} \end{cases} \quad \text{A2.3}$$

as shown in Fig. A2.1a, where the ratio $\beta = f_w/f_c$ is called the rolloff

factor. Equation A2.3 can be written as

$$H(f) = \begin{cases} T + H_1(f) & , f_c - f_x < |f| < f_c \\ H_1(f) & , f_c < |f| < f_c + f_x \\ 0 & , \text{elsewhere} \end{cases} \quad \text{A2.4}$$

where $1/f_c = 1/2T$ and

$$H_1(f) = \begin{cases} \frac{T}{2} \left(\cos \frac{\pi[|f| - (f_c - f_x)]}{2f_x} - 1 \right) & , f_c - f_x < |f| < f_c \\ \frac{T}{2} \left(\cos \frac{\pi[|f| - (f_c - f_x)]}{2f_x} + 1 \right) & , f_c < |f| < f_c + f_x \\ 0 & , \text{elsewhere} \end{cases} \quad \text{A2.5}$$

Assume that the overall filter has zero phase shift. (A linear phase term of course results in a corresponding time delay.) Assume further that $H_1(f)$ has odd symmetry about f_c . Then

$$H_1(f_c + |f|) = -H_1(f_c - |f|) \quad , \text{for } f_x < |f| \quad \text{A2.6}$$

The sinusoidal rolloff spectrum has this property, as shown in Fig. A2.1b, with the overall characteristic shown in Fig. A2.1a.

Taking the Fourier transform of Eqn A2.4, by superposition, the impulse is given by

$$h(t) = \frac{\sin(\pi t/T)}{\pi t/T} + h_1(t) \quad \text{A2.7}$$

as can be seen from Eqn. A2.2, and

$$h_1(t) = \int_{-\infty}^{\infty} H_1(f) \exp(j2\pi ft) df \quad \text{A2.8}$$

But $H_1(f)$, having zero (or linear) phase shift, must be even in f

(Fig. A2.1b) [4, p.182]. Then

$$\begin{aligned}
 h_1(t) &= \int_{-\infty}^{\infty} H_1(f) \exp(j2\pi ft) df \\
 &= 2 \int_{f_c - f_x}^{f_c + f_x} H_1(f) \cos 2\pi ft df \\
 &= 2 \int_{f_c - f_x}^{f_c} H_1(f) \cos 2\pi ft df + 2 \int_{f_c}^{f_c + f_x} H_1(f) \cos 2\pi ft df \quad \text{A2.9}
 \end{aligned}$$

using the fact that $H_1(f)=0$, for $|f|>f_c+f_x$.

Using the property of odd symmetry about f_c by letting $f=f_c-x$ in the first integral of Eqn. A2.9 and $f=f_c+x$ in the second integral. The new dummy variable x ranges between 0 and f_x in both integrals, and the two may be combined into the following one integral, after using the odd-symmetry property:

$$\begin{aligned}
 h_1(t) &= -2 \int_{f_x}^0 H_1(f_c-x) \cos 2\pi(f_c-x)t dx \\
 &\quad + 2 \int_0^{f_x} H_1(f_c+x) \cos 2\pi(f_c+x)t dx \\
 &= 2 \int_0^{f_x} H_1(f_c+x) \cos 2\pi(f_c+x)t + H_1(f_c-x) \cos 2\pi(f_c-x)t dx \quad \text{A2.10}
 \end{aligned}$$

After using the odd-symmetry property (Eqn. A2.6), it becomes

$$\begin{aligned}
 h_1(t) &= 2 \int_0^{f_x} H_1(f_c+x) \cos 2\pi(f_c+x)t - H_1(f_c+x) \cos 2\pi(f_c-x)t dx \\
 &= 2 \int_0^{f_x} H_1(f_c+x) [\cos 2\pi(f_c+x)t - \cos 2\pi(f_c-x)t] dx \\
 &= -4 \sin 2\pi f_c t \int_0^{f_x} H_1(f_c+x) \sin 2\pi x t dx \\
 &= -4 \sin(\pi t/T) \int_0^{f_x} H_2(f) \sin 2\pi x t dx \quad \text{A2.11}
 \end{aligned}$$

where
$$H_2(f) = \begin{cases} \frac{T}{2} \left(1 - \sin \frac{\pi x}{2f_x} \right) & , x < f_x \\ 0 & , x > f_x \end{cases} \quad \text{A2.12}$$

as shown in Fig. A2.1c.

Using Eqn. A2.11, A2.7 can be written as

$$\begin{aligned} h(t) &= \frac{\sin(\pi t/T)}{\pi/T} \left\{ \frac{1}{t} - 2\pi \int_0^{f_x} \left(1 - \sin \frac{\pi x t}{2f_x} \right) \sin 2\pi x t \, dx \right\} \\ &= \frac{\sin(\pi t/T)}{\pi/T} \left\{ \frac{1}{t} - 2\pi \int_0^{f_x} \sin 2\pi x t + \frac{1}{2} \cos \left(\frac{\pi}{2f_x} + 2\pi t \right) x - \frac{1}{2} \cos \left(\frac{\pi}{2f_x} - 2\pi t \right) x \, dx \right\} \\ &= \frac{\sin(\pi t/T)}{\pi/T} \left\{ \frac{1}{t} - 2\pi \left[\frac{-\cos 2\pi x t}{2\pi t} + \frac{\frac{1}{2} \sin \left(\frac{\pi x}{2f_x} + 2\pi t \right)}{\pi / (2f_x) + 2\pi t} - \frac{\frac{1}{2} \sin \left(\frac{\pi x}{2f_x} - 2\pi t \right)}{\pi / (2f_x) - 2\pi t} \right] \right\}_{0}^{f_x} \\ &= \frac{\sin(\pi t/T)}{\pi/T} \left\{ \frac{1}{t} - 2\pi \left[\frac{1 - \cos 2\pi f_x t}{2\pi t} + \frac{\frac{1}{2} \cos 2\pi f_x t}{\pi / 2f_x + 2\pi t} - \frac{\frac{1}{2} \cos 2\pi f_x t}{\pi / 2f_x - 2\pi t} \right] \right\} \\ &= \frac{\sin(\pi t/T)}{\pi/T} \left\{ \frac{1}{t} - \left[\frac{1 - \cos 2\pi f_x t}{t} + \frac{\cos 2\pi f_x t}{1/2f_x + 2t} - \frac{\cos 2\pi f_x t}{1/2f_x - 2t} \right] \right\} \\ &= \frac{\sin(\pi t/T)}{\pi/T} \left\{ \frac{\cos 2\pi f_x t}{t} + \frac{2f_x \cos 2\pi f_x t}{1 + 4f_x t} - \frac{2f_x \cos 2\pi f_x t}{1 - 4f_x t} \right\} \\ &= \frac{\sin(\pi t/T)}{\pi/T} \cos 2\pi f_x t \left[2f_x \left\{ \frac{1}{2f_x t} + \frac{1}{1 + 4f_x t} - \frac{1}{1 - 4f_x t} \right\} \right] \\ &= \frac{\sin(\pi t/T)}{\pi/T} \frac{\cos 2\pi f_x t}{t[1 - 4f_x t]^2} \end{aligned} \quad \text{A2.13}$$

But $\beta = f_x/f_c$ and so $f_x = \beta f_c = \beta/2T$, thus Eqn. A2.13 can be written as

$$h(t) = \frac{\sin(\pi t/T)}{\pi t/T} \frac{\cos(\beta \pi t/T)}{1 - 4\beta^2 t^2/T^2} \quad \text{A2.14}$$

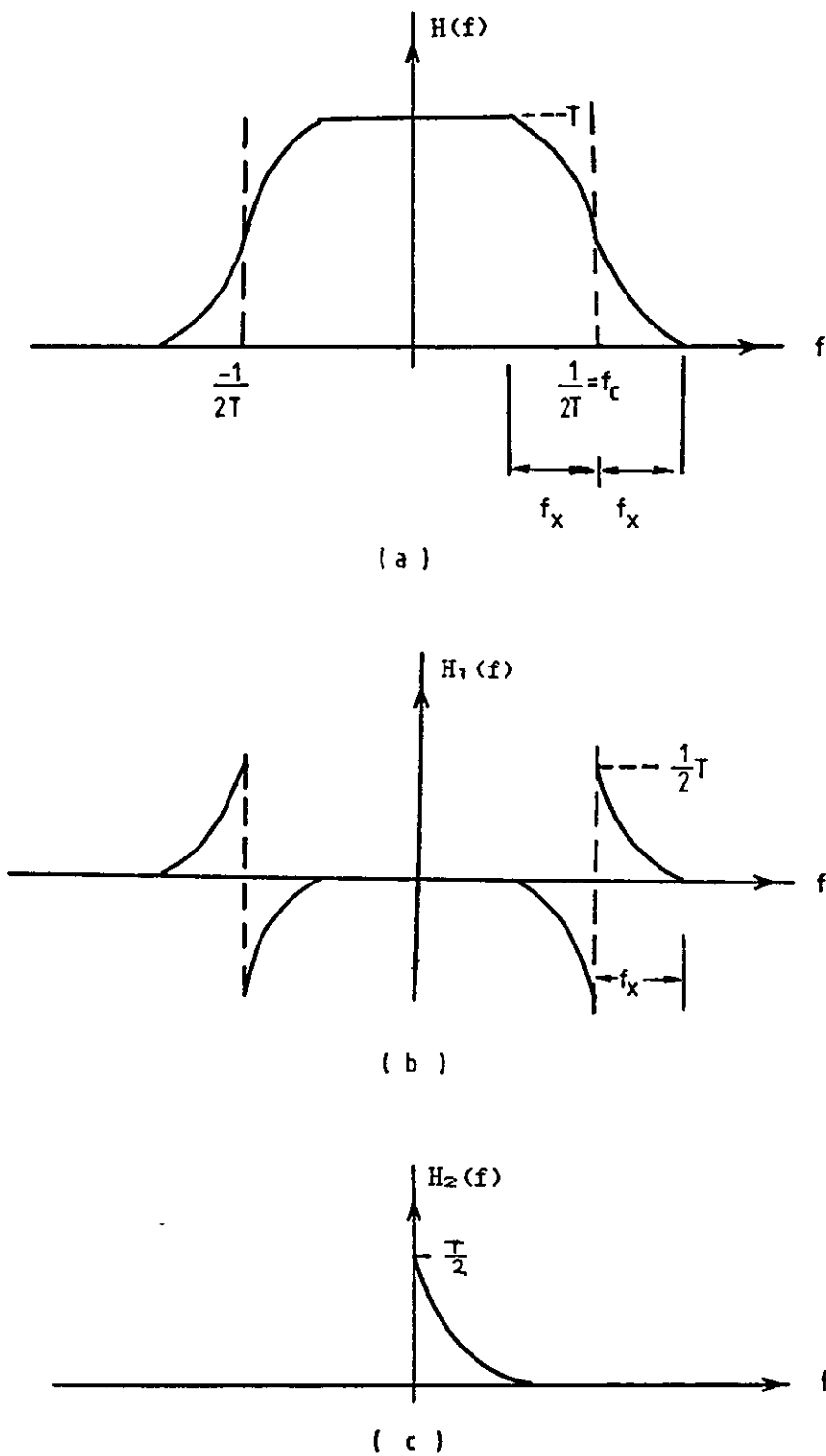


Figure A2.1 (a) Sinusoidal rolloff spectrum. (b) and (c) spectra of $H_1(f)$ and $H_2(f)$, respectively.

APPENDIX A3THE RELATIONSHIP OF $2E_b/N_o$ BETWEEN THE UPLINK AND DOWNLINK
OF A SATELLITE CHANNEL

In conventional amplifier satellite transponders, the noise contributions of the uplink and downlink are added according to the following expression [6, ch.2, p6], [7, p42]:

$$(2E_b/N_o)_T^{-1} = (2E_b/N_o)_U^{-1} + (2E_b/N_o)_D^{-1} \quad A3.1$$

where E_b is the energy per bit, N_o is the two-sided noise power spectral density, and the subscripts U, D, and T denote the uplink, downlink and total, respectively. In Eqn. A3.1, the quantities are in ratios and not dBs.

Normally the value of $2E_b/N_o$ in the uplink is made high enough to compensate for the restricted performance caused by the fact that less power is available in the downlink. This is because the noise and interference contributions in the uplink are passed together with the wanted signal to the downlink where further noise and interference are added. If the same value of E_b/N_o is used for both up and downlink, so that

$$(2E_b/N_o)_T = (2E_b/N_o)_U = (2E_b/N_o)_D \quad A3.2$$

then $2E_b/N_o$ must be at least 3 dB greater than before in order to achieve the required value of $(2E_b/N_o)_T$.

APPENDIX A4

BASEBAND EQUIVALENT MODELS OF SYMMETRICAL BANDPASS FILTERS

Figure A4.1 shows the baseband equivalent model of bandpass modulated signals. The bandpass filter, with a limited bandwidth, represents the cascade of the transmitter BPF (bandpass filter), the channel filter, and receiver BPF. It is assumed that perfect carrier and symbol timing synchronization signals are available, the noise is negligible on the channel, and the channel is linear. Note that due to the linearity of the system, the conclusions are not restricted to the noiseless case.

A4.1 Baseband equivalent model of the BPF at the transmitter [7, p131]

In Fig. A4.1b, the modulator contains only a premodulation lowpass filter, LPF_r . The modulated signal is

$$s_r(t) = [a(t) * h_L(t)]c(t) \quad A4.1$$

where $a(t)$ is the input signal, $h_L(t)$ is the impulse response of the lowpass filter, $c(t)$ is the sinusoidal carrier signal, and $*$ denotes the convolution, defined by

$$a(t) * h_L(t) = \int_{-\infty}^{\infty} a(\tau) h_L(t-\tau) d\tau \quad A4.2$$

Taking the Fourier transform of Eqn. A4.1 and noting that convolution in the time domain corresponds to multiplication in frequency domain, and that convolution in the frequency domain corresponds to multiplication in time domain, the spectrum of $s_r(t)$ can be written as

$$S_r(f) = [A(f)H_L(f)] * C(f) \quad A4.3$$

where $A(f)$, $H_L(f)$ and $C(f)$ are the Fourier transforms of $a(t)$, $h_L(t)$ and $c(t)$, respectively. Since convolution of a baseband spectrum with a

sinusoidal carrier results in a double-side band spectrum centered around the carrier frequency f_c , Equation A4.3 can be written as

$$S_1(f) = \frac{1}{2}(A(f-f_c)H_L(f-f_c) + A(f+f_c)H_L(f+f_c)) \quad A4.4$$

In Fig. A4.1c, the linear modulator contains only a postmodulation bandpass filter, BPF_T . The modulating signal is

$$s_2(t) = [a(t)c(t)] * h_B(t) \quad A4.5$$

where $h_B(t)$ is the impulse response of the BPF_T . The corresponding Fourier transform is

$$\begin{aligned} S_2(f) &= [A(f)*C(f)]H_B(f) \\ &= \frac{1}{2}[A(f-f_c) + A(f+f_c)]H_B(f) \end{aligned} \quad A4.6$$

where $H_B(f)$ is the Fourier transform of $h_B(t)$.

The amplitude spectra of the predemodulated and postmodulated filter signals, represented by Eqns. A4.4 and A4.6, respectively, are the same if $S_1(f) = S_2(f)$, that is

$$H_L(f-f_c) = H_L(f+f_c) = H_B(f) \quad A4.7$$

bearing in mind that the bandpass filter has a limited bandwidth. Hence, the equivalent condition is satisfied if the bandpass filter, $H_B(f)$, has the same transfer function as lowpass filter, $H_L(f)$, shifted so as to be centered around the carrier frequency f_c . Thus if a transmitter bandpass filter is symmetrical around the center frequency, the baseband equivalent model of it can be easily obtained by shifting the center frequency to zero frequency.

A4.2 Baseband equivalent model of the BPF at the receiver

In Fig. A4.1d, the demodulator contains a predemodulated bandpass filter, BPF_R. The signal to the demodulator is

$$s_{11}(t) = [a(t)c(t)] * h_B(t)c(t)$$

The corresponding spectrum is

$$\begin{aligned} S_{11}(f) &= \mathcal{F}\{[A(f-f_c) + A(f+f_c)]H_B(f)*C(f)\} \\ &= \mathcal{F}\{[A(f-f_c)H_B(f) + A(f+f_c)H_B(f)]*C(f)\} \\ &= \mathcal{F}\{[A(f-f_c-f_c)H_B(f-f_c) + A(f-f_c+f_c)H_B(f+f_c) \\ &\quad + A(f+f_c-f_c)H_B(f-f_c) + A(f+f_c+f_c)H_B(f+f_c)]\} \end{aligned} \quad \text{A4.8}$$

The wide LFP will block the second-order spectral components, so that amplitude spectrum of the signal to the detector is

$$\hat{S}_{11}(f) = \mathcal{F}\{A(f)[H_B(f-f_c) + H_B(f+f_c)]\} \quad \text{A4.9}$$

In Fig. A4.1e, the linear demodulator contains only a postdemodulator lowpass filter, LPF_R. The demodulated signal is

$$s_{22}(t) = [a(t)c(t)c(t)] * h_L(t)$$

The corresponding Fourier transform is

$$\begin{aligned} S_{22}(f) &= [A(f)*C(f)]H_L(f) \\ &= \mathcal{F}\{[A(f-f_c)+A(f+f_c)]*C(f)\}H_L(f) \\ &= \mathcal{F}\{[A(f-f_c-f_c)+A(f-f_c+f_c)+A(f+f_c-f_c)+A(f+f_c+f_c)]\}H_L(f) \end{aligned} \quad \text{A4.10}$$

The second-order spectral components are blocked by the LPF_R, so that the amplitude spectrum of the signal to the detector becomes

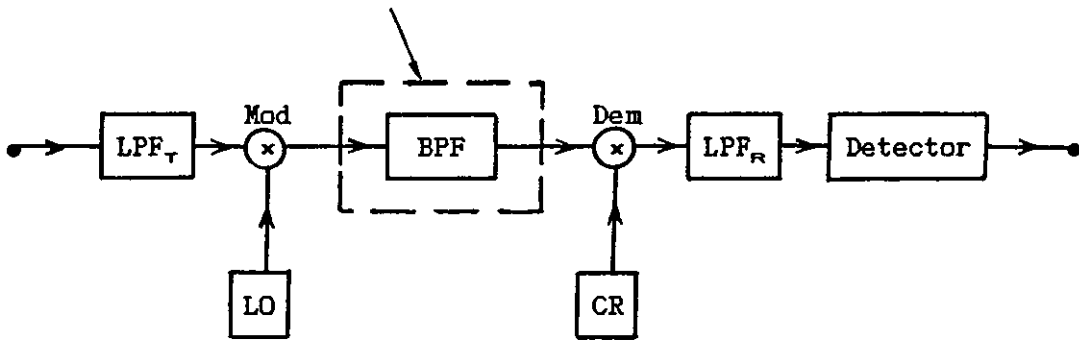
$$\hat{S}_{22}(f) = \mathcal{F}\{A(f)H_L(f) + A(f)H_L^*(f)\} \quad \text{A4.11}$$

The amplitude spectra to the detector, represented by Eqns. A4.9 and A4.11, are the same if $\hat{S}_{11}(f) = \hat{S}_{22}(f)$, that is

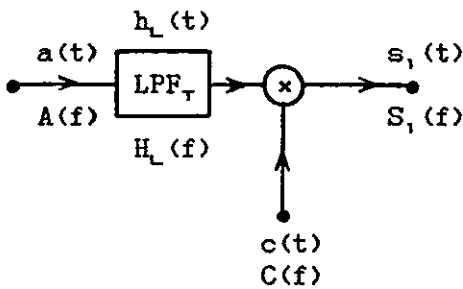
$$H_L(f) = H_B(f-f_c) = H_B(f+f_c) \quad \text{A4.12}$$

bearing in mind that the bandpass filter has a limited bandwidth. Therefore the equivalent condition is satisfied if the bandpass filter, $H_B(f)$, has the same transfer function as the lowpass filter, $H_L(f)$, shifted so as to be centered around the zero frequency. Thus if a receiver bandpass filter is symmetrical around the center frequency, the baseband equivalent model of it can be easily obtained by shifting the center frequency to zero frequency.

Represents cascade
of transmitter BPF,
channel filter, and
receiver BPF.

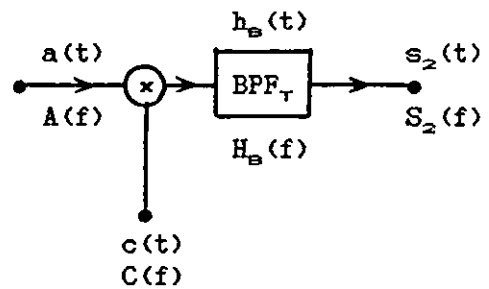


(a)

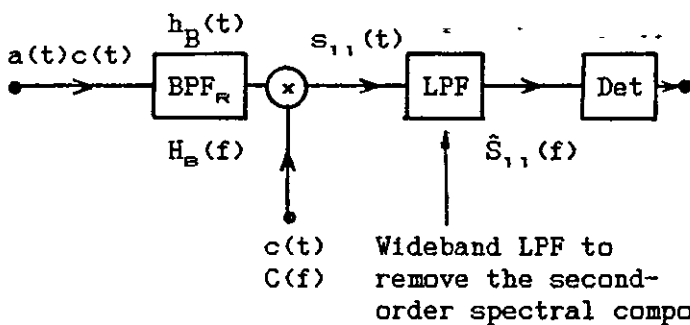


(b)

Equivalent modulator

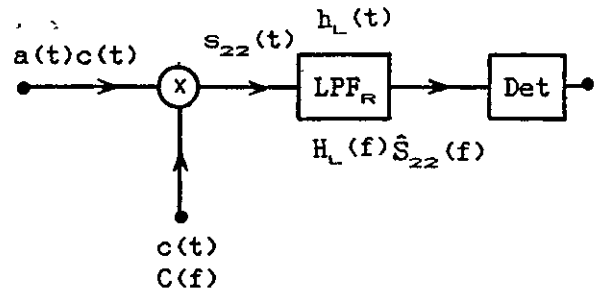


(c)



(d)

Equivalent demodulator



(e)

Figure A4.1 Baseband equivalent model of bandpass modulated signals. (a) Modulator, channel, demodulator. Mod is modulator, Dem is demodulator, LPF is lowpass filter, BPF is bandpass filter, LO is local oscillator, CR is carrier recovery, and Det is detector. (b) Linear modulator having a premodulation LPF only. (c) Modulator having a postmodulation BPF only. h_L and h_B are impulse responses of the LPF and BPF, respectively. (d) demodulator having a predetection BPF. (e) demodulator having a postdetection LPF only.

APPENDIX A5ANALYSIS OF QUADRATURE CROSSTALK IN BANDPASS SIGNALS [8]

Consider a bandpass signal $s(t)$ is given by

$$\begin{aligned} s(t) &= a(t)\cos 2\pi f_c t - b(t)\sin 2\pi f_c t \\ &= \frac{1}{2}c(t)\exp(j2\pi f_c t) + \frac{1}{2}c^*(t)\exp(-2\pi f_c t) \end{aligned} \quad \text{A5.1}$$

where $c(t) = a(t) + jb(t),$ A5.2a

$$c^*(t) = a(t) - jb(t), \quad \text{A5.2b}$$

$j = \sqrt{-1}$ and f_c is the carrier frequency.

The signal $c(t)$ is the complex lowpass envelope of $s(t)$ while $a(t)$ and $b(t)$ are the inphase and quadrature components of $s(t)$, respectively.

Hence, the Fourier transform of $s(t)$, giving by the frequency translation theorem, is

$$S(f) = \frac{1}{2}C(f-f_c) + \frac{1}{2}C^*(-f-f_c) \quad \text{A5.3}$$

where $C(f)$ is the Fourier transform of $c(t)$.

The process of bandpass filtering $s(t)$ through a bandpass filter is

$$y(t) = h(t)*s(t) \quad \text{A5.4}$$

where $h(t)$ is the impulse response of the bandpass filter and $*$ denotes the convolution (see Eqn. A4.2 for the definition).

The corresponding Fourier transform is

$$Y(f) = H(f)S(f) \quad \text{A5.5}$$

where $Y(f)$, $H(f)$ and $S(f)$ are the Fourier transforms of $y(t)$, $h(t)$ and $s(t)$, respectively.

The impulse response of the bandpass filter can be expressed as

$$h(t) = r(t)\cos 2\pi f_c t - q(t)\sin 2\pi f_c t \quad A5.6$$

$$= \frac{1}{2}d(t)\exp(j2\pi f_c t) + \frac{1}{2}d^*(t)\exp(-j2\pi f_c t) \quad A5.7$$

where $d(t) = r(t) + jq(t), \quad A5.8a$

$$d^*(t) = r(t) - jq(t), \quad A5.8b$$

and f_c is the centered frequency of the bandpass filter. (Assume it is the same as the carrier frequency of $s(t)$).

The signal $d(t)$ is the complex lowpass envelope of $h(t)$, while $r(t)$ and $q(t)$ are the inphase and quadrature components of $h(t)$, respectively.

The Fourier transform of $h(t)$ is given by

$$H(f) = D(f-f_c) + D^*(-f-f_c) \quad A5.9$$

where $D(f)$ is the Fourier transform of $d(t)$.

The bandpass signals of $d(t)$ and $d^*(t)$ in Eqn. A5.7 can be written as

$$d(t)\exp(j2\pi f_c t) = r(t)\exp(j2\pi f_c t) + jq(t)\exp(j2\pi f_c t) \quad A5.10a$$

and $d^*(t)\exp(j2\pi f_c t) = r(t)\exp(j2\pi f_c t) - jq(t)\exp(j2\pi f_c t) \quad A5.10b$

The corresponding Fourier transforms are

$$D(f-f_c) = R(f-f_c) + jQ(f-f_c) \quad A5.11a$$

and $D^*(-f-f_c) = R(f-f_c) - jQ(f-f_c) \quad A5.11b$

where $R(f)$ and $Q(f)$ are the Fourier transforms of $r(t)$ and $q(t)$, bearing in mind that $r(t)$ and $q(t)$ are the inphase and quadrature components of the impulse response. Thus

$$R(f-f_c) = \frac{1}{2}[D(f-f_c) + D^*(-f-f_c)] \quad A5.12$$

and $jQ(f-f_c) = \frac{1}{2}[D(f-f_c) - D^*(-f-f_c)] \quad A5.13$

If the signal from the output of the baseband equivalent model of the filter is not real for a real input, or if the output from it is not purely imaginary for an imaginary input, there is crosstalk introduced by the bandpass filter. From Eqn. A5.13, the crosstalk interference (CI) is represented by

$$CI = jQ(f-f_c) \quad A5.14$$

Case I Symmetrical bandpass filter

If the bandpass filter transfer function $H(f)$ is symmetrical in amplitude and asymmetrical in phase about f_c (i.e., $D(f-f_c) = D^*(-f-f_c)$), then $jQ(f-f_c)=0$ and so $CI=0$. Since there is no interference between the inphase and quadrature components, there is no crosstalk.

Case II Nonsymmetrical bandpass filter

If the bandpass filter transfer function $H(f)$ is not symmetrical in amplitude or not asymmetrical in phase about f_c (i.e., $D(f-f_c) \neq D^*(-f-f_c)$), then $jQ(f-f_c) \neq 0$ and $CI=jQ(f-f_c)$. There is crosstalk between the inphase and quadrature components, introduced by the bandpass filter.

APPENDIX A6PROOF OF THE COMPLEX SIGNAL REPRESENTATION OF SYSTEMS USING
QUADRATURE MODULATED SIGNAL [91]A6.1 Representation of the modulated signal

Let $R(\cdot)$ represent the real part part of (\cdot) . If $a(t)$ and $b(t)$ are the information bearing signals then:

$$S(t) = \sqrt{2} \{a(t)\cos\omega_c t - b(t)\sin\omega_c t\} \quad \text{A6.1}$$

$$= \sqrt{2} \{a(t)\cos\omega_c t - b(t)\cos(\omega_c t - \pi/2)\} \quad \text{A6.2}$$

$$= \sqrt{2}R\{a(t)\exp(j\omega_c t) - b(t)\exp(j\omega_c t - \pi/2)\} \quad \text{A6.3}$$

$$= \sqrt{2}R\{a(t)\exp(j\omega_c t) - b(t)\exp(j\omega_c t)\exp(-j\pi/2)\} \quad \text{A6.4}$$

$$\text{now } \exp(-j\pi/2) = \cos(-\pi/2) + j\sin(-\pi/2) \quad \text{A6.5}$$

$$= 0 - j \quad \text{A6.6}$$

where $j = \sqrt{-1}$.

$$\therefore S(t) = \sqrt{2}\{a(t) + jb(t)\} R\{\exp(j\omega_c t)\} \quad \text{A6.7}$$

If

$$s(t) = a(t) + jb(t) \quad \text{A6.8}$$

$$\text{then } S(t) = \sqrt{2}s(t) R\{\exp(j\omega_c t)\} \quad \text{A6.9}$$

The auto-correlation function of $S(t)$ is

$$y_{\infty}(\tau) = 2 \int_{-\infty}^{\infty} s(t-\tau)\cos\omega_c(t-\tau) s(t)\cos\omega_c t dt \quad \text{A6.10}$$

The energy of the waveform $S(t)$ is

$$y_{\infty}(0) = 2 \int_{-\infty}^{\infty} [s(t)\cos\omega_c t]^2 dt \quad \text{A6.11}$$

$$= \int_{-\infty}^{\infty} [s(t)]^2 + \cos 2\omega_c t dt \quad \text{A6.12}$$

$$= \int_{-\infty}^{\infty} s^2(t) dt \quad \text{after lowpass filtering} \quad \text{A6.13}$$

which is also the energy of the modulating waveform. Hence, the process of

modulation does not alter the energy content of the waveform to be transmitted. Consequently, the modulation of the two waveforms $a(t)$ and $b(t)$ can, from Eqn. A6.7, be represented as

$$s(t) = a(t) + jb(t) \quad \text{A6.14}$$

in a baseband equivalent model, because the term $\sqrt{2}R(\exp(j\omega_c t))$ in Eqn. A6.7 only represents a shift of the spectrum of $s^2(t)$ by ω_c rad/sec and has a modulus of unity.

A6.2 Representation of the demodulated signal

Let the demodulated signal be represented by $r'(t)$ and let the received information bearing signal before demodulation be represented by $m(t)$, then

$$r'(t) = \sqrt{2}m_a(t)\cos(\omega_c t + \phi) - \sqrt{2}m_b(t)\sin(\omega_c t - \phi)$$

where $m_a(t)$ and $m_b(t)$ are the inphase and quadrature components of $m(t)$, and ϕ is an arbitrary phase. Hence

$$r'(t) = \sqrt{2} \{m_a(t)\cos(\omega_c t + \phi) - m_b(t)\cos(\omega_c t + \phi - \pi/2)\} \quad \text{A6.15}$$

$$= \sqrt{2}R\{m_a(t)\exp[j(\omega_c t + \phi)] - m_b(t)\exp[j(\omega_c t + \phi - \pi/2)]\} \quad \text{A6.16}$$

$$= \sqrt{2}R\{m_a(t)\exp[j(\omega_c t + \phi)] - m_b(t)\exp[j(\omega_c t + \phi)]\exp[-j\pi/2]\} \quad \text{A6.17}$$

$$= \sqrt{2}R\{m_a(t) + jm_b(t)\} \exp[j(\omega_c t + \phi)] \quad \text{A6.18}$$

where $\exp(-j\pi/2) = 0 - j$, ($j = \sqrt{-1}$);

$$\text{hence } r'(t) = \sqrt{2}R\{[m_a(t) + jm_b(t)] \exp(j\omega_c t) \exp(j\phi)\} \quad \text{A6.19}$$

From Eqns. A6.7 and A6.9, the term $\sqrt{2}(\exp[j\omega_c t])$ in Eqn. A6.19 only represents a shift of the spectrum of $m(t)$ by ω_c rad/sec and has an average value of unity. Thus, the demodulation of $m(t)$ into two separate waveforms, representing the demodulation of two double sideband suppressed

carrier amplitude modulated signals which are in phase quadrature, gives

$$r(t) = \{m_a(t) + jm_b(t)\} \exp(j\phi) \quad \text{A6.20}$$

$$= \{m_a(t)\cos\phi - m_b(t)\sin\phi\} + j\{m_a(t)\sin\phi + m_b(t)\cos\phi\} \quad \text{A6.21}$$

in a baseband equivalent model.

If the channel introduces no signal distortion or noise then the representation of the bandpass signal in the baseband equivalent model from Eqns. A6.14 and A6.20, is

$$r(t) = s(t) \exp(j\phi) \quad \text{A6.22}$$

The result of Eqn. A6.22 can be verified by demodulating the signal in Eqn. A6.9 with $\sqrt{2}R\{\exp[j(\omega_c t + \phi)]\}$ and gives

$$\begin{aligned} r(t) &= \sqrt{2}s(t) R\{\exp[j\omega_c t]\} \sqrt{2}\{\exp[j(\omega_c t + \phi)]\} \\ &= 2s(t) \exp(j\phi)\cos^2\omega_c t \\ &= s(t) \exp(j\phi)\{1 + \cos 2\omega_c t\} \\ &= s(t) \exp(j\phi) \quad \text{after lowpass filtering} \quad \text{A6.23} \end{aligned}$$

Equations A6.22 and A6.23 are the same. Thus a system using quadrature amplitude modulated signals can use the complex signal representation given by Eqns. A6.15, A6.21 and A6.22 to represent a baseband equivalent model.

APPENDIX A7

NARROWBAND NOISE REPRESENTATION PROPERTIES

Consider a white Gaussian noise of zero-mean and spectral density $\frac{1}{2}N_0$ which is passed through an ideal narrow bandpass filter (i.e., the center frequency f_c is large compared with the half-bandwidth of the filter) of unit gain, midband frequency f_c , and bandwidth $2B$ Hz. The spectral density characteristic of the filtered noise process $N(t)$ will therefore be as shown in Fig. A7.1a. It may be written [10] that

$$N(t) = N_c(t)\cos 2\pi f_c t - N_q(t)\sin 2\pi f_c t \tag{A7.1}$$

where $N_c(t)$ and $N_q(t)$ are referred as the inphase and quadrature components of the narrowband noise $N(t)$. Some properties of this expansion are as follows [10],[11]:

- (1) Gaussian. If $N(t)$ is a sample function of a Gaussian process, then $N_c(t)$ and $N_q(t)$ are also sample functions of Gaussian random processes.
- (2) Independence. The functions $N_c(t)$ and $N_q(t)$ are statistically independent.
- (3) Mean. If $N(t)$ has zero mean, then $N_c(t)$ and $N_q(t)$ also have zero mean.
- (4) Spectra and variance. Both $N_c(t)$ and $N_q(t)$ have the same spectral density, which related to the spectral density $\psi_n(f)$ of the narrowband noise $N(t)$ as follows.

$$\psi_c(f) = \psi_q(f) = \begin{cases} \psi_n(f+f_c) + \psi_n(f-f_c) & , -B < f < B \\ 0 & , \text{elsewhere} \end{cases} \tag{A7.2}$$

where $\psi_n(f)$, and $\psi_c(f)$ and $\psi_q(f)$ are the spectral density of $N(t)$, $N_c(t)$ and $N_q(t)$, respectively, and $2B$ Hz is the bandwidth of $N(t)$. $N_c(t)$ and $N_q(t)$ each occupy the frequency band from zero frequency to $\pm B$ Hz. Since $N(t)$ has a

two-sided power spectral density of $\frac{1}{2}N_0$ over the frequency bandwidth, Eqn. A7.2 reduces to

$$\psi_c(f) = \psi_n(f) = \begin{cases} 2\psi_n(f+f_c) & , -B \leq f \leq B \\ 0 & , \text{elsewhere} \end{cases} \quad \text{A7.3}$$

$$= \begin{cases} N_0 & , -B \leq f \leq B \\ 0 & , \text{elsewhere} \end{cases} \quad \text{A7.4}$$

The two-sided power spectral density of $N_c(t)$ and $N_m(t)$ are twice that of $N(t)$. The variance of $N_c(t)$ and $N_m(t)$, is

$$\overline{N_c^2(t)} = \overline{N_m^2(t)} = \int_{-B}^B \psi_c(f) df = 2N_0B \quad \text{A7.5}$$

The variance of $N(t)$ is

$$\begin{aligned} \overline{N^2(t)} &= \int_{-f_c-B}^{-f_c+B} \psi_n(f) df + \int_{f_m-B}^{f_c+B} \psi_n(f) df \\ &= 2N_0B \end{aligned} \quad \text{A7.6}$$

Thus, the variance of $N_c(t)$, $N_m(t)$ and $N(t)$ are equal.

(5) Autocorrelation function of $N_c(t)$ and $N_m(t)$.

The autocorrelation function of $N(t)$ is the inverse Fourier transform of the spectral density characteristic, i.e., [11, p.208]

$$\begin{aligned} R_n(\tau) &= \int_{-f_c-B}^{-f_c+B} \frac{1}{2}N_0 \exp(j2\pi f\tau) df + \int_{f_c-B}^{f_c+B} \frac{1}{2}N_0 \exp(2\pi f\tau) df \\ &= N_0B \frac{\sin 2\pi B\tau}{2\pi B\tau} [\exp(-j2\pi f_c\tau) + \exp(j2\pi f_c\tau)] \\ &= 2N_0B \frac{\sin 2\pi B\tau}{2\pi B\tau} \cos 2\pi f_c\tau \end{aligned} \quad \text{A7.7}$$

which is shown in Fig. A7.1b.

Applying Eqn. A7.4 to the spectral density characteristic of Fig. A7.1, which is symmetrical about $\pm f_c$, the corresponding spectral density characteristic of the inphase and quadrature noise components, $N_c(t)$ or $N_m(t)$, as shown in Fig. A7.1c. The autocorrelation function of $N_c(t)$ or $N_m(t)$ is therefore

$$\begin{aligned} R_n(\tau) = R_c(\tau) &= \int_{-B}^B N_o \exp(j2\pi f\tau) df \\ &= 2N_o B \frac{\sin 2\pi B\tau}{2\pi B\tau} \end{aligned} \quad \text{A7.8}$$

It can be seen that $R_c(\tau)$ or $R_m(\tau)$ passes through zero at $\tau = \pm n/B$, where $n=1, 2, 3, \dots$, if $N_c(t)$ or $N_m(t)$ is sampled at the rate of $2B$ samples per second, the resulting noise samples are uncorrelated, being Gaussian, they are statistically independent.

(6) Equivalent baseband signal of $N(t)$.

From Appendix A6, the narrowband noise $N(t)$ can be represented as the complex-valued signal

$$N(t) = [N_c(t) + jN_m(t)]R[\exp(j\omega_c t)] \quad \text{A7.9}$$

in a baseband equivalent model, where $j = \sqrt{-1}$, $\omega_c = 2\pi f_c$ and $R(\cdot)$ represents the real part of (\cdot) . The demodulation of $N(t)$ with $\sqrt{2}R[\exp(j\omega_c t)]$ gives

$$\begin{aligned} N(t)\sqrt{2}R[\exp(j\omega_c t)] &= [N_c(t) + jN_m(t)]R[\exp(j\omega_c t)] \sqrt{2}R[\exp(j\omega_c t)] \\ &= \sqrt{2}[N_c(t) + jN_m(t)]\cos^2\omega_c t \\ &= [\sqrt{1/2}N_c(t) + j\sqrt{1/2}N_m(t)][1 + \cos 2\omega_c t] \\ &= n(t)[1 + \cos 2\omega_c t] \\ &= n(t) \quad \text{after lowpass filtering} \end{aligned} \quad \text{A7.10}$$

where $n(t) = \sqrt{1/2}N_c(t) + j\sqrt{1/2}N_m(t)$ A7.11

$$= n_c(t) + jn_m(t) \quad \text{A7.12}$$

with $n_c(t) = \sqrt{1/2}N_c(t)$ and $n_m(t) = \sqrt{1/2}N_m(t)$.

Since the variance of $N_c(t)$ and $N_m(t)$ are $2N_0B$, the variance of $n_c(t)$ and $n_m(t)$ are

$$\overline{n_c^2(t)} = \frac{\overline{N_c^2(t)}}{2} = \frac{2N_0B}{2} = N_0B \quad \text{A7.13a}$$

and

$$\overline{n_m^2(t)} = \frac{\overline{N_m^2(t)}}{2} = N_0B \quad \text{A7.13b}$$

respectively.

The equivalent baseband signal of the narrowband noise is therefore

$$n(t) = n_c(t) + jn_m(t)$$

where $n_c(t)$ and $n_m(t)$ each occupy a bandwidth of $\pm B$ Hz with a two-sided power spectral density of $\frac{1}{2}N_0$ over the frequency bandwidth (Fig. A7.1d).

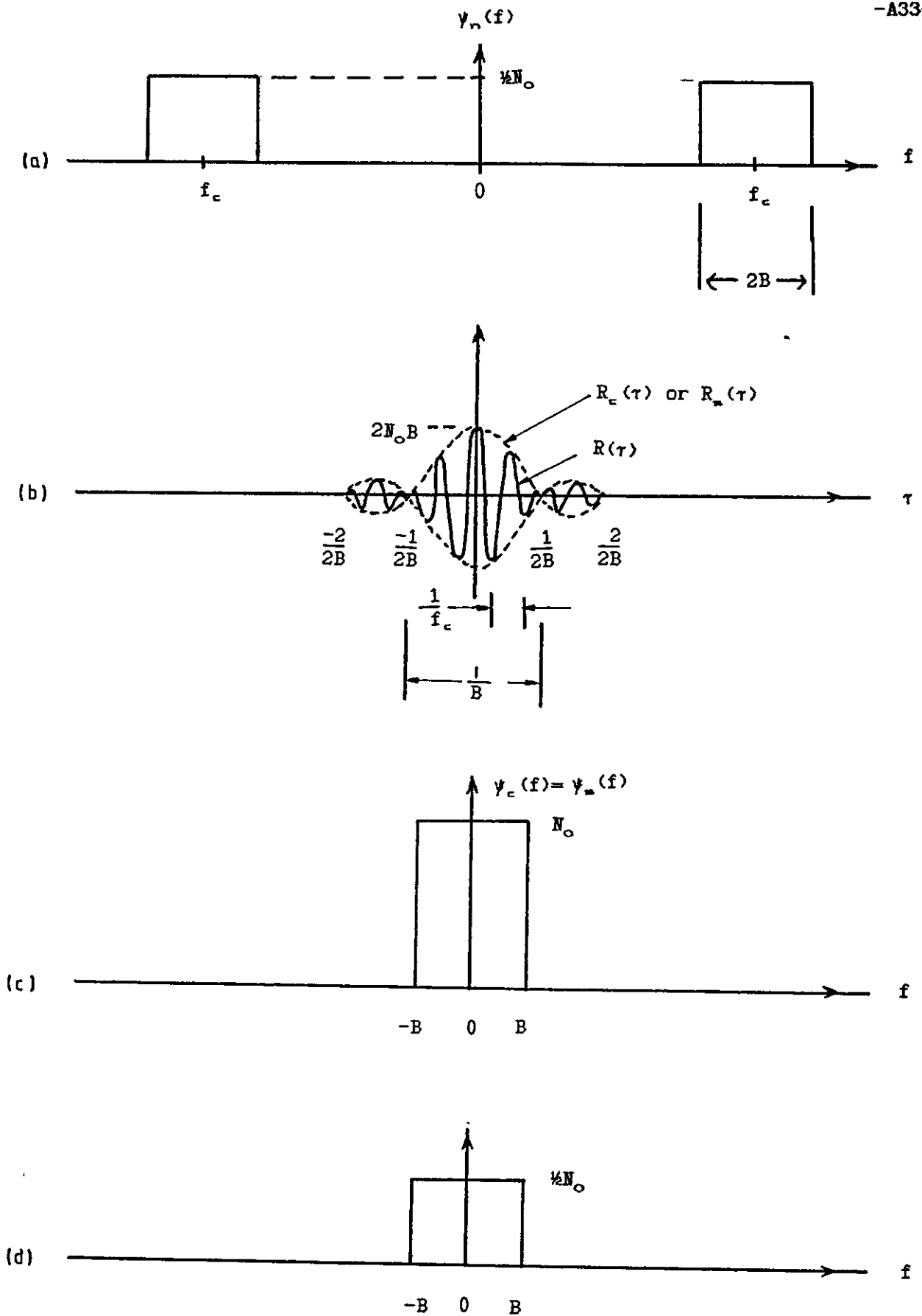


Figure A7.1 Characteristics of ideal bandpass filtered white noise. (a) Spectral density. (b) Autocorrelation function. (c) Spectral density of inphase and quadrature components. (d) Spectral density of the baseband inphase and quadrature components.

APPENDIX A8BIT-ENERGY-TO-NOISE POWER DENSITY RATIO ($2E_b/N_0$)CALCULATION FOR COMPUTER SIMULATIONA8.1 $\%N_0$ determination for computer simulation

It is mentioned in Section 2.2.4 that the bit-energy-to-noise power spectral density ratio, $E_b/\%N_0$ is frequently used in digital communication systems to enable a comparison of systems having variable transmission rates and of the performances of various modulation and coded systems in a complex interference environment. E_b is the energy per bit at the input to the receiver and $\%N_0$ is the white Gaussian two-sided noise power spectral density measured at the same point. Here, it is to determine the white Gaussian two-sided noise power spectral density at the input to the receiver, for the different values of noise variance and sampling rate used in the simulation tests.

Consider a white Gaussian noise of zero mean and a two-sided power spectral density of $\%N_0$ which is passed through an ideal narrow receiver bandpass filter of unit gain, mid-band frequency f_c , and bandwidth $2B$ Hz (Fig. A7.1). The baseband equivalent of the noise signal at the output of the filter can be written (Appendix A7) as the complex signal:

$$n(t) = n_c(t) + jn_m(t) \quad \text{A8.1}$$

where $j=\sqrt{-1}$, and $n_c(t)$ and $n_m(t)$ are sample functions of Gaussian random processes with zero mean and a two-sided power spectral density of $\%N_0$ over the frequency band from $-B$ Hz to B Hz (Fig. A7.3).

If $n(t)$ is sampled, at the time instants $\{iT\}$, where i takes all positive integer values, and

$$T = 1/2B \quad \text{A8.2}$$

or $2B = 1/T \quad \text{A8.3}$

to give the noise sample value, at time $t=iT$,

$$n_i = n_{c,i} + jn_{s,i} \quad \text{A8.4}$$

where $n_i = n(iT)$, $n_{c,i} = n_c(iT)$ and $n_{s,i} = n_s(iT)$, the resulting samples $\{n_i\}$ are uncorrelated and statistically independent (Appendix A7). The $\{n_{c,i}\}$ and $\{n_{s,i}\}$ each have the variance (Eqn. A7.13)

$$\sigma^2 = N_0 B \quad \text{A8.5}$$

Thus, the two-sided noise power spectral density, $\frac{1}{2}N_0$, at the input to the ideal bandpass filter, in terms of variance σ^2 and bandwidth B Hz of the baseband equivalent model, can be written as

$$\frac{1}{2}N_0 = \sigma^2 / (2B) \quad \text{A8.6}$$

Hence, if the variance and bandwidth of the baseband equivalent model of the noise signal are known, the two-sided noise power spectral density at the input to the receiver filter can be found using Eqn. A8.6.

Now suppose a Gaussian random number generator generates the complex-valued samples, at the time instants $\{mT_m\}$, where m takes all positive integer values and

$$T_m = T/k \quad \text{A8.7}$$

where k is an integer. The generating rate is k/T samples per second. So that at time $t=mT_m$, the generated complex-value sample is

$$n_m = n_{c,m} + jn_{s,m} \quad \text{A8.8}$$

where $n_{c,m}$ and $n_{s,m}$ are sample values of uncorrelated and statistically independent Gaussian random variables with zero mean and fixed variance σ^2 . This process is equivalent to obtaining the complex-valued Gaussian noise samples from the equivalent baseband model of an ideal narrow

bandpass filter (Fig. A8.1). The ideal bandpass filter has a passband gain of one and a bandwidth of

$$2B = 1/T_m = k/T \quad \text{A8.9}$$

as can be seen in an exactly analogous fashion expressed in Eqn. A8.3. So that by substituting $B=k/2T$ into Eqn. A8.6, the two-sided noise spectral power density at the input to the ideal bandpass filter can be found as

$$\frac{N_o}{2} = \frac{\sigma^2 T}{k} \quad \text{A8.10}$$

Note that $\frac{1}{2}N_o$ is dependent on the generating rate k/T . This equation is very important in calculating the bit-energy-to-noise power density ratio in the computer simulation tests, because it relates the noise variance σ^2 and sampling rate used in the tests to the two-sided power density $\frac{1}{2}N_o$ at the input to the receiver.

Thus a Gaussian random number generator, generates uncorrelated complex-value samples (n_m) with zero mean and fixed variance σ^2 , at a rate of k/T samples per second, is equivalent to obtaining the complex-valued Gaussian noise samples from the baseband equivalent model of an ideal bandpass filter (Fig. A8.1). The ideal bandpass filter has a bandwidth k/T Hz and a gain of one. The two-sided noise power spectral density at the input to the baseband equivalent model of the ideal bandpass filter is

$$\frac{N_o}{2} = \frac{\sigma^2 T}{k} \quad \text{A8.11}$$

This value can be used to compute the value $2E_b/N_o$ in the computer simulation tests.

A8.2 $2E_b/N_0$ value calculation for computer simulation

The equivalent baseband of a transmitted quadrature modulation signal (Section 2.6) can be represented as the complex signal (Appendix A6):

$$s(t) = a(t) + jb(t) \quad \text{A8.12}$$

where $j = \sqrt{-1}$, and $a(t)$ and $b(t)$ are the equivalent baseband of the inphase and quadrature signal components, respectively.

The transmitted signal energy during the n^{th} T interval is

$$E_{\text{tr}}(n) = \int_{(n-1)T}^{nT} |s(t)|^2 dt \quad \text{A8.13}$$

where T is the symbol duration.

Suppose the continuous waveform $s(t)$ of the transmitted signal is sampled at the time instants $\{mT_s\}$, for $m=1, 2, 3, \dots$, where

$$T = kT_s \quad \text{A8.14}$$

and k takes a positive integer value (Eqn. A8.7), to give a sequence of samples $\{s_m\}$, where $s_m = s(mT_s)$ has a complex value. Assume that the sampling rate, $1/T_s = k/T$, is high enough to prevent aliasing and L symbols are transmitted. There are altogether kL samples in the sequence $\{s_m\}$. The average energy per sample in $\{s_m\}$ is

$$P_s = \frac{1}{kL} = \frac{\sum_{m=1}^{kL} |s_m|^2}{kL} \quad \text{A8.15}$$

Thus the average transmitted signal energy over a period of T seconds is

$$E_{\text{tr}} = P_s T \quad \text{A8.16}$$

This is also the average transmitted energy per signal element, and so the average transmitted bit energy (for DEQPSK, CE8PSK and CDE8PSK signals) can be written as

$$E_b = E_m/2 = P_m T/2 \quad A8.17$$

Suppose the Gaussian noise sample values $\{n_m\}$ with zero mean and fixed variance σ^2 , as described in Appendix A8.1, are used to add to the signal sample values at the time instants $\{mT_m\}$. So that at time $t=mT_m$, the added noise sample is

$$n_m = n_{c,m} + jn_{s,m} \quad A8.18$$

with $n_{c,m}$ and $n_{s,m}$ the same definitions as in Eqn. A8.8.

From Appendix A8.1, it can be said that, under these assumed conditions, the two-sided power spectral density of $\frac{1}{2}N_o$ of the noise, measure at the same point as E_b , can be written as

$$\frac{N_o}{2} = \frac{\sigma^2 T}{k} \quad A8.19$$

as can be seen in Eqn. A8.10. Of course, the signal is assumed to be all covered by the white Gaussian noise.

Using Eqns. A8.17 and A8.19, the bit-energy-to-noise power spectral density ratio can be written as

$$\frac{2E_b}{N_o} = \frac{P_m T k}{2\sigma^2 T} = \frac{P_m k}{2\sigma^2} \quad A8.20$$

and the variance of the noise can be written as

$$\sigma^2 = \frac{N_o P_m k}{4E_b} \quad A8.21$$

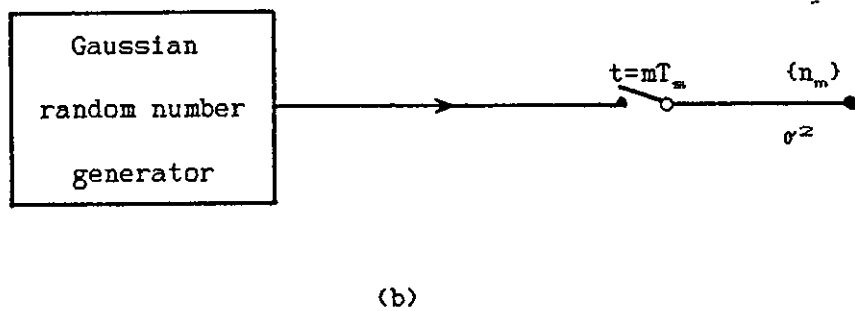
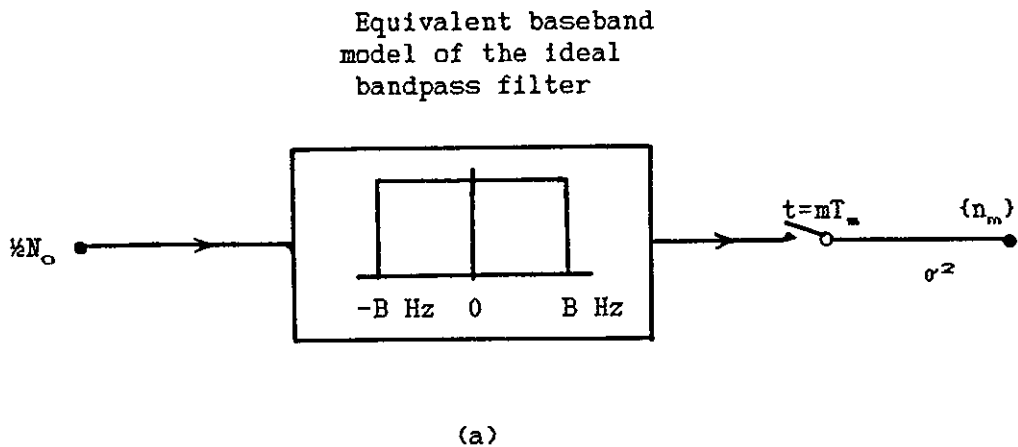


Figure A8.1 Equivalence of the noise model for computer simulation. (a) Model for obtaining the noise samples from the baseband equivalent model of the ideal bandpass filter. (b) Model for generating the noise samples for computer simulation. This is equivalent to the model shown in (a).

APPENDIX 9

THE SCALING RELATIONSHIP BETWEEN THE CONTINUOUS SIGNAL AND THE SAMPLED SIGNAL

Let $y(t)$ be a continuous waveform which is sampled at not less than the Nyquist rate to give the samples $\{y_m\}$, where

$$y_m = y(mT_s) \quad \text{A9.1}$$

and T_s is the sampling period. Now $y(t)$ may be expressed as [23]

$$y(t) = \sum_{m=-\infty}^{\infty} y_m \frac{\sin(t/T_s - m)}{\pi(t/T_s - m)} \quad \text{A9.2}$$

where the $\left\{ \frac{\sin(t/T_s - m)}{\pi(t/T_s - m)} \right\}$, are a set of orthonormal functions. Thus

$$\int_{-\infty}^{\infty} |y(t)|^2 dt = \sum_{m=-\infty}^{\infty} |y_m|^2 \int_{-\infty}^{\infty} \frac{[\sin(t/T_s - m)]^2}{[\pi(t/T_s - m)]^2} dt \quad \text{A9.3}$$

The integral on the right-hand side is equal to T_s [24]. Therefore, Eqn. A9.3 becomes,

$$\int_{-\infty}^{\infty} |y(t)|^2 dt = T_s \sum_{m=-\infty}^{\infty} |y_m|^2 \quad \text{A9.4}$$

which means that the sampled signal must be scaled by the sampling interval T_s in order to give the same energy level as the continuous signal $y(t)$.

APPENDIX A10PROBABILITY OF ERROR CALCULATION FOR BINARY SIGNALS [12,p499]

Consider two signal vectors S_1 and S_2 with a distance of $d_{1,2}$ units apart. With the two signals equally likely to be transmitted (as assumed here) it is to determine the probability of error for either one. By symmetry this is the same as for the other, and, averaging over both, is the system probability of error. This shows up in the decision regions of Fig. A10.1, since it is apparent that a signal vector V anywhere in the right-half plane should be associated with S_1 , while any value in the left-half plane is associated with S_2 . It is clear from Fig. A10.1 that the locus of all points ρ equally distant from S_1 and S_2 is the ρ_2 axis. Thus an error occurs when S_2 is transmitted if and only if the noise component N_2 exceeds $d_{1,2}/2$, where $d_{1,2}$ is the Euclidean distance between the two signals:

$$P[E|S_1] = P[N_2 > d_{1,2}/2], \quad A10.1$$

where

$$d_{1,2}^2 = |S_1 - S_2|^2 = \int_{-\infty}^{\infty} [s_1(t) - s_2(t)]^2 dt \quad A10.2$$

is the square Euclidean distance, and $s_1(t)$ and $s_2(t)$ are the two corresponding timing signals in time domain. $P[E|S_1]$ is the conditional probability of error when S_1 has been transmitted.

Let N_2 be zero-mean Gaussian with variance $\frac{1}{2}N_0$, so that

$$P[E|S_1] = \int_{d_{1,2}/2}^{\infty} \frac{1}{\sqrt{\pi N_0}} \exp\left(-\frac{\alpha^2}{N_0}\right) d\alpha \quad A10.3$$

Setting $\gamma = \alpha / 2 / N_0$, Eqn. A10.3 becomes

$$P[E|S_1] = \int_{d_{1j}/2}^{\infty} \frac{1}{\sqrt{2\pi}} \exp\left(\frac{-\gamma^2}{2}\right) d\gamma \quad A10.4$$

$$\frac{1}{\sqrt{N_0/2}}$$

$$= Q\left(\frac{d_{1j}}{\sqrt{2N_0}}\right) \quad A10.5$$

where
$$Q(y) = \int_y^{\infty} \frac{1}{\sqrt{2\pi}} \exp\left(\frac{-w^2}{2}\right) dw$$

Since, by symmetry, the conditional probability of error is the same for either signal, so the probability of error is

$$P_e = P(E) = P[S_1]P[E|S_1] + P[S_2]P[E|S_2] \quad A10.6$$

$$= \frac{1}{2}P[E|S_1] + \frac{1}{2}P[E|S_2] \quad A10.7$$

$$= Q\left(\frac{d_{1j}}{\sqrt{2N_0}}\right) \quad A10.8$$

$$= Q\left(\sqrt{\frac{d_{1j}^2}{2N_0}}\right) \quad A10.9$$

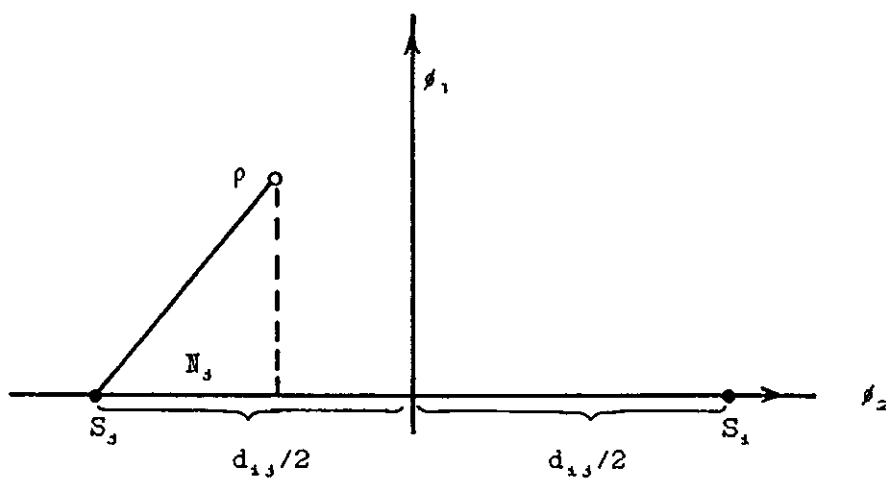


Figure A10.1 Two signal vectors and decision boundary in a subspace.

APPENDIX A11

FUNDAMENTALS OF CARRIER RECOVERY TECHNIQUES

Several different types of carrier recovery techniques are described in this appendix. These include the analog phase-locked loop (APLL) and digital phase-locked loop (DPLL) which are used for the signals with a spectral component existing at the carrier frequency, and the M^{th} power loop, the Costas loop and the decision-feedback loop which are used for the signals with suppressed carrier. In order to simplify the description of the loops, noise free conditions are assumed.

A11.1 Analog phase-locked loop (APLL)

A PLL is a device which continuously tries to track the phase of the incoming signal. It is realized by a phase detector (PD), a loop filter, and a voltage-controlled oscillator (VCO). The configuration is shown in Fig. A11.1a. The PD compares the phase of the incoming signal with that of the VCO, and its output voltage is filtered and applied to the VCO whose output frequency moves in a direction so as to reduce the phase difference of the incoming signal and output of VCO. When the loop is "locked", the short-term frequency of the VCO is exactly or very nearly equal to the average frequency of the input signal. A number of different kinds of phase detectors have been used (viz., sinusoidal, triangular, and sawtooth) though sinusoidal is the most common one.

A11.1.1 Linear model of APLL

Consider the basic model of an APLL consisting of a PD, a loop filter, and a VCO as shown in Fig. A11.1b. The incoming signal has a phase of $\theta(t)$, and the VCO output has a phase $\hat{\theta}(t)$. For the present, assume that the loop is locked, that the PD is linear and the PD output voltage is

proportional to the difference in phase between its inputs; that is

$$\hat{e}(t) = K_p[\theta(t) - \hat{\theta}(t)] \quad \text{A11.1.1}$$

$$= K_p \epsilon(t) \quad \text{A11.1.2}$$

where K_p is the PD gain factor and is measured in unit of volts/rad, and

$$\epsilon(t) = \theta(t) - \hat{\theta}(t) \quad \text{A11.1.3}$$

is the phase error signal.

The phase error voltage $\hat{e}(t)$ is filtered by the loop filter. The noise and high frequency signal components are suppressed. The filter helps to determine the dynamic performance of the loop. The filter transfer function is given by $F(s)$.

The frequency of the VCO is determined by the control voltage e . The deviation of frequency of the VCO from its center frequency is given by $\Delta\omega = K_v e$, where K_v is the VCO gain factor and has units of rad/sec-V. Since frequency is the derivative of phase, the VCO operation may be described as $d\hat{\theta}/dt = K_v e$. By taking Laplace transforms

$$L[d\hat{\theta}(t)/dt] = s\hat{\theta}(s) = K_v E(s) \quad \text{A11.1.4}$$

therefore,
$$\hat{\theta}(s) = K_v E(s)/s \quad \text{A11.1.5}$$

where $E(s) = L[e(t)]$. In other words, the phase of the VCO output is linearly related to the integral of the control voltage.

By using Laplace notation (e.g., $E(s) = L[e(t)]$) the following equations are applicable:

$$\hat{E}(s) = K_p[\theta(s) - \hat{\theta}(s)] \quad \text{A11.1.6}$$

$$E(s) = F(s)\hat{E}(s) \quad \text{A11.1.7}$$

$$\hat{\theta}(s) = K_v E(s)/s \quad \text{A11.1.8}$$

hence
$$\frac{\hat{\theta}(s)}{\theta(s)} = H(s) = \frac{K_v K_p F(s)}{s + K_v K_p F(s)} \quad \text{A11.1.9}$$

where $H(s)$ is the closed-loop transfer function. The loop noise bandwidth

and A11.1.12, the CE becomes

$$s^2 + Ks + K\mu = 0 \quad \text{A11.1.15}$$

$$\text{or } s^2 + 2\zeta\omega_n + \omega_n^2 = 0 \quad \text{A11.1.16}$$

to give

$$\omega_n = \sqrt{K\mu} \quad \text{A11.1.17}$$

$$\zeta = \frac{1}{2} \sqrt{K/\mu} \quad \text{A11.1.18}$$

When noise is present, for a fixed signal/noise power ratio, the noise phase variance at the output of the loop depends on B_L , consequently ω_n should be chosen to be just small enough so that the tracking error stays within acceptable bounds for the smallest signal/noise power ratio for which the PLL is expected to give satisfactory operation. If ω_n is too small, the transient response of the PLL may be very slow. The value of the damping constant ζ which minimises Eqn. A11.1.13 is $\zeta = \frac{1}{2}$, but this is not the optimum response [14].

Stiffler [15, ch.5] has shown that $\zeta = \sqrt{\frac{1}{2}}$ gives the optimum type 2 2nd order loop, in the sense that it minimises the output phase variance and the pull-in time.

A11.1.2 Nonlinear model of APLL

Consider the PD in Fig. A11.1a to be a perfect multiplier. When the two inputs are $v_1(t)$ and $v_2(t)$, its output is $K_m v_1(t)v_2(t)$, where K_m is a constant with dimensions of volt⁻¹. Let one input to the multiplier be the incoming signal

$$v(t) = \sqrt{2V} \sin[\omega_c t + \theta(t)] \quad \text{A11.1.19}$$

The other input to the multiplier comes from the VCO and has the form

$$\hat{v}(t) = \sqrt{2\hat{V}} \cos[\omega_c t + \hat{\theta}(t)] \quad \text{A11.1.20}$$

The output of the multiplier is found to be

$$\begin{aligned} \hat{e}(t) &= K_m v(t)\hat{v}(t) \\ &= K_m V\hat{V} \sin[\theta(t) - \hat{\theta}(t)] + K_m V\hat{V} \sin[2\omega_c t + \theta(t) + \hat{\theta}(t)] \end{aligned} \quad \text{A11.1.21}$$

Ignoring the term at $2\omega_c$, which is removed by the loop filter, and

defining $K_d = K_m V \hat{V}$ yields

$$\begin{aligned} e(t) &= K_d \sin[\theta(t) - \hat{\theta}(t)] \\ &= K_d \sin[\epsilon(t)] \end{aligned} \quad \text{A11.1.22}$$

where $\epsilon(t)$ is defined by Eqn. A11.1.3.

An exact equivalent model of the PLL shown in Fig. A11.1a, with the PD a perfect multiplier, is shown in Fig. A11.1c. No linearizing approximation has yet been imposed.

The signal-linearizing approximation invariably made requires that $\epsilon(t)$ to be small so that $\sin[\epsilon(t)] \approx \epsilon(t)$, and the useful output of the PD is approximated by $K_d \epsilon(t)$, as given by Eqn. A11.1.2. Thus, in fact, the PD has a sinusoidal characteristic as shown in Fig. A11.1d. An examination of the sinusoidal PD characteristic indicates that the zero null is stable whereas the $-\pi$ null is not. With a phase error near the zero null the PLL tends to remain locked, whereas for a phase error near $-\pi$ the pull tends to drift away from the null. The rate of correction in the PLL depends upon the PD output voltage. If the PLL state initially results in a $-\pi$ null, the error control voltage is small. The loop state is unstable at this null. However the rate of divergence will be slow, as will be the rate of convergence to a stable null. This is known as the "hangup" phenomenon and the PLL requires excessive acquisition times [17].

A11.2 Digital phase-locked loop (DPLL)

To be classified as digital, a loop ought to have at least these two properties [13]:

- 1) Output phase is generated in a discrete increment, not a continuous function.
- 2) Error signal is generated as a digital number, not as an analog voltage.

A DPLL is shown in Fig. A11.2a. Let the received signal be

$$r(t) = \sqrt{2}V \sin[\omega_c t + \theta(t)] \quad \text{A11.2.1}$$

where ω_c is the VCO centre frequency and $\theta(t)$ is the time varying input phase relative to ω_c . The signal is sampled to give at time $t=iT$

$$r_i = \sqrt{2}V \sin(\omega_c iT + \theta_i) \quad \text{A11.2.2}$$

where $\theta_i = \theta(iT)$ and $r_i = r(iT)$. The sampled input signal is multiplied by a reference signal

$$\hat{r}_i = \sqrt{2}\hat{V} \cos(\omega_c iT + \hat{\theta}_{i/i-1}) \quad \text{A11.2.3}$$

where $\hat{\theta}_{i/i-1}$ is the predicted phase of $\hat{\theta}$ at time $t=iT$ from the received information at time $t=(i-1)T$, to give an error signal \hat{e}_i which is dependent on the phase and frequency difference between the signals r_i and \hat{r}_i . The samples are assumed to be taken at a rate such that the effects of aliasing are negligible.

The error signal at the PD output (multiplier in Fig. A11.2a) is

$$\hat{e}_i = \sqrt{2}V \sin(\omega_c iT + \theta_i) \sqrt{2}\hat{V} \cos(\omega_c iT + \hat{\theta}_{i/i-1}) \quad \text{A11.2.4}$$

$$= V\hat{V} \{ \sin(\theta_i - \hat{\theta}_{i/i-1}) + \sin(2\omega_c iT + \theta_i + \hat{\theta}_{i/i-1}) \} \quad \text{A11.2.5}$$

Thus
$$e_i = V\hat{V} \sin \epsilon_i \quad \text{A11.2.6}$$

- neglecting the term centered at $2\omega_c$ because of the lowpass filtering action of the PLL, and where ϵ_i is the phase error

$$\epsilon_i = \epsilon(iT) = \theta_i - \hat{\theta}_{i/i-1} \quad \text{A11.2.7}$$

with $\hat{\theta}_{i/i-1}$ the predicted value of $\hat{\theta}_i$ at time $t=iT$ from the received information at time $t=(i-1)T$. Now

$$\hat{\theta}_{i/i-1} = \hat{\theta}_{i-1/i-2} + K_v e_{i-1} \quad \text{A11.2.8}$$

hence $\hat{\theta}_{1/i-1} - \hat{\theta}_{1-1/i-2} = K_V e_{i-1}$ A11.2.9

$$\hat{\theta}_{1/i-1} [1-z^{-1}] = K_V e_{i-1}$$
 A11.2.10

$$\hat{\theta}_{1/i-1} = \frac{K_V}{1-z^{-1}} e_{i-1}$$
 A11.2.11

where z^{-1} is a delay of one sample period and K_V is the VCO gain factor.

From Eqns. A11.2.7 and A11.2.11, ϵ_1 becomes

$$\epsilon_1 = \theta_1 - K_V e_{i-1} \frac{z}{z-1}$$
 A11.2.12

$$= \theta_1 - \hat{e}_1 K_V \frac{z}{z-1} F(z) \frac{1}{z}$$
 A11.2.13

where $e_{i-1} = \hat{e}_{i-1} F(z) = \hat{e}_1 F(z) z^{-1}$ has been used.

Thus, from Eqns. A11.2.5, A11.2.6 and A11.2.13,

$$\epsilon_1 = \theta_1 - \frac{KF(z)}{z-1} (V \sin \epsilon_1)$$
 A11.2.14

where $K=K_V \hat{V}$ is the product of all loop gain. The model of the DPLL is shown in Fig. A11.2b. Since the phase error signal (Eqn. A11.2.6) is a sinusoidal function of the phase error, the loop suffers from the "hangup" phenomenon [17] (Appendix A11.2.2). When ϵ_1 is small, the approximation $\sin \epsilon_1 \approx \epsilon_1$ is valid and the sinusoidal nonlinearity can be removed from the model of Fig. A11.2b. Assuming a linear model, then the Closed Loop Transfer Function is given by

$$\frac{\hat{\theta}_{1/i-1}}{\theta_1} = H(z) = \frac{VKF(z)/(z-1)}{1 + VKF(z)/(z-1)}$$
 A11.2.15

$$= \frac{VKF(z)}{(z-1) + VKF(z)}$$
 A11.2.16

For a Type 1 Order 1 PLL $F(z)=1$ A11.2.17

Type 2 Order 2 PLL $F(z)=1+\mu z/(z-1)$ A11.2.18

Let $\gamma=VK$, then for a Type 2 Order 2 PLL

$$H(z) = \frac{\gamma(z-1) + \mu\gamma z}{(z-1)^2 + \gamma(z-1) + \mu\gamma z}$$
 A11.2.19

As for an APLL, a 1st order Type 1 (Eqn. A11.2.17) DPLL can track a phase step $\Delta\theta/(1-z^{-1})$ with no steady state error, and can track a frequency step $\Delta\theta_m/(1-z^{-1})^2$ with a steady state error of $\Delta\theta_m/VK$. Furthermore, a 2nd order Type 2 DPLL (Eqn. A11.2.18) can track both phase and frequency steps with no steady state error [22],[21]. A 2nd Type 2 APLL is optimum for tracking phase and frequency offsets[16,ch.6] but the optimum DPLL for tracking phase and frequency offsets has an ORDER number one degree higher than that for an APLL [18]. However, if the expected difference between the frequency of $r(iT)$ and $\tilde{r}(iT)$ is much less than $1/T$, where $1/T$ is the sampling rate, then the constants μ and γ in Eqn. A11.2.19 can be chosen such that $\mu, \gamma \ll 1$. Consequently the DPLL is for practical purpose, an optimum PLL for tracking phase and frequency offsets [19].

Drawing a servo terminology, the Characteristic Equation (CE) is the denominator of the Closed Loop Transfer Function (Eqn. A11.2.19). Hence the CE is

$$(z-1)^2 + \gamma(z-1) + \mu\gamma z = 0 \quad \text{A11.2.20}$$

$$(z-1)^2 + (\gamma + \mu\gamma)(z-1) + \mu\gamma = 0 \quad \text{A11.2.21}$$

$$\theta \quad (z-1)^2 + 2\zeta\omega_n(z-1) + \omega_n^2 = 0 \quad \text{A11.2.22}$$

where

$$\omega_n = \sqrt{\mu\gamma}$$

and

$$\zeta = (\gamma + \mu\gamma)/2\sqrt{\mu\gamma} \quad \text{A11.2.24}$$

are the natural frequency and damping factor, respectively, of the loop. The roots of the CE are

$$a_1, a_2 = \frac{1}{2}(2 - \gamma - \mu\gamma) \pm \frac{1}{2}\sqrt{(\gamma + \mu\gamma)^2 - 4\mu\gamma} \quad \text{A11.2.25}$$

For critical damping, the term $\frac{1}{2}\sqrt{(\cdot)}$ in Eqn. A11.2.25 is zero, giving

$$(a_1, a_2)_{\text{CRITICAL}} = 1 - \sqrt{\mu\gamma} \quad \text{A11.2.26}$$

and results in (Eqn. A11.2.24)

$$s = \frac{\gamma + \mu\gamma}{2\sqrt{\mu\gamma}} = \frac{1 - \frac{1}{2}(2-\gamma-\mu\gamma)}{1 - [1 - \sqrt{\mu\gamma}]} \quad \text{A11.2.27}$$

$$= \frac{1}{2}(1+\mu) \sqrt{\gamma/\mu} \quad \text{A11.2.28}$$

As for the APLL, s has an optimum value of $\sqrt{1/2}$ [19]. so Eqn. A11.2.28 becomes, for $\mu \ll 1$

$$\mu = \gamma(1 + 2\mu)/2 \approx \gamma/2 \quad \text{A11.2.29}$$

A11.3 Mth power loop

In M-ary PSK systems the set of phase states is a multiple of $2\pi/M$ and raising the signal to the power of M (by using an M-power device) will provide a component at M times the carrier frequency. This can be seen by an expansion. Let the noise free received signal be given by

$$r(t) = \cos(\omega_c t + \theta) \quad , 0 \leq t < T \quad \text{A11.3.1}$$

where $\theta = 2\pi k/M$; $k=0, 1, \dots, M-1$. Passing $r(t)$ through the nonlinearity and using the well-known Fourier series expansion of $\cos^M x$ yield [16,p71], [20,p137]

$$\begin{aligned} r^M(t) &= \cos^M(\omega_c t + \theta) = \cos^{2p}(\phi) \\ &= \frac{1}{2^{2p}} {}_{2p}C_p + \frac{1}{2^{2p-1}} [\cos 2p\phi + {}_{2p}C_1 \cos(2p-2)\phi + \dots + {}_{2p}C_{p-1} \cos 2\phi] \quad \text{A11.3.2} \end{aligned}$$

where ${}_{2p}C_p = 2p! / p!(2p-p)!$, $p=M/2$ and $\phi = \omega_c t + \theta$. Thus the nonlinearity output contains a component at even harmonic of ω_c and the component at $M\omega_c$ has zero phase modulo- 2π . A PLL, as shown in Fig. A11.3, then can be used to track the $M\omega_c$ component. Frequency division by M of the PLL output signal yields the required carrier reference with an M-fold phase ambiguity. Since a PLL is used, the Mth power loop also suffers from the "hangup" phenomenon [17] (Appendix A11.1.2). With $M=4$ and 8, the loop can be used for DEQPSK and CDE8PSK signals, respectively.

A11.4 Costas loop

The error control signal to the VCO can be derived by means of baseband processing. In the 4-phase Costas loop shown in Fig. A11.4a, the received 4-phase signal is multiplied by outputs of a VCO with phase shifts of $k\pi/2$, where $k=0, 1, 2$ and 3 . The filters in the four channels are used to remove the high frequency components in the outputs of the multipliers A, B, C and D. Multiplication of the four lowpass filter outputs produces an error signal that is a function of $\sin[4\epsilon(t)]$, where $\epsilon(t)=\theta(t)-\hat{\theta}(t)$. Eqn. A11.1.22 is the inphase channel phase error, which is used to control the phase of the VCO signal. It has been shown [16] that the Costas loop and the 4th loop provide the same performance provided that

- 1) the Costas arms filters provide the same noise filtering as that of the lowpass equivalent of the 4th power loop IF filters,
- 2) the VCO prefilters are identical, and
- 3) the Costas VCO gain measured in rad/s-V must be one-quarter of the 4th loop's VCO because of operation at ω_c rather than $4\omega_c$.

It should be noted that, since the phase signal is a sinusoidal function of the phase error, the loop also suffers from the "hangup" phenomenon (Appendix A11.2.2). The Costas loop for M-ary PSK signal is shown in Fig. A11.4b.

A11.5 Decision-feedback loop [16],[21]

Figure A11.5a shows one possible implementation of a biphasic decision-feedback loop [16],[21]. Let the received suppressed carrier signal be

$$r(t) = \sqrt{2}V m(t) \sin[\omega_c t + \theta(t)] \quad \text{A11.5.1}$$

where V is a constant and the linear modulation $m(t)$ possesses no continuous d.c. component in its power spectrum. $r(t)$ is demodulated by a

reference signal

$$r'_m(t) = r(t) \{ \sqrt{2} \hat{V} \cos[\omega_c t + \hat{\theta}(t)] \} \quad \text{A11.5.2}$$

$$= \hat{V} \hat{m}(t) \sin[\theta(t) - \hat{\theta}(t)] + \hat{V} \hat{m}(t) \sin[2\omega_c t + \theta(t) + \hat{\theta}(t)] \quad \text{A11.5.3}$$

where \hat{V} is a constant and $\hat{\theta}(t)$ is the loop phase estimate. The lowpass filters only remove the high frequency components, but do not distort the data signal, so at the output of the lowpass filter in the upper loop is

$$r_m(t) = \hat{V} \hat{m}(t) \sin \epsilon(t) \quad \text{A11.5.4}$$

with $\epsilon(t)$ the phase error $\theta(t) - \hat{\theta}(t)$. The signal is then delayed by one symbol interval T and multiplied by an estimate of the data produced at the output of the data demodulator $\hat{m}(t-T)$. The modulating signal has the form

$$m(t) = \left(\sum_i q_i g(t-iT) \right) \exp[j\epsilon(t)] \quad \text{A11.5.5}$$

where the $\{q_i\}$ are the transmitted data symbols. $g(t)$ is the equivalent baseband impulse response of the transmitter shaping filter and $\epsilon(t)$ is the phase error waveform. The corresponding estimate of the modulating waveform $m(t)$ is, neglecting any phase error,

$$\hat{m}(t) = \sum_i \hat{q}_i g(t-iT) \quad \text{A11.5.6}$$

where the $\{\hat{q}_i\}$ are the detected signal elements. Assume the channel introduces no signal distortion and the transmitted signal element $q_i g(t-iT)$ has a duration of T seconds, the modulation estimator of Fig. A11.5a becomes that shown in Fig. A11.5b. In Fig. A11.5b, the matched filter $g(T-t)$ is matched to the transmitted pulse $\{q_i g(t-iT)\}$. The detection process shown in Fig. A11.5b is the optimum detector for detecting q_i from $r_m(t)$ in the presence of AWGN in the sense that it minimises the probability of error in the $\{\hat{q}_i\}$ [1].

The estimate of the modulation $m(t-T)$ is then multiplied with $r_m(t-T)$ to give, at the input of the filter $F(s)$

$$e(t) = r_m(t-T) \hat{m}(t-T) \quad \text{A11.5.7}$$

$$= V\hat{V}m(t)\hat{m}(t) \exp(-j\omega T) \quad \text{A11.5.8}$$

where $\exp(-j\omega T)$ is a delay of T seconds. When the bandwidth of the loop is small relative to the signalling data rate, $1/T$, i.e., the phase error is essentially constant for several time intervals (each of length T), then the product $m(t)\hat{m}(t)$ can be replaced by its average value [16]:

$$E\{m(t)\hat{m}(t)\} = (+1) \times \text{Prob}\{m(t)=\hat{m}(t)\} + (-1) \times \text{Prob}\{m(t) \neq \hat{m}(t)\} \quad \text{A11.5.9}$$

$$= 1 - 2P_e[\epsilon(t)] \quad \text{A11.5.10}$$

where $P_e[\epsilon(t)]$ is the error probability of the data detector conditional on the loop phase error [16]. Under this assumption, the error signal to the loop filter is (Eqns. A11.5.8 and A11.5.10)

$$e(t) = \hat{V} [\exp(-j\omega T) \{ V (1-2P_e[\epsilon(t)]) \text{sinc}(t) \}] \quad \text{A11.5.11}$$

which is also a sinusoidal function of the loop error $\epsilon(t)$, so the loop also suffers from the "hangup" phenomenon [17] (Appendix A11.9.2). Note that the error signal is dependent on the error rate.

For a 4 phase signal, the received signal, in Fig. A11.5c, can be written as

$$r(t) = Vm_1(t) \sin[\omega_c t + \theta(t) - \pi/4] + Vm_2(t) \cos[\omega_c t + \theta(t) - \pi/4] \quad \text{A11.5.12}$$

where	$[m_1(t), m_2(t)] = +1, +1$	for $h=1, iT < t < (i+1)T$
	$= -1, +1$	for $h=2, iT < t < (i+1)T$
	$= -1, -1$	for $h=3, iT < t < (i+1)T$
	$= +1, -1$	for $h=4, iT < t < (i+1)T$

h being the particular phase being transmitted. The required extension to

4 phase signal requires the addition of a quadrature loop to Fig. A11.5a as shown in Fig. A11.5c. After the lowpass filtering, the upper and lower reference signals $r_u(t)$ and $r_l(t)$ become

$$r_u(t) = \hat{V} \times [V_{m_1}(t) \sin \epsilon(t) + V_{m_2}(t) \cos \epsilon(t)] / \sqrt{2} \quad \text{A11.5.13}$$

$$r_l(t) = \hat{V} \times [V_{m_1}(t) \cos \epsilon(t) - V_{m_2}(t) \sin \epsilon(t)] / \sqrt{2} \quad \text{A11.5.14}$$

Following the development given for the biphasic decision-feedback loop, the signals $e_u(t)$ and $e_l(t)$ are given by [15]

$$\begin{aligned} e_u(t) &= r_u(t) \hat{m}_1(t) \exp(-j\omega T) \\ &= \hat{V} \exp(-j\omega T) [m_1(t) \hat{m}_1(t) \sin \epsilon(t) + m_2(t) \hat{m}_1(t) \cos \epsilon(t)] / \sqrt{2} \end{aligned} \quad \text{A11.5.15}$$

and

$$\begin{aligned} e_l(t) &= r_l(t) \hat{m}_2(t) \exp(-j\omega T) \\ &= \hat{V} \exp(-j\omega T) [m_1(t) \hat{m}_2(t) \cos \epsilon(t) - m_2(t) \hat{m}_2(t) \sin \epsilon(t)] / \sqrt{2} \end{aligned} \quad \text{A11.5.16}$$

Following the same averaging argument as given in arriving at Eqn. A11.5.9, and the fact that $E[m_i(t) \hat{m}_j(t)] = 0$ for $i \neq j$, Eqns A11.5.15 and A11.5.16 reduce to

$$e_u(t) = \hat{V} \exp(-j\omega T) \{ 1 - 2P_{e1}[\epsilon(t)] \} \sin \epsilon(t) \quad \text{A11.5.17}$$

$$\text{and} \quad e_l(t) = \hat{V} \exp(-j\omega T) \{ 1 - 2P_{e2}[\epsilon(t)] \} \sin \epsilon(t) \quad \text{A11.5.18}$$

respectively, with P_{e1} and P_{e2} the error probabilities in the upper and lower loops, respectively. Letting $e(t) = e_u(t) + e_l(t)$, the error signal at the input of the filter $F(s)$ is

$$e(t) = 2\hat{V} \exp(-j\omega T) \{ 1 - P_{e1}[\epsilon(t)] - P_{e2}[\epsilon(t)] \} \sin \epsilon(t) \quad \text{A11.5.19}$$

This quadriphase loop, in principle, can be extended to M phases where M phase loop requires $M/2$ 'arms' giving $M/2$ decisions $\hat{m}_h(t)$, for $h=0, 1, \dots, (M/2-1)$, where the $\{\hat{m}_h(t)\}$ are again ± 1 waveforms whose transitions

occur at T second intervals. The VCD output would be phase shifted by $(h-1)\pi/M$, $h=0, 1, 2, \dots, (M/2-1)$, to provide $M/2$ coherent reference signals [6].

The disadvantages of the decision-feedback loops as follows.

- 1) It is very difficult to design an analogue filter with the wanted impulse response of $g(T-t)$,
- 2) With large value of M , the circuit becomes complicated and less efficiency.
- 3) It also suffers from the "hangup" phenomenon.

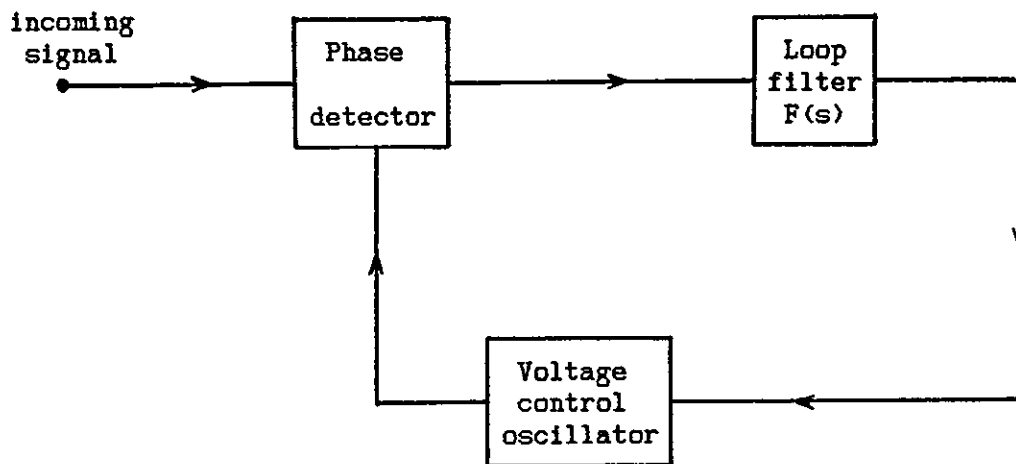


Figure A11.13 Phase-locked loop (PLL).

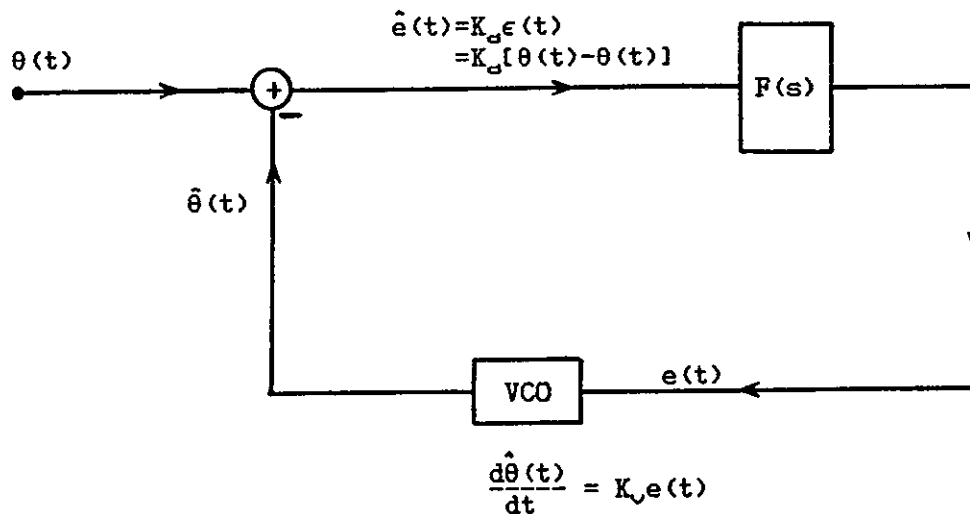


Figure A11.1b Linearised APLL basic block diagram.

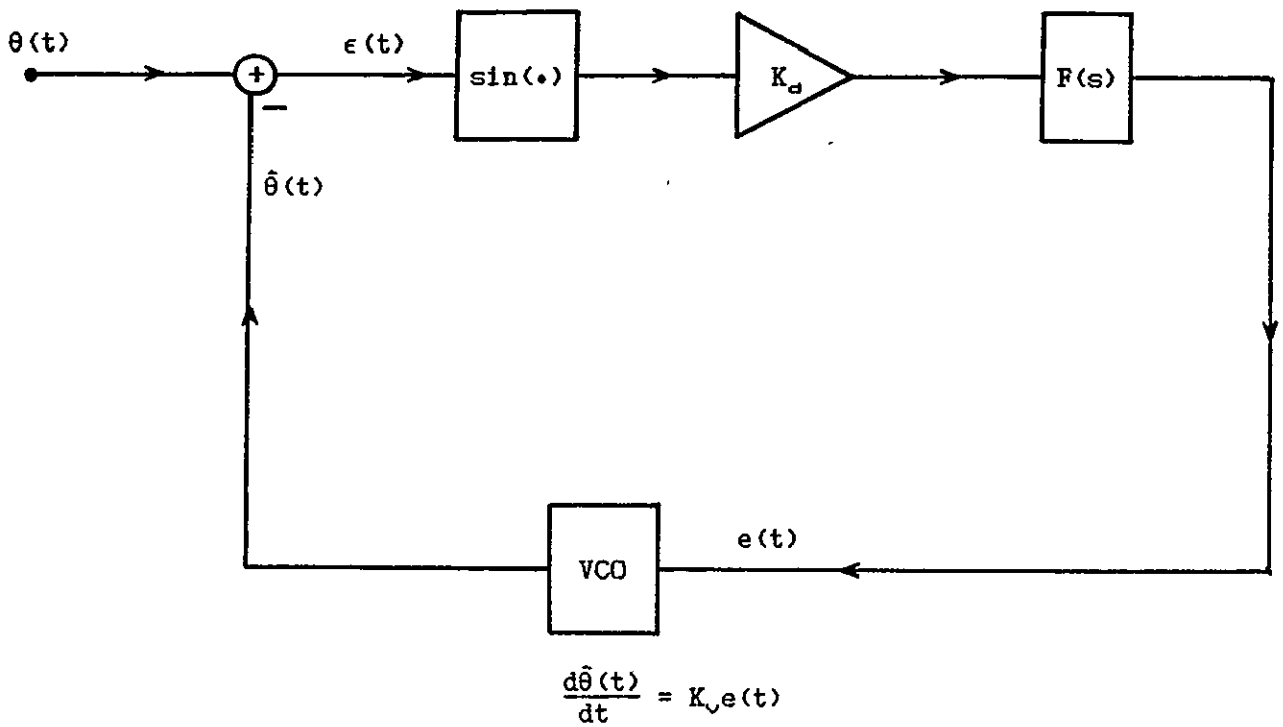


Figure A11.1c Nonlinearised APLL basic block diagram.

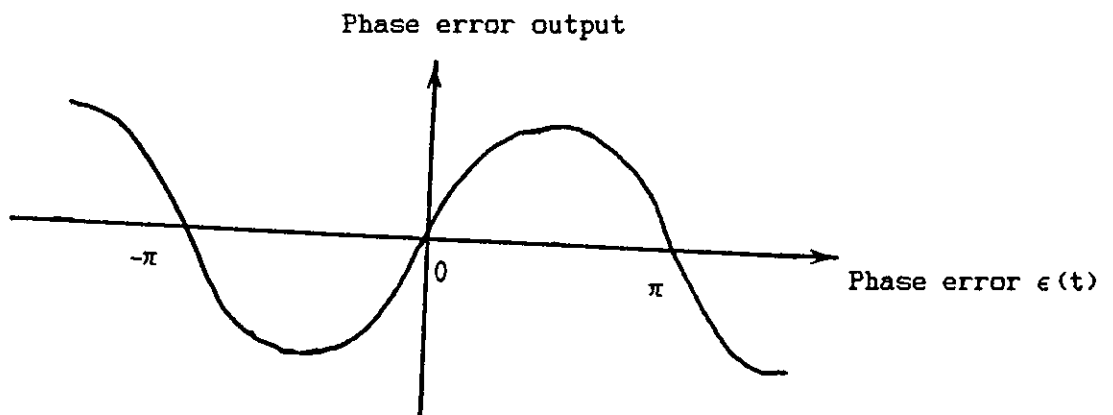


Figure A11.1d Sinusoidal phase detector characteristic.

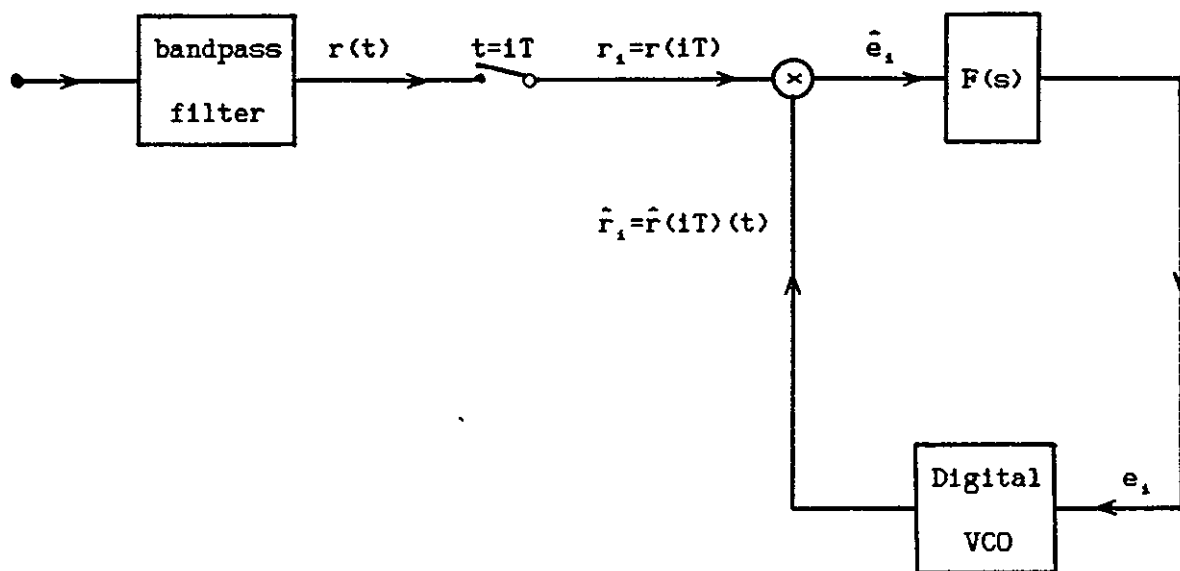
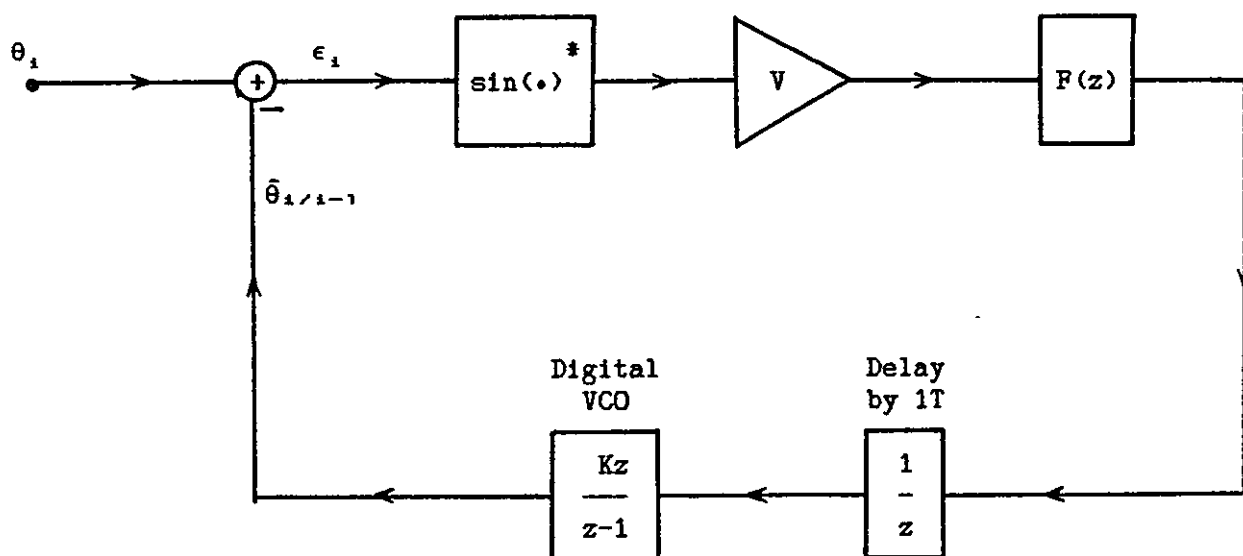


Figure A11.2a Digital phase-locked loop (DPLL) structure.



* omit for a linear model

Figure A11.2b Model of a DPLL.

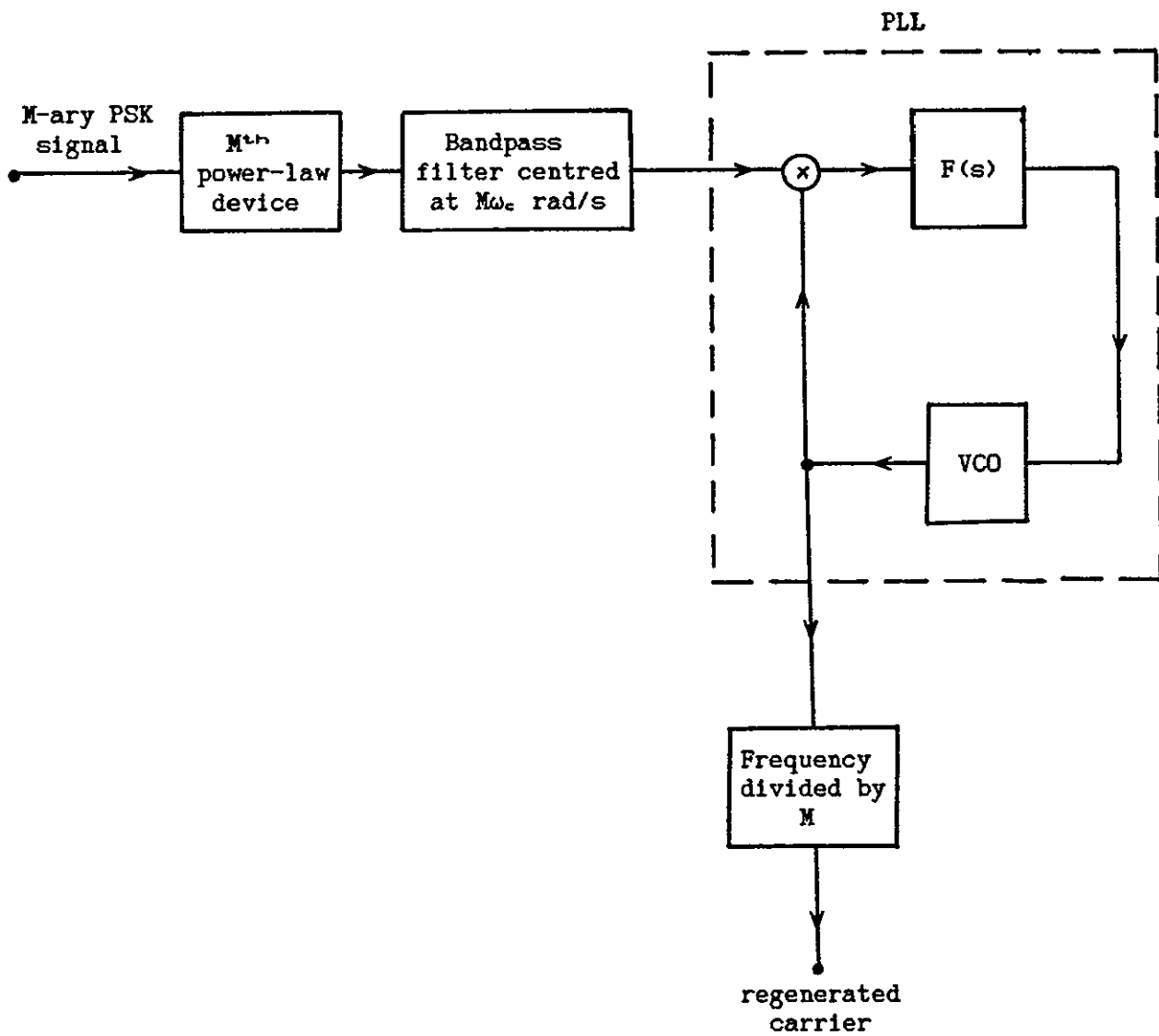


Figure A11.3 The M^{th} power loop.

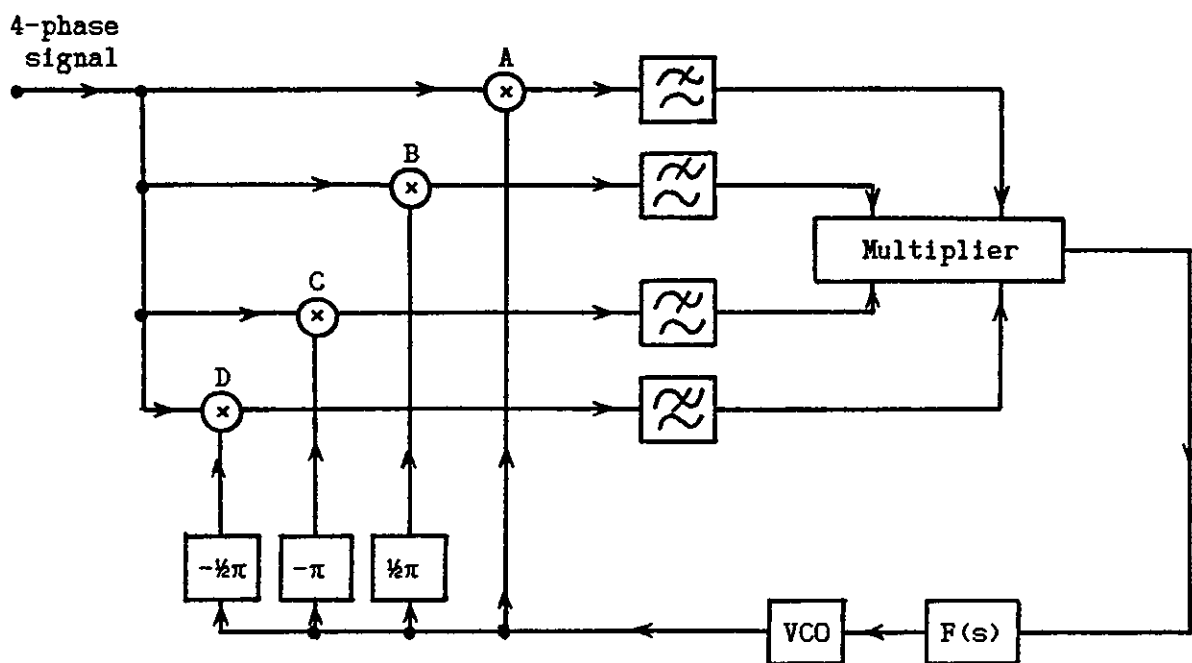


Figure A11.4a The 4-phase Costas loop.

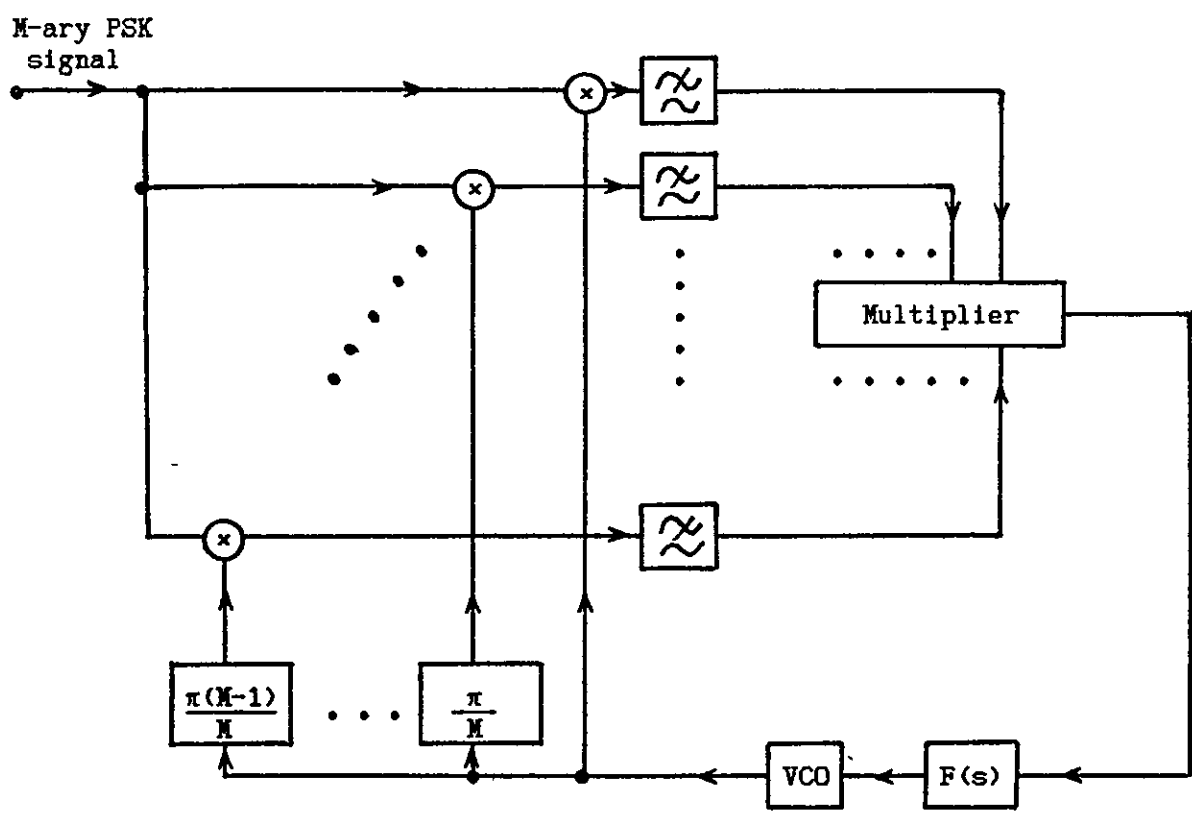


Figure A11.4b The M-phase Costas loop.

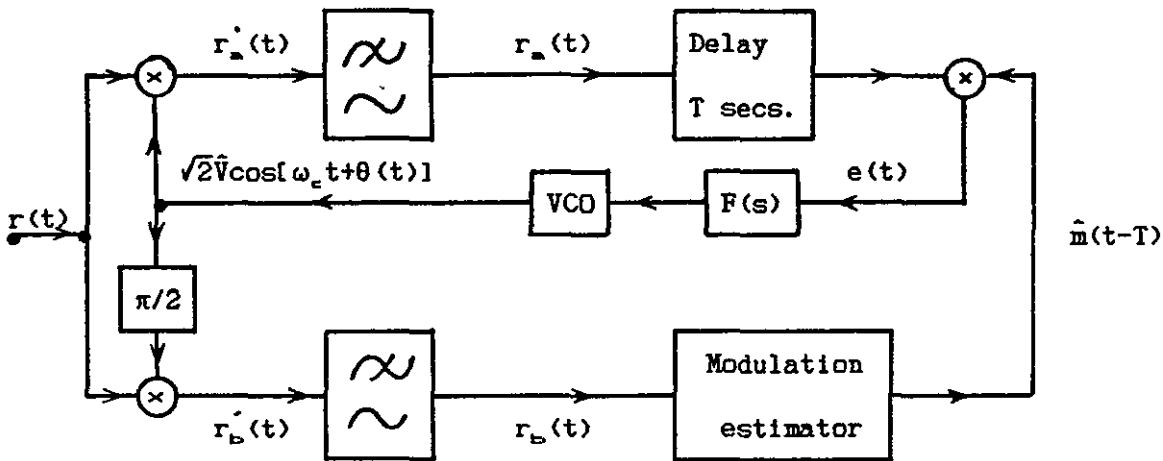


Figure A11.5a The biphase decision-feedback loop.

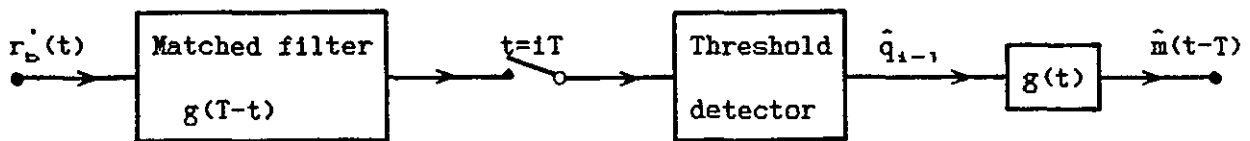


Figure A11.5b Modulation estimation for non-overlapping T seconds duration signal pulses.

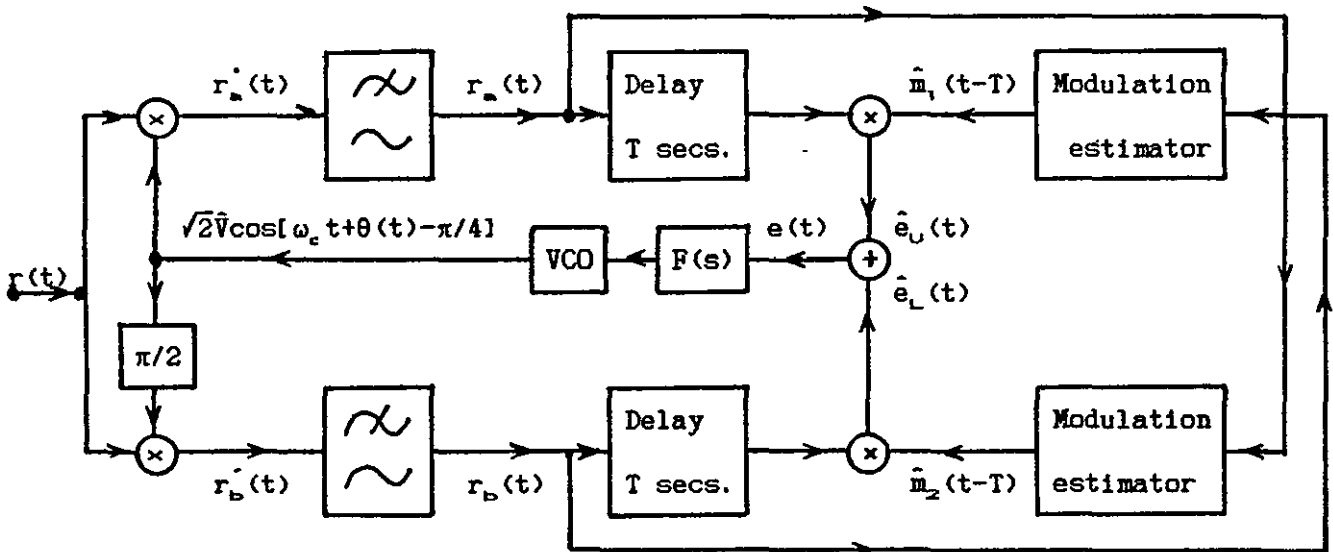


Figure A11.5c The quadriphase decision-feedback loop.

APPENDIX A12

SIMULATOR FOR DEQPSK SIGNALS WITH THE USE OF THE MDPL

THIS PROGRAM IS USED TO EVALUATE THE ERROR-RATE PERFORMANCES OF SIGNALS 1A, 2A, 3A AND 4A, OVER A NONLINEAR AND BANDLIMITED SATELLITE CHANNEL, WITH THE USE OF THE SUBOPTIMUM FILTERS, THE PREDISTORTER, THE AMPLIFIER LIMITER, PHASE DEMODULATOR A OR B AND THE MDPL AND IN AN ACI ENVIRONMENT

```
/*JOB D1,EUELSWC,ST=MFY,C=S,TI=1280,
/* PW=SWC
FTN5,DB=0/PMD,L=0.
LIBRARY(PROCLIB,*)
NAG(FTN5)
LGO.
####S
```

```
PROGRAM SWCAB(INPUT,OUTPUT,TAPE1=INPUT,TAPE2=OUTPUT)
DIMENSION BSF(-200:200),FF1(0:63),FF2(0:63),FF3(0:63),FF4(0:63)
DATA (FF1(I),I=0,63)/1.0,.943,.786,.566,.334,.135,.0,-.064,-.068,
*-.038,-.001,.024,.029,.017,-.001,-.014,-.017,-.011,
*-.001,.008,.01,.007,-.001,-.007,-.008,
*-.006,-.001,.004,.005,.003,-.001,-.004,-.005,-.004,
*.0,.003,.004,.002,.0,-.003,-.004,-.003,-.001,.002,.003,
*.002,.0,-.003,-.003,-.002,.0,.001,.002,.001,.0,-.002,
*-.003,-.002,-.001,.001,.002,.001,.0,-.002/
```

C

```
DATA (FF2(I),I=0,63)/1.0,.954,.825,.638,.425,.223,.06,-.047,
*-.095,-.096,-.067,-.028,.005,.022,.022,.01,-.006,-.018,-.022,
*-.018,-.008,.003,.011,.012,.009,
*.002,-.004,-.007,-.007,-.003,.002,.006,.006,.004,.0,-.005,
*-.007,-.008,-.005,-.002,.001,.003,.002,.0,-.002,-.004,-.004,
*-.002,.001,.004,.005,.005,.003,.0,-.002,-.003,-.002,.0,
*.001,.002,.001,.0,-.003,-.005/
```

C

```
DATA (FF3(I),I=0,63)/1.0,.963,0.858,0.7,0.511,0.316,0.139,-0.001,
*-0.094,-0.138,-0.14,-0.112,-0.068,-0.022,0.035,0.039,0.03,0.014,
*0.014,-0.003,-0.015,-0.02,-0.017,-0.008,0.002,
*.011,.016,.015,.01,.003,-.005,-.01,-.011,-.009,
*-.005,.001,.005,.008,.007,.003,-.001,-.005,
*-.008,-.008,-.006,-.002,.002,.005,.006,
*.005,.002,-.002,-.005,-.006,-.006,-.004,.0,
*.003,.005,.005,.003,.001,-.003,-.005/
```

C

```
DATA (FF4(I),I=0,48)/1.0,.970,.884,.751,.585,.405,
```

```

*.227,.068,-.058,-.144,-.188,-.192,-.164,-.115,-.056,
*.002,.049,.08,.091,.085,.065,.036,.006,-.02,-.039,
*-.047,-.045,-.034,-.019,-.003,.011,.021,.024,.021,.014,
*.004,-.005,-.012,-.016,-.015,-.011,-.004,.003,.009,
*.013,.013,.01,.005,-.002/

```

C

```

DO 10009 NR=1,7
PRINT*, 'INPUT BASEBAND FILTER R.O.F (SQ.)=1,0.75,0.5,0.25'
READ*,ROF
PRINT*, 'INPUT THE TRUNCATION LENGTH'
READ*,KT12
PRINT*, 'INPUT THE NOISE VARIANCE'
READ*,P
PRINT*, 'INPUT THE RANDOM SEED'
READ*,IIQQ
PRINT*, 'INPUT NO. OF TESTED SYMBOLS'
READ*,L

```

C

```

IF(ROF.EQ.1) THEN
DO 100 I=0,63
100 BSF(I)=FF1(I)
PBOP=7.9
CT BOP=5.74
BOP=6.46
ELSEIF(ROF.EQ.0.75) THEN
DO 101 I=0,63
101 BSF(I)=FF2(I)
PBOP=9.096
CT BOP=6.7
BOP=7.39
ELSEIF(ROF.EQ.0.5) THEN
DO 102 I=0,63
102 BSF(I)=FF3(I)
PBOP=10.408
CT BOP=7.67
BOP=8.43
ELSEIF(ROF.EQ.0.25) THEN
DO 103 I=0,63
103 BSF(I)=FF4(I)
PBOP=11.955
CT BOP=8.75
BOP=9.645
ELSE
PRINT*, 'NO REQUIRED FILTER'
STOP
ENDIF

```

C

```

CALL QPSKSUB(KT12,ROF,BSF,P,IIQQ,L,BOP,PBOP)
10009 CONTINUE
STOP
END

```

C

```

SUBROUTINE QPSKSUB(KT12,ROF,BSF,P,IIQQ,L,BOP,PBOP)
DIMENSION IX2(-50:50),X2(-400:400),XX2(-400:400),
1XXX1(-400:400),XXX2(-400:400),FR(-200:200),GQ(0:38),GR(0:38),
1BSF(-200:200),FM(-200:200),
2IX1(-50:50),FT(-200:200),
2X1(-300:300),XX1(-300:300),
2XU1(-300:100),XU2(-300:100),
2BF(-400:400),PGR(0:38),PGQ(0:38),

```

```

2PHDL(-8:0),
2XL1(-300:100),XL2(-300:100),
2IS(-1:0),ISSD(-1:0),ISD(-1:0),
2RS(320),QS(320),ADJI(16),ADJQ(16)
COMMON /PPII/PI0,PI1,PI2,PI3
DATA(FT(I),I=0,24)/1.0,0.935,0.758,0.512,0.256,0.041,-0.099,
*-0.157,-0.146,-0.094,-0.031,0.02,0.048,0.052,0.039,0.017,-0.004,
*-0.017,-0.021,-0.017,-0.008,0.002,0.009,0.011,0.008/

```

C

```

DATA(FR(I),I=0,24)/1.0,0.935,0.758,0.512,0.256,0.041,-0.099,
*-0.157,-0.146,-0.094,-0.031,0.02,0.048,0.052,0.039,0.017,-0.004,
*-0.017,-0.021,-0.017,-0.008,0.002,0.009,0.011,0.008/

```

C

```

DATA(GQ(I),I=0,38)/0.17,0.34,0.48,0.58,0.65,0.70,0.75,
*0.78,0.82,0.84,0.85,0.85,0.84,0.83,0.84,0.85,0.83,
*0.82,0.80,0.78,0.75,0.73,0.7,0.67,0.65,0.61,0.58,0.56,
*0.53,0.50,0.48,0.43,0.4,0.38,0.37,0.36,0.34,0.36,0.35/

```

C

```

DATA(GR(I),I=0,38)/3.57,3.17,2.83,2.55,2.33,2.15,1.99,
*1.83,1.69,1.55,1.44,1.30,1.20,1.09,1.0,0.92,0.86,0.80,
*0.74,0.68,0.63,0.58,0.54,0.50,0.46,0.43,0.4,0.37,0.352,
*0.352,0.332,0.332,0.31,0.3,0.3,0.29,0.29,0.28,0.28/

```

C

```

DATA(PGR(I),I=0,38)/0.280,0.280,0.280,0.285,0.309,0.309,
*0.319,0.341,0.357,0.358,0.386,0.399,0.418,0.432,0.453,
*0.468,0.492,0.504,0.574,0.594,0.594,0.594,0.594,0.594,
*0.594,0.594,0.594,0.594,0.594,0.594,0.594,0.594,0.594,
*0.594,0.594,0.594,0.594,0.594,0.594/

```

C

```

DATA(PGQ(I),I=0,38)/-0.005,-0.012,-0.015,-0.020,-0.033,-0.038,
*-0.051,-0.063,-0.076,-0.086,-0.104,-0.122,-0.136,-0.157,-0.188,
*-0.218,-0.251,-0.315,-0.425,-0.544,-0.544,-0.544,-0.544,-0.544,
*-0.544,-0.544,-0.544,-0.544,-0.544,-0.544,-0.544,-0.544,-0.544,
*-0.544,-0.544,-0.544,-0.544,-0.544,-0.544/

```

C

```

RR=SQRT(PGR(20)**2+PGQ(20)**2)
DO 136 I=0,38
  PGQ(I)=PGQ(I)/RR
  PGR(I)=PGR(I)/RR

```

136

C

```

PI1=ACOS(-1.0)
PI0=PI1/2.0
PI2=PI0*3.0
PI3=2.0*PI1

```

C

```

PI4=PI0/2
PI5=PI4*3
PI6=PI4*5
PI7=PI4*7

```

C

```

KS1: NO OF THE SAMPLES IN ONE T.
KT1: SYMBOL LENGTH OF THE TRUNCATED IMPULSE RESPONSE WAVEFORM
OF THE BASEBAND SHAPPING FILTER IN CASCADED WITH THE BPF.
KS2: THE BASEBAND SHAPPING ARRAY EXTENDS FROM -KS3 TO +KS2.
KT2: SYMBOL TIME FOR THE 1ST SAMPLE INSTANCE
KS3: ARRAY ELEMENT FOR THE 1ST SAMPLE.
KT12: TRUNCATED OF THE BASEBAND SHAPPING FILTER.
KT4: SYMBOL LENGTH OF THE IMPULSE RESPONSE OF FT IN THE TX
KS4: THE LAST ELEMENT IN FT
KT5: SYMBOL LENGTH OF THE IMPULSE RESPONSE OF FT IN THE RX

```

C

C KS5: THE LAST ELEMENT IN FR
C KTM1: SYMBOL LENGTH OF THE IMPULSE RESPONSE OF THE MATCHED-FILTER
C KSM1: THE LAST ELEMENT IN MF
C

KS1=8

C***SETUP SYNC PARAMETERS***

PRINT*, 'OFFSET(HZ) INIT PHASE ERROR(DEG)'

READ*, FOS, PHI

FPH=0

FPH1=0

FPH2=0

RCOR=1

QCOR=0

PHCOR=0

PHEF=0

PHI=PHI*PI1/180

PHF=PI3*FOS/(32.0E3*KS1)

F1=PHI

C*****

C

KT4=3

KT1=2*(KT12+KT4)

KT3=KT1*(-1)/2

KS1=8

KS2=KT1*KS1/2

KS3=KS2*(-1)

KS4=KT4*KS1

KT5=3

KS5=KT5*KS1

KS12=KT12*KS1

KTM1=KT12+KT5

KSM1=KTM1*KS1

KT2=-KT1/2-KTM1

DO 165 I=KS4+1,200

165 FT(I)=0.0

DO 166 I=0,200

166 FT(-I)=FT(I)

DO 167 II=0,KS2

RR=BSF(0)*FT(II)

DO 168 I=1,KS12

168 RR=RR+BSF(I)*(FT(II+I)+FT(II-I))

167 BF(II)=RR

DO 150 I=0,KS2

BF(-I)=BF(I)

150 FM(I)=BF(I)

KS10=320

C

CSP=5

F=PI3*CSP/32.0

DO 164, I=1,KS10

FF=F*REAL(I)

RS(I)=COS(FF)

164 QS(I)=SIN(FF)

C

C INITIALISE ID

C

KT6=KT2

DO 104 I=KT6,0

IX1(I)=-1

104 IX2(I)=-1

```

C
C
C
INITIALISATION
KS6=KS3-KS1+1-2*KSM1
KS7=KS3-KS5
DO 105 I=KS6,KS2+KS1
  X1(I)=0.0
  X2(I)=0.0
  XXX1(I)=0.0
  XXX2(I)=0.0
  XX1(I)=0.0
  XX2(I)=0.0
  XU1(I)=0.0
  XU2(I)=0.0
  XL1(I)=0.0
105  XL2(I)=0.0
C
C
DX1=1.0
DX2=1.0
ISD(0)=0
C
DO 127 J=KT6,0
DX1=-DX1
DX2=-DX2
ISD(0)=2+ISD(0)
IF(ISD(0).EQ.4) ISD(0)=ISD(0)-4
DO 126 I=KS6,KS2
  II=I+KS1
  X1(I)=X1(II)
  X2(I)=X2(II)
  XU1(I)=XU1(II)
  XU2(I)=XU2(II)
  XL1(I)=XL1(II)
126  XL2(I)=XL2(II)
  DO 125 I=KS3,KS2
  X1(I)=BF(I)*DX1+X1(I)
  X2(I)=BF(I)*DX2+X2(I)
  XU1(I)=X1(I)
  XU2(I)=X2(I)
  XL1(I)=X1(I)
125  XL2(I)=X2(I)
127  CONTINUE
C
IS(0)=0
C
PRINT*, 'INPUT PREDBK AND BK'
READ*, PREDBK, BK
PAV=SQRT(4.0*PBOP)
AV=SQRT(4.0*BOP)
AV1=PREDBK/PAV
AV2=BK/AV
I=PREDBK
SUM1=SQRT(PGR(I)**2+PGQ(I)**2)
A1=PGR(I)/SUM1
B1=-PGQ(I)/SUM1
I=BK
SUM2=SQRT(GR(I)**2+GQ(I)**2)
A2=GR(I)/SUM2
B2=-GQ(I)/SUM2

```

```

A=A1*A2-B1*B2
B=A1*B2+B1*A2
DO 141 N=KS6,KS3
RN=X1(N)
QN=X2(N)
I=INT(AV1*SQRT(RN*RN+QN*QN))
PR=RN*PGR(I)-QN*PGQ(I)
PQ=RN*PGQ(I)+QN*PGR(I)
I=INT(AV2*SQRT(PR*PR+PQ*PQ))
141 X1(N)=PR*GR(I)-PQ*GQ(I)
C X2(N)=PR*GQ(I)+PQ*GR(I)

DO 146 N=KS6,KS3
R1=X1(N)
Q1=X2(N)
X1(N)=A*R1-B*Q1
X2(N)=A*Q1+B*R1

C
F1=F1+PHF
IF(F1.GT.PI3) THEN
  F1=F1-PI3
ELSEIF(F1.LT.-PI3) THEN
  F1=F1+PI3
ENDIF
R1=X1(N)
Q1=X2(N)
R2=COS(F1)
Q2=SIN(F1)
X1(N)=R1*R2-Q1*Q2
X2(N)=Q1*R2+R1*Q2
146 XX1(N)=X1(N)
C XX2(N)=X2(N)

DO 130 II=KS6+KS5,KS3-KS5
XXX1(II)=XX1(II)*FR(O)
XXX2(II)=XX2(II)*FR(O)
DO 135 I=1,KS5
R1=XX1(II+I)
R2=XX1(II-I)
Q1=XX2(II+I)
Q2=XX2(II-I)
XXX1(II)=XXX1(II)+FR(I)*(R1+R2)
135 XXX2(II)=XXX2(II)+FR(I)*(Q1+Q2)
130 CONTINUE
C

DO 133 I=KS6+KS5,KS3-KS5
CT RR=1/SQRT(XXX1(I)**2+XXX2(I)**2)
RR=1/(ABS(XXX1(I))+ABS(XXX2(I)))

C
C CORRECT OFFSETS
C
FPH=FPH+PHF
IF(FPH.GT.PI3) THEN
  FPH=FPH-PI3
ELSEIF(FPH.LT.-PI3) THEN
  FPH=FPH+PI3
ENDIF
R1=XXX1(I)
Q1=XXX2(I)
R2=COS(FPH)

```

```
Q2=SIN(FPH)
XXX1(I)=R1*R2+Q1*Q2
XXX2(I)=Q1*R2-R1*Q2
  XXX1(I)=XXX1(I)*RR
  XXX2(I)=XXX2(I)*RR
133
C
  KT7=KT2-1
  ISSD(0)=2
C
  I1: THE MAIN SAMPLING INSTANCE
  I1=KS3-KSM1
  I2: THE OFFSET SAMPLING INSTANCE.
  I2=I1
C
  XXXM1=XXX1(I1)*BSF(0)
  XXXM2=XXX2(I1)*BSF(0)
  DO 138 I=1,KS12
    XXXM1=XXXM1+BSF(I)*(XXX1(I1-I)+XXX1(I1+I))
    XXXM2=XXXM2+BSF(I)*(XXX2(I1-I)+XXX2(I1+I))
138
C
  CALL ANGSUB1(XXXM1,XXXM2,PH)
  PH1=PH
C
  PRINT*, 'INPUT GAMMA1 & ALPHA1'
  READ*, GAMMA1, ALPHA1
  GAMMA=0.1
  ALPHA=0.05
  NTEST2=600
  NTEST1=1
  P1=0
  ISW=0
  F2=F1
  F3=F1
  KS11=1
C
1006 CALL G05CBF(IIQQ)
C
  INITIALISE ALL COUNTERS.
  IE=0
  IA1=0
  IA2=0
  IA3=0
  IB1=0
  IB2=0
  IB3=0
  IBE=0
  E=0.0
  E1=0.0
  E2=0.0
C
C
C
  START
C
  DO 111 LLL=1,NTEST1
  DO 111 LL=1,NTEST2
C
C
C
  SHIFT IX
C
  DO 112 I=KT6,-1
    J=I+1
    IX1(I)=IX1(J)
```

```
112 IX2(I)=IX2(J)
C
C SHIFT IS & ISD FOR DIFF CODING & ENCODING
C
IS(-1)=IS(0)
ISD(-1)=ISD(0)
ISSD(-1)=ISSD(0)
C
C GENERATE DATA IX(0) AND GRAY CODE IT INTO R & Q.
C
U=G05DAF(0.000,4.000)
IF(U.LT.1.0) THEN
IX1(0)=-1
IX2(0)=-1
IS(0)=2
ELSEIF(U.LT.2.0) THEN
IX1(0)=-1
IX2(0)=1
IS(0)=1
ELSEIF(U.LT.3.0) THEN
IX1(0)=1
IX2(0)=-1
IS(0)=3
ELSE
IX1(0)=1
IX2(0)=1
IS(0)=0
ENDIF
C
IF(ISW.EQ.0) THEN
IX1(0)=-1
IX2(0)=-1
IS(0)=2
ENDIF
C
ISD(0)=IS(0)+ISD(-1)
IF(ISD(0).GE.4) ISD(0)=ISD(0)-4
IF(ISD(0).EQ.1) THEN
DX1=-1
DX2=1
ELSEIF(ISD(0).EQ.2) THEN
DX1=-1
DX2=-1
ELSEIF(ISD(0).EQ.3) THEN
DX1=1
DX2=-1
ELSE
DX1=1
DX2=1
ENDIF
C
C SHIFT ARRAY.
C
DO 113 I=KS6,KS2
II=I+KS1
X1(I)=X1(II)
X2(I)=X2(II)
XXX1(I)=XXX1(II)
XXX2(I)=XXX2(II)
XX1(I)=XX1(II)
```

```

      XX2(I)=XX2(II)
      XU1(I)=XU1(II)
      XU2(I)=XU2(II)
      XL1(I)=XL1(II)
113  XL2(I)=XL2(II)
C
      DO 114 I=KS3,KS2
      X1(I)=BF(I)*DX1+X1(I)
114  X2(I)=BF(I)*DX2+X2(I)
C
      DO 143 N=KS3-KS1+1,KS3
      RN=X1(N)
      QN=X2(N)
      E2=RN*RN+QN*QN+E2
      I=INT(AV1*SQRT(RN*RN+QN*QN))
      PR=RN*PGR(I)-QN*PGQ(I)
      PQ=RN*PGQ(I)+QN*PGR(I)
      E1=PR*PR+PQ*PQ+E1
      I=INT(AV2*SQRT(PR*PR+PQ*PQ))
      R1=PR*GR(I)-PQ*GQ(I)
      Q1=PR*GQ(I)+PQ*GR(I)
C
      X1(N)=A*R1-B*Q1
143  X2(N)=A*Q1+B*R1
C
      U=G05DAF(0.000,4.000)
      IF(U.LT.1.0) THEN
      RU=1.0
      QU=1.0
      ELSEIF(U.LT.2.0) THEN
      RU=-1.0
      QU=1.0
      ELSEIF(U.LT.3.0) THEN
      RU=1.0
      QU=-1.0
      ELSE
      RU=-1.0
      QU=-1.0
      ENDIF
C
      DO 151 I=KS3,KS2
      XU1(I)=BF(I)*RU+XU1(I)
151  XU2(I)=BF(I)*QU+XU2(I)
C
      DO 155 N=KS3-KS1+1,KS3
      RN=XU1(N)
      QN=XU2(N)
      I=INT(AV1*SQRT(RN*RN+QN*QN))
      PR=RN*PGR(I)-QN*PGQ(I)
      PQ=RN*PGQ(I)+QN*PGR(I)
      I=INT(AV2*SQRT(PR*PR+PQ*PQ))
      R1=PR*GR(I)-PQ*GQ(I)
      Q1=PR*GQ(I)+PQ*GR(I)
C
      XU1(N)=A*R1-B*Q1
155  XU2(N)=A*Q1+B*R1
C
      U=G05DAF(0.000,4.000)
      IF(U.LT.1.0) THEN
      RL=1.0

```

```

QL=1.0
ELSEIF(U.LT.2.0) THEN
RL=-1.0
QL=1.0
ELSEIF(U.LT.3.0) THEN
RL=1.0
QL=-1.0
ELSE
RL=-1.0
QL=-1.0
ENDIF

```

```

C
DO 157 I=KS3,KS2
157 XL1(I)=BF(I)*RL+XL1(I)
C XL2(I)=BF(I)*QL+XL2(I)
C
DO 161 N=KS3-KS1+1,KS3
RN=XL1(N)
QN=XL2(N)
I=INT(AV1*SQRT(RN*RN+QN*QN))
PR=RN*PGR(I)-QN*PGQ(I)
PQ=RN*PGQ(I)+QN*PGR(I)
I=INT(AV2*SQRT(PR*PR+PQ*PQ))
R1=PR*GR(I)-PQ*GQ(I)
Q1=PR*GQ(I)+PQ*GR(I)
C
XL1(N)=A*R1-B*Q1
161 XL2(N)=A*Q1+B*R1
C
C CALCU. TOTAL ENERGY PER SYMBOL
C
DO 124 I=KS3-KS1+1,KS3
124 E=X1(I)**2+X2(I)**2+E
C
J=1
DO 163 I=KS3-KS1+1,KS3
C ADD OFFSETS
C
F2=F2+F+PHF
IF(F2.GT.PI3) THEN
F2=F2-PI3
ELSEIF(F2.LT.-PI3) THEN
F2=F2+PI3
ENDIF
R2=COS(F2)
Q2=SIN(F2)
F3=F3+F-PHF
IF(F3.GT.PI3) THEN
F3=F3-PI3
ELSEIF(F3.LT.-PI3) THEN
F3=F3+PI3
ENDIF
R3=COS(F3)
Q3=SIN(F3)
ADJI(J)=XU1(I)*R2-XU2(I)*Q2
*+XL1(I)*R3+XL2(I)*Q3
ADJQ(J)=XU1(I)*Q2+XU2(I)*R2
*-XL1(I)*Q3+XL2(I)*R3
163 J=J+1
C

```

```
IF(ISW.EQ.0) THEN
  DO 142 I=1,8
  ADJI(I)=0
  ADJQ(I)=0
  ENDIF
142
C
  J=1
  DO 119 I=KS3-KS1+1,KS3
  W1=G05DDF(0.000,P1)
  W2=G05DDF(0.000,P1)
  R1=X1(I)+W1+ADJI(J)
  Q1=X2(I)+W2+ADJQ(J)
C
  F1=F1+PHF
  IF(F1.GT.PI3) THEN
    F1=F1-PI3
  ELSEIF(F1.LT.-PI3) THEN
    F1=F1+PI3
  ENDIF
  R2=COS(F1)
  Q2=SIN(F1)
  XX1(I)=R1*R2-Q1*Q2
  XX2(I)=Q1*R2+R1*Q2
119
C
  DO 134 II=KS7-KS1+1,KS7
  XXX1(II)=XX1(II)*FR(0)
  XXX2(II)=XX2(II)*FR(0)
  DO 137 I=1,KS5
  R1=XX1(II+I)
  R2=XX1(II-I)
  Q1=XX2(II+I)
  Q2=XX2(II-I)
  XXX1(II)=XXX1(II)+FR(I)*(R1+R2)
  XXX2(II)=XXX2(II)+FR(I)*(Q1+Q2)
137
134
CONTINUE
C
  FPH1=PHEF*GAMMA
  FPH2=FPH1*ALPHA+FPH2
  FPH3=FPH1+FPH2
  DO 132 I=KS7-KS1+1,KS7
  RR=1/SQRT(XXX1(I)**2+XXX2(I)**2)
  RR=1/(ABS(XXX1(I))+ABS(XXX2(I)))
  FPH=FPH+FPH3
  IF(FPH.GT.PI3) THEN
    FPH=FPH-PI3
  ELSEIF(FPH.LT.-PI3) THEN
    FPH=FPH+PI3
  ENDIF
  R1=XXX1(I)
  Q1=XXX2(I)
  R2=COS(FPH)
  Q2=SIN(FPH)
  XXX1(I)=R1*R2+Q1*Q2
  XXX2(I)=Q1*R2-R1*Q2
  XXX1(I)=XXX1(I)*RR
  XXX2(I)=XXX2(I)*RR
132
C
  XXXM1=XXX1(I1)*BSF(0)
  XXXM2=XXX2(I1)*BSF(0)
```

```
DO 131 I=1,KS12
  XXXM1=XXXM1+BSF(I)*(XXX1(I1-I)+XXX1(I1+I))
  XXXM2=XXXM2+BSF(I)*(XXX2(I1-I)+XXX2(I1+I))
CALL ANGSUB1(XXXM1,XXXM2,PHPOSF)

PHPOS=PHPOSF
IF(PHPOS.LT.0) PHPOS=PHPOS+PI3

THRESHOLD DETECTION

IF(PHPOS.LT.PI0) THEN
  ISSD(0)=0
  PHASTI=PI4
ELSEIF(PHPOS.LT.PI1) THEN
  ISSD(0)=1
  PHASTI=PI5
ELSEIF(PHPOS.LT.PI2) THEN
  ISSD(0)=2
  PHASTI=PI6
ELSE
  ISSD(0)=3
  PHASTI=PI7
ENDIF

IF(ISW.EQ.1) THEN

PHEF=PHPOS-PHASTI
IF(ABS(PHEF).GT.PI1) THEN
  IF(PHEF.GT.0) THEN
    PHEF=PHEF-PI3
  ELSE
    PHEF=PHEF+PI3
  ENDIF
ENDIF
ELSE

IF(LL.GE.200) THEN
PHEF=PHPOS-PHASTI
IF(ABS(PHEF).GT.PI1) THEN
  IF(PHEF.GT.0) THEN
    PHEF=PHEF-PI3
  ELSE
    PHEF=PHEF+PI3
  ENDIF
ENDIF
ELSE
  IF(LL.EQ.199) GAMMA=0.03
  IF(LL.EQ.199) ALPHA=0.015

PHEF=PHPOSF-PH1
PH1=PHPOSF
IF(PHEF.GT.0) THEN
  PHEF=PHEF-PI1
ELSE
  PHEF=PHEF+PI1
ENDIF
ENDIF
ENDIF
```

```

ISS=ISSD(0)-ISSD(-1)
IF(ISS.LT.0) ISS=ISS+4
IF(ISS.EQ.0) THEN
  IXXX1=1
  IXXX2=1
ELSEIF(ISS.EQ.1) THEN
  IXXX1=-1
  IXXX2=1
ELSEIF(ISS.EQ.2) THEN
  IXXX1=-1
  IXXX2=-1
ELSE
  IXXX1=1
  IXXX2=-1
ENDIF

```

C
C
C

```

COUNT ERROR BURSTS

```

```

IB3=IB3+1
IB1=IB1+1
IB2=IB2+1
IF(IXXX1.EQ.IX1(KT2).AND.IXXX2.EQ.IX2(KT2)) GOTO 111
IF(IX1(KT2).NE.IXXX1) IBE=IBE+1
IF(IX2(KT2).NE.IXXX2) IBE=IBE+1
IF(IB1.GT.3) IA1=IA1+1
IB1=0
IF(IB2.GT.5) IA2=IA2+1
IB2=0
IF(IB3.GT.10) IA3=IA3+1
IB3=0

```

111

```

CONTINUE
IF(ISW.EQ.0) THEN
  NTEST1=L
  NTEST2=10000
  P1=P
  GAMMA=GAMMA1
  ALPHA=ALPHA1
  ISW=1
  GOTO 1006
ENDIF
PRINT*,'THE CHANNAL SPACING IS (M HZ)',CSP
PRINT*,'THE BASEBAND SHAPPING FILTER IS R.O. (SQ.RT=)',ROF
PRINT*,'GAMMA & ALPHA ARE',GAMMA,ALPHA
PRINT*,'THE TRUNCATED LENGTH OF THE BASEBAND FILTER IS',KT12
PRINT*,'THE SEED INTEGER IS',IIQQ
PRINT*,'NO. OF SYMBOL TRANSMITTED=',L*10000
PRINT*,'THE FREQ. OFFSET IS',FOS
E1=E1/(REAL(L*10000)*4.0*KS1)
E2=E2/(REAL(L*10000)*4.0*KS1)
PRINT*,'THE PERDISTORTOR AND TWT VALUES ARE',INT(PREDBK),INT(BK)
PRINT*,'THE PREDISTORTION BACKOFF POINT IS',PBOP
PRINT*,'ENERGY PER BIT AT THE INPUT TO THE PREDISTORTOR IS',E2
PRINT*,'THE BACKOFF POINT IS',BOP
PRINT*,'ENERGY PER BIT AT THE INPUT OF THE TWT',E1
EB=E/REAL(L*10000)/REAL(KS1)
PRINT*,'ENERGY PER BIT AT THE OUTPUT OF THE DEMODULATOR IS',EB
PRINT*,'VARIANCE OF NOISE IS',P
IJ=2*L*10000
PRINT*,'THE SNR IS',10.0*LOG10(EB*KS1/2/(P*P))
BER=REAL(IBE)/REAL(IJ)

```

```

PRINT*, 'BIT ERROR RATE IS', BER
PRINT*, 'ERROR BURST IA1 IS', IA1
PRINT*, 'ERROR BURST IA2 IS', IA2
PRINT*, 'ERROR BURST IA3 IS', IA3
RETURN
END

```

C

```

SUBROUTINE ANGSUB1(RE, AIM, PHASE)
COMMON /PPII/PIO, PI1, PI2, PI3
IF (RE.EQ.0.AND.AIM.EQ.0) THEN
  PHASE=0
ELSEIF (RE.EQ.0.AND.AIM.GT.0) THEN
  PHASE=PIO
ELSEIF (RE.EQ.0.AND.AIM.LT.0) THEN
  PHASE=-PIO
ELSE
  PHASE=ATAN(AIM/RE)
  IF (RE.LT.0) THEN
    PHASE=PI1+PHASE
  ELSEIF (RE.GT.0.AND.AIM.LT.0) THEN
    PHASE=PHASE+PI3
  ENDIF
ENDIF
RETURN
END

```

####S

```

0.5
2
6.95
1
2
2000 0
18 15
0.03 0.015
0.5
2
6.2
2
3
2000 0
18 15
0.03 0.015
0.5
2
5.52
3
6
2000 0
18 15
0.03 0.015
0.5
2
4.92
4
6
2000 0
18 15
0.03 0.015
0.5
2

```

4.38
5
8
2000 0
18 15
0.03 0.015
0.5
2
3.91
6
12
2000 0
18 15
0.03 0.015
0.5
2
3.48
7
25
2000 0
18 15
0.03 0.015
####S

APPENDIX A13SIMULATOR FOR CE8PSK SIGNALS

THIS PROGRAM IS USED TO EVALUATE THE ERROR-RATE PERFORMANCES OF SIGNALS 1B, 2B, 3B AND 4B, OVER A NONLINEAR AND BANDLIMITED SATELLITE CHANNEL, WITH THE USE OF THE SUBOPTIMUM FILTERS, THE PREDISTORTER, THE AMPLIFIER LIMITER, PHASE DEMODULATOR A OR B AND THE DISTANCE MEASURE D AND IN AN ACI ENVIRONMENT

```

/*JOB PP27,EUELSWC,ST=MFY,C=S,TI=1280,
/* PW=SWC
FTNS,DB=0/PMD,L=0.
LIBRARY(PROCLIB,*)
NAG(FTNS)
LGO.
####S
PROGRAM SWCAB(INPUT,OUTPUT,TAPE1=INPUT,TAPE2=OUTPUT)
DIMENSION FF1(0:63),FF2(0:63),FF3(0:63),FF4(0:63)
DIMENSION X2(-400:400),XXX2(-400:400),
1XX1(-400:400),XX2(-400:400),FR(-200:200),GQ(0:38),GR(0:38),
1BSF(-200:200),FM(-200:200),
2FT(-200:200),
2X1(-300:300),XXX1(-400:400),STPH(-300:300),
2XU1(-300:100),XU2(-300:100),
2BF(-400:400),PGR(0:38),PGQ(0:38),
2XL1(-300:100),XL2(-300:100),
2RU(-2:0),QU(-2:0),RL(-2:0),QL(-2:0),
2RS(320),QS(320),ADJI(16),ADJQ(16)
DIMENSION IX1(-100:0),IX2(-100:0),
1IV(16,-200:0),IVV(16,-200:0)
COMMON /VMAP/VIO,VI1,VI2,VI3,VI4,VI5,VI6,VI7,VQ0,VQ1,
1VQ2,VQ3,VQ4,VQ5,VQ6,VQ7
COMMON /PPII/PI0,PI1,PI2,PI3
COMMON /COST/CE1(8),CIO(64),CQ0(64),C(64),CC(16),CE(64)
DATA(FT(I),I=0,24)/1.0,0.935,0.758,0.512,0.256,0.041,-0.099,
*-0.157,-0.146,-0.094,-0.031,0.02,0.048,0.052,0.039,0.017,-0.004,
*-0.017,-0.021,-0.017,-0.008,0.002,0.009,0.011,0.008/
C
DATA(FR(I),I=0,24)/1.0,0.935,0.758,0.512,0.256,0.041,-0.099,
*-0.157,-0.146,-0.094,-0.031,0.02,0.048,0.052,0.039,0.017,-0.004,
*-0.017,-0.021,-0.017,-0.008,0.002,0.009,0.011,0.008/
C
DATA(GQ(I),I=0,38)/0.17,0.34,0.48,0.58,0.65,0.70,0.75,
*0.78,0.82,0.84,0.85,0.85,0.84,0.83,0.84,0.85,0.83,

```

*0.82,0.80,0.78,0.75,0.73,0.7,0.67,0.65,0.61,0.58,0.56,
*0.53,0.50,0.48,0.43,0.4,0.38,0.37,0.36,0.34,0.36,0.35/

C

DATA(GR(I),I=0,38)/3.57,3.17,2.83,2.55,2.33,2.15,1.99,
*1.83,1.69,1.55,1.44,1.30,1.20,1.09,1.0,0.92,0.86,0.80,
*0.74,0.68,0.63,0.58,0.54,0.50,0.46,0.43,0.4,0.37,0.352,
*0.352,0.332,0.332,0.31,0.3,0.3,0.29,0.29,0.28,0.28/

C

DATA(PGR(I),I=0,38)/0.280,0.280,0.280,0.285,0.309,0.309,
*0.319,0.341,0.357,0.358,0.386,0.399,0.418,0.432,0.453,
*0.468,0.492,0.504,0.574,0.594,0.594,0.594,0.594,0.594,
*0.594,0.594,0.594,0.594,0.594,0.594,0.594,0.594,0.594,
*0.594,0.594,0.594,0.594,0.594,0.594/

C

DATA(PGQ(I),I=0,38)/-0.005,-0.012,-0.015,-0.020,-0.033,-0.038,
*-0.051,-0.063,-0.076,-0.086,-0.104,-0.122,-0.136,-0.157,-0.188,
*-0.218,-0.251,-0.315,-0.425,-0.544,-0.544,-0.544,-0.544,-0.544,
*-0.544,-0.544,-0.544,-0.544,-0.544,-0.544,-0.544,-0.544,-0.544,
*-0.544,-0.544,-0.544,-0.544,-0.544,-0.544/

C

C

RR=SQRT(PGR(20)**2+PGQ(20)**2)
DO 136 I=0,38
PGQ(I)=PGQ(I)/RR
136 PGR(I)=PGR(I)/RR

136

C

DATA (FF1(I),I=0,63)/1.0,.943,.786,.566,.334,.135,.0,-.064,-.068,
*-.038,-.001,.024,.029,.017,-.001,-.014,-.017,-.011,
*-.001,.008,.01,.007,-.001,-.007,-.008,
*-.006,-.001,.004,.005,.003,-.001,-.004,-.005,-.004,
*.0,.003,.004,.002,.0,-.003,-.004,-.003,-.001,.002,.003,
*.002,.0,-.003,-.003,-.002,.0,.001,.002,.001,.0,-.002,
*-.003,-.002,-.001,.001,.002,.001,.0,-.002/

C

DATA (FF2(I),I=0,63)/1.0,.954,.825,.638,.425,.223,.06,-.047,
*-.095,-.096,-.067,-.028,.005,.022,.022,.01,-.006,-.018,-.022,
*-.018,-.008,.003,.011,.012,.009,
*.002,-.004,-.007,-.007,-.003,.002,.006,.006,.004,.0,-.005,
*-.007,-.008,-.005,-.002,.001,.003,.002,.0,-.002,-.004,-.004,
*-.002,.001,.004,.005,.005,.003,.0,-.002,-.003,-.002,.0,
*.001,.002,.001,.0,-.003,-.005/

C

DATA (FF3(I),I=0,63)/1.0,.963,0.858,0.7,0.511,0.316,0.139,-0.001,
*-0.094,-0.138,-0.14,-0.112,-0.068,-0.022,0.035,0.039,0.03,0.014,
*0.014,-0.003,-0.015,-0.02,-0.017,-0.008,0.002,
*.011,.016,.015,.01,.003,-.005,-.01,-.011,-.009,
*-.005,.001,.005,.008,.007,.003,-.001,-.005,
*-.008,-.008,-.006,-.002,.002,.005,.006,
*.005,.002,-.002,-.005,-.006,-.006,-.004,.0,
*.003,.005,.005,.003,.001,-.003,-.005/

C

DATA (FF4(I),I=0,48)/1.0,.970,.884,.751,.585,.405,
*.227,.068,-.058,-.144,-.188,-.192,-.164,-.115,-.056,
*.002,.049,.08,.091,.085,.065,.036,.006,-.02,-.039,
*-.047,-.045,-.034,-.019,-.003,.011,.021,.024,.021,.014,
*.004,-.005,-.012,-.016,-.015,-.011,-.004,.003,.009,
*.013,.013,.01,.005,-.002/

C

DO 1005 NR=1,1
PRINT*, 'INPUT BASEBAND FILTER R.O.F (SQ.)=1,0.75,0.5,0.25'

```
READ*,ROF
PRINT*, 'INPUT THE TRUNCATION LENGTH'
READ*,KT12
PRINT*, 'INPUT THE NOISE VARIANCE'
READ*,P
PRINT*, 'INPUT THE RANDOM SEED'
READ*,IIQQ
PRINT*, 'INPUT NO. OF TESTED SYMBOLS'
READ*,L
```

```
C
IF(ROF.EQ.1) THEN
  DO 172 I=0,63
172  BSF(I)=FF1(I)
  PBOP=3.953
  BOP=3.21
CT   BOP=2.84
ELSEIF(ROF.EQ.0.75) THEN
  DO 173 I=0,63
173  BSF(I)=FF2(I)
  PBOP=4.551
  BOP=3.715
CT   BOP=3.31
ELSEIF(ROF.EQ.0.5) THEN
  DO 174 I=0,63
174  BSF(I)=FF3(I)
  PBOP=5.207
  BOP=4.22
CT   BOP=3.83
ELSEIF(ROF.EQ.0.25) THEN
  DO 175 I=0,63
175  BSF(I)=FF4(I)
  PBOP=5.98
  BOP=4.83
CT   BOP=4.39
ELSE
  PRINT*, 'NO REQUIRED FILTER'
  STOP
ENDIF
```

```
C
PI1=ACOS(-1.0)
PI0=PI1/2.0
PI2=PI0*3.0
PI3=2.0*PI1
```

```
C
C   MAP-SETTING
C
```

```
V10=0.924
VQ0=0.383
V11=0.383
VQ1=0.924
V12=-0.383
VQ2=0.924
V13=-0.924
VQ3=0.383
V14=-0.924
VQ4=-0.383
V15=-0.383
VQ5=-0.924
V16=0.383
VQ6=-0.924
```

VI7=0.924
VQ7=-0.383

C

CALL COSTSUB(1,C10,CQ0,0,0,0,0,0,0)
CALL COSTSUB(2,C10,CQ0,0,0,0,1,0,0)
CALL COSTSUB(3,C10,CQ0,1,0,0,0,0,0)
CALL COSTSUB(4,C10,CQ0,1,0,0,1,0,0)
CALL COSTSUB(5,C10,CQ0,0,0,0,0,1,0)
CALL COSTSUB(6,C10,CQ0,0,0,0,1,1,0)
CALL COSTSUB(7,C10,CQ0,1,0,0,0,1,0)
CALL COSTSUB(8,C10,CQ0,1,0,0,1,1,0)
CALL COSTSUB(9,C10,CQ0,0,1,0,0,0,0)
CALL COSTSUB(10,C10,CQ0,0,1,0,1,0,0)
CALL COSTSUB(11,C10,CQ0,1,1,0,0,0,0)
CALL COSTSUB(12,C10,CQ0,1,1,0,1,0,0)
CALL COSTSUB(13,C10,CQ0,0,1,0,0,1,0)
CALL COSTSUB(14,C10,CQ0,0,1,0,1,1,0)
CALL COSTSUB(15,C10,CQ0,1,1,0,0,1,0)
CALL COSTSUB(16,C10,CQ0,1,1,0,1,1,0)
CALL COSTSUB(17,C10,CQ0,0,0,0,0,0,1)
CALL COSTSUB(18,C10,CQ0,0,0,0,1,0,1)
CALL COSTSUB(19,C10,CQ0,1,0,0,0,0,1)
CALL COSTSUB(20,C10,CQ0,1,0,0,1,0,1)
CALL COSTSUB(21,C10,CQ0,0,0,0,0,1,1)
CALL COSTSUB(22,C10,CQ0,0,0,0,1,1,1)
CALL COSTSUB(23,C10,CQ0,1,0,0,0,1,1)
CALL COSTSUB(24,C10,CQ0,1,0,0,1,1,1)
CALL COSTSUB(25,C10,CQ0,0,1,0,0,0,1)
CALL COSTSUB(26,C10,CQ0,0,1,0,1,0,1)
CALL COSTSUB(27,C10,CQ0,1,1,0,0,0,1)
CALL COSTSUB(28,C10,CQ0,1,1,0,1,0,1)
CALL COSTSUB(29,C10,CQ0,0,1,0,0,1,1)
CALL COSTSUB(30,C10,CQ0,0,1,0,1,1,1)
CALL COSTSUB(31,C10,CQ0,1,1,0,0,1,1)
CALL COSTSUB(32,C10,CQ0,1,1,0,1,1,1)
CALL COSTSUB(33,C10,CQ0,0,0,1,0,0,0)
CALL COSTSUB(34,C10,CQ0,0,0,1,1,0,0)
CALL COSTSUB(35,C10,CQ0,1,0,1,0,0,0)
CALL COSTSUB(36,C10,CQ0,1,0,1,1,0,0)
CALL COSTSUB(37,C10,CQ0,0,0,1,0,1,0)
CALL COSTSUB(38,C10,CQ0,0,0,1,1,1,0)
CALL COSTSUB(39,C10,CQ0,1,0,1,0,1,0)
CALL COSTSUB(40,C10,CQ0,1,0,1,1,1,0)
CALL COSTSUB(41,C10,CQ0,0,1,1,0,0,0)
CALL COSTSUB(42,C10,CQ0,0,1,1,1,0,0)
CALL COSTSUB(43,C10,CQ0,1,1,1,0,0,0)
CALL COSTSUB(44,C10,CQ0,1,1,1,1,0,0)
CALL COSTSUB(45,C10,CQ0,0,1,1,0,1,0)
CALL COSTSUB(46,C10,CQ0,0,1,1,1,1,0)
CALL COSTSUB(47,C10,CQ0,1,1,1,0,1,0)
CALL COSTSUB(48,C10,CQ0,1,1,1,1,1,0)
CALL COSTSUB(49,C10,CQ0,0,0,1,0,0,1)
CALL COSTSUB(50,C10,CQ0,0,0,1,1,0,1)
CALL COSTSUB(51,C10,CQ0,1,0,1,0,0,1)
CALL COSTSUB(52,C10,CQ0,1,0,1,1,0,1)
CALL COSTSUB(53,C10,CQ0,0,0,1,0,1,1)
CALL COSTSUB(54,C10,CQ0,0,0,1,1,1,1)
CALL COSTSUB(55,C10,CQ0,1,0,1,0,1,1)
CALL COSTSUB(56,C10,CQ0,1,0,1,1,1,1)
CALL COSTSUB(57,C10,CQ0,0,1,1,0,0,1)

```

CALL COSTSUB(58,CIO,CQ0,0,1,1,1,0,1)
CALL COSTSUB(59,CIO,CQ0,1,1,1,0,0,1)
CALL COSTSUB(60,CIO,CQ0,1,1,1,1,0,1)
CALL COSTSUB(61,CIO,CQ0,0,1,1,0,1,1)
CALL COSTSUB(62,CIO,CQ0,0,1,1,1,1,1)
CALL COSTSUB(63,CIO,CQ0,1,1,1,0,1,1)
CALL COSTSUB(64,CIO,CQ0,1,1,1,1,1,1)

```

C

```

PRINT*,'TWT AND ACI'
PRINT*,'WHAT MEASURE ?'
PRINT*,'1-CX ,2-PH**2, 3-LIMITER, 4-PH, 5-R*PH, 6-R*PH**2',
1' ,7-COS ,8-R*COS'
READ*,MEAS
IF(MEAS.NE.1.AND.MEAS.NE.3) THEN
DO 122 I=1,64
  RE=CIO(I)
  AIM=CQ0(I)
  CALL ANGSUB(RE,AIM,PHASE)
122 CIO(I)=PHASE
  ELSEIF(MEAS.EQ.1) THEN
    DO 129 I=1,64
      CIO(I)=CIO(I)
129 CQ0(I)=CQ0(I)
ENDIF

```

C

```

C
C KS1: NO OF THE SAMPLES IN ONE T.
C KT1: SYMBOL LENGTH OF THE TRUNCATED IMPULSE RESPONSE WAVEFORM
C OF THE BASEBAND SHAPPING FILTER IN CASCADED WITH THE BPF.
C KS2: THE BASEBAND SHAPPING ARRAY EXTENDS FROM -KS3 TO +KS2.
C KT2: SYMBOL TIME FOR THE 1ST SAMPLE INSTANCE
C KS3: ARRAY ELEMENT FOR THE 1ST SAMPLE.
C KT12: TRUNCATED OF THE BASEBAND SHAPPING FILTER.
C KT4: SYMBOL LENGTH OF THE IMPULSE RESPONSE OF FT IN THE TX
C KS4: THE LAST ELEMENT IN FT
C KT5: SYMBOL LENGTH OF THE IMPULSE RESPONSE OF FT IN THE RX
C KS5: THE LAST ELEMENT IN FR
C KTM1: SYMBOL LENGTH OF THE IMPULSE RESPONSE OF THE MATCHED-FILTER
C KSM1: THE LAST ELEMENT IN MF
C

```

```

KT4=3
KT1=2*(KT12+KT4)
KT3=KT1*(-1)/2
KS1=8
KS2=KT1*KS1/2
KS3=KS2*(-1)
KS4=KT4*KS1
KT5=3
KS5=KT5*KS1
KS12=KT12*KS1
KTM1=KT12+KT5
KSM1=KTM1*KS1
KT2=-KT1/2-KTM1

```

C

```

DO 165 I=KS4+1,200
165 FT(I)=0.0
DO 166 I=0,200
166 FT(-I)=FT(I)
DO 167 II=0,KS2
  RR=BSF(0)*FT(II)
DO 168 I=1,KS12

```

```
168 RR=RR+BSF(I)*(FT(II+I)+FT(II-I))
167 BF(II)=RR
DO 150 I=0,KS2
BF(-I)=BF(I)
150 FM(I)=BF(I)
```

```
C
KS10=320
KT13=-32
KT14=KT13-1
KT15=KT13+KT2
```

```
C
C DETECTOR INITIALISATION
C
```

```
DO 120 I=1,16
CC(I)=1.0E+6
DO 120 J=KT14,0
120 IV(I,J)=0
```

```
C
CC(1)=0
DO 102 I=1,16,4
IV(I,0)=0
IV(I+1,0)=1
IV(I+2,0)=2
102 IV(I+3,0)=3
```

```
C
KT6=KT14+KT2
```

```
C
CSP=5
F=PI3*CSP/32.0
DO 164, I=1,KS10
FF=F*REAL(I)
RS(I)=COS(FF)
164 QS(I)=SIN(FF)
```

```
C
C INITIALISATION
C
```

```
DO 104 I=KT6,0
IX1(I)=0
104 IX2(I)=0
```

```
C
DO 138 I=-2,0
RU(I)=0
QU(I)=0
RL(I)=0
138 QL(I)=0
```

```
C
KS6=KS3-KS1+1-2*KSM1
KS7=KS3-KS5
DO 105 I=KS6,KS2+KS1
X1(I)=0.0
X2(I)=0.0
XX1(I)=0.0
XX2(I)=0.0
XXX1(I)=0.0
XXX2(I)=0.0
XU1(I)=0.0
XU2(I)=0.0
XL1(I)=0.0
STPH(I)=0.0
```

```

105 XL2(I)=0.0
C
C
CDI=V10
CDQ=VQ0
C
DO 127 J=KT6,0
DO 126 I=KS6,KS2
  II=I+KS1
  X1(I)=X1(II)
  X2(I)=X2(II)
  XU1(I)=XU1(II)
  XU2(I)=XU2(II)
  XL1(I)=XL1(II)
126 XL2(I)=XL2(II)
  DO 125 I=KS3,KS2
  X1(I)=BF(I)*CDI+X1(I)
  X2(I)=BF(I)*CDQ+X2(I)
  XU1(I)=X1(I)
  XU2(I)=X2(I)
  XL1(I)=X1(I)
125 XL2(I)=X2(I)
127 CONTINUE
C
PREDBK=18
BK=15
PAV=SQRT(4.0*PBOP)
AV=SQRT(4.0*BOP)
AV1=PREDBK/PAV
AV2=BK/AV
I=PREDBK
SUM1=SQRT(PGR(I)**2+PGQ(I)**2)
A1=PGR(I)/SUM1
B1=-PGQ(I)/SUM1
I=BK
SUM2=SQRT(GR(I)**2+GQ(I)**2)
A2=GR(I)/SUM2
B2=-GQ(I)/SUM2
A=A1*A2-B1*B2
B=A1*B2+B1*A2
DO 141 N=KS6,KS3
RN=X1(N)
QN=X2(N)
I=INT(AV1*SQRT(RN*RN+QN*QN))
PR=RN*PGR(I)-QN*PGQ(I)
PQ=RN*PGQ(I)+QN*PGR(I)
I=INT(AV2*SQRT(PR*PR+PQ*PQ))
X1(N)=PR*GR(I)-PQ*GQ(I)
141 X2(N)=PR*GQ(I)+PQ*GR(I)
C
DO 146 N=KS6,KS3
R1=X1(N)
Q1=X2(N)
X1(N)=A*R1-B*Q1
X2(N)=A*Q1+B*R1
  XX1(N)=X1(N)
146  XX2(N)=X2(N)
C
DO 130 II=KS6+KS5,KS3-KS5
  XXX1(II)=XX1(II)*FR(0)

```

```

      XXX2(II)=XX2(II)*FR(0)
      DO 135 I=1,KS5
      R1=XX1(II+I)
      R2=XX1(II-I)
      Q1=XX2(II+I)
      Q2=XX2(II-I)
      XXX1(II)=XXX1(II)+FR(I)*(R1+R2)
      XXX2(II)=XXX2(II)+FR(I)*(Q1+Q2)
135  CONTINUE
130  C
      DO 133 I=KS6+KS5,KS3-KS5
      RR=1/SQRT(XXX1(I)**2+XXX2(I)**2)
      RR=1/(ABS(XXX1(I))+ABS(XXX2(I)))
      XXX1(I)=XXX1(I)*RR
      XXX2(I)=XXX2(I)*RR
133  C
      C
      C   ASSUME THE 1ST DETECTION IS CORRECT
      C
      C   KT7=KT2-1
      C
      C   I1: THE MAIN SAMPLING INSTANCE
      C   I1=KS3-KSM1
      C   I2: THE OFFSET SAMPLING INSTANCE.
      C   I2=I1
      C
      C   CALL G05CBF(IIQQ)
      C
      C   INITIALISE ALL COUNTERS.
      C
      C   IE=0
      C   IA1=0
      C   IA2=0
      C   IA3=0
      C   IB1=0
      C   IB2=0
      C   IB3=0
      C   IBE=0
      C   E=0.0
      C   E1=0.0
      C   E2=0.0
      C   E3=0
      C
      C   KS11=1
      C
      C   START
      C
      C   DO 111 LLL=1,L
      C   DO 111 LL=1,10000
      C
      C   SHIFT ID
      C
      C   DO 112 I=KT6,-1
      C   J=I+1
      C   IX1(I)=IX1(J)
      C   IX2(I)=IX2(J)
112  C
      C   U=G05DAF(0.000,4.000)
      C   IF(U.LT.1.0) THEN
      C   IX1(0)=0
      C   IX2(0)=0

```

```

ELSEIF(U.LT.2.0) THEN
IX1(0)=0
IX2(0)=1
ELSEIF(U.LT.3.0) THEN
IX1(0)=1
IX2(0)=1
ELSE
IX1(0)=1
IX2(0)=0
ENDIF

```

```

C
K1=IX1(0)+IX1(-2)+IX2(-1)
K2=IX1(-2)+IX2(0)+IX2(-1)+IX2(-2)
K3=IX1(-1)
K4=MOD(K1,2)
K5=MOD(K2,2)
K6=MOD(K3,2)
K7=4*K4+2*K5+K6+1
GOTO(1,2,3,4,5,6,7,8),K7

```

```

C
1  CDI=VI0
   CDQ=VQ0
   GOTO 9

```

```

C
2  CDI=VI1
   CDQ=VQ1
   GOTO 9

```

```

C
3  CDI=VI2
   CDQ=VQ2
   GOTO 9

```

```

C
4  CDI=VI3
   CDQ=VQ3
   GOTO 9

```

```

C
5  CDI=VI4
   CDQ=VQ4
   GOTO 9

```

```

C
6  CDI=VI5
   CDQ=VQ5
   GOTO 9

```

```

C
7  CDI=VI6
   CDQ=VQ6
   GOTO 9

```

```

C
8  CDI=VI7
   CDQ=VQ7

```

```

C
9  DO 113 I=KS6,KS2
   II=I+KS1
   X1(I)=X1(II)
   X2(I)=X2(II)
   XX1(I)=XX1(II)
   XX2(I)=XX2(II)
   XXX1(I)=XXX1(II)
   XXX2(I)=XXX2(II)
   XU1(I)=XU1(II)

```

```

XU2(I)=XU2(II)
XL1(I)=XL1(II)
STPH(I)=STPH(II)
113 XL2(I)=XL2(II)
C
DO 114 I=KS3,KS2
X1(I)=BF(I)*CDI+X1(I)
114 X2(I)=BF(I)*CDQ+X2(I)
C
DO 143 N=KS3-KS1+1,KS3
RN=X1(N)
QN=X2(N)
E2=RN*RN+QN*QN+E2
I=INT(AV1*SQRT(RN*RN+QN*QN))
PR=RN*PGR(I)-QN*PGQ(I)
PQ=RN*PGQ(I)+QN*PGR(I)
E1=PR*PR+PQ*PQ+E1
I=INT(AV2*SQRT(PR*PR+PQ*PQ))
X1(N)=PR*GR(I)-PQ*GQ(I)
143 X2(N)=PR*GQ(I)+PQ*GR(I)
C
DO 144 N=KS3-KS1+1,KS3
R1=X1(N)
Q1=X2(N)
X1(N)=A*R1-B*Q1
144 X2(N)=A*Q1+B*R1
C
C CALCU. TOTAL ENERGY PER SYMBOL
C
DO 124 I=KS3-KS1+1,KS3
124 E=X1(I)**2+X2(I)**2+E
C
DO 101 I=-2,-1
J=I+1
RU(I)=RU(J)
QU(I)=QU(J)
RL(I)=RL(J)
101 QL(I)=QL(J)
C
U=G05DAF(0.000,4.000)
IF(U.LT.1.0) THEN
RU(0)=0
QU(0)=0
ELSEIF(U.LT.2.0) THEN
RU(0)=0
QU(0)=1
ELSEIF(U.LT.3.0) THEN
RU(0)=1
QU(0)=1
ELSE
RU(0)=1
QU(0)=0
ENDIF
C
K1=RU(0)+RU(-2)+QU(-1)
K2=RU(-2)+QU(0)+QU(-1)+QU(-2)
K3=RU(-1)
K4=MOD(K1,2)
K5=MOD(K2,2)
K6=MOD(K3,2)

```

K7=4*K4+2*K5+K6+1
 GOTO (21,22,23,24,25,26,27,28),K7

```

C
21  CDUI=VI0
    CDUQ=VQ0
    GOTO 29

C
22  CDUI=VI1
    CDUQ=VQ1
    GOTO 29

C
23  CDUI=VI2
    CDUQ=VQ2
    GOTO 29

C
24  CDUI=VI3
    CDUQ=VQ3
    GOTO 29

C
25  CDUI=VI4
    CDUQ=VQ4
    GOTO 29

C
26  CDUI=VI5
    CDUQ=VQ5
    GOTO 29

C
27  CDUI=VI6
     CDUQ=VQ6
    GOTO 29

C
28  CDUI=VI7
     CDUQ=VQ7

C
29  DO 151 I=KS3,KS2
     XU1(I)=BF(I)*CDUI+XU1(I)
151  XU2(I)=BF(I)*CDUQ+XU2(I)
C
     DO 155 N=KS3-KS1+1,KS3
     RN=XU1(N)
     QN=XU2(N)
     I=INT(AV1*SQRT(RN*RN+QN*QN))
     PR=RN*PGR(I)-QN*PGQ(I)
     PQ=RN*PGQ(I)+QN*PGR(I)
     I=INT(AV2*SQRT(PR*PR+PQ*PQ))
     XU1(N)=PR*GR(I)-PQ*GQ(I)
155  XU2(N)=PR*GQ(I)+PQ*GR(I)
C
     DO 156 N=KS3-KS1+1,KS3
     R1=XU1(N)
     Q1=XU2(N)
     XU1(N)=A*R1-B*Q1
156  XU2(N)=A*Q1+B*R1
C
     U=G05DAF(0.000,4.000)
     IF(U.LT.1.0) THEN
     RL(0)=0
     QL(0)=0
     ELSEIF(U.LT.2.0) THEN
     RL(0)=0
  
```

```
QL(0)=1
ELSEIF(U.LT.3.0) THEN
RL(0)=1
QL(0)=1
ELSE
RL(0)=1
QL(0)=0
ENDIF
```

```
C
K1=RL(0)+RL(-2)+QL(-1)
K2=RL(-2)+QL(0)+QL(-1)+QL(-2)
K3=RL(-1)
K4=MOD(K1,2)
K5=MOD(K2,2)
K6=MOD(K3,2)
K7=4*K4+2*K5+K6+1
GOTO(31,32,33,34,35,36,37,38),K7
```

```
C
31 CDLI=VI0
CDLQ=VQ0
GOTO 40
```

```
C
32 CDLI=VI1
CDLQ=VQ1
GOTO 40
```

```
C
33 CDLI=VI2
CDLQ=VQ2
GOTO 40
```

```
C
34 CDLI=VI3
CDLQ=VQ3
GOTO 40
```

```
C
35 CDLI=VI4
CDLQ=VQ4
GOTO 40
```

```
C
36 CDLI=VI5
CDLQ=VQ5
GOTO 40
```

```
C
37 CDLI=VI6
CDLQ=VQ6
GOTO 40
```

```
C
38 CDLI=VI7
CDLQ=VQ7
```

```
C
40 DO 157 I=KS3,KS2
XL1(I)=BF(I)*CDLI+XL1(I)
157 XL2(I)=BF(I)*CDLQ+XL2(I)
```

```
C
DO 161 N=KS3-KS1+1,KS3
RN=XL1(N)
QN=XL2(N)
I=INT(AV1*SQRT(RN*RN+QN*QN))
PR=RN*PGR(I)-QN*PGQ(I)
PQ=RN*PGQ(I)+QN*PGR(I)
I=INT(AV2*SQRT(PR*PR+PQ*PQ))
```

```

161 XL1(N)=PR*GR(I)-PQ*GQ(I)
C XL2(N)=PR*GQ(I)+PQ*GR(I)

DO 162 N=KS3-KS1+1,KS3
R1=XL1(N)
Q1=XL2(N)
162 XL1(N)=A*R1-B*Q1
C XL2(N)=A*Q1+B*R1

IF(KS11.GE.KS10) KS11=1
J=1
DO 163 I=KS3-KS1+1,KS3
ADJI(J)=RS(KS11)*(XU1(I)+XL1(I))+QS(KS11)*(XL2(I)
*-XU2(I))
ADJQ(J)=RS(KS11)*(XU2(I)+XL2(I))+QS(KS11)*(XU1(I)
*-XL1(I))
KS11=KS11+1
163 J=J+1
C

J=1
DO 119 I=KS3-KS1+1,KS3
W1=G05DDF(0.000,P)
W2=G05DDF(0.000,P)
XX1(I)=X1(I)+W1+ADJI(J)
XX2(I)=X2(I)+W2+ADJQ(J)
119 J=J+1
C

DO 134 II=KS7-KS1+1,KS7
XXX1(II)=XX1(II)*FR(0)
XXX2(II)=XX2(II)*FR(0)
DO 137 I=1,KS5
R1=XX1(II+I)
R2=XX1(II-I)
Q1=XX2(II+I)
Q2=XX2(II-I)
XXX1(II)=XXX1(II)+FR(I)*(R1+R2)
137 XXX2(II)=XXX2(II)+FR(I)*(Q1+Q2)
134 CONTINUE
C

DO 132 I=KS7-KS1+1,KS7
RR=1/SQRT(XXX1(I)**2+XXX2(I)**2)
CT RR=1/(ABS(XXX1(I))+ABS(XXX2(I)))
XXX1(I)=XXX1(I)*RR
132 XXX2(I)=XXX2(I)*RR
C

XXXM1=XXX1(I1)*BSF(0)
XXXM2=XXX2(I1)*BSF(0)
DO 131 I=1,KS12
131 XXXM1=XXXM1+BSF(I)*(XXX1(I1-I)+XXX1(I1+I))
C XXXM2=XXXM2+BSF(I)*(XXX2(I1-I)+XXX2(I1+I))

CALL ANGSUB(XXXM1,XXXM2,PH)

C
C VIT-DETECTION
C
GOTO(11,12,13,14,15,16,17,18),MEAS
11 CALL SUB1(XXXM1,XXXM2)
GOTO 20
12 CALL SUB2(XXXM1,XXXM2)
GOTO 20

```

13 CALL SUB3 (XXXM1 ,XXXM2)
GOTO 20
14 CALL SUB4 (PH)
GOTO 20
15 CALL SUB5 (XXXM1 ,XXXM2)
GOTO 20
16 CALL SUB6 (XXXM1 ,XXXM2)
GOTO 20
17 CALL SUB7 (XXXM1 ,XXXM2)
GOTO 20
18 CALL SUB8 (XXXM1 ,XXXM2)

C
20 C(1)=CE1(1)+CC(1)
C(7)=CE1(1)+CC(7)
C(18)=CE1(1)+CC(2)
C(24)=CE1(1)+CC(8)
C(36)=CE1(1)+CC(4)
C(38)=CE1(1)+CC(6)
C(51)=CE1(1)+CC(3)
C(53)=CE1(1)+CC(5)

C
C(9)=CE1(2)+CC(9)
C(15)=CE1(2)+CC(15)
C(26)=CE1(2)+CC(10)
C(32)=CE1(2)+CC(16)
C(44)=CE1(2)+CC(12)
C(46)=CE1(2)+CC(14)
C(59)=CE1(2)+CC(11)
C(61)=CE1(2)+CC(13)

C
C(2)=CE1(3)+CC(2)
C(8)=CE1(3)+CC(8)
C(17)=CE1(3)+CC(1)
C(23)=CE1(3)+CC(7)
C(35)=CE1(3)+CC(3)
C(37)=CE1(3)+CC(5)
C(52)=CE1(3)+CC(4)
C(54)=CE1(3)+CC(6)

C
C(10)=CE1(4)+CC(10)
C(16)=CE1(4)+CC(16)
C(25)=CE1(4)+CC(9)
C(31)=CE1(4)+CC(15)
C(43)=CE1(4)+CC(11)
C(45)=CE1(4)+CC(13)
C(60)=CE1(4)+CC(12)
C(62)=CE1(4)+CC(14)

C
C(4)=CE1(5)+CC(4)
C(6)=CE1(5)+CC(6)
C(19)=CE1(5)+CC(3)
C(21)=CE1(5)+CC(5)
C(33)=CE1(5)+CC(1)
C(39)=CE1(5)+CC(7)
C(50)=CE1(5)+CC(2)
C(56)=CE1(5)+CC(8)

C
C(12)=CE1(6)+CC(12)
C(14)=CE1(6)+CC(14)
C(27)=CE1(6)+CC(11)

C(29)=CE1(6)+CC(13)
C(41)=CE1(6)+CC(9)
C(47)=CE1(6)+CC(15)
C(58)=CE1(6)+CC(10)
C(64)=CE1(6)+CC(16)

C

C(3)=CE1(7)+CC(3)
C(5)=CE1(7)+CC(5)
C(20)=CE1(7)+CC(4)
C(22)=CE1(7)+CC(6)
C(34)=CE1(7)+CC(2)
C(40)=CE1(7)+CC(8)
C(49)=CE1(7)+CC(1)
C(55)=CE1(7)+CC(7)

C

C(11)=CE1(8)+CC(11)
C(13)=CE1(8)+CC(13)
C(28)=CE1(8)+CC(12)
C(30)=CE1(8)+CC(14)
C(42)=CE1(8)+CC(10)
C(48)=CE1(8)+CC(16)
C(57)=CE1(8)+CC(9)
C(63)=CE1(8)+CC(15)

C

M1=1
II1=0
DO 103 M=1,16,4
CCC=C(M1)
J=M1
DO 106 I=M1+1,M1+3
IF((C(I)-CCC).GE.0.0) GOTO 106
CCC=C(I)
J=I

106

CONTINUE
J=MOD(J,16)
IF(J.EQ.0) J=16
IVV(M,0)=II1
CC(M)=CCC

107

DO 107 I=KT14,-1
IVV(M,I)=IV(J,I+1)
CCC=C(M1+4)
J=M1+4
DO 110 I=M1+5,M1+7
IF((C(I)-CCC).GE.0.0) GOTO 110
CCC=C(I)
J=I

110

CONTINUE
J=MOD(J,16)
IF(J.EQ.0) J=16
IVV(M+1,0)=II1
CC(M+1)=CCC

108

DO 108 I=KT14,-1
IVV(M+1,I)=IV(J,I+1)
CCC=C(M1+8)
J=M1+8
DO 109 I=M1+9,M1+11
IF((C(I)-CCC).GE.0.0) GOTO 109
CCC=C(I)
J=I

109

CONTINUE

```
J=MOD(J,16)
IF(J.EQ.0) J=16
IVV(M+2,0)=II1
CC(M+2)=CCC
DO 121 I=KT14,-1
121 IVV(M+2,I)=IV(J,I+1)
CCC=C(M1+12)
J=M1+12
DO 128 I=M1+13,M1+15
IF((C(I)-CCC).GE.0.0) GOTO 128
CCC=C(I)
J=I
128 CONTINUE
J=MOD(J,16)
IF(J.EQ.0) J=16
IVV(M+3,0)=II1
CC(M+3)=CCC
DO 115 I=KT14,-1
115 IVV(M+3,I)=IV(J,I+1)
II1=II1+1
103 M1=M1+16
C
C SEARCH THE MIN. COST VECTOR
C
CCC=1.0E+7
DO 116 I=1,16
IF((CC(I)-CCC).GE.0.0) GOTO 116
CCC=CC(I)
JJ=I
116 CONTINUE
C
C SUBTRACT ALL THE COSTS BY CCC
C
DO 117 I=1,16
117 CC(I)=CC(I)-CCC
C
C MOVE THE VECTORS IVV BACK TO THE IV VECTORS
C
DO 118 J=1,16
DO 118 I=KT14,0
118 IV(J,I)=IVV(J,I)
C
ISS=IV(JJ,KT13)
IF(ISS.EQ.0) THEN
  IXXX1=0
  IXXX2=0
ELSEIF(ISS.EQ.1) THEN
  IXXX1=0
  IXXX2=1
ELSEIF(ISS.EQ.2) THEN
  IXXX1=1
  IXXX2=0
ELSE
  IXXX1=1
  IXXX2=1
ENDIF
C
C COUNT ERROR BURSTS
C
```

C

```

IB3=IB3+1
IB1=IB1+1
IB2=IB2+1
IF(IXXX1.EQ.IX1(KT15).AND.IXXX2.EQ.IX2(KT15)) GOTO 111
IF(IX1(KT15).NE.IXXX1) IBE=IBE+1
IF(IX2(KT15).NE.IXXX2) IBE=IBE+1
IF(IB1.GT.3) IA1=IA1+1
IB1=0
IF(IB2.GT.10) IA2=IA2+1
IB2=0
IF(IB3.GT.28) IA3=IA3+1
IB3=0

```

111

```

CONTINUE
IF(MEAS.NE.1.AND.MEAS.NE.3) PRINT*,'PHASE DEMODULATION IS USED'
PRINT*,'-----'
IF(MEAS.EQ.1) THEN
PRINT*,'CX IS USED'
ELSEIF(MEAS.EQ.2) THEN
PRINT*,'PH**2 IS USED'
ELSEIF(MEAS.EQ.3) THEN
PRINT*,'LIMITER IS USED'
ELSEIF(MEAS.EQ.4) THEN
PRINT*,'PH IS USED'
ELSEIF(MEAS.EQ.5) THEN
PRINT*,'R*PH IS USED'
ELSEIF(MEAS.EQ.6) THEN
PRINT*,'R*PH*PH IS USED'
ELSEIF(MEAS.EQ.7) THEN
PRINT*,'COS(PH) IS USED'
ELSE
PRINT*,'R*COS(PH) IS USED'
ENDIF
PRINT*,'-----'
PRINT*,'SINE WAVE PD IS USED'
PRINT*,'EX-OR GATE PD IS USED'

```

CT

```

PRINT*,'THE CHANNAL SPACING IS (M HZ)',(CSP)
PRINT*,'THE BASEBAND SHAPPING FILTER IS R.O. (SQ.RT=)',ROF
PRINT*,'THE TRUNCATED LENGTH OF THE BASEBAND FILTER IS',KT12
PRINT*,'THE SEED INTEGER IS',IIQQ
PRINT*,'NO. OF SYMBOL TRANSMITTED=',L*10000
E1=E1/(REAL(L*10000)*4.0*KS1)
E2=E2/(REAL(L*10000)*4.0*KS1)
PRINT*,'THE PERDISTORTOR AND TWT VALUES ARE',INT(PREDBK),INT(BK)
PRINT*,'THE PREDISTORTION BACKOFF POINT IS',PBOP
PRINT*,'ENERGY PER BIT AT THE INPUT TO THE PREDISTORTOR IS',E2
PRINT*,'THE BACKOFF POINT IS',BOP
PRINT*,'ENERGY PER BIT AT THE INPUT OF THE TWT',E1
EB=E/REAL(L*10000)/REAL(KS1)
PRINT*,'ENERGY PER BIT AT THE OUTPUT OF THE DEMODULATOR IS',EB
PRINT*,'VARIANCE OF NOISE IS',P
IJ=2*L*10000
PRINT*,'THE SNR IS',10.0*LOG10(EB*KS1/2/(P*P))
BER=REAL(IBE)/REAL(IJ)
PRINT*,'BIT ERROR RATE IS',BER
PRINT*,'ERROR BURST IA1 IS',IA1
PRINT*,'ERROR BURST IA2 IS',IA2
PRINT*,'ERROR BURST IA3 IS',IA3
1005 CONTINUE
STOP

```

END

C

```
SUBROUTINE COSTSUB(N,CIO,CQO,ISI1,ISI2,ISI3,  
1 ISQ1,ISQ2,ISQ3)  
DIMENSION CIO(64),CQO(64)  
COMMON /VMAP/VIO,VI1,VI2,VI3,VI4,VI5,VI6,VI7,VQ0,VQ1,  
1 VQ2,VQ3,VQ4,VQ5,VQ6,VQ7  
I1=ISI3+ISI1+ISQ2  
I2=ISI1+ISQ3+ISQ2+ISQ1  
I3=ISI2  
I4=MOD(I1,2)  
I5=MOD(I2,2)  
I6=MOD(I3,2)  
I7=4*I4+2*I5+I6+1  
GOTO(1,2,3,4,5,6,7,8),I7
```

C

```
1 CIO(N)=VIO  
CQO(N)=VQ0  
GOTO 9
```

C

```
2 CIO(N)=VI1  
CQO(N)=VQ1  
GOTO 9
```

C

```
3 CIO(N)=VI2  
CQO(N)=VQ2  
GOTO 9
```

C

```
4 CIO(N)=VI3  
CQO(N)=VQ3  
GOTO 9
```

C

```
5 CIO(N)=VI4  
CQO(N)=VQ4  
GOTO 9
```

C

```
6 CIO(N)=VI5  
CQO(N)=VQ5  
GOTO 9
```

C

```
7 CIO(N)=VI6  
CQO(N)=VQ6  
GOTO 9
```

C

```
8 CIO(N)=VI7  
CQO(N)=VQ7
```

C

```
9 I=I  
RETURN  
END
```

C

```
SUBROUTINE ANGSUB(RE,AIM,PHASE)  
COMMON /PPII/PIO,PI1,PI2,PI3  
IF(RE.EQ.0.AND.AIM.EQ.0) THEN  
PHASE=0  
ELSEIF(RE.EQ.0.AND.AIM.GT.0) THEN  
PHASE=PIO  
ELSEIF(RE.EQ.0.AND.AIM.LT.0) THEN  
PHASE=-PIO  
ELSE
```

```

    PHASE=ATAN(AIM/RE)
    IF(PHASE.GT.0.AND.RE.LT.0.AND.AIM.LT.0) THEN
      PHASE=-PI1+PHASE
    ELSEIF(PHASE.LT.0.AND.RE.LT.0.AND.AIM.GT.0) THEN
      PHASE=PHASE+PI1
    ENDIF
    ENDIF
    RETURN
  END

```

C

```

SUBROUTINE SUB2(RE,AIM)
COMMON /PPII/PI0,PI1,PI2,PI3
COMMON /COST/CE1(8),CIO(64),CQO(64),C(64),CC(16),CE(64)
CALL ANGSUB(RE,AIM,PH)

```

C

```

CE1(1)=ABS(CIO(1)-PH)
CE1(2)=ABS(CIO(9)-PH)
CE1(3)=ABS(CIO(2)-PH)
CE1(4)=ABS(CIO(10)-PH)
CE1(5)=ABS(CIO(4)-PH)
CE1(6)=ABS(CIO(12)-PH)
CE1(7)=ABS(CIO(3)-PH)
CE1(8)=ABS(CIO(11)-PH)
DO 104 I=1,8
IF(CE1(I).GT.PI1) CE1(I)=PI3-CE1(I)
104 CONTINUE

```

104

C

```

CE1(1)=CE1(1)**2
CE1(2)=CE1(2)**2
CE1(3)=CE1(3)**2
CE1(4)=CE1(4)**2
CE1(5)=CE1(5)**2
CE1(6)=CE1(6)**2
CE1(7)=CE1(7)**2
CE1(8)=CE1(8)**2
RETURN
END

```

C

```

SUBROUTINE SUB1(RE,AIM)
COMMON /PPII/PI0,PI1,PI2,PI3
COMMON /COST/CE1(8),CIO(64),CQO(64),C(64),CC(16),CE(64)

```

C

```

CE1(1)=(RE-CIO(1))**2+(AIM-CQO(1))**2
CE1(2)=(RE-CIO(9))**2+(AIM-CQO(9))**2
CE1(3)=(RE-CIO(2))**2+(AIM-CQO(2))**2
CE1(4)=(RE-CIO(10))**2+(AIM-CQO(10))**2
CE1(5)=(RE-CIO(4))**2+(AIM-CQO(4))**2
CE1(6)=(RE-CIO(12))**2+(AIM-CQO(12))**2
CE1(7)=(RE-CIO(3))**2+(AIM-CQO(3))**2
CE1(8)=(RE-CIO(11))**2+(AIM-CQO(11))**2
RETURN
END

```

C

```

SUBROUTINE SUB3(RE,AIM)
COMMON /PPII/PI0,PI1,PI2,PI3
COMMON /COST/CE1(8),CIO(64),CQO(64),C(64),CC(16),CE(64)
RR=SQRT(RE**2+AIM**2)
RE=RE/RR
AIM=AIM/RR

```

C

```
CE1(1)=(RE-CI0(1))**2+(AIM-CQ0(1))**2
CE1(2)=(RE-CI0(9))**2+(AIM-CQ0(9))**2
CE1(3)=(RE-CI0(2))**2+(AIM-CQ0(2))**2
CE1(4)=(RE-CI0(10))**2+(AIM-CQ0(10))**2
CE1(5)=(RE-CI0(4))**2+(AIM-CQ0(4))**2
CE1(6)=(RE-CI0(12))**2+(AIM-CQ0(12))**2
CE1(7)=(RE-CI0(3))**2+(AIM-CQ0(3))**2
CE1(8)=(RE-CI0(11))**2+(AIM-CQ0(11))**2
RETURN
END
```

C

```
SUBROUTINE SUB4(PH)
COMMON /PPII/PI0,PI1,PI2,PI3
COMMON /COST/CE1(8),CI0(64),CQ0(64),C(64),CC(16),CE(64)
```

C

```
106 IF(PH.GT.PI3) THEN
      PH=PH-PI3
    ELSEIF(PH.LT.-PI3) THEN
      PH=PH+PI3
    ENDIF
    IF(ABS(PH).GT.PI3) GOTO 106
    IF(PH.GT.PI1) PH=PH-PI1
    IF(PH.LT.-PI1) PH=PH+PI1
```

C

```
CE1(1)=ABS(CI0(1)-PH)
CE1(2)=ABS(CI0(9)-PH)
CE1(3)=ABS(CI0(2)-PH)
CE1(4)=ABS(CI0(10)-PH)
CE1(5)=ABS(CI0(4)-PH)
CE1(6)=ABS(CI0(12)-PH)
CE1(7)=ABS(CI0(3)-PH)
CE1(8)=ABS(CI0(11)-PH)
DO 104 I=1,8
IF(CE1(I).GT.PI1) CE1(I)=PI3-CE1(I)
```

104

C

```
CONTINUE
RETURN
END
```

C

```
SUBROUTINE SUB5(RE,AIM)
COMMON /PPII/PI0,PI1,PI2,PI3
COMMON /COST/CE1(8),CI0(64),CQ0(64),C(64),CC(16),CE(64)
R1=SQRT(RE**2+AIM**2)
CALL ANGSUB(RE,AIM,PH)
```

C

```
CE1(1)=ABS(CI0(1)-PH)
CE1(2)=ABS(CI0(9)-PH)
CE1(3)=ABS(CI0(2)-PH)
CE1(4)=ABS(CI0(10)-PH)
CE1(5)=ABS(CI0(4)-PH)
CE1(6)=ABS(CI0(12)-PH)
CE1(7)=ABS(CI0(3)-PH)
CE1(8)=ABS(CI0(11)-PH)
DO 104 I=1,8
IF(CE1(I).GT.PI1) CE1(I)=PI3-CE1(I)
```

104

C

```
CONTINUE
CE1(1)=R1*CE1(1)
CE1(2)=R1*CE1(2)
CE1(3)=R1*CE1(3)
```

```
CE1(4)=R1*CE1(4)
CE1(5)=R1*CE1(5)
CE1(6)=R1*CE1(6)
CE1(7)=R1*CE1(7)
CE1(8)=R1*CE1(8)
RETURN
END
```

C

```
SUBROUTINE SUB6(RE,AIM)
COMMON /PPII/PI0,PI1,PI2,PI3
COMMON /COST/CE1(8),CIO(64),CQO(64),C(64),CC(16),CE(64)
R1=SQRT(RE**2+AIM**2)
CALL ANGSUB(RE,AIM,PH)
```

C

```
CE1(1)=ABS(CIO(1)-PH)
CE1(2)=ABS(CIO(9)-PH)
CE1(3)=ABS(CIO(2)-PH)
CE1(4)=ABS(CIO(10)-PH)
CE1(5)=ABS(CIO(4)-PH)
CE1(6)=ABS(CIO(12)-PH)
CE1(7)=ABS(CIO(3)-PH)
CE1(8)=ABS(CIO(11)-PH)
DO 104 I=1,8
IF(CE1(I).GT.PI1) CE1(I)=PI3-CE1(I)
CONTINUE
```

104

C

```
CE1(1)=R1*CE1(1)**2
CE1(2)=R1*CE1(2)**2
CE1(3)=R1*CE1(3)**2
CE1(4)=R1*CE1(4)**2
CE1(5)=R1*CE1(5)**2
CE1(6)=R1*CE1(6)**2
CE1(7)=R1*CE1(7)**2
CE1(8)=R1*CE1(8)**2
RETURN
END
```

C

```
SUBROUTINE SUB7(RE,AIM)
COMMON /PPII/PI0,PI1,PI2,PI3
COMMON /COST/CE1(8),CIO(64),CQO(64),C(64),CC(16),CE(64)
CALL ANGSUB(RE,AIM,PH)
```

C

```
CE1(1)=ABS(CIO(1)-PH)
CE1(2)=ABS(CIO(9)-PH)
CE1(3)=ABS(CIO(2)-PH)
CE1(4)=ABS(CIO(10)-PH)
CE1(5)=ABS(CIO(4)-PH)
CE1(6)=ABS(CIO(12)-PH)
CE1(7)=ABS(CIO(3)-PH)
CE1(8)=ABS(CIO(11)-PH)
DO 104 I=1,8
IF(CE1(I).GT.PI1) CE1(I)=PI3-CE1(I)
CONTINUE
```

104

C

```
CE1(1)=-COS(CE1(1))
CE1(2)=-COS(CE1(2))
CE1(3)=-COS(CE1(3))
CE1(4)=-COS(CE1(4))
CE1(5)=-COS(CE1(5))
CE1(6)=-COS(CE1(6))
```

```

CE1(7)=-COS(CE1(7))
CE1(8)=-COS(CE1(8))
RETURN
END

```

C

```

SUBROUTINE SUB8(RE,AIM)
COMMON /PPII/PI0,PI1,PI2,PI3
COMMON /COST/CE1(8),CI0(64),CQ0(64),C(64),CC(16),CE(64)
R1=SQRT(RE**2+AIM**2)
CALL ANGSUB(RE,AIM,PH)

```

C

```

CE1(1)=ABS(CI0(1)-PH)
CE1(2)=ABS(CI0(9)-PH)
CE1(3)=ABS(CI0(2)-PH)
CE1(4)=ABS(CI0(10)-PH)
CE1(5)=ABS(CI0(4)-PH)
CE1(6)=ABS(CI0(12)-PH)
CE1(7)=ABS(CI0(3)-PH)
CE1(8)=ABS(CI0(11)-PH)
DO 104 I=1,8
IF(CE1(I).GT.PI1) CE1(I)=PI3-CE1(I)
CONTINUE

```

104

C

```

CE1(1)=-R1*COS(CE1(1))
CE1(2)=-R1*COS(CE1(2))
CE1(3)=-R1*COS(CE1(3))
CE1(4)=-R1*COS(CE1(4))
CE1(5)=-R1*COS(CE1(5))
CE1(6)=-R1*COS(CE1(6))
CE1(7)=-R1*COS(CE1(7))
CE1(8)=-R1*COS(CE1(8))
RETURN
END

```

```

####S
0.25
4
3.09
38
48
4
0.25
4
4.36
2
20
4
0.25
4
4.12
3
20
4
####S

```

APPENDIX A14SIMULATOR FOR CDE8PSK SIGNALS WITH THE USE OF THE DDL

THIS PROGRAM IS USED TO EVALUATE THE ERROR-RATE PERFORMANCES OF SIGNALS 1A, 2A, 3A AND 4A, OVER A NONLINEAR AND BANDLIMITED SATELLITE CHANNEL, WITH THE USE OF THE SUBOPTIMUM FILTERS, THE PREDISTORTER, THE AMPLIFIER LIMITER, PHASE DEMODULATOR A OR B, THE DISTANCE MEASURE D AND THE DDL AND IN AN ACI ENVIRONMENT

```

/*JOB C1,EUELSWC,ST=MFY,C=S,TI=1280,
/* PW=SWC
FTN5,DB=0/PMD,L=0.
LIBRARY(PROCLIB,*)
NAG(FTN5)
LGO.
####S
PROGRAM SWCAB(INPUT,OUTPUT,TAPE1=INPUT,TAPE2=OUTPUT)
DIMENSION BSF(-200:200),FF1(0:63),FF2(0:63),FF3(0:63),FF4(0:63)
DATA (FF1(I),I=0,63)/1.0,.943,.786,.566,.334,.135,.0,-.064,-.068,
*-.038,-.001,.024,.029,.017,-.001,-.014,-.017,-.011,
*-.001,.008,.01,.007,-.001,-.007,-.008,
*-.006,-.001,.004,.005,.003,-.001,-.004,-.005,-.004,
*.0,.003,.004,.002,.0,-.003,-.004,-.003,-.001,.002,.003,
*.002,.0,-.003,-.003,-.002,.0,.001,.002,.001,.0,-.002,
*-.003,-.002,-.001,.001,.002,.001,.0,-.002/
C
DATA (FF2(I),I=0,63)/1.0,.954,.825,.638,.425,.223,.06,-.047,
*-.095,-.096,-.067,-.028,.005,.022,.022,.01,-.006,-.018,-.022,
*-.018,-.008,.003,.011,.012,.009,
*.002,-.004,-.007,-.007,-.003,.002,.006,.006,.004,.0,-.005,
*-.007,-.008,-.005,-.002,.001,.003,.002,.0,-.002,-.004,-.004,
*-.002,.001,.004,.005,.005,.003,.0,-.002,-.003,-.002,.0,
*.001,.002,.001,.0,-.003,-.005/
C
DATA (FF3(I),I=0,63)/1.0,.963,0.858,0.7,0.511,0.316,0.139,-0.001,
*-0.094,-0.138,-0.14,-0.112,-0.068,-0.022,0.035,0.039,0.03,0.014,
*0.014,-0.003,-0.015,-0.02,-0.017,-0.008,0.002,
*.011,.016,.015,.01,.003,-.005,-.01,-.011,-.009,
*-.005,.001,.005,.008,.007,.003,-.001,-.005,
*-.008,-.008,-.006,-.002,.002,.005,.006,
*.005,.002,-.002,-.005,-.006,-.006,-.004,.0,
*.003,.005,.005,.003,.001,-.003,-.005/
C
DATA (FF4(I),I=0,48)/1.0,.970,.884,.751,.585,.405,
*.227,.068,-.058,-.144,-.188,-.192,-.164,-.115,-.056,

```

```
*.002,.049,.08,.091,.085,.065,.036,.006,-.02,-.039,  
*-.047,-.045,-.034,-.019,-.003,.011,.021,.024,.021,.014,  
*.004,-.005,-.012,-.016,-.015,-.011,-.004,.003,.009,  
*.013,.013,.01,.005,-.002/
```

C

```
DO 10000 NR=1,3  
PRINT*,'INPUT BASEBAND FILTER R.O.F (SQ.)=1,0.75,0.5,0.25'  
READ*,ROF  
PRINT*,'INPUT THE TRUNCATION LENGTH'  
READ*,KT12  
PRINT*,'INPUT THE NOISE VARIANCE'  
READ*,P  
PRINT*,'INPUT THE RANDOM SEED'  
READ*,IIQQ  
PRINT*,'INPUT NO. OF TESTED SYMBOLS'  
READ*,L
```

C

```
IF(ROF.EQ.1) THEN  
DO 100 I=0,63  
100 BSF(I)=FF1(I)  
PBOP=3.953  
BOP=3.21  
CT BOP=2.84  
ELSEIF(ROF.EQ.0.75) THEN  
DO 101 I=0,63  
101 BSF(I)=FF2(I)  
PBOP=4.551  
BOP=3.715  
CT BOP=3.31  
ELSEIF(ROF.EQ.0.5) THEN  
DO 102 I=0,63  
102 BSF(I)=FF3(I)  
PBOP=5.207  
BOP=4.22  
CT BOP=3.83  
ELSEIF(ROF.EQ.0.25) THEN  
DO 103 I=0,63  
103 BSF(I)=FF4(I)  
PBOP=5.98  
BOP=4.83  
CT BOP=4.39  
ELSE  
PRINT*,'NO REQUIRED FILTER'  
STOP  
ENDIF
```

C

```
CALL QPSKSUB(KT12,ROF,BSF,P,IIQQ,L,BOP,PBOP)  
10000 CONTINUE  
STOP  
END
```

C

```
SUBROUTINE QPSKSUB(KT12,ROF,BSF,P,IIQQ,L,BOP,PBOP)  
DIMENSION X2(-400:400),XXX2(-400:400),  
1XX1(-400:400),XX2(-400:400),FR(-200:200),GQ(0:38),GR(0:38),  
1BSF(-200:200),FM(-200:200),  
2FT(-200:200),  
2X1(-300:300),XXX1(-400:400),STPH(-300:300),  
2XU1(-300:100),XU2(-300:100),  
2BF(-200:200),PGR(0:38),PGQ(0:38),  
2PHDL(-8:0),
```

2C1(128),C(512),CC(16),
 2XL1(-300:100),XL2(-300:100),
 2RU(-2:0),QU(-2:0),RL(-2:0),QL(-2:0),
 2RS(320),QS(320),ADJI(16),ADJQ(16)
 DIMENSION IX1(-100:0),IX2(-100:0),
 1IV(16,-200:0),IVV(16,-200:0)
 COMMON /VMAP/VIO,VI1,VI2,VI3,VI4,VI5,VI6,VI7,VQ0,VQ1,
 1VQ2,VQ3,VQ4,VQ5,VQ6,VQ7
 COMMON /PPII/PIO,PI1,PI2,PI3
 COMMON /COST/CE1(8),CIO(64),CQ0(64)
 DATA(FT(I),I=0,24)/1.0,0.935,0.758,0.512,0.256,0.041,-0.099,
 *-0.157,-0.146,-0.094,-0.031,0.02,0.048,0.052,0.039,0.017,-0.004,
 *-0.017,-0.021,-0.017,-0.008,0.002,0.009,0.011,0.008/

C

DATA(FR(I),I=0,24)/1.0,0.935,0.758,0.512,0.256,0.041,-0.099,
 *-0.157,-0.146,-0.094,-0.031,0.02,0.048,0.052,0.039,0.017,-0.004,
 *-0.017,-0.021,-0.017,-0.008,0.002,0.009,0.011,0.008/

C

DATA(GQ(I),I=0,38)/0.17,0.34,0.48,0.58,0.65,0.70,0.75,
 *0.78,0.82,0.84,0.85,0.85,0.84,0.83,0.84,0.85,0.83,
 *0.82,0.80,0.78,0.75,0.73,0.7,0.67,0.65,0.61,0.58,0.56,
 *0.53,0.50,0.48,0.43,0.4,0.38,0.37,0.36,0.34,0.36,0.35/

C

DATA(GR(I),I=0,38)/3.57,3.17,2.83,2.55,2.33,2.15,1.99,
 *1.83,1.69,1.55,1.44,1.30,1.20,1.09,1.0,0.92,0.86,0.80,
 *0.74,0.68,0.63,0.58,0.54,0.50,0.46,0.43,0.4,0.37,0.352,
 *0.352,0.332,0.332,0.31,0.3,0.3,0.29,0.29,0.28,0.28/

C

DATA(PGR(I),I=0,38)/0.280,0.280,0.280,0.285,0.309,0.309,
 *0.319,0.341,0.357,0.358,0.386,0.399,0.418,0.432,0.453,
 *0.468,0.492,0.504,0.574,0.594,0.594,0.594,0.594,0.594,
 *0.594,0.594,0.594,0.594,0.594,0.594,0.594,0.594,0.594,
 *0.594,0.594,0.594,0.594,0.594,0.594/

C

DATA(PGQ(I),I=0,38)/-0.005,-0.012,-0.015,-0.020,-0.033,-0.038,
 *-0.051,-0.063,-0.076,-0.086,-0.104,-0.122,-0.136,-0.157,-0.188,
 *-0.218,-0.251,-0.315,-0.425,-0.544,-0.544,-0.544,-0.544,-0.544,
 *-0.544,-0.544,-0.544,-0.544,-0.544,-0.544,-0.544,-0.544,-0.544,
 *-0.544,-0.544,-0.544,-0.544,-0.544,-0.544/

C

RR=SQRT(PGR(20)**2+PGQ(20)**2)
 DO 136 I=0,38
 PGQ(I)=PGQ(I)/RR
 PGR(I)=PGR(I)/RR

136

C

PI1=ACOS(-1.0)
 PIO=PI1/2.0
 PI2=PIO*3.0
 PI3=2.0*PI1
 PI4=PI1/4.0
 P4I=1.0/PI4
 PI8=PI1/8.0
 P8I=1.0/PI8

C

C

C

MAP-SETTING

VIO=0.924
 VQ0=0.383
 VI1=0.383
 VQ1=0.924

VI2=-0.383
VQ2=0.924
VI3=-0.924
VQ3=0.383
VI4=-0.924
VQ4=-0.383
VI5=-0.383
VQ5=-0.924
VI6=0.383
VQ6=-0.924
VI7=0.924
VQ7=-0.383

C

CALL COSTSUB(1,C10,CQ0,0,0,0,0,0,0)
CALL COSTSUB(2,C10,CQ0,0,0,0,1,0,0)
CALL COSTSUB(3,C10,CQ0,1,0,0,0,0,0)
CALL COSTSUB(4,C10,CQ0,1,0,0,1,0,0)
CALL COSTSUB(5,C10,CQ0,0,0,0,0,1,0)
CALL COSTSUB(6,C10,CQ0,0,0,0,1,1,0)
CALL COSTSUB(7,C10,CQ0,1,0,0,0,1,0)
CALL COSTSUB(8,C10,CQ0,1,0,0,1,1,0)
CALL COSTSUB(9,C10,CQ0,0,1,0,0,0,0)
CALL COSTSUB(10,C10,CQ0,0,1,0,1,0,0)
CALL COSTSUB(11,C10,CQ0,1,1,0,0,0,0)
CALL COSTSUB(12,C10,CQ0,1,1,0,1,0,0)
CALL COSTSUB(13,C10,CQ0,0,1,0,0,1,0)
CALL COSTSUB(14,C10,CQ0,0,1,0,1,1,0)
CALL COSTSUB(15,C10,CQ0,1,1,0,0,1,0)
CALL COSTSUB(16,C10,CQ0,1,1,0,1,1,0)
CALL COSTSUB(17,C10,CQ0,0,0,0,0,0,1)
CALL COSTSUB(18,C10,CQ0,0,0,0,1,0,1)
CALL COSTSUB(19,C10,CQ0,1,0,0,0,0,1)
CALL COSTSUB(20,C10,CQ0,1,0,0,1,0,1)
CALL COSTSUB(21,C10,CQ0,0,0,0,0,1,1)
CALL COSTSUB(22,C10,CQ0,0,0,0,1,1,1)
CALL COSTSUB(23,C10,CQ0,1,0,0,0,1,1)
CALL COSTSUB(24,C10,CQ0,1,0,0,1,1,1)
CALL COSTSUB(25,C10,CQ0,0,1,0,0,0,1)
CALL COSTSUB(26,C10,CQ0,0,1,0,1,0,1)
CALL COSTSUB(27,C10,CQ0,1,1,0,0,0,1)
CALL COSTSUB(28,C10,CQ0,1,1,0,1,0,1)
CALL COSTSUB(29,C10,CQ0,0,1,0,0,1,1)
CALL COSTSUB(30,C10,CQ0,0,1,0,1,1,1)
CALL COSTSUB(31,C10,CQ0,1,1,0,0,1,1)
CALL COSTSUB(32,C10,CQ0,1,1,0,1,1,1)
CALL COSTSUB(33,C10,CQ0,0,0,1,0,0,0)
CALL COSTSUB(34,C10,CQ0,0,0,1,1,0,0)
CALL COSTSUB(35,C10,CQ0,1,0,1,0,0,0)
CALL COSTSUB(36,C10,CQ0,1,0,1,1,0,0)
CALL COSTSUB(37,C10,CQ0,0,0,1,0,1,0)
CALL COSTSUB(38,C10,CQ0,0,0,1,1,1,0)
CALL COSTSUB(39,C10,CQ0,1,0,1,0,1,0)
CALL COSTSUB(40,C10,CQ0,1,0,1,1,1,0)
CALL COSTSUB(41,C10,CQ0,0,1,1,0,0,0)
CALL COSTSUB(42,C10,CQ0,0,1,1,1,0,0)
CALL COSTSUB(43,C10,CQ0,1,1,1,0,0,0)
CALL COSTSUB(44,C10,CQ0,1,1,1,1,0,0)
CALL COSTSUB(45,C10,CQ0,0,1,1,0,1,0)
CALL COSTSUB(46,C10,CQ0,0,1,1,1,1,0)
CALL COSTSUB(47,C10,CQ0,1,1,1,0,1,0)

```

CALL COSTSUB(48,CIO,CQO,1,1,1,1,1,0)
CALL COSTSUB(49,CIO,CQO,0,0,1,0,0,1)
CALL COSTSUB(50,CIO,CQO,0,0,1,1,0,1)
CALL COSTSUB(51,CIO,CQO,1,0,1,0,0,1)
CALL COSTSUB(52,CIO,CQO,1,0,1,1,0,1)
CALL COSTSUB(53,CIO,CQO,0,0,1,0,1,1)
CALL COSTSUB(54,CIO,CQO,0,0,1,1,1,1)
CALL COSTSUB(55,CIO,CQO,1,0,1,0,1,1)
CALL COSTSUB(56,CIO,CQO,1,0,1,1,1,1)
CALL COSTSUB(57,CIO,CQO,0,1,1,0,0,1)
CALL COSTSUB(58,CIO,CQO,0,1,1,1,0,1)
CALL COSTSUB(59,CIO,CQO,1,1,1,0,0,1)
CALL COSTSUB(60,CIO,CQO,1,1,1,1,0,1)
CALL COSTSUB(61,CIO,CQO,0,1,1,0,1,1)
CALL COSTSUB(62,CIO,CQO,0,1,1,1,1,1)
CALL COSTSUB(63,CIO,CQO,1,1,1,0,1,1)
CALL COSTSUB(64,CIO,CQO,1,1,1,1,1,1)

```

C

```

PRINT*,'WHAT MEASURE ?'
PRINT*,'1-CX ,2-PH**2, 3-LIMITER, 4-PH, 5-R*PH, 6-R*PH**2',
1' ,7-COS ,8-R*COS'
READ*,MEAS
IF(MEAS.NE.1.AND.MEAS.NE.3) THEN
DO 122 I=1,64
RE=CIO(I)
AIM=CQO(I)
CALL ANGSUB(RE,AIM,PHASE)
122 CIO(I)=PHASE
ENDIF

```

C

```

C
C KS1: NO OF THE SAMPLES IN ONE T.
C
C KT1: SYMBOL LENGTH OF THE TRUNCATED IMPULSE RESPONSE WAVEFORM
C OF THE BASEBAND SHAPPING FILTER IN CASCADED WITH THE BPF.
C
C KS2: THE BASEBAND SHAPPING ARRAY EXTENDS FROM -KS3 TO +KS2.
C
C KT2: SYMBOL TIME FOR THE 1ST SAMPLE INSTANCE
C
C KS3: ARRAY ELEMENT FOR THE 1ST SAMPLE.
C
C KT12: TRUNCATED OF THE BASEBAND SHAPPING FILTER.
C
C KT4: SYMBOL LENGTH OF THE IMPULSE RESPONSE OF FT IN THE TX
C
C KS4: THE LAST ELEMENT IN FT
C
C KT5: SYMBOL LENGTH OF THE IMPULSE RESPONSE OF FT IN THE RX
C
C KS5: THE LAST ELEMENT IN FR
C
C KTM1: SYMBOL LENGTH OF THE IMPULSE RESPONSE OF THE MATCHED-FILTER
C
C KSM1: THE LAST ELEMENT IN MF

```

C

KS1=8

C***SETUP SYNC PARAMETERS***

```

PRINT*,'OFFSET(HZ) INIT PHASE ERROR(DEG)'
READ*,FOS,PHI
FPH=0
FPH1=0
FPH2=0
FPH3=0
RCOR=1
QCOR=0
PHCOR=0
PHF=PI3*FOS/(32.0E3*KS1)
PHI=PHI*PI1/180
FPH1=0
F1=PHI
PHE=0

```

PHEF=0

```

C
C*****
C
  KT13=32
  KT13=-KT13
  KT4=3
  KT1=2*(KT12+KT4)
  KT3=KT1*(-1)/2
  KS2=KT1*KS1/2
  KS3=KS2*(-1)
  KS4=KT4*KS1
  KT5=3
  KS5=KT5*KS1
  KS12=KT12*KS1
  KTM1=KT12+KT5
  KSM1=KTM1*KS1
  KT2=-KT1/2-KTM1
DO 165 I=KS4+1,200
  FT(I)=0.0
DO 166 I=0,200
  FT(-I)=FT(I)
DO 167 II=0,KS2
  RR=BSF(0)*FT(II)
DO 168 I=1,KS12
  RR=RR+BSF(I)*(FT(II+I)+FT(II-I))
DO 167 BF(II)=RR
DO 150 I=0,KS2
  BF(-I)=BF(I)
DO 150 FM(I)=BF(I)
C
  KS10=320
  KT13=-32
  KT14=KT13-1
  KT15=KT13+KT2
C
C   DETECTOR INITIALISATION
C
DO 120 I=1,16
  CC(I)=1.0E+6
  DO 120 J=KT14,0
    IV(I,J)=0
C
DO 123 I=1,128
  C1(I)=0.0
C
DO 102 I=1,16,4
  IV(I,0)=0
  IV(I+1,0)=1
  IV(I+2,0)=2
DO 102 IV(I+3,0)=3
C
  KT6=KT14+KT2
C
C
  PRINT*,'INPUT CHANNAL SPACING (M HZ)'
  READ*,CSP
  F=PI3*CSP/32.0
  DO 164, I=1,KS10
  FF=F*REAL(I)

```

```
RS(I)=COS(FF)
164 QS(I)=SIN(FF)
C
C INITIALISE IX
C
DO 104 I=KT6,0
  IX1(I)=1
104  IX2(I)=0
DO 140 I=-2,0
  RU(I)=0
  QU(I)=0
  RL(I)=0
140  QL(I)=0
C
KS6=KS3-KS1+1-2*KSM1
KS7=KS3-KS5
DO 105 I=KS6,KS2+KS1
  X1(I)=0.0
  X2(I)=0.0
  XX1(I)=0.0
  XX2(I)=0.0
  XXX1(I)=0.0
  XXX2(I)=0.0
  XU1(I)=0.0
  XU2(I)=0.0
  XL1(I)=0.0
  STPH(I)=0.0
105  XL2(I)=0.0
C
CDI=VIO
CDQ=VQO
C
PH=-PI8
K8=0
DO 127 J=KT6,0
  PH=PH+PI1
  K8=K8+4
  CDI=COS(PH)
  CDQ=SIN(PH)
  IF(PH.GT.PI3) PH=PH-PI3
DO 126 I=KS6,KS2
  II=I+KS1
  X1(I)=X1(II)
  X2(I)=X2(II)
  XU1(I)=XU1(II)
  XU2(I)=XU2(II)
  XL1(I)=XL1(II)
126  XL2(I)=XL2(II)
  DO 125 I=KS3,KS2
  X1(I)=BF(I)*CDI+X1(I)
  X2(I)=BF(I)*CDQ+X2(I)
  XU1(I)=X1(I)
  XU2(I)=X2(I)
  XL1(I)=X1(I)
125  XL2(I)=X2(I)
127 CONTINUE
C
PREDBK=18
BK=15
PAV=SQRT(4.0*PBOP)
```

```

AV=SQRT(4.0*BOP)
AV1=PREDBK/PAV
AV2=BK/AV
I=PREDBK
SUM1=SQRT(PGR(I)**2+PGQ(I)**2)
A1=PGR(I)/SUM1
B1=-PGQ(I)/SUM1
I=BK
SUM2=SQRT(GR(I)**2+GQ(I)**2)
A2=GR(I)/SUM2
B2=-GQ(I)/SUM2
A=A1*A2-B1*B2
B=A1*B2+B1*A2
DO 141 N=KS6,KS3
RN=X1(N)
QN=X2(N)
I=INT(AV1*SQRT(RN*RN+QN*QN))
PR=RN*PGR(I)-QN*PGQ(I)
PQ=RN*PGQ(I)+QN*PGR(I)
I=INT(AV2*SQRT(PR*PR+PQ*PQ))
X1(N)=PR*GR(I)-PQ*GQ(I)
141 X2(N)=PR*GQ(I)+PQ*GR(I)
C
DO 146 N=KS6,KS3
R1=X1(N)
Q1=X2(N)
X1(N)=A*R1-B*Q1
X2(N)=A*Q1+B*R1
C
C   ADD OFFSETS
C
F1=F1+PHF
IF(F1.GT.PI3) THEN
  F1=F1-PI3
ELSEIF(F1.LT.-PI3) THEN
  F1=F1+PI3
ENDIF
R1=X1(N)
Q1=X2(N)
R2=COS(F1)
Q2=SIN(F1)
X1(N)=R1*R2-Q1*Q2
X2(N)=Q1*R2+R1*Q2
146 XX1(N)=X1(N)
C   XX2(N)=X2(N)
DO 130 II=KS6+KS5,KS3-KS5
  XXX1(II)=XX1(II)*FR(0)
  XXX2(II)=XX2(II)*FR(0)
DO 135 I=1,KS5
  R1=XX1(II+I)
  R2=XX1(II-I)
  Q1=XX2(II+I)
  Q2=XX2(II-I)
  XXX1(II)=XXX1(II)+FR(I)*(R1+R2)
135 XXX2(II)=XXX2(II)+FR(I)*(Q1+Q2)
130 CONTINUE
C
C   ADD THE LIMITER BEFORE THE RX LPF
C

```

```
DO 133 I=KS6+KS5,KS3-KS5
CT   RR=1/SQRT(XXX1(I)**2+XXX2(I)**2)
      RR=1/(ABS(XXX1(I))+ABS(XXX2(I)))
C
C   CORRECT OFFSETS
C
FPH=FPH+FPH
IF(FPH.GT.PI3) THEN
  FPH=FPH-PI3
ELSEIF(FPH.LT.-PI3) THEN
  FPH=FPH+PI3
ENDIF
R1=XXX1(I)
Q1=XXX2(I)
R2=COS(FPH)
Q2=SIN(FPH)
XXX1(I)=R1*R2+Q1*Q2
XXX2(I)=Q1*R2-R1*Q2
      XXX1(I)=XXX1(I)*RR
133   XXX2(I)=XXX2(I)*RR
C
C   ASSUME THE 1ST DETECTION IS CORRECT
C
KT7=KT2-1
C
C   I1: THE MAIN SAMPLING INSTANCE
I1=KS3-KSM1
C   I2: THE OFFSET SAMPLING INSTANCE.
I2=I1
C
C
      XXXM1=XXX1(I1)*BSF(0)
      XXXM2=XXX2(I1)*BSF(0)
      DO 147 I=1,KS12
147   XXXM1=XXXM1+BSF(I)*(XXX1(I1-I)+XXX1(I1+I))
      XXXM2=XXXM2+BSF(I)*(XXX2(I1-I)+XXX2(I1+I))
C
      CALL ANGSUB1(XXXM1,XXXM2,PH)
PH1=PH
KT7=KT2-1
K8=MOD(K8,8)
IF(K8.EQ.0) K8=8
C
CT   PRINT*, 'INPUT GAMMA1 & ALPHA1'
CT   READ*, GAMMA1, ALPHA1
      GAMMA1=0.01
      ALPHA1=0.005
C
      GAMMA=0.1
      ALPHA=0.05
      P1=0
      NTEST2=600
      NTEST1=1
      ISW=0
C   KS11:FREQ. SHIFT ARRAY VARIABLE
      KS11=1
      F2=F1
      F3=F1
1006 CALL G05CBF(IIQQ)
C
```

```
C      INITIALISE ALL COUNTERS.
      IE=0
      IA1=0
      IA2=0
      IA3=0
      IB1=0
      IB2=0
      IB3=0
      IBE=0
      E=0.0
      E1=0.0
      E2=0.0
      E3=0

C
C      START
      DO 111 LLL=1,NTEST1
      DO 111 LL=1,NTEST2

C
C      SHIFT IX
C
      DO 112 I=KT6,-1
         J=I+1
         IX1(I)=IX1(J)
112    IX2(I)=IX2(J)

C
C      GENERATE DATA IX(0) AND GRAY CODE  IT INTO R & Q.
C
      U=G05DAF(0.000,4.000)
      IF(U.LT.1.0) THEN
         IX1(0)=0
         IX2(0)=0
      ELSEIF(U.LT.2.0) THEN
         IX1(0)=0
         IX2(0)=1
      ELSEIF(U.LT.3.0) THEN
         IX1(0)=1
         IX2(0)=1
      ELSE
         IX1(0)=1
         IX2(0)=0
      ENDIF
      IF(ISW.EQ.0) THEN
         IX1(0)=1
         IX2(0)=0
      ENDIF

C
C
      K1=IX1(0)+IX1(-2)+IX2(-1)
      K2=IX1(-2)+IX2(0)+IX2(-1)+IX2(-2)
      K3=IX1(-1)
      K4=MOD(K1,2)
      K5=MOD(K2,2)
      K6=MOD(K3,2)
      K7=4*K4+2*K5+K6+1

C
      K8=K7+K8
      IF(K8.GT.8) K8=K8-8
      K7=K8
      GOTO(1,2,3,4,5,6,7,8),K7

C
```

```
1   CDI=V10
    CDQ=VQ0
    GOTO 9

C
2   CDI=V11
    CDQ=VQ1
    GOTO 9

C
3   CDI=V12
    CDQ=VQ2
    GOTO 9

C
4   CDI=V13
    CDQ=VQ3
    GOTO 9

C
5   CDI=V14
    CDQ=VQ4
    GOTO 9

C
6   CDI=V15
    CDQ=VQ5
    GOTO 9

C
7   CDI=V16
    CDQ=VQ6
    GOTO 9

C
8   CDI=V17
    CDQ=VQ7

C
9   DO 113 I=KS6,KS2
      II=I+KS1
      X1(I)=X1(II)
      X2(I)=X2(II)
      XX1(I)=XX1(II)
      XX2(I)=XX2(II)
      XXX1(I)=XXX1(II)
      XXX2(I)=XXX2(II)
      XU1(I)=XU1(II)
      XU2(I)=XU2(II)
      XL1(I)=XL1(II)
      STPH(I)=STPH(II)
113  XL2(I)=XL2(II)
C
      DO 114 I=KS3,KS2
        X1(I)=BF(I)*CDI+X1(I)
114  X2(I)=BF(I)*CDQ+X2(I)
C
      DO 143 N=KS3-KS1+1,KS3
        RN=X1(N)
        QN=X2(N)
        E2=RN*RN+QN*QN+E2
        I=INT(AV1*SQRT(RN*RN+QN*QN))
        PR=RN*PGR(I)-QN*PGQ(I)
        PQ=RN*PGQ(I)+QN*PGR(I)
        E1=PR*PR+PQ*PQ+E1
        I=INT(AV2*SQRT(PR*PR+PQ*PQ))
        X1(N)=PR*GR(I)-PQ*GQ(I)
```

```

143 X2(N)=PR*GQ(I)+PQ*GR(I)
C
DO 144 N=KS3-KS1+1,KS3
R1=X1(N)
Q1=X2(N)
X1(N)=A*R1-B*Q1
144 X2(N)=A*Q1+B*R1
C
DO 101 I=-2,-1
J=I+1
RU(I)=RU(J)
QU(I)=QU(J)
RL(I)=RL(J)
101 QL(I)=QL(J)
C
U=G05DAF(0.000,4.000)
IF(U.LT.1.0) THEN
RU(0)=0
QU(0)=0
ELSEIF(U.LT.2.0) THEN
RU(0)=0
QU(0)=1
ELSEIF(U.LT.3.0) THEN
RU(0)=1
QU(0)=1
ELSE
RU(0)=1
QU(0)=0
ENDIF
C
K1=RU(0)+RU(-2)+QU(-1)
K2=RU(-2)+QU(0)+QU(-1)+QU(-2)
K3=RU(-1)
K4=MOD(K1,2)
K5=MOD(K2,2)
K6=MOD(K3,2)
K7=4*K4+2*K5+K6+1
GOTO(21,22,23,24,25,26,27,28),K7
C
21 CDUI=V10
CDUQ=VQ0
GOTO 29
C
22 CDUI=V11
CDUQ=VQ1
GOTO 29
C
23 CDUI=V12
CDUQ=VQ2
GOTO 29
C
24 CDUI=V13
CDUQ=VQ3
GOTO 29
C
25 CDUI=V14
CDUQ=VQ4
GOTO 29
C
26 CDUI=V15

```

CDUQ=VQ5
GOTO 29

C
27 CDUI=VI6
CDUQ=VQ6
GOTO 29

C
28 CDUI=VI7
CDUQ=VQ7

C
29 DO 151 I=KS3,KS2
XU1(I)=BF(I)*CDUI+XU1(I)
151 XU2(I)=BF(I)*CDUQ+XU2(I)

C
DO 155 N=KS3-KS1+1,KS3
RN=XU1(N)
QN=XU2(N)
I=INT(AV1*SQRT(RN*RN+QN*QN))
PR=RN*PGR(I)-QN*PGQ(I)
PQ=RN*PGQ(I)+QN*PGR(I)
I=INT(AV2*SQRT(PR*PR+PQ*PQ))
XU1(N)=PR*GR(I)-PQ*GQ(I)
XU2(N)=PR*GQ(I)+PQ*GR(I)

C
R1=XU1(N)
Q1=XU2(N)
155 XU1(N)=A*R1-B*Q1
XU2(N)=A*Q1+B*R1

C
U=G05DAF(0.000,4.000)
IF(U.LT.1.0) THEN
RL(0)=0
QL(0)=0
ELSEIF(U.LT.2.0) THEN
RL(0)=0
QL(0)=1
ELSEIF(U.LT.3.0) THEN
RL(0)=1
QL(0)=1
ELSE
RL(0)=1
QL(0)=0
ENDIF

C
K1=RL(0)+RL(-2)+QL(-1)
K2=RL(-2)+QL(0)+QL(-1)+QL(-2)
K3=RL(-1)
K4=MOD(K1,2)
K5=MOD(K2,2)
K6=MOD(K3,2)
K7=4*K4+2*K5+K6+1
GOTO(31,32,33,34,35,36,37,38),K7

C
31 CDLI=VI0
CDLQ=VQ0
GOTO 40

C
32 CDLI=VI1
CDLQ=VQ1
GOTO 40

```
C
33  CDLI=VI2
    CDLQ=VQ2
    GOTO 40

C
34  CDLI=VI3
    CDLQ=VQ3
    GOTO 40

C
35  CDLI=VI4
    CDLQ=VQ4
    GOTO 40

C
36  CDLI=VI5
    CDLQ=VQ5
    GOTO 40

C
37  CDLI=VI6
    CDLQ=VQ6
    GOTO 40

C
38  CDLI=VI7
    CDLQ=VQ7

C
40  DO 157 I=KS3,KS2
    XL1(I)=BF(I)*CDLI+XL1(I)
157  XL2(I)=BF(I)*CDLQ+XL2(I)
C
    DO 161 N=KS3-KS1+1,KS3
    RN=XL1(N)
    QN=XL2(N)
    I=INT(AV1*SQRT(RN*RN+QN*QN))
    PR=RN*PGR(I)-QN*PGQ(I)
    PQ=RN*PGQ(I)+QN*PGR(I)
    I=INT(AV2*SQRT(PR*PR+PQ*PQ))
    XL1(N)=PR*GR(I)-PQ*GQ(I)
    XL2(N)=PR*GQ(I)+PQ*GR(I)

C
    R1=XL1(N)
    Q1=XL2(N)
    XL1(N)=A*R1-B*Q1
161  XL2(N)=A*Q1+B*R1
C
C
C
C  CALCU. TOTAL ENERGY PER SYMBOL
C
    DO 124 I=KS3-KS1+1,KS3
124  E=X1(I)**2+X2(I)**2+E
C
    J=1
    DO 163 I=KS3-KS1+1,KS3
    F2=F2+F+PHF
    IF(F2.GT.PI3) THEN
        F2=F2-PI3
    ELSEIF(F2.LT.-PI3) THEN
        F2=F2+PI3
    ENDIF
    R2=COS(F2)
    Q2=SIN(F2)
```

```

F3=F3+F-PHF
IF(F3.GT.PI3) THEN
  F3=F3-PI3
ELSEIF(F3.LT.-PI3) THEN
  F3=F3+PI3
ENDIF
R3=COS(F3)
Q3=SIN(F3)
ADJI(J)=XU1(I)*R2-XU2(I)*Q2
*+XL1(I)*R3+XL2(I)*Q3
ADJQ(J)=XU1(I)*Q2+XU2(I)*R2
*-XL1(I)*Q3+XL2(I)*R3
163 J=J+1
C
IF(ISW.EQ.0) THEN
  DO 142 I=1,8
  ADJI(I)=0
142 ADJQ(I)=0
ENDIF
J=1
DO 119 I=KS3-KS1+1,KS3
W1=G05DDF(0.000,P1)
W2=G05DDF(0.000,P1)
R1=X1(I)+W1+ADJI(J)
Q1=X2(I)+W2+ADJQ(J)
C
C
  ADD OFFSETS

F1=F1+PHF
IF(F1.GT.PI3) THEN
  F1=F1-PI3
ELSEIF(F1.LT.-PI3) THEN
  F1=F1+PI3
ENDIF
R2=COS(F1)
Q2=SIN(F1)
XX1(I)=R1*R2-Q1*Q2
XX2(I)=Q1*R2+R1*Q2
119 J=J+1
C
DO 134 II=KS7-KS1+1,KS7
XXX1(II)=XX1(II)*FR(0)
XXX2(II)=XX2(II)*FR(0)
  DO 137 I=1,KS5
  R1=XX1(II+I)
  R2=XX1(II-I)
  Q1=XX2(II+I)
  Q2=XX2(II-I)
  XXX1(II)=XXX1(II)+FR(I)*(R1+R2)
137 XXX2(II)=XXX2(II)+FR(I)*(Q1+Q2)
134 CONTINUE
C
FPH1=PHEF*GAMMA
FPH2=FPH1*ALPHA+FPH2
FPH3=FPH1+FPH2
DO 132 I=KS7-KS1+1,KS7
CT RR=1/SQRT(XXX1(I)**2+XXX2(I)**2)
  RR=1/(ABS(XXX1(I))+ABS(XXX2(I)))
C
FPH=FPH+FPH3
IF(FPH.GT.PI3) THEN

```

```

    FPH=FPH-PI3
ELSEIF(FPH.LT.-PI3) THEN
    FPH=FPH+PI3
ENDIF
R1=XXX1(I)
Q1=XXX2(I)
R2=COS(FPH)
Q2=SIN(FPH)
XXX1(I)=R1*R2+Q1*Q2
XXX2(I)=Q1*R2-R1*Q2
    XXX1(I)=XXX1(I)*RR
    XXX2(I)=XXX2(I)*RR

```

132
C

```

    XXXM1=XXX1(I1)*BSF(0)
    XXXM2=XXX2(I1)*BSF(0)
    DO 131 I=1,KS12
        XXXM1=XXXM1+BSF(I)*(XXX1(I1-I)+XXX1(I1+I))
        XXXM2=XXXM2+BSF(I)*(XXX2(I1-I)+XXX2(I1+I))

```

131
C

```

CALL ANGSUB1(XXXM1,XXXM2,PHPOSF)
PH=PHPOSF
IF(PH.LT.-PI1) PH=PH+PI3
IF(PH.GT.PI1) PH=PH-PI3

```

C
C
C

VIT-DETECTION

```

GOTO(11,12,13,14,15,16,17,18),MEAS

```

```

11  CALL SUB1(XXXM1,XXXM2)
    GOTO 20
12  CALL SUB2(XXXM1,XXXM2)
    GOTO 20
13  CALL SUB3(XXXM1,XXXM2)
    GOTO 20
14  CALL SUB4(PH)
    GOTO 20
15  CALL SUB5(XXXM1,XXXM2)
    GOTO 20
16  CALL SUB6(XXXM1,XXXM2)
    GOTO 20
17  CALL SUB7(XXXM1,XXXM2)
    GOTO 20
18  CALL SUB8(XXXM1,XXXM2)

```

C
20

```

CE=CE1(1)
C(1)=C1(8)+CE
C(35)=C1(56)+CE
C(130)=C1(16)+CE
C(164)=C1(64)+CE
C(260)=C1(32)+CE
C(290)=C1(48)+CE
C(387)=C1(24)+CE
C(417)=C1(40)+CE

```

C

```

CE=CE1(3)
C(10)=C1(16)+CE
C(44)=C1(64)+CE
C(137)=C1(8)+CE
C(171)=C1(56)+CE
C(267)=C1(24)+CE
C(297)=C1(40)+CE

```

C(396)=C1(32)+CE
C(426)=C1(48)+CE

C

CE=CE1(7)
C(27)=C1(24)+CE
C(57)=C1(40)+CE
C(156)=C1(32)+CE
C(186)=C1(48)+CE
C(282)=C1(16)+CE
C(316)=C1(64)+CE
C(409)=C1(8)+CE
C(443)=C1(56)+CE

C

CE=CE1(5)
C(20)=C1(32)+CE
C(50)=C1(48)+CE
C(147)=C1(24)+CE
C(177)=C1(40)+CE
C(273)=C1(8)+CE
C(307)=C1(56)+CE
C(402)=C1(16)+CE
C(436)=C1(64)+CE

C

CE=CE1(2)
C(69)=C1(72)+CE
C(103)=C1(120)+CE
C(198)=C1(80)+CE
C(232)=C1(128)+CE
C(328)=C1(96)+CE
C(358)=C1(112)+CE
C(455)=C1(88)+CE
C(485)=C1(104)+CE

C

CE=CE1(4)
C(78)=C1(80)+CE
C(112)=C1(128)+CE
C(205)=C1(72)+CE
C(239)=C1(120)+CE
C(335)=C1(88)+CE
C(365)=C1(104)+CE
C(464)=C1(96)+CE
C(494)=C1(112)+CE

C

CE=CE1(8)
C(95)=C1(88)+CE
C(125)=C1(104)+CE
C(224)=C1(96)+CE
C(254)=C1(112)+CE
C(350)=C1(80)+CE
C(384)=C1(128)+CE
C(477)=C1(72)+CE
C(511)=C1(120)+CE

C

CE=CE1(6)
C(88)=C1(96)+CE
C(118)=C1(112)+CE
C(215)=C1(88)+CE
C(245)=C1(104)+CE
C(341)=C1(72)+CE
C(375)=C1(120)+CE

```
C(470)=C1(80)+CE
C(504)=C1(128)+CE
DO 180 I=1,7
J=4*I
CE=CE1(I+1)
C(1+J)=C1(I)+CE
C(35+J)=C1(I+48)+CE
C(130+J)=C1(I+8)+CE
C(164+J)=C1(I+56)+CE
C(260+J)=C1(I+24)+CE
C(290+J)=C1(I+40)+CE
C(387+J)=C1(I+16)+CE
C(417+J)=C1(I+32)+CE
```

180
C

```
DO 181 I=1,5
J=4*I
CE=CE1(I+3)
C(10+J)=C1(I+8)+CE
C(44+J)=C1(I+56)+CE
C(137+J)=C1(I)+CE
C(171+J)=C1(I+48)+CE
C(267+J)=C1(I+16)+CE
C(297+J)=C1(I+32)+CE
C(396+J)=C1(I+24)+CE
C(426+J)=C1(I+40)+CE
```

181
C

```
DO 182 I=0,2
J=4*I
CE=CE1(I+1)
C(2+J)=C1(I+14)+CE
C(36+J)=C1(I+62)+CE
C(129+J)=C1(I+6)+CE
C(163+J)=C1(I+54)+CE
C(259+J)=C1(I+22)+CE
C(289+J)=C1(I+38)+CE
C(388+J)=C1(I+30)+CE
C(418+J)=C1(I+46)+CE
```

182
C

```
CE=CE1(8)
C(31)=C1(17)+CE
C(61)=C1(33)+CE
C(160)=C1(25)+CE
C(190)=C1(41)+CE
C(286)=C1(9)+CE
C(320)=C1(57)+CE
C(413)=C1(1)+CE
C(447)=C1(49)+CE
```

C

```
DO 183 I=0,5
J=4*I
CE=CE1(I+1)
C(3+J)=C1(I+18)+CE
C(33+J)=C1(I+34)+CE
C(132+J)=C1(I+26)+CE
C(162+J)=C1(I+42)+CE
C(258+J)=C1(I+10)+CE
C(292+J)=C1(I+58)+CE
C(385+J)=C1(I+2)+CE
C(419+J)=C1(I+50)+CE
```

183
C

```
DO 184 I=1,3
J=4*I
CE=CE1(I+5)
C(20+J)=C1(I+24)+CE
C(50+J)=C1(I+40)+CE
C(147+J)=C1(I+16)+CE
C(177+J)=C1(I+32)+CE
C(273+J)=C1(I)+CE
C(307+J)=C1(I+48)+CE
C(402+J)=C1(I+8)+CE
C(436+J)=C1(I+56)+CE
```

184
C

```
DO 185 I=0,3
J=4*I
CE=CE1(I+1)
C(4+J)=C1(I+28)+CE
C(34+J)=C1(I+44)+CE
C(131+J)=C1(I+20)+CE
C(161+J)=C1(I+36)+CE
C(257+J)=C1(I+4)+CE
C(291+J)=C1(I+52)+CE
C(386+J)=C1(I+12)+CE
C(420+J)=C1(I+60)+CE
```

185
C

```
DO 186 I=1,6
J=4*I
CE=CE1(I+2)
C(69+J)=C1(I+64)+CE
C(103+J)=C1(I+112)+CE
C(198+J)=C1(I+72)+CE
C(232+J)=C1(I+120)+CE
C(328+J)=C1(I+88)+CE
C(358+J)=C1(I+104)+CE
C(455+J)=C1(I+80)+CE
C(485+J)=C1(I+96)+CE
```

186
C

```
CE=CE1(1)
C(65)=C1(71)+CE
C(99)=C1(119)+CE
C(194)=C1(79)+CE
C(228)=C1(127)+CE
C(324)=C1(95)+CE
C(354)=C1(111)+CE
C(451)=C1(87)+CE
C(481)=C1(103)+CE
```

C

```
DO 187 I=1,4
J=4*I
CE=CE1(I+4)
C(78+J)=C1(I+72)+CE
C(112+J)=C1(I+120)+CE
C(205+J)=C1(I+64)+CE
C(239+J)=C1(I+112)+CE
C(335+J)=C1(I+80)+CE
C(365+J)=C1(I+96)+CE
C(464+J)=C1(I+88)+CE
C(494+J)=C1(I+104)+CE
```

187
C

```
DO 188 I=0,2
J=4*I
```

```
CE=CE1(I+1)
C(66+J)=C1(I+77)+CE
C(100+J)=C1(I+125)+CE
C(193+J)=C1(I+69)+CE
C(227+J)=C1(I+117)+CE
C(323+J)=C1(I+85)+CE
C(353+J)=C1(I+101)+CE
C(452+J)=C1(I+93)+CE
188 C C(482+J)=C1(I+109)+CE
DO 189 I=0,6
J=4*I
CE=CE1(I+1)
C(67+J)=C1(I+81)+CE
C(97+J)=C1(I+97)+CE
C(196+J)=C1(I+89)+CE
C(226+J)=C1(I+105)+CE
C(322+J)=C1(I+73)+CE
C(356+J)=C1(I+121)+CE
189 C C(449+J)=C1(I+65)+CE
C(483+J)=C1(I+113)+CE
DO 190 I=1,2
J=4*I
CE=CE1(I+6)
C(88+J)=C1(I+88)+CE
C(118+J)=C1(I+104)+CE
C(215+J)=C1(I+80)+CE
C(245+J)=C1(I+96)+CE
C(341+J)=C1(I+64)+CE
C(375+J)=C1(I+112)+CE
190 C C(470+J)=C1(I+72)+CE
C(504+J)=C1(I+120)+CE
DO 191 I=0,4
J=4*I
CE=CE1(I+1)
C(68+J)=C1(I+91)+CE
C(98+J)=C1(I+107)+CE
C(195+J)=C1(I+83)+CE
C(225+J)=C1(I+99)+CE
C(321+J)=C1(I+67)+CE
C(355+J)=C1(I+115)+CE
191 C C(450+J)=C1(I+75)+CE
C(484+J)=C1(I+123)+CE
M1=1
II1=0
DO 103 M=1,16,4
CCC=C(M1)
J=M1
DO 106 I=M1+1,M1+31
IF((C(I)-CCC).GE.0.0) GOTO 106
CCC=C(I)
J=I
106 C CONTINUE
J=MOD(J,32)
IF(J.EQ.0) J=32
J=MOD(J,4)
IF(J.EQ.0) J=4
```

```
IVV(M,0)=II1
CC(M)=CCC
DO 107 I=KT14,-1
107 IVV(M,I)=IV(J,I+1)
CCC=C(M+32)
J=M1+4
DO 110 I=M1+33,M1+63
IF((C(I)-CCC).GE.0.0) GOTO 110
CCC=C(I)
J=I
110 CONTINUE
J=MOD(J,32)
IF(J.EQ.0) J=32
J=MOD(J,4)
IF(J.EQ.0) J=4
IVV(M+1,0)=II1
CC(M+1)=CCC
J=J+4
DO 108 I=KT14,-1
108 IVV(M+1,I)=IV(J,I+1)
CCC=C(M+64)
J=M1+8
DO 109 I=M1+65,M1+95
IF((C(I)-CCC).GE.0.0) GOTO 109
CCC=C(I)
J=I
109 CONTINUE
J=MOD(J,32)
IF(J.EQ.0) J=32
J=MOD(J,4)
IF(J.EQ.0) J=4
IVV(M+2,0)=II1
CC(M+2)=CCC
J=J+8
DO 121 I=KT14,-1
121 IVV(M+2,I)=IV(J,I+1)
CCC=C(M1+96)
J=M1+12
DO 128 I=M1+97,M1+127
IF((C(I)-CCC).GE.0.0) GOTO 128
CCC=C(I)
J=I
128 CONTINUE
J=MOD(J,32)
IF(J.EQ.0) J=32
J=MOD(J,4)
IF(J.EQ.0) J=4
IVV(M+3,0)=II1
CC(M+3)=CCC
J=J+12
DO 115 I=KT14,-1
115 IVV(M+3,I)=IV(J,I+1)
II1=II1+1
103 M1=M1+128
C
C SEARCH THE MIN. COST VECTOR
C
CCC=1.0E+7
DO 116 I=1,16
IF((CC(I)-CCC).GE.0.0) GOTO 116
```

```

CCC=CC(I)
JJ=I
116 CONTINUE
C
C   CHOOSE THE 128 COSTS
C
J=1
DO 138 I=1,512,32
R1=C(I)
R2=C(I+1)
R3=C(I+2)
R4=C(I+3)
C1(J)=MIN(R1,R2,R3,R4)
R5=C(I+4)
R6=C(I+5)
R7=C(I+6)
R8=C(I+7)
C1(J+1)=MIN(R5,R6,R7,R8)
R9=C(I+8)
R10=C(I+9)
R11=C(I+10)
R12=C(I+11)
C1(J+2)=MIN(R9,R10,R11,R12)
R13=C(I+12)
R14=C(I+13)
R15=C(I+14)
R16=C(I+15)
C1(J+3)=MIN(R13,R14,R15,R16)
R17=C(I+16)
R18=C(I+17)
R19=C(I+18)
R20=C(I+19)
C1(J+4)=MIN(R17,R18,R19,R20)
R21=C(I+20)
R22=C(I+21)
R23=C(I+22)
R24=C(I+23)
C1(J+5)=MIN(R21,R22,R23,R24)
R25=C(I+24)
R26=C(I+25)
R27=C(I+26)
R28=C(I+27)
C1(J+6)=MIN(R25,R26,R27,R28)
R29=C(I+28)
R30=C(I+29)
R31=C(I+30)
R32=C(I+31)
C1(J+7)=MIN(R29,R30,R31,R32)
138 J=J+8
C
C   SUBTRACT ALL THE COSTS BY CCC
C
DO 117 I=1,128
C1(I)=C1(I)-CCC
IF(C1(I).EQ.0.0) JJJ=I
117 CONTINUE
C
C   IF(ISW.EQ.1) THEN
C
PHPOS=PH

```

```
IF(PH.LT.0) PHPOS=PH+PI3
JJJ=MOD(JJJ,8)
IF(JJJ.EQ.0) JJJ=8
PHASTI=JJJ*PI4-PI8
PHEF=PHPOS-PHASTI
IF(ABS(PHEF).GT.PI1) THEN
  IF(PHEF.GT.0) THEN
    PHEF=PHEF-PI3
  ELSE
    PHEF=PHEF+PI3
  ENDIF
ENDIF
ELSE
```

C

```
IF(LL.GE.200) THEN
PHPOS=PH
IF(PH.LT.0) PHPOS=PH+PI3
JJJ=MOD(JJJ,8)
IF(JJJ.EQ.0) JJJ=8
PHASTI=JJJ*PI4-PI8
PHEF=PHPOS-PHASTI
IF(ABS(PHEF).GT.PI1) THEN
  IF(PHEF.GT.0) THEN
    PHEF=PHEF-PI3
  ELSE
    PHEF=PHEF+PI3
  ENDIF
ENDIF
ELSE
```

C

```
IF(LL.EQ.199) GAMMA=0.03
IF(LL.EQ.199) ALPHA=0.015
PHEF=PHPOSF-PH1
PH1=PHPOSF
IF(PHEF.GT.0) THEN
  PHEF=PHEF-PI1
ELSE
  PHEF=PHEF+PI1
ENDIF
ENDIF
ENDIF
```

C

C

C

MOVE THE VECTORS IVV BACK TO THE IV VECTORS

118

C

```
DO 118 J=1,16
  DO 118 I=KT14,0
    IV(J,I)=IVV(J,I)
```

```
ISS=IV(JJ,KT13)
IF(ISS.EQ.0) THEN
  IXXX1=0
  IXXX2=0
ELSEIF(ISS.EQ.1) THEN
  IXXX1=0
  IXXX2=1
ELSEIF(ISS.EQ.2) THEN
  IXXX1=1
  IXXX2=0
ELSE
  IXXX1=1
```

```

    IXXX2=1
  ENDIF

```

C
C
C
C

```

COUNT ERROR BURSTS

```

```

IB3=IB3+1
IB1=IB1+1
IB2=IB2+1
IF(IXXX1.EQ.IX1(KT15).AND.IXXX2.EQ.IX2(KT15)) GOTO 111
IF(IX1(KT15).NE.IXXX1) IBE=IBE+1
IF(IX2(KT15).NE.IXXX2) IBE=IBE+1
IF(IB1.GT.3) IA1=IA1+1
IB1=0
IF(IB2.GT.10) IA2=IA2+1
IB2=0
IF(IB3.GT.28) IA3=IA3+1
IB3=0

```

111

```

CONTINUE
IF(ISW.EQ.0) THEN
  NTEST1=L
  NTEST2=10000
  P1=P
  GAMMA=GAMMA1
  ALPHA=ALPHA1
  ISW=1
  GOTO 1006
ENDIF
IF(MEAS.NE.1.AND.MEAS.NE.3) PRINT*,'PHASE DEMODULATION IS USED'
PRINT*,'-----'
IF(MEAS.EQ.1) THEN
  PRINT*,'CX IS USED'
ELSEIF(MEAS.EQ.2) THEN
  PRINT*,'PH**2 IS USED'
ELSEIF(MEAS.EQ.3) THEN
  PRINT*,'LIMITER IS USED'
ELSEIF(MEAS.EQ.4) THEN
  PRINT*,'PH IS USED'
ELSEIF(MEAS.EQ.5) THEN
  PRINT*,'R*PH IS USED'
ELSEIF(MEAS.EQ.6) THEN
  PRINT*,'R*PH*PH IS USED'
ELSEIF(MEAS.EQ.7) THEN
  PRINT*,'COS(PH) IS USED'
ELSE
  PRINT*,'R*COS(PH) IS USED'
ENDIF
PRINT*,'-----'
CT PRINT*,'SINE WAVE PD IS USED'
PRINT*,'EX-OR GATE PD IS USED'
PRINT*,'THE CHANNAL SPACING IS (M HZ)',(CSP)
PRINT*,'THE BASEBAND SHAPPING FILTER IS R.O. (SQ.RT=)',ROF
PRINT*,'THE FREQ OFFSET IS',INT(FOS)
PRINT*,'GAMMA & ALPHA ARE',GAMMA,ALPHA
PRINT*,'THE TRUNCATED LENGTH OF THE BASEBAND FILTER IS',KT12
PRINT*,'THE SEED INTEGER IS',IIQQ
PRINT*,'NO. OF SYMBOL TRANSMITTED=',L*10000
E1=E1/(REAL(L*10000)*4.0*KS1)
E2=E2/(REAL(L*10000)*4.0*KS1)
PRINT*,'THE PERDISTORTOR AND TWT VALUES ARE',INT(PREDBK),INT(BK)

```

```
PRINT*, 'THE PREDISTORTION BACKOFF POINT IS', PBOP
PRINT*, 'ENERGY PER BIT AT THE INPUT TO THE PREDISTORTOR IS', E2
PRINT*, 'THE BACKOFF POINT IS', BOP
PRINT*, 'ENERGY PER BIT AT THE INPUT OF THE TWT', E1
EB=E/REAL(L*10000)/REAL(KS1)
PRINT*, 'ENERGY PER BIT AT THE OUTPUT OF THE DEMODULATOR IS', EB
PRINT*, 'VARIANCE OF NOISE IS', P
IJ=2*L*10000
PRINT*, 'THE SNR IS', 10.0*LOG10(EB*KS1/2/(P*P))
BER=REAL(IBE)/REAL(IJ)
PRINT*, 'BIT ERROR RATE IS', BER
PRINT*, 'NO. OF ERROR IS', IBE
PRINT*, 'ERROR BURST IA1 IS', IA1
PRINT*, 'ERROR BURST IA2 IS', IA2
PRINT*, 'ERROR BURST IA3 IS', IA3
RETURN
END
```

C

```
SUBROUTINE COSTSUB(N,CIO,CQ0,ISI1,ISI2,ISI3,
1ISQ1,ISQ2,ISQ3)
DIMENSION CIO(64),CQ0(64)
COMMON /VMAP/VIO,VI1,VI2,VI3,VI4,VI5,VI6,VI7,VQ0,VQ1,
1VQ2,VQ3,VQ4,VQ5,VQ6,VQ7
I1=ISI3+ISI1+ISQ2
I2=ISI1+ISQ3+ISQ2+ISQ1
I3=ISI2
I4=MOD(I1,2)
I5=MOD(I2,2)
I6=MOD(I3,2)
I7=4*I4+2*I5+I6+1
GOTO(1,2,3,4,5,6,7,8),I7
```

C

```
1 CIO(N)=VIO
CQ0(N)=VQ0
GOTO 9
```

C

```
2 CIO(N)=VI1
CQ0(N)=VQ1
GOTO 9
```

C

```
3 CIO(N)=VI2
CQ0(N)=VQ2
GOTO 9
```

C

```
4 CIO(N)=VI3
CQ0(N)=VQ3
GOTO 9
```

C

```
5 CIO(N)=VI4
CQ0(N)=VQ4
GOTO 9
```

C

```
6 CIO(N)=VI5
CQ0(N)=VQ5
GOTO 9
```

C

```
7 CIO(N)=VI6
CQ0(N)=VQ6
GOTO 9
```

C

8 CIO(N)=VI7
CQO(N)=VQ7

C
9 I=I
RETURN
END

C
SUBROUTINE ANGSUB(RE,AIM,PHASE)
COMMON /PPII/PI0,PI1,PI2,PI3
IF(RE.EQ.0.AND.AIM.EQ.0) THEN
PHASE=0
ELSEIF(RE.EQ.0.AND.AIM.GT.0) THEN
PHASE=PI0
ELSEIF(RE.EQ.0.AND.AIM.LT.0) THEN
PHASE=-PI0
ELSE
PHASE=ATAN(AIM/RE)
IF(PHASE.GT.0.AND.RE.LT.0.AND.AIM.LT.0) THEN
PHASE=-PI1+PHASE
ELSEIF(PHASE.LT.0.AND.RE.LT.0.AND.AIM.GT.0) THEN
PHASE=PHASE+PI1
ENDIF
ENDIF
RETURN
END

C
SUBROUTINE SUB2(RE,AIM)
COMMON /PPII/PI0,PI1,PI2,PI3
COMMON /COST/CE1(8),CIO(64),CQO(64)
CALL ANGSUB(RE,AIM,PH)

C
CE1(1)=ABS(CIO(1)-PH)
CE1(2)=ABS(CIO(9)-PH)
CE1(3)=ABS(CIO(2)-PH)
CE1(4)=ABS(CIO(10)-PH)
CE1(5)=ABS(CIO(4)-PH)
CE1(6)=ABS(CIO(12)-PH)
CE1(7)=ABS(CIO(3)-PH)
CE1(8)=ABS(CIO(11)-PH)
DO 104 I=1,8
IF(CE1(I).GT.PI1) CE1(I)=PI3-CE1(I)
104 CONTINUE

C
CE1(1)=CE1(1)**2
CE1(2)=CE1(2)**2
CE1(3)=CE1(3)**2
CE1(4)=CE1(4)**2
CE1(5)=CE1(5)**2
CE1(6)=CE1(6)**2
CE1(7)=CE1(7)**2
CE1(8)=CE1(8)**2
RETURN
END

C
SUBROUTINE SUB1(RE,AIM)
COMMON /PPII/PI0,PI1,PI2,PI3
COMMON /COST/CE1(8),CIO(64),CQO(64)

C
CE1(1)=(RE-CIO(1))**2+(AIM-CQO(1))**2
CE1(2)=(RE-CIO(9))**2+(AIM-CQO(9))**2

```
CE1(3)=(RE-CIO(2))*2+(AIM-CQ0(2))*2  
CE1(4)=(RE-CIO(10))*2+(AIM-CQ0(10))*2  
CE1(5)=(RE-CIO(4))*2+(AIM-CQ0(4))*2  
CE1(6)=(RE-CIO(12))*2+(AIM-CQ0(12))*2  
CE1(7)=(RE-CIO(3))*2+(AIM-CQ0(3))*2  
CE1(8)=(RE-CIO(11))*2+(AIM-CQ0(11))*2  
RETURN  
END
```

```
C  
SUBROUTINE SUB3(RE,AIM)  
COMMON /PPII/PI0,PI1,PI2,PI3  
COMMON /COST/CE1(8),CIO(64),CQ0(64)  
RR=SQRT(RE**2+AIM**2)  
RE=RE/RR  
AIM=AIM/RR
```

```
C  
CE1(1)=(RE-CIO(1))*2+(AIM-CQ0(1))*2  
CE1(2)=(RE-CIO(9))*2+(AIM-CQ0(9))*2  
CE1(3)=(RE-CIO(2))*2+(AIM-CQ0(2))*2  
CE1(4)=(RE-CIO(10))*2+(AIM-CQ0(10))*2  
CE1(5)=(RE-CIO(4))*2+(AIM-CQ0(4))*2  
CE1(6)=(RE-CIO(12))*2+(AIM-CQ0(12))*2  
CE1(7)=(RE-CIO(3))*2+(AIM-CQ0(3))*2  
CE1(8)=(RE-CIO(11))*2+(AIM-CQ0(11))*2  
RETURN  
END
```

```
C  
SUBROUTINE SUB4(PH)  
COMMON /PPII/PI0,PI1,PI2,PI3  
COMMON /COST/CE1(8),CIO(64),CQ0(64)
```

```
C  
106 IF(PH.GT.PI3) THEN  
    PH=PH-PI3  
ELSEIF(PH.LT.-PI3) THEN  
    PH=PH+PI3  
ENDIF  
IF(ABS(PH).GT.PI3) GOTO 106  
IF(PH.GT.PI1) PH=PH-PI1  
IF(PH.LT.-PI1) PH=PH+PI1
```

```
C  
CE1(1)=ABS(CIO(1)-PH)  
CE1(2)=ABS(CIO(9)-PH)  
CE1(3)=ABS(CIO(2)-PH)  
CE1(4)=ABS(CIO(10)-PH)  
CE1(5)=ABS(CIO(4)-PH)  
CE1(6)=ABS(CIO(12)-PH)  
CE1(7)=ABS(CIO(3)-PH)  
CE1(8)=ABS(CIO(11)-PH)  
DO 104 I=1,8  
104 IF(CE1(I).GT.PI1) CE1(I)=PI3-CE1(I)  
CONTINUE
```

```
C  
RETURN  
END
```

```
C  
SUBROUTINE SUB5(RE,AIM)  
COMMON /PPII/PI0,PI1,PI2,PI3  
COMMON /COST/CE1(8),CIO(64),CQ0(64)  
R1=SQRT(RE**2+AIM**2)  
CALL ANGSUB(RE,AIM,PH)
```

```
C
CE1(1)=ABS(CIO(1)-PH)
CE1(2)=ABS(CIO(9)-PH)
CE1(3)=ABS(CIO(2)-PH)
CE1(4)=ABS(CIO(10)-PH)
CE1(5)=ABS(CIO(4)-PH)
CE1(6)=ABS(CIO(12)-PH)
CE1(7)=ABS(CIO(3)-PH)
CE1(8)=ABS(CIO(11)-PH)
DO 104 I=1,8
IF(CE1(I).GT.PI1) CE1(I)=PI3-CE1(I)
104 CONTINUE
```

```
C
CE1(1)=R1*CE1(1)
CE1(2)=R1*CE1(2)
CE1(3)=R1*CE1(3)
CE1(4)=R1*CE1(4)
CE1(5)=R1*CE1(5)
CE1(6)=R1*CE1(6)
CE1(7)=R1*CE1(7)
CE1(8)=R1*CE1(8)
RETURN
END
```

```
C
SUBROUTINE SUB6(RE,AIM)
COMMON /PPII/PIO,PI1,PI2,PI3
COMMON /COST/CE1(8),CIO(64),CQO(64)
R1=SQRT(RE**2+AIM**2)
CALL ANGSUB(RE,AIM,PH)
```

```
C
CE1(1)=ABS(CIO(1)-PH)
CE1(2)=ABS(CIO(9)-PH)
CE1(3)=ABS(CIO(2)-PH)
CE1(4)=ABS(CIO(10)-PH)
CE1(5)=ABS(CIO(4)-PH)
CE1(6)=ABS(CIO(12)-PH)
CE1(7)=ABS(CIO(3)-PH)
CE1(8)=ABS(CIO(11)-PH)
DO 104 I=1,8
IF(CE1(I).GT.PI1) CE1(I)=PI3-CE1(I)
104 CONTINUE
```

```
C
CE1(1)=R1*CE1(1)**2
CE1(2)=R1*CE1(2)**2
CE1(3)=R1*CE1(3)**2
CE1(4)=R1*CE1(4)**2
CE1(5)=R1*CE1(5)**2
CE1(6)=R1*CE1(6)**2
CE1(7)=R1*CE1(7)**2
CE1(8)=R1*CE1(8)**2
RETURN
END
```

```
C
SUBROUTINE SUB7(RE,AIM)
COMMON /PPII/PIO,PI1,PI2,PI3
COMMON /COST/CE1(8),CIO(64),CQO(64)
CALL ANGSUB(RE,AIM,PH)
```

```
C
CE1(1)=ABS(CIO(1)-PH)
CE1(2)=ABS(CIO(9)-PH)
```

```
CE1(3)=ABS(CIO(2)-PH)
CE1(4)=ABS(CIO(10)-PH)
CE1(5)=ABS(CIO(4)-PH)
CE1(6)=ABS(CIO(12)-PH)
CE1(7)=ABS(CIO(3)-PH)
CE1(8)=ABS(CIO(11)-PH)
DO 104 I=1,8
IF(CE1(I).GT.PI1) CE1(I)=PI3-CE1(I)
CONTINUE
```

104
C

```
CE1(1)=-COS(CE1(1))
CE1(2)=-COS(CE1(2))
CE1(3)=-COS(CE1(3))
CE1(4)=-COS(CE1(4))
CE1(5)=-COS(CE1(5))
CE1(6)=-COS(CE1(6))
CE1(7)=-COS(CE1(7))
CE1(8)=-COS(CE1(8))
RETURN
END
```

C

```
SUBROUTINE SUB8(RE,AIM)
COMMON /PPII/PIO,PI1,PI2,PI3
COMMON /COST/CE1(8),CIO(64),CQO(64)
R1=SQRT(RE**2+AIM**2)
CALL ANGSUB(RE,AIM,PH)
```

C

```
CE1(1)=ABS(CIO(1)-PH)
CE1(2)=ABS(CIO(9)-PH)
CE1(3)=ABS(CIO(2)-PH)
CE1(4)=ABS(CIO(10)-PH)
CE1(5)=ABS(CIO(4)-PH)
CE1(6)=ABS(CIO(12)-PH)
CE1(7)=ABS(CIO(3)-PH)
CE1(8)=ABS(CIO(11)-PH)
DO 104 I=1,8
IF(CE1(I).GT.PI1) CE1(I)=PI3-CE1(I)
CONTINUE
```

104
C

```
CE1(1)=-R1*COS(CE1(1))
CE1(2)=-R1*COS(CE1(2))
CE1(3)=-R1*COS(CE1(3))
CE1(4)=-R1*COS(CE1(4))
CE1(5)=-R1*COS(CE1(5))
CE1(6)=-R1*COS(CE1(6))
CE1(7)=-R1*COS(CE1(7))
CE1(8)=-R1*COS(CE1(8))
RETURN
END
SUBROUTINE ANGSUB1(RE,AIM,PHASE)
COMMON /PPII/PIO,PI1,PI2,PI3
IF(RE.EQ.0.AND.AIM.EQ.0) THEN
  PHASE=0
ELSEIF(RE.EQ.0.AND.AIM.GT.0) THEN
  PHASE=PIO
ELSEIF(RE.EQ.0.AND.AIM.LT.0) THEN
  PHASE=-PIO
ELSE
  PHASE=ATAN(AIM/RE)
IF(RE.LT.0) THEN
```

```
PHASE=PI1+PHASE  
ELSEIF(RE.GT.0.AND.AIM.LT.0) THEN  
PHASE=PHASE+PI3  
ENDIF  
ENDIF  
RETURN  
END
```

```
####S  
0.5  
2  
4.38  
1  
8  
4  
2000 0  
5  
0.5  
2  
4.14  
2  
10  
4  
2000 0  
5  
0.5  
2  
3.91  
3  
13  
4  
2000 0  
5  
####S
```

REFERENCES

- [1] Clark, A.P., *Principles of Digital Data Transmission*, Pentech Press, London (1976)
- [2] Thomas, J.B., *An Introduction to Statistical Communication Theory*, pp.614-620, Wiley, New York (1969)
- [3] Lathi, B.P., *Random Signals and Communication Theory*, Intertext Books, London (1968)
- [4] Schwartz, M., *Information Transmission, Modulation, and Noise*, 2nd Ed., McGraw-Hill Kogakusha, Tokyo (1970)
- [5] Clark, A.P., *Advanced Data-Transmission Systems*, Pentech Press, London (1977)
- [6] Barton, S.K. et al, "*Communications Engineering Research*", Final Report of Project Definition Phase (PD1) Study of Experimental Payload and Earth Stations, March 1984
- [7] Feher, K., *Digital Communications : Satellite/Earth Station Engineering*, Prentice-Hall, Englewood Cliffs, NJ (1983)
- [8] Brayer, K., "Analysis of Quadrature Crosstalk in Bandpass Signals", *Proc. IEEE*, pp.292-294, Feb. 1971
- [9] Harvey, J.D., *Adaptive Detection of Digital Suppressed-Carrier A.M. Signals*", pp.362-365, PhD Thesis, Loughborough University of Technology (1978)
- [10] Taub, H. and Schilling, D.L., *Principles of Communication Systems*, pp.235-281, McGraw-Hill (1971)
- [11] Haykin, S., *Communication Systems*, pp.206-207, John Wiley & Sons, Inc., New York (1979)
- [12] Wozencraft, J.M. and Jacobs, I.M., *Principles of Communication Engineering*, John Wiley & Sons, N.Y. (1967)
- [13] Gardner, F.M. *Phaselock Techniques*, 2nd Ed., John Wiley & Sons (1979)
- [14] Stiffler, J.J., *Theory of Synchronous Communications*, Prentice-Hall, Englewood Cliffs, N.J. (1973)
- [15] Lindsey, W.C. and Simon, M.K., *Telecommunication Systems Engineering*, Prentice Hall, Englewood Cliffs, N.J. (1971)
- [16] Viterbi, A.J., *Principles of Coherent Communication*, McGraw-Hill (1966)
- [17] Gardner, F.M., "Hang-up in Phase-Lock Loop", *IEEE Trans. on Commun.*, Vol. COM-25, NO.10, Oct. 1977
- [18] Gupta, S.C., "On Optimum Digital Phase Locked Loops", *IEEE Trans. on Commun.*, COM-16, pp.340-344, April 1968
- [19] Gupta, S.C., "Phase-Locked Loops", *Proc. IEEE*, 63, pp. 291-306, Feb. 1975

- [20] Bhargava, U.K., Haccoun, D., Matyas, R. and Nuspl, P.P., *Digital Communications by Satellite*, John Wiley & Sons (1981)
- [21] Harvey, J.D., *Synchronisation Techniques*, Internal report, Loughborough University of Technology
- [22] Lindsey, W.C. and Chie, C.M., "A Survey of Digital Phase-Locked Loops", *Proc. IEEE*, vol. 69, NO. 4, pp. 410-431, April 1981
- [23] Openheim, A.V. and Shafer, R.W., *Digital signal processing*, Prentice-Hall, 1975
- [24] Maisel, L., *Probability, statistics and random processes*, Simon and Schuster Inc., NY, 1971

